AERODYNAMICS AND MODELLING OF VANE-SWIRLED FLAMES IN FURNACES

by

S.A. Beltagui, B.Sc.

Thesis submitted for the Degree of Ph.D.
to the Faculty of Engineering,
The University of Glasgow.

May, 1974.

ProQuest LLC.
789 East Eisenhower Parkway
P.O. Box 1346
Ann Arbor, MI 48106 – 1346

ACKNOWLEDGEMENT

The author wishes to thank Professor R.S. Silver and Dr. N.R.L. Maccallum for their encouragement and advice throughout the course of this work. The work of the departmental technicians is gratefully acknowledged.

The author wishes also to thank the Science Research Council and the Faculty of Engineering, Glasgow University for financial assistance.

SUMMARY

Swirl produces notable effects on flames, generally making them shorter and highly stable over a wide range of air and fuel flows. One common method of generating a swirling jet is to employ a vane swirler. In this work the aerodynamics of vane-swirled premixed town gas-air flames are investigated in two furnaces, using the same swirlers. Variables investigated include the swirler vane angle, geometry, degree of confinement, Reynolds Number and fuel/air ratio. Cold tests were also carried out for the purpose of modelling.

Significant changes in the flow and the combustion patterns were produced by swirl. Strong swirl created a central recirculation zone which when well established had a maximum diameter and length of nearly fixed proportions of the furnace diameter. The jet spread rate was found to increase mainly with the swirler-vane angle and to vary slightly with combustion and confinement particularly at strong swirl. The presence of a central hub in the swirler had little effect on the flow and combustion pattern.

The survey of previous work and the present results showed the need for a revised measure of swirl. This was taken as the ratio of the tangential to axial velocity momentum fluxes divided by the furnace diameter. The values of this Swirl Number obtained by integrations of the flow properties were found to be a valuable index of the flow and combustion patterns. A critical value at which the flow reversal occurs was found to be the same for all input conditions tested.

The strong relation between combustion and flow patterns shows the value of isothermal model results for furnace design. For a non-swirled flame a parameter was derived on the basis of the ratio of source to shear momenta. For swirling flames, the use of the Swirl Number defined above proved to be a satisfactory modelling criterion since it has a fixed relation to the flow pattern under both cold and burning conditions.

A mathematical model was developed for the prediction of the flow and combustion patterns of confined swirling flows. The results obtained for weak and medium degrees of swirl were reasonably similar to those experimentally measured.

The study of the measured combustion patterns shows that swirling flames are stabilized by a mechanism of mixing between the fresh charge and the recirculated gases. These contained direct combustion products and entrained gases from the surroundings. The effective fuel/air ratio at the reaction zone versus blow-off velocity relations were obtained and found to be the same for both free and confined swirling flames.

Finally some recommendations to the choice of the optimum swirl range and suggestions for further work are presented.

A paper presented at the Combustion Institute European Symposium (1973) is included as an Appendix.

CONTENTS

		Page
Acknowledgement		i
Summary		ii
Contents		iv
Nomenclature		ix
CHAPTER 1.	INTRODUCTION	1
CHAPTER 2.	THEORY OF SWIRLING FLAMES	6
2.1	Introduction	6
2.2	The Simple Free Jet	7
2.2.1	Characteristics of axially symmetric jets	7
2.2.2	Jet entrainment	8
2.3	The Confined Jet	9
2.3.1	Recirculation theory of Thring-Newby	10
2.3.2	Recirculation theory of Craya-Curtet	12
2.3.3	Experimental work on confined jets	13
2.4	The Swirling Jet	14
2.4.1	Isothermal free swirling jet	14
2.4.2	Methods of swirl generation	17
2.4.3	Efficiency of swirl generation	18
2.4.4	Quantitative measure of swirl	20
2.4.5	Validity of Kerr's swirl number	22
2.5	Similarity criteria for the study of furnace flames by means of models	24
2.5.1	Modelling for aerodynamic studies	25
2.5.2	Modelling for mixing studies	26
2.5.3	Isothermal modelling of turbulent flames	26
2.5.4	A new approach to the isothermal modelling of furnaces	32
2.6	Aerodynamic measurements in swirling flames	34

			Page
2.7	Turbulence in swirling flames		35
	2.7.1	The interaction of swirl and turbulence	35
	2.7.2	Measurements of turbulence in isothermal swirling jets	37
	2.7.3	Turbulence measurements in flames	38
2.8	Review of work in Glasgow University		40
	2.8.1	The work of D. Fraser (1964)	40
	2.8.2	The work of N.M. Kerr (1965)	40
	2.8.3	The work of M.L. Mathur (1967)	42
	2.8.4	The work of G.G. Bafuwa (1970)	43
CHAPTER 3.	EXPERIMENTAL PROCEDURE		45
3.1	Introduction		45
3.2	Construction of furnaces		45
3.3	Design of vane swirlers		46
3.4	Flow systems and reactants		47
	3.4.1	Compressors	47
	3.4.2	The flow lines	48
	3.4.3	Safety devices	49
	3.4.4	The flow metering	51
	3.4.5	The town gas	52
	3.4.6	Flue ducting	53
3.5	Measurements		53
	3.5.1	Velocity and static pressure measurements	53
	3.5.2	Temperature measurements	60
	3.5.3	Concentration measurements	62
3.6	The traversing mechanism		64
3.7	Flame visual observation		65
3.8	Ignition of the flame in the furnace		66
3.9	Furnace start-up procedure		66
CHAPTER 4.	EXPERIMENTAL RESULTS		67
4.1	Introduction		67
4.2	Variables and measurements		67
	4.2.1	Input parameters	67
	4.2.2	Output or measured parameters	68
4.3	Distributions of axial velocity component		69
	4.3.1	Flow patterns of Category A	70
	4.3.2	Flow patterns of Category B	72
	4.3.3	Flow patterns of Category C	73
	4.3.4	Flow patterns of Category D	74
	4.3.5	Decay of maximum axial velocity along the furnace	75

Page

4.4	Distributions of tangential velocities		78
	4.4.1	Flow patterns in Categories A and B	78
	4.4.2	Flow patterns in Categories C and D	79
	4.4.3	Variation of the maximum tangential velocity along the furnace	79
4.5	Distributions of radial velocity component		80
4.6	Distributions of static pressure		81
	4.6.1	Flow patterns in Categories A and B	82
	4.6.2	Flow patterns in Category C	83
	4.6.3	Flow patterns in Category D	83
	4.6.4	Recovery of static pressure along the axis	84
4.7	Distributions of Temperatures		85
	4.7.1	Flow patterns in Categories A and B	85
	4.7.2	Flow patterns in Categories C and D	86
	4.7.3	Distributions of carbon dioxide concentrations	87
	4.7.4	Variation of maximum temperature along the furnace	88
	4.7.5	Variation of the centre-line temperature along the furnace	89
4.8	Axial momentum flux		89
	4.8.1	Dynamic axial momentum flux	90
	4.8.2	Total axial momentum flux	91
4.9	Axial flux of tangential momentum		92
4.10	Swirl Number S^*		93
4.11	General conclusions from experimental results		94
CHAPTER 5.	DISCUSSION OF EXPERIMENTAL RESULTS		96
5.1	Introduction		96
5.2	Some problems with experimental measurements		98
	5.2.1	The three-dimensional probe	98
	5.2.2	The effect of turbulence on velocity measurements	99
	5.2.3	Problem of flow asymmetry	100
5.3	Jet Spread		102
	5.3.1	Effect of input parameters	102
	5.3.2	Predicted relation of jet spread to pressure distributions and density changes	104

Page

	5.4	The effect of combustion	107
	5.5	Central Recirculation Zones (CRZ)	108
		5.5.1 Mechanism of creation	108
		5.5.2 Prediction of the CRZ	109
		5.5.3 Size of CRZ	111
		5.5.4 Velocities and mass flows in CRZ	112
	5.6	Shear forces in swirling flames	112
	5.7	Amplification of turbulence level by combustion	113
	5.8	Axial fluxes of axial and tangential momenta	115
CHAPTER 6.		MATHEMATICAL MODELLING OF SWIRLING FLAMES	119
	6.1	Introduction	119
	6.2	The numerical solutions of Navier-Stokes equations	120
	6.3	Turbulence transport modelling	122
		6.3.1 Conceptional models	122
		6.3.2 Mathematical models	123
	6.4	Chemical reaction representation	125
	6.5	Some relevant predictions	126
	6.6	Theory for the prediction procedure	129
		6.6.1 The principal equations	129
		6.6.2 Physical inputs	132
		6.6.3 Finite difference formulation	134
		6.6.4 The boundary conditions	135
		6.6.5 The computer programme	138
	6.7	Results and Discussion	139
		6.7.1 Cold flow	139
		6.7.2 Burning flow	140
	6.8	Suggestions for further work	140
CHAPTER 7.		STABILIZATION OF PRE-MIXED SWIRLING FLAMES	142
	7.1	Introduction	142
	7.2	Review of published work	142
	7.3	Theories of flame stabilization in recirculation zones	144
	7.4	Factors which influence entrainment	148
		7.4.1 Effect of fuel/air ratio	148
		7.4.2 Effect of end wall	150
	7.5	Effect of scale on stability limits of free flames	151

		Page
7.6	Effect of quarl on the flame stability	152
7.7	Stabilization in furnaces	153
7.8	Suggestions for further work	154
CHAPTER 8.	GENERAL CONCLUSIONS AND SUGGESTIONS	155
8.1	Aerodynamics of confined swirling flows	155
8.2	Physical modelling of flames	157
8.3	Mathematical modelling of swirling flames	157
8.4	Stability of premixed swirling flames	158
8.5	Optimum swirl range	158
8.6	Suggestions for further work	159
Bibliography		161
List of Tables		175
List of Figures		176
Tables		180
Figures		185
Appendix:	Aerodynamics of swirling flames, vane generated type. (Paper presented at the Combustion Institute, European Symposium (1973)).	

NOMENCLATURE

a	constant in Equation 4.2	
a, b, c, d	coefficients of Equation 6.8	
Ct	Craya-Curtet parameter - Equation 2.11	
C_v, C_p	specific heats, constant volume and pressure respectively	
D	furnace or confinement diameter,	m
d	swirler or nozzle diameter,	m
d_e, d_t, d_i	swirler equivalent, torque, inner diameter respectively,	m
E	time mean kinetic energy of the flow, Equation 5.5	
E	activation energy, Equation 6.13	kcal/kg mole
F	boundary shear force	N
G	flux of axial momentum, velocity term,	N
H	enthalpy	kcal/kg
h	grid spacing used for numerical solution	m
K	ratio of the surrounding flow momentum to nozzle momentum, Equation 2.11	
K	global reaction rate constant, Equation 6.13	$m^3/kg\ mole.S.K^{\frac{1}{2}}$
K	stretch factor for flame stretch theory, Equation 7.3	
k	constant, Equation 2.1	
k_1, k_2	coefficients of entrainment, Equation 2.33	m
L	length along streamlines of fresh charge flow, Equation 7.2	m
l	turbulence mixing length,	m
l_e	radius of the excess jet flow area, Equation 2.9,	m

$\dot{m}$	mass flow rate,	kg/s
m	mass fraction of the different species	
Nu	Nusselt Number	
$\bar{p}$	static pressure,	mm H_2O
p_1, p_2, p_3	3-dimensional probe pressure readings,	"
p^*	minimum static pressure at jet centreline behind swirler,	"
Q	total volume rate of flow, (jet and base) Equation 2.10,	m^3/s
q	volume rate of jet flow, Equation 2.9	"
R_c	confinement radius, Equation 2.10.	m
Re	Reynolds Number	
r	local radius	m
S	Swirl Number defined by T/Gd	
S^*	Swirl Number defined by T/GD	
S_u	laminar burning velocity	m/s
S_b, S_t	turbulent burning velocity components, Figure 5.1	
T	axial flux of tangential momentum	N.m
T	absolute temperature	^oK
U	velocity of flow along a streamline,	m/s
u,v,w	axial, radial and tangential velocity components respectively (Time-mean value)	m/s
u',v',w'	fluctuating components of u,v,w	"
u', u",	fluctuating components defined Figure 5.1	"
$\bar{V}$	total velocity vector	"

x	distance along the jet axis,	m
$\bar{x}$	axial distance in units of furnace diameter	
y	distance normal to the wall in radial direction, Section 6.6.4.a	m
y	distance normal to streamline measured from the CRZ boundary, Equation 7.2,	m
Z	hub diameter to outer swirler diameter ratio	

Suffixes:

a	ambient value
b	burner or burned gases
e	entrainment flow, excess velocity
f	furnace or full size installation, for fuel
i	impingement
i, j	index of grid lines in the x and r directions
l	values for base flow
m	model
0	values at nozzle or swirler exit section
Ox	oxident
pr	products of combustion
r	recirculation
s	shear for force, static for pressure
t	total
th	theoretical
u	unburned gases
θ	in the θ direction

Greek letters:

α	pitch angle	o
β	yaw angle	o
γ	volume ratio q/Q	
δ	boundary layer thickness	m
ϵ	emissivity or small quantity	
η	efficiency of swirl generation	
η_b	flame thickness	m
Θ	Thring-Newby parameter, Equation 2.7	
θ	swirler vane angle to the axis	o
λ	furnace size scaling factor	
μ	dynamic viscosity	kg/m.s.
ρ	density	m^3/kg
σ	Stefans constant	$kcal/m^2.s.{}^oK^4$
ψ	stream function	kg/s
$\mathcal{T}$	contact time, Equation 7.2	s
τ	shear stress	N/m^2
ϕ	any variable of the general Equation 6.8	
ω	vorticity component in the x-plane	s^{-1}

CHAPTER 1

INTRODUCTION

A furnace designer is faced with many requirements to satisfy. Although much effort has been put into the development of many practical furnaces and burners, relatively little has gone into the development of the quantitative understanding of the processes involved.

Some of the major requirements are that the flame should be stable, efficient, it should release its heat in the desired zones, and it should not produce pollutants. A further, and most important requirement, is that it should be matched to the combustion chamber.

It has been found that giving swirl to the entering gases is a convenient method of achieving at least some of the above requirements. This use of swirl has been progressively increasing in industrial applications. The methods by which swirl achieves these favourable effects are as follows:

a) Better flame stabilization, through more intense mixing especially with recirculated products of combustion.

b) Higher combustion intensity by increasing the shear stresses and their effective areas and thus the total mixing.

c) Varying the residence time towards the ideal one for complete and efficient combustion.

d) Ability to control the flow pattern by varying the degree of swirl during operation. This also leads to a good performance with wide turn-down ratios.

Most of these effects were put into use in industrial furnaces even before the fundamental knowledge of the phenomena explaining them had been understood. Studies to gain this knowledge started only very recently (in the last 10-15 years) in different institutions, (B.P., Delft Univ., Glasgow Univ., International flame research foundation, Sheffield Univ., Shell, SOGREAH, and other institutions in Japan and the U.S.S.R., etc.).

It was realised that of all the different factors governing the processes in the furnace, the aerodynamics of the flow, before and after combustion, have the greatest effect. These aerodynamics are dictated by both burner design and furnace size relative to the burner.

Predictions of the aerodynamics of swirling flames are needed, and to produce them the following methods are possible and have been used in the present work:-

1) The solution of the differential equations relating the physical and chemical laws governing the flow and combustion processes. Although some success has been achieved in some combustion problems using this method for simple flows, there are two difficulties in the case of a swirling flame:

(a) The mathematical problem of solving these equations for turbulent flows with recirculations. However with the use of numerical analysis finite-difference techniques on high-speed computers this is no longer a major problem.

(b) The physical problem of the representation of turbulent transport processes, especially where turbulence is non-isotropic and is influenced by chemical reaction. No satisfactory answer to this has yet been found. Work on the finite-difference prediction method is described in Chapter 6.

2) Direct experimental measurements on a prototype system. In addition to being expensive this method involves many limitations on the variables and their ranges. The results may only be valid for the system tested because of the interference of the factors which vary from one system to another.

However, in a specially designed test rig, variables could be separated and varied as required, giving results which will be comparable to a full-scale test and will show the effect of the different variables. Results of such experiments are essential for testing the validity of any other mathematical or physical model.

3) Use of a scaled-down model, (frequently isothermal) and relating flow conditions in the model to those in the prototype. This method has been widely applied but with different degrees of success. The success of the method depends on the careful choice of the scaling similarity criteria to be adopted when designing the model and interpreting the results. A review of the modelling criteria in use, and their application to model and full-scale tests is given in Chapter 2. Some discrepancies are shown, with a suggested new criterion for swirl flames.

The above analysis shows the need for a consistent set of experimental data, both on full-size plant and on scaled models, to test the results of the mathematical models and to define the relation between the isothermal models and full-scale furnaces. The acquisition of such data is the main object of the present work. Aerodynamic measurements were taken on two experimental furnaces for burning pre-mixed town gas-air mixtures, supplied to the furnace through vane-swirl burners with different degrees of swirl. Tests were carried out under both isothermal and combustion conditions.

Flow and combustion patterns were assessed by the following measurements at different radial locations on cross-sections along the flame or jet in the two furnace sizes:

(1) Velocity components and static pressure, using a specially designed and calibrated 3-dimensional, 3-hole probe and a disc probe.

(2) Temperatures using a thermocouple.

(3) Concentrations of carbon-dioxide using a specially designed sampling probe and a radiation absorption type analyser.

A description of the experimental set-up is given in Chapter 3. Results of measurements are presented in Chapter 4 showing a detailed picture of the flow and combustion. In Chapter 5 the results are further discussed and used to support the modelling theory. The results are also used to test the validity of the numerical predictions reported in Chapter 6.

The mechanism of flame stabilization in swirling jets is discussed in Chapter 7 and correlations are presented which are related to velocities and mixing rates.

In the final Chapter, the major conclusions of the work are summarised, and suggestions are made for further work.

CHAPTER 2

THEORY OF SWIRLING FLAMES

2.1 Introduction:

This review of the theory relating to swirling flames in furnaces starts with a brief description of the main aerodynamic features of unswirled axisymmetric isothermal free jets. The effects of confinement in a furnace, of introducing swirl and of combustion are then considered, separately and in various combinations. The various theoretical analyses, where they exist, of these arrangements are discussed (with the exception of finite-difference methods which are described separately in Chapter 6). Where experimental results offering comparisons are available, they are introduced alongside the appropriate theories. There then follows a review of relevant work which is mainly experimental. This introduces descriptions of methods of generating swirl and the definition of swirl number.

The above review of the aerodynamic theory is followed by a description of the modelling methods that have been used to predict flows in furnaces from models (usually isothermal). The various parameters for satisfactory modelling of both unswirled and swirled flames are introduced.

A review is then given of experimental work in turbulent swirling flames, a considerable proportion of this work originating from full-scale furnace tests.

The Chapter ends with a summary of the previous work carried out in the Department of Mechanical Engineering, Glasgow University.

2.2 The Simple free Jets:-

2.2.1 Characteristics of axially symmetric jets: (free, unswirled, isothermal)

Experimental measurements of free jets are numerous and mostly consistent, (e.g. Pai (1954), Schlichting (1968)). They all seem to agree on the following main features:

(a) Jet width is proportional to axial distance.

(b) Jet angle is independent of initial velocity and nozzle diameter.

(c) Jet momentum is conserved.

(d) Radial distributions of axial velocities and concentrations of nozzle fluid are similar in the fully developed region, (axial distances beyond eight nozzle diameters). For the velocity distributions, the best fit was found to be the Gaussian or Error Curve suggested by Reichardt (1941) as:

$$\frac{u}{u_m} = \exp\left[-k\left(\frac{r}{x}\right)^2\right] \quad \ldots \quad 2.1$$

where u axial velocity at radius r

u_m maximum axial velocity at the section (centreline)

x axial distance from nozzle

k a constant which varies between 73 and 117 according to different experimentators, e.g. Kerr (1965).

A similar formula represents the concentrations, only with a different constant (Hinze and Zijnen (1949)).

2.2.2 Jet entrainment:

A jet issuing into a reservoir of fluid at rest will entrain some of the surrounding, this is due to the total movement of the eddies formed at the very turbulent boundary of the jet. For an isothermal free jet this could be calculated through the integration of the velocity profiles at different axial locations. The various investigators agree to the following formula:

$$\frac{\dot{m}_e}{\dot{m}_o} = k_e \left(\frac{x}{d} \right) \quad \cdots \quad 2.2$$

where $\dot{m}_e$ is the mass flow entrained up to the section

$\dot{m}_o$ " mass flow rate from the nozzle

d " nozzle diameter

k_e " constant of proportionality, again varying from 0.25 to 0.45 according to the investigator.

A different method for measuring the mass entrainment was used by Ricou and Spalding (1961) and gave a value of 0.32. Their method involves surrounding the jet with a porous wall and adjusting the flow, which is taken to be the entrained one, so as to keep the pressure inside constant, thus simulating a free jet. However they measured the pressure only along the axis, and with a blank wall at the nozzle plane there is a chance for radial pressure gradient to be set up. The present writer considers that this leads to a wider jet than usual which is what was reported.

2.3 The confined jet:

Basically, the confined jet has some of the features of the free jet and some of the features of entrance flows. One of the fundamental differences between the confined and the free jets is the existence of pressure gradients, both in the direction of and normal to the main flow, caused by the presence of the confining walls. The effect of this is to modify the jet spread, the rate of growth of the boundary layer, and the velocity profile shape. Confined jets differ also from free jets in that the axial momentum flux is not conserved.

However, some of the theoretical methods used in studying free jets are readily extendable to confined flows. The intermediate problem of a jet in a free moving stream with a lower velocity was solved by Squire and Trouncer (1944). They assumed cosine curves for the jetting flow superimposed on the uniform base stream. Using a mixing length type turbulent viscosity and the condition of momentum conservation, they predicted the axial decay of the jet velocity and the jet boundary.

A step further was introduced by Mikhail (1960), by considering the same flow in a closed boundary. This meant no entrainment and also a non-conserved momentum. For the wall friction he used Darcy's formula and this was introduced into the total momentum balance. The decay of the maximum axial velocity was reasonably predicted but jet boundary and centreline static pressure predictions were only approximate when compared with experimental measurements for x/d values up to 34.

The work of Razinsky and Brighton (1971) included more detailed experimental measurements of the same type of flow. These consisted of wall static pressure, mean velocity and turbulent velocities and Reynolds stresses for different velocity ratios and diameter ratios. The main changes were the initial increase of static pressure and Reynolds stresses in the first two or three diameters of axial distance, followed by decay. Fully developed flow was reached within eight diameters from the nozzle, this being shorter for lower velocity ratios.

In the above works, the entrainment was supplied by the base flow which is not always available in actual confined furnaces. Calculation of the entrainment is the main feature of the two following analyses. In both a surrounding stream is assumed but this could be taken as zero for a solid wall confinement.

2.3.1 Recirculation Theory of Thring-Newby:

Thring and Newby (1953) assumed the confined jet to expand in the same manner as the free one up to the point of wall impingement. The entrainment was supplied by the surrounding fluid m_a, and when this was exhausted, by recirculated fluid m_r from the main flow. This mass flow entrained was expressed by the equation given by Hinze and Zijnen (1949):

$$m_e = m_o \left(0.4 \frac{x}{d} - 1\right) \quad \cdots \quad 2.3$$

Thus m_a will be exhausted at a distance x_a

$$\frac{x_a}{d} = 2.5 \frac{m_o + m_a}{m_o} \quad \ldots \quad 2.4$$

They further assume that the axial distance to impingement x_i is related to the confinement diameter D by the relation:

$$x_i = 2.25\ D \quad \ldots \quad 2.5$$

At this distance, the total entrained mass is m_{ei}.

$$m_{ei} = m_a + m_r \quad \ldots \quad 2.6$$

substituting Equations 2.3 to 2.6

$$m_r = m_o \left(0.9 \frac{D}{d} - 1\right) - m_a$$

$$\frac{m_r}{m_o + m_a} = \frac{0.9}{\theta} - 1 \quad \ldots \quad 2.7$$

where $$\theta = \frac{m_o + m_a}{m_o} \cdot \frac{d}{D}$$

Thus the recirculation is a function of θ only which is why it is taken as a recirculation parameter.

2.3.2 Recirculation theory of Craya-Curtet (1955)

This theory considered the mixing of two co-axial streams with different velocities within a circular chamber. The flow can be considered in two parts, within and surrounding the mixing zone of the central jet. A uniform surrounding flow of velocity u_e was assumed, with a jet stream superimposed on it having a velocity u_e (excess velocity). Thus

$$u_e = u - u_1 \quad \ldots \quad 2.8$$

The jet stream is assumed to have the error curve profile and to occupy an imaginary effective area ofradius l_e given by

$$q = \pi \, u_o \, l_e^2 \quad \ldots \quad 2.9$$

where u_o is the excess velocity at the axis. Applying continuity, the total flow is given by:

$$Q = \pi \, u_1 \, (R_c - \delta)^2 + \pi \, u_o \, l_e^2 \quad \ldots \quad 2.10$$

where R_c is the radius of the confinement

δ the wall boundary layer thickness.

With the above assumptions introduced into the integral momentum equations for boundary layer flow, they arrive at a similarity parameter Ct given by:

$$Ct = -\frac{3}{2} \gamma^2 + \gamma + K \gamma^2 \left(\frac{R_c}{l} \right)^2 \quad \ldots \quad 2.11$$

where γ is the volumetric flow ratio q/Q

K is the axial momentum flux ratio of the surrounding fluid to the nozzle fluid.

When d/D is small with respect to θ they show that

$$Ct = 1/\theta^2 \qquad 2.12$$

2.3.3 Experimental work on confined jets:

These were carried out mainly to test and verify the above two theories, the degree of agreement between them and their range of applicability.

Curtet (1958) found that the theoretical and experimental curves are not exactly the same especially near the recirculation eye. In fact the region beyond this point cannot be approached by the Craya-Curtet theory, since most of the assumptions made in establishing it cease to be valid. In a further study Curtet and Ricou (1964) proved that the terms neglected in deriving the theory were small but the jet spread parameter has to be modified. They suggested experimentally derived coefficients to do this. Velocity fluctuations were also measured but they showed only a tendency towards the assumed similarity. Further, measurements of velocity fluctuations by Barchilon and Curtet (1964) showed that high turbulence levels exist in the jet and in the reverse flow.

Predictions of the length of the recirculation eddy and of the maximum recirculated mass flow using both theories are shown to be in reasonable agreement with experiment (Thring-Newby (1953), Curtet (1958), Hubbard (1962), Brown and Thring (1965) and Chedaille et al (1966)).

2.4 The swirling jet:-

2.4.1 Isothermal free swirling jet:-

Application of swirl to a free jet is found to cause the jet to spread more rapidly, with faster rates of decay of the maximum axial velocity. The position of the maximum axial velocity is shifted radially from the centreline. Axial and radial pressure gradients are set up. Turbulence becomes anisotropic and the maximum values of the axial component move from the very outer boundary of the jet to a position nearer to the centreline.

With stronger degrees of swirl, the adverse axial pressure gradient along the axis could be high enough to create a stagnation point followed by a Central Recirculation Zone (CRZ) with reverse flow towards the swirler, Brown and Thring (1965).

Swirl alters the character of the radial motion. Whereas the radial motion is directed away from the jet axis in the central region of an unswirled jet, Rose (1962) described it as predominantly towards the centre in the swirling jet.

Theoretical analyses of swirling jets were mainly concerned with weakly swirled jets where the swirl was not strong enough to set up a CRZ. This condition made it possible to use the momentum conservation equations (Navier-Stokes equations) in their simplified Boundary layer form.

Loitsyanskii (1953) used these equations for laminar flow and then extended his method to turbulent flow using a constant value eddy viscosity. With the knowledge of jet constants, namely jet axial and tangential momenta and mass entrainment, he produced expressions for velocity components and static pressure. Similar solutions were

produced by Görtler (1954), who used the same assumptions, with an additional one of negligible radial pressure gradient. These solutions show the swirl velocity component decay to be proportional to x^{-2} compared to axial and radial velocity components which decay proportional to x^{-1}. Axial decay of static pressure was fastest and proportional to x^{-4}. Experimental verification of these results was made by Rose (1962) whose measurements agree quantitatively with the above results for the weak swirled jet tested.

A different method is to use the Karman momentum integral equations for swirling jets and assume functional forms for the velocity distributions (Steiger and Bloom (1962)), or assume similarity of the velocity distributions (Lee (1965)). Predictions of jet spread rate and axial decay of velocities were made. Lee's predictions agreed closely with Rose's experimental results.

Craya and Darrigol (1967) extended the boundary layer equation solution to predict the axial velocity and shear stress components with the help of some chosen family of profiles. Their experimental work covers a wider range of swirl, a case with CRZ being reported. Their observations were more comprehensive than those of earlier workers, axial and tangential mean and fluctuating velocity components being measured.

Contributions towards the understanding of strongly swirling free jets, i.e. strong enough to create a CRZ, are solely experimental. The swirl numbers used are based on the definition:

$$S = \frac{T}{Gd} \qquad \cdots \qquad 2.13$$

where T is the axial flux of the tangential momentum,

G " flux of axial momentum.

Distributions of axial and tangential velocity components, and fluctuations of the axial component for swirling jets were measured by Kawaguchi and Sato (1971). They also measured the static pressure along the axis. Swirl was increased up to a value of 0.35 where a CRZ was created but no detailed measurements were taken inside it.

Swirling jets issuing from a burner having tangential entry guide vanes were tested by Shagalova et al (1965) for velocities and static pressure distributions. Central recirculation zones were recorded with reverse velocities of the same order as the forward ones. Recirculated mass flows were about 0.10 of the burner flow and the maximum width of the CRZ was 0.4 of the burner diameter. Concentrations of a hot primary jet fluid in the main stream were measured as temperature distributions and rates of decay at different degrees of swirl.

Velocity and static pressure measurements in swirling jets were carried out at the International flame research foundation (IFRF) by Beer and Chigier (1963). Swirl numbers were varied up to 1.16 using a tangential entry type swirler. Measured pressures and tangential velocities at high degrees of swirl were in agreement with:

$$\frac{\partial p}{\partial r} = \rho \frac{w^2}{r} \qquad \ldots\ldots 2.14$$

Profiles of axial velocities indicated CRZ's to occur at $S > 0.39$, with recirculated mass flow increasing with swirl, a typical value being 0.12 of nozzle flow at $S = 0.785$. Integrations were made of the velocities and static pressure to calculate the mass flow and the axial and tangential momenta. The pressure term in the axial

momentum equation increased with swirl and was of comparable magnitude to the velocity term. However the sum did not vary the swirl. The tangential momentum of course increased with swirl. Both momenta showed the conservation principle to hold, within experimental limits of accuracy.

A comparative study of the CRZ's produced by different techniques (swirl, annular jet, bluff body or divergent nozzle) was made by Chigier and Gilbert (1968). Swirl appears to be a very efficient and versatile method of producing a CRZ, whether alone or coupled with other methods.

The work of Chervinsky (1969) includes isothermal and burning measurements for a low swirl jet, $S \leq 0.116$. Velocity and temperature distributions were measured and results compared with the theoretical analysis. This involved the solution of the boundary layer-type conservation equations, after being transformed to the Von Mises plane. Turbulent exchange coefficients were adjusted to the experimental measurements to vary with swirl.

2.4.2 Methods of swirl generation:

Different workers have used various methods for generating swirl and it is appropriate that these methods should be compared here.

(a) Rotation of the nozzle pipe: This method was used by Rose (1962), it produces only weak swirl even with very high rotational speed, e.g. $S = 0.095$ at 9500 rpm.

(b) Tangential entry: of part or all of the flow to the swirler. There have been different techniques of introducing the flow tangentially. Radial guide vanes were used by McEwan (1972), tangential pipe by IFRF and Sheffield groups, and nozzles were used by Kawaguchi and Sato (1971). A recent swirler used by the IFRF consisted of movable radial blocks. The main feature of this method is the ability to change the degree of swirl easily and progressivly.

(c) Swirl vanes: This is the method most widely used in industrial applications. A typical arrangement was used by Kerr (1965) and Fraser (1964). Ivanov (1968) reports five different swirlers of this type in use. An axial-tangential vane type burner designed by Akhmedov and Rashidov (1969) is claimed to have the most versatile performance.

The swirlers used in the present work are a simplified design of this type.

2.4.3 Efficiency of swirl generators:

With the number of swirlers in operation and the new designs to come, a need for a measure of the efficiency of swirl generation is evident. The cost of pumping the air, fuel or both through the swirler represents the input to a swirler. Part of this input energy is transformed to kinetic energy at exit from the swirler. An expression for the efficiency of a swirler is suggested by Ivanov (1968) as:

$$\eta = \frac{\rho_o [u_o^2 + v_o^2 + w_o^2]}{\rho_i u_i^2 + p_i .2g} \quad \ldots\ 2.15$$

where ρ_i , ρ_o fluid density at inlet and outlet of swirler.

u_i , p_i average axial velocity and static pressure at inlet to the swirler.

u_o, v_o, w_o average axial, radial and tangential velocity components at exit from swirler.

Using this formula he compares efficiencies of six different burners of different designs and concludes that a 45^o vane axial swirler has the best efficiency, of about 80%.

What appears to be a similar formula is used by Leuckel (1968) to compare tangential entry and vane swirlers of different designs, again the vane type swirler gave an efficiency in the range 70-80%.

However, two comments should be given here about the above formula:

(a) It neglects the static pressure term at the exit section from the swirler. Experimental measurements do not justify this approximation.

(b) The non-uniformity of velocity distributions should be considered, especially at higher degrees of swirl.

Considering these comments, the following expression is proposed for future work:-

$$\eta = \frac{\Sigma [\frac{\rho_o}{2g} (u_o^2 + v_o^2 + w_o^2) + p_o]}{\Sigma [\frac{\rho_i}{2g} u^2 + p_i]} \quad \ldots\ 2.16$$

Unfortunately, comparisons between different swirlers could not be made because of the lack of some of the information in the published results.

2.4.4 Quantitative measure of swirl:

The need for a measure of the degree of swirl was felt by the early workers in this field. Drake and Hubbard (1963) suggested the following two definitions:

(a) The ratio of tangential to axial momentum fluxes.

(b) The tangent of the median angle, i.e. the angle that will divide the mass flow in two equal parts.

Neither was regarded as acceptable, the first because it is dimensionally unsound and the second because it considers only the radial spread of the jet and omits the main factor which is the tangential momentum.

Kerr (1965), working from dimensional analysis, took the ratio of the torque to the (thrust x nozzle diameter), as a definition for swirl. The same definition was used by the workers at the IFRF, with the only difference of using the nozzle radius instead of diameter. Subsequent workers have continued to use this definition.

The torque or tangential momentum flux is given by

$$T = 2\pi \int_0^{d/2} \rho\, u\, w\, r^2\, dr \qquad \ldots\ 2.17$$

The thrust or axial momentum flux is given by

$$G_t = 2\pi \int_0^{d/2} (\rho u^2 + p_{rel}) r \, dr \quad .... \quad 2.18$$

Thus the swirl number is given by

$$S = \frac{T}{G d_e} \quad .... \quad 2.19$$

where d_e is the swirler equivalent diameter

$$d_e = (d_o^2 - d_i^2)^{\frac{1}{2}}$$

where d_o swirler outer diameter

d_i swirler hub diameter (zero for a hubless swirler)

Kerr assumed uniform profiles for the velocities u and w at the exit plane of the swirler and that they are related by the equation

$$w = u \tan \theta \quad .... \quad 2.20$$

where θ is the vane angle to the swirler axis.

Further he neglected the pressure term in the thrust equation. Thus a torque mean diameter was defined as

$$d_t = \frac{2}{3} \frac{d_o^3 - d_i^3}{d_o^2 - d_i^2} = \frac{2}{3} d_o \frac{1 - Z^3}{1 - Z^2} \quad ... \quad 2.21$$

where Z is the hub ratio defined as d_i / d_o and the swirl number is reduced to the form

$$S = \frac{1}{3} \tan \theta . \frac{1 - Z^3}{(1-Z^2)^{1.5}} \quad ... \quad 2.22$$

For annular swirlers and

$$S = \frac{1}{3} \tan \theta \qquad \ldots \quad 2.23$$

for hubless swirlers.

This means that the swirl number is a function of the swirler geometry only. For combined concentric jets with swirl on both of them, the swirl number is based on the sum of the torques divided by the sum of thrusts and the equivalent diameter of a nozzle to pass the total mass with the same thrust.

2.4.5 Validity of Kerr's swirl number:

The ratio $\frac{T}{Gd}$ was used by most investigators and correlated results of swirling jets and flames with a good degree of success. However, the following experimental findings have to be considered.

(a) Measurements of velocities issuing from swirlers show non-uniform profiles contrary to the assumption of Kerr and others.

(b) The increase in the axial momentum flux caused by the higher swirler exit static pressure required when combustion occurs, was not considered.

(c) Measurements of velocity profiles showed that in cold tests the same swirler gave different flow patterns for free jets as compared to confined jets. In the latter case, patterns varied with different degrees of confinement.

(d) Using the same swirler and under the same confinement conditions, results of flow patterns under isothermal and burning conditions were different.

(e) Flow patterns of free open cold jets are different from those of free burning ones.

(f) Flow pattern tests on prototype and isothermal models with the same vane angle, and with the burner diameter scaled according to the Thring-Newby (1953) criteria, gave different results.

The above findings are compiled from the results of the experimental work reported here and from the experiments of previous workers, (e.g. Mathur (1966), Bafuwa (1970), Afrosimova (1967), Wu and Fricker (1971), McEwan (1972) .. etc.).

It was thought in the present investigation that the discrepancies, c, d, e, f, are the results of the false assumptions described in a, b, plus the fact that the size of the combustion chamber relative to the swirler does affect the flow pattern and should be considered. Another factor to be considered is the pressure rise upstream of the flame which is partly responsible for the differences indicated in d, e, f.

Thus it was decided to calculate the swirl number using the experimental results numerically integrated by equations 2.17 and 2.18 to determine the values of T and G. As to the consideration of the combustion chamber size, the use of the chamber diameter, instead of the swirler diameter, as the characteristic length in the swirl number is suggested, where the degree of confinement is significant. The limiting case will be a function of the jet spread as will be seen from the following analysis. The development of these extensions to the original forms of swirl number is described subsequently in Chapters 4 and 5.

2.5 Similarity criteria for the study of furnace flames by means of models:-

Model studies in furnaces can often offer the quickest and least expensive route to the information for development and design. The purpose of modelling furnace systems is to predict conditions inside existing or projected equipment by carrying out experiments on models which are smaller in size than the prototype, or work at lower temperature, or both.

The success of modelling depends largely on ensuring that similarity, between the processes investigated in the model and the prototype, exists. Johnston and Thring (1957) distinguished five types of similarity for flow systems:

(a) Geometric similarity: The shapes of the model and prototype to be similar.

(b) Kinematic similarity: Traces of particles to be similar in both.

(c) Dynamic similarity: Similarity of the ratios of the important forces.

(d) Thermal similarity: Effects of temperature differences and gradients to be the same.

(e) Chemical similarity: Effects of concentration differences and residence-time distributions to be the same.

The similarity criteria are dimensionless groups which are usually established by the use of either dimensional analysis or from the differential equations relating the processes studied.

These groups have to be equal in model and prototype. However, the strict requirements of similarity are so numerous and restrictive that complete modelling of a combustion system is practically impossible. In fact it is never necessary to aim at complete modelling and the central task of the problem is the critical selection of the groups which need to be retained for successful partial modelling.

In the work reported here, interest is focussed on the aerodynamic, mixing and combustion processes.

2.5.1 Modelling for aerodynamic studies:-

The similarities required are,

(a) Geometric similarity: However when a cold model is used to represent a combustion system, this similarity has to be distorted to allow for the density changes accompanying the combustion process. This distortion will be discussed later.

(b) Dynamic similarity: When the flow Reynolds number is sufficiently high to ensure fully developed turbulent flow, a regime similarity will suffice and values need not be equal, Hulse (1960). Further, when the flow is fully turbulent, it is not necessary for the Prandtl, Schmidt and Froude numbers to be the same in the model as in the prototype.

(c) Swirl similarity: The obvious choice of similarity criteria is that the swirl number (T/Gd) should be the same in model and prototype. However tests (Section 2.4.6) have shown the inadequacy of this parameter. An alternative suggestion initiated by Kerr (1965), is that the swirl number should use the furnace diameter D, rather than the burner diameter d as the characteristic dimension.

This is supported by the present work (Chapters 4 and 5). This use of the furnace diameter confirms the deduction mentioned in Section 2.4.6 which was simply based on the effect of furnace size relative to the swirler.

2.5.2 Modelling for mixing studies:

Since the distribution of fluid composition depends strongly on the aerodynamic aspects of the process, especially in the case of the gas flame considered here where no solids or liquid particles are involved, it is clear that a model which is satisfactory for aerodynamic study will give equally good results for mixing and will also give the same residence-time distribution. This was suggested by Thring and Newby (1953), and confirmed experimentally for unswirled flows. Beer and Lee (1965) extended the theoretical treatment to swirled flows and again obtained experimental verification. Further, Drake and Hubbard (1966) measured residence-time distributions of the cold flow in a furnace and found it to agree with Beer and Lee's hypothesis of a stirred flow region followed by a plug flow one, the proportions varying with swirl. Though they measured this in cold flow, the aerodynamics of the cold flow were similar, at least quantitatively, to those of the burning flow.

2.5.3 Isothermal modelling of turbulent flames:

The geometry of the burners and combustion chambers, coupled with the great density gradients that exist within the furnace, make the problem of studying the furnace aerodynamics and modelling quite complex. A way round the problem is to simplify it to the best understood arrangement, which is an isothermal free jet and then

consider in turn the additional complications of a non-isothermal jet, an enclosed jet, and a swirling jet.

(a) Non-isothermal jet:

For a jet of density ρ_o moving into surroundings of density ρ_a to be modelled, this density difference has to be considered. It is known that a free jet development is governed mainly by its momentum, thus an equivalence of momentum has to be considered. Thus a nozzle has to be designed to carry the same mass flow with the same momentum but with the nozzle fluid having the density of the surrounding fluid.

Since
$$G = 2\pi \int_0^\infty \rho u^2 \, r dr = \frac{\pi}{4} d^2 \rho u_o^2$$

$$d_o^2 \rho_o u_o^2 = d_e \rho_a u_o^2$$

Thus the equivalent nozzle diameter is

$$d_e = d_o \left(\rho_o / \rho_a \right)^{\frac{1}{2}} \quad \ldots \quad 2.24$$

where ρ_o and ρ_a are nozzle fluid and surrounding fluid densities respectively.

(b) Enclosed jet:

Two cases are to be considered separately:

(i) When the furnace diameter to the burner diameter ratio (D/d) is sufficiently large, the jet expands as a free one with enough surrounding fluid for entrainment. This case can be treated in the same manner as the free jet above. The limiting minimum value for (D/d) in this case is given by Thring-Newby (1953) as 5 for an unswirled jet. For swirling jets, Mathur (1967) indicated that

velocity profiles for jets with different degrees of swirl in a D/d = 10.0 enclosure were not different from those of the free jets.

(ii) When the ratio D/d is small, the surrounding fluid is not sufficient for the jet entrainment and thus an external recirculation flow is set up. For aerodynamic and mixing similarity, the Thring-Newby parameter θ (section 2.3) has to be equal in model and prototype; Thus we should have

$$\left(\frac{m_a + m_o}{m_o} \cdot \frac{d}{D} \right)_f = \left(\frac{m_a + m_o}{m_o} \cdot \frac{d}{D} \right)_m \quad \ldots 2.25$$

where f and m stand for prototype and model.

This condition is to be coupled with the equivalent nozzle diameter concept given in Equation 2.24 to give:

$$d_e = d\lambda \sqrt{\frac{\rho_o}{\rho_f}} \quad \ldots 2.26$$

where λ is the model scaling factor on furnace size.

ρ_f is the density of the furnace fluid.

A similar expression was derived by Thurlow (1959) using dimensional analysis, he also extended it to be used for double concentric jets. Robertson (1965) has modified this criterion for a U-fired soaking pit furnace where the width to length ratio is significant and has to be distroted in scaling the furnace. Brown and Thring (1965) also used this criterion for modelling a multi-burner marine boiler furnace.

Many investigators have used this criterion for modelling furnaces but very few produced comparative model and furnace results. Beer (1962) compared his measurements on an oil-fired furnace with those produced from a cold model at SOGREAH (Hubbard (1962)). The model was designed according to the above criterion. Comparisons showed that cold model experiments give a good approximation of the maximum flow rate of the recirculated gases and of the position of this maximum.

(c) The swirling jet:

Kerr (1965) was the first to suggest that, in addition to the Thring-Newby parameter, for a swirling flame to be modelled, torque ratios at burner and furnace have to be equal for model and prototype. One would expect that the torque, or flux of tangential momentum, in the furnace will be almost equal to the burner torque, in both model and prototype. Kerr stated this, and wrote

$$\frac{T_f}{T_m} = \frac{T_{bf}}{T_{bm}}$$

where b stands for burner.

He then inferred that the 'Swirl numbers' at equivalent furnace cross-sections should be equal, by writing

$$\frac{T_f}{T_m} = \frac{G_f}{G_m} \cdot \frac{l}{\lambda} \qquad \ldots \quad 2.27$$

Using S from Equations 2.22 or 2.23, the above criterion is reduced to

$$\frac{\tan \theta_m}{\tan \theta_f} = \left(\frac{\rho_f}{\rho_m} \right)^{\frac{1}{2}} \quad \ldots \quad 2.28$$

This means that the swirl angle has to be distorted in the same manner as the burner diameter.

This principle was used by various investigators to model swirl but it took different forms. Robertson (1966) used the group (Sd) = T/G as a modelling criterion for the swirl burner of a U-fired soaking pit furnace. Cold and burning flow patterns were similar only when this group was equal for both. McEwan (1972) used Kerr's formula to model the swirl in a water model of an oil fired square furnace, and produced similar flow patterns in furnace and model.

Isothermal and burning flow measurements in furnaces were also carried out by Shagalova et al (1967)and(1969), and also by Afrosimova (1967), at different degrees of swirl. They showed the differences in the aerodynamics when combustion takes place. They emphasized the need for experimental data on both models and prototypes in order to establish the relation between them, but no attempt was made by them to produce any parameters.

The swirl number $\frac{T}{Gd}$ was used by Wu and Fricker (1971) as a modelling parameter for small D/d furnaces. They conclude that a much smaller swirl number has to be used for the cold model than in the prototype for aerodynamic and mixing similarities to be achieved.

If the burner diameter, d, used by them is replaced by the furnace diameter D, the new swirl numbers for the prototype and for the model when producing the same flow patterns are very similar. There would be even better agreement if the pressure term in the axial momentum equation, which they did not measure, is considered.

The above analysis shows that the new definition for swirl number suggested earlier (Section 2.4) will be successful as a modelling parameter as well as a measure for the intensity of swirl. Detailed experimental evidence will be presented in Chapter 5.

(d) Isothermal modelling and the pre-combustion zone:

Use of the Thring-Newby parameter for isothermal modelling of combustion systems gives good simulation of the post-combustion zone where densities are very nearly uniform, but the pre-combustion zone is not considered. In this zone very high density changes occur across the flame front with subsequent increase in the volume flow rate. Davison (1968) proposes two techniques for the simulation of these changes, - one is to enlarge the nozzle and then absorb the excess momentum by a wire gauze set in the flame front location, - the other is to introduce part of the flow at the nozzle and the rest at the flame front zone with zero momentum flux. Although he states that these techniques are being tried, no results appear to have been published.

2.5.4 A new approach to the isothermal modelling of flames:-

While the previous analyses were based on the mean flow gross forces, this new analysis is based on the dynamic nature of the turbulent flow for both the flame and the isothermal jet. A simple jet is considered but the analysis can be extended to more complex flows.

The criterion for similarity is taken as the ratio between the two most significant external forces, namely the source momentum flux and the turbulent shear forces. The nozzle momentum flux is expressed as

$$G_o \propto \rho_o u_o^2 d^2 \quad \ldots 2.29$$

The turbulent shear force will be proportional to the product of an average shear stress and the jet or flame peripheral area. The former will be taken as

$$\tau \propto \rho u' l \frac{\partial u}{\partial r}$$

where u and u' are mean and fluctuating components of the axial velocity. l is a turbulent mixing length.
u' and l could be taken as proportional to u and ∂r respectively. The area of the jet is proportional to the square of its diameter which could be taken as the confinement diameter for small D/d values.

Thus the turbulent shear total force F_s is written as

$$F_s \propto \left(\rho u' l \frac{\partial u}{\partial r} \right) \times D^2$$

$$\propto \rho u^2 D^2 \quad \ldots 2.30$$

Using the mass continuity equation between the nozzle and a general section on the jet or flame

$$\rho_o \; u_o \; d^2 = \rho \; u \; D^2$$

Therefore the ratio of the nozzle momentum given by Equation 2.29 to the jet shear force is given by

$$\frac{G_o}{F_s} = \frac{u_o}{u} = \frac{\rho \; D^2}{\rho_o \; d^2} \qquad \ldots \quad 2.31$$

For the isothermal modelling of a combustion system this ratio should be the same for both the isothermal model and the prototype. For the isothermal jet, nozzle density is the same as in the jet, but for the prototype this changes from ρ_o to ρ_f in the flame. Thus the similarity condition is written as

$$\left[\frac{D}{d} \right]_m = \left[\left(\frac{\rho_f}{\rho_o} \right)^{\frac{1}{2}} . \; \frac{D}{d} \right]_f$$

Rearranging and taking the scaling factor $\lambda = \frac{D_m}{D_f}$

$$d_m = d \; . \; \frac{1}{\lambda} \sqrt{\frac{\rho_o}{\rho_f}} \qquad \ldots \quad 2.32$$

This is the same result as was reached by Thring-Newby, stated as Equation 2.26.

2.6 Aerodynamic measurements in swirling flames:

Most of the early experimental studies were carried out on industrial furnaces which were already available for investigation. While this was convenient and saved the expense of rig construction, on the other hand it made the results more difficult to interpret and correlate. One of the first specially constructed swirling flame rigs was used by Chigier and Chervinsky (1967) to study turbulent pre-mixed propane-air flames. Swirl intensities were low, with a maximum value of 0.107. The flame which was shorter than an unswirled one, was stabilized at an axial distance of 4d from the nozzle in the form of an annular ring with an apparently high turbulent flame velocity. The profiles of velocity and temperature showed reasonably good similarity. The decay of axial and tangential velocities was slower than in the cold jet with the same swirl number.

Brown and Thring (1965), working on an oil-fired marine boiler furnace, studied the aerodynamics of cold and burning swirling flows. Swirl was shown to increase the jet width and to concentrate the peak velocities into a cylinder which surrounds the CRZ. The reverse mass flow was about one third of the burner main flow.

A study of the solid particles and sulpher trioxide emission from a heavy oil-fired furnace led Drake and Hubbard to investigate the effect of swirl on improving the mixing in the combustion chamber. They demonstrated the effect of swirl in changing the jet width and characteristics. The existence of a CRZ was recorded and the maximum recirculated mass was found to be 0.3 of the burner flow.

Optimum conditions for burn-out of carbon solids were found to exist at a certain intermediate value of swirl of about 0.2. They also showed that under these conditions the effect of the angle of the oil spray was not critical. Tests of residence-time distributions in the cold flow with the introduction of a tracer gas were conducted. Results agreed with the stirred-plug flow assumptions of Beer and Lee (1965). Moreover, the ratio of the stirred part of the residence time to the total was a minimum at the optimum swirl.

Observations have also been made by other workers in full-scale furnaces, with flames and with cold flow, or in scaled models. As these studies were relevant to modelling, they have been described in the previous section on modelling (2.5). Some of their results are listed in Table 4.1, and will be discussed in Chapter 5.

2.7 Turbulence in swirling flames:

2.7.1 The interaction of swirl and turbulence:

Swirl has been found to change the turbulence characteristics of a jet. This might be attributed, wholly or partly, to the flow rotational instability. Since an entity of the fluid in rotational motion tends to conserve its angular momentum even when it moves radially, the stability criterion is a function of the radial gradient of the angular momentum distribution. This was first suggested by Raleigh (1916) who stated that flow is rotationally stable when the gradient $\frac{\partial}{\partial r}\left(\rho w^2 r^2\right)$ is positive, unstable when negative and neutrally stable when zero. This can be explained as follows.

In the case of a negative gradient, if an entity is displaced to a larger radius, in its new location it will possess larger angular momentum than its neighbours. The centrifugal force on this displaced entity $\left(\rho \frac{w^2}{r} \right)$ will be greater than the centripetal pressure gradient that exists at the new location, thus the particle will tend to be displaced to a still larger radius, i.e. unstable radial equilibrium. By this same reasoning a solid body rotation motion $(w \propto r)$ is seen to be stable and a free vortex $(w \propto 1/r)$ is only neutrally stable.

This principle explains two important features of a swirling jet:

(i) The importance of the type of swirl and the method of generation, since this will decide the type of vortex motion produced. In other words the degree of stability and its effect on the turbulence and mixing rates. Leuckel (1968) showed the various tangential velocity profiles produced by different swirl generators and related them to the pure free and forced vortices. Emmons (1967) applied this principle to explain the difference between the swirling burner flame and the fire whirl in a rotating atmosphere. The first was unstable and thus shortened the flame, while the second was stable and swirl made the flame longer than the unswirled one.

(ii) The effect of swirl on turbulence:

Rotational stability mentioned here, would lead to a reduction in turbulence intensities and vice versa. Rubel (1972) developed this analysis to produce the effect as a multiple factor to the flow eddy diffusivity given by $\left[1 + 91.1 \left(\frac{u}{w} \right)^2 \right]^{\frac{1}{2}}$.

Using this formula in a numerical solution of the equations of conservation of momentum and energy, he predicted mean velocity and temperature profiles comparable to those measured by Chervinsky (1969).

2.7.2 Measurements of turbulence in isothermal swirling jets:-

Rose (1962) was the first to publish turbulence measurements in swirling jets. He measured the fluctuating component of the total velocity vector. Swirl being very weak, the results showed only slight change from the unswirled jet case. Craya and Darrigol (1967) also measured the fluctuations of the velocity components in three directions. These show an increase over the unswirled jet values. They also show that eddy diffusivities in both axial and tangential directions are quite comparable. Kawaguchi and Sato (1971), assuming isotropic turbulence, measured the axial velocity fluctuating component in an open swirling jet. With weak swirl, turbulence intensity distributions tended to be similar to those for non-swirling jets, that is, nearly uniform with maxima on the boundary. For high degrees of swirl where reverse flows occur, e.g. $S = 0.35$, this tendency changed and values are generally higher with broad peaks near the centre.

Distributions of the six shear stress components have been determined from the measurements of mean and fluctuating components of velocity by Syred et al (1971-a,-b), using aspecial technique for analysing the hot-wire anemometer signals. Interest was focussed on the region near the swirler exit, both inside and outside it. A swirl number of 1.1 was used and turbulence intensities relative to the nozzle average velocity were recorded. The maximum intensity occurred at the separation point at the swirler exit and had a value of 150%,

the corresponding value of turbulent kinetic energy being 300% of that of the mean nozzle flow. Values of effective viscosities were calculated from the mean and fluctuating components. These confirmed the anisotropic nature of turbulence in this case, with components of shear in the u-w plane more important than those in the other two planes.

The flow in a cyclone chamber is less complicated than a swirling flow in a furnace, the motion being mainly rotational and with negligible radial velocities. A complete set of isothermal measurements of mean and fluctuating velocities and of static pressure was taken by Ustimenko and Bukhman (1968). These results showed similarity of profiles for both mean and fluctuating components. Correlation coefficients, kinetic energy of turbulence and values for eddy diffusivities for axial and tangential directions were calculated from the above measurements. Compared with molecular viscosities, these were one to three orders of magnitude higher.

2.7.3 Turbulence measurements in flames:

In addition to measuring the velocity fluctuations in a combustion system fluctuations of temperature and concentrations are also needed. Various techniques are in use. Velocity fluctuations can be measured by special hot wires, either directly or through a microphone, or by tracer diffusion or by ionization probe techniques. Static pressure fluctuations can also be measured by a microphone. Total emission spectral emission, ionization and thermocouple with compensation are used for temperature fluctuations. Conductivity of a special hot wire and calculations from mean values were used for concentration fluctuation

measurements. These methods were reviewed by Gunther (1970) who pointed out the need for fluctuation measurements in flames. Unfortunately every measuring technique has its limitations and reported results for simple flow flames show large discrepancies, thus there is a clear need for better techniques and more measurements. Recently, optical methods, using laser doppler shift technique, have come into use in this field and seem to be the most promising for velocity fluctuation measurements. Such results for a swirling flame have been very recently reported by Baker et al (1973). These reveal the very high turbulence intensities that exist especially at the locations where the flow reverses.

A numerical technique for calculating turbulence intensities from mean time measurements was used by some investigators and will be discussed in Chapter 6.

On the theoretical side, there is no established theory for the flame turbulence interaction as yet. An example of the work in this is the phenomenon of flame generated turbulence proposed by Karloritz (1953). Recently some of its assumptions have been challenged by measurements in a simple jet system with and without reaction, (Dashchuk (1971), Parker and Guillon (1971) and Eickhoff (1973))

2.8 Review of work in Glasgow University:

This work started as a study of the flow pattern inside a full-scale furnace fitted with a vane swirl burner. The first worker, Kerr, found thet there were too many factors in this full-size furnace to allow a complete understanding of the problem. He therefore initiated programmes of research by Fraser and Mathur on the basic phenomena. They started on symmetric free isothermal jets. Thereafter the complications of confinement, swirl and combustion were added one at a time, and then in combinations. The work on free, swirling burning jets was carried out by Bafuwa, and in the present work the effects of confinement have been studied

2.8.1 The work of D. Fraser (1964):

He developed measuring techniques for mass flow, torque and thrust of a swirl burner, both by integration of velocity measurements and by direct mechanical force balancing. Agreement between the two methods was reasonable. He showed that in the free jets the axial thrust and the torque, obtained from velocity integrations, remained constant along the jet axis. Further, as the degree of swirl was increased, the torque increased but the axial thrust remained constant, at a constant burner mass flow.

2.8.2 The work of N.M. Kerr (1965):

Kerr extended the theory of similarity for isothermal jets to the swirling jet by introducing the non-dimensional swirl number $S = \frac{T}{Gd}$, this being derived by dimensional analysis.

For the mass flow rate along the jet he modified the equation of the nonswirled jet, Equation 2.2, to be

$$\frac{\dot{m}}{\dot{m}_o} = \frac{x}{d} (k_1 + k_2 \cdot S) \quad \ldots \quad 2.33$$

Similar modifications were applied to the expressions for velocity decay, for jet spread and for jet half-angle. Velocity profiles were assumed to follow an error curve with an exponent which is influenced by swirl. Measurements in the fully developed region of the isothermal swirling jet supported this theory and the constants were determined.

Tests on the full-sized oil-fired boiler furnace were conducted with different combinations of primary and secondary degrees of swirl and the effect of each was studied. A combined swirl number was suggested and found to correlate the results, although not perfectly. An optimum range of this swirl number was found necessary to produce stable, efficient and smokeless combustion. Lower swirl flames gave an oil-chilled core near the burner, (this case has no CRZ), and higher swirl tended to split the flame into smaller, smoky sub-flames.

Kerr suggested a new criterion for isothermal modelling of furnaces with swirl burners as discussed in Section 2.5, namely, the same ratio of torque in the furnace to torque in the burner in both prototype and model, coupled with the dimensionless swirl number in the furnaces being the same. With these conditions satisfied he found the same range of optimum swirl numbers in an isothermal water model as in the full-size furnace.

2.8.3 The work of M.L. Mathur (1967):

Mathur's work was the start of a more systemmatic project stimulated both by the findings of Fraser and Kerr and by the difficulties that limited their measurements to the fully developed region of the flame. The earlier workers had not been able to study the initial part of the jet. This part is the most important from a combustion point of view, because it is here that mixing and flame stabilization occurs and from here the flame develops.

A simple efficient design of swirler was made using vane angles in the range 15° to 75°. The pressure drops measured across them were found to be proportional to $(u_o \tan \theta)^2$, thus confirming the theoretical analysis put forward. Static pressures relative to ambient on the axis at the swirler exit were proportional to $u_o^2 \tan \theta$. Measurements were made of velocity profiles, both axial and tangential, and of concentrations of a tracer at different axial locations for swirlers with a central hub or without, under free and confined boundaries. The profiles, particularly near the swirler, differed markedly from the error curve distributions. It was only at weak swirl and at distances well downstream that the error curve distribution was approached. When the ratio D/d was about 10, the confined flow profiles were very similar to the free jets. Recirculation flows at the centre of the jet were established with swirlers of 30° and higher in the confined case, and 45° and higher with the free jets.

The rates of spread of the jets in the confined flow were more rapid than in the free one for the same vane angle, although

velocity profiles were similar up to the impingement point. Maxima in the wall static pressure in the confined jets correlated with the impingement points and the centres of the CRZ. Minima in the wall static pressure coincided with the centres of the outer recirculation zones.

In studies of mixing between two concentric jets, the length of the stoichiometric contour between the two streams was shortened by swirl.

Visual tests on a water model confirmed the flow patterns obtained in the air model.

2.8.4 The work of G.G. Bafuwa (1970):

Using the same design of swirlers as Mathur, Bafuwa built up a combustion rig for burning pre-mixed town gas and air in free surroundings. Radial distributions of velocity components, axial and tangential, static pressure and temperature along the flame were measured. He recorded CRZ's with reverse flow of combustion products. Compared with cold flow, they were shorter and wider. Velocity profiles of the flames had the same general pattern as of the cold flow, although the rates of expansion of the flames were higher, particularly in the early stages of the expansion, before air entrainment had a significant effect.

Swirl was found to shorten the flame bringing the position of maximum temperature nearer to the burner.

The numerical solution of the mass, momentum, energy and species conservation equations by finite difference methods was carried out to predict velocity components in cold and burning jets. Reasonable predictions were obtained for the isothermal jet from the 15° swirler.

The work on flame stabilization included the determination of the weak and rich stability limits which were found to occur at higher fuel-air ratios as the swirl was increased.

CHAPTER 3

EXPERIMENTAL PROCEDURE

3.1 Introduction:

Experimental aerodynamic measurements were made in a rig both with cold flow and when burning a pre-mixed town gas-air flow. Two furnace sizes were used with the same set of burners, the smaller furnace being an isothermal model of the larger, according to the modelling criteria discussed in Chapter 2.

This chapter describes the design and construction of the furnaces, swirlers, flow system and sensing probes.

3.2 Construction of furnaces:

(a) Geometry:

Since the object of the experimental work is to produce results which could be correlated to the input variables and also to verify the results of mathematical predictions, a reasonably simple geometry was selected. The furnaces were both of cylindrical shape to produce axi-symmetric flows. No quarl was introduced. The ratios of furnace diameter to burner diameter were very nearly 5 for the bigger furnace and 2.5 for the smaller one.

(b) Materials:

Fire bricks were used for the large furnace and high temperature cement for the small furnace. This use of materials permitted the assumption of adiabatic flow. The large furnace was built using side-arch fire bricks to make a cylinder of 460 mm (18 in) diameter. The fire bricks were supplied by GR-Stein

and were to stand a service temperature of 1500°C. The small furnace was cast from heat resisting cement inside a steel shell to form a furnace diameter of 220 mm. The furnaces were supported upon a steel structure so that they were at a reasonable working level.

3.3 Design of vane swirlers:-

One of the main objectives of this work is to make a comparative study of the present results with previous work on free burning and cold swirled flows, for this reason the main design features of Mathur's swirlers were employed here (Mathur (1967)). Swirlers with vane angles 0°, 15°, 22.5°, 30°, 45°, 60° and 70° were manufactured. The main point was to produce as full deflection of the flow as possible with simple and symmetric vanes. This was achieved by having vanes with dimensions according to the geometry shown in Figure 3.1. The angle of overlap between each pair of adjacent vanes was 30° for swirlers of vane angle 30° and higher. For the 22.5° swirler an overlap of 15° only was practically possible. No overlap was possible for the 15° swirler, the reason being the impractical increase in the length of the vanes.

Due to the effect of the excessive heat in the current tests, the materials and the dimensions had to be changed from those of Mathur and Bafuwa. Vanes were made of stainless steel plates 1.6 mm thick with the inner and outer tubes of mild steel.

Two types of vane swirlers were prepared, annular and hubless. The reason for investigating these two types was to

determine the effect of the central hub. The net flow areas of all the swirlers, after allowing for vane blockage effects, were equal to within ±6%. An annular swirler is illustrated in Figure 3.1 which also shows the leading dimensions of all the swirlers, Table 3.1.

Burner Mounting:

The swirlers, or burners, were inserted into the inner tube of a cooling water jacket. The jacket consisted of two tubes with a helical strip in the annular space in order to keep a continuous flow of the cooling water. A heat sink coating material was applied to the swirler to reduce the effect of the insulating air gap between the swirler and the cooling jacket. The swirler was inserted in the inner tube against a shoulder in the furnace end and prevented from any rotation by a feather key on the other end. Two flanges were welded on the outer tube, one to fix it to the furnace face wall, and the other to fit the end of the pipe line supplying the air-gas mixture. This end is a movable part to allow for changing the swirlers.

3.4 Flow systems and reactants:

3.4.1 Compressors:

Two 14-piston Wellworthy-Ricardo superchargers, each driven by a 10 h.p. motor through a variable speed drive, were used to deliver the required air and gas flows. Both delivered an oil-free discharge at steady rates with very minimal pulsations. Since the required gas flow was only a fraction of the air one, a belt drive speed reduction system was fitted between the motor and the compressor for the gas system.

Motor speed control:

For the continuous control of the flows of the reactants it was needed to have the metering orifice plate readings together with the motor speed controls at one place. This was done by transmitting the motion from handwheels adjacent to the orifice manometers through long rods to pinion sprockets of chain drives which end at the compressor speed control devices.

3.4.2 The flow lines:-

These include the air, the gas and then the mixture lines. A schematic drawing is given in Figure 3.2.

(a) The air flow line:

The 3 in. (76 mm) nominal bore line from the air compressor carried an adjustable bleed to the atmosphere followed by a gate valve. The bleed and gate valve are used if ever the required air flow is very low. This was never the case in the present investigation and the bleed was kept closed and the gate valve open. Twenty one pipe diameters downstream from the valve a square edged orifice with pressure taps at D and D/2 was installed, in accordance with B.S.1042. A thermometer pocket was placed downstream of the orifice. The air line discharged into a mixing box.

(b) The gas flow line:

Town gas was supplied from the mains to the blower through a 3 in nominal bore pipe. The blower discharged into a 1.5 in. (38 mm) nominal bore steel pipe which carried a gate valve, followed at about 40 diameters by a square edged orifice plate with D and D/2 pressure tappings and a thermometer pocket. A quick closing,

electrically operated, valve was fitted in this line just before its delivery point into the mixing box.

(c) The mixture flow line:

The discharge from the mixing box was delivered to a distributing box through a wire mesh and a 0.5 m long 3 in nominal bore pipe. Originally this included a convergent-divergent section which was thought to increase the mixing, but a considerable pressure loss occurred in this section and without any extra gain in the mixing. Consequently this convergent-divergent section was replaced by a straight pipe.

The mixture from the distribution box was discharged either to a 3 in or to a 1.5 in nominal, bore pipe, both meeting again through a 90^{o} elbow into a coaxial line feeding the swirler. The 3 in pipe was used in the present work, and the 1.5 in pipe was only used when a smaller swirler was being employed for furnace heating or for stability tests. The arrangement of two pipes will be used for future work on non-premixed flames. Each line had a gate valve at its upstream end and a flame trap at the downstream end.

3.4.3 Safety devices:

Several devices were used to ensure that the flame is not started under unsafe conditions and to stop the gas supply if the flame is extinguished or flashes back. These devices are as follows:-

(i) A padlock was fitted to the gate valve in the line from the gas main to the gas compressor.

(ii) Low-pressure cut-off: The object of this cut-off is to prevent the starting or the continuing of the gas compressor operation if the gas supply pressure falls to under half its normal value of 12.5 mm Hg. A u-tube mercury manometer was connected to the gas supply line. Under normal pressure, the mercury column is raised to complete the circuit between two contacts lowered down the atmospheric limb. If the gas pressure drops, to open this circuit, this closes a relay which breaks the electrical supply to the driving motor. This prevents the compressor from drawing air into the gas line in case of gas supply failure.

(iii) Coil-operated quick-closing valve:

If, in an emergency, the gas compressor is cut-off, it will not stop instantly, because of the inertia of the moving parts. This means it is continuing to supply gas at a reduced rate for about 30 seconds. A coil-operated valve was actuated by the gas compressor starter current, so that it closes exactly when the compressor is switched off, thus reducing any gas flow to a minimum.

(iv) Flame traps:

Flame traps were fitted in the mixture lines near their downstream ends to extinguish any flame flashing back. The flame traps were those designed by the Gas Council.

(v) Bursting Discs:

To prevent any pressure being built up, a 0.6 mm thick Polythene disc was fitted at the bottom of each of the mixing and distributing boxes and at the meeting point of the two mixture lines just before the swirler.

3.4.4 The flow metering:

Square-edged orifice plates were used for measuring flow rates of reactants with four D and $\frac{1}{2}$D pressure tappings (D is pipe diameter). For air flow an orifice plate of bore diameter 0.6 D was used, while for gas flow the usual orifice plate was 0.5 D; however a 0.8 D was sometimes used, especially for stability tests. All plates, tappings and pipe lengths upstream and downstream from the orifice were designed in accordance with B.S.1042. The thermometer pockets were positioned downstream from the orifice plate locations where they did not disturb the pressure recordings. The fluid temperature measured in this way has to be corrected as determined by Bafuwa (1970).

Pressure differences across the plates were measured with water manometers, and pressures upstream of the plates with mercury manometers. All manometers were positioned in one location near the blower speed controls.

3.4.5 The town gas:

The composition of town gas used in the experiments fluctuated slightly from day to day about the average composition given in Table 3.2

TABLE 3.2

Town gas composition

Constituent	% by volume
H_2	48.2
CH_4	29.4
C_2H_6	00.8
C_3H_8	00.1
C_4H_{10}	00.1
CO	01.3
CO_2	11.1
O_2	01.8
N_2	07.2

For the purpose of calculating the gas flow rate, the gas specific gravity, relative to air, was measured twice daily using a Gas Specific Gravity Meter supplied by Alexander Wright and Co.. The time to discharge a certain volume of gas through a small orifice on the top of a bell immersed in water was measured. The gas was changed from air to town gas.

$$\text{Relative specific gravity} = \left[\frac{\text{Gas time}}{\text{Air time}}\right]^2$$

Some properties of the town gas calculated from the average composition in Table 3.2 are given in Table 3.3.

TABLE 3.3

Properties of Town Gas

Stoichiometric fuel/air by volume	0.245
Molecular weight	13.85
Net calorific value kcal/m^3	3700

The net calorific value was calculated at 16°C and 76 cm Hg.

3.4.6 Flue ducting:

Combustion products were directed from the furnace straight into a water-cooled canopy 900 by 900 mm at inlet connected to a 460 mm diameter duct which rose to a large chimney 4.5 m from the floor level.

3.5 Measurements:

Measurements were made of the following parameters. Axial, tangential and radial velocity components, static pressure, temperature and gas concentrations. These were to be measured under cold and firing conditions. In the latter case all probes were water cooled.

3.5.1 Velocity and static pressure measurements:

Of the many techniques available, the following are the most suitable methods of measuring flow velocities of gases:

(a) Pitot-tube type velocity probes, developed for three-dimensional flow measurements by having three to five holes.

(b) Hot wire anemometers.

(c) Laser-Doppler anemometers.

Although the last two methods should be capable of providing more information than the first method in the type of flow encountered in these furnaces, the problems discussed below arise.

With hot wire anemometers there are problems of compensations for the gas temperature variations and also the interpretation of the reading as to the interaction between the different components of the velocity vector. Although a method has been developed it is still open to question particularly under firing conditions, Syred (1970) and Beer and Chigier (1972).

Laser-Doppler anemometry is now a promising tool for velocity measurements in flames, but it was still in the developing stage at the time this work started.

Accordingly the 3-dimensional, 3-hole probe was chosen. This probe measures only the time average values of the velocity components. An influencing factor in this choice was the successful use of these probes in the previous investigations at Glasgow University. Mass flows calculated, from the integrated velocity measurements, by Kerr (1965) and Fraser (1964) were only 5% different from the actual flow value.

The 3-dimensional-3 hole probe:

A study of the pressure distribution around a cylinder in a cross-flow reveals the appearance of the static pressure at a certain angular position from the total pressure or stagnation point. This angular displacement was found to vary with the size of the tube and the holes, being 40°-45° for 6.35 mm tube and 51° for a 2.46 mm tube, Fechheimer (1926) and, Albright and Alexander (1957). These angles varied slightly with the flow Reynolds Number.

Thus a tube with two holes (Holes 1 and 2) at an angle of approximately 80° will give the yaw angle of a 2-dimensional flow, when both holes read the static pressure, and hence the total velocity vector from measuring the total pressure when the probe is rotated 40° back to bring hole 1 into the velocity vector plane. For 3-dimensional flows, another angle has to be measured, the pitch angle, and a third hole (No.3) in the same plane as the velocity vector has to be introduced at an angle to the first one but as near as possible to it to reduce the effect of variations due to flow pressure and velocity gradients.

On this basis the 3-dimensional probe of Hiett and Powell (1962) was designed having a V-groove at a fixed distance (2 probe tip diameters) from the end. Two holes (Nos. 1 and 2) were drilled in one flank of the 120° V groove at an angle of 72°, and the third hole on the opposite flank facing one of the first two.

For the present work, the probe tip, which was made of heat resistant alloy, Nimonic 105, had a diameter of 6.35 mm (0.25 in) to reduce the flow disturbances by the probe to a minimum and to improve the local resolution. The smallest size of holes to give a reasonable response time was used, this being 0.75 mm. These holes were connected to hypodermic stainless steel tubes of 0.8 mm inside diameter through 1.5 mm diameter axial holes in the probe tip. The tubes were soldered to the probe tip using a special high-melting silver solder supplied by Johnson Matthey Metals. The probe tip was also soldered to the outer tube of the probe cooling system. Details of the probe tip and the cooling system are shown in Figure 3.3. The cooling water system consisted of two concentric stainless steel tubes of outer diameters 9.5 and 6.35 mm, thus giving nearly equal flow areas for the inlet and outlet water flows. A continuous flow of water at a velocity which was always above 2.3 m/s was maintained. It was observed that the probe tip should not be too cold otherwise carbon deposits developed. The probe holes were occasionally blocked by dust which was blown off by compressed air.

Probe Calibration:

The 3-dimensional probe was calibrated both for velocity measurements and for static pressure measurements by inserting it in a free jet issuing from a vertical pipe of 63.5 mm (2.5 in) diameter. A uniform velocity profile at outlet from the pipe was obtained by supplying air to the pipe which is 1 m long from a settling chamber, and by inserting three wire gauses at the inlet to the pipe.

The probe was mounted in a special attachment that allowed the probe to be rotated about its own axis to find the yaw angle, β, and to be tilted to vary the pitch angle in the range 20° to 160°. A pitot-static tube could be mounted at the same attachment to establish the jet velocity and static pressure.

For the calibration, the probe was rotated at any pitch angle to get zero yaw angle where the pressure difference $(p_1 - p_2)$ is zero, then the probe was rotated back 36° and the pressures p_1, p_2 and p_3 were recorded. The pressures p_1, p_2 and p_3 represent the pressures sensed by the probe holes 1, 2 and 3 respectively. This procedure was repeated for pitch angles from 20° to 160° at intervals of 5°. The whole calibration was repeated at four different flow velocities to ensure the independence of the calibration from the Reynolds Number.

Values of $(p_1 - p_3)$, $(p_t - p_s)$ and $(p_s - p_2)$ as ratios of the corresponding $(p_1 - p_2)$ at different Reynolds Numbers were plotted against the pitch angle. Curves at the different Reynolds numbers were very close or overlapped for most of the pitch angle range. An average curve was therefore taken to represent all values. Figure 3.4 illustrates a typical set of calibration curves.

The Use of the probe:

The probe was first rotated to obtain a zero value of $(p_1 - p_2)$ and the yaw angle β was then recorded. The probe was then rotated back 36° to bring holes 1 and 3 facing the flow and all three pressures p_1, p_2 and p_3 were recorded.

The ratio $(p_1 - p_3)/(p_1 - p_2)$ was calculated and used as an entry to the calibration chart from which we get the pitch angle α and using the known p_1, p_2 and p_3 we find the total velocity head and the static pressure. With the velocity head and the density calculated using the local measured temperatures, the total velocity vector $\bar{V}$ is obtained. This is resolved into the three components u, v and w using the following relations, (see Figure 3.5),

$$\begin{aligned} u &= \bar{V} \sin \alpha \cos \beta \\ v &= \bar{V} \cos \alpha \\ w &= \bar{V} \sin \alpha \sin \beta \end{aligned} \qquad \ldots \quad 3.1$$

Static pressure:

Static pressures could be determined from the 3-dimensional probe calibration curves. However when these were plotted, sometimes there were discontinuities at points of great pressure and velocity gradients. Since this probe had not been used before for static pressure measurements, a different probe was used to check static pressures at those discontinuities. This was a disc probe to the design of Miller and Comings (1957). This is shown in Figure 3.6 and consists of a very smooth surface disc of 12.5 mm diameter having a 0.5 mm diameter hole in its centre and connected to a pressure transducer. When the disc is in the plane of the velocity vector, which was already decided from the 3-dimensional probe readings, this will read the static pressure.

Values of static pressures read by this probe agreed with those read by the 3-dimensional probe except for a few points where pressure and velocity gradients were high. It was decided that static pressure values indicated by the disc probe in this region were more reliable than those obtained from the 3-dimensional probe.

Pressure measurement and recording:

Pressure signals from the three holes of the 3-dimensional probe and from the disc static pressure probe were measured by a diaphragm-capacitance type micromanometer supplied by Furness Controls Ltd. This has 3-ranges of pressures covering the ranges $\pm$ 12.5, $\pm$ 25.0 and $\pm$62.5 mm water with an accuracy of 1%, of the base scale full deflection. The instrument gave stable calibration and non-significant zero shift over long periods of operation and ambient temperature variations.

The output from the micromanometer was read and recorded by a Kent recorder on a 250 mm wide chart. Full scale deflection was obtained with any input between 1 and 50 millivolt according to the range selected. The accuracy of the recorder was $\pm$ 0.2% of full scale deflection.

With the combined arrangement of the micromometer and the recorder it was possible to read velocity differences of 0.2 m/s around a 3 m/s flow.

3.5.2 Temperature measurements:

A thermocouple made of 0.25 mm diameter of Pt-5% Rh/Pt-20% Rh wires was found suitable for this investigation and recommended by the B.S.1041. The thermocouple bead of 0.5 mm diameter was made by an electric arc welding of the two wire ends in a reducing atmosphere of town gas to prevent oxidation. This thermocouple was known to serve at temperatures in the range up to 1600°C with negligible catalytic effects, Spiers (1962), Pein and Fetting (1970), even without coating.

The wires were passed through a twin-bore ceramic insulator which was carried in a water cooled probe stem. The cooling water arrangement was the same as for the 3-dimensional probe.

The thermocouple millivolt output was measured by a galvanometer-type potentiometer.

Correction of the temperature reading:

Enough immersion of the hot junction was ensured to reduce the conduction error, which was already small, to a minimum.

Radiation correction was estimated using the following formula, given by McAdams (1954) for heat convection to a sphere in a cross-stream, as a relation between Nusselt and Reynolds numbers:

$$Nu = 0.37\ Re^{0.6} \quad \ldots \quad 3.2$$

Under steady state conditions, this is balanced by the heat radiation from the sphere, thus:

$$h \Delta T = \epsilon \sigma T^4 \quad \ldots \quad 3.3$$

where h is the coefficient of heat transfer

T the thermocouple temperature ^{o}K

ΔT the temperature difference across the film of gas around the sphere

ϵ the thermocouple material emissivity

σ Stefan's constant

From 3.2 and 3.3 the temperature correction is given by

$$\Delta T = \frac{\epsilon \sigma d_s^{0.4} T^4}{0.37 k} \left(\frac{\mu}{\rho \bar{V}}\right)^{0.6} \quad \ldots \quad 3.4$$

where d_s is the thermocouple bead diameter, m

k is the film thermal conductivity, kcal/cm sec ^{o}K

μ is the film viscosity, kg/m sec

$\bar{V}$ is the gas velocity, m/sec

The transport properties of the mixture of gases were taken to be equal to those of air at the same temperature as a reasonable approximation (B.S.1041).

The viscosity was calculated using the following equation given by Spiers (1962):

$$\mu = \frac{145.8 T^{1.5}}{T + 110.4} 10^{-7} \quad \text{poise} \quad \ldots \quad 3.5$$

The thermal conductivity variation with temperature is given by

$$k = k_o \frac{\mu C_v}{\mu_o C_{vo}} \quad \ldots \quad 3.6$$

with suffix o representing values at $0^{o}C$ and the constant pressure specific heat given by:

$$c_p = 0.160 + 4.039 \times 10^{-5} T \quad \ldots \quad 3.7$$

Emissivity values for different materials were given by Wiebelt (1966) as functions of temperature. Since the thermocouple was made of both Platinum and Rohdium, an interpolation was made to the data of both and it was found that values could be represented by the formula

$$\epsilon = 0.0052 + 1.011 \times 10^{-4} T \quad \ldots \quad 3.8$$

Feeding this information into Equation 3.4 the temperature correction due to the radiation from the thermocouple was calculated. This has to be reduced by the amount of radiation to the thermocouple from the walls since their temperatures were high. The net effect was applied to the results of measurements.

3.5.3 Concentration measurements:

Sampling probe:

A special probe was designed for this purpose. The main features of this design were simplicity and efficient cooling of the sample as it enters the probe to ensure quenching of the reaction in the sample. The probe tip was a stainless steel block 12.5 mm long and 9.5 mm diameter with a 2.6 mm diameter sample hole normal to its axis. A continuous flow of cooling water was maintained on both sides of this block and through it from one side to the other, as shown in Figure 3.7. The rest of the cooling system was the same as for the other probes.

Samples were drawn at a velocity of about 4 m/s by a small sampling pump. This speed was thought to be a reasonable average for the flow, thus making the process as near as possible to being isokinetic sampling for most locations. A higher velocity would mean higher pressure on the mica windows of the gas analyser than required for safe operation. The metering of the samples was done by a specially calibrated capillary tube system, Maccallum (1956). In sampling, the probe was rotated at each location so that the sampling hole was brought to face the flow direction which was known from the 3-dimensional probe measurements.

The Infra Red Gas Analyser:

A 3-box Infra Red Gas Analyser, supplied by Grubb-Parsons, was used for the carbon dioxide concentration measurements. Some carbon monoxide tests were also carried out with the same instrument. The principle of operation is described by Martin (1953). An outline of this is given below.

Intermittent radiation from a michrome heater is passed through 2 variable-length absorption tubes and then to absorbing vessels which are filled with the gas to be detected. The absorbing vessels are separated by a diaphragm partition which forms one side of an electric condenser. A steady flow of the sample is passed through one absorption tube and of air free from CO_2 through the other. Both flows were freed from any water vapour which could affect the readings. A sketch of the arrangement of these flows is given in Figure 3.8. The difference of composition between the two absorption tubes due to the presence of the detected gas causes the proportions of the radiation reaching the absorbing vessels to be altered,

thus creating a pressure difference which moves the diaphragm, and consequently varying the condenser capacitance. This variation is amplified and indicated as milliampers.

The instrument was used for both CO_2 and CO by changing the condenser unit. For each, three different ranges were possible. Special care was required during operation because of the instrument's sensitivity to zero shift, ample setting time was given. Care was taken to avoid applying excessive pressure to the mica windows of the cells. The instrument was supported on soft rubber mounts to isolate it from vibrations.

Calibration of the gas analyser:

A calibration was supplied by the manufacturer. After some preliminary tests it was felt necessary to check the calibration at the time of use. This was carried out using standard samples of air with 2,4 and 6 percent CO_2 supplied by Mine Safety Appliances. The calibrations were noticed to have shifted from the original ones and the new curves were used.

Some samples were also analysed for the concentration of combustibles by the use of a Gascope supplied by Mine Safety Appliances.

3.6 The traversing mechanism:

A traversing mechanism was used to support and position the various probes where they were being used. The mechanism was built onto the steel structure carrying the furnace and carefully aligned with the furnace axis.

This system permitted the movement of the probe horizontally, parallel to the furnace axis from one section to another. At any section the probe could be traversed radially with an accuracy of 0.25 mm. Once the probe was located in the measuring position, it was required to rotate it about its own axis to define the yaw angle; this was achieved by a sleeve-protractor unit. This unit consisted of a split tube inside a sleeve carried on a disc with a pointer and a locking mechanism. The sleeve was located inside a block which carried a chrome plated mirror and a protractor to define the angle of rotation of the sleeve.

Probe access holes:

Probe access holes of 12.5 mm were drilled through the furnace bricks on a horizontal line parallel to the furnace axis at the sections where probe traverses were to be made. Asbestos rods were used to plug those not in use. Spacings of the holes for the two furnaces are shown in Figure 3.9.

3.7 Flame visual observation:

This was needed for the starting and adjusting of the flame. Also it was necessary for the stability tests in the furnace. A stainless steel plate of mirror finish quality was placed in the corner of the canopy where it could be seen from the furnace side.

3.8 Ignition of the flame in the furnace:

A premixed mixture of Butane and air was supplied to a 20 mm nozzle having a 3 mm rod stabilizer to produce a pilot flame for ignition of the furnace flame. This was introduced into the furnace through a 23 mm hole near the burner. Once the main flame was stabilized, this hole was plugged.

3.9 Furnace start-up procedure:

(a) Larger Furnace:

After the larger furnace was built, it was dried out slowly with the flame temperature being gradually raised. For this work, a small nozzle of 28 mm diameter with a crossed wire stabilizer was used. This warming-up run was followed by the normal runs with the full-size swirler.

To test the transient time of the furnace, a run with thermocouple beads attached to the furnace walls was carried out. The results (Figure 3.10) showed that a temperature rise in the brick work equal to 90% of the asymptotic value was reached within 3 hours. This time varied slightly with axial position and jet impingement point.

Thus it was decided that for normal aerodynamic runs, no readings were taken before 3.5 hours from starting up the flame. Pressure readings were then taken followed by CO_2 measurements and finally temperature readings.

(b) Smaller Furnace:

The same procedure was adopted as for the larger furnace. In this case it was found that the transient time was less, about 2 hours.

CHAPTER 4

EXPERIMENTAL RESULTS

4.1 Introduction:

This Chapter starts with a brief statement of the different parameters involved in the experimental programme. These are divided into two groups. The first group contains those held constant or varied independently as input variables. The second group contains parameters measured in the experiments directly or after further calculations. The main purpose is to define the flow and combustion patterns and how they change with the input parameters, particularly swirl.

4.2 Variables and measurements:

4.2.1 Input parameters:

The following are the parameters controlled as inputs. The object of the experiments is to study the effect of their variation upon the flow and combustion patterns. The methods of varying these parameters were described in Chapter 3.

(a) The swirler vane angle, as a means of varying swirl which is the principal parameter in the experiments.

(b) The change of the geometry of the swirler due to having a central hub which might have a bluff-body effect.

(c) The Reynolds number of the flow at exit from the swirler.

(d) The degree of confinement of the flow, being controlled by the ratio of furnace diameter to swirler diameter D/d.

(e) Combustion and its effect on changing the flow pattern from that of the cold isothermal flow.

(f) The variation of the fuel to air ratio and its effect on the flow pattern especially when swirl is near the critical value, i.e. when the flow near the centreline behind the burner is just about to reverse to form a central recirculation zone (CRZ).

The above parameters are detailed in Table 4.1.

4.2.2 Output, or measured parameters:

The full study of the flow and combustion patterns under different conditions is the object of this work. Measured parameters will be described and discussed in the following sections. These include the profiles or radial distributions of axial, tangential and radial components of velocity, static pressure, temperature and CO_2 concentrations at different axial locations (six or seven in number), downstream from the burner. From these profiles, the variation of the maximum and centreline values with the axial distance from the furnace are produced and plotted.

Numerical integrations of the axial velocity components to calculate the mass flows at different regions of the flow were performed. Also, integrations were carried out to calculate the axial fluxes of both axial and tangential momenta according to Equations 2.18 and 2.17. A new Swirl Number defined by

$$S^* = \frac{T}{GD} \qquad \ldots \quad 4.1$$

where G is the dynamic component of the axial momentum flux. This Number

was calculated for the different swirlers running under the various input conditions. Flow patterns are better correlated by these swirl numbers than by vane angles of the swirlers, as will be shown later.

The rate of jet spread, the point of impingement or jet reattachment to the furnace wall and the size of the peripheral recirculation zone (PRZ) were also defined for the different tests. The CRZ's which were created with higher degrees of swirl were also investigated by defining in each case its dimensions, maximum reverse velocity and ratio of mass flow recirculated to the main flow.

Several repeat tests were carried out at identical flow conditions and these showed good reproducability. The scatter of the experimental points was not more than 3% for cold flows and 6% for reacting flows, except close to the points of flow reversal where values of velocities were fluctuating about zero and were small. However, the dimensions of the recirculation zones were reproduced within the above range.

4.3 Distributions of axial velocity component:

This section contains a discussion of the develcpment of the axial velocity profiles from those of a non-swirled jet to those of a strongly swirling jet. The effects of this development on the different zones of forward and backward flow are shown.

Flow patterns are classified into four categories A, B, C and D and each is described in turn. It should be emphasised that there is no definite line of separation between these categories

and the division is mainly to help in demonstrating the effect of the different parameters in changing the flow and combustion patterns.

Axial velocity profiles are shown in Figure 4.1 to 4.4. For easy comparisons, all values of the dimensions of both CRZ's and PRZ's together with ratios of maximum velocity and mass flow in the CRZ to the main flow values are compiled in Table 4.2. The Table shows also the calculated values of the Swirl Number S^*.

4.3.1 Flow patterns in Category A: $S^* < 0.08$

These are obtained when there is no swirl or very weak swirl. The velocity distrubutions with the very weak swirl are similar to the unswirled distributions. They consist of a nearly flat region of the peak velocities around the centreline and, at the boundaries, surrounded by a very weak PRZ, i.e. having very low velocities. The radial velocity gradient is very high in the area between the two zones but this decreases as the velocity distribution approaches the Gaussian error curve shape at large distances from the swirler exit. Generally in this case the jet spread is very slow and sometimes the jet would not reach the furnace wall before an axial distance $\bar{x} = 2$, where

$$\bar{x} = \frac{x}{D} = \text{distance in units of furnace diameter}$$

In fact the walls seem to have little effect on the jet expansion.

This type of distribution occurs in the following cases:

- 0^{o} Hubless and Annular burners in both furnaces, i.e. D/d = 5 and 2.5, under both burning and cold isothermal conditions. See Figures 4.1.b, 4.3.a, 4.4.a.

  In the last case, Figure 4.4.a, the effect of the presence of the central hub is noticed to result in a small dip on the axial velocity plateau near the centreline, but this soon disappears.

- 15^{o} Hubless and Annular swirlers in both furnaces, both burning and isothermal. The isothermal tests are shown in Figures 4.1.a, 4.3.b. In these two cases a phenomenon similar to that known as Coanda effect is recorded. The flow is attached earlier to one side of the furnace and a large recirculation eddy is formed on the other side. This phenomenon will be discussed in Chapter 5.

  The effect of the hub in the annular swirlers is less pronounded than with the 0^{o} burners, at least partly because it lies at a distance of some 50 mm upstream of the swirler exit section.

  It is to be noted here that the jet spread is faster than for the 0^{o} swirler and also it is faster when D/d = 2.5 than with D/d = 5. It is noticed that some of these profiles are not quite symmetrical; they are seen to be distorted slightly.

- 22.5^{o} Hubless swirler, burning in D/d = 5 furnace at fuel/air of 0.143. These velocity distributions are very similar to those of the 15^{o} swirler flame in the D/d = 2.5 furnace, as can be seen from Figure 4.3.c.

4.3.2 Flow patterns in Category B:

These are obtained with weak to medium swirl where S^* is near the critical value of 0.11 but no CRZ exists. In this case the axial velocity profiles have a two crest-trough shape with a minimum, but positive value, at the centreline. Radial gradients are high on both sides of the peak velocity values, but they decay rapidly to almost zero. Thus the profiles at a distance of $\bar{x} \geq 1.5$ are mostly uniform.

The jet expands faster than in the case of flow type A, leading to a reduced size of the PRZ, the maximum length now being about 1D. But in this case the velocities in the PRZ are higher and they have a more effective mixing influence.

Cases that produce this type of flow are as follows:

- 30° Hubless swirler flame with f/a = 0.141 in D/d = 2.5 furnace shown in Figure 4.1.c.
- 22.5° Hubless swirler flame with f/a = 0.125 in the D/d = 5 furnace also the isothermal jet in the same furnace by the same swirler, both shown in Figure 4.3.c.
- 30° Hubless and Annular swirler flames in the D/d = 5 furnace as shown in Figures 4.3.d and 4.4.c respectively.

The effect of the central hub is seen again here to produce a lower minimum velocity at the centreline and a more extensive subsequent trough than in the hubless case. This effect led to peak velocity values being shifted radially towards the walls. Near $\bar{x} = 1.8$ a central reverse flow was recorded.

4.3.3 Flow patterns in Category C:

These are obtained with medium swirl. S^* is near the critical value of 0.11 and with a small CRZ.

By increasing the swirl above the values giving flow pattern B, the double crest-trough shape is developed to higher maxima and a lower minimum with sharp intermediate velocity gradients. The minimum value at the centreline reaches a stagnation value followed by negative velocities. Thus a CRZ is created. Initially it is of a small size and has only a small recirculated mass. These increase steadily with swirl. Only cases where this mass flow is less than 0.1 of the burner flow are considered as being in this category, otherwise they will be treated as Category D. The PRZ's are again small with maximum length of 1D. The velocity profiles developed beyond $\bar{x} = 1.5$ are almost uniform with slight peaks at the sides near the walls and smaller values near the centreline.

The following cases are representative of this type of flow:

- 22.5° Hubless swirler isothermal jet in D/d = 2.5 furnace as shown in Figure 4.1.b.
- 30° Hubless swirler flame with f/a = 0.106 in D/d = 2.5 furnace shown in Figure 4.1.c where a CRZ of reasonable size is recorded but the reverse mass flow is still small, viz. 0.065 of swirler flow.
- 30° Annular swirler flames in D/d = 2.5 furnace, Figure 4.2.a.

The two cases at the different fuel/air ratios 0.137 and 0.107 have the same flow pattern but with a bigger size of the CRZ in the case

of the lower fuel/air ratio. However, in both cases the recirculated mass flow is less than 0.1 of the inlet flow, viz. 0.04 and 0.07 respectively.

4.3.4 Flow patterns in Category D:

These occur with strong swirl where S^* is greater than 0.18. These differ from the previous one, C, only in that the size of the CRZ is greater and the reverse velocities and recirculated masses are larger, e.g. mass flows recirculated are generally greater than 0.15.

The length and maximum diameter of the CRZ in this case seem to vary very little with the degree of swirl and both tend to be fixed proportions of the furnace diameter. These proportions are, however, different from one furnace size, or D/d, to the other. With further increase of swirl the maximum diameter of the CRZ does not change but the length increases and sometimes a long thin tail of the CRZ extends up to as far as 3.7 D (maximum length investigated). However, the mass flow in this is very small and the length of the most active part of the CRZ is nearly equal to that of the closed ones. The axial position where the maximum width of the CRZ occurs always moves nearer to the swirler with increasing the swirl. As to the maximum flow in the CRZ, it continuously increased with swirl. The ratio of the maximum reverse velocity in the CRZ to the average swirler axial velocity, also increased with swirl but at a slower rate.

The main flow starts with a cylinder of peak velocities surrounding the CRZ. At the same time this cylinder is surrounded by the PRZ. Thus on both sides of the peak velocities there are very high axial velocity gradients in the radial direction. Due to the very fast spread of the jet, the PRZ is very short and the flow impinges on the furnace walls within an axial distance of 0.6 D at most. At impingement, the positions of maximum velocity are near the wall but thereafter they move slowly towards the centre. Velocity profiles thus develop to an almost uniform flow, though sometimes with slightly lower values near the centre.

To represent this type of flow pattern, the following cases are shown:

- 30° Hubless and annular swirlers cold isothermal flow in both furnaces, Figures 4.1.c, 4.2.a, 4.3.d.
- All 45° and 60° swirler flows both cold and burning and in both furnaces are of this type with all the features mentioned above. For these profiles see the Figures 4.1.d, e - 4.2.b,c - 4.3.e, f - 4.4.d,e.

4.3.5 Decay of maximum axial velocity along the furnace:

In this section the change of the maximum axial velocity at any section of the flow along the furnace length is discussed in relation to the flow pattern classification A to D. These velocities are presented in Figures 4.25.a to h plotted versus axial distance from the swirler exit for the different cases studied.

Flow Pattern A:

The maximum velocity value suffers little or no decay for the length of expansion before the jet touches the wall, after which it decays almost uniformly along the remainder of the furnace length investigated. Thus in the D/d = 2.5 furnace, a constant maximum velocity region is followed by an approximately linear decay for the cases of 0° and 15° Hubless swirlers in cold flow. For the 0° and 15° swirler flames, both hubless and annular, in the D/d = 5 furnace the curves show little decay over the entire length studied of 1.8 D.

Flow Patterns B and C:

The axial decays of the maximum velocity for both types B and C follow similar patterns. The decay starts from the first point measured and at a much higher rate than in the case of type A flow. The decay virtually ceases after a certain axial distance which decreases with increasing swirl. The starting points of this range have velocity values still in the same range as in case A, viz. about 1.5 - 2.0 u_o (where u_o is the swirler average axial velocity). The faster rate of decay is attributed to the jet expansion rate being higher and to the jet impingement on the walls being nearer to the swirler exit.

Flow Pattern D - Isothermal flow:

With still higher rate of jet spread and closer wall impingement, the rate of decay is, as expected, much faster in this case than in the previous cases. Within an axial distance of about 1D the maximum axial velocity decays to its minimum value,

which is preserved for the remainder of the length investigated. The maximum values along the length lie nearest to the swirler exit and they show values as high as 2.5 u_o, because of the strong centrifugal effect of the swirler.

Flow Pattern D - Burning:

Some of the cases tested show trends similar to the isothermal flows of type D, while others produce some apparent differences.

In the D/d = 5 furnace, the 45° and 60° Annular swirler flames, initially the maximum axial velocities decay rapidly then maintain their new peak velocities for some distance before the final decay commences. The lengths over which the peak velocities remain constant are $\bar{x} = 0.45$ to $\bar{x} = 0.7$ for the 45° swirler and $\bar{x} = 0.5$ to $\bar{x} = 0.6$ for the 60° swirler. The 45° Hubless swirler shows no decay, in fact a slight rise, in the length $\bar{x} = 0.35$ to $\bar{x} = 0.85$.

In the D/d = 2.5 furnace, there is an increase in the maximum velocity in the first 0.5 D length of the furnace for both 45° swirlers. This is explained by applying the mass continuity equation along the area of forward flow. In this region, the forward mass increases because it is, the sum of the burner flow plus the reversed flow entrained from the two recirculation zones. The volume also increases because of the chemical reaction which occurs in this region, as will be seen later. While the volume is increasing (principally due to the reaction), the net area of the forward flow is decreasing. Thus the flow has to accelerate until the area starts to increase again beyond the end of the PRZ, or beyond the maximum width of the CRZ, or both. This explanation is confirmed by

comparing the net forward flow areas forthe above cases with those cases giving the same type D flow but having decay curves that follow the same pattern as the isothermal.

4.4 Distributions of tangential velocities:

Radial distributions of tangential velocities for the different cases studied are plotted in Figures 4.5 to 4.7. The values of these velocities increase with swirler vane angle, but the patterns of the profiles are more related to the Swirl Number. The different types of profiles are discussed below on the same basic classification as for the axial velocities.

4.4.1 Flow patterns in Categories A and B:

The tangential velocity increases from zero at the centreline to a maximum at a radius which increases with the jet width, or swirl. Sometimes two peaks are recorded with a trough in between. The tangential velocity in the PRZ decreases slowly with increasing radius. However, at larger axial distances from the swirler, as the maximum velocity at the section is reduced and shifted to a greater radius, the profiles consist of a forced vortex core surrounded by a constant tangential velocity area and then a tangential velocity decreasing to zero at the wall, which is similar to a free vortex. The ratios of the areas occupied by the different regions depend on both swirl and axial distance.

4.4.2 Flow patterns in Categories C and D:

With the presence of a CRZ and an annular cylinder of high axial velocity surrounding it, the tangential velocity profiles are modified. In the CRZ the tangential velocities are very small when $\bar{x}$ is small, but they follow a forced vortex type flow at larger $\bar{x}$, particularly after the maximum width of the CRZ is reached. In the PRZ the tangential velocities are small again. As to the main forward flow, it has a high tangential velocity region, having a maximum which coincides with the maximum axial velocity. At larger axial distances, the distributions become more uniform in this region with a decrease towards a zero value at the walls.

4.4.3 Variation of the maximum tangential velocity along the furnace:

The maximum tangential velocities are plotted versus axial distance from the swirler in Figure 4.2.8.a to h. The main common feature of these results is that for each swirler type, the asymptotic value reached at large axial distance increases with the vane angle. These values are thus different from swirler to another, unlike the axial velocities. The values for the maximum tangential velocities are higher for annular swirlers than for hubless ones.

For flow patterns of type A and B the rate of decay with axial distance is similar in most cases, the decay virtually ceasing at a distance of about 1D.

Flow patterns of type C follow nearly the same trend as in B but with a higher rate of decay followed by a slight rise after the minimum is reached.

For flow pattern of type D, the initial rate of decay is very high and increases with swirl. This is followed by a noticeable increase to another peak followed by the asymptotic value either directly or after further decay, the decay this time being less rapid. When an increase in the tangential velocity occurs, it is not always accompanied by an increase in axial velocity, particularly in cold flows. These increases are discussed in Chapter 5.

4.5 Distributions of radial velocity components

Although most of the previous workers ignored the radial velocity components on the basis of their being small, in this work they were measured and found to be of considerable magnitude. At small values of $\bar{x}$ where the jet was expanding these were of the same order of magnitude as the axial components. But, at large values of $\bar{x}$ they were generally small. Values for the radial velocities are plotted for the different cases studied in Figures 4.9 to 4.12. The sign convention for these figures is now given. In the upper half of any diagram, positive values mean flow towards the centreline and negative ones flow away from the centreline, the opposite being the case for the lower half. Thus for a perfectly symmetrical flow, distributions should be diagonally symmetric. Unfortunately this was not always observed and in most cases there was a slight shift towards the side farthest from the probe access holes. Before, discussing the results, it should be borne

in mind that the 3-hole probe used in this work may not be the most suitable for measuring large radial components of velocity. The probe itself may cause disturbances to the flow due to its body being in a radial position.

In general the radial velocities defined the jet expansion zone, the jet impingement and the location of the maximum width of the CRZ. When the jet is expanding the radial velocities are high and directed away from the centre. Just after the impingement point, a reverse of direction occurs. In the PRZ the radial velocities are small and directed towards the centre. In addition to the above general features, the following are particular to the different flow patterns.

For flow patterns A and B, the asymmetry of the flow is magnified in the radial velocity profiles. The main flow shows expansion of the outer layers and, nearer the centreline, inward radial flow with velocities rising to about u_o.

For flow patterns C and D, the radial velocities are more symmetrical with only slight apparent displacement towards the farthest wall. In the CRZ the radial velocities are low and directed towards the centreline. After the jet impingement on the walls, the main flow moves towards the centre thus reducing the diameter of the CRZ.

4.6 Distributions of static pressure:

All measured static pressure values are subatmospheric except for a few points near the furnace wall at large values of $\bar{x}$. The radial distributions of static pressure at different axial distances for all the cases tested are shown in Figures 4.13 to 4.16.

The effect of combustion is always to raise closer to atmospheric the static pressure in the vicinity of the centre-line. In many cases the pressures near the walls are lowered slightly. For flows with CRZ, confinement caused the pressures near the centreline to be depressed further below atmospheric. This effect increases as the confinement is made more pronounced, i.e. as D/d is lowered.

Since the profiles are related to the velocity distributions, in the following sections they will be treated according to the same classification. The strong interrelation between the static pressure and the flow velocities, especially with reference to jet spread, is discussed later in Section 5.3.

4.6.1 Flow patterns in Categories A and B:

With these patterns the pressure profiles have similar trends. The main forward flow is in the central region and this is the region of lowest static pressure, the minimum value occurring on the axis. On moving from the axis to the jet boundary, the pressure rises progressively, until the PRZ is reached where the pressure is constant. The depression in static pressure at the centreline increases with swirl. With larger values of $\bar{x}$ this distribution moves towards uniformity but with values near the walls equal to atmospheric. When there was a shift of the axial velocity profiles towards one side of the furnace, this was accompanied by a similar trend in the static pressure profiles, the minimum being to the same side as the axial velocity maximum.

4.6.2 Flow patterns in Category C:

In this category a CRZ is just established, and the corresponding effect in pressure is a sudden raising of the minimum value which occurred at the centre of the jet near the swirler. Static pressure distributions in both CRZ and PRZ are uniform with slight variations in the area between them which carries the main flow. With larger values of $\bar{x}$ these profiles are gradually readjusted to have a minimum at the centreline and values increasing with radius until the wall is reached with a value equal to atmospheric. As swirl is increased, all centreline pressures are slowly reduced.

4.6.3 Flow patterns in Category D:

The centreline values continue to decrease with swirl. With a very small PRZ and a much higher velocity flow in both PRZ and CRZ, the pressure distributions in them are no longer uniform. A minimum occurs at the centreline, and a maximum near the walls at atmospheric pressure, or even higher at large axial distances.

The case of the cold flow issuing from the 30° Hubless swirler in the D/d = 5 furnace is an interesting one. Here a CRZ exists but it starts very thin until $\bar{x} = 0.4$ where it widens suddenly. The static pressure shows a sudden rise at the same value of $\bar{x}$.

4.6.4 Recovery of static pressure along the axis:

Figures 4.29.a to h show how the pressure reduction below atmospheric at the jet centreline decays along the furnace. The greatest reduction in pressure occurs either at the swirler exit or within a distance of 0.5 D downstream. Thereafter it decays with x. For flow patterns A and B the rate of decay is high and increases with swirl. When some maximum decay rate is reached, the centreline flow reverses and the flow pattern changes to category C where a CRZ exists. With flow patterns of type D, the pressures on the axis lie further below atmospheric than for type C flows. The depression of the pressure increases with swirl, as also does the decay with axial distance of the sub-atmospheric pressure.

The value of the largest reductions in pressure at the jet axis have a definite relation to the swirl and flow pattern. Figure 4.34 gives plots of this relation which is an exponential increase of this largest pressure reduction (p^*) with the Swirl Number S^*.

$$p^* = a\, e^{m S^*} \qquad \ldots \quad 4.2$$

where a and m are constants.

The slope of the lines m varies with the type of flow, i.e. whether isothermal or flame. It is also affected by the confinement (D/d) ratio. The constant a is equal to the pressure drop below atmospheric at the centreline of an unswirled jet in the same confinement.

The important point to note from this Figure is that, for the same type of flow and in the same confinement, points for flow patterns A and B fall together on one line, while those for flow patterns C and D fall together on a different line. The transition from the first line to the second occurs when the degree of swirl (measured by S^*) is just sufficient to establish the CRZ.

4.7 Distribution of Temperatures:

Temperature distributions are reported in Figures 4.17 to 4.20. A study of these will help in defining the combustion pattern and the effect of the flow pattern upon it. The study will also be of value in indicating the heat release rates from the different sections of the furnace. In this analysis the relation between the flow pattern and the combustion pattern will be shown by following the same classification of flow patterns A to D.

4.7.1 Flow patterns in Categories A and B:

In this case, combustion starts at the centreline and spreads to the rest of the input charge radially. Thus the temperature profiles show a peak at the centreline and a minimum at the jet boundary. With increasing swirl, the peak at the centre becomes wider at a shorter axial distance. The temperature of the fluid in the PRZ is much lower than the section peak temperature, e.g. lower by $400^{\circ}C$ in the case of no swirl.

This is because of the very slow movement of the gases in this zone and the lower mixing rates between the recirculating gases and the main jet, and the low temperature of the outer boundary of the main jet.

The walls are cold in this case due to the jet not impinging on the walls until a considerable axial distance. Also the gases that impinge are comparatively cold. It is to be noted here that any fuel-air mixture entering this PRZ will not react due to the quenching effect of the cold walls. In the cases where no impingement occurs within the furnace, there is a possibility of an induced flow of air from the downstream end of the furnace. As swirl is increased the jet impinges earlier, the flow in the PRZ is more intense and the flame is wider. Consequently the temperatures in the PRZ are higher. The full profile tends to be uniform with larger axial distances and with increasing swirl.

4.7.2 Flow patterns in Categories C and D:

In this case the flame starts at an axial distance downstream from the swirler. Both PRZ and CRZ contain products of combustion at high temperatures, corresponding to about 90% of the adiabatic temperature rise. Within a short axial distance , which decreases with swirl, the combustion is completed and the temperature profiles are uniform. The maximum values of temperature here were less than in the previous patterns. This is because of the early jet impingement causing more heat to be convected to the furnace walls.

At the extreme case of a CRZ which was still open until the furnace exit (60^{o} swirler flames in the D/d = 2.5 furnace), this CRZ introduced colder gases into the flow. This caused a lower temperature at the centreline near the exit.

4.7.3 Distributions of carbon dioxide concentrations:

The distributions of carbon dioxide concentrations are shown in Figures 4.21 - 4.24 as fractions of the concentration corresponding to complete combustion. These distributions follow exactly the same pattern as the temperature and therefore serve to confirm the conclusions drawn from the temperature profiles.

These conclusions are as follows:-

(i) For flow pattern A, combustion starts quickly in the centreline. There is incomplete combustion in the PRZ and at the boundary of the main jet.

(ii) For flow pattern B, there is a wider central peak of temperature and carbon dioxide concentration close to the swirler and a more uniform distribution further downstream than for flow of type A.

(iii) In flow patterns C and D, with a CRZ, complete combustion is somewhat delayed and the gases in the CRZ are products of combustion.

As a further check on this, measurements of the concentrations of combustibles near the swirler were made using a Gascope (M.S.A.). No traces of combustibles were found in the CRZ.

4.7.4 Variation of maximum temperature along furnace:

Values of maximum temperature at any section are plotted to a base of axial distance in Figures 4.30.a to e.

For flow patterns A and B, the maximum temperature at any section lies on or very near the centreline. The maximum temperature always occurs in the forward flow. In these two types of flow, the maximum temperature starts to rise slowly along the axial direction until it reaches its largest value at x of about 2.5 d. This dimension is independent of the furnace size. After the maximum is reached there is a slow decay which continues till the furnace exit. In both cases the rates of rise and of decay are both increased with swirl, thus being higher in pattern B than in pattern A. The maximum temperature at exit is reduced by increasing swirl due to the early jet impingement causing more heat convection to the walls.

With flow patterns C and D, moving downstream from the swirler, initially the maximum temperatures are the CRZ temperatures and these are rising. After a short distance the maximum temperature at a section moves to the reacting gases in the forward flow. This maximum value remains constant for a distance and finally decays, the decay being reduced at higher swirl. This is due to the lower swirl flames retaining their high velocities near the wall and thus increasing the convective loss. In the larger furnace the region of temperature rise is very short, and does not extend beyond the first traverse plane.

4.7.5 Variation of the centreline temperature along the furnace:

This is shown for the different cases in Figures 4.31.a to d. For flow patterns A and B the maximum temperature at any section lies very near or on the centreline, thus these plots are only very slightly different from these of the maximum temperature.

For flow patterns C and D, the centreline values are those of the CRZ flow and although this flow consists of products of combustion its temperature varies along the axis. To follow this flow it is more convenient to start from the downstream end of the CRZ and move towards the swirler, to find that the temperature increases slowly to a maximum at $\bar{x}$ about 1, then decreases to a lower value nearest to the swirler. This change is explained by the convective heat transport with the surroundings, whether products of combustion or fresh change, causing the temperature to increase or decrease respectively.

4.8 Axial momentum flux:

Values of axial momentum flux were obtained by numerical integration of velocity and pressure distributions at any cross-section of the flow according to the Equation 2.18. The flux of axial momentum can be divided into two parts, the dynamic term and the static pressure term. Figures 4.32.a to h show the variation of the values of these fluxes along the furnace length for the different flow cases investigated. In each graph the dynamic contributions are plotted on the top part and the total fluxes on the lower part.

4.8.1 Dynamic axial momentum flux:

For cold flows, as shown in Figures 4.32.a to c, the value nearest to the swirler increases with swirl and so does the initial rate of decay. At an axial distance of about 1.7 D and beyond, the axial momentum fluxes are constant and equal each other for all swirlers. However, for the case of no swirl or very weak swirl, where the jet does not impinge on the furnace walls, the downstream value is higher. In the case of the 45° hubless swirler in the $D/d = 5$ furnace, where the rate of flow was varied to test the effect of Reynolds Number, there was a difference in proportion to the square of the velocity ratio, as expected. The averages of the scaled values are plotted in Figure 4.32.c.

In the case of burning jets, the main features described above are reproduced except in the cases where the flow pattern is of type D in the $D/d = 2.5$ furnace. In these cases, mainly 45° and 60° swirlers, there is an apparent rise in the axial momentum flux in the region around $\bar{x} = 0.2$ to 0.4. Upstream of this, the fluxes are not as high, relative to other swirlers, as in the cold flow.

At large axial distances ($\bar{x} > 2.0$) values are all nearly equal for all swirlers, and greater than the corresponding values for the cold flow by a ratio equal to the density ratio of the two flows.

Finally the effect of increasing the fuel/air ratio for the case of the 22.5° Hubless swirler in the $D/d = 5$ furnace is shown in Figure 4.32.h together with the results for the cold isothermal flow. As found in the other cases, the momentum fluxes in the burning case differ from that in the cold flow by the appropriate density ratio.

4.8.2 Total axial momentum flux:

This includes both dynamic and static pressure terms. The values of the static pressures to be integrated for this calculation should be those relative to a certain reference pressure. For the choice of this reference pressure there are many alternatives. The following were considered:

(a) The atmospheric pressure outside the furnace. This was rejected on the argument that the general static pressure level in the furnace varies with the flow and the chimney suction.

(b) The static pressure at the exit section of the furnace. This again was variable and affected by the flow currents at this section.

(c) The static pressure at the centre of the PRZ for each case. The only objection to this choice is that this value is affected by swirl since the tangential velocities do not vanish at the PRZ. Also it is affected by the jet spread rate.

(d) The static pressure at the centre of the PRZ for the non-swirled cold flow in the furnace tested. This choice was taken since it avoids the objections mentioned in (c). Thus the net value of the static pressure will show the effects of swirl and of combustion in the same confinement.

The total axial momentum fluxes calculated using this last reference static pressure value (d) are those plotted in Figures 4.32.a to h (lower plots).

For lower degrees of swirl, flow types A and B, the total axial momentum flux value is approximately conserved along the furnace, with some variations at the sections near the swirler.

For higher degrees of swirl, and at the first 1D length of the furnace, the apparent variations of the total axial momentum fluxes were considerable. The reasons for these variations are the effects of turbulence shear and also wall friction, as will be discussed in Chapter 5. However, after this length, the total momentum values show a reasonable trend towards preservation.

Comparison of these values between cold and burning flows show the latter to be higher by an amount which is proportional to the fuel/air ratio, provided the flow pattern has not changed with the f/a. This value corresponds to the "flame pressure" which will be discussed in Section 5.4.

4.9 Axial flux of tangential momentum:

The values of the axial flux of tangential momentum, calculated from Equation 2.17, along the furnace length are shown in Figures 4.33.a to h. The rate of decay is much lower than that for the axial momentum flux.

In the D/d = 2.5 furnace, Figures 4.33.a, b, d, e, for $\bar{x}$ up to 1.5, the values show some scatter which is followed by an almost constant value along the remainder of the length investigated (up to $\bar{x} = 4$) for both cold and burning flows. These values are higher for the burning jets than for the corresponding ones for the same swirler under cold flow conditions. These tangential momentum

fluxes are higher by a factor of 25%, whereas, as mentioned in 4.8, the axial momentum fluxes are higher by a factor of about 4. The Swirl Numbers, S^*, in the burning cases are thus lower by a factor of about 3 than the isothermal values with the same swirler.

Similar features are represented by Figures 4.33.c, f, g, h for the flow in the D/d = 5 furnace. Because of the shorter relative length investigated in this case, only the tendency towards the conservation of angular momentum flux is noted.

The effect of the variation of the fuel/air ratio is shown in Figure 4.33.h for the 22.5° Swirler flow in the D/d = 5 furnace together with the cold flow results.

4.10 Swirl Number, S^*:

With values of the axial fluxes of the axial and tangential momenta available, Swirl Numbers for the different swirlers, under different flow conditions were calculated according to the new definition in Equation 4.1. The relation between these values and the swirler vane angles was generally an increase in S^* with an increase in vane angle, but at different rates depending on flow type. Near the critical degree of swirl, a slight variation in the fuel/air ratio caused a pronounced difference in the Swirl Numbers of the flows.

This relation is given as plots of the averaged S^* values versus the vane angle θ on a log-linear scale in Figure 4.35. These plots show that for a certain flow state (cold or burning) a straight line relation exists between log S^* and θ, but with a sudden change of slope at S^* value of about 0.11, after which the line is less steep.

These relations were the same for both confinements tested, i.e. D/d = 5 and 2.5. The presence of a central hub in the swirler, does not seem to have a noticeable effect on this Swirl Number.

It is important to note here that the point of change of slope corresponds with the point of change of flow pattern from Category B to Category C, i.e. the start of a CRZ. Moreover, this value of the Swirl Number S^*, representing the critical value where the CRZ is started, is the same for all conditions of flow and confinement.

Comparisons with other research workers show that the flow reversal in their experiments started at almost the same value of this parameter, Section 5.5.

4.11 General conclusions from experimental results:

The flow parameters of velocities (three components), and static pressure were found to be the deciding factors controlling the combustion pattern, as indicated by the temperature and product concentration distributions.

Four different patterns of flow are described through the plots of both radial and axial distributions of velocity components and static pressure. Whether the flow is cold air or burning mixture, it fell into one of the four categories. When combustion exists the flow from a certain swirler is readjusted and may move from one category to another.

A valuable parameter in correlating the results was found to be the Swirl Number S^* suggested by the discussion in Chapter 2 and given by Equation 4.1. Flow patterns were always related to the values of this Swirl Number which was affected by combustion, fuel/air ratio as well as the swirler vane angle. The confinement ratio D/d does not change this Swirl Number relation to the vane angle θ for a certain flow state (cold or burning). The transition from a totally forward central flow to flow with CRZ always occurred at the same value of this parameter S^* about 0.11.

CHAPTER 5

DISCUSSION OF THE EXPERIMENTAL RESULTS

5.1 Introduction:

In the previous Chapter the experimental findings were presented in a manner which attempted to group them so as to bring out the common features and to show the differences. The main parameter was swirl, represented here by the Swirl Number S^* suggested in Chapter 2. The use of this measure of swirl as a modelling parameter for confined swirling flows is justified by its success in correlating the flow and combustion patterns.

The presentation in Chapter 4 shows that there are two distinctive groups of swirling flames, namely patterns A and D. The intermediate states where the flow reversal starts to occur are divided into patterns B and C which could be attached to A and D respectively if broader lines are to be used. There is a strong relation between this classification and the Swirl Number S^* over the whole range of flow conditions. This Swirl Number proved to be a good measure of both flow and combustion patterns, taking account of all the factors considered as input parameters, as listed in Table 4.1. Thus the problem of isothermal modelling of swirling flames is reduced to that of having a Swirl Number similarity. Swirl Number variation with the different input variables, together with their relation to the resultant flow patterns as classified by categories A to D, are represented in Figures 4.35.

A general discussion of the experimental results will be presented in the following sections, with special attention being given to the main features of the flow which affect the combustion, stability and intensity. The features of importance to the transport of heat and momentum are also discussed. An example of this is the jet impingement on the furnace walls which has a great part to play with respect to the heat transfer mode and the furnace wall life. These main parameters can be classified as -

(i) the jet spread,

(ii) CRZ, and

(iii) the momentum fluxes, including a study of the effect of shear forces.

The extent to which the results are applicable to industrial furnaces can be assessed on the following factors:

(a) The size and materials used in the design and construction of the experimental rig are very similar to those used in actual practice, the only difference being that geometrically the rig is less complicated.

(b) Comparisons of the results of this work with those produced from measurements in industrial furnaces reported by previous workers (e.g. Kerr (1965), Afrosimova (1967), etc.) show good agreement. The general conclusions drawn in the following sections are confirmed by results of other research workers, where they are relevant.

Before proceeding with the discussion it is useful to consider some of the problems with measurements which might be responsible for the scatter of some results. It is to be noted also that some scatter could develop by accumulation of experimental errors when they enter in further calculations. One example is the integration of the velocity profiles to produce axial and tangential momentum fluxes. The element of integration in this case is (density x $(\text{velocity})^2$ x radius). All three are measured quantities which are subject to errors, particularly the velocity.

5.2 Some problems with experimental measurements:

5.2.1 The three-dimensional probe:

The calibration of this probe shows that the total velocity parameter $\left[\frac{p_t - p_2}{p_1 - p_2}\right]$ becomes too sensitive to the changes in the pitch angle when this becomes near to either 0° or 180°. This is the case when the total velocity vector becomes mainly radial where the axial component is reversing direction. In this case the probe lies on its own wake and results are less reliable. This was remedied by interpolating the velocity component values on both sides of the point in question, thus more reasonable values were obtained, particularly for axial and tangential components. The static pressure values were corrected by the use of the disc probe as mentioned in Chapter 3.

5.2.2 The effect of turbulence on velocity measurements:

Little information is available about the effect of turbulence intensities on pitot tube readings, but the effect is undoubtedly pronounced for turbulence intensities higher than 20%. The 3-dimensional probe used in this work is a development of the simple pitot tube, which reads the time mean average total and static pressures $\bar{p}_t$, $\bar{p}_s$. For a turbulent flow having a time mean velocity vector, in the normal direction to the pitot probe total pressure hole, of $\bar{V}$ and fluctuating velocity components u', v', w', the total pressure $\bar{p}_t$ is given by Dean (1953) as,

$$\bar{p}_t = \bar{p}_s + \rho \frac{\bar{V}^2}{2} + \frac{\rho}{2} \cdot \frac{1}{3} (u'^2 + v'^2 + w'^2) \quad \ldots 5.1$$

The last term represents the turbulence contribution leading to a higher velocity reading than the true time mean value. It is to be noted here that u', v', w' are not exactly the main flow fluctuating components because of the effect of the presence of the probe body in readjusting the local turbulence.

A very simple statistical analysis, assuming that the velocity values have a normal distribution about the time mean value, was carried out. The results show the measured velocity is higher than the true mean by an amount which is proportional to the square of the turbulence intensity. For example for 20% and 40% turbulence intensities the corresponding apparent increases in the measured velocities are 2% and 8% respectively. Similar values are given by Dean (1953). A more comprehensive study is reported by Barat (1965),

in which he considered the effect of probe direction relative to the flow and the probe diameter relative to the size of turbulent eddies. Of his results, the following equation is the one nearest to being applicable to our work:

$$V = V_m / (1 - 0.25 \frac{\overline{v'^2}}{\bar{V}^2}) \quad \ldots \quad 5.2$$

where V and V_m are true and measured time mean velocities

v' is the fluctuating component of the velocity.

The corrections using this equation are of the same order as those from the above mentioned simple analysis, although they are considerably higher at lower intensities, (5% and 11% as compared to 2% and 8%, above).

However both of these analyses are too simple to represent the case of the present measurements. This is because of the complexity of the probe geometry, because the flow is three-dimensional and because combustion is taking place.

5.2.3 Problem of flow assymmetry:

The velocity profiles showed some departure from the generally assumed symmetry about the axis. These departures were more apparent in cases of weak swirl or no swirl, while increasing the degree of swirl made the flows more symmetric. The extreme case occurred with cold flows issuing from 0° and 15° swirlers, where a large recirculation eddy was formed near one wall and the main flow was attached to the other.

Many previous workers, see Chapter 2, have reported this unsymmetrical nature of the flow profiles. Average symmetrical profiles were frequently presented with no analysis of the problem.

Factors contributing to the unsymmetric nature of the jet are:

(a) Constructional:

The swirler construction could be distorted either during manufacture or operation. Another factor could be some misalignment of the swirler in the furnace. Leakage through the probe access hole could also have some effect. However the effect of these is probably very small and should be scattered on both sides of the centreline, which is not the case with the reported results.

(b) Flow attachment phenomenon:

This is a well known phenomenon of flows expanding in ducts or diffusers of increasing sectional area, sometimes known as the Coanda effect. Experimental and theoretical studies of the phenomenon of the reattachment of a two-dimensional air jet to an adjacent wall were carried out by Taga et al (1971) and Kirkpatrick and Walker (1972). They studied the effect of the angle of the jet relative to the wall and their results showed that for a case similar to the type investigated in the present work, the jet is almost invariably deflected in one direction or another, by any slight disturbance.

(c) Vortex effect:

There is now considerable evidence that there is another effect which may cause asymmetry in swirling flows, (Syred and Beer (1973)).

This arises from the existence under some conditions of vortices which form between the main forward flow and the recirculation zones. These vortices precess around the jet, either on the axis of the jet or on an axis inclined to the jet. In the latter case the jet will be observed to be asymmetric.

Usually these precessing vortices are damped by combustion, a phenomenon which explains the better axisymmetry of the burning flow profiles.

5.3 Jet Spread:

5.3.1 Effect of input parameters

The outer boundary of the forward moving jet is defined by the points where the axial velocity is zero. In this section the effects are considered of the experimental variables, particularly swirl, on the spread of the jet up to the point where the jet impinges on the wall. The length to the point of jet impingement (defined by the intersection of the zero velocity contour with the wall) can also be taken as a measure of the rate of jet spread. The zero velocity contours are plotted in Figures 4.27.a to g, and values of the distance to impingement divided by the appropriate furnace diameter ($\bar{x}_i$) are given in Table 4.2.

(a) Effect of confinement:

It had previously been found that the effect of confinement on cold swirling jets was to cause a rapid increase in the spreading rate, (Mathur (1967)). This effect was due to the jet entraining air from the PRZ in the confined case, instead of from the surrounding atmosphere. This lowers the pressure surrounding the jet and enhances the spread.

The present work on isothermal jets confirmed Mathur's results.

Free burning swirling jets expand more rapidly than isothermal jets, (Bafuwa (1967)). The effect of confinement on the spread is less noticeable in the burning case. The expansion in the smaller furnace (D/d = 2.5) has to be compared with early stages of the free burning jets where the spread is rapid. In this case there is little effect on the spread. However, at the free jet diameters corresponding to the larger furnace (D/d = 5) the free jet expansion is less rapid. The confinement by this furnace maintains a more rapid spread.

On comparing the two confinements, the lengths to impingement, divided by the appropriate furnace diameter, are very similar for a given swirler (Table 4.2).

(b) Effect of combustion:

Combustion can alter the flow from one of the patterns described in Chapter 4 to another. For example, the flow from the 30^{o} Hubless Swirler in the D/d = 5 furnace is of type C when there is no combustion, but becomes of type B when combustion takes place. A comparison therefore of the spreads of these two jets is complicated by the change of flow regime. However, useful comparisons can be made where there is no change of flow pattern.

For flows of types A and B, combustion increases the rate of jet spread, similar to the increase in free systems.

For flows of types C and D there is little change in the jet spread due to combustion. The only noticeable effect occurs with the 60^{o} swirler where the cold jet is slightly faster, impingement distances,

which are very short already, being reduced by about 15% in the larger furnace.

(c) Effect of hub:

The effect in the smaller furnace is not noticeable. In the larger furnace (D/d = 5), jets from annular swirlers spread less rapidly than those from hubless swirlers when the flow is of type D, i.e. strong CRZ. For other flow types the effect of the hub is to make the spreads slightly faster.

(d) Summary of effects:

Summing these effects for systems with established CRZ's, it can be concluded that, for practical purposes, the spread of the confined jets (measured by x_i/D) is controlled by the vane angle of the swirler, for values of confinement diameter ratios D/d up to 5. The effects of combustion, of a hub in the swirler and of the value D/d, provided it is less than 5, appear to be of second order.

It should be noted that the presence of combustion in the above cases can alter the Swirl Number S^* by a factor of about 3 (see Figure 4.35) for the same swirler. Thus spread cannot be related to this Swirl Number.

For flow patterns of types A and B, the above mentioned effects of combustion and confinement cause a noticeable increase in the rate of jet spread.

5.3.2 Predicted relation of jet spread to density changes and pressure distributions:

(a) Density changes:

The density gradient at the jet boundary, or in other words the relation between the nozzle fluid and surrounding fluid

densities is known to have some effect on the rate of jet expansion. It was shown by Thring and Newby that the rate of spread of a simple jet in a surrounding fluid of different density is inversely proportional to the square root of the ratio of jet flow to surrounding fluid densities. In the burning tests reported in Chapter 4, the initial jets, which are of an air-fuel mixture, are expanding in an atmosphere of PRZ gases which are of lower density. In the open flames reported by Bafuwa (1970), the same air-fuel mixtures were expanding in an atmosphere of cold air at the same density, or only slightly higher. After combustion has taken place, a confined jet is expanding in surroundings of the same density while an open one is expanding in a much higher density atmosphere. This argument explains the faster spread, in a confined furnace than in an open atmosphere, of flames issuing from the same swirler as shown in Figure 4.27.g. This density effect also explains the change in the rate of the jet spread along the flame length, being different before and after combustion takes place. Bafuwa (1970) also reports faster spread of the open flames than their corresponding cold flows. Comparisons based on the results described in this work are complicated by the effects of pressure gradients which are now discussed.

(b) Pressure gradients:

Generally the radial pressure gradient created by a jet expanding in a confinement is higher than in a free surrounding. This pressure gradient will also increase with the confinement being narrower.

The effect of this pressure gradient together with the other relevant forces, e.g. centrifugal force, shear forces, etc., are considered by the radial momentum equilibrium equation:

$$\rho u \frac{\partial v}{\partial x} + \rho v \frac{\partial v}{\partial r} - \frac{\rho w^2}{r} = - \frac{\partial p}{\partial r} + \mu_t \nabla^2 v \quad \ldots \quad 5.3$$

where μ_t is the effective viscosity

A preliminary attempt has been made to assess the magnitudes of the three terms on the left hand side of this equation and compare the result with the observed pressure differences between the wall and the centreline. The isothermal arrangement of a free jet and of furnaces of D/d = 5 and 2.5 were considered, using the 45° swirler.

The second term ($\rho v \frac{\partial v}{\partial r}$) always comes to zero when integrated from the outer boundary to the centreline.

The third term ($-\rho \frac{w^2}{r}$) could be assessed and integrated. In the free jet this term is of much greater magnitude than in the enclosed cases due to the higher tangential velocities in the free jets. It is considered that this term is responsible for the observed centreline pressures in the free jets being significantly lower than in the larger furnace.

It has not yet been possible to assess with any accuracy the remaining term on the left side ($\rho u \frac{\partial v}{\partial x}$), nor the shear force term. It is thought that the changes in these terms between the two furnace sizes contain the explanation for the centreline pressures in the smaller furnace being of lower magnitude than in the larger one.

5.4 The effect of combustion:

One of the important effects of combustion is the pressure drop which occurs across the flame front. The value of this for a simple plane laminar wave is given by, (Lewis and von Elbe (1961)),

$$\Delta p = \rho_u S_u^2 \left[\frac{\rho_u}{\rho_b} - 1 \right] \qquad \ldots 5.4$$

where ρ_u , ρ_b are fluid densities before and after the wave

S_u is the laminar burning velocity.

For the curved turbulent wave, this will be more complicated to calculate, especially for 3-dimensional flow. Tests were carried out to observe this phenomenon and the magnitude of the pressure rise. The static pressure upstream of a swirler was measured when passing a certain air-fuel mixture in two cases. The mixture was exhausted unburned in the first and was ignited in the second. A considerable pressure rise was recorded when the mixture was ignited. The pressure rise exceeded that predicted by Equation 5.4 (using the laminar burning velocity), by an order of magnitude. This is due to the combustion being turbulent. The pressure rise was also a function of the fuel/air ratio. The static pressure profiles discussed in Chapter 4 also show such a rise for the same flow patterns. This pressure rise produces higher axial velocities and thus increases the axial momentum flux which leads to a reduced Swirl Number from that of the cold flow issuing from the same swirler. At the same time it reduces the adverse pressure gradient along the axis, and thus a higher swirler vane angle is needed to produce a CRZ. Both effects of this pressure rise move in parallel and the Critical Swirl Number stays the same for both

cold and burning flows, in spite of the fact that combustion changes the relation between the Swirl Number and the vane angle. Combustion was found to reduce the Swirl Number by a factor of about 3. This factor was found to be the same for both confinements tested. As an example of the agreement with other workers, the case of McEwan (1972) is considered. Working in a square furnace with $D/d = 4$, using a swirler with radial vanes and a cup shaped quarl, he found that combustion reduced the Swirl Number by a ratio of 4. Other workers report qualitatively such changes but no other numerical comparisons are reported.

5.5 Central Recirculation Zones (CRZ):

The presence of a CRZ caused a drastic change in the flow and combustion patterns as seen from the results reported in Chapter 4. The mechanism of the creation of the CRZ, its size and the mass flow recirculated in it are discussed. The use of the Swirl Number in predicting it is also discussed.

5.5.1 Mechanism of creation:

Swirling jets possess an angular momentum which causes them, where the constraint of the swirler is released, to spread outwards producing lower pressure and velocity at the centreline of the jet. Along the length of the jet, while the main flow is decelerating, the pressure is rising and thus an adverse pressure gradient is built up downstream from the swirler. This pressure gradient continues to increase with increasing swirl as long as it is balanced by the

shear forces of the axial flow. This balance is given in the limiting case of a stagnation point by:

$$\frac{\partial p}{\partial x} = - \mu_t \frac{\partial^2 u}{\partial x^2}$$

Beyond a certain pressure gradient, the balance will not be possible and the flow reaches a stagnation point followed by reversal of the axial velocity. This readjustment of the flow causes the pressure upstream of the stagnation point to be raised and the pressure gradient to be reduced.

This analysis is confirmed quantitatively by the values of pressure gradients shown in Figure 4.29.a to g. These figures of the change of the measured static pressure along the jet axis exhibit a sudden increase in the static pressure value nearest to the swirler when the flow changes from pattern B to pattern C, (i.e. when a CRZ occurs). Similar evidence is given by Bafuwa (1970) for open swirling flames and Kawaguchi and Sato (1971) for open swirling jets.

5.5.2 Prediction of the CRZ:

The sudden rise in the static pressure value when the CRZ is started, as mentioned above, could be used as an index of a CRZ occurrence. Figure 4.34 gives the relation between the minimum static pressure at the jet centreline and the Swirl Number S^*. The figure shows this relation to be linear but with a different line representing the flows with CRZ from that representing flows with no CRZ. The transition from one line to the other happens suddenly and not gradually. For a new system the same figure could be readily produced experimentally,

since, all that is needed is the minimum static pressure value along the centreline for different degrees of swirl. Even if the Swirl Numbers are not known, an early indication could be obtained if this pressure is plotted versus the vane angle. A reasonable design method is also available by the use of Figure 4.35. For any given conditions of flow, (cold or burning, degree of confinement) there is a change of slope of the straight line, representing the relation log S^* - θ, which coincides with the Swirl Number at which a CRZ occurs. For all the conditions represented on Figure 4.35. this value of Swirl Number where the transition occurs varies only within a very small range which could simply be an experimental scatter. Thus it could be said that for all confined swirling flows, whether cold or burning, a CRZ is started at the same value of Swirl Number S^* of about 0.11.

To generalise this conclusion, a survey of other workers' results to find the corresponding value was carried out. The following are some examples (main features are listed in Table 4.2).

Mathur (1966) used the same annular swirlers as those used in the present work in a study of isothermal flow in a square cross-sectional model. His results showed the presence of a CRZ when the swirler vane angle was 30°, but not when it was 15°. Using the same relation between the Swirl Number and the vane angle as in Figure 4.35.a, these two points lie on the two sides of the 0.11 critical value of S^*. Similar results are reported by Afrosimova (1967) for cold tests in a D/d = 3 furnace. His results for burning flows agrees with the present work where the reverse flow occurs at a vane angle between 30° and 45°. Critical S^* values reported by Wu and Fricker (1971) are much smaller than 0.11, but they are all equal for a D/d range of 2.35 to 5. The results of McEwan (1972) give critical S^* value of about 0.1.

5.5.3 Size of CRZ:

Details of the development of the CRZ were given in Chapter 4. Figure 4.27.a to g, shows the boundaries of these zones related to the furnace dimensions. In Table 4.2 the characteristic dimensions of the CRZ's measured in this work are given together with other workers' results where relevant.

For flows of pattern C the size of a CRZ increases with the Swirl Number until pattern D is reached. In this pattern, over a wide range of Swirl Numbers, the CRZ's have fixed dimensions relative to the furnace diameter, particularly the maximum width of the CRZ. The ratio of this width to the furnace diameter is seen to vary slightly with D/d. Average values are 0.69 for D/d = 5 and 0.6 for D/d = 2.5. As for the elngth of the CRZ, as a ratio of the furnace diameter, it increases slowly with swirl up to a Swirl Number of 0.7. With higher degrees of swirl the CRZ's do not have a closed end, and a long thin tail extends beyond the furnace exit.

Results of Mathur (1967) and McEwan (1972) agree with the above conclusions as can be seen from Table 4.2. However, those of Afrosimova (1967) showed smaller CRZ dimensions, which is a result of using a long cylindrical quarl after the swirler.

Comparing with open flows (Mathur (1967), Bafuwa (1970)), generally the size of the CRZ is larger in the confined situation.

The reason for this is the higher fraction of the radial pressure gradient set up in the confined flow which is not balanced by the centripetal forces.

5.5.4 Velocities and mass flows in CRZ:

The flow in the CRZ was shown to be mainly axially towards the swirler with low tangential and radial components.

Swirl increases the maximum reverse velocities and the maximum reverse flows, the latter at a higher rate. These quantities are listed in Table 4.2. The recirculated mass flows were calculated by integrating the reverse velocities at different sections.

It is interesting to compare these results with the free jet results obtained by Mathur (1967) and Bafuwa (1970) using similar swirlers. In the confined cases the maximum reverse mass flows are higher, though the maximum reverse velocities are lower, for both isothermal and burning cases. As the D/d ratio of the confinement increased from 2.5 to 5, the reverse mass flow increased, due to the larger cross sectional area of the CRZ.

5.6 Shear forces in swirling flows:

Although no turbulence measurements were carried out in this work, it is thought that a simple analysis would be a useful guide to the extent of the shear forces and to their effect upon the main flow. Also a study of the interaction between turbulence and combustion is presented in the next section. Results of turbulence intensity

measurements in swirling flows, mainly cold, carried out by different investigators were mentioned in Section 2.7. From these results, two main features are evident:

(a) The values of the shear forces are higher than those in an unswirled jet and increase with swirl.

(b) The distribution of these forces follows the same principle as the free shear flow, i.e. the maximum shear forces occur on the jet boundary where velocity gradients are highest. In the case of flow with a CRZ there are two jet boundaries, these being adjacent to the PRZ and to the CRZ. Beyond the wall impingement point one expects a turbulent boundary layer to develop. Initially this will be very thin because of the high velocity gradients.

The overall effect of the two factors (viz. having a more intense shear force integrated over a larger area) leads to a much higher contribution to the flow forces. Neglecting this mainly negative contribution to the momentum means that the values of momenta, at a given cross-sectional plane, calculated from Equations 2.17 and 2.18 are the sums of the net momenta at the furnace exit and the integrations of the boundary shear forces from that plane to the furnace exit.

5.7 Amplification of turbulence level by combustion:

At the flame front, the kinetic energy of the gas increases because of the rapid acceleration, and it is accepted that the energy of turbulence increases simultaneously, (Mizutani (1972)). The increase in turbulence energy could be assumed to be proportional to the increase in the main flow kinetic energy raised to some power.

The turbulence of the approach flow also affects this turbulence increase. Mizutani proposes the following relation:

$$\frac{\bar{u}'^2_f}{2} = \frac{\bar{u}'^2_1}{2} + k_1 \left(\frac{\bar{u}'^2_1}{2} \right)^{\alpha} (\Delta E)^{\beta} \quad .. \quad 5.5$$

where u'_1, u'_f are the fluctuating velocity components before and after the flame front respectively.

ΔE is the time averaged flow kinetic energy increase across the wave, and

k_1, α, β, are constants to be determined experimentally.

The term ΔE is calculated for the two extreme cases of flow acceleration when the combustion wave takes either of the two following geometries shown in Figure 5.1, (where all symbols are defined),

(a) An infinite plane wave, thus acceleration would be in the direction normal to the wave only:

$$\Delta E_1 = \tfrac{1}{2} (u_{b1}^2 - u^2) = \tfrac{1}{2} (S_b^2 - S_t^2)$$

$$= \tfrac{1}{2} S_t^2 \left[\left(\frac{\rho_u}{\rho_b} \right)^2 - 1 \right] \quad \ldots \quad 5.6$$

(b) A curved wave such that the flow directions are not changed in the wave, giving accelerations both along and normal to the mean flame position,

$$\Delta E_2 = \tfrac{1}{2} (u_{b2}^2 - u^2) = \tfrac{1}{2} u^2 \left[\left(\frac{\rho_u}{\rho_b} \right)^2 - 1 \right] \quad \ldots \quad 5.7$$

The actual acceleration mode falls between these two cases and thus ΔE is assumed to have the form,

$$\Delta E = (\Delta E_1)^a (\Delta E_2)^{1-a}$$

$$= \tfrac{1}{2} S_t^{2a} u^{2(1-a)} \left[\left(\frac{\rho_u}{\rho_b}\right)^2 - 1 \right] \quad \ldots \quad 5.8$$

This equation combined with Equation 5.5 indicates that the turbulent kinetic energy increase across the combustion wave can be expressed as a function of approach flow mean and fluctuating velocity, density, flame velocity and direction relative to the flame front.

Thus the effect of the presence of the combustion wave is to increase the overall effect of turbulence; in other words to increase the integrated shear forces.

5.8 Axial fluxes of axial and tangential momenta:

The integration of the full Navier-Stokes equations for 3-dimensional axisymmetric flow gives the following expressions for the axial and tangential momenta at any axial distance, (using the appropriate boundary conditions),

$$G_{th} = 2\pi \int_0^{D/2} \left[\rho u^2 - \mathcal{T}_{xx} + (p - p_{ref}) \right] r dr - F_x \quad .. \quad 5.9$$

$$T_{th} = 2\pi \int_0^{D/2} \left[\rho uw - \mathcal{T}_{\theta x} \right] r^2 dr - F_\theta \quad \ldots \quad 5.10$$

where $\mathcal{T}_{xx}$ and $\mathcal{T}_{\theta x}$ are the shear stresses on the (x-x) and (θ-x) planes respectively

F_x and F_θ are the wall friction force in the axial direction and tangential torque respectively.

suffix th refers to theoretical values.

In the former expressions given by Equations 2.17 and 2.18 used for calculating T and G through integration of experimental results, the shear stresses and wall friction forces were not considered. This implies that the calculated values differ from the true ones by the amount of these forces. The effect of each is considered in the following discussion.

First, considering the wall friction, this will always be in a direction opposite to the flow adjacent to the wall, whether forward or backward (in the PRZ it is backward), thus adding or subtracting from the total value of G. The magnitude of these forces will be proportional to the velocity gradient near the wall. The effect of the walls on the term T will be always in one direction, i.e. additive.

The second effect is that of the shear stresses, and this will always add to G and T an amount which is the total integration of the flow shear forces discussed in Sections 5.6 and 5.7.

Another factor to be considered is the effect of turbulence upon the velocity readings of the 3-dimensional probe. This was discussed in Section 5.2 and was found to be proportional to the square of the turbulence intensity.

Thus the total discrepancy, due to the shear forces, between the experimentally observed fluxes, and their true values, will increase with increasing turbulence. The turbulence is caused by the sudden expansion at the swirler exit and also by the combustion wave.

With higher swirl, these increases occur across a shorter axial distance because of the faster expansion and the more intense combustion. The study of the temperature and CO_2 concentrations show that, while combustion starts earlier in the flows with no CRZ and proceeds for a certain axial distance which is shortened by swirl, for flows with CRZ combustion is delayed for some distance downstream but thereafter it is more intense and goes to completion in a shorter distance.

To sum up, apparent increases in the values of G and T are caused by shear forces being neglected. These forces are proportional to turbulence levels, which increase with swirl and combustion intensities. Wall friction forces are proportional to the velocity gradients adjacent to the wall and they have an additive effect for forward flow and an opposite one when reverse flow occurs adjacent to the wall. The magnitude of the above contributions will decay along the furnace length, more quickly so with larger swirl which causes faster decay of velocity gradients. Experimental measurements of turbulence intensities show that shear stresses, as compared to those of an unswirled jet, are initially higher but lower after an axial distance, x/d = 3, Allen (1970).

The shear forces contributions to the momentum fluxes are shown in the results presented in Figures 4.32 and 4.33, where the resultant effect of the above factors explains the variations of the G and T values along the first 1 to 2 D length of the furnace, with greater variations where swirl is higher. After this distance, the flow reaches an almost settled turbulent situation and the flow is entirely forward. The values of G and T approach constant magnitudes

in an asymptotic fashion.

The effect of turbulence in isolation from the other factors (confinement and combustion), can be seen from the free swirling isothermal jet results reported by Beer and Chigier (1963). The total momentum values, calculated in the same manner as in this work, show a decay along the axial distance from the swirler. This decay can only be due to the shear stresses set up by turbulent motion.

Unfortunately there appear to be no other published results of momentum integrations relevant to this work.

CHAPTER 6

MATHEMATICAL MODELLING OF SWIRLING FLAMES

6.1 Introduction:

The main object of the work described in this Chapter is to develop a mathematical procedure which can adequately predict a priori the information required for the design and performance of a confined swirling flame. The aim of this is to reduce the amount of experimental work on physical models or prototypes. To be able to predict this information, namely the flow and combustion patterns, a mathematical representation of the processes and materials involved is needed. These include the physical processes of the flow aerodynamics, the thermodynamic relations between species and the energy release, and the chemical processes occurring during combustion. Some of the laws governing these processes are already formulated and these include the laws of conservation of mass, momentum, energy and species. But these formulations include some transport coefficients which still need specification, particularly for turbulent flows.

The next step is to solve these formulae which mostly are non-linear coupled partial differential equations. The present state of the art of solution of partial differential equations does not give analytical solutions except to a few simple flow problems. Even then, the solutions are not in a form to help the designer. For example, Chervinsky's (1969) solution for a weak swirling flame, with over-simplified assumptions, is difficult to interpret. For these reasons,

the alternative method, which is the numerical solution using finite-difference techniques, has greatly progressed, particularly due to the availability of high-speed computers.

For a complete procedure to be possible, the information from the fields of mathematics, fluid mechanics, thermodynamics and chemical kinetics have to be related. A brief review of relevant work is given here followed by the actual procedure and the results which was possible to obtain in the time available after completing the experimental work.

The sequence adopted in this Chapter is present difficulties, describe developments, demonstrate that useful predictions are already being made and indicate in what areas further research may be useful.

6.2 The Numerical solutions of Navier-Stokes Equations:

Before proceeding to the numerical side of the procedure, it is necessary to realise the type of equation to be solved. The conservation of momentum equations of the flow (Navier-Stokes equations, (NSE)), for the case to be considered of flow with recirculation can be reduced to an elliptic type partial differential equation. Similar equations will represent the conservation of energy and species. For the very weak swirling unconfined case the flow has no recirculation and the boundary layer approximations apply. These reduce the equations to the parabolic type which are easier to solve. For the solution of the elliptic type equations, boundary conditions along a closed boundary and initial guesses over the field of solution are necessary to start the solution.

The use of numerical finite-difference techniques in solving the NSE is not new. As early as 1928, Thom produced such solutions and others followed. The early work up to 1960 was summarised by Thom and Apelt (1961). This work was limited to laminar flows with very low Reynolds Numbers, up to 100. All attempts to solve problems of higher Reynolds Numbers led to divergence of the solution. It was only about 1965 that this obstacle was overcome by the use of a special formulation for the differences in the non-linear term of the equation, as will be explained later. The technique known as uni-directional or upwind differencing, was used by Runchal and Wolfshtein (1966) and Greenspan (1968) and made it possible to obtain convergence of the solutions for any Reynolds Number. The extensive use of modern computers also facilitated the application of the solutions to a variety of problems. It should be noted here that this technique offers a lower degree of accuracy because of the special non-symmetric formulation (error of order ϵ instead of ϵ^2). The truncation errors when accumulated seem to work as an artificial viscosity term which has a stabilising effect on the solution.

The amount of work produced in this field is so varied and diverse that it cannot be comprehensively reviewed here. Some relevant investigations will be mentioned later. However, a review of some recent numerical work on solutions of NSE is given by Salah (1971), who developed a variety of numerical methods and applied them to different problems to indicate the superiority or otherwise of each method.

The NSE are solved either in their usual form for velocity and pressure or in the stream function and vorticity form after eliminating

the pressure. The latter method has the advantage of reducing the non-linearity produced by the pressure term, which is regained after the solution has converged. But it has the disadvantages of the necessity of using one eddy viscosity for the two equations of directions x and r, and the need to specify boundary conditions for the vorticity which has some singularities and is not a direct physical parameter. Thus for work on 3-dimensional flows the former approach is necessary.

6.3 Turbulence transport modelling:

The possibility of solving the flow equations for higher Reynolds Numbers meant the extension of the solutions to turbulent flows. Most analyses accept the NSE to represent turbulent flow as a follow up of the eddy viscosity concept. The centre of the problem of representing turbulent flows has thus become the search for a satisfactory model for this eddy viscosity. The other approach is to model the shear stresses for the Reynolds equation.

Two main approaches to the turbulence transport representation are:

6.3.1 Conceptional models:

The earliest of these was put forward by Prandtl (1925) as an analogy to the kinetic theory of gases. Various implementations of this model were used in many engineering problems, especially of boundary layer type flows. The choice for this model is based on its simplicity and the small amount of empirical knowledge needed to specify the mixing length. It also has the advantage that it

could be extended to include two or three directions, although with more information needed to specify the mixing lengths.

A more realistic and complete conceptional model is presented by Tyldesley and Silver (1968). Starting with an entity of fluid and integrating the forces of interaction with neighbouring entities, they were able to find an expression for the eddy viscosity. This type of model could be developed to include more situations by adding the different forces one at a time and testing the model against specially designed experiments.

6.3.2 Mathematical models:

In this approach one differential equation or more is derived for the turbulent properties of the flow and solved together with the time-mean flow equations. These equations are generally produced by separating the fluctuating components from the time-mean ones in the NSE. The variables in these equations vary according to the authors but they generally include kinetic energy of turbulence, length scale, vorticity fluctuations or a direct calculation of the shear stresses. The constants needed for these equations are determined or adjusted to produce agreement with experimental measurements. With more complicated flows, the number of constants increases and their determination becomes more difficult with no guarantee of their universality (i.e. having same values for different situations). It should be mentioned that this increases the computing time considerably. There is also the problem of the accuracy of the numerical method of solving the equations and adjusting the constants which may affect the agreement with measurements. This becomes clear

when solutions are compared and it is found that the simpler conceptional models sometimes produced the same or better agreement than the mathematical ones which had to be adjusted and were more expensive to use. A review of these mathematical models is given by Launder and Spalding (1972), and a collection of papers on both types of models is presented by Harlow (1973). A more general approach appears to be the use of conceptional modelling for simple turbulence processes to determine the constants and the mathematical models to relate them to each other and produce solutions. In this way the turbulence modelling could be separated from the numerical solution, which could be used for testing the final model.

For swirling isothermal flows, two extra effects have to be considered. Firstly there is the effect of rotational motion which changes the turbulence in the flow. One method of including this in a simple model is the rotational stability effect discussed in Section 2.7. The second effect is that of the curvature of the streamlines caused by the jet expansion, the confinement and the CRZ. This curvature is known to have more effect on the turbulence properties of the flow than on the mean flow itself, a recent review of relevant work is given by Bradshaw (1973).

From experimental measurements, it is evident that anisotropy of the eddy viscosity for swirling flows is significant. The combined effects of swirl and 3-dimensionality seem to be inseparable and numerical methods that are known to work satisfactorily for simpler flows need further developments for swirling flows.

For a combustion system other transport coefficients for mass and heat are also needed. These are usually related to the momentum coefficients through the Schmidt and Prandtl numbers.

To test the validity of available turbulence models for swirling flows and help modify or formulate new ones, the transport coefficients were worked out using time-mean experimental measurements as input to the conservation equations. The results of the work on this method will be discussed later.

6.4 Chemical Reaction representation:

The rate at which the chemical reaction will proceed needs to be specified in any mass species conservation equation. The generally used model is the one that applies the Arrhenius type equation for this rate. This means that the reaction is controlled mainly by the temperature and concentration of the reactants. The two constants required are taken from experiments on specially designed well-stirred reactors, Herbert (1957).

Another limit was suggested by Spalding (1971) where the degree of mixing is the major factor. This model assumes that turbulence has a strong influence on the local reaction rate, in most cases a dominant one. This acts either through its effect on the fluctuations of the concentrations or its effect on breaking up the "lumps" of unburned reactants to be small enough for heat conduction and chemical reaction to be significant. The latter effect is referred to as eddy break-up.

6.5 Some relevant predictions:

The flow of a confined swirling flame is of a complicated nature, and as discussed in Chapter 2, it can be better understood if the analysis is built up from simple elements. In this Section a brief review of predictions for relevant problems is presented.

(a) Sudden expansion in a confinement:

This problem was dealt with for laminar flow by Macagno and Hung (1967). They presented predictions for Reynolds Numbers up to 70 which compared favourably with their experimental measurements. They present a good analysis of shear forces in this case.

The problem was considered for higher Reynolds Numbers by Kirkpatrick and Walker (1972) where the nozzle velocity was as high as 0.4 Mach No.. They used a semi-empirical turbulent viscosity developed from Prandtl's mixing length theory given by,

$$\mu_t = u_o x/2 \ \sigma^2$$

where σ is a constant.

Using a differential equation turbulence model Runchal et al (1971) solved this problem and produced good agreement with measurements. McBride (1972) extended this solution to a similar flow in a furnace and he reported that a constant eddy viscosity model gave better predictions than a 2-differential equation model.

(b) Swirling flow in pipes:

This case is simpler than swirl in a furnace because the radial velocities are negligible. Lavan et al (1969), produced numerical

solutions for the decay of swirl in a pipe flow using a constant eddy viscosity model. Roberts (1971) found that a scalar representation of the eddy viscosity did not produce reasonable results. Next he used two values, one for the axial motion from a 2-differential equation model (for turbulence kinetic energy and vorticity fluctuations) and another for the rotating motion using an extension of the mixing length concept. This produced better agreement with experimental measurements.

(c) Boundary layer type swirling flows:

The main feature of this type is that the principal equations are of the parabolic type after applying the boundary layer approximations. This type includes swirling flow on rotating bodies (wall type B.L.) and free expanding weak swirling jets. The former type was dealt with by Koosinlin and Lockwood (1973) with special interest on producing a turbulence model. Two models were used, a 2-differential equation model, for kinetic energy and length scale, and an extension of the mixing length model to allow for flow anisotropy, which could not be done with the former model. Better predictions were made when the latter model was used.

The jet type swirling flows, cold and burning were dealt with by Gibson and Morgan (1970), and Pai and Lowes (1972), using a constant value for μ_t and Arrhenius type reaction equation. Both predicted reasonable results for cold or nonswirling flows, but the addition of swirl, and/or, combustion made the predictionsless satisfactory.

Rubel (1972) produced better agreement for weak swirl, cold and burning, using a turbulent viscosity mixing length model modified for swirl,(Section 2.7).

Similar work to that of Koosinlin and Lockwood was performed by Lilley (1973 a,b) on both cold and burning jets, who arrived at the same conclusion as to the better turbulence modelling. In the burning case he used the eddy break-up model with an extra condition by which no combustion starts where the velocity is higher than 24 m/sec (following the experimental results of Chervinsky with which he compared his predictions).

(d) Recirculating swirling flows:

Gosman et al (1969) gave a procedure for solving a swirling diffusion flame. They produced velocity components, axial and tangential, and temperature distributions. The shortening of the flame caused by swirl was reasonably predicted, although no comparisons with experiments were presented. A similar procedure was used by Odlozinski (1968) to predict the flow and combustion in a flame stabilized by a bluff body. Predictions of velocities and temperatures were made, which seem reasonable qualitatively, although they were not compared with any experimental results.

This procedure was developed by Bafuwa (1970) for the prediction of flow patterns of free swirling flows. Cold flow predictions were made for 15^{o} and 45^{o} swirlers which were in good agreement with experimental measurements. Predictions for the 15^{o} swirler's burning flow were also made but there is some doubt about the validity of these because of an error in one constant of the

chemical reaction equation.

(e) Transport coefficients from mean values measurements:

Lilley and Chigier (1971) obtained local values of shear stresses in weak swirling unconfined cold and burning flows by numerical solutions of the conservation equations, using time-mean values of velocities and temperatures. The results show that for very weak swirl, the values are not very different from the nonswirling jets where a constant μ_t along a section is sufficient although $\mu_{r\theta}$ is smaller than μ_{rx}. With increasing swirl to about S = 0.3 (S based on d), values of $\mu_{r\theta}$, μ_{rx} increase with swirl but decay faster with the axial distance from the swirler. The results also show that an isotropic model will not be satisfactory for swirling flows.

Scott and Rask (1973) performed similar solutions for swirling isothermal flow in an annular pipe. Similar results were found and for the variation with radius, it was shown that μ_t is nearly equal to μ (molecular) near the inner wall but increases with radius until the outer wall is reached.

6.6 Theory for the prediction procedure:

6.6.1 The principal equations:

These include the momentum conservation equation, the Navier-Stokes equations for the steady state $\left(\frac{\partial}{\partial t} = 0\right)$ two-dimensional axisymmetric $\left(\frac{\partial}{\partial \theta} = 0\right)$ flow in the polar cylindrical coordinates.

The third component is solved for the tangential velocity. Added to these is the continuity equation. For the case of combustion more than one mass species exists and thus a conservation equation is solved for each and another one for the conservation of energy (enthalpy). Here follows a listing of these equations.

The continuity equation:

$$\frac{\partial}{\partial x}(\rho u) + \frac{1}{r}\frac{\partial}{\partial r}(r \rho v) = 0 \qquad \ldots 6.1$$

The Navier-Stokes equations for this case are -

$$u \frac{\partial}{\partial x}(\rho u) + v \frac{\partial}{\partial r}(\rho u) = - \frac{\partial p}{\partial x} + \frac{\partial}{\partial x} \mathcal{T}_{xx} + \frac{1}{r} \frac{\partial}{\partial r}(r \mathcal{T}_{rx}) \ldots 6.2$$

$$u \frac{\partial}{\partial x}(\rho v) + v \frac{\partial}{\partial r}(\rho v) - \rho \frac{w^2}{r} = - \frac{\partial p}{\partial r} + \frac{\partial}{\partial x}(\mathcal{T}_{rx}) + \frac{1}{r} \frac{\partial}{\partial r}(r \mathcal{T}_{rr}) - \frac{\mathcal{T}_{\theta\theta}}{w} \ldots 6.3$$

$$u \frac{\partial}{\partial x}(\rho w) + v \frac{\partial(\rho w)}{\partial r} + \rho \frac{vw}{r} = \frac{\partial}{\partial x}(\mathcal{T}_{\theta x}) + \frac{1}{r^2} \frac{\partial}{\partial r}(r^2 \mathcal{T}_{r\theta}) \qquad \ldots 6.4$$

The shear stresses $\mathcal{T}$'s are related to the velocity gradients and the effective viscosity in the normal way, Schlichting (1968).

For the numerical solution the pressure term was eliminated from Equations 6.2 and 6.3 to give together with 6.1 two new equations for vorticity and stream function which were defined as

$$\omega = \frac{\partial v}{\partial x} - \frac{\partial u}{\partial r} \qquad \ldots \quad 6.5$$

$$\frac{\partial \psi}{\partial r} = \rho\, ur \qquad \ldots \quad 6.6$$

$$\frac{\partial \psi}{\partial x} = -\rho\, vr \qquad \ldots \quad 6.7$$

These equations will have the general form, (Gosman et al (1969),

$$a\left[\frac{\partial}{\partial x}\left(\phi \frac{\partial \psi}{\partial r}\right) - \frac{\partial}{\partial r}\left(\phi \frac{\partial \psi}{\partial x}\right)\right] = \frac{\partial}{\partial x}\left[b \frac{\partial}{\partial x}(c\phi)\right] + \frac{\partial}{\partial r}\left[b \frac{\partial}{\partial r}(c\phi)\right] + d \qquad \ldots \quad 6.8$$

← Convection term ——→ ←—— Diffusion term ——→ Source term

where ϕ stands for any variable.

and a,b,c,d coefficients given for every variable in Table 6.1. The three terms of the above Equation 6.8 can be identified as convection, diffusion and source terms respectively.

The tangential velocity Equation 6.4 could be also cast in the same form as 6.8.

The equations for the conservation of the mass species, one for each species, and the enthalpy could also be fitted to the same form. For derivation of these equations see Bird et al (1960).

6.6.2 Physical Input:

(a) Eddy Viscosity:

In this work as a starting point, the free jet eddy viscosity empirically derived by Squire (1951) was used. This was given as:

$$\mu_t = 0.0162\ \rho\ u_o\ d \qquad \ldots \quad 6.9$$

This was further developed to include effects of density changes and swirl by using the absolute velocity instead of the axial one. Later a factor similar to that given by Rubel (1972) was incorporated.

Turbulent Schmidt and Prandtl numbers were taken as unity.

(b) Combustion representation:

A simple one-step reaction between fuel and oxidant was assumed,

$$m_{fu} + m_{ox} \longrightarrow m_{pr} \qquad \ldots \quad 6.10$$

where m is the mass fraction of any species.

For a premixed confined flame, the following extra relations apply:

$$m_{fu} + m_{ox} + m_{pr} = 1 \qquad \ldots \quad 6.11$$

and

$$m_{fu} - \frac{m_{ox}}{(f/a)_s} = \text{const.} \qquad \ldots \quad 6.12$$

where $(f/a)_s$ is the stoichiometric fuel/air ratio. Using these relations means that one needs to solve only one equation to find all three mass fractions. This equation will have the form of Equation 6.8 and it was chosen to solve for m_{fu}. The reaction was considered

to be chemically controlled with the following equation for the rate of m_{fu} dissipation

$$\dot{m} = - K\, m_{fu}\, m_{ox}\, \rho^2 \sqrt{T}\; e^{-\frac{E}{RT}} \qquad \ldots \quad 6.13$$

where E is the activation energy taken as 40,000 kcal/kg mole, and K is the global reaction rate constant given by Longwell and Weiss (1955) as 1.13×10^{11} m^3/kg mole sec $K^{\frac{1}{2}}$. This was measured in a specially designed well stirred reactor where mixing is as near as possible to perfect. Weiss et al (1958) recommended the use of the above constants for most hydrocarbons.

(c) Energy equation:

For a confined system, the only heat transfer is that through the walls, mainly by radiation, in the case of refrectory walls. For the first solution the flow was assumed adiabatic, thus the enthalpy H is given by

$$H = C_p\, T + m_{fu} \cdot C.V. = \text{Constant} \qquad \ldots \quad 6.14$$

where C_p was taken as 0.3011 which is the value for the products of combustion at the corresponding flame temperature. The above equation replaces the general differential equation for enthalpy conservation.

Density calculations were based on the usual equation of state using the gas constant for the products of combustion, which is nearly the same as for air. Temperatures were calculated from the enthalpy Equation 6.14.

6.6.3 Finite-difference formulation:

The flow field is divided into a variable size grid, with closer points where flow gradients are higher, and the differential equations are replaced by difference equations for each grid point. The general method of using the central differences was used except for the convection term, where the upwind differencing mentioned in Section 6.2 was used. The general grid arrangement and an element of the grid are shown in Figure 6.1. For the point (i,j) we can express the differentials as

$$\left(\frac{\partial \phi}{\partial x}\right)_{i,j} = \frac{1}{2h} (\phi_{i+1} - \phi_{i-1}) + \epsilon^2 \quad \ldots \quad 6.15$$

where ϵ is a small quantity of the order h, h being the grid spacing as a fraction of the main regime dimensions.

The convection terms are formulated according to the following principle. The flow direction is determined by finding the value of $(\psi_{i,j+1} - \psi_{i,j-1})$. If this value is ≥ 0.0 one takes

$$\frac{\partial \omega}{\partial x}_{i,j} = \frac{1}{h} (\omega_{i,j} - \omega_{i-1,j}) + \epsilon \quad \ldots \quad 6.16$$

otherwise take

$$\frac{\partial \omega}{\partial x}_{i,j} = \frac{1}{h} (\omega_{i+1,j} - \omega_{i,j}) + \epsilon \quad \ldots \quad 6.17$$

similarly for the normal direction.

Applying these relations to all differential terms in the equations of the form 6.8 at each grid node and summing coefficients the final equation could be reduced to the form

$$\phi_{i,j} = C_1 \phi_{i-1,j} + C_2\phi_{i+1,j} + C_3 \phi_{i,j-1} + C_4 \phi_{i,j+1} + C_5 \quad .. \ 6.18$$

There exists now one such equation for each node and for each variable. These equations are solved by successive substitution. Initial values must be prescribed to each internal point together with the conditions at the boundary enclosing the system. Thus the solution is started by these values which are updated in each cycle of iterations until the convergence criterion is satisfied, i.e. the difference of the value of a variable between two cycles of iterations is below a prescribed limit, taken as 0.01 of the maximum value of the variable in the field in this solution.

6.6.4 The boundary conditions:

These are necessary for the solution to proceed and some have a major influence on the success of the procedure. However, they are not all known before the solution starts and thus they can only be specified as related to neighbouring internal points. Special care was given to these conditions and several trials were made to select the best formulation for them, on the basis of the correct representation of the flow and to give reasonable predictions. The following is a brief description of the ones chosen for the work.

(a) Inlet section:

It was very important for the conditions to be as realistic as possible. A profile for the axial velocity distribution was assumed for each swirl vane angle, an example is given in Figure 6.2. The tangential velocity component was assumed to be related to the axial one by:

$$w = u \tan \theta \qquad \ldots \quad 6.19$$

Numerical integrations of the axial velocity give the values of stream function according to the equation

$$\psi = \int_{r_1}^{r_2} \rho u r \, dr \qquad \ldots 6.20$$

For the vorticity, differentiation of the velocity profiles were made using the unsymmetrical relation, Greenspan (1968)

$$\left.\frac{\partial \phi}{\partial y}\right)_o = \frac{1}{2h} (3 \phi_o - 4 \phi_1 + \phi_2)$$

where o, 1, 2 indicate the points along the section starting from one end, next to a wall.

The fuel mass fractions along the inlet plane were specified corresponding to the inlet fuel/air ratio.

(b) Walls:

For stream function, a constant value for the walls was taken. Tangential velocities are zero along the walls. For the vorticity, special formulations were used as follows.

For vertical walls, the condition derived by Macagno and Hung (1967) using a Taylor expansion near the wall was used; this was given by

$$\omega_o = \frac{3}{h^2 r} \left[\psi_1 - \psi_o \right] - \omega_1 \quad \ldots \quad 6.21$$

where o, 1 indicate the wall point and the nearest internal node respectively. A different expansion was derived in the same way for the horizontal walls. Similar expressions were derived by Cosman et al (1969) and were also used. At the corner points the vorticity was taken to be the average of the two neighbouring points.

For the fuel mass fractions, gradient type boundary conditions were used, i.e. gradient of the fuel mass fraction vanishes as the wall is reached.

(c) Axis of symmetry:

The stream function was taken constant along the axis, being a condition of symmetry. Also this condition implies that the tangential velocity is zero along the axis. Although the vorticity might be assumed zero, the variable used in the calculations was $\frac{\omega}{r}$ which should have a definite value at the axis. Thus a gradient type boundary condition was assumed. The same type was used for the fuel mass fraction.

(d) Exit section:

There is no previous knowledge about the conditions at the exit section when the procedure is started, but it has to be defined for the closing of the solution. An extrapolation formula is thus used for this purpose. The one used here was that given by Milne (1953),

$$\phi_{i,j} = \phi_{i-4,j} - 2\,\phi_{i-3,j} + 2\,\phi_{i-1,j} \quad \ldots 6.22$$

This formula was used for all variables.

6.6.5 The computer programme:

The main structure of the programme used by Bafuwa was adopted in the present work but some details were altered for simplicity, economy and efficiency of program use. These led to reducing the time for compiling the programme which was run on both the UNIVAC 1108 and the IBM 370/155 computers.

The following modifications were also made:

(i) The main geometry was changed to that for confined flow.

(ii) For the confined adiabatic flow, the enthalpy equation became the algebraic one given by Equation 6.14.

(iii) The relaxation parameter was varied to give best convergence.

(iv) A different eddy viscosity model was used, Section 6.6.2.

(v) The values in the chemical kinetic rate Equation 6.13 were corrected.

(vi) Most of the boundary conditions were changed as in Section 6.6.4, to suit the new flow conditions, or to give better representation.

6.7 Results and Discussion:

6.7.1 Cold flows:

Figures 6.3 a and b give a sample of the predictions for cold flow to show the effect of swirl through variation of the vane angle. Although the predictions seem reasonable, they predict less rapid jet spread than the experimentally measured profiles. The CRZ was predicted, but again smaller than the measured one for the same swirler. There could be two reasons for these differences.

(a) The effect of swirl is not strongly linked to the stream function and vorticity equations. It appears only in the source term of the latter. The pressure term is not represented explicitly to introduce this effect.

(b) The effect of the eddy viscosity representation may be over-simplified. This effect was tested by varying the constant in the Equation 6.9 giving it the values 0.012, 0.024 and 0.080. The results show that the jet spread is made faster by increasing the eddy viscosity, as given by the jet impingement point in Figure 6.4. A more realistic representation with values that vary locally with the velocity and momentum gradients is expected to produce better predictions.

The general conclusion is that while predictions of the flow patterns of types A, B and C were possible with the procedure in this form, more input information is needed to predict the flow type D.

6.7.2 Burning flows:

Converged solutions of the cold flow were taken as initial guesses for the burning solution. Even with this, the convergence was more difficult to achieve than the cold flow and thus required more computing time. The extra information needed as input to the procedure are the effect of combustion on the eddy viscosity and the rate of the chemical reaction. The results of computations using the chemical kinetics rate Equation 6.13 showed a faster reaction rate than that experimentally observed. This could be attributed to the model constants being measured for a perfectly stirred reactor where the mixing is better than in the case considered here. This could be remedied by using different constants in the Equation 6.13 or by using a model related directly to the mixing rates, i.e. turbulence, for example, as in the "eddy break-up" model.

The effects of heat losses through the walls should also be considered since these were found to affect not only the near wall flow, but also the CRZ flow through entrainment as will be discussed in Chapter 7.

A sample of the flow and temperature patterns for a 30^{o} swirler flow is given in Figure 6.5.

6.8 Suggestions for further work:

The main improvements to this procedure are needed in the physical inputs. These include the flow dynamics, the chemical reaction and the heat transfer. The main factor in the flow dynamics is the need for a turbulence model which could be varied with the

different flow conditions and be reasonably economic to use. As suggested in Section 6.3, development of a conceptional model seems appropriate. The chemical reaction model has also to be related to the flow mixing. This seems to be an easier task if the turbulence representation is improved. Heat transfer to the walls by radiation and convection should be included in the solution, especially as most furnaces are not adiabatic.

For a more general model to include flows which are not generally axisymmetric a 3-dimensional solution procedure is needed. This should be better based on the solution of the NSE in their velocities and pressure form as discussed in Section 6.2.

CHAPTER 7

STABILIZATION OF PREMIXED SWIRLING FLAMES

7.1 Introduction:

The patterns which swirling flames follow in furnaces are important to designers and these have been discussed in the preceding chapters. The mechanism of flame stabilization is also of great importance to the designer, and therefore a study of how a premixed flame is stabilized in a swirling jet should be included in this Thesis.

This Chapter contains a review of previously published work on stabilization in a free jet. There then follows a description of experiments that were carried out to test one of the assumptions of a published theory. Experiments were also performed on the effect of scale. A side effect due to a small quarl was observed in these tests and briefly investigated. Finally, stability limits are reported for the enclosed furnace, and these are related to the free jet stability limits.

7.2 Review of published work:

Bafuwa (1970) has given a description of the shapes that the flames can take in pre-mixed jets issuing from vane-type swirlers similar to those used in the present work. Under typical flow conditions which are not near the stability limit, the flame anchors itself in the wakes of the vanes. Under conditions of low flow

velocity and high mixture burning velocity, the flame may move into the swirler, stabilizing itself within the separation bubble that exists near the leading edge of the "suction" surface of the vanes. This of course can cause serious damage to the swirler. These types of flames were also observed in the present work. However it was observed that, for flows which had a CRZ, as the stability limits were approached, the flame moved away from the vanes, and combustion was maintained by the hot gases in the CRZ.

Weak stability limits were published by Bafuwa for these flames stabilized in jets issuing from hubless vane swirlers into the atmosphere. The results were later analysed by Bafuwa and Maccallum (1973). Other stability limits were published by Lutzhoft and Fetting (1968). In both cases, increasing swirl, in the range of established CRZ, was found to cause a deterioration of the weak limits.

Bafuwa and Maccallum suggested that the explanation for this lay in the fact that ambient air was entrained by the swirling jet and some of it is recirculated back in the CRZ. This air entrainment of fresh air into the CRZ was also detected by Albright and Alexander (1956) in a cyclone flame system, but no attempt was made to estimate the amount of this air nor did they consider its effect on the stability limits. Bafuwa and Maccallum (1970) had demonstrated the reduction in the CRZ temperature that occurred when swirl was increased. By assuming that the fractional dilution, as indicated by the temperature reduction at the edge of the CRZ near the swirler, remains the same at other fuel/air ratios, they estimated temperatures in this zone corresponding to the stability limit conditions.

It was found that the flow velocities at the weak limits for the three swirlers tested, (vane angles 30^{o}, 45^{o} and 60^{o}) could be correlated by these temperatures.

7.3 Theories of flame stabilization in Recirculation Zones:

Three theories which had been used with success for correlating stability limits of flames behind bluff bodies were applied by Bafuwa and Maccallum to their results. The theories were the "contact time" theory of Zukoski and Marble (1955, 1956), the "flame stretch" theory described by Lewis and von Elbe (1963), and a recirculation model proposed by Spalding (1953).

In Bafuwa and Maccallum's 1973 paper, the discussion of these theories was very brief. A more complete analysis will be given by Bafuwa et al (1974). As this latter paper has not yet been published, a more extensive description of this analysis is given here.

In their "contact time" theory, Zukoski and Marble consider the time, $\mathcal{T}$, that an element is in contact with the hot recirculation zone behind the bluff body. They found that this time, which is taken as the length, L, of the recirculation zone, divided by the approach stream velocity, u, is a function only of the fuel/air ratio of the mixture and is essentially independent of the variables of flame holder shape and size. In applying this concept to the stabilization of free swirling flames there is the problem of selecting the effective fuel/air ratio for the mixture. The two extremes are the fuel/air of the jet leaving the swirler and the fuel/air ratio of the mixture at the edge of the CRZ after ambient air has been entrained.

Taking the latter extreme, Bafuwa et al (1974) compared the stability data for the 30° and 60° swirlers, (Bafuwa and Maccallum (1973)). The CRZ length with the 60° swirler was about 4.2 swirler diameters (d), while with the 30° swirler it was about 2.3 d. The axial component of velocity corresponding to the weak limits at the same "effective" fuel/air ratio were in the ratio $u_{60}/u_{30} = 0.9$. Thus comparing the contact times they found,

$$\frac{\mathcal{T}_{30}}{\mathcal{T}_{60}} = \frac{2.3}{4.2} \times 0.9 = 0.5 \qquad \ldots \quad 7.1$$

If the approach fuel/air ratio had been used (the other extreme) the ratio $\mathcal{T}_{30}/\mathcal{T}_{60}$ had a value less than 0.15. If the contact time theory is applicable, one of these ratios, or an intermediate value should be unity. On this evidence, Bafuwa and Maccallum discarded this theory.

In the flame stretch theory, Lewis and von Elbe interpreted the above time, $\mathcal{T}$, as also being the time which a wave element takes to advance, with the burning velocity, S_u, from the anchoring point which is adjacent to the stabilizer through a distance, y, across the stream to meet the fresh element which just touches the end of the recirculation zone, thus,

$$\mathcal{T} = \frac{L}{u_{max}} = \frac{y}{S_u} \qquad \ldots \quad 7.2$$

The test for stability is the stretch of the flame front when this element is "on its own" at the downstream end of the recirculation zone. A stretch parameter K is defined as,

$$K = \frac{\eta_o}{u} \frac{du}{dy} \quad \ldots \quad 7.3$$

where η_o is the flame thickness given by $\frac{k}{C_p \rho_u S_u}$.

Extinction occurs when the flame stretch parameter exceeds a critical value of about unity. This development of Lewis and von Elbe partially explained the dependence of the contact time on fuel/air ratio which Zukoski and Marble found with their bluff-body stability limits. When Bafuwa and Macçallum applied this theory to their results, again they had to decide what effective fuel/air ratio to use. Taking the one extreme using values of η_o and S_u corresponding to the fuel/air ratio at the edge of the CRZ after entrainment of ambient air, the application of the 30^o and 60^o swirler data to Equation 7.2 gave,

$$y_{30} = 0.5\, y_{60} \quad \ldots \quad 7.4$$

Integration of the flame stretch factor equation between velocities S_u and u gives (Lewis and von Elbe),

$$\log (u/S_u) = (y/\eta_o)\, K \quad \ldots \quad 7.5$$

Inserting appropriate values for S_u and η_o, and the result of Equation 7.4 leads to the relation at the extinction limits:

$$K_{30} = 2.1\ K_{60} \quad \ldots \quad 7.6$$

If the fuel/air ratio of the flow from the swirler had been used as the "effective" value (the other extreme), K_{30} was larger than K_{60} by a factor of 8. Bafuwa and Maccallum concluded that this theory did not offer a satisfactory explanation for stabilization in free swirling jets with CRZ's.

However a modified version of Spalding's (1953) model looked promising to them. Spalding's model, for bluff body stabilization, is shown in Figure 7.1.a and b. The modification suggested by Bafuwa and Maccallum is to draw the reaction curves in Figure 7.1.b, corresponding to the fuel/air ratio of the diluted stream after entraining ambient air. They suggested that raising the degree of swirl increases the diluting effect to such an extent that the values of T_1, at a flow velocity, are effectively unaltered at the blow-off limits, although the approach fuel/air is very much higher.

This model can be further discussed as a result of the present work. In the model, the flow of the combustible mixture from the swirler is considered as layers which flow along the stream lines but all the time mixing with each other radially. The mixing is more intense in this case than in the flow behind a bluff-body stabilizer due to the effect of swirl. Thus the inner layers are mixed with the

flow of the ambient air (or PRZ flow if inside a furnace). After a certain distance of contact the fresh charge will start to react and the flame is thus started. This distance will become longer, for the same flow velocity, as the fuel/air ratio of the charge is reduced, also as swirl is increased and more air is entrained in the CRZ. This increase of the contact length becomes more obvious if temperature profiles measured in the two furnaces, reported in Chapter 4, are compared. The distance is seen to be longer in the smaller furnace where a leaner mixture is used than in the larger furnace for 45^{o} and 60^{o} swirlers. By the time the gases reach the downstream stagnation point and start to recirculate they are a mixture of the input charge, either with entrained air from the surroundings (for free jets) so that the CRZ contains a leaner mixture, or with entrained (and somewhat cooled) products from the PRZ.

In concluding this discussion of the theories of flame stabilization, it should be stated that the theories of contact time and flame stretch might well be applicable to the stability limits of swirling flames which do not have a CRZ. Unfortunately there was data available on only one such arrangement - that with the 15^{o} swirler.

7.4 Factors which influence entrainment:

7.4.1 Effect of fuel/air ratio:

Bafuwa and Maccallum estimated fractional entrainment of ambient air into the CRZ from temperature traverses. They then

assumed that the fractional entrainment at the stability limit was the same as at the conditions corresponding to the temperature traverse, i.e. it was independent of the fuel/air ratio. In the present work this assumption has been examined.

To reduce the relative effect on the flow due to the traversing probes, the experiments were carried out using one of the hubless swirlers prepared in the present work, which are of 93 mm (3.66 in) diameter instead of the smaller swirlers 24 mm (0.93 in) used by Bafuwa. Temperature traverses were made across the CRZ behind the 45° swirler at three fuel/air ratio and the results are given in Figure 7.2. From the traverses, the temperatures at the edges of the recirculation zone were found and hence the corresponding fractional entrainment of ambient air. At the fuel/air ratios of 0.119, 0.133 and 0.144 (by volume), the fractional entrainments were 0.36, 0.32 and 0.28 respectively. For comparison, the fraction which Bafuwa and Maccallum found with the smaller swirler was 0.40. It must be concluded that there is some effect of fuel/air ratio on the entrainment, and strictly one should use the entrainment appropriate to the limit condition. However, there are discontinuities in the temperature variations, frequently due to the wakes of the vanes, and this makes the estimation of the effective entrainment difficult. There is of course the other problem of the choice of the axial distance where the temperature traverse should be made. Bafuwa and Maccallum selected a distance of 1 swirler diameter downstream. This distance was also used for the above calculations. But owing to the

conclusion drawn in the previous section about the location of the effective reaction zone varying with fuel/ratio, it is suggested that for further work, several temperature traverses be made at a range of distances and using a fuel/air ratio near to the stability limit. The results of the traverse nearest to the reaction zone should be used for correlations.

Gas samples were also withdrawn across the plane used for temperature traverses, and analysed for carbon dioxide and unburned fuel. No significant quantity of unburned fuel was found within the CRZ. The carbon dioxide levels showed troughs in the CRZ similar to the temperature troughs. The magnitudes of the troughs did not appear as great, compared to the completely burnt fresh mixture, as those in temperature, but the discrepancy is probably at least partly due to the insensitivity of the gas analyser in this range and also to the effect of the probe in the flow. Again, the above suggestion about additional temperature traverses applies here, preferably with a more sensitive gas analyser either measuring carbon dioxide or oxygen.

7.4.2 Effect of end wall:

In the arrangement used by Bafuwa for stability limits measurements, the hubless swirlers had an end wall in the plane of the swirler exit end concentric with the swirler and of diameter 100 mm and a swirler of 24 mm diameter. Also in a furnace such a wall always exists. Thus, it was thought that the presence of an end wall might have an effect on the entrainment of air into the CRZ and on the weak stability limits. Tests to study this effect were carried out, again using the hubless swirlers of 93 mm diameter and an end wall of outer

diameter 450 mm (18 in) was used. It was found to have no effect on the entrainment, nor on the stability limits of the 30° and 45° swirlers. Only a slight effect was observed with 60° swirler. In this case the presence of the wall slightly widened the recirculation zone (by about 3%) and caused a deterioration of about 2% in the weak limit fuel/air ratio values. The change in the entrainment corresponding to the temperature change at the edge of the recirculation zone was too small to detect.

7.5 Effect of scale on stability limits of free flames:

Bafuwa (1970) obtained stability limits of premixed town-gas air flames issuing from hubless vane swirlers of 24 mm diameter. It was decided to observe the weak stability limits for the corresponding hubless swirlers of 93 mm diameter that had been used in the present work. The air compressor capacity limited the maximum velocity to about 20 m/sec. The results are shown in Figure 7.3 where they are plotted as swirler axial velocity to a base of fuel/air ratio leaving the swirler. The results are compared with those obtained by Bafuwa. It is seen that for a given vane angle of swirler, the axial velocity leaving the swirler provides a satisfactory method of correlating the limits for the two sizes. The correlation is excellent for the 30° and 60° swirlers, but less satisfactory for the 45° swirler. Similar agreement would be found if the average absolute velocities leaving the swirler were plotted to a base of fuel/air ratio.

Although some uncertainties about the accuracy of the estimations of the ambient air entrainment have been found, as discussed in Section 7.4, it was decided, pending further investigation, to continue using the entrainment factors taken by Bafuwa and Maccallum (1973) for the three swirlers (viz. 0.26, 0.40 and 0.53 for the 30°, 45° and 60° swirlers respectively). On this basis the average absolute velocities leaving the swirler have been plotted on Figure 7.4 to a base of the temperature at the edge of the CRZ at an axial distance of 1 swirler diameter downstream. Again, the results of Bafuwa are shown alongside. The general correlation shown can be considered as reasonably satisfactory.

7.6 Effect of quarl on the flame stability:

The construction of the rig for the 93 mm diameter swirlers included a small shoulder of 3 mm after the swirler exit. This shoulder acted as a very small quarl which, however, had no effect on the stability of the flames issuing from swirlers with vane angles up to and including 45°. As to the 60° swirler flame, this quarl had no effect on the flame in the furnace but when used to produce an open flame, the flow formed a wall jet which could not ignite and no flame was possible. The construction was changed to remove this shoulder effect and make the swirler exit plane flush with the end wall. With this new arrangement the flow reverted to type D again, and it was possible to ignite the flame in the normal way.

7.7 Stabilization in Furnaces:

In the flames burning in free jets issuing into atmosphere, described in the previous sections, the flow entrains cold, ambient air.

On the other hand, in a furnace, the main flow entrains on its outer surface from the PRZ. The gases in the PRZ are generally at a significantly lower temperature than that corresponding to adiabatic combustion. Part of this reduction in temperature is due to heat loss to the walls, and part is due to incomplete combustion. These gases have a much reduced chilling effect on the gases in the CRZ than would ambient air.

There are two problems in applying the method used above to correlate the stability limits of similar swirlers in furnaces. One problem is to know the temperature reduction of the gases in the PRZ due to heat loss to the walls. The other is to know the fractional entrainment of the PRZ gases into the CRZ. While the fractional entrainment in the open flames could be found by analysis of samples, this is impossible in an enclosed furnace. The problems of reading troughs in the temperature distribution to the required accuracy are great.

The technique adopted here has been to take the average temperature loss in the PRZ and assume this to be entirely due to the wall heat transfer and then use the entrainment fraction corresponding to the open flames. This method has been applied to the stability limits taken in this work with type D flows (strong CRZ) in the larger furnace ($D/d = 5$). No stability limits were attempted in the smaller furnace due to the onset of significant oscillations.

The unadjusted results are shown in Figure 7.5 as absolute swirler exit velocities, to a base of inlet fuel/air ratio. It is seen that, although there is considerable scatter, the limiting fuel/air ratio is virtually independent of flow velocity in this range of velocities. The adjusted results are shown in Figure 7.6, in this case the abscissae are the fuel/air ratios corresponding to the adiabatic combustion to achieve the temperatures resulting from entraining the PRZ gases. This is an alternative method, instead of using the CRZ temperatures as in Figure 7.4. The "effective" fuel/air ratios calculated in this way are 13% and 20% lower than the inlet fuel/air ratios for the 45° and 60° swirlers respectively. The effect of this change can be seen by comparing Figure 7.6 with Figure 7.4. There are no significant differences between the results for the hubless and annular swirlers. Figure 7.6 also gives the corresponding results for the open stability limits. This approach provides reasonable agreement between all the sets of stability limits.

It should be mentioned that the stability limits were usually taken after the furnace had been heated for some hours. When a different set of limits was taken quickly after the first light up, there was a slight increase in the fuel/air ratio at extinction.

7.8 Suggestions for further work:

For improvements to the model, experiments ought to be carried out to estimate more accurately the air entrainment by temperature and concentration traverses, as suggested in Section 7.4. As for the stability limits in the furnace, more measurements are needed to cover a higher range of velocities. For experimental convenience these could be performed in small size swirlers since the effect of scale was found to be minimal, as reported in Section 7.5

CHAPTER 8

GENERAL CONCLUSIONS AND SUGGESTIONS

8.1 Aerodynamics of confined swirling flows:

The experimental measurements presented gave a detailed picture of the flow and combustion patterns produced by vane swirled jets, (cold or burning) in confinements. The flow patterns were represented by distributions of the three velocity components and the static pressure, and the combustion patterns by the temperature and the product concentration distributions. The flow and combustion patterns were closely related and any changes in one produced changes in the other.

The patterns were classified into four categories. The extreme cases A and D were produced by very weak and strong swirl respectively. With pattern A, the changes from the non-swirled flow were small, but pattern D was completely different, where the main flow in a cylinder with reverse flow inside and a much faster rate of spread than type A. While combustion started in the central flow for type A, in type D it started in the main flow at a radial distance from the centreline. The intermediate types of patterns were taken as B and C, the transition being where the central reverse flow occurs. The CRZ onset was caused by a high adverse pressure gradient along the axis, which collapsed when the flow reversed its direction.

The size of the CRZ increased with swirl in type C flows up to the almost fixed proportion of the confinement size observed in type D flows. The maximum reverse velocity and maximum reverse flow increased with swirl.

The jet spread rates were found to be affected mainly by the swirler vane angles and slightly by confinement and combustion.

Turbulence in swirling flows was affected by the rotational motion, the curvature of the streamlines and the increased velocity gradients compared with unswirled flow. Weak swirl produced solid body rotation in the central part of the jet which reduced turbulence intensities, but with strong swirl, flow reversal cancelled this effect. The overall effect of swirl was to increase the turbulence levels and thus the mixing rates which leads to more intense and stable combustion.

The integrations of the time-mean values of velocities and static pressures were performed to calculate the axial fluxes of axial and tangential momenta. These were analysed and were seen to change with combustion and swirl. Their variations along the axial length caused by the shear forces, flow and wall, were found to be considerable.

A Swirl Number was calculated from these momenta according to the definition, $S^* = T/GD$, suggested after the analysis of previous investigations. This Swirl Number was found to vary with the swirler vane angle according to an exponential relation of the form $S^* = a\, e^{m\theta}$. The coefficients a and m were functions of the flow state, cold or burning, the fuel/air ratio and the flow pattern. A direct relation between these Swirl Numbers and the types of flow patterns A to D existed. For the same Swirl Number, the same flow pattern was obtained irrespective of the other independent variables. The linear, $\log S^* - \theta$, relation showed a sudden change of slope when the flow reversal occurred.

8.2 Physical modelling of flames:

While there is a good prospect that numerical predictions will be suitable for design use in the near future, physical modelling is at present a powerful tool of engineering design and it will still be needed for predicting the complex geometries usual in industrial furnaces. The success of this modelling depends on the use of the appropriate similarity criteria.

For the non-swirling flames, a criterion based on the ratio of source to shear momenta was derived for isothermal modelling and was found to be the same as that of Thring-Newby.

For swirling flames, the Swirl Number, S^*, when calculated, from experimentally measured momenta, was demonstrated to correlate the flow patterns on both full scale burning and model cold flows. The utility of this Swirl Number was further demonstrated by its ability to predict the change of the flow pattern from type B to C. This change occurred at the same value of $S^* = 0.11$ for all the cases investigated in this work and by other investigators.

The required aerodynamic pattern could thus be produced in a model and scaled to the prototype through the use of this Swirl Number. This will allow good use of the swirl by employing the most appropriate value for the operation required and avoiding the undesirable effects.

8.3 Mathematical modelling of swirling flows:

A prediction procedure was developed for confined swirling flows. Some results were obtained and these showed reasonable similarity to the experimentally measured patterns A, B and C. The physical and chemical inputs need more consideration for the case of strong swirl, i.e.

flow pattern D.

8.4 Stability of swirling flames:

The stability limits measured in this work and those for open flames were correlated to the absolute velocity at exit from the swirler. The mechanism of stability for flames with CRZ's was demonstrated. This is a self-stabilizing mechanism where the mixing between the fresh charge and the recirculated gases sustains the flame. The recirculated gases were found to be products of combustion together with entrained gases from the surrounding atmosphere. The amounts of these were estimated.

8.5 Optimum swirl range:

This will be different according to the nature of the process but the general indications from the results presented are that the flows with an established CRZ are recommended. The reason for this is that these achieve most of the desirable features in a flame, viz. higher intensity and efficiency of combustion, self-stability, uniformity of velocities and temperatures. Weak swirl produces low mixing rates and stability depends on the bluff body effect of the vanes which is less effective. Very strong swirl is not economic to produce, and in an oil fired furnace it leads to the scatter of the oil fuel before it burns. It also increases the entrainment of the surrounding flow into the CRZ.

The values of swirl selected should ensure the existence of a reasonable CRZ for the whole, or at least most, of the operation range. The relation between the Swirl Number S^* and the swirler vane angle could be determined for an installation and used as a performance chart.

8.6 Suggestions for further research:

There are several lines of further research that follow from the work presented in this Thesis. These include both fields of fundamental studies and design applications.

More fundamental knowledge is needed about the nature of turbulence, its variation with swirl, combustion and other parameters. The relation between momentum transport and mass transport, i.e. mixing, is also necessary for complete modelling of the combustion process. The chemical reaction rates need further investigation to determine the limiting factor for the reaction, either kinetics or concentration fluctuations, and how this is to be mathematically represented. This knowledge will be the basis for predicting the products of combustion particularly those causing pollution.

Extensions of the project, are also required, to include the effect of the type of fuel, gas, liquid or solid, and the effect of introducing non-premixed streams of fuel and air.

Work on the mechanism of the combustion oscillations observed in the small furnace is essential if such a furnace is to be used in practice.

The effect of having a quarl together with swirl could produce desirable aerodynamic features which needs investigation.

The determination of the relation between the Swirl Number and swirler vane angle could be produced by some mechanical balancing system developed from the one used by Fraser.

Swirler design could be improved aerodynamically by using aerofoiled vanes with the appropriate leading angles to produce the required deflection of the flow but with less pressure loss.

More concentrations and temperature measurements near the stability limits are required for more accurate calculations of the entrainment of the peripheral gases into the central recirculation zone.

BIBLIOGRAPHY

1. AFROSIMOVA, V.N. (1967) — Study of the aerodynamics of a furnace space. Thermal Engineering, vol.14(1),p.10-15.

2. AKHMEDOV, R.B. and RASHIDOV, F.K. (1969) — The aerodynamic characteristics of vortex burners with axial-tangential vane units. Thermal Engineering, vol.16(8), p.78-82.

3. ALBRIGHT, L.F. and ALEXANDER, L.G. (1956) — Stable cyclone flames of Natural gas and air. Jet Propulsion, vol.26, p.867-873.

4. ALBRIGHT, L.F. and ALEXANDER, L.G. (1957) — Flame stabilization in gases following cyclonically: Flow characteristics, temperature and gas analyses. 6th Symposium (Int.) on Combustion, Reinhold Publishing Corp., New York, p.464-472.

5. ALLEN, R.A. (1970) — Ph.D. Thesis, Department of Fuel Technology and Chemical Engineering, Sheffield University.

6. BAFUWA, G.G. (1970) — Characteristics of Swirling Flames Issuing from Vane Swirlers. Ph.D. Thesis, Mechanical Engineering Department, Glasgow University.

7. BAFUWA, G.G., BELTAGUI, S.A. and MACCALLUM, N.R.L. (1974) — Stabilization of Vane-Swirled Pre-mixed Flames. Mechanical Engineering Department Report, University of Glasgow (May). (To be submitted to Combustion and Flame).

8. BAFUWA, G.G. and MACCALLUM, N.R.L. (1970) — Turbulent swirling flames issuing from vane swirlers. International Flame Research Foundation, 18th Meeting of Aerodynamic Panel, Paris, September, Document no. G02/ca/3.

9. BAFUWA, G.G. and MACCALLUM, N.R.L. (1973) — Flame stabilization in swirling jets. Combustion Institute, European Symposium, September 1973, Weinberg, F.J. Editor. Academic Press, London, p.565-570.

10. BAKER, R.J., HUTCHINSON, P and WHITELAW, J.H. (1973)
Detailed measurements of flow in the recirculation region of an industrial burner by laser anemometry.
The Combustion Institute, European Symposium, September 1973, Weinberg, F.J. Editor, Academic Press, London. p.583-588.

11. BARAT, M. (1965)
Difficultes relatives aux determinations des champs de pression et de vitesse dans les ecoulements turbulents.
Eurovent, Paris. See also Chedaille and Braud (1972).

12. BARCHILON, M., and CURTET, R. (1964)
Some details of the structure of an axisymmetric confined jet with back flow.
J. of Basic Engineering, vol.86, p.777-787.

13. BEER, J.M. (1962)
International Flame Research Foundation.
Some results of the first trials on the pressure jet oil flames in the Ijmuiden furnace.
Journal Institute of Fuel, vol.36, p.3-15.

14. BEER, J.M. and CHIGIER, N.A. (1963)
Swirling jet flames issuing from an annular burner.
5^{me} Journee d'Etudes sur les Flammes, Paris, IFRF Doc.no. K20/a/9.

15. BEER, J.M. and CHIGIER, N.A. (1972)
Combustion Aerodynamics.
Applied Science Publishers, London.

16. BEER, J.M. and LEE, K.B. (1965)
The effect of the residence time distribution on the performance and efficiency of combustors.
10th Symposium (Int.) on Combustion, The Combustion Institute, Pittsburgh, p.1187-1202.

17. BIRD, R.B., STEWART, W.E. and LIGHTFOOT, E.N. (1960)
Transport Phenomena.
John Wiley and Son, New York.

18. BRADSHAW, P. (1973) — Effects of Streamline Curvature on Turbulent Flow, AGARDograph No.169.

19. BROWN, A.M. and THRING, N.W. (1965) — The Application of pressure jet burners to marine boilers. 10th Symposium (Int.) on Combustion. The Combustion Institute, Pittsburgh, p.1203-1218.

20. B.S. 1041 (1943) — Temperature Measurement. British Standards Institution, London.

21. B.S. 1042 (1964) — Methods for the measurements of flow in pipes. British Standards Institution, London.

22. CHEDAILLE, J. and BRAUD, Y. (1972) — Measurements and Flames. Edward Arnold (Publishers) London.

23. CHEDAILLE, J., LEUCKEL, W. and CHESTERS, A.K. (1966) — Aerodynamic studies carried out on turbulent jets by the IFRF. J. Institute of Fuel, vol.39, p.506-521.

24. CHERVINSKY, A. (1969) — Turbulent swirling jet diffusion flames. AIAA Journal, vol.7, no.10, p.1877-1883.

25. CHIGIER, N.A. and CHERVINSKY, A. (1967) — Aerodynamic study of turbulent burning free jet with swirl. 11th Symposium (Int.) on Combustion. The Combustion Institute, Pittsburgh. p.489.

26. CHIGIER, N.A. and GILBERT, J.L. (1968) — Recirculation eddies in the wake of flame holders. J. Institute of Fuel, vol.42, p.105-112.

27. CRAYA, A. and CURTET, R. (1955) — Sur L'evolution d'un jet en espace confine. Compte Rand. Acad. Science, Paris, vol.241, p.621-622.

28. CRAYA, A. and DARRIGOL, M. (1967) — Turbulent swirling jet. The Physics of Fluids, Supplement III, vol.10. p.S197-S199.

29. CURTET, R. (1958) — Confined jets and recirculation phenomena with cold air. Combustion and Flame, vol.2, no.4, p.383-411.

30. CURTET, R. and RICOU, F.P. (1964) — On the tendency of self-preservation in axisymmetric ducted jets. J. of Basic Engineering, vol.86, p.765-776.

31. DASHCHUK, M. (1971) — Preservation of approach flow velocity and turbulence in burner flames. 13th Symposium (Int.) on Combustion, The Combustion Institute, Pittsburgh, p.659-665.

32. DAVISON, F.J. (1968) — Nozzle scaling in isothermal furnace models. J. Inst. of Fuel, vol.42, p.470-475.

33. DEAN, R.C. (1953) — Aerodynamic Measurements. M.I.T., Gas Turbine Laboratory, Cambridge, Massachusetts.

34. DRAKE, P.F. and HUBBARD, E.G. (1963) — Note: Effect of air swirl on the completeness of combustion. J. Institute of Fuel, vol.36, p.389-390.

35. DRAKE, P.F. and HUBBARD, E.H. (1966) — Combustion system aerodynamics and their effect on the burning of heavy fuel oil. J. Institute of Fuel, vol.39, p.98-109.

36. EICKHOFF, H.E. (1973) — Experimental investigation of the influence of combustion on turbulent transport in jet diffusion flames. The Combustion Institute, European Symposium, F.J. Weinburg, Editor. Academic Press, p.513-517.

37. EMMONS, H.W. (1967) — Discussion on Chigier and Chervinsky (1967)

38. FECHHEIMER (1926) — Measurements of static pressure. ASME Transactions, vol.48, p.965-977.

39. FRASER, D. (1964)
Investigation into swirl in air jets with application to an oil-fired furnace.
M.Sc. Thesis, Mechanical Engineering Department, Glasgow University.

40. GIBSON, M.M. and MORGAN, M.A. (1970)
Mathematical model of combustion of solid particles in a turbulent stream with recirculation.
J. Institute of Fuel, vol.43, p.517-523. Also in AGARD Conference Proceedings No.52, Paper 21.

41. GORTLER, H. (1954)
Decay of swirl in an axially symmetrical jet far from the orifice.
Revista Matematica Hispano Americanas, Series 4, vol.14, p.143-178.

42. GOSMAN, A.D., PUN, W.M., RUNCHAL, A.K., SPALDING, D.B. and WOLFSHTEIN, M. (1969)
Heat and Mass Transfer in Recirculation Flows.
Academic Press, London.

43. GREENSPAN, D. (1968)
Lectures on the Numerical Solution of Linear, Singular and Non-Linear Differential Equations.
Prentice-Hall.

44. GUNTHER, R. (1970)
Measurements of flame turbulence: aims, methods and results.
J. Institute of Fuel, vol.44, p.187-192.

45. HARLOW, F.H., Editor, (1973)
Turbulence Transport Modelling.
AIAA Selected Reprints Series, No.14.

46. HERBERT, M.V. (1957)
Theoretical analysis of reaction rate controlled systems, Part 1.
AGARDograph No.15, Combustion Researches and Reviews. Butterworth, London, p.76-109.

47. HIETT, G.F. and POWELL, G.E. (1962)
Three-dimensional probe for investigation of flow patterns.
The Engineer, vol.213, p.165-170.

48. HINZE, J.O. and Van der HEGGE ZIJNEN, B.G. (1949)
Transfer of heat and matter in the turbulent mixing zone of an axially symmetrical jet.
Applied Scientific Research, vol.A1, p.435-461.

49. HUBBARD, E.H. (1962)
Recirculation in cold models of furnaces: A review of work carried out at SOGREAH.
J. Institute of Fuel, vol.35, p.160-173.

50. HULSE, C. (1960)
The aerodynamics of open-hearth furnace regenerators.
J. Iron and Steel Institute, vol.196, p.264-274.

51. IVANOV, A.G. (1968)
A method of estimating the flow section of vortex burners.
Thermal Engineering, vol.15(5), p.44-49.

52. JOHNSTON, R.E. and THRING, M.W. (1957)
Pilot Plants, Models and Scale-up Methods in Chemical Engineering.
McGraw-Hill Book Co. Inc., N.Y., London.

53. KARLOVITZ, B. (1953)
Open turbulent flames.
4th Symposium (Int.) on Combustion. Williams and Wilkins, Baltimore, p.60-67.

54. KAWAGUCHI, O. and SATO, G.T. (1971)
Experimental investigation of premixed swirling jet flames (Velocity and turbulence intensity of swirling air jets).
Bulletin of JSME, vol.14, no.69, p.248-256.

55. KERR, N.M. (1965)
An Aerodynamic Study of Swirling Jets and Flames.
Ph.D. Thesis, Mechanical Engineering Department, Glasgow University.

56. KERR, N.M. and FRASER, D. (1965)
Swirl, Part 1: Effect on axisymmetrical turbulent jets.
J. Institute of Fuel, vol.38, p.519-526.

57. KERR, N.M. (1965) — Swirl, Part 2: Effect on flame performance and the modelling of swirling flames. J. Institute of Fuel, vol.38, p.527-538.

58. KIRKPATRICK, J.R., and WALKER, W.F. (1972) — Numerical methods for describing turbulent compressible, subsonic separated jet flows. Journal of Computational Physics, vol.10, p.185-201.

59. KOOSINLIN, M.L. and LOCKWOOD, F.C. (1973) — The prediction of axisymmetrical turbulent swirling boundary layers. Imperial College of Science and Technology, London, Department of Mechanical Engineering, Report HTS/73/1.

60. LAUNDER, B.E. and SPALDING, D.B. (1972) — Lectures in Mathematical Models of Turbulence. Academic Press, London.

61. LAVAN, Z., NIELSON, H. and FEJER, A.A. (1969) — Separation and flow reversal in swirling flows in circular ducts. Physics of Fluids, vol.12, No.9, p.1747-1757.

62. LEE, S. (1965) — Axisymmetrical turbulent swirling jets. J. Applied Mechanics, vol.32, p.258-262.

63. LEUCKEL, W. (1968) — The aerodynamics of swirling flows. Rev. Gen. Thermique, vol.7, p.1367-1383.

64. LEWIS, B. and von ELBE, G. (1961) — Combustion, Flames and Explosions of Gases. Academic Press, London.

65. LEWIS, B. and von ELBE, G. (1963) — The concept of flame stretch. Z. Phys. Chem. vol.37, p.287.

66. LILLEY, D.G. and CHIGIER, N.A. (1971-a) — Non-isotropic turbulent stress distribution in swirling flows. Int. J. Heat and Mass Transfer, vol.14, p.573-585.

67. LILLEY, D.G. and CHIGIER, N.A. (1971- b)
Non-isotropic exchange coefficients in turbulent swirling flames, from mean value distributions.
Combustion and Flame, vol.16, p.177-189.

68. LILLEY, D.G. (1973-a)
Prediction of inert turbulent swirl flows.
AIAA Journal, vol.11, no.7, p.955-960.

69. LILLEY, D.G. (1973-b)
Turbulent swirling flame prediction.
AIAA Paper No.73-651, presented at the AIAA 6th Fluid and Plasma Dynamics Conference, Palm-Spring, California.

70. LOITSYANSKII, L.G. (1953)
The propagation of a twisted jet in an unbounded space filled with the same fluid.
Prikladnaya Matematic i Mekhanika, vol.17, p.3-16.

71. LONGWELL, J.P. and WEISS, M.A. (1955)
High temperature reaction rates in hydrocarbon combustion.
Industrial and Engineering Chemistry, vol.47, No.8, p.1634-1643.

72. LUTZHOFT, V.W. and FETTING, F. (1968)
Der Einfluss des Dralls die Stabilitat von Drallflammen.
Brennst-Warme-Kraft, 20, Nr.12, p.572-576.

73. MACAGNO, E.O. and HUNG, T.K. (1967)
Computational and experimental study of a captive annular eddy.
J. Fluid Mechanics, vol.28, 1, p.43-64.

74. MATHUR, M.L. (1966)
An aerodynamic Study of Swirling Jets with Application to Burners.
Ph.D. Thesis, Mechanical Engineering Department, Glasgow University.

75. MATHUR, M.L. and MACCALLUM, N.R.L. (1967)
Part 1: Free jets
Part 2: Enclosed jets
J. Institute of Fuel, vol.41, p.214-245.

76. MARTIN, A.E. (1953)
The present status of the Infra-Red Gas Analyser.
Heaton Works Journal, vol.6, No.35

77. McADAMS, W.H. (1954) — Heat Transmission. McGraw-Hill, New York, 3rd Edition.

78. McBRIDE, R.N. (1972) — Prediction of a convective heating system. 4th Symposium on Flames and Industry, London.

79. MACCALLUM, N.R.L. (1956) — Combustion in a Gas Stream. Ph.D. Thesis, Department of Mechanical Engineering, Glasgow University.

80. McEWAN, M.W. (1972) — Hot and cold studies on an oil-fired burner with swirler fitted in a refinery oil heater. J. Institute of Fuel, vol.46, p.107-112.

81. MIKHAIL, S. (1960) — Mixing of coaxial streams inside a closed conduit. J. of Mechanical Engineering Science, Vol.2, No.1, p.59-68.

82. MILLER, D.R. and COMINGS, E.W. (1957) — Static pressure distribution in the free turbulent jet. J. Fluid Mechanics, vol.3,p.1-16.

83. MILNE, W.E. (1953) — Numerical Solutions of Differential Equations. John Wiley and Sons, New York.

84. MIZUTANI, Y. (1972) — Amplification of turbulence level by a flame and turbulent flame velocity. Combustion and Flame, vol.19, p.203-212.

85. ODLOSINSKI, G. (1968) — A procedure for predicting the distributions of velocity and temperature in a flame stabilized behind a bluff body. Department of Mechanical Engineering, Imperial College of Science and Technology, London, Report EF/R/G/2.

86. PAI, S. (1954) — Fluid Dynamics of Jets. Van Nostrand, London.

87. PAI, B.R. and LOWES, T.M. (1972) — Flow and mixing in confined axial flows. 20th Meeting of the Aerodynamic Panel, University of Grenoble, IFRF Doc. No. G02/a/21.

88. PARKER, K.H. and GUILLON, O. (1971)
Local measurements in a turbulent flame by hot-wire anemometry.
13th Symposium (Int.) on Combustion. The Combustion Institute, Pittsburgh (1971) p.667-674.

89. PEIN, R., PESCHEL, H. and FETTING, F. (1970)
Recirculation zone concentrations and temperature of bluff-body stabilized turbulent flames.
Combustion Science and Technology, vol. 1, p.327-330.

90. PRANDTL, L. (1925)
Bericht uber Untersuchungen Zur Ausgebildeten Turbulenz.
Z.A.M.M., vol.5, p.136.

91. RALEIGH, J.W.S. (1916)
On the dynamics of revolving fluids.
Proc. Roy. Soc., Series A, vol.93, p.148-154.

92. RAZINSKY, E. and BRIGHTON, J.A. (1971)
Confined jet mixing for nonseparating conditions.
J. Basic Engineering, vol.93, p.333-349.

93. REICHARDT, H. (1941)
On a new theory of free turbulence.
Z.A.M.M., vol.21, no.5, 1941.

94. RICOU, F.P. and SPALDING, D.B. (1961)
Measurements of entrainment by axisymmetrical turbulent jets.
J. of Fluid Mechanics, vol.11, p.21-32.

95. ROBERTS, L.W. (1971)
The prediction of turbulent swirling pipe flows.
Imperial College of Science and Technology, London. Mechanical Engineering Department, Report No. EF/TN/A/37.

96. ROBERTSON, A.D. (1965)
Modification of the Thring-Newby criterion for problems where flow pattern and mixing are equally important.
J. Institute of Fuel, vol.38, p.481-482.

97. ROBERTSON, A.D. (1966) Scaling and modelling criteria for burner design with swirl addition. J. Institute of Fuel, vol.39, p.335-342.

98. ROSE, W.G. (1962) A swirling round turbulent jet, 1-mean flow measurements. J. Applied Mechanics, vol.29, p.615-625.

99. RUBEL, A. (1972) Some effects of swirl on turbulent mixing and combustion. NASA CR-1956.

100. RUNCHAL, A.K., KANPUR, I.I.T. and SPALDING, D.B. (1971) Steady turbulent flow and heat transfer downstream of a sudden enlargement in a pipe of circular cross-section. Imperial College of Science and Technology, London, Department of Mechanical Engineering. Report EF/TN/A/39.

101. RUNCHAL, A.K. and WOLFSHTEIN, M. (1966) A finite-difference procedure for the integration of the Navier-Stokes equations. Imperial College of Science and Technology, London. Department of Mechanical Engineering. Report SF/TN/1.

102. SALAH, M.S.M. (1971) Numerical solutions of the Navier-Stokes Equations with Fluid Mechanics and Heat Transfer Applications. Ph.D. Thesis, Department of Computing Science, Glasgow University.

103. SCHLICHTING, H. (1968) Boundary Layer Theory. McGraw-Hill, New York, London.

104. SCOTT, C.J. and RASK, D.R. (1973) Turbulent viscosities for swirling flow in a stationary annulus. J. of Fluid Engineering, vol.95, no.4, p.557-566.

105. SHAGALOVA, S.L., SHNITSER, I.N. and GROMOV, G.V. (1965) Aerodynamic chatacteristics of flow produced by a burner with guide vanes. Thermal Engineering, vol.12, no.6, p.31-37.

106. SHAGALOVA, S.L., RUBIN, M.M., SHNISTER, I.N. and PARPAROV, D.I. (1967)
Investigation of the aerodynamics and combustion processes in the TP-100 boiler furnace.
Thermal Engineering, vol.14, no.11, p.93-99.

107. SHAGALOVA, S.L., SHINSTER, I.N. and PARPAROV, D.I. (1969)
Aerodynamic characteristics of vortex burner flames.
Thermal Engineering, vol.16, no.6, p.39-44.

108. SPALDING, D.B. (1953)
Theoretical aspects of flame stabilization.
Aircraft Engineering, 25, p.264-286.

109. SPALDING, D.B. (1971)
Mixing and chemical reaction in steady confined turbulent flames.
13th Symposium (Int.) on Combustion. The Combustion Institute, Pittsburgh, p.649-657.

110. SPIERS, H.M. (1962)
Technical Data on Fuel-World Power Conference, London.

111. SQUIRE, H.B. (1951)
The round laminar jet.
Quarterly Journal of Mechanics and Applied Mathematics, vol.14, 3, p.321-329.

112. SQUIRE, H.B. and TROUNCER, J. (1944)
Round jets in a general stream.
Aeronautical Research Council, London, R & M No. 1974

113. STEIGER, M.H. and BLOOM, M.B. (1962)
Lincarised swirling wakes.
Physics of Fluids, vol.5, no.9, p.1027-1032.

114. SYRED, N. (1970)
Velocity measurements in turbulent flow fields.
IFRF Doc. no. Fig/ca/4, also as Department of Fuel Technology and Chemical Engineering, Sheffield University. Report FTCE/27/NS/12/70.

115. SYRED, N. and BEER, J.M. (1973)
Effect of combustion upon precessing vortex cores generated by swirl combustors.
14th Symposium (Int.) on Combustion. The Combustion Institute, Pittsburgh, p.537-550.

116. SYRED, N., BEER, J.M. and CHIGIER, N.A. (1971-a)
Turbulence measurements in swirling recirculating flows.
Symposium on Internal Flows, University of Salford. p. B27.

117. SYRED, N., CHIGIER, N.A. and BEER, J.M. (1971-b)
Flame stabilization in recirculation zones of jets with swirl.
13th Symposium (Int.) on Combustion. The Combustion Institute, Pittsburgh, p.617-624.

118. TAGA, M., AKAGAWA, K. and NISHIJIMA, M. (1971)
Flow characteristics of the curved turbulent jet in the two-dimensional passage.
Bulletin of the JSME, vol.14, no.69, p.217-223.

119. THOM, A., and APELT, C.J. (1961)
Field Computations in Engineering and Physics.
D. van Nostrand Co., London.

120. THRING, M.W. and NEWBY, M.P. (1953)
Combustion length of enclosed turbulent jet flames.
4th Symposium (Int.) on Combustion. The Combustion Institute, Williams and Wilkins, Baltimore, p.789-796.

121. THURLOW, G.G. (1959)
Similarity criteria for the study of furnace flames by means of cold models.
Combustion and Flame, vol.3, no.3, p.373-388.

122. TYLDESLEY, J.R. and SILVER, R.S. (1968)
The prediction of the transport properties of a turbulent fluid.
Int. J. Heat and Mass Transfer, vol.11, p.1325-1340.

123. USTIMENKO, B.P. and BUKHAM, M.A. (1968)
Turbulent flow structure in a cyclone chamber.
Thermal Engineering, vol.15(2), p.90-94.

124. WEISS, M.A., LANG, R.J. and LONGWELL, J.D. (1958)
Combustion rates in spherical reactors: Effect of inlet temperature and fuel type.
Industrial Engineering Chemistry, vol. 50, no.2, p.257-264.

125. WEIBELT, J.A. (1966)
Engineering Radiation Heat Transfer. Hott, Reinhart and Winston.

126. WU, H.I. and FRICKER, N. (1971)
An investigation of the behaviour of swirling jet flames in a narrow cylindrical furnace.
2nd Members Conference, IFRF, Ijmuiden Doc. G02/a/61.

127. ZUKOSKI, E.E. and MARBLE, F.E. (1955)
The rate of wake transition in the process of flame stabilization on bluff bodies.
AGARD "Combustion Researches and Reviews", Butterworth Pub., London. p.167-180.

128. ZUKOSKI, E.E. and MARBLE, F.E. (1956)
Experiments concerning the mechanism of flame blow-off from bluff bodies.
Proceedings of the Gas Dynamics Symposium on Aerothermochemistry, Nosthwestern University. p.205-210.

LIST OF TABLES

Table No.	Title	Page
4.1	Input variables	180
4.2	Characteristic dimensions, Swirl Numbers and flow types	181
6.1	Coefficients in equations of the form 6.8	184

LIST OF FIGURES

Figure No.	Title	Page
3.1	Geometry of vane swirlers	185
3.2	Flow lines for reactants	186
3.3	3-dimensional probe and cooling water system	187
3.4	Typical set of calibration curves for 3-dimensional probe	188
3.5	Total velocity vector with components	189
3.6	Static-pressure disc-probe	189
3.7	Gas sampling probe	190
3.8	Arrangement of sample flow	190
3.9 (a,b)	Distances of sections for traverse along furnaces	191
3.10	Furnace wall transient temperature rise	192
4.1.a to e	Axial velocity profiles, Hubless swirlers, D/d = 2.5	193
4.2.a to c	Axial velocity profiles, Annular swirlers, D/d = 2.5	198
4.3.a to f	Axial velocity profiles, Hubless swirlers, D/d = 5	201
4.4.a to e	Axial velocity profiles, Annular swirlers, D/d = 5	207
4.5.a to c	Tangential velocity profiles, Hubless swirlers, D/d = 2.5	212
4.6.a to c	Tangential velocity profiles, Annular swirlers, D/d = 2.5	215
4.7.a to e	Tangential velocity profiles, Hubless swirlers, D/d = 5	218
4.8.a to d	Tangential velocity profiles, Annular swirlers, D/d = 5	223
4.9.a to c	Radial velocity profiles, Hubless swirlers, D/d = 2.5	227

Figure No.	Title	Page
4.10.a to c	Radial velocity profiles, Annular swirlers, D/d = 2.5	230
4.11.a to f	Radial velocity profiles, Hubless swirlers, D/d = 5	233
4.12.a to e	Radial velocity profiles, Annular swirlers, D/d = 5	239
4.13.a to e	Static pressure profiles, Hubless swirlers, D/d = 2.5	244
4.14.a to c	Static pressure profiles, Annular swirlers, D/d = 2.5	249
4.15.a to f	Static pressure profiles, Hubless swirlers, D/d = 5	252
4.16.a to e	Static pressure profiles, Annular swirlers, D/d = 5	258
4.17.a to d	Temperature profiles, Hubless swirlers, D/d = 2.5	263
4.18.a to c	Temperature profiles, Annular swirlers, D/d = 2.5	267
4.19.a to f	Temperature profiles, Hubless swirlers, D/d = 5	270
4.20.a to e	Temperature profiles, Annular swirlers, D/d = 5	276
4.21.a to d	CO_2 concentration profiles, Hubless swirlers, D/d = 2.5	281
4.22.a to c	CO_2 concentration profiles, Annular swirlers, D/d = 2.5	285
4.23.a to f	CO_2 concentration profiles, Hubless swirlers, D/d = 5	288
4.24.a to e	CO_2 concentration profiles, Annular swirlers, D/d = 5	294

Figure No.	Title	Page
4.25.a to h	Decay of maximum axial velocity along the furnace	299
4.26.a to g	Variation of the maximum central reverse velocity along the furnace	303
4.27.a to g	Jet width and CRZ dimensions	306
4.28.a to h	Decay of maximum tangential velocity along the furnace	313
4.29.a to h	Recovery of centreline static pressure along the furnace	317
4.30.a to e	Maximum temperature variation along the furnace	323
4.31.a to d	Centreline temperature variation along the furnace	326
4.32.a to h	Axial momentum fluxes	328
4.33.a to h	Axial flux of tangential momentum	336
4.34	Minimum static pressure-Swirl Number relation	342
4.35	Swirl Number relation to input conditions and flow types	343
5.1	Idealised flow pattern across a flame front	344
6.1	Furnace geometry and grid arrangement	345
6.2	Assumed velocity distribution at swirler exit section	345
6.3 (a,b)	Predicted velocity profiles for cold flow	346
6.4	Jet spread variation with effective viscosity	348
6.5	Predicted velocity and temperatures for 30° swirler	349
7.1	Mixing model for flame stabilization	351
7.2	Temperature traverses for 45° swirler free flame	352

Figure No.	Title	Page
7.3	Effect of scale on weak stability limits of hubless swirler free flames	353
7.4	Correlation of weak stability limits by temperature at the edge of the CRZ	354
7.5 (a,b)	Weak stability limits of enclosed swirling flames	355
7.6	Correlation of weak stability limits of swirling flames (free and enclosed)	357

TABLE 4.1

Input Variables

Variable	Range investigated
Swirler vane angle	0°, 15°, 22.5°, 30°, 45° and 60°
Swirler type	Hubless, diameter 93 mm Annular, outside diameter 98 mm hub diameter 32 mm
Flow Reynolds Number	7.5×10^5 to 10.25×10^4 for 45° hubless swirler cold flow in D/d = 5 furnace; otherwise all at about 9×10^5, i.e. average axial velocity 15.25 m/s at swirler exit
Degree of Confinement	Ratio of furnace diameter D to swirler diameter d = 2.5 and 5
Chemical reaction	Cold flow and burning flow
Fuel/air ratio	- For D/d = 5 furnace: 22.5° hubless swirler, f/a= 0.125, 0.143 by volume; otherwise all at f/a = 0.125. - For D/d = 2.5 furnace: 15° Hubless swirler-- f/a = 0.131 30° Hubless swirler-- f/a = 0.106, 0.141 (i) 30° Annular swirler-- f/a = 0.108, 0.137 (i) 45°, 60° swirlers -- f/a = 0.100 to 0.106 (ii)

(i) Combustion oscillations occurred at f/a ratios between these two values.

(ii) For these swirlers, f/a had to be kept low to avoid combustion oscillations.

TABLE 4.2

Characteristic dimensions, Swirl Numbers and Flow types

Swirler vane angle	Swirler type H hubless A annular	D/d	Flow state I = isothermal B = burning (f/a)	Swirl Number S^*	Flow type	Impingement length $\bar{x}_i$	CRZ			
							Length/D	Max. diameter/D	Max. $\frac{u_{rev}}{u_o}$	Max. $\frac{m_{rev}}{m_o}$
15.0	H	2.5	I	0.0738	A	1.11	-	-	-	-
22.5	H	2.5	I	0.1195	C	1.15	0.44	0.150	0.33	0.044
30	H	2.5	I	0.3290	D	0.565	1.5	0.575	0.32	0.273
45	H	2.5	I	0.5825	D	0.445	⟶	0.670	0.335	0.290
60	H	2.5	I	1.1590	D	0.164	⟶	0.65	0.335	0.800
30	A	2.5	I	0.3645	D	0.700	1.85	0.26	0.35	0.094
45	A	2.5	I	0.5716	D	0.510	⟶	0.62	0.255	0.293
60	A	2.5	I	1.1487	D	0.300	⟶	0.61	0.455	0.470
15	H	5	I	0.0790	A	⟶	-	-	-	-
22.5	H	5	I	0.1190	B	1.9	-	-	-	-
30	H	5	I	0.3630	D	0.82	⟶	0.63	0.18	1.13
45	H	5	I	0.5530	D	0.48	⟶	0.70	0.30	1.80
60	H	5	I	1.250	D	0.12	⟶	0.70	0.31	2.6
15	H	2.5	B	0.0296	A	0.90	-	-	-	-
30	H	2.5	B (0.141)	0.0951	B	0.51	-	-	-	-
30	H	2.5	B (0.106)	0.1030	C	0.51	1.0	0.41	0.44	0.06
45	H	2.5	B	0.1981	D	0.38	1.0	0.56	0.54	0.24
60	H	2.5	B	0.3242	D	0.22	1.6	0.56	0.59	0.19
30	A	2.5	B (0.137)	0.1371	C	0.62	0.85	0.15	0.38	0.01
30	A	2.5	B (0.108)	0.1189	C	0.62	1.35	0.41	0.42	0.07

Table 4.2 (Cont)

Swirler vane angle	Swirler type H hubless A annular	D/d	Flow state I = isothermal B = burning (f/a)	Swirl Number S^*	Flow type	Impingement $\bar{x}_i$	CRZ			
							Length/D	Max. diameter/D	Max. $\frac{u_{rev}}{u_o}$	Max. $\frac{m_{rev}}{m_o}$
45	A	2.5	B	0.1939	D	0.49	1.63	0.53	0.43	0.15
60	A	2.5	B	0.3823	D	0.31	1.80	0.57	0.53	0.25
0	H	5	B	0.0000	A	→	-	-	-	-
15	H	5	B	0.0368	A	→	-	-	-	-
22.5	H	5	B (0.125)	0.0543	B	1.20	-	-	-	-
22.5	H	5	B (0.143)	0.0589	A	1.20	-	-	-	-
30	H	5	B	0.0877	B	1.05	-	-	-	-
45	H	5	B	0.3020	D	0.52	1.50	0.71	0.48	0.59
60	H	5	B	0.5198	D	0.20	1.83	0.71	0.52	0.75
0	A	5	B	0.0000	A	→	-	-	-	-
15	A	5	B	0.0472	A	1.60	-	-	-	-
30	A	5	B	0.1061	B	1.20	-	-	-	-
45	A	5	B	0.2332	D	0.50	1.72	0.63	0.41	0.49
60	A	5	B	0.4361	D	0.41	1.72	0.70	0.51	0.81
Results of Mathur and Maccallum (1967)							Results of Mathur and Maccallum (1967)			
0	A	2.6	I		A	1.67	-	-	-	-
15	A	2.6	I		A	1.02	-	-	-	-
30	A	2.6	I		D	0.41	1.35	0.60	0.29	0.36
45	A	2.6	I		D	0.34	1.35	0.65	0.43	0.67
60	A	2.6	I		D	0.33	1.30	0.65	0.50	0.95
70	A	2.6	I		wall jet	< 0.1	→	0.57	0.41	1.05
75	A	2.6	I		wall jet	< 0.1	→	0.54	0.42	1.17

Table 4.2. (Contd.)

Swirler vane angle	Swirler type H hubless A annular	D/d	Flow state I = isothermal B = burning (f/a)	Swirl Number S^*	Flow type	Impingement $\bar{x}_i$	CRZ			
							Length/D	Max. diameter/D	Max. $\frac{u_{rev}}{u_o}$	Max. $\frac{m_{rev}}{m_o}$
Results of Afrosimova (1967)										
0	A with Quarl	3	I		A	0.83	-	-	-	-
30	A with Quarl	3	I		D	0.56	0.57	0.27		0.23
45	A with Quarl	3	I		D	0.52	0.57	0.21		0.40
60	A with Quarl	3	I		D	0.42	→	0.89		0.33
0	A with Quarl	3	B		A	0.58	-	-	-	-
30	A with Quarl	3	B		B	0.58	-	-	-	-
45	A with Quarl	3	B		D	0.54	0.71	0.39		0.10
60	A with Quarl	3	B		D	0.44	0.71	0.54		0.36

TABLE 6.1

Coefficients in equations of the form 6.8

0	a	b	c	d
$\frac{\partial \Gamma}{r}$	1	1	μ_e	$\frac{1}{r}\frac{\partial \rho}{\partial r}\cdot\frac{\partial}{\partial x}\left(\frac{V^2}{2}\right) - \frac{\partial \rho}{\partial x}\cdot\frac{\partial}{\partial r}\left(\frac{V^2}{2}\right) + \frac{\partial}{\partial x}\left(\rho\frac{w^2}{r}\right) + 2\mu_e\frac{\partial}{\partial r}\left(\frac{\omega}{r}\right)$
ψ	0.0	$1/r^2$	1	$\rho\left(\frac{\omega}{r}\right) - \frac{1}{\rho r^2}\left(\frac{\partial \psi}{\partial x}\cdot\frac{\partial \rho}{\partial x} + \frac{\partial \psi}{\partial r}\cdot\frac{\partial \rho}{\partial r}\right)$
w	1	μ_e	1	$-\frac{w}{r}\left(\frac{\mu_e}{r} + \rho v + \frac{\partial \mu_e}{\partial r}\right.$
m_f	1	1	1	$-K\, m_f\, m_{ox}\, \rho^2\, T^{\frac{1}{2}}\, e^{-E/RT}$

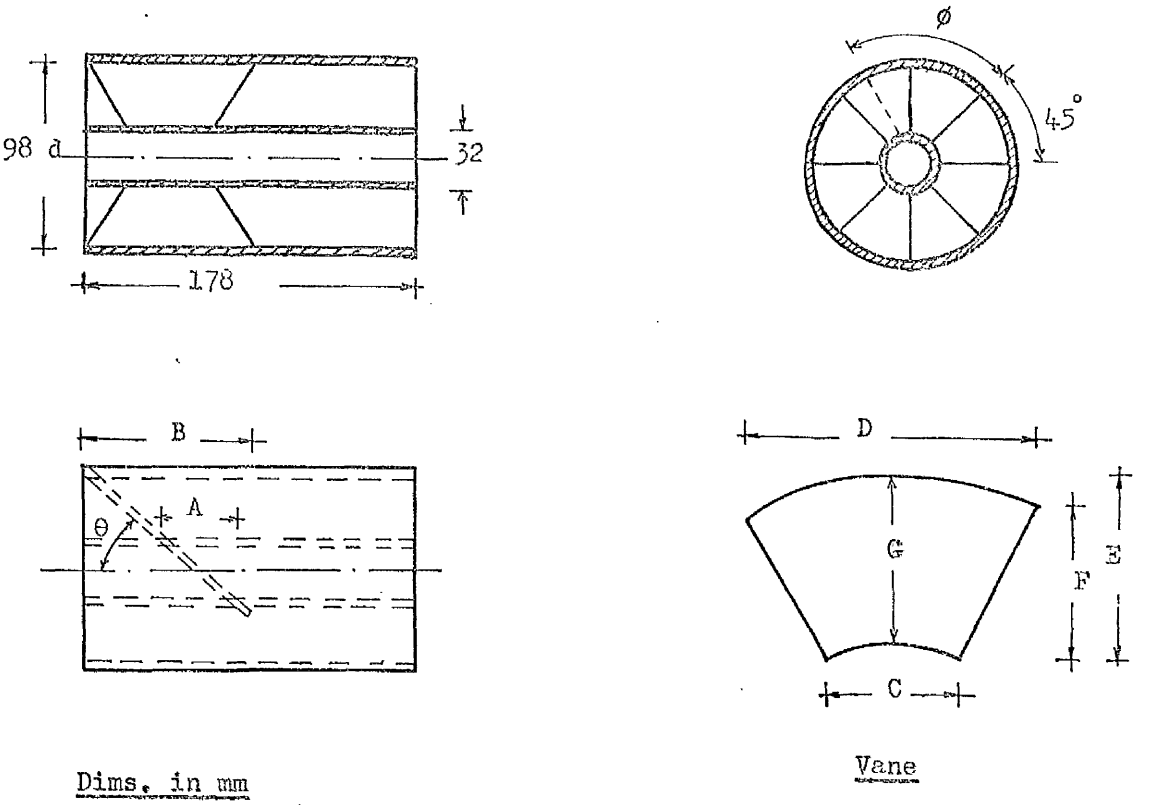

TABLE 3.1

Vane dimensions for different swirlers

Dimension	Value
A	$d_i \sin \frac{\phi}{2} / \tan \theta$
B	$d_o \sin \frac{\phi}{2} / \tan \theta$
C	$d_i \sin \frac{\phi}{2} / \sin \theta$
D	$d_o \sin \frac{\phi}{2} / \sin \theta$
E	$\frac{1}{2}(d_o - d_i \cos \frac{\phi}{2})$
F	$\frac{1}{2}(d_o - d_i)\cos \frac{\phi}{2}$
G	$\frac{1}{2}(d_o - d_i)$

FIGURE 3.1: Geometry of Vane Swirlers

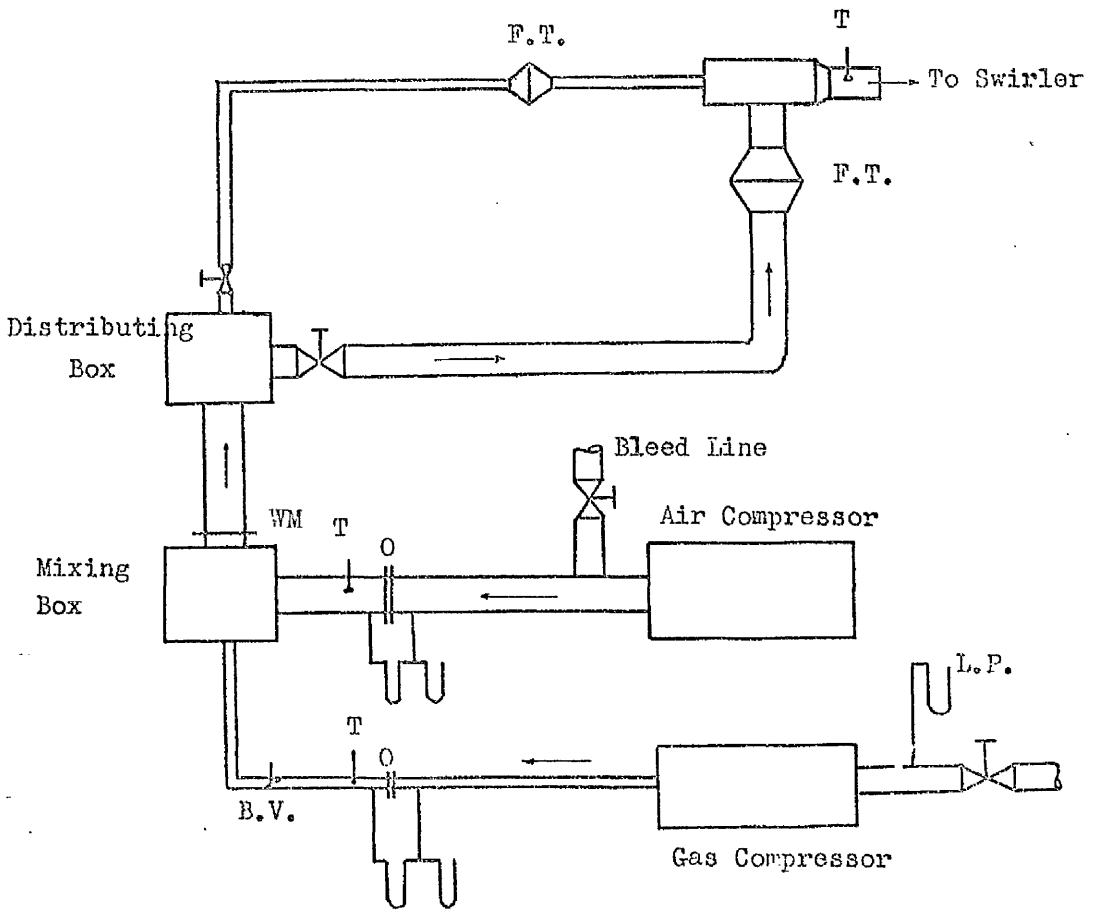

B.V.	Butter Fly Valve	} Safety Devices
F.T.	Flame Trap	
L.P.	Low Pressure Cut-off Trigger	
O	Orifice Plate	
T	Thermometer	
WM	Wire Mesh	

FIG. 3.2. Flow Lines of Reactants

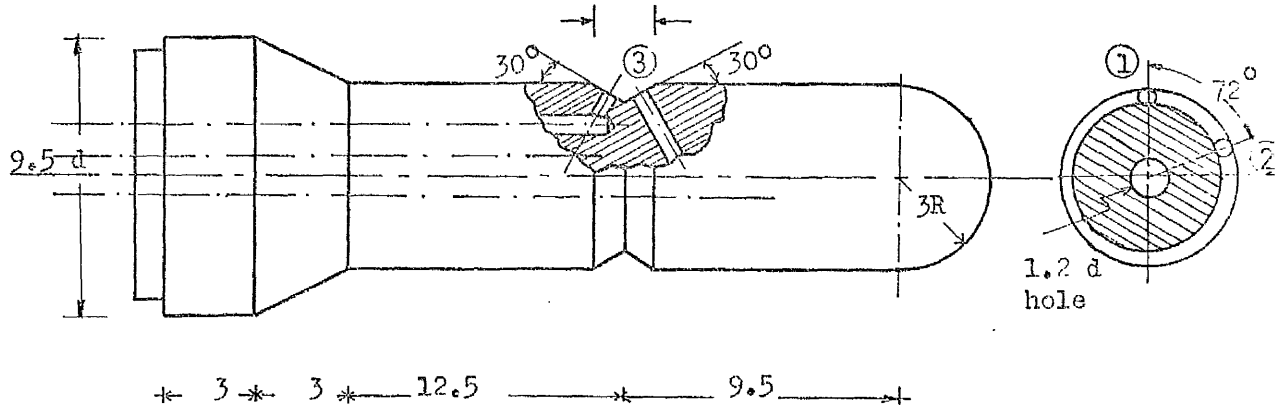

- Pressure holes 1,2,3 : diam.=0.75 mm

- Dims. in mm

Three-Dimensional Probe Tip

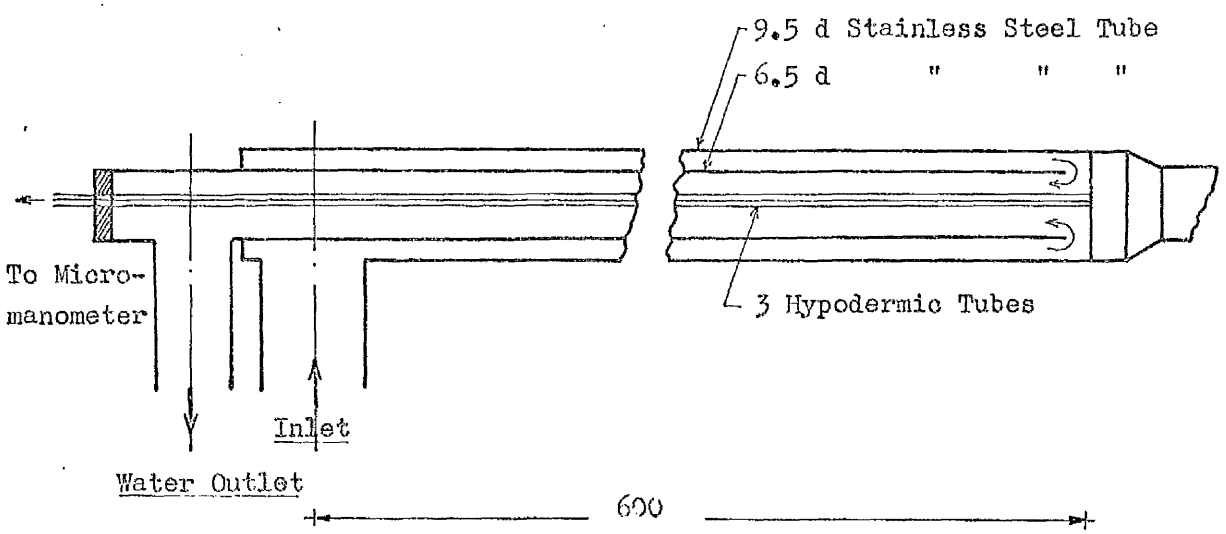

- Dims. in mm

Probe Cooling Water System

FIG. 3.3. Three-dimensional Probe Tip and Cooling Water System

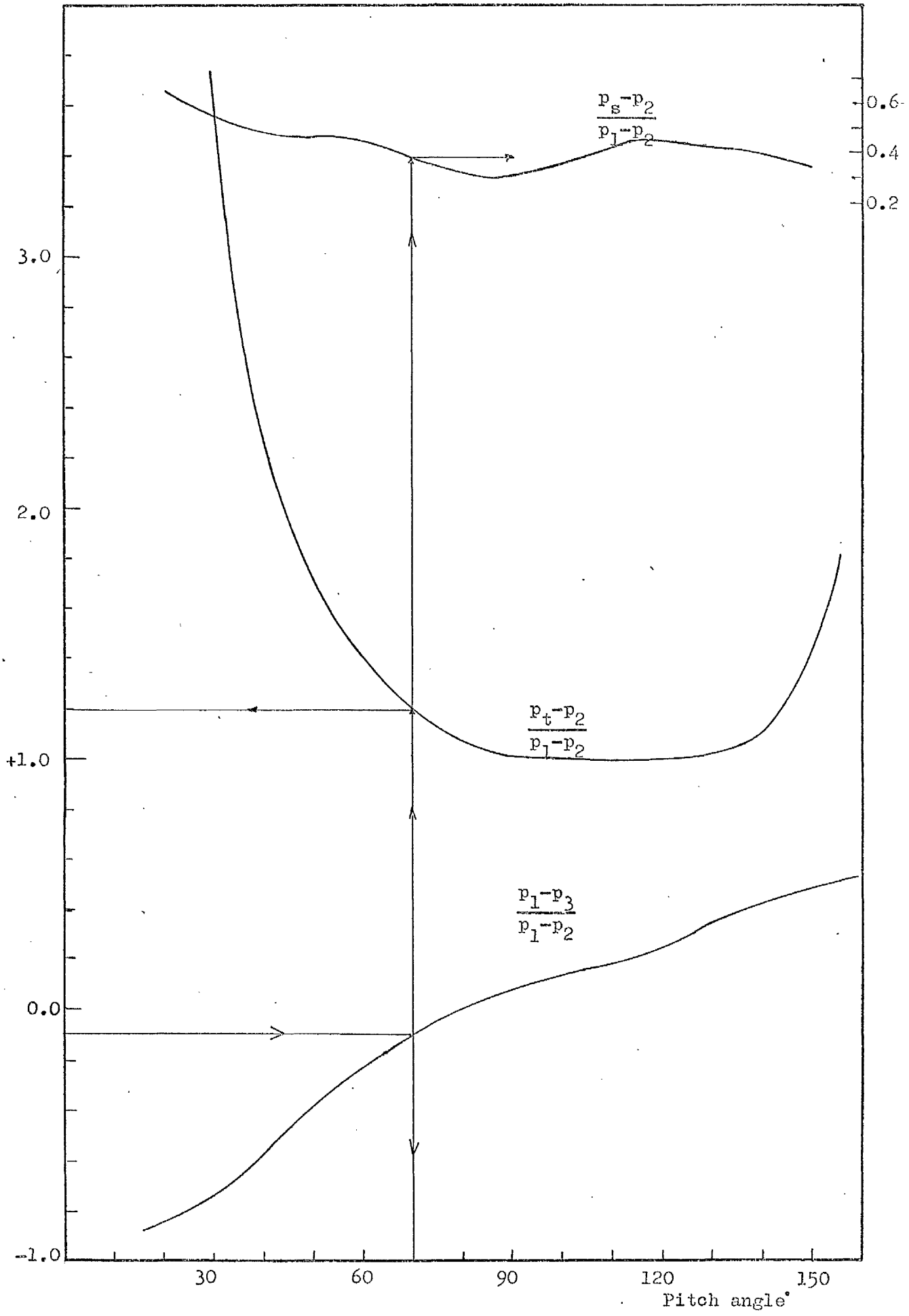

Figure 3.4 :- Typical set of calibration curves for 3-dimensional probe.

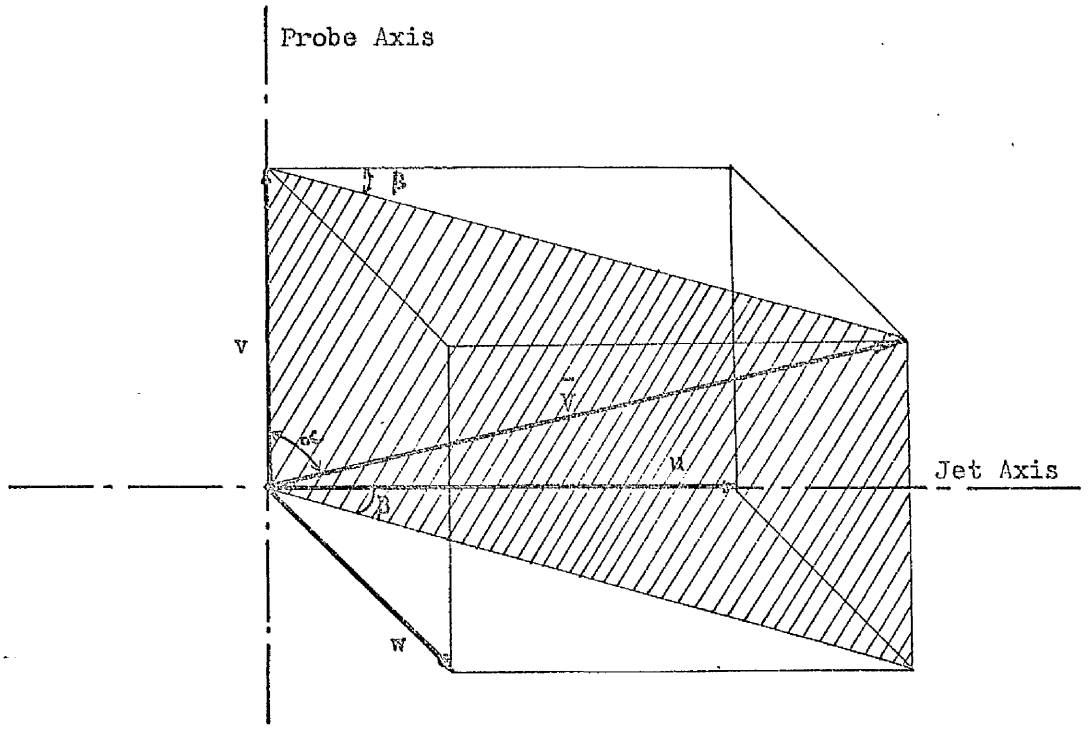

FIG. 3.5. Total velocity vector with components.

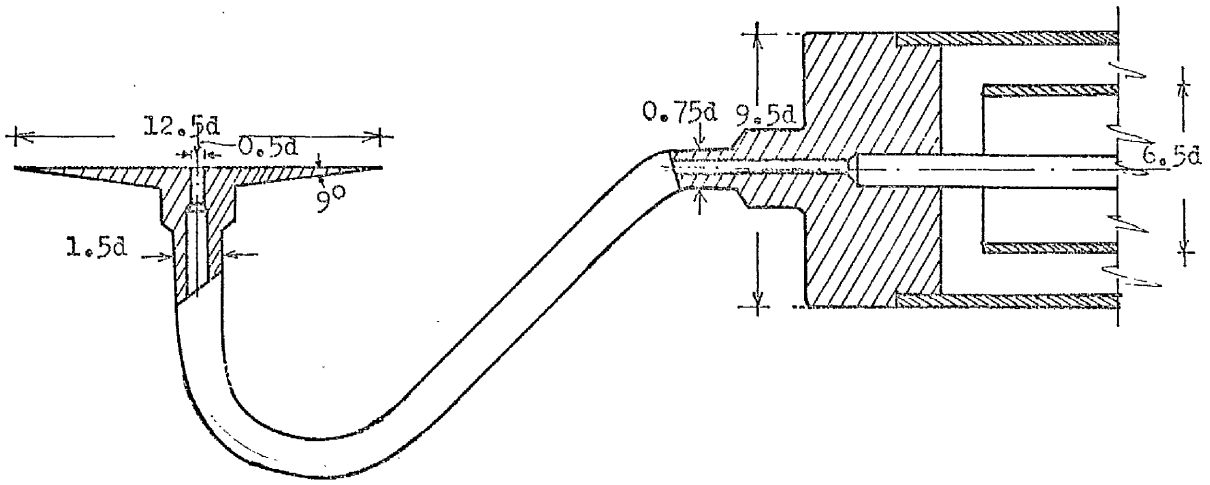

- Dims. in mm

FIG. 3.6. Static Pressure Disc Probe

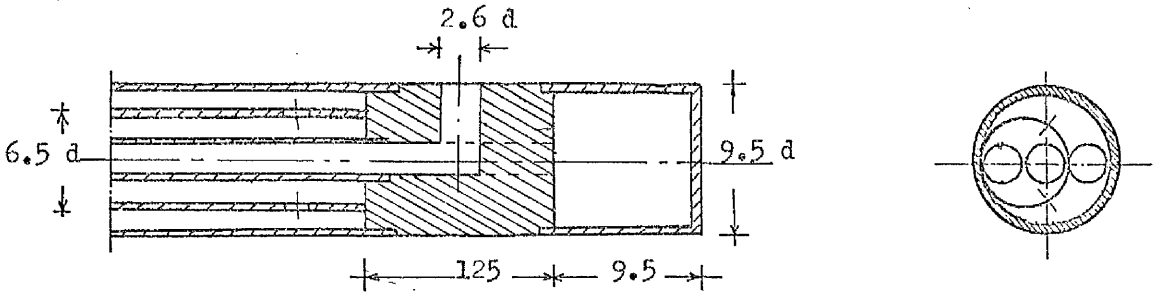

Silver solder

- Dims in mm

FIG. 3.7. Gas Sampling Probe

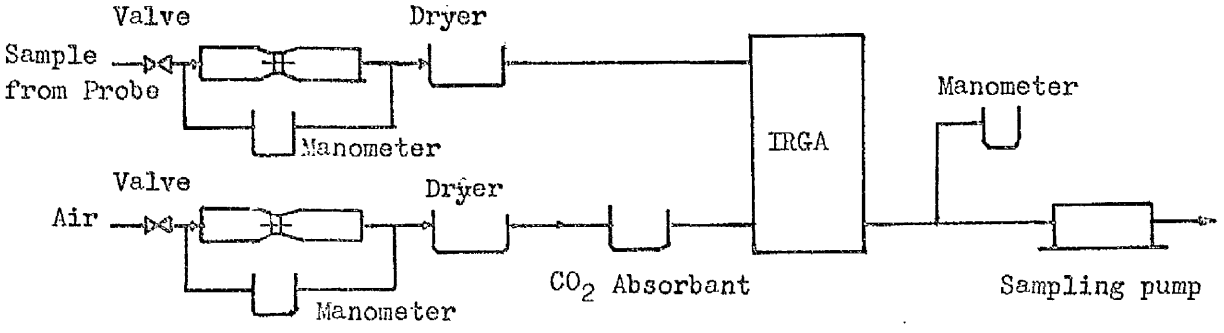

FIG. 3.8. Arrangement for Gas Sample Flow

(a) Big furnace: D/d=5

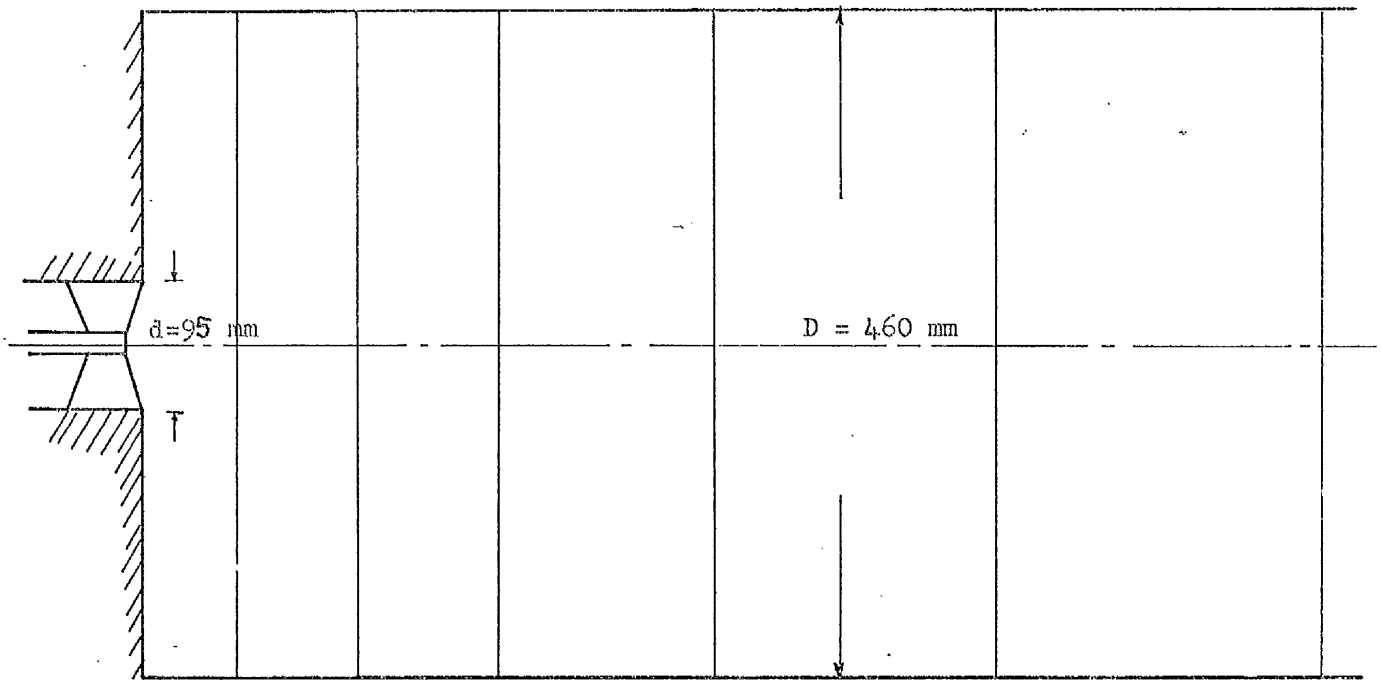

$\bar{x} = \frac{X}{D}$	0.13	0.32	0.54	0.86	1.28	1.81
x (mm)	12	60	147	246	393	576	827

(b) Small furnace: D/d=2.5

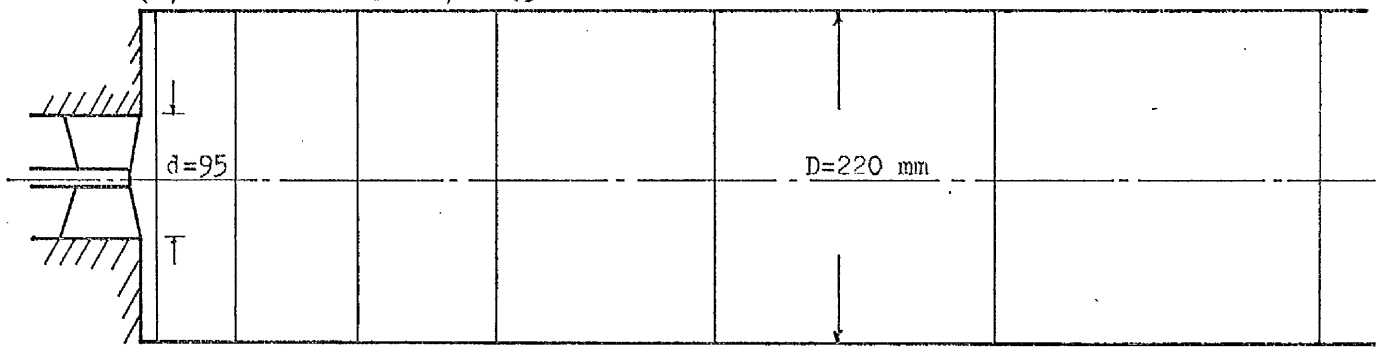

$\bar{x} = \frac{x}{D}$	0.06	0.27	0.66	1.11	1.77	2.63	3.77

FIG. 3.9. Distances of Sections for Traverce Along Furnaces

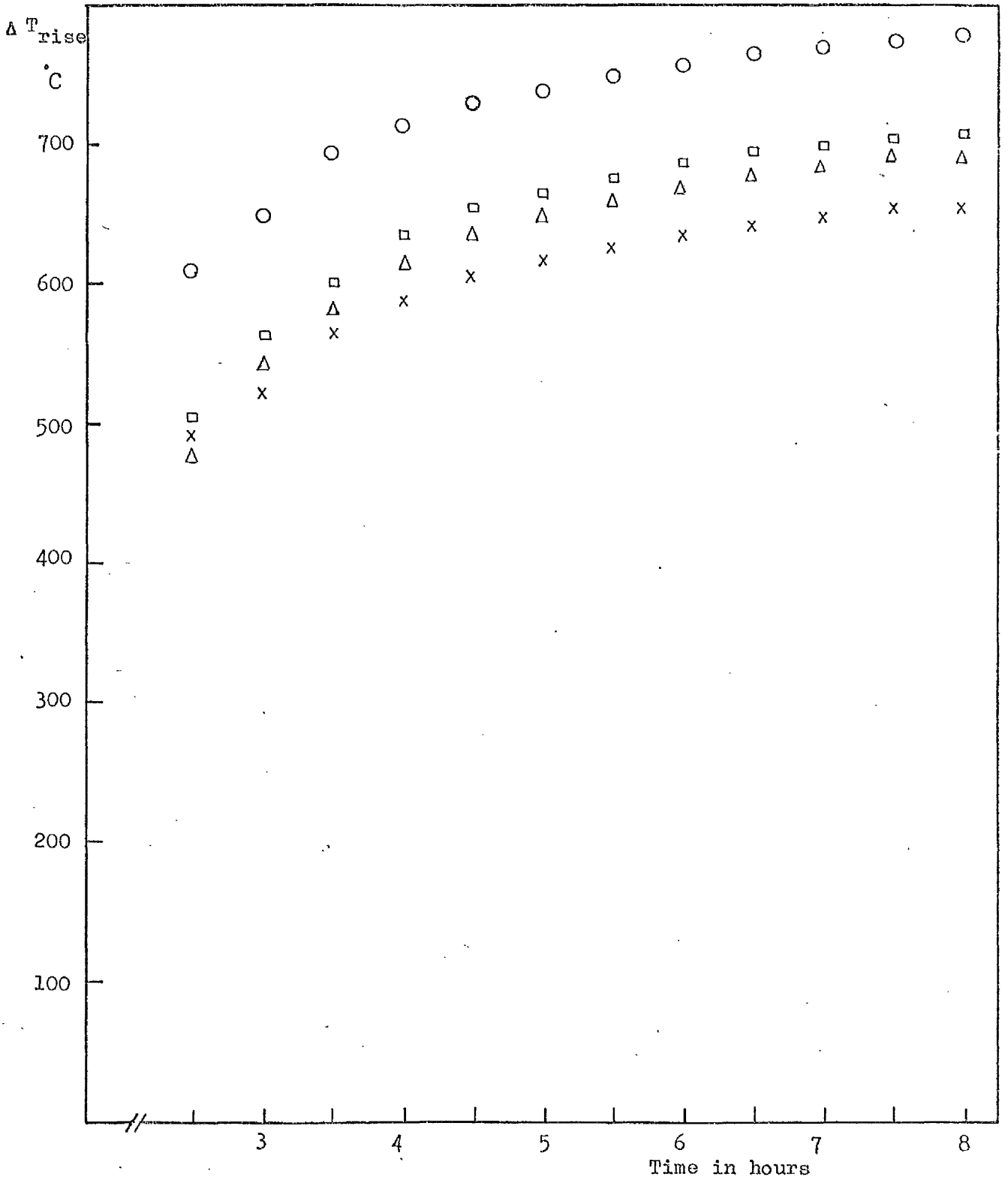

Figure 3.10 :- Furnace wall transient temperature rise.

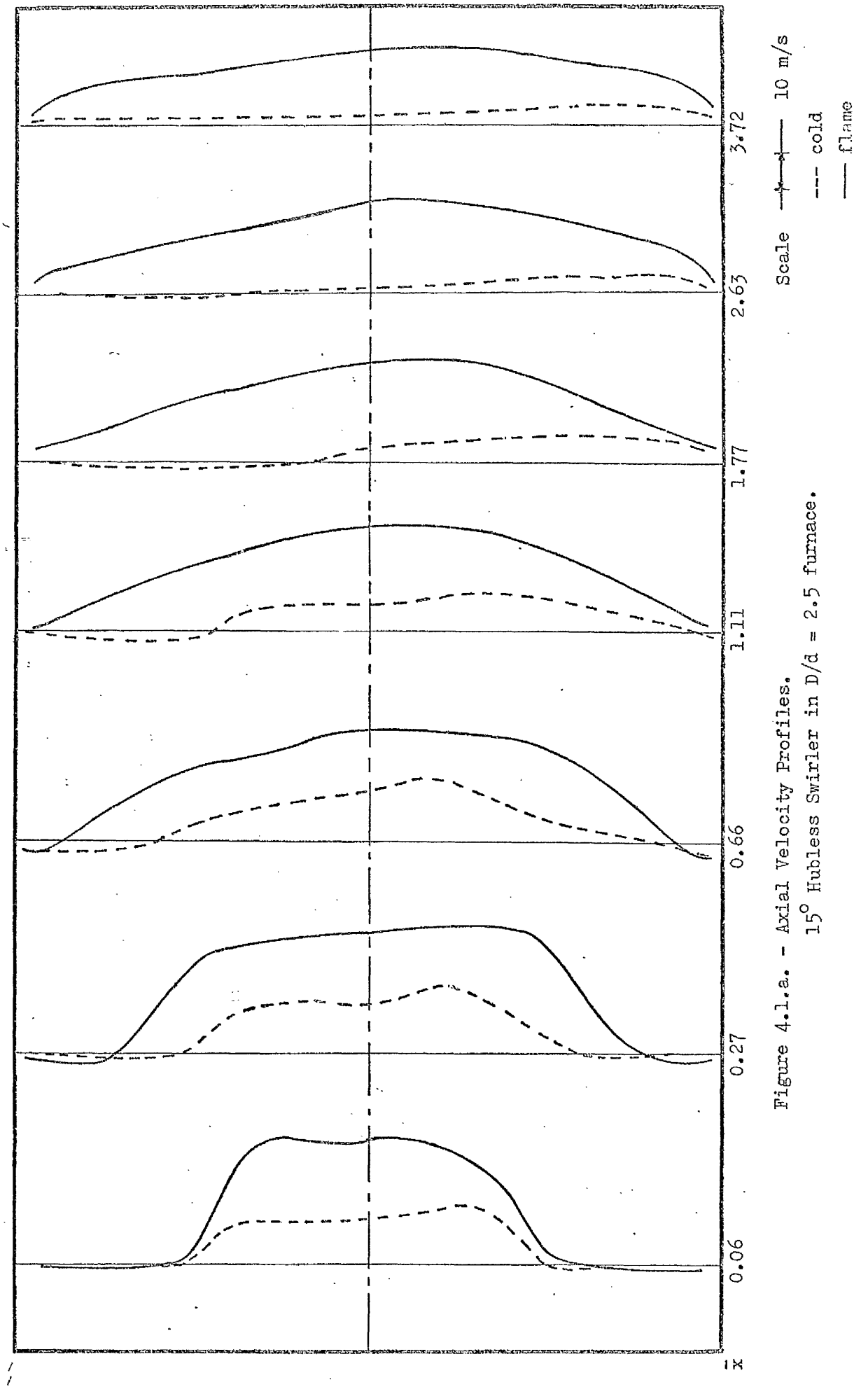

Figure 4.1.a. - Axial Velocity Profiles.
15° Hubless Swirler in D/d = 2.5 furnace.

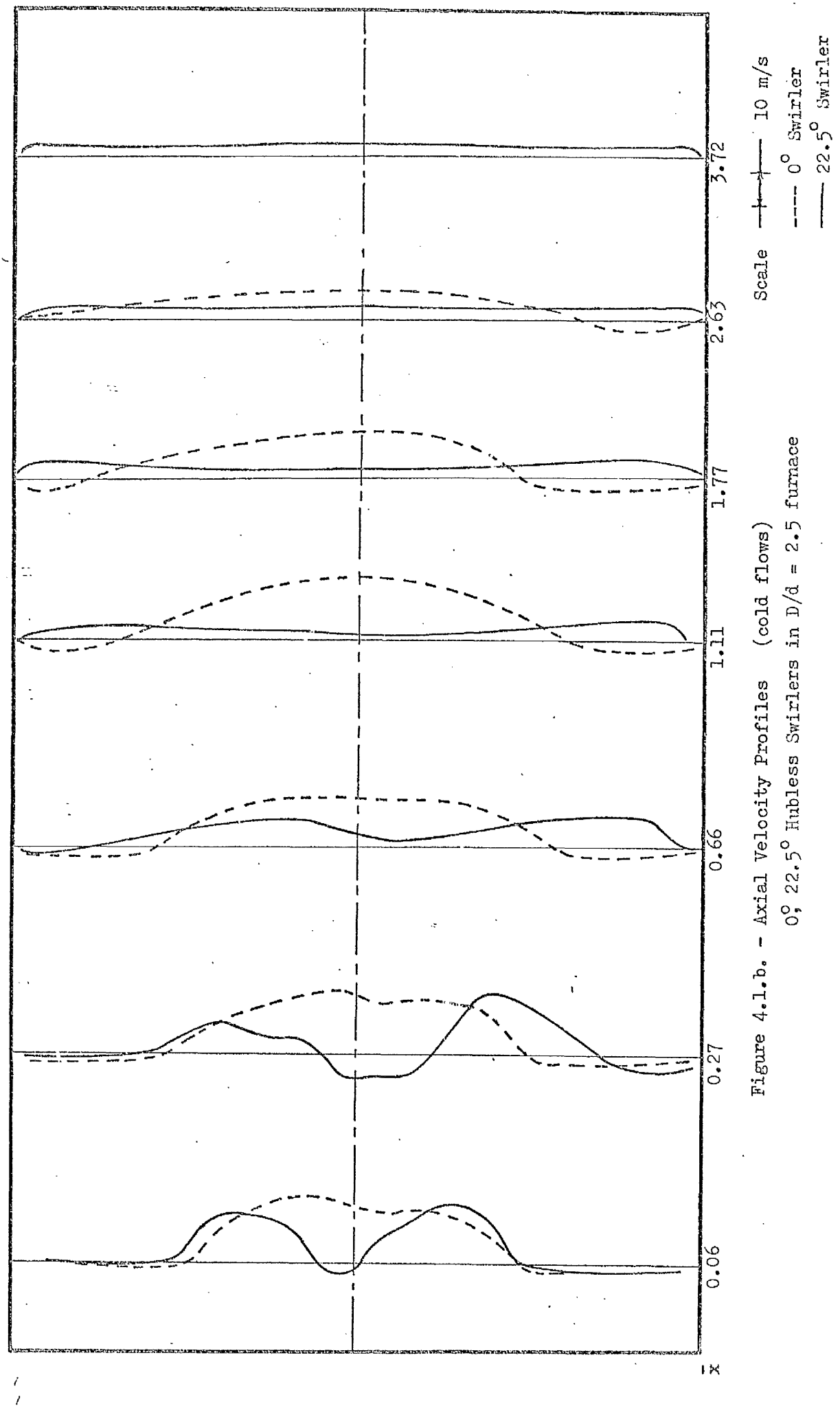

Figure 4.1.b. - Axial Velocity Profiles (cold flows)
0°, 22.5° Hubless Swirlers in D/d = 2.5 furnace

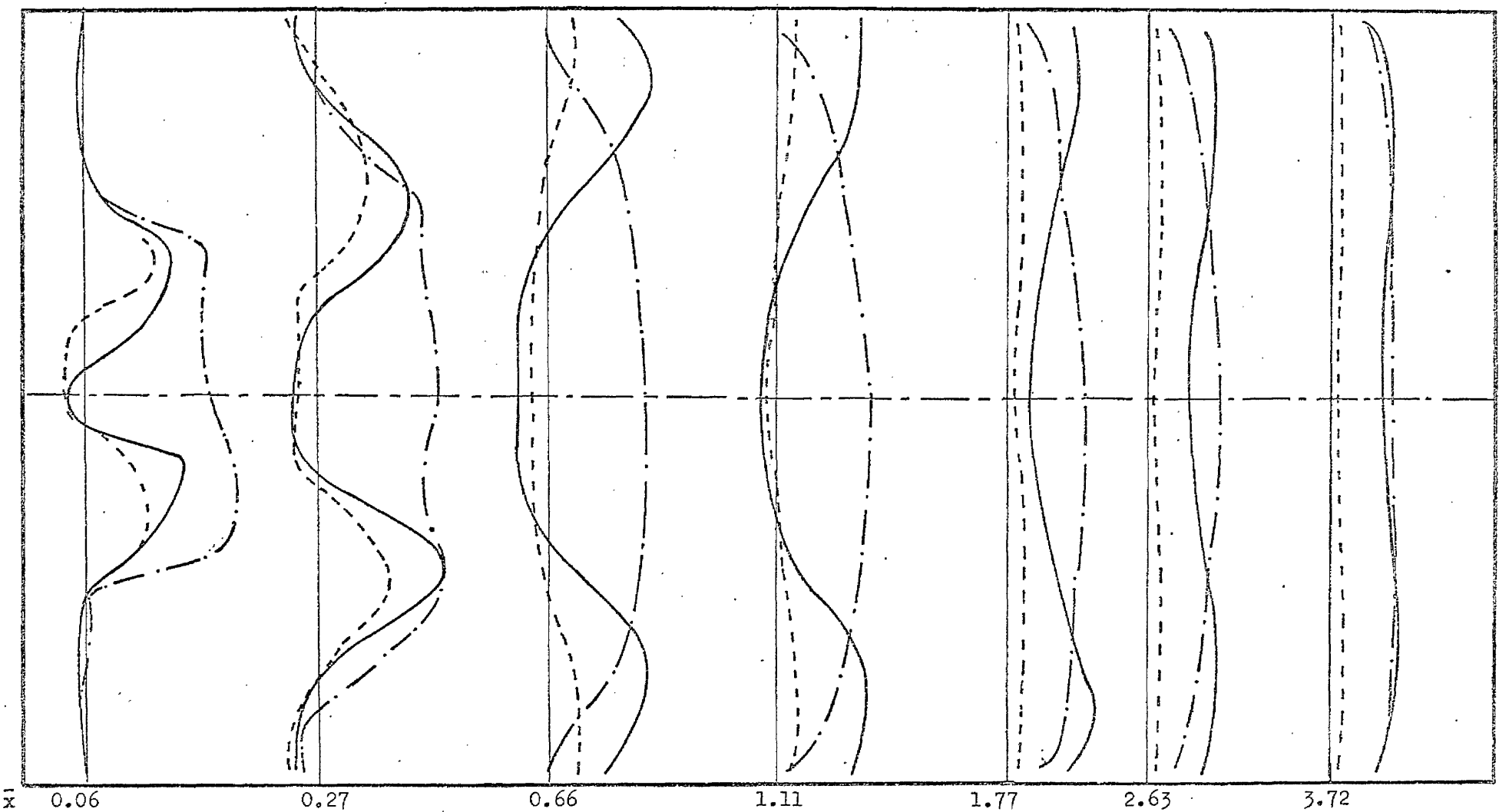

Figure 4.1.c. - Axial Velocity Profiles.

30° Hubless Swirler in D/d = 2.5 furnace.

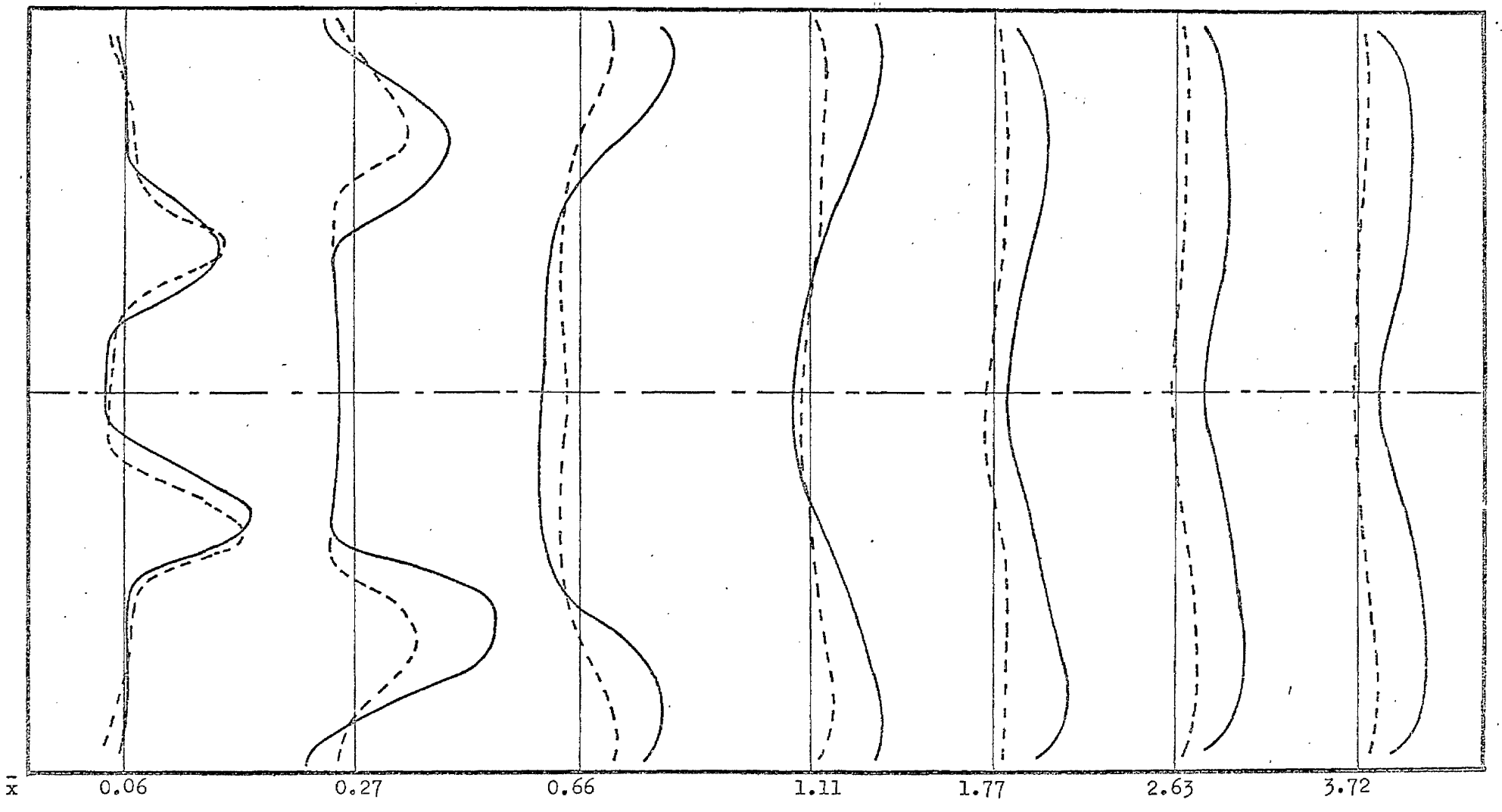

Figure 4.1.d. - Axial Velocity Profiles.
45° Hubless Swirler in D/d = 2.5 furnace.

Scale —|—|— 10 m/s
--- cold
—— flame

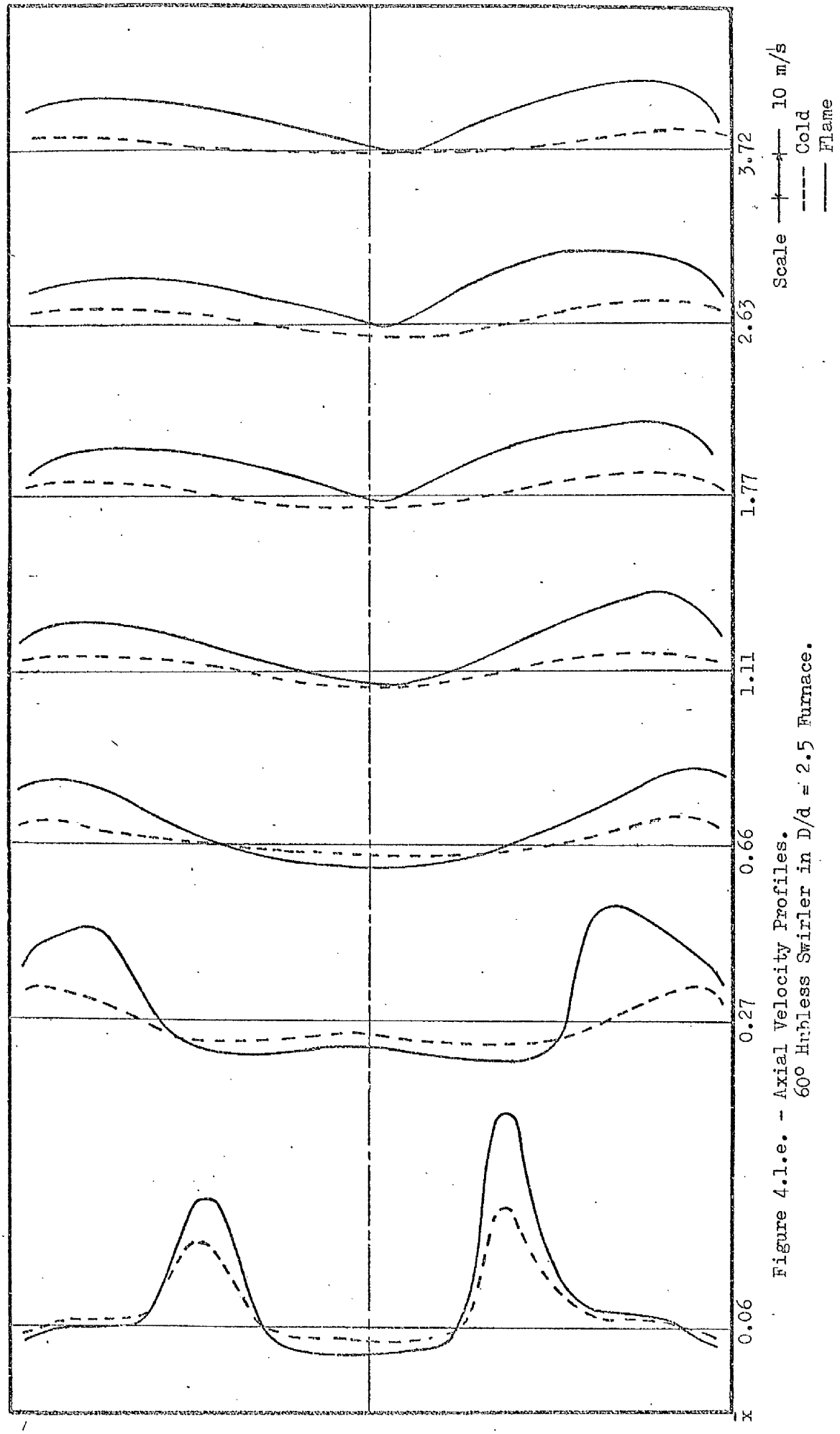

Figure 4.1.e. - Axial Velocity Profiles.
60° Hubless Swirler in D/d = 2.5 Furnace.

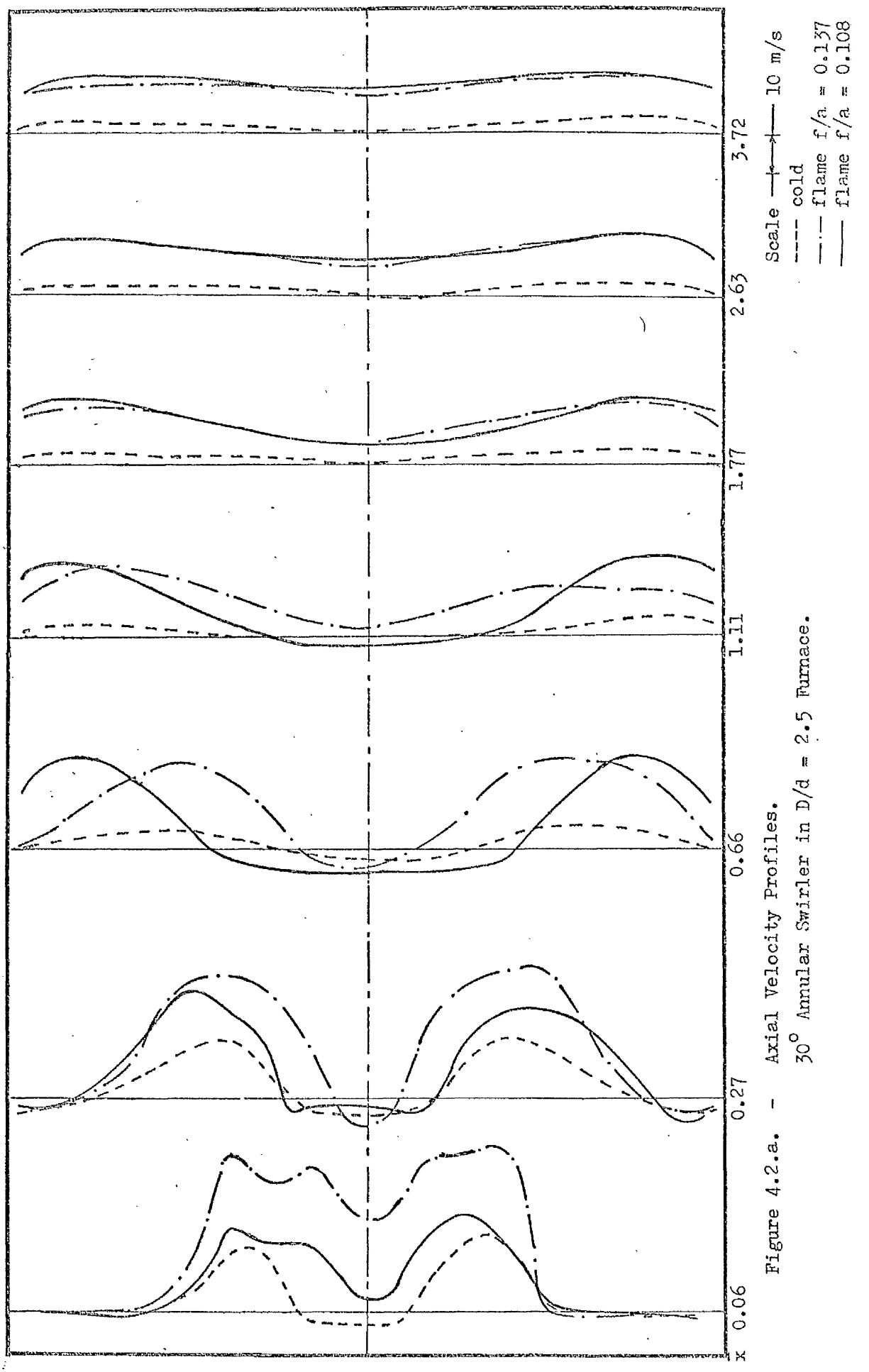

Figure 4.2.a. - Axial Velocity Profiles.
30° Annular Swirler in D/d = 2.5 Furnace.

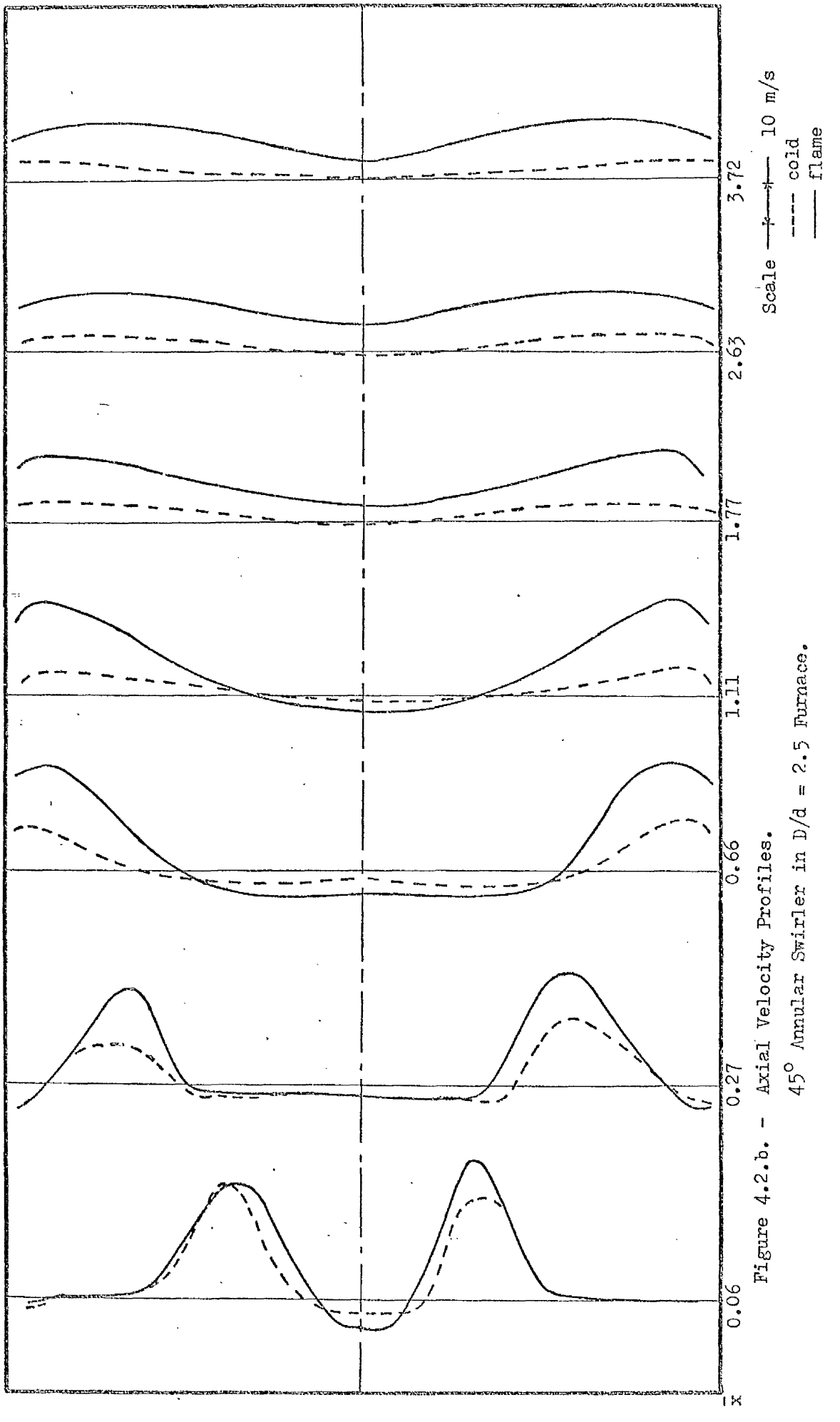

Figure 4.2.b. - Axial Velocity Profiles.
45° Annular Swirler in D/d = 2.5 Furnace.

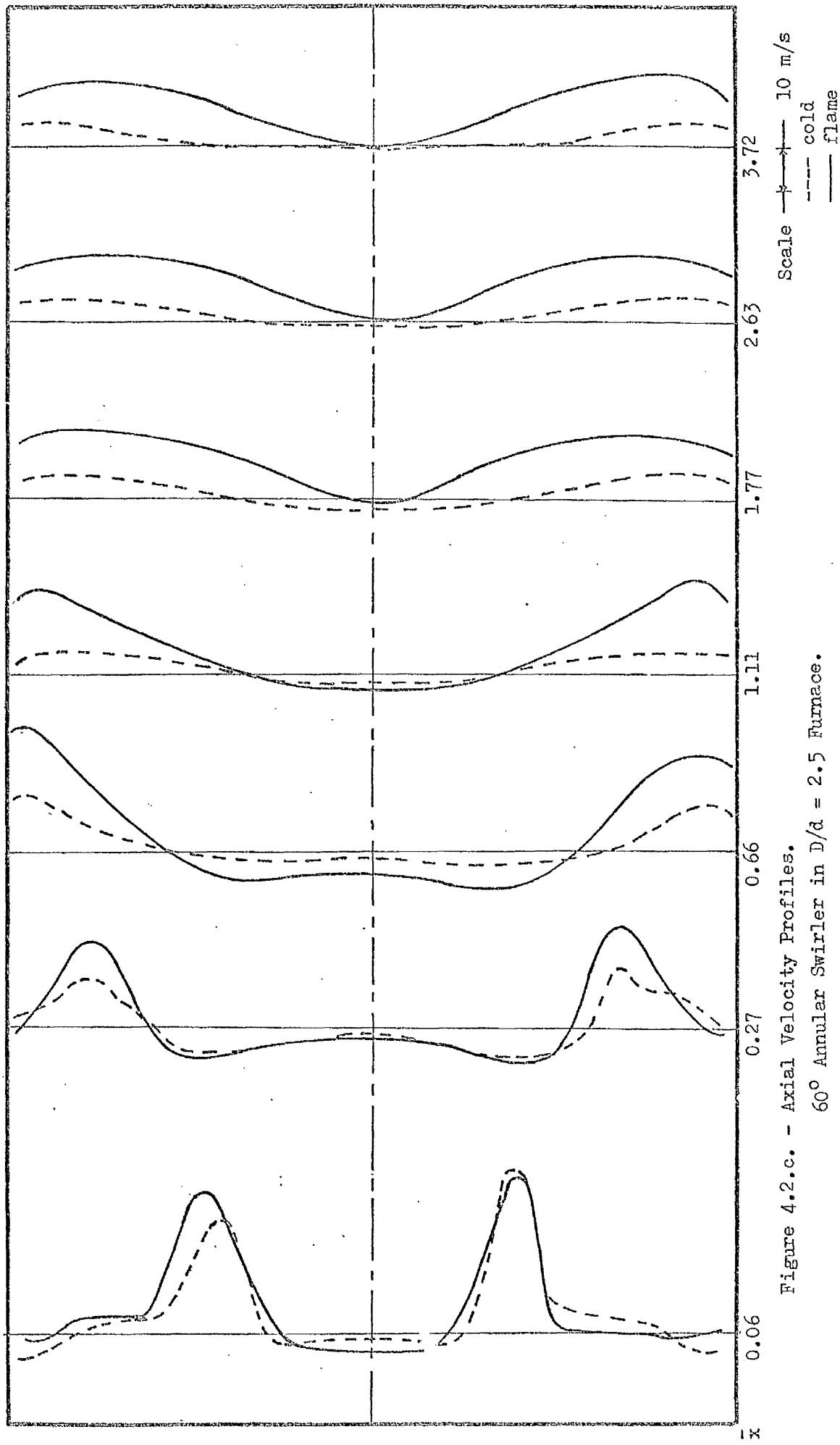

Figure 4.2.c. - Axial Velocity Profiles.
60° Annular Swirler in D/d = 2.5 Furnace.

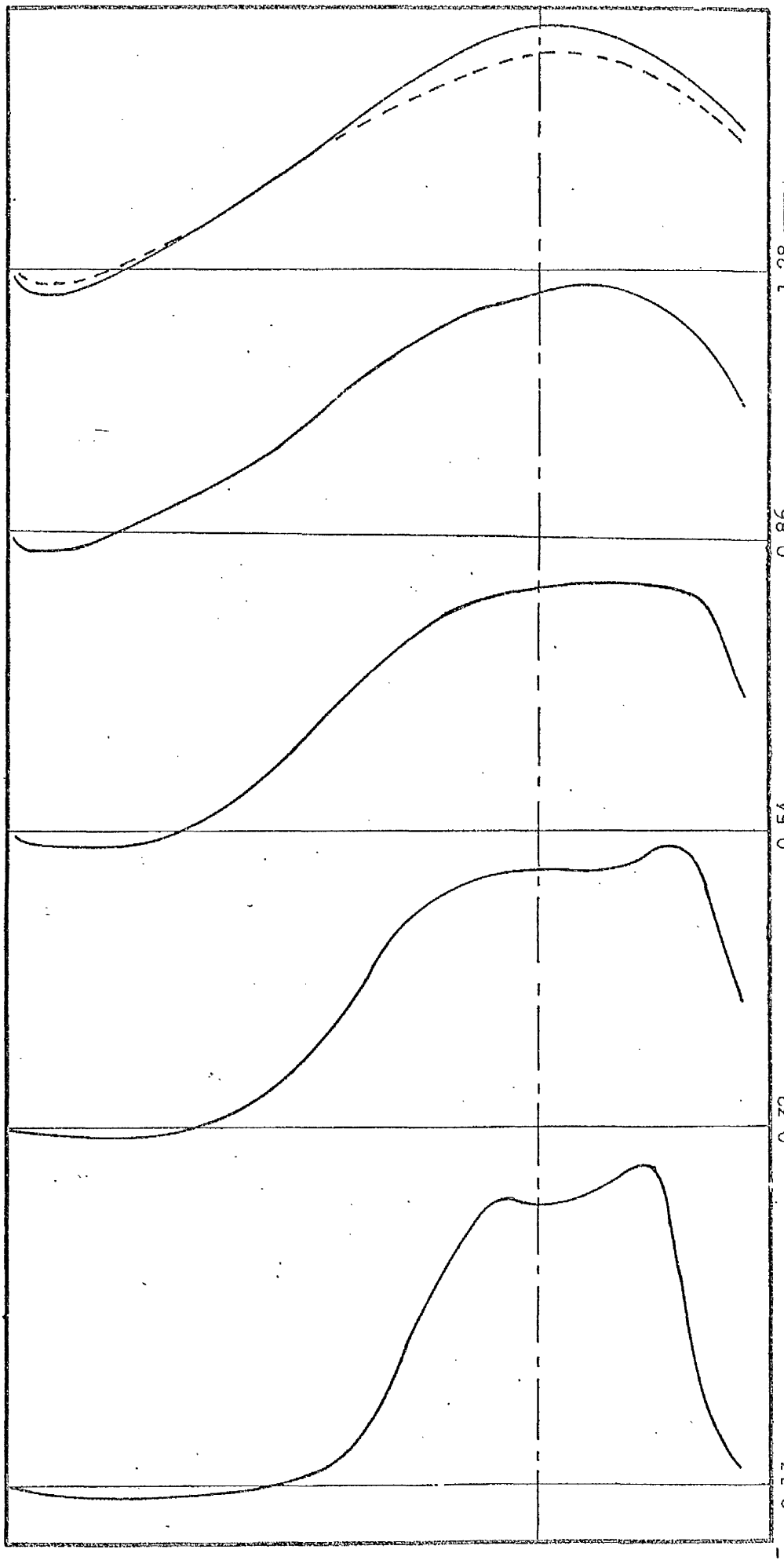

Figure 4.3.a. - Axial Velocity Profiles.
0^{o} Hubless Swirler flame in D/d = 5 Furnace.

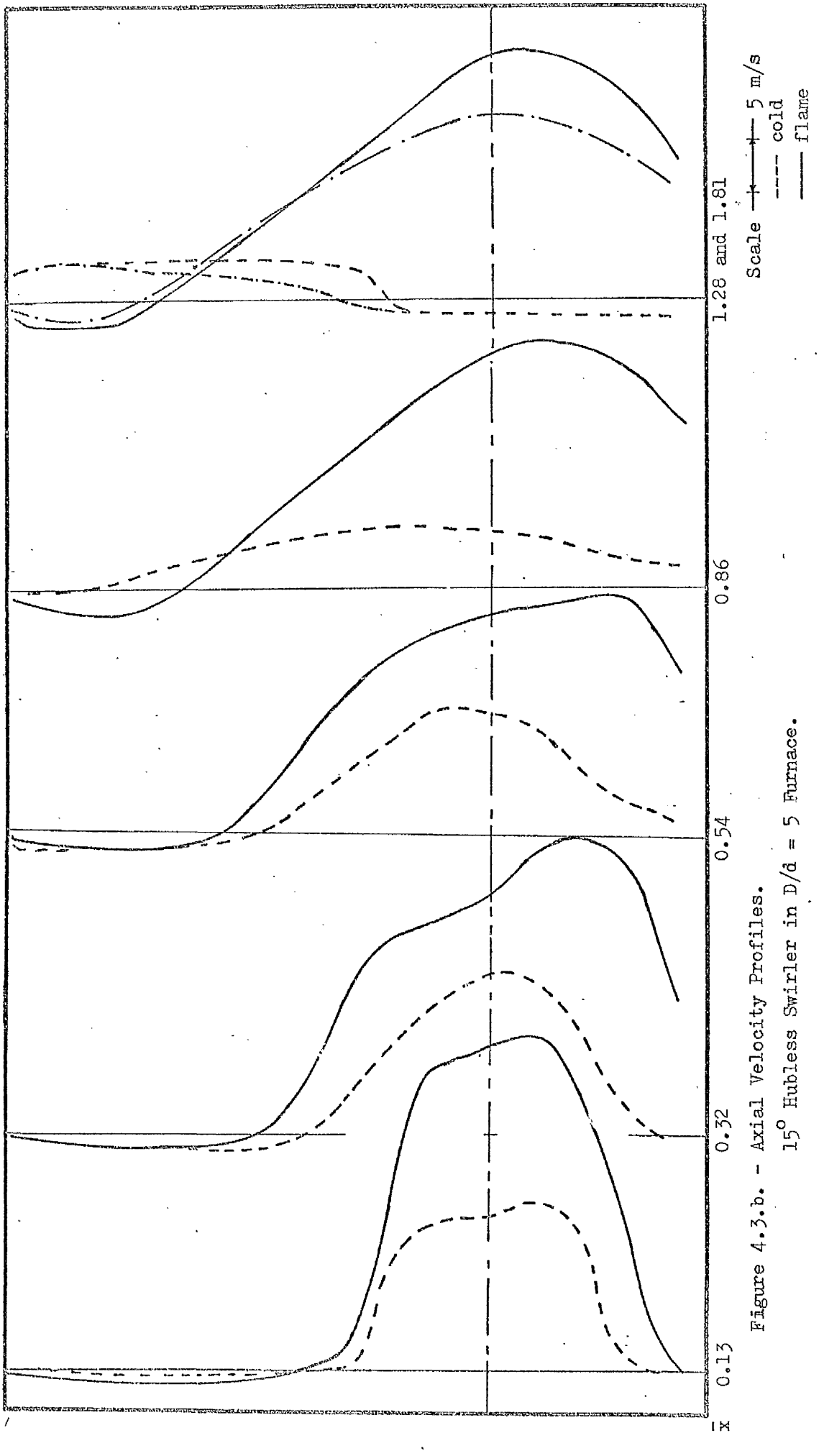

Figure 4.3.b. - Axial Velocity Profiles.
15^{o} Hubless Swirler in D/d = 5 Furnace.

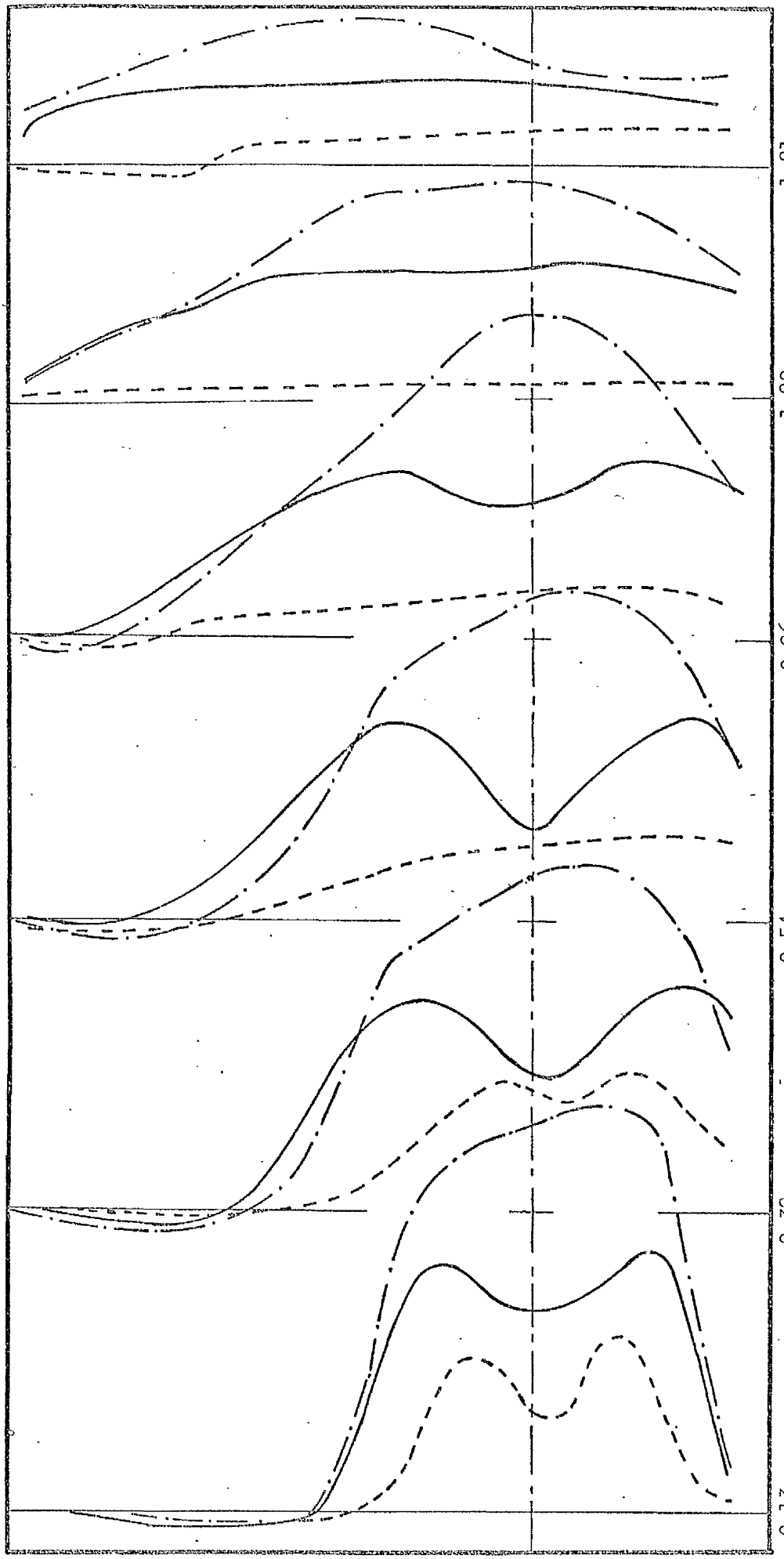

Figure 4.3.c. - Axial Velocity Profiles.
22.5° Hubless Swirler in D/d = 5 Furnace.

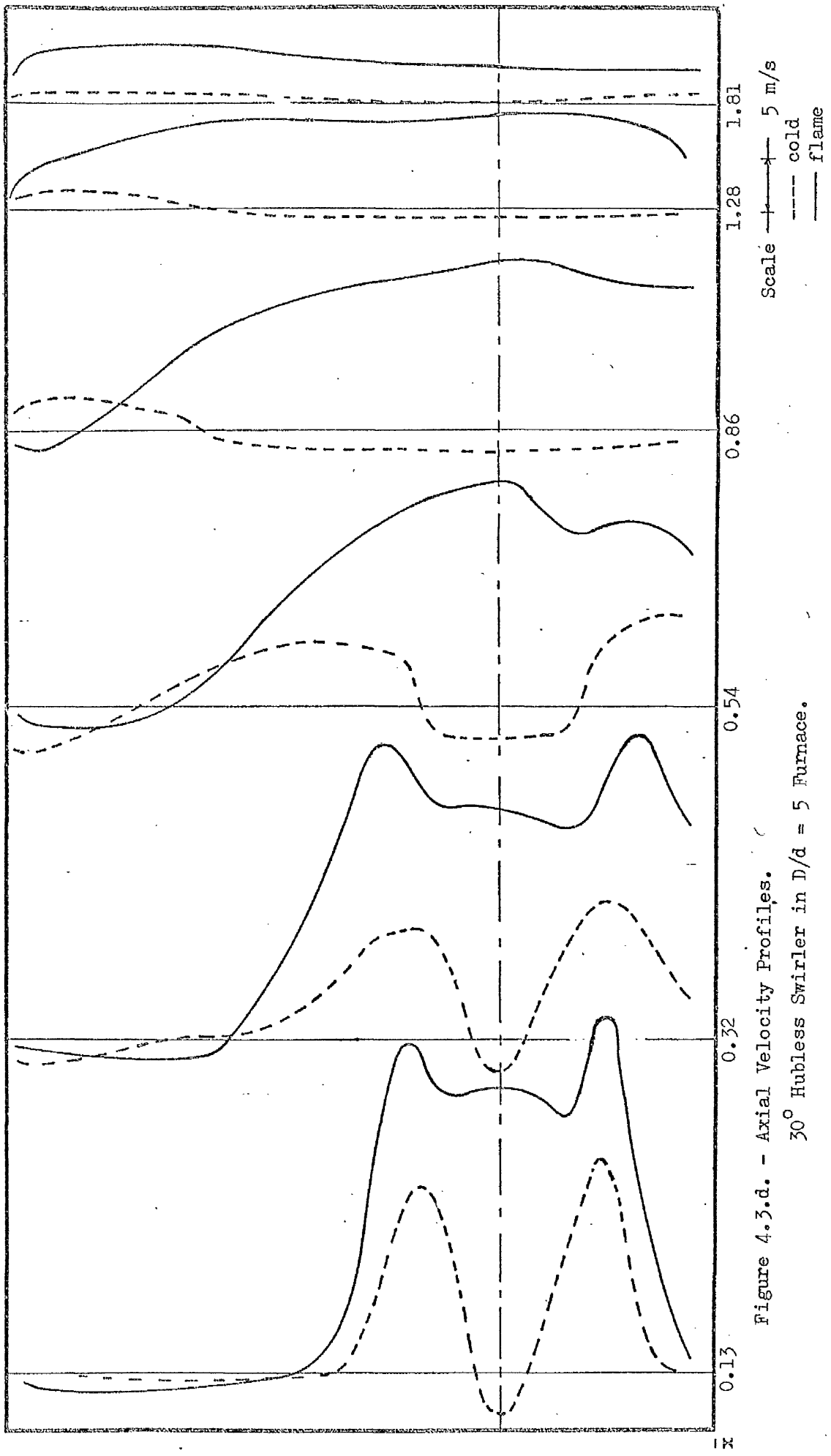

Figure 4.3.d. - Axial Velocity Profiles.
30° Hubless Swirler in D/d = 5 Furnace.

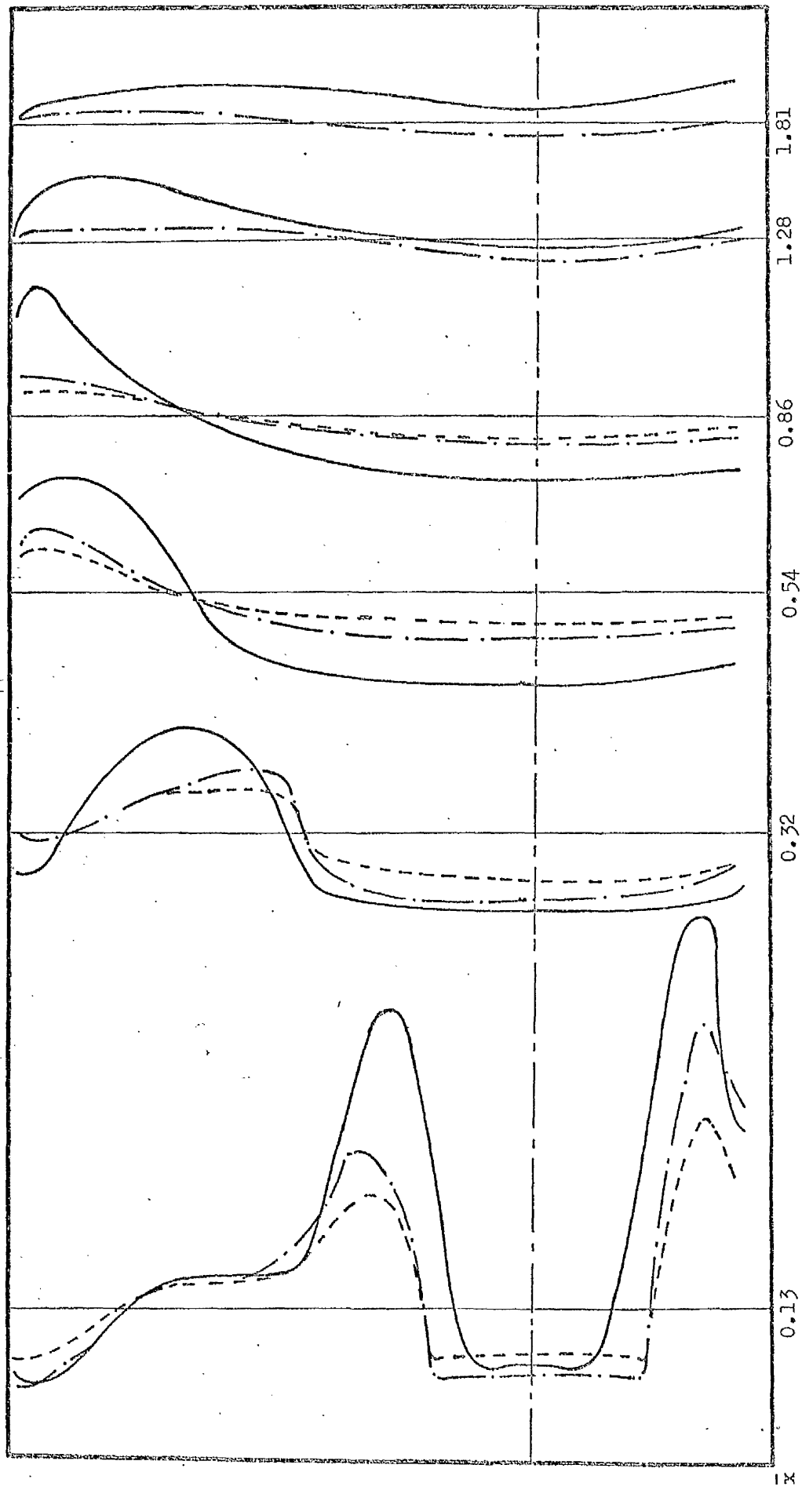

Figure 4.3.e. - Axial Velocity Profiles.
45° Hubless Swirler in D/d = 5 Furnace.

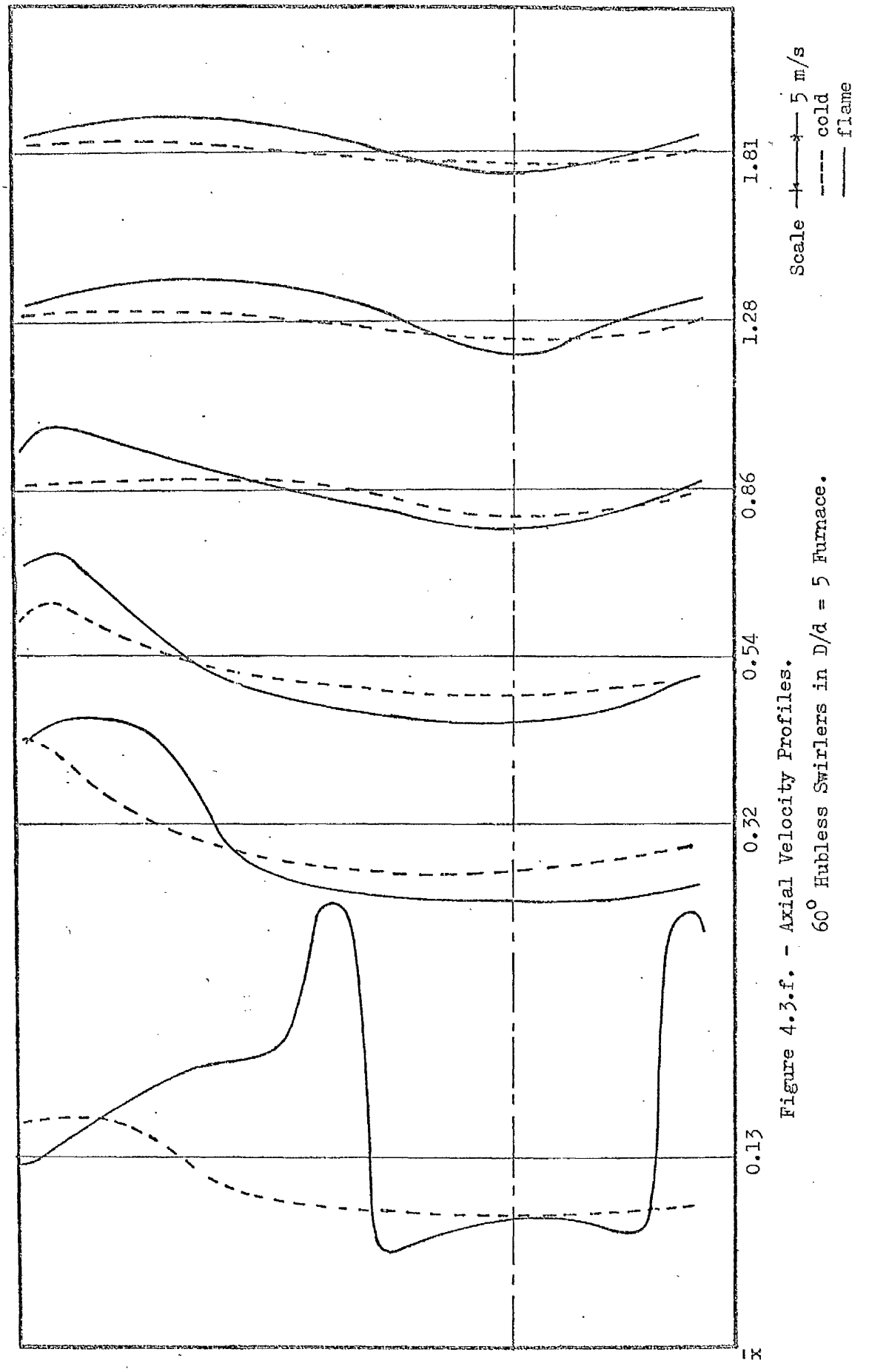

Figure 4.3.f. - Axial Velocity Profiles.
60° Hubless Swirlers in D/d = 5 Furnace.

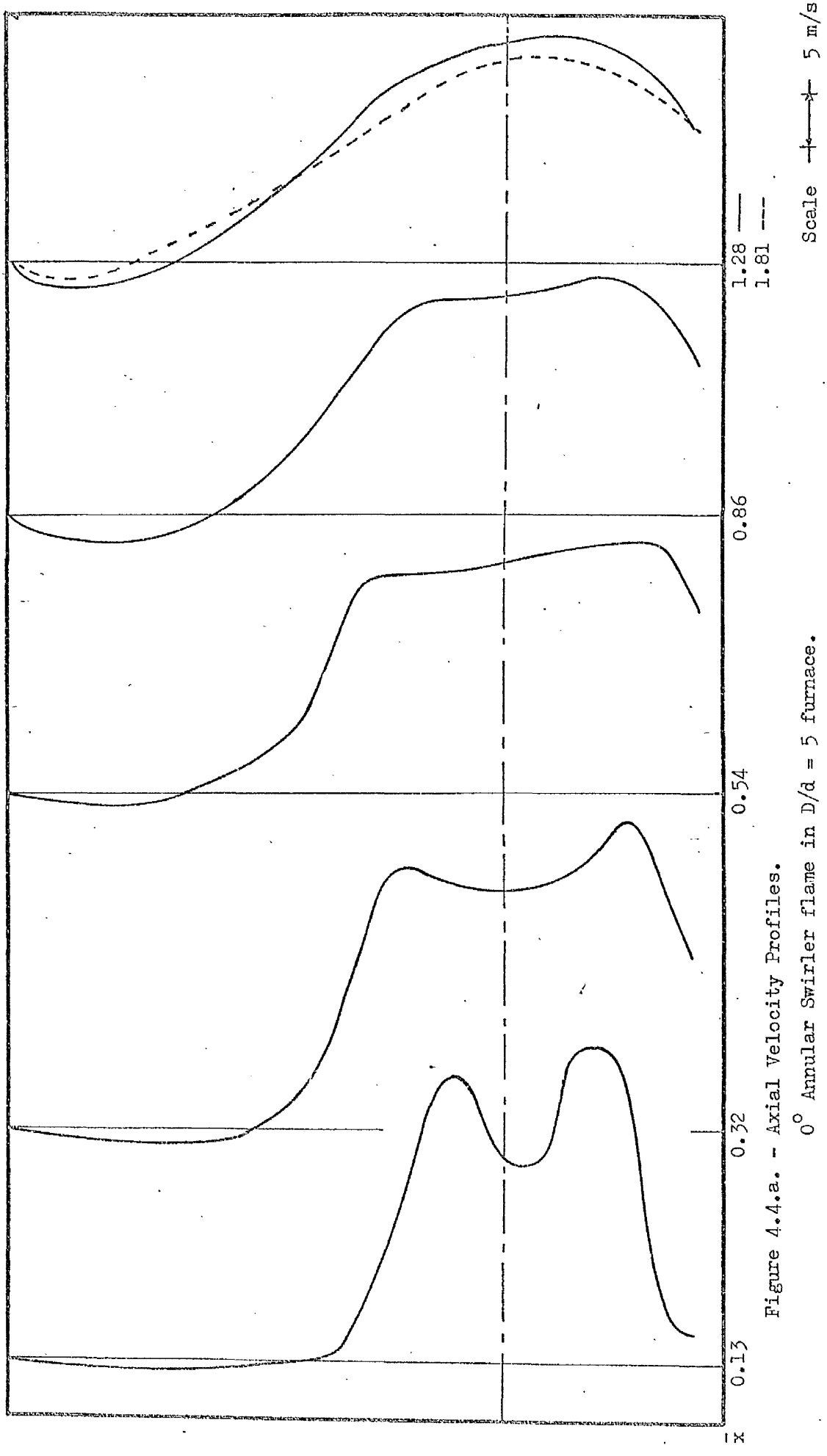

Figure 4.4.a. - Axial Velocity Profiles.
0^{o} Annular Swirler flame in D/d = 5 furnace.

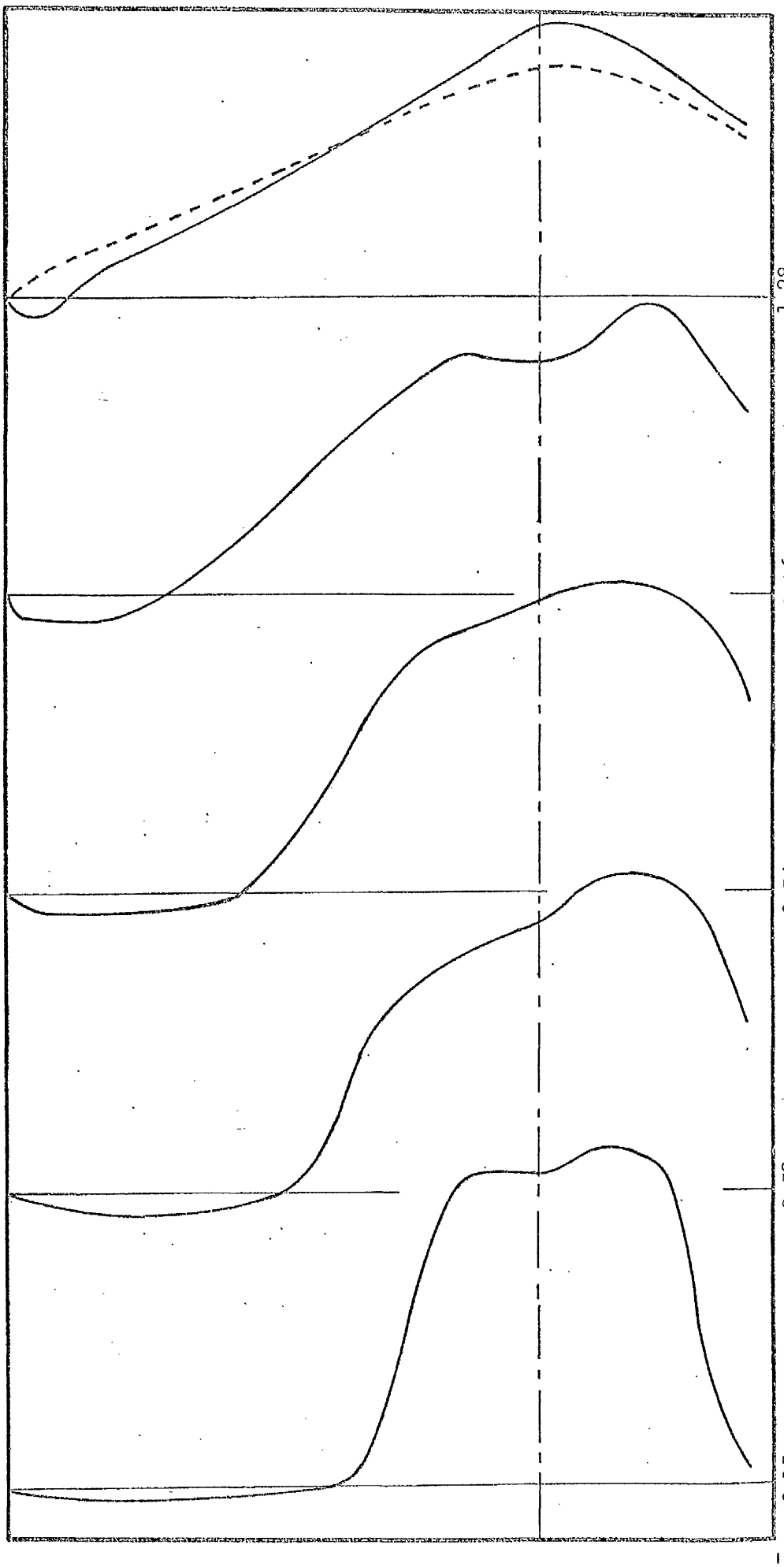

Figure 4.4.b. - Axial Velocity Profiles.
15° Annular Swirler flame in D/d = 5 furnace.

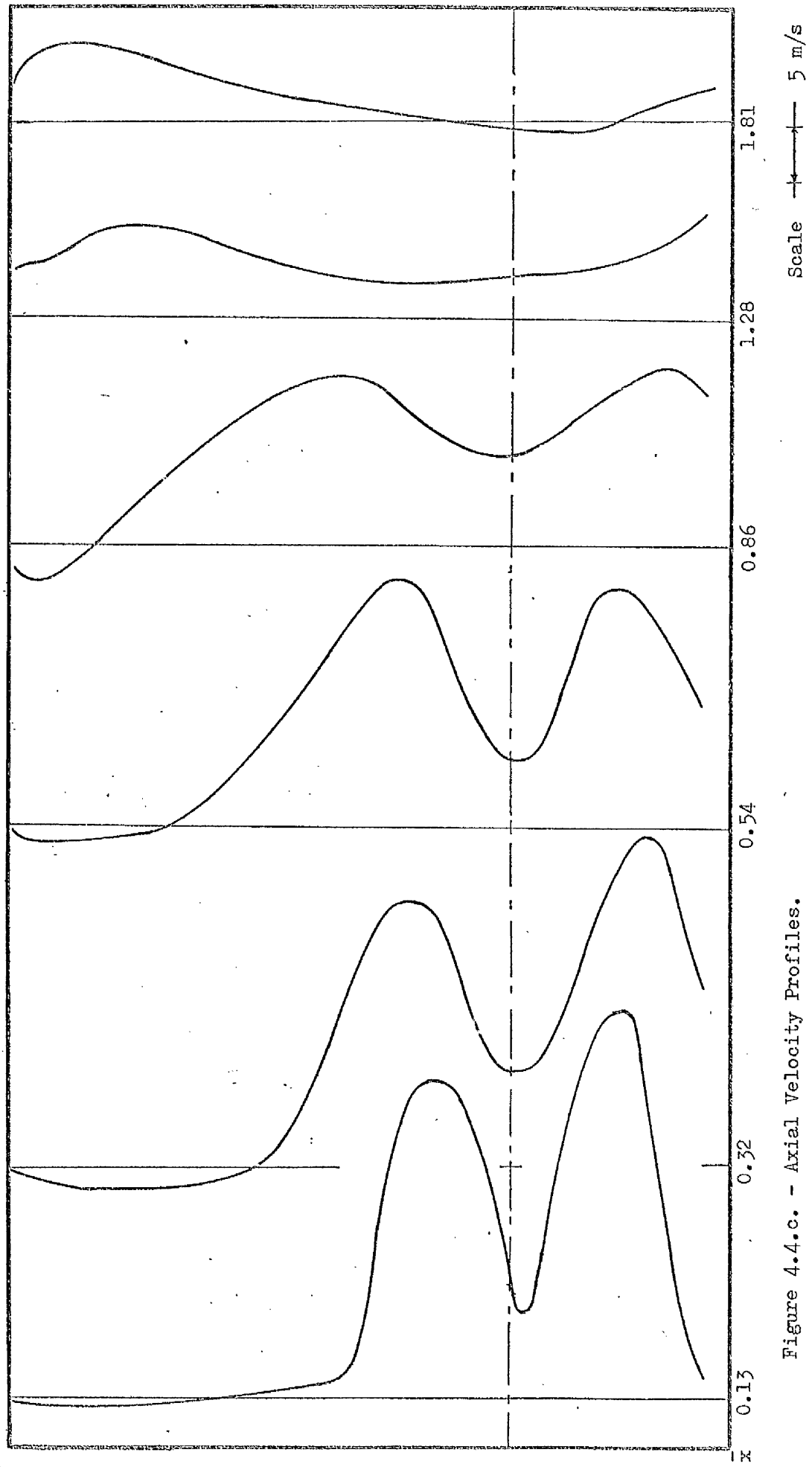

Figure 4.4.c. - Axial Velocity Profiles.
30° Annular Swirler flame in D/d = 5 furnace.

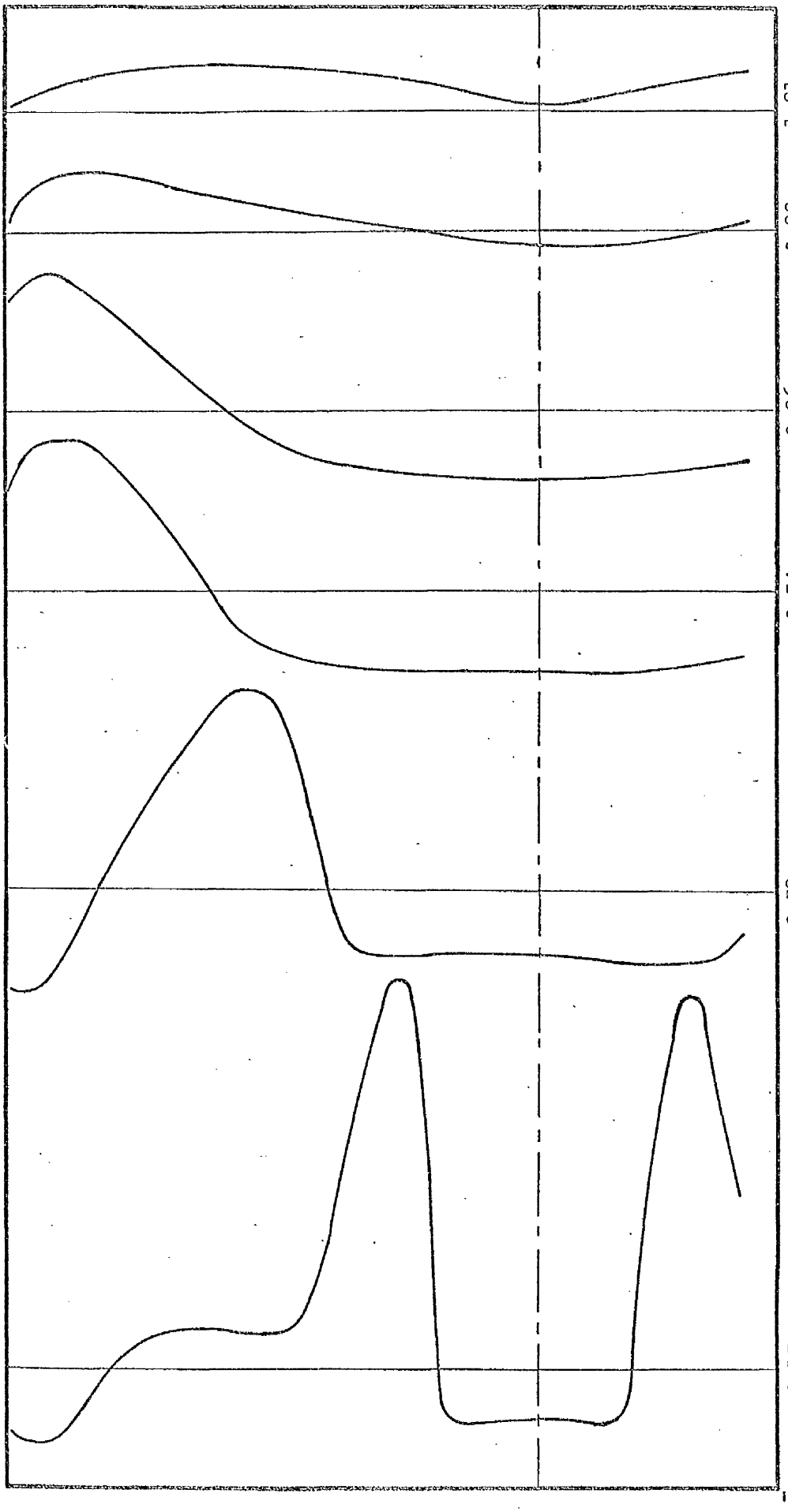

Figure 4.4.d. - Axial Velocity Profiles.
45° Annular Swirler flame in D/d = 5 furnace.

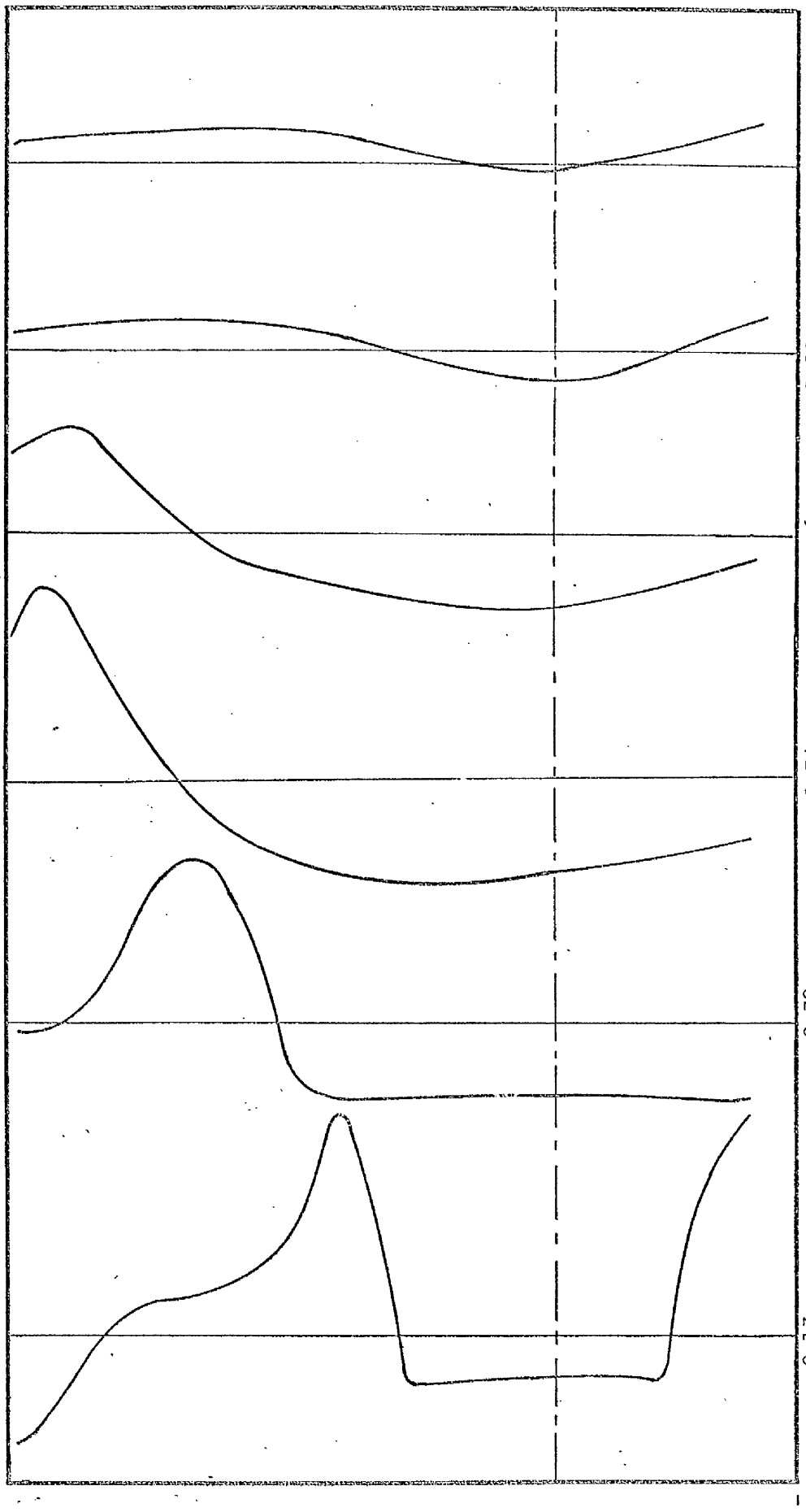

Figure 4.4.e. - Axial Velocity Profiles.
68 Annular Swirler flame in D/d = 5 furnace.

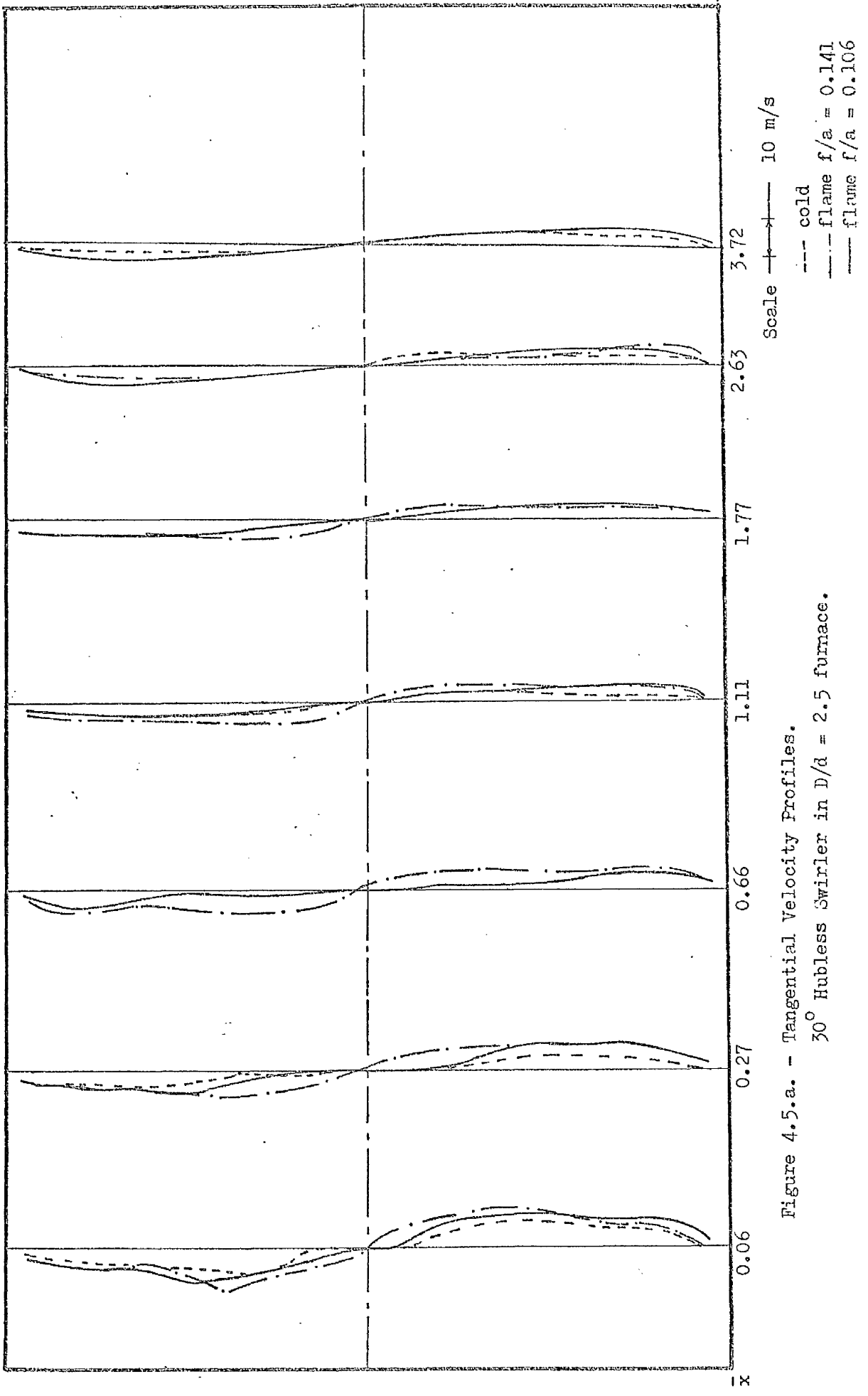

Figure 4.5.a. - Tangential Velocity Profiles.
30° Hubless Swirler in D/d = 2.5 furnace.

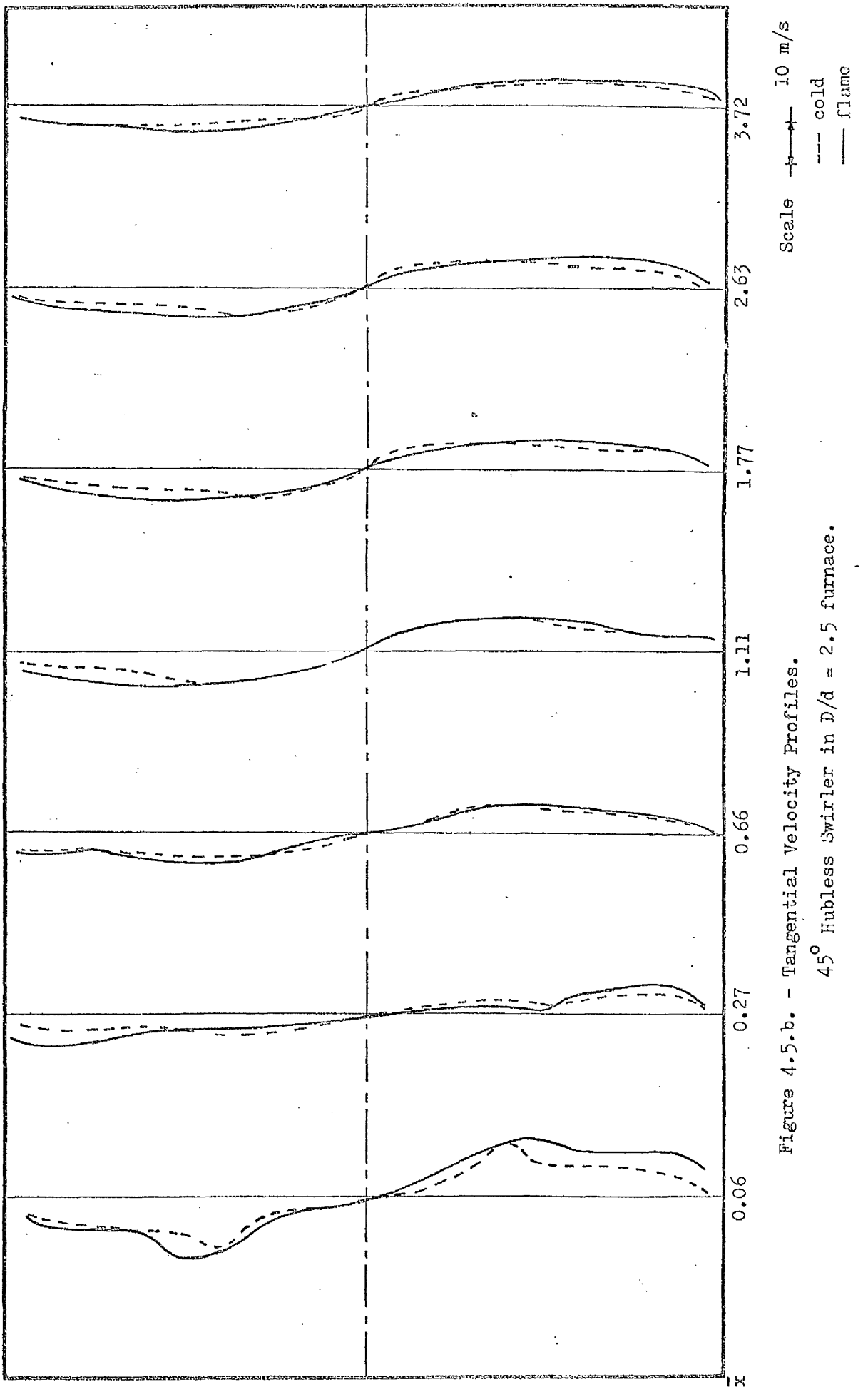

Figure 4.5.b. - Tangential Velocity Profiles.
45° Hubless Swirler in D/d = 2.5 furnace.

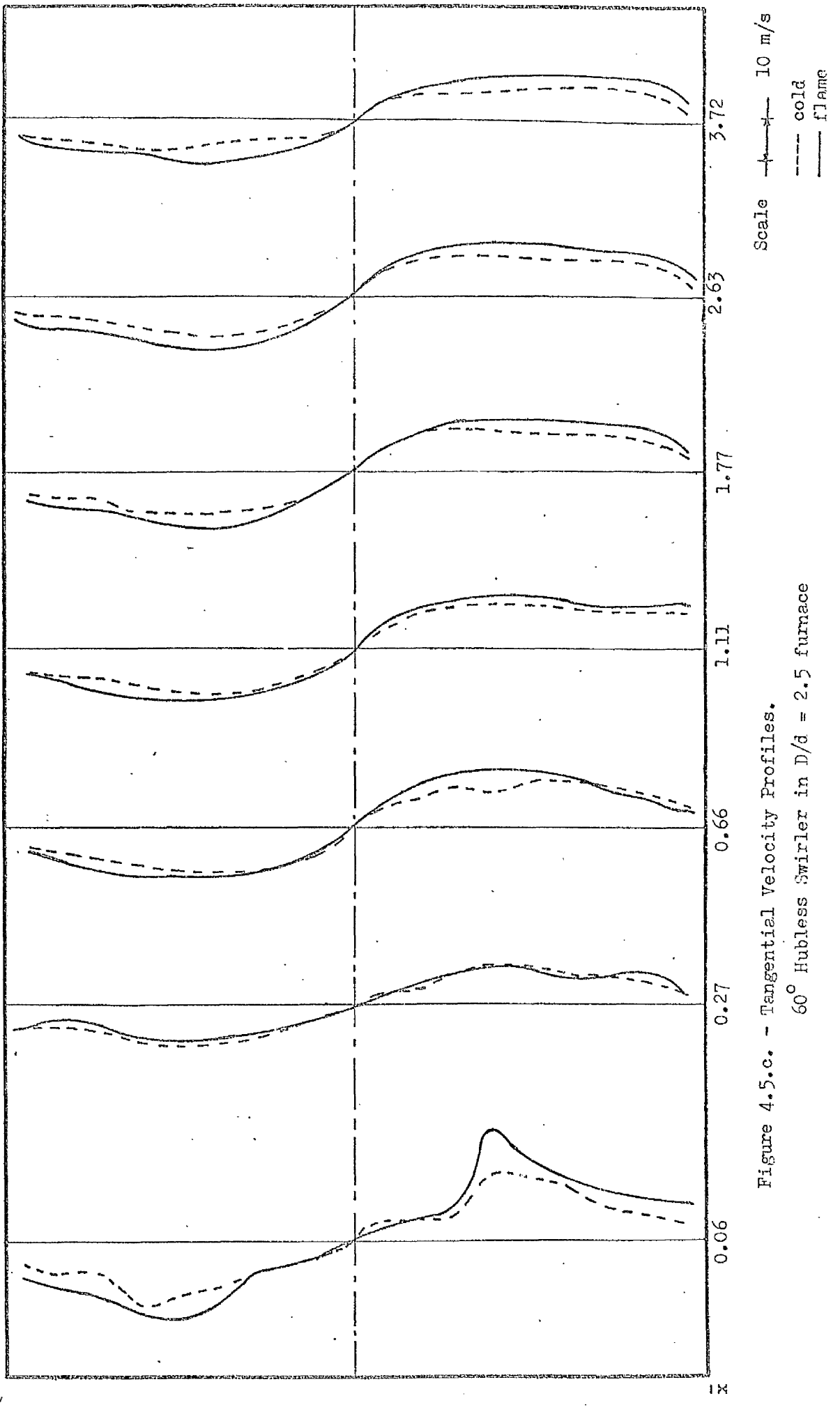

Figure 4.5.c. - Tangential Velocity Profiles.
60° Hubless Swirler in D/d = 2.5 furnace

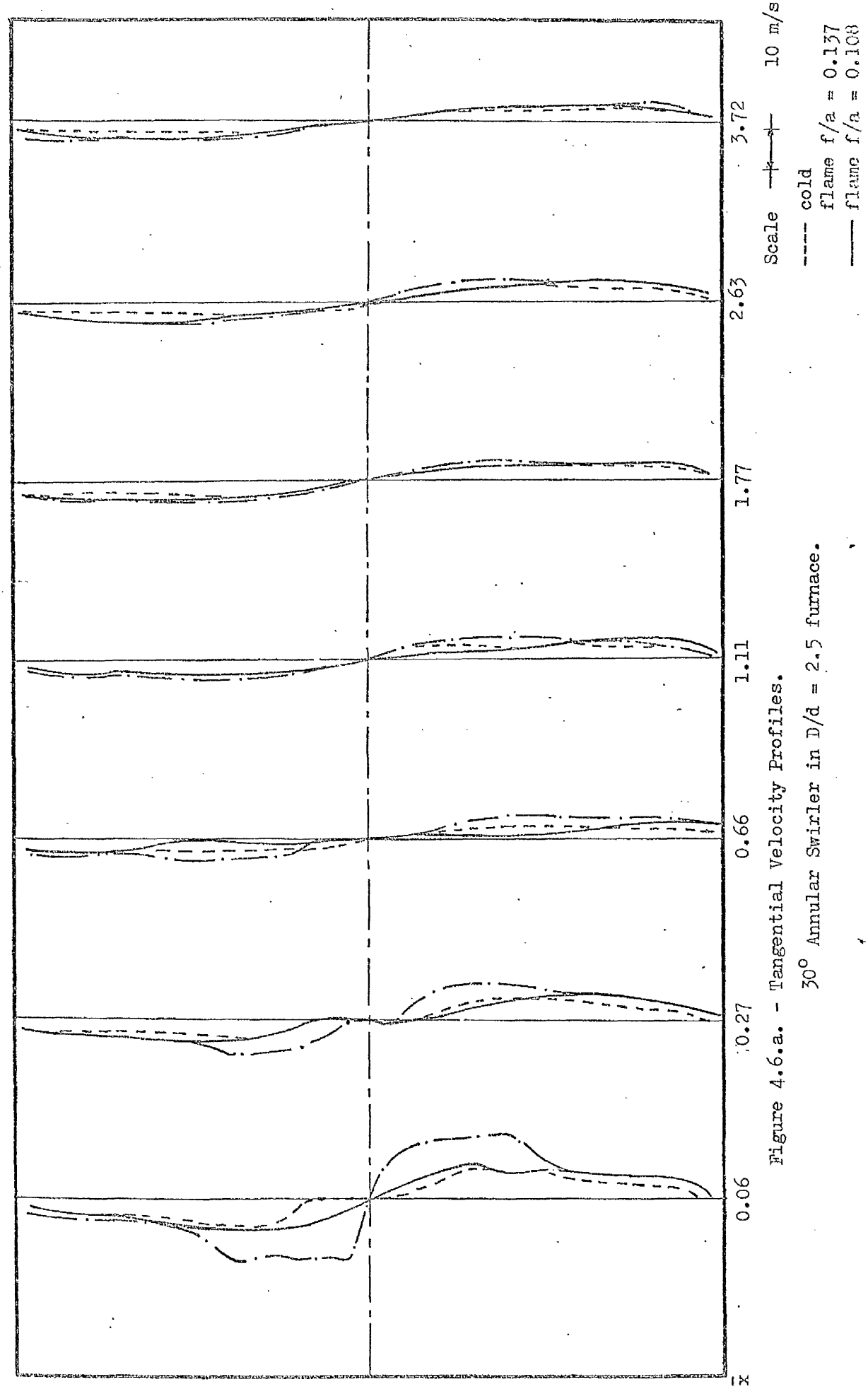

Figure 4.6.a. - Tangential Velocity Profiles.
30° Annular Swirler in D/d = 2.5 furnace.

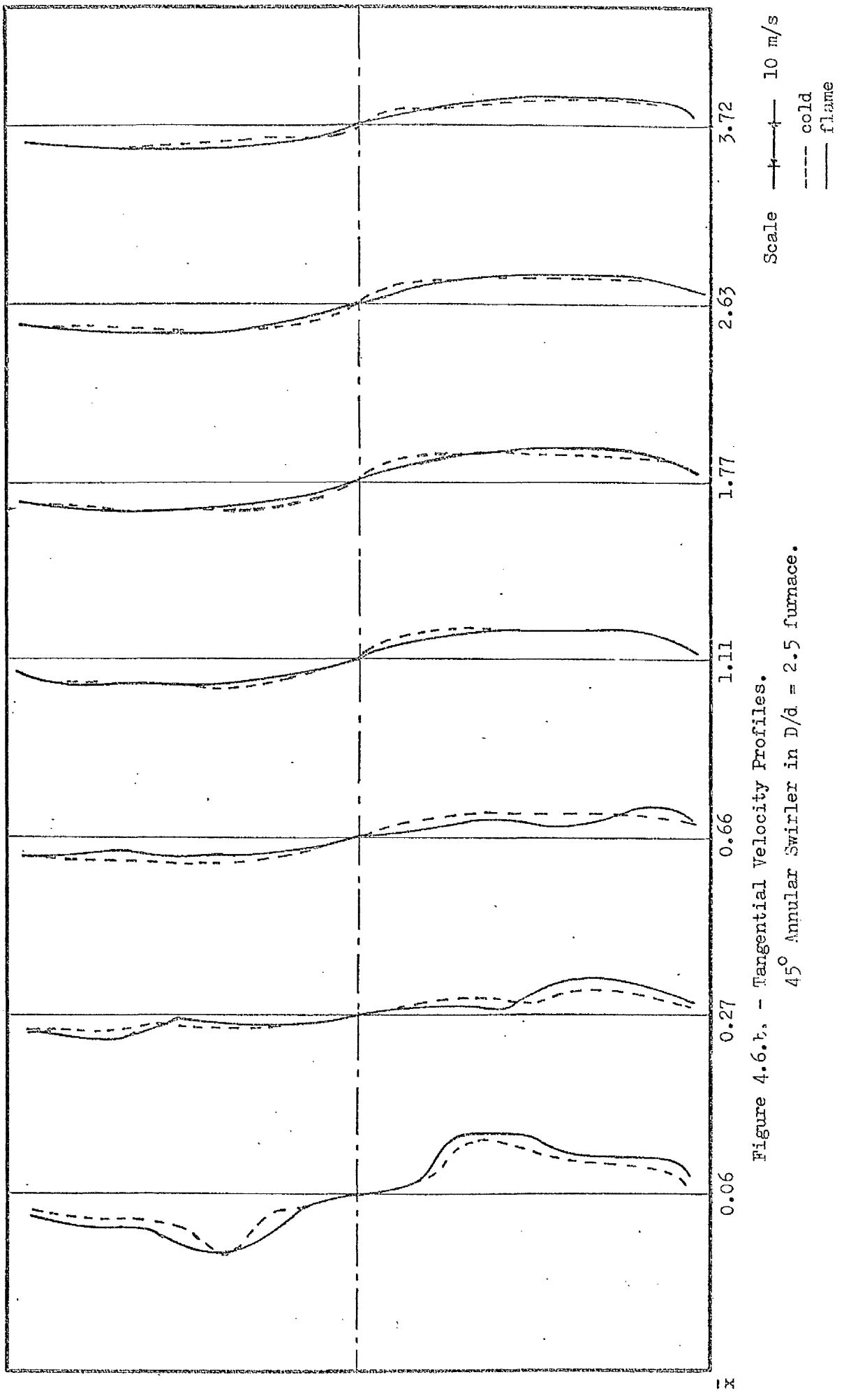

Figure 4.6.b. - Tangential Velocity Profiles.
45° Annular Swirler in D/d = 2.5 furnace.

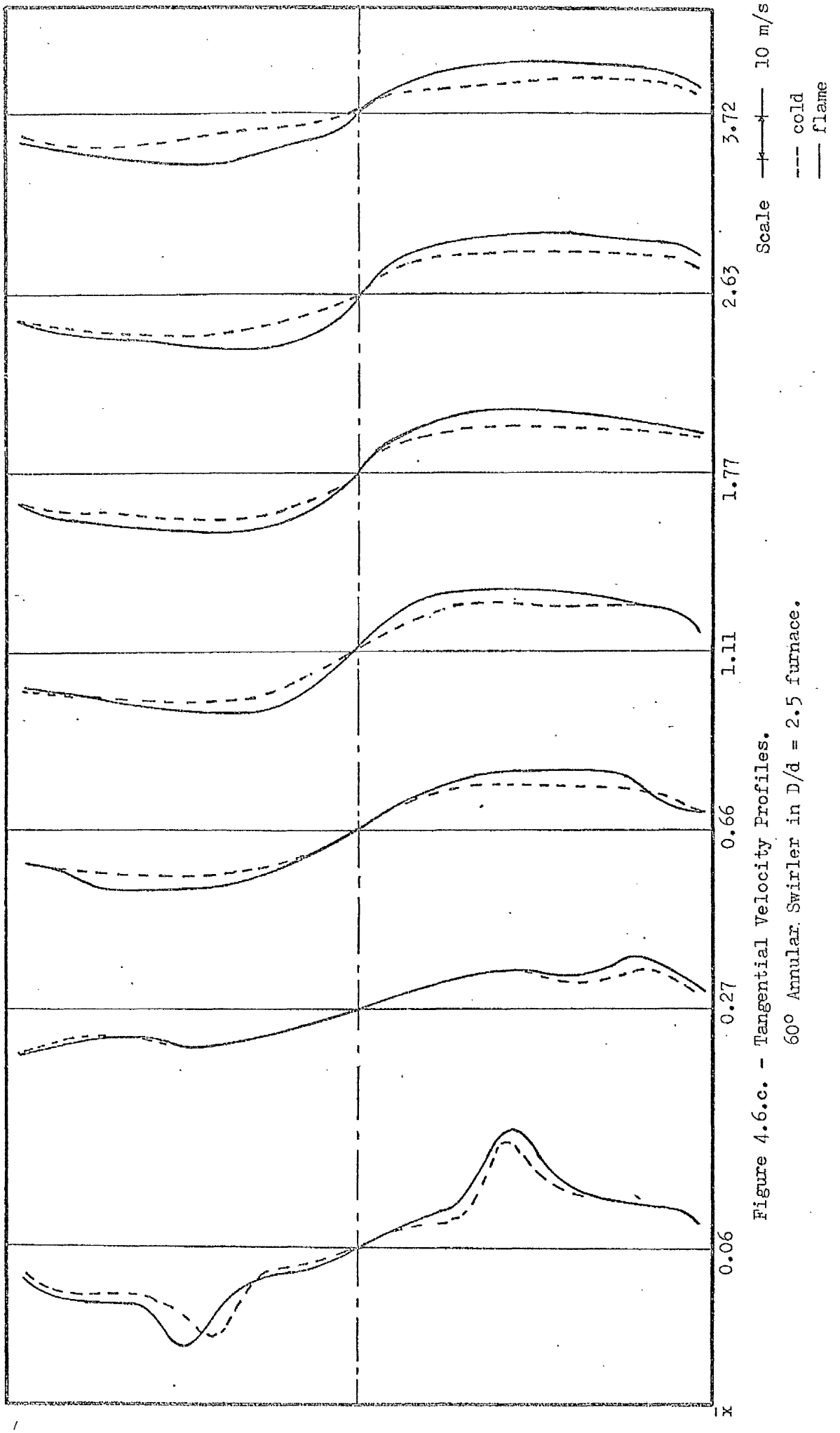

Figure 4.6.c. - Tangential Velocity Profiles.
60° Annular Swirler in D/d = 2.5 furnace.

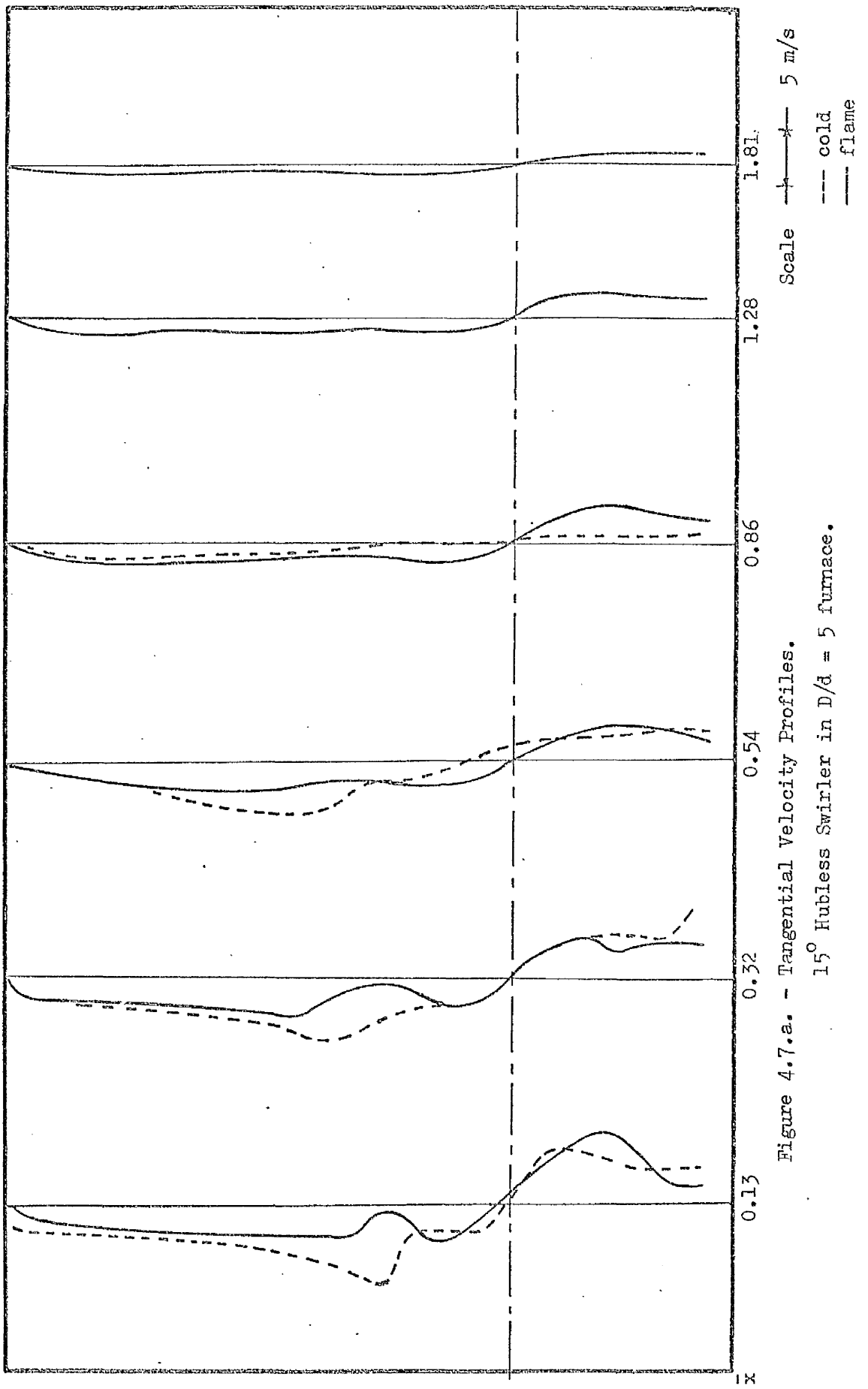

Figure 4.7.a. - Tangential Velocity Profiles.
15^{o} Hubless Swirler in D/d = 5 furnace.

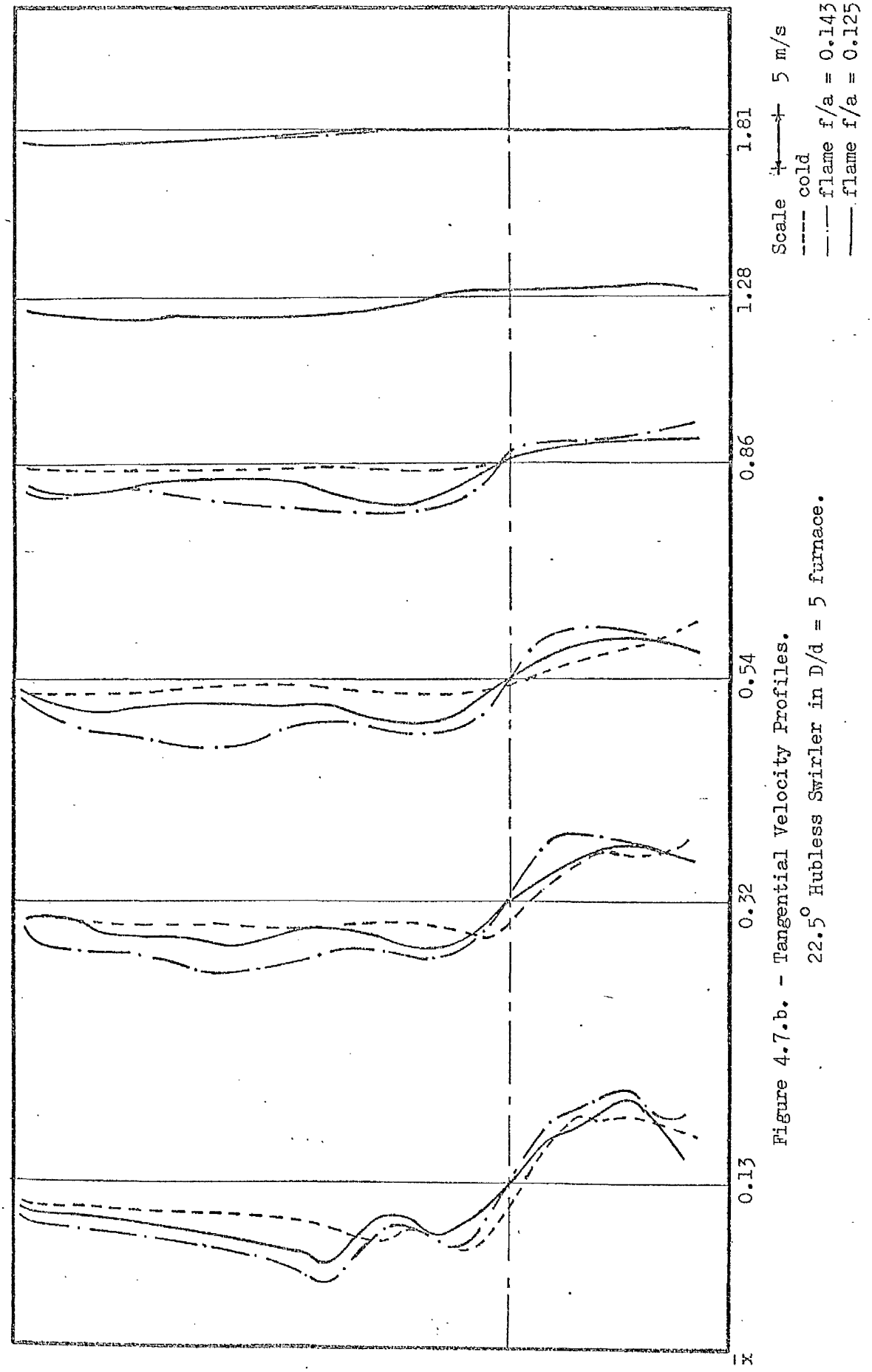

Figure 4.7.b. - Tangential Velocity Profiles.
22.5^{o} Hubless Swirler in D/d = 5 furnace.

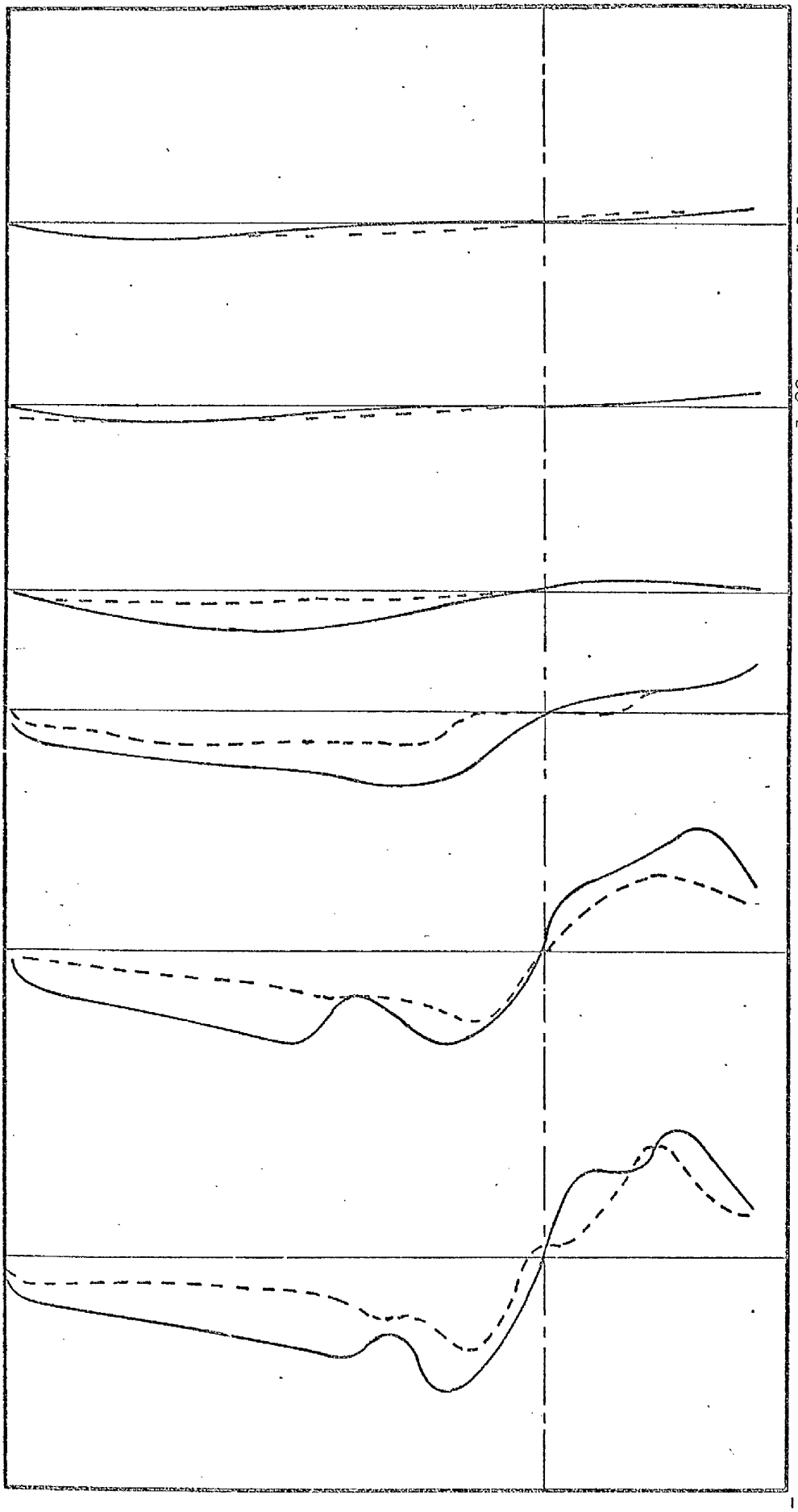

Figure 4.7.c. - Tangential Velocity Profiles.
30^{o} Hubless Swirler in D/d = 5 furnace.

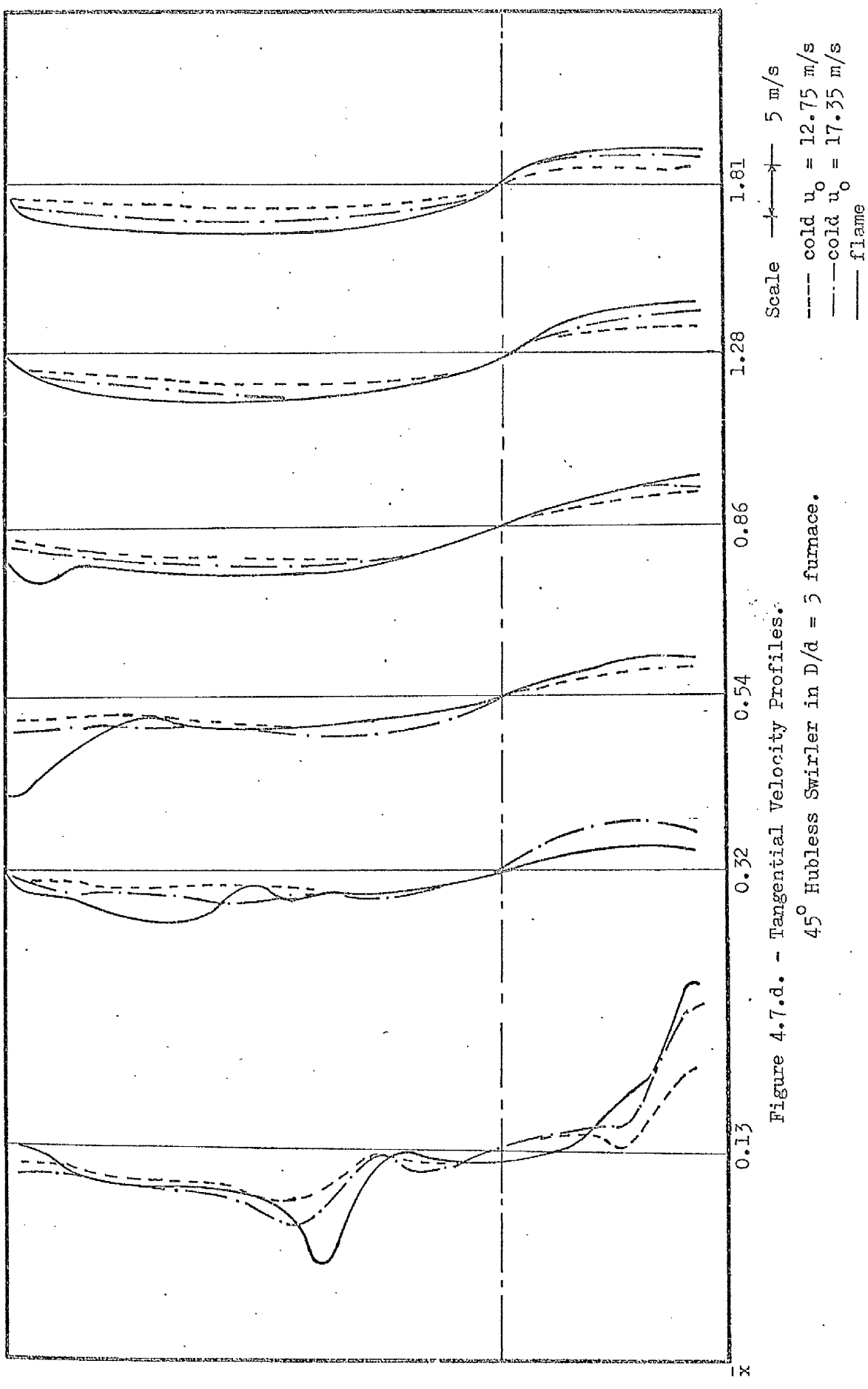

Figure 4.7.d. - Tangential Velocity Profiles.
45° Hubless Swirler in D/d = 3 furnace.

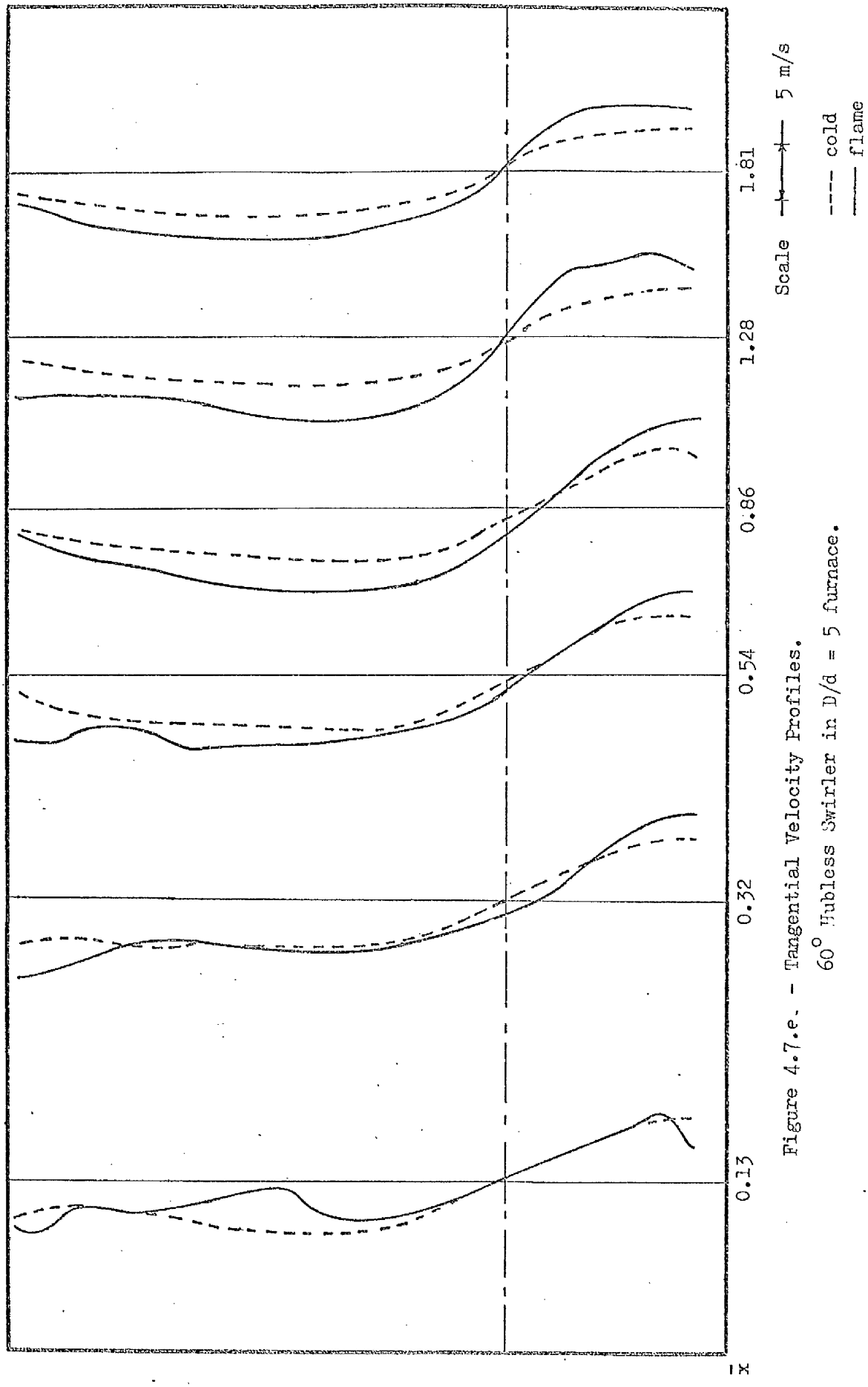

Figure 4.7.e. - Tangential Velocity Profiles.
60^{o} Hubless Swirler in D/d = 5 furnace.

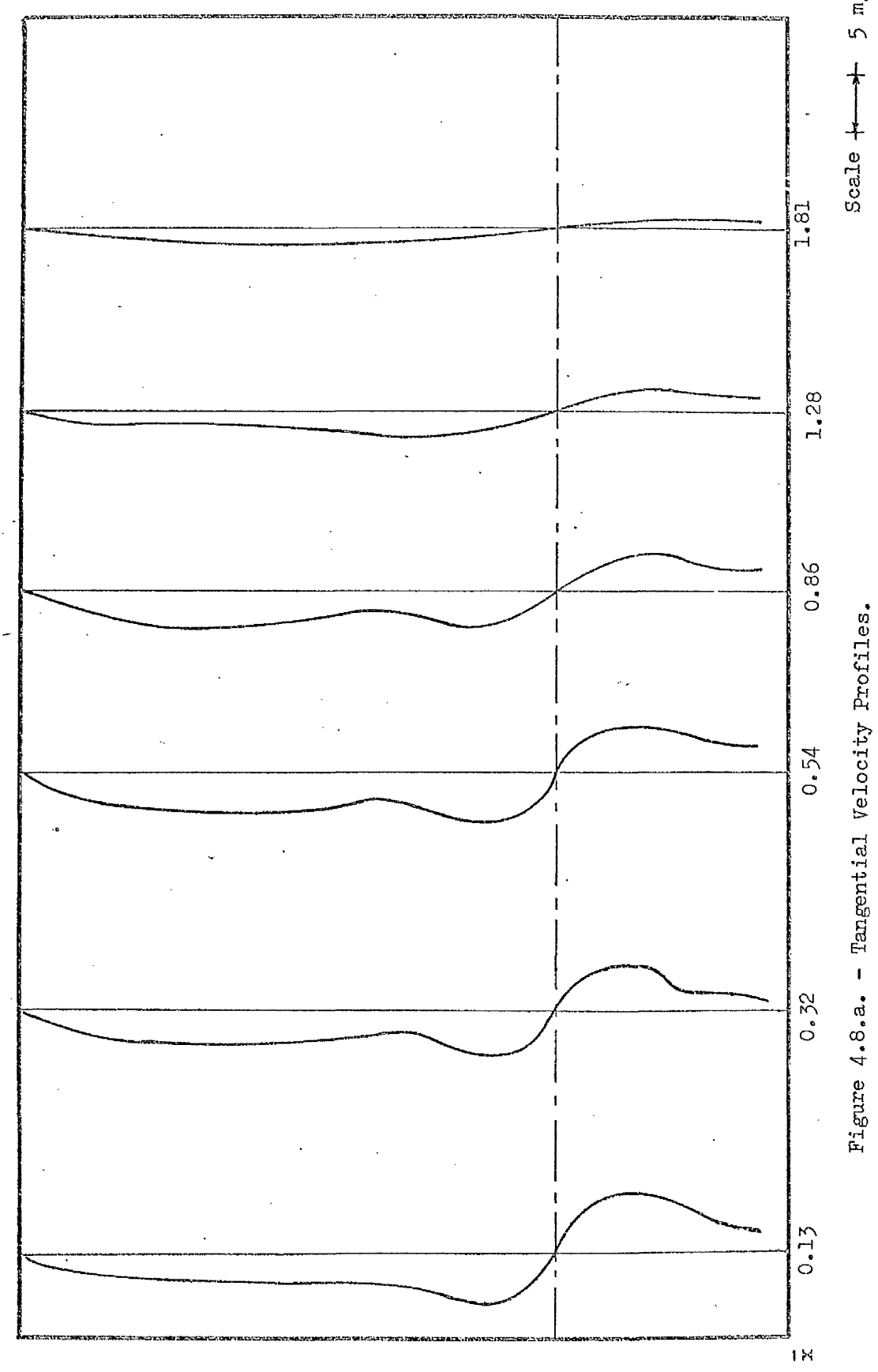

Figure 4.8.a. - Tangential Velocity Profiles.
15° Annular Swirler flame in D/d = 5 furnace.

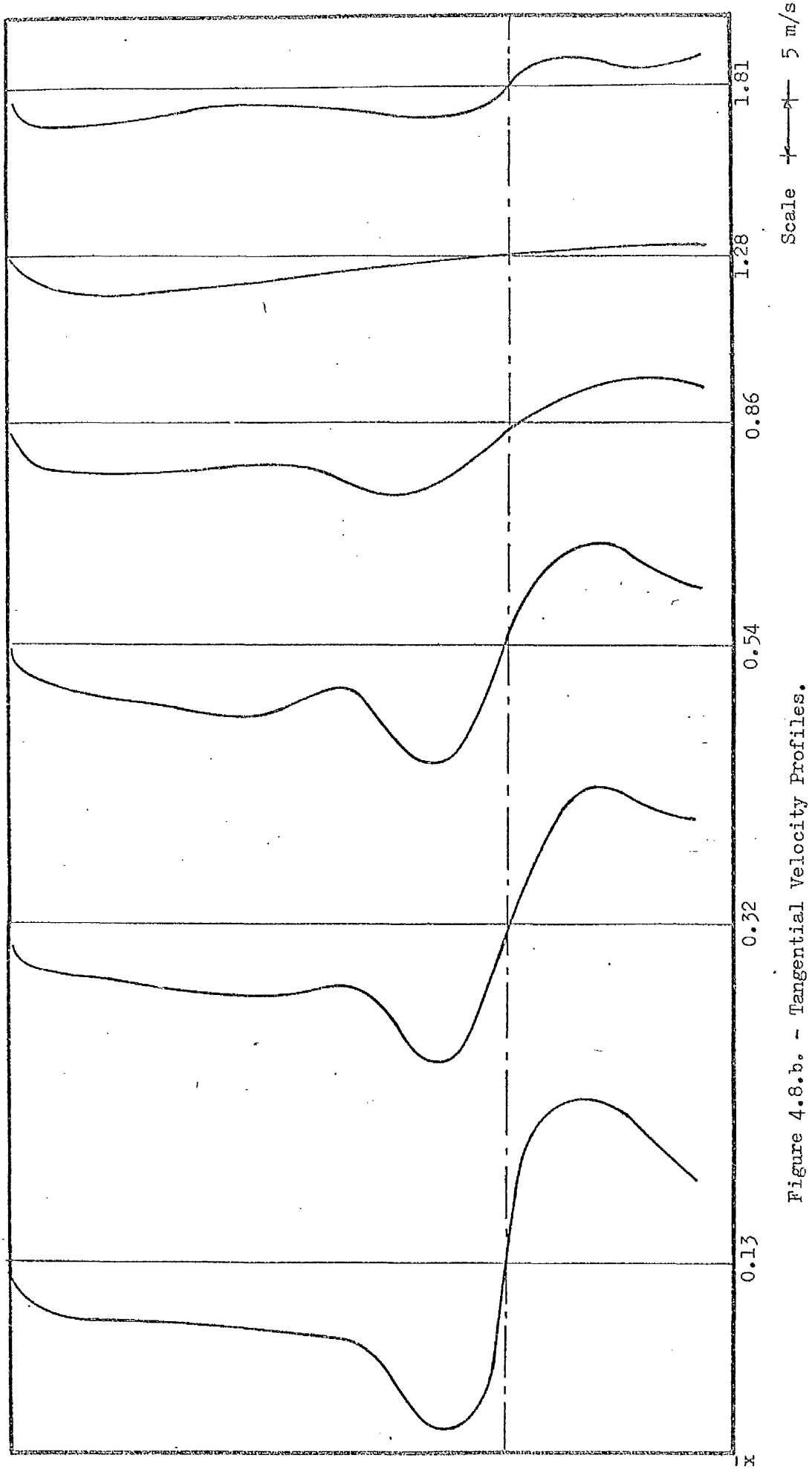

Figure 4.8.b. - Tangential Velocity Profiles.
30° Annular Swirler flame in D/d = 5 furnace.

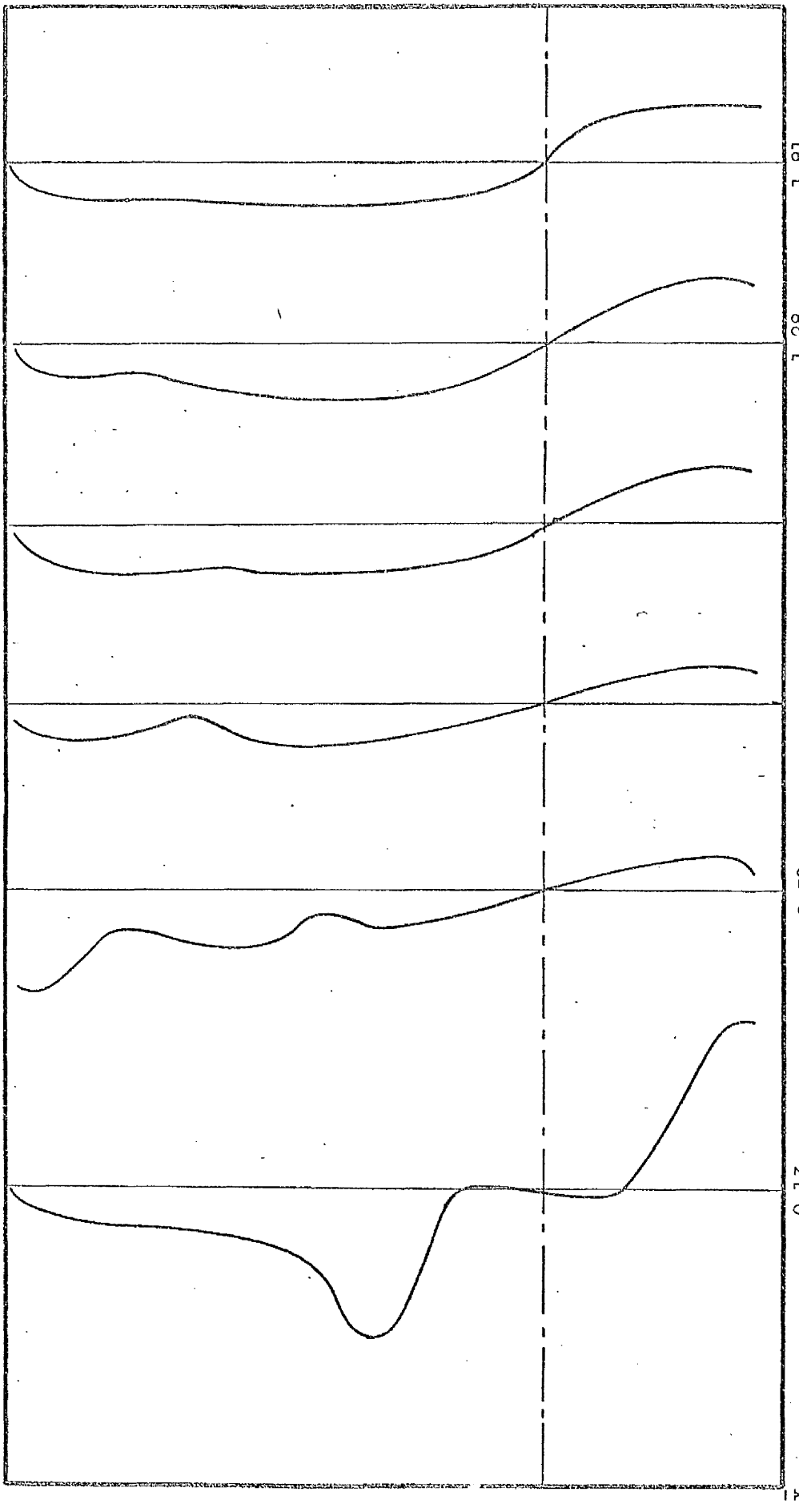

Figure 4.8.c. - Tangential Velocity Profiles.
45° Annular Swirler flame in D/d = 5 furnace.

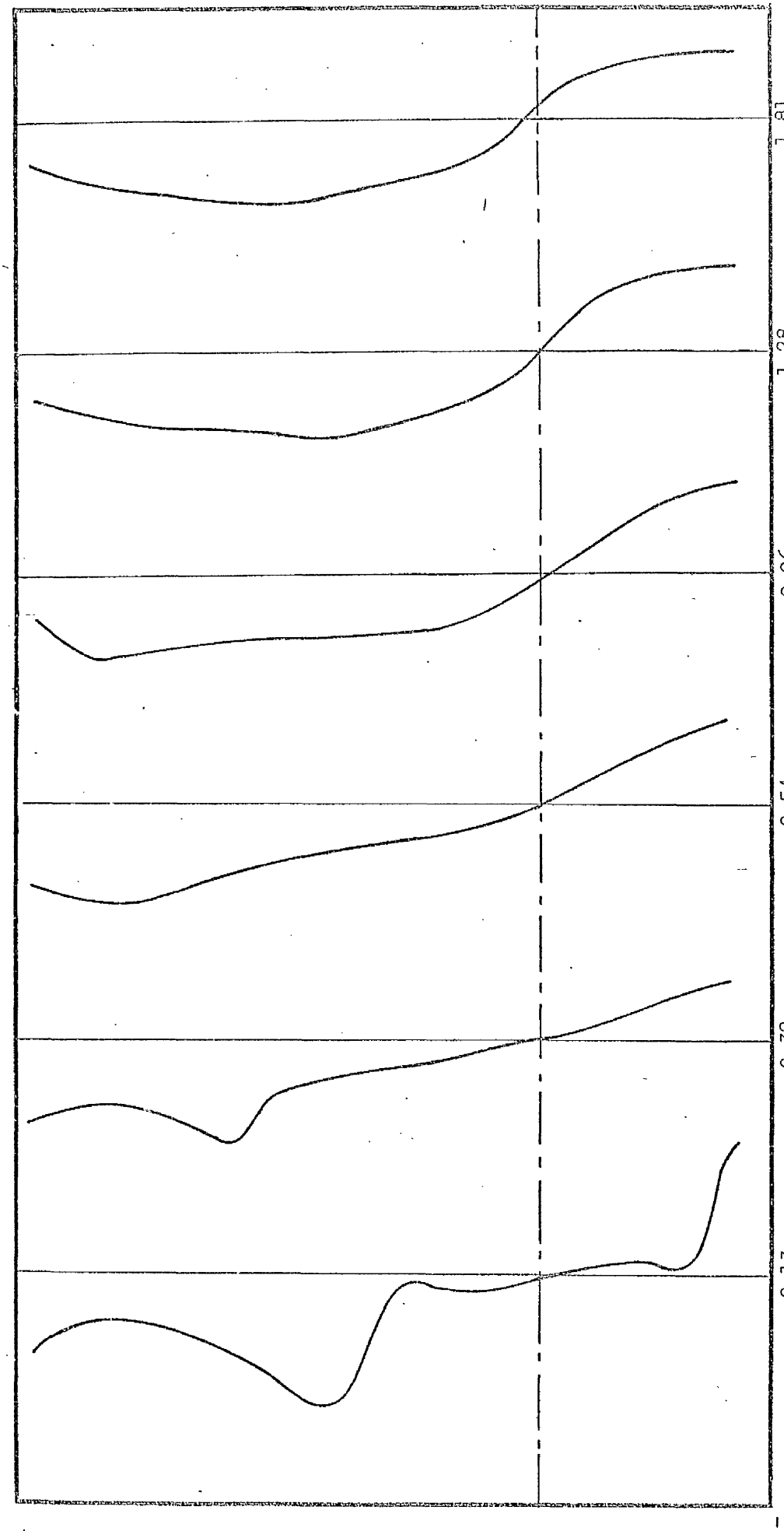

Figure 4.8.d. - Tangential Velocity Profiles.
60^{o} Annular Swirler flame in D/d = 5 furnace.

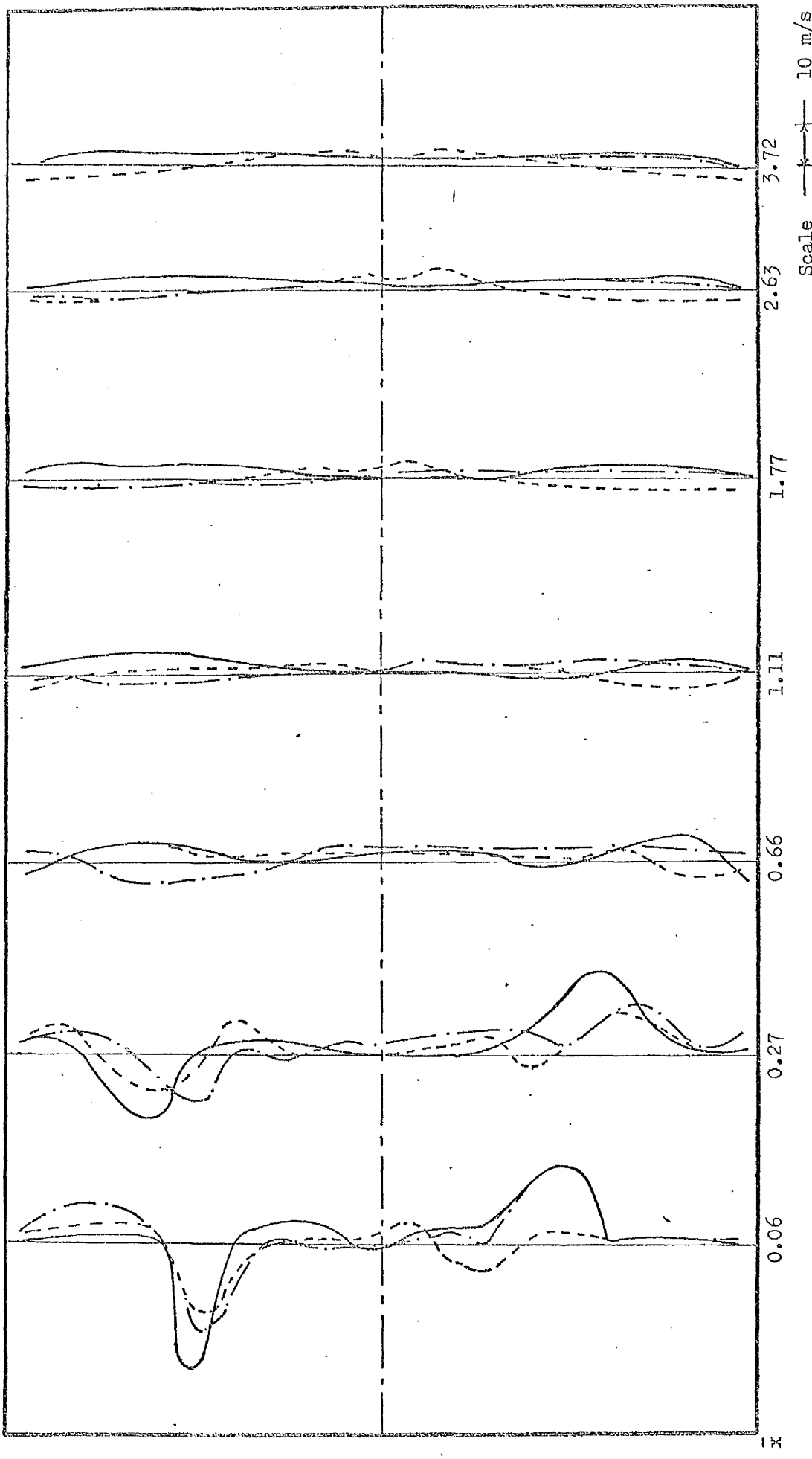

Figure 4.9.a. - Radial Velocity Profiles.
30° Hubless Swirler in D/d = 2.5 furnace.

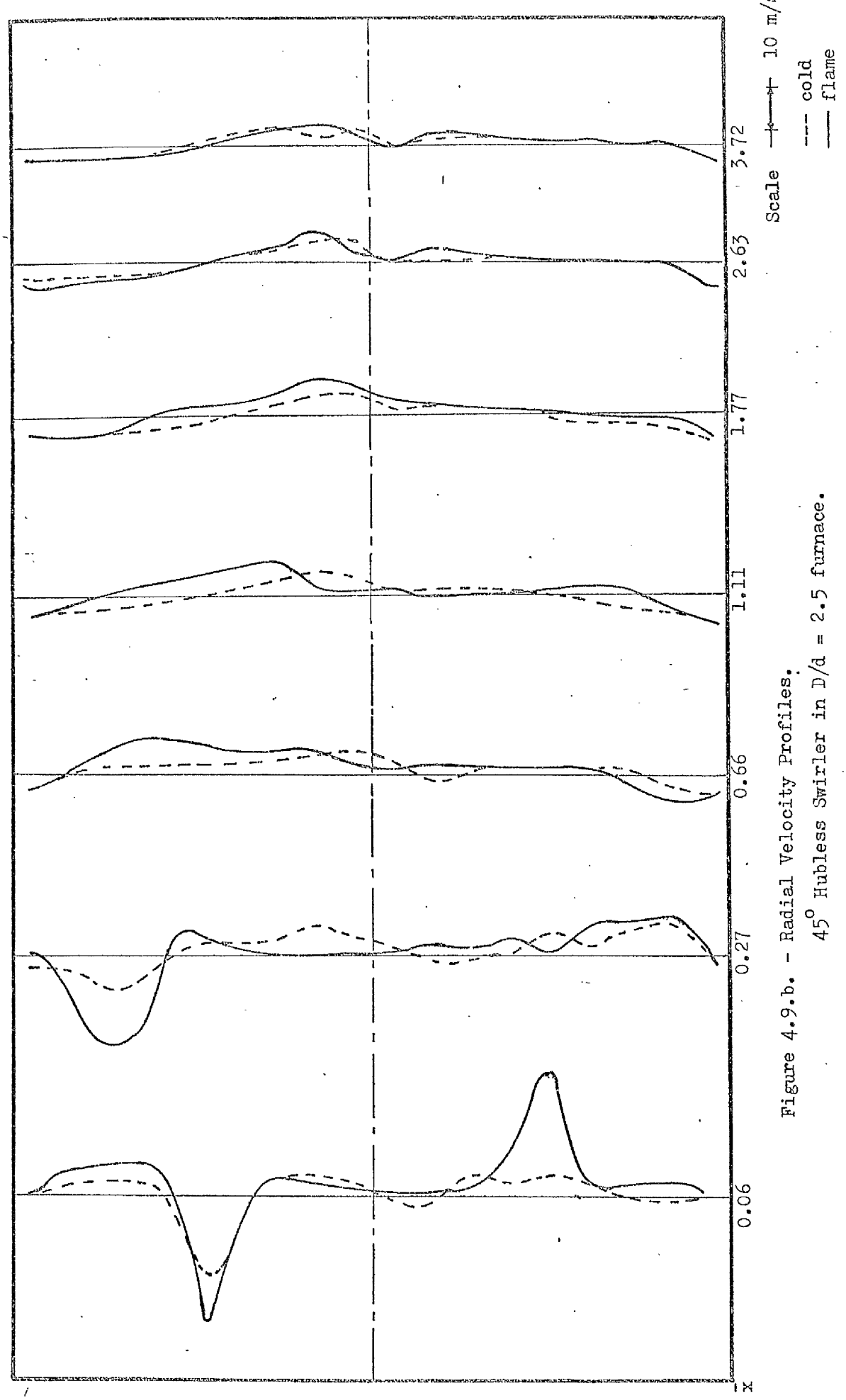

Figure 4.9.b. - Radial Velocity Profiles.
45° Hubless Swirler in D/d = 2.5 furnace.

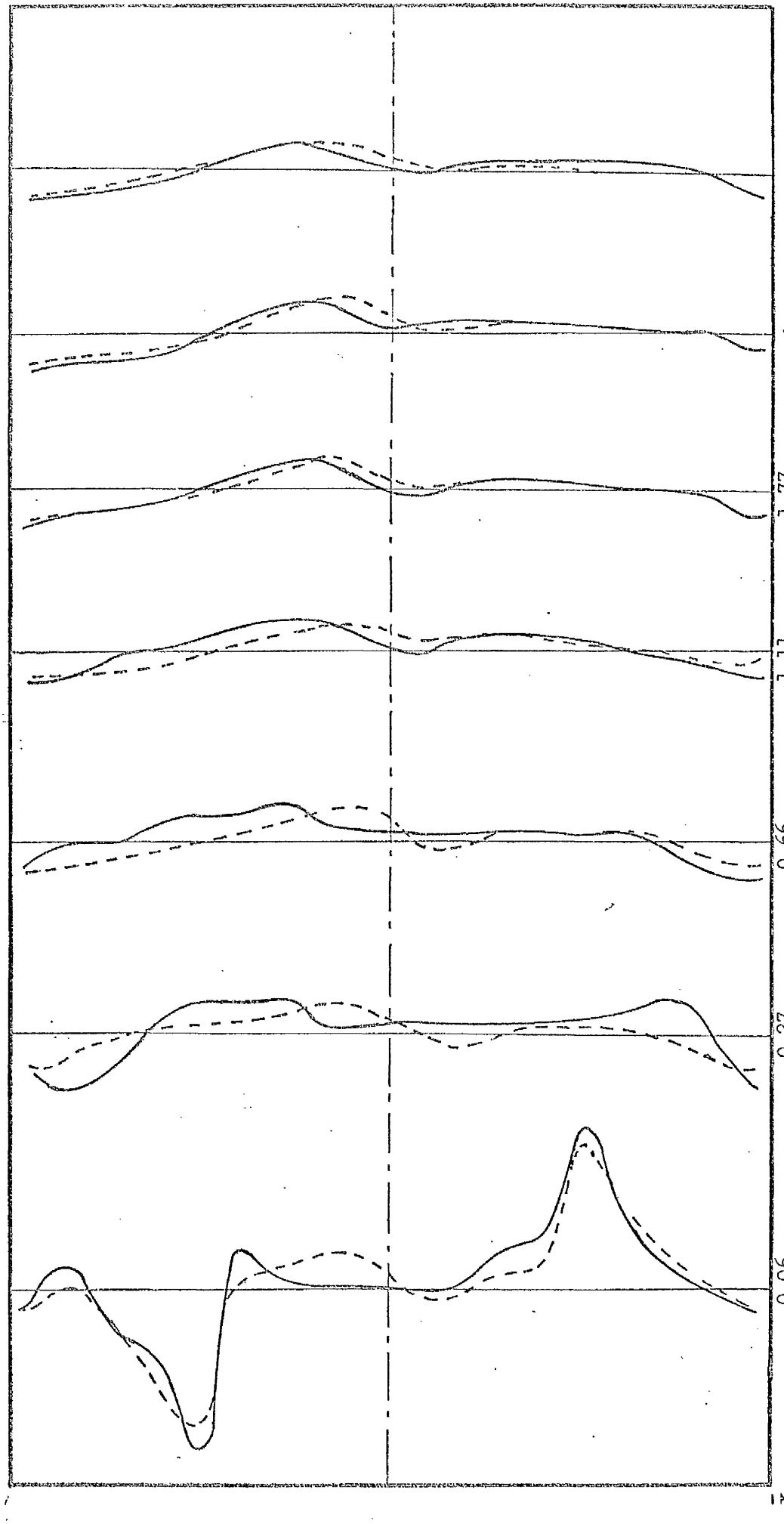

Figure 4.9.c. - Radial Velocity Profiles.
60^{o} Hubless Swirler in D/d = 2.5 furnace.

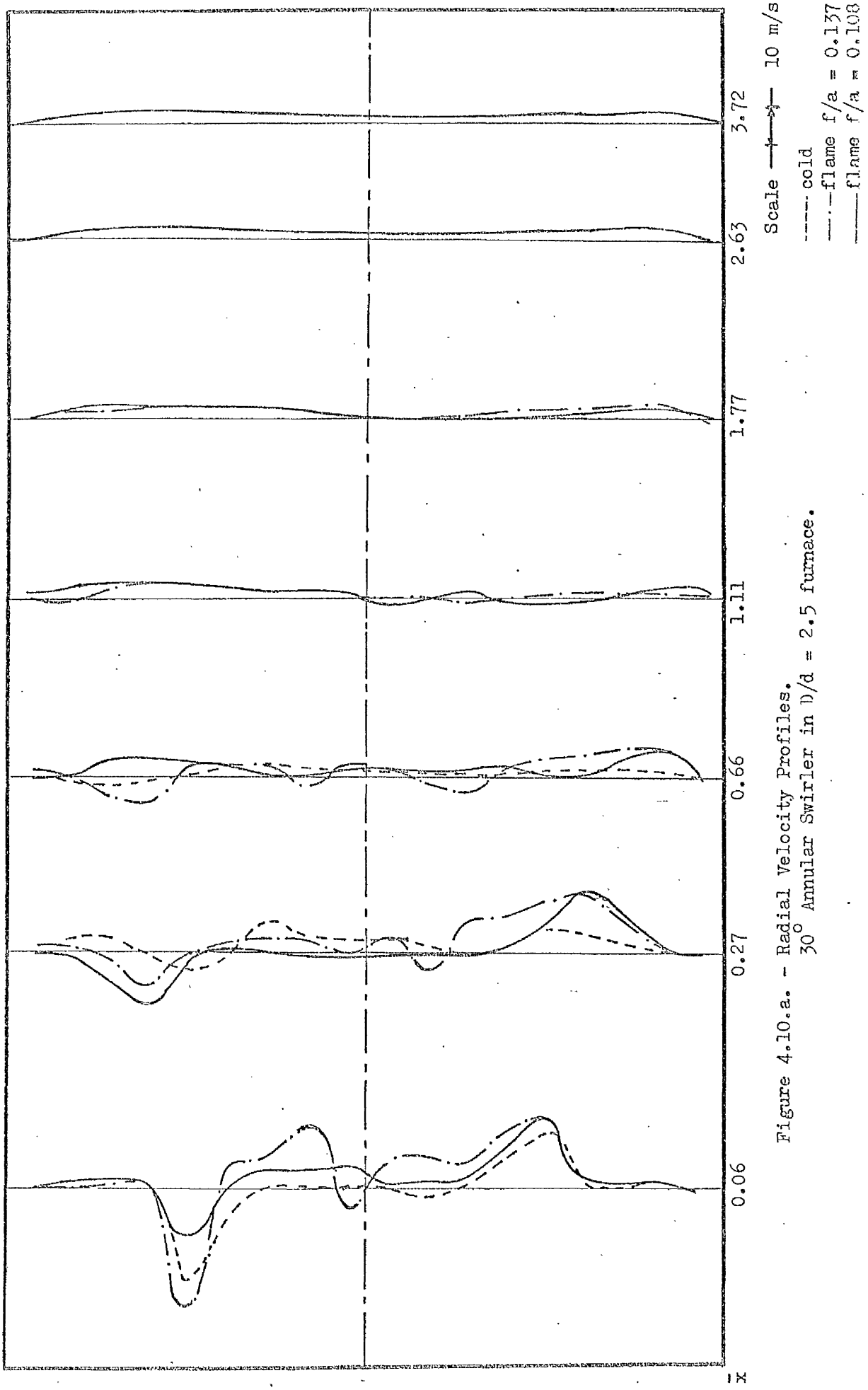

Figure 4.10.a. - Radial Velocity Profiles.
30° Annular Swirler in D/d = 2.5 furnace.

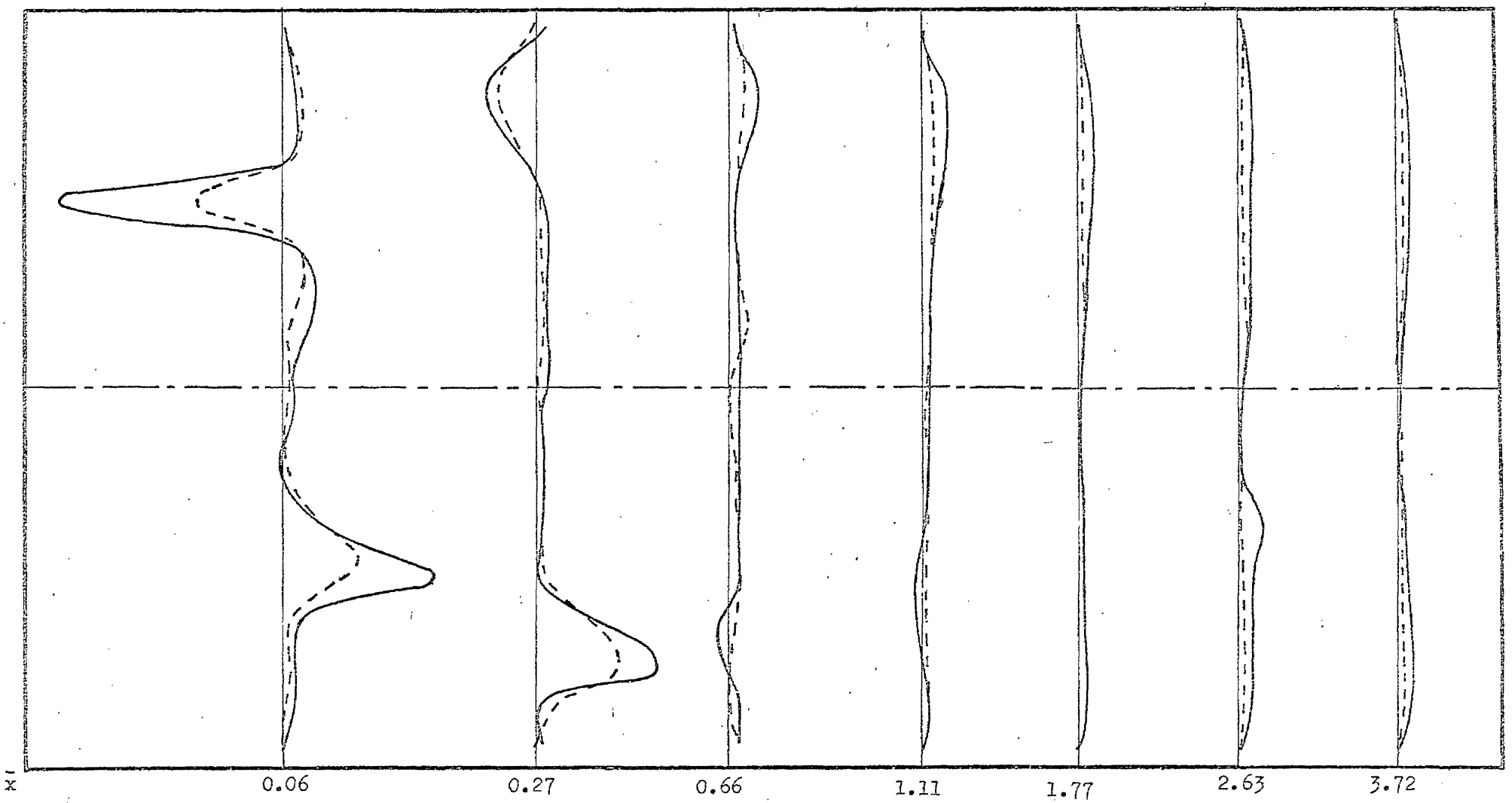

Figure 4.10.b. - Radial Velocity Profiles.
45° Annular Swirler in D/d = 2.5 furnace.

Scale ⟷ 10 m/s
--- cold
—— flame

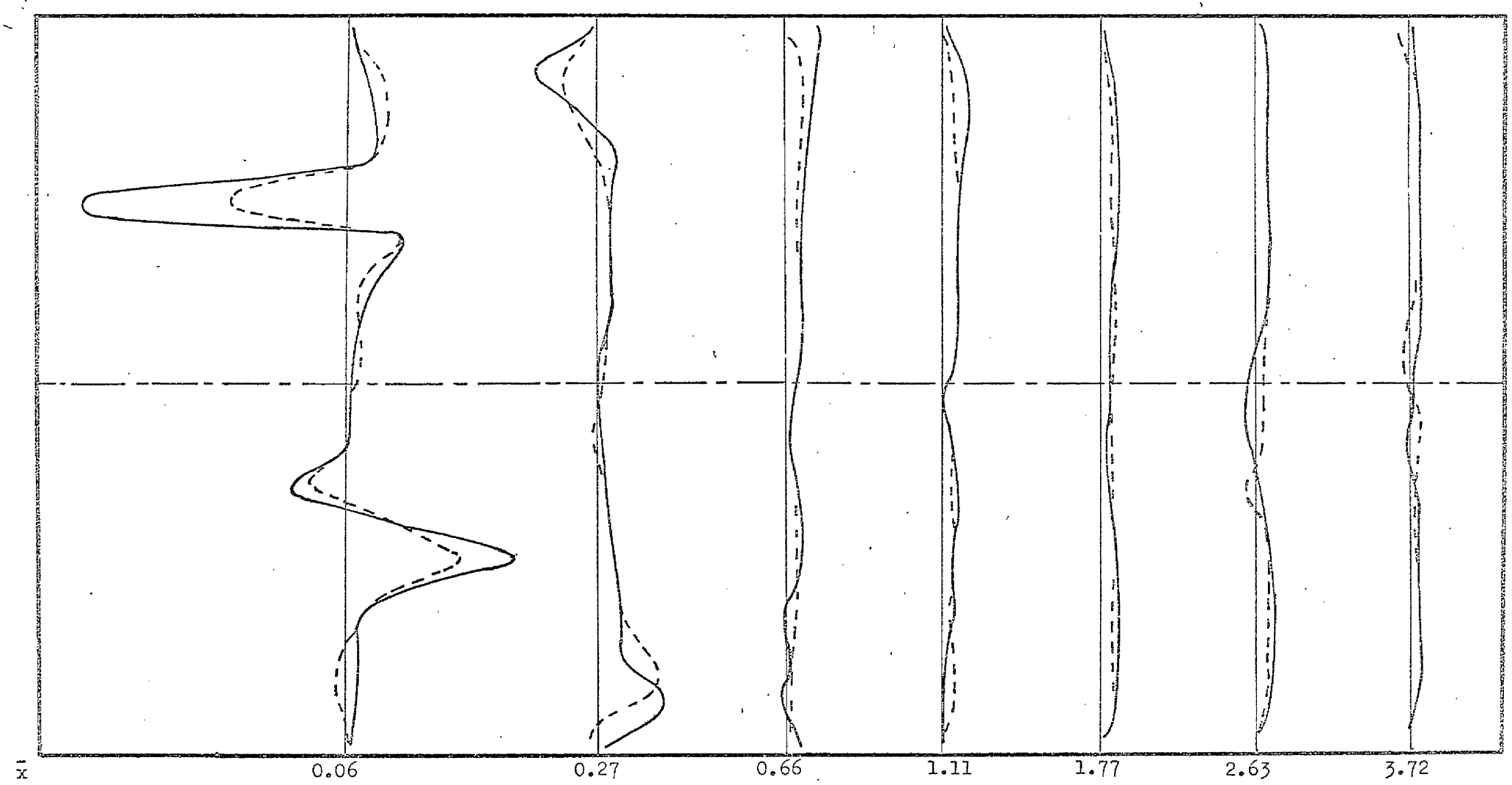

Figure 4.10.c. - Radial Velocity Profiles.
60° Annular Swirler in D/d = 2.5 furnace.

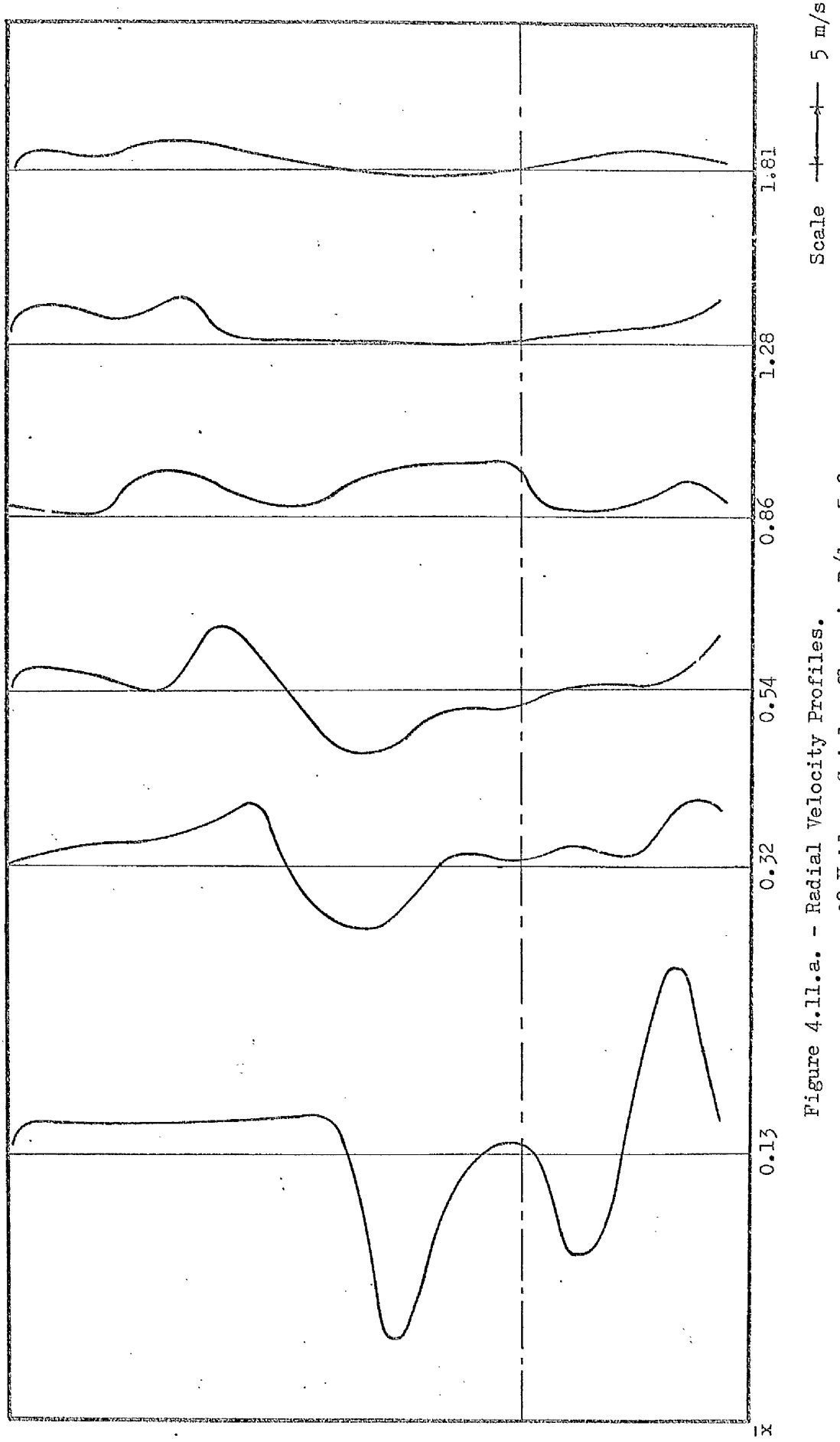

Figure 4.11.a. - Radial Velocity Profiles.
0° Hubless Swirler flame in D/d = 5 furnace.

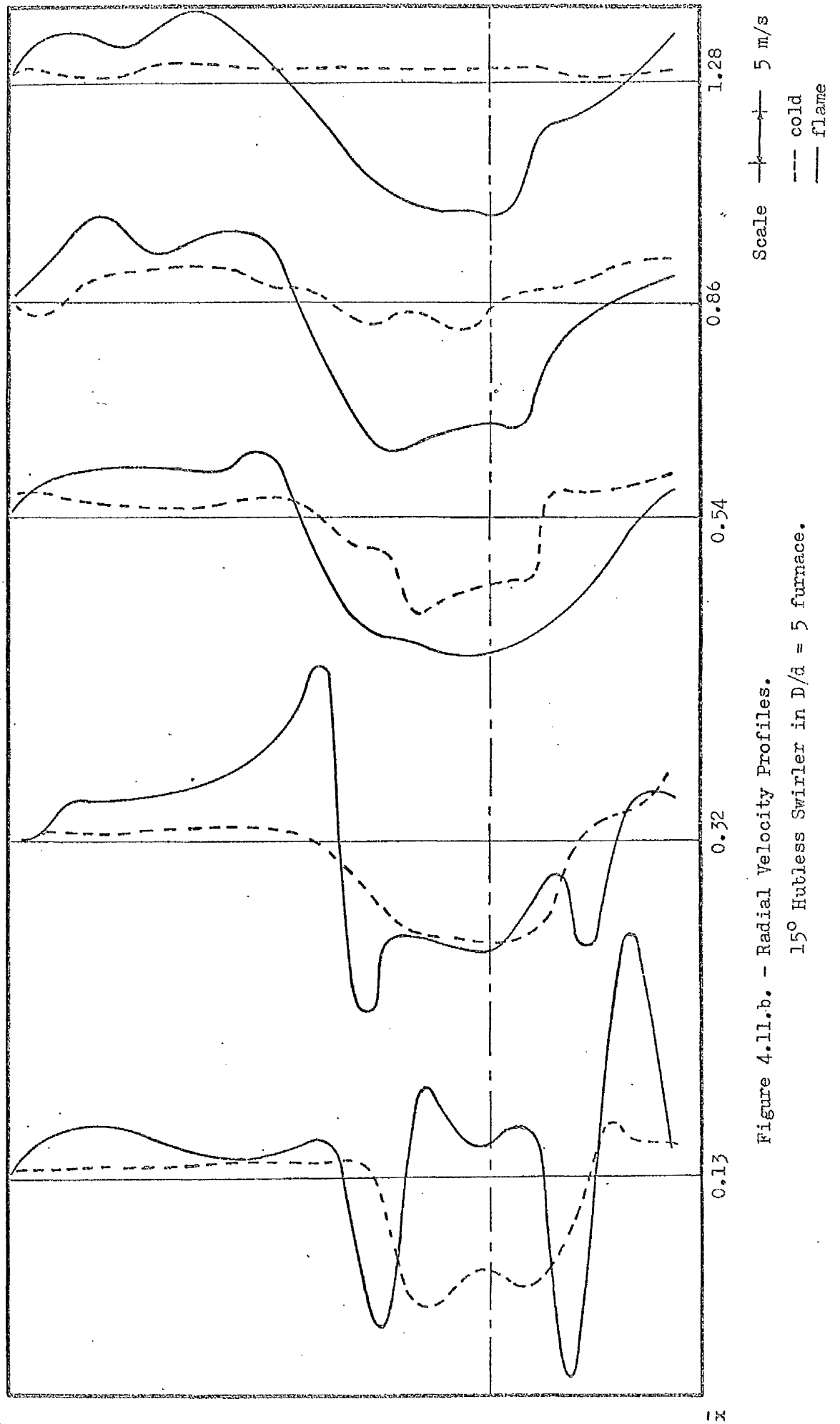

Figure 4.11.b. - Radial Velocity Profiles.
15° Hubless Swirler in D/d = 5 furnace.

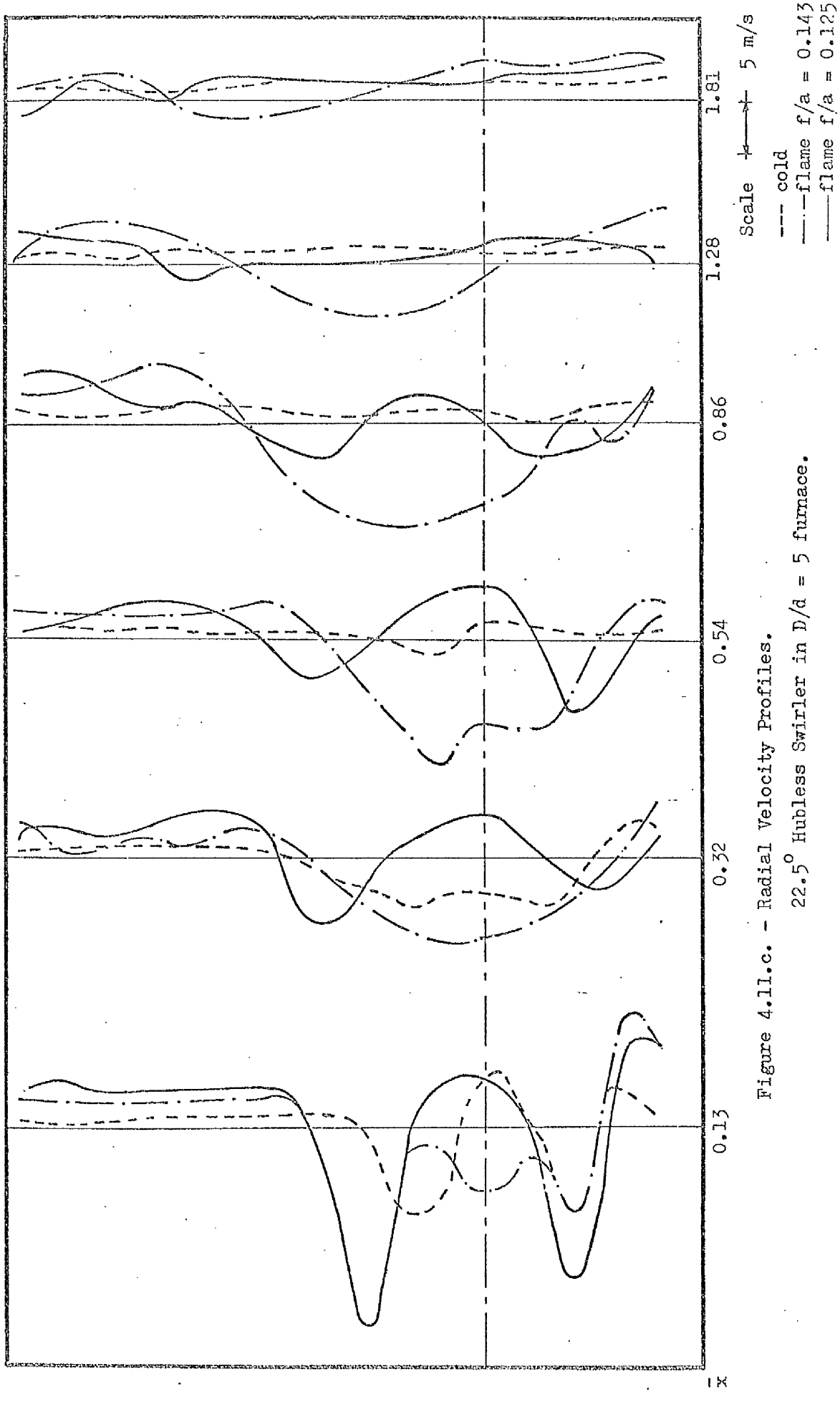

Figure 4.11.c. - Radial Velocity Profiles.
22.5^{o} Hubless Swirler in D/d = 5 furnace.

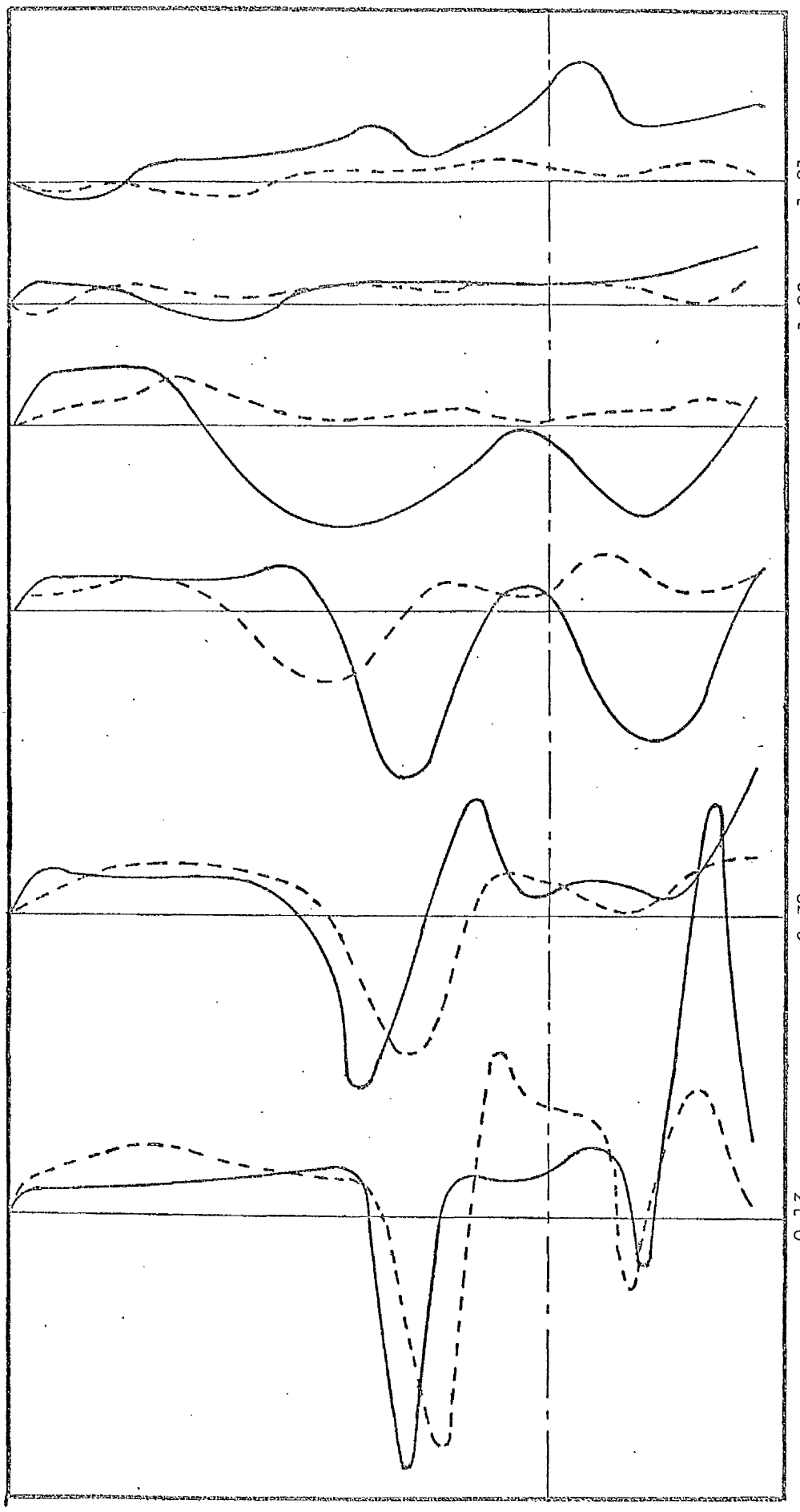

Figure 4.11.d. - Radial Velocity Profiles.
30° Hubless Swirler in D/d = 5 furnace.

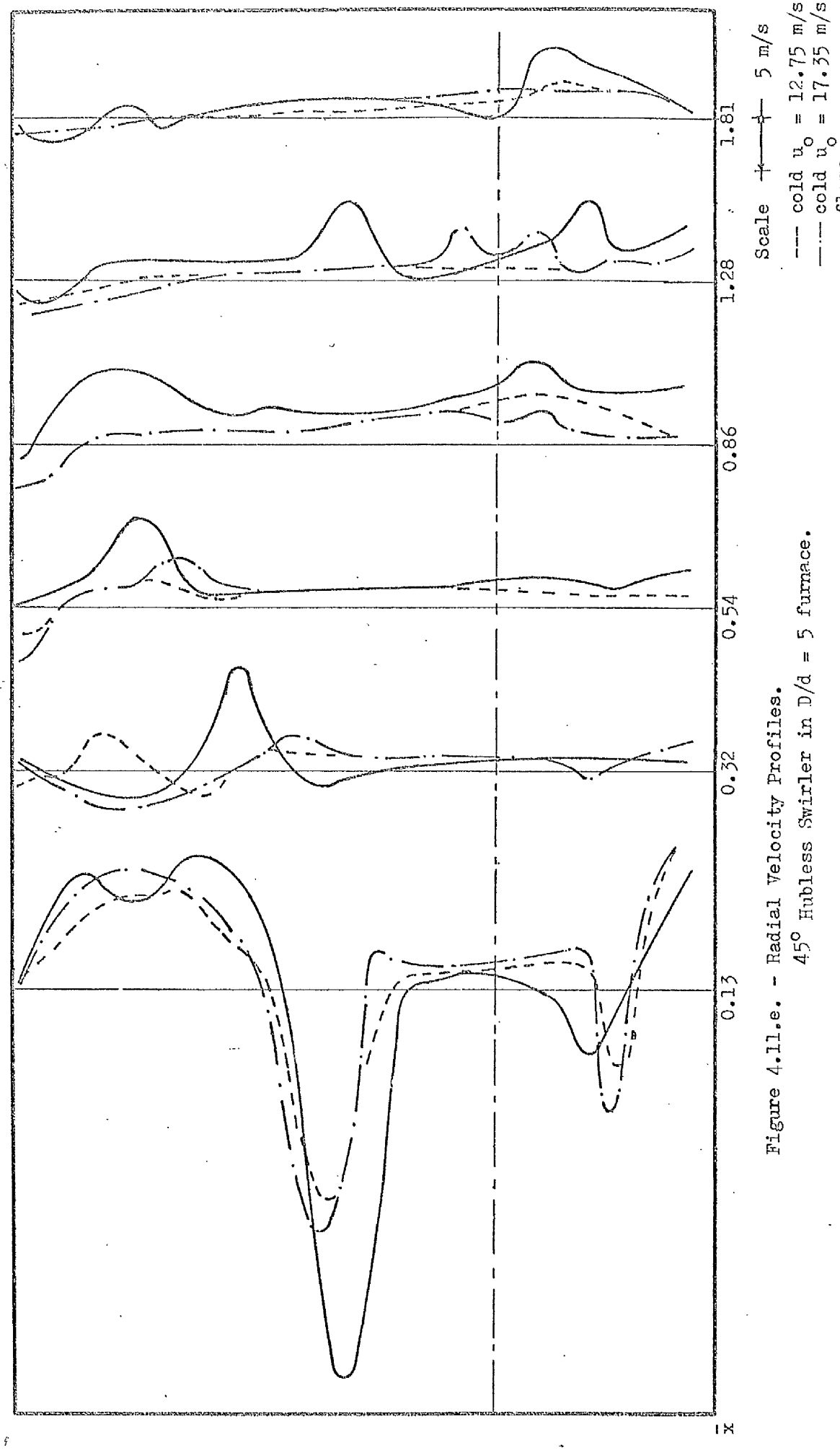

Figure 4.11.e. - Radial Velocity Profiles.
45° Hubless Swirler in D/d = 5 furnace.

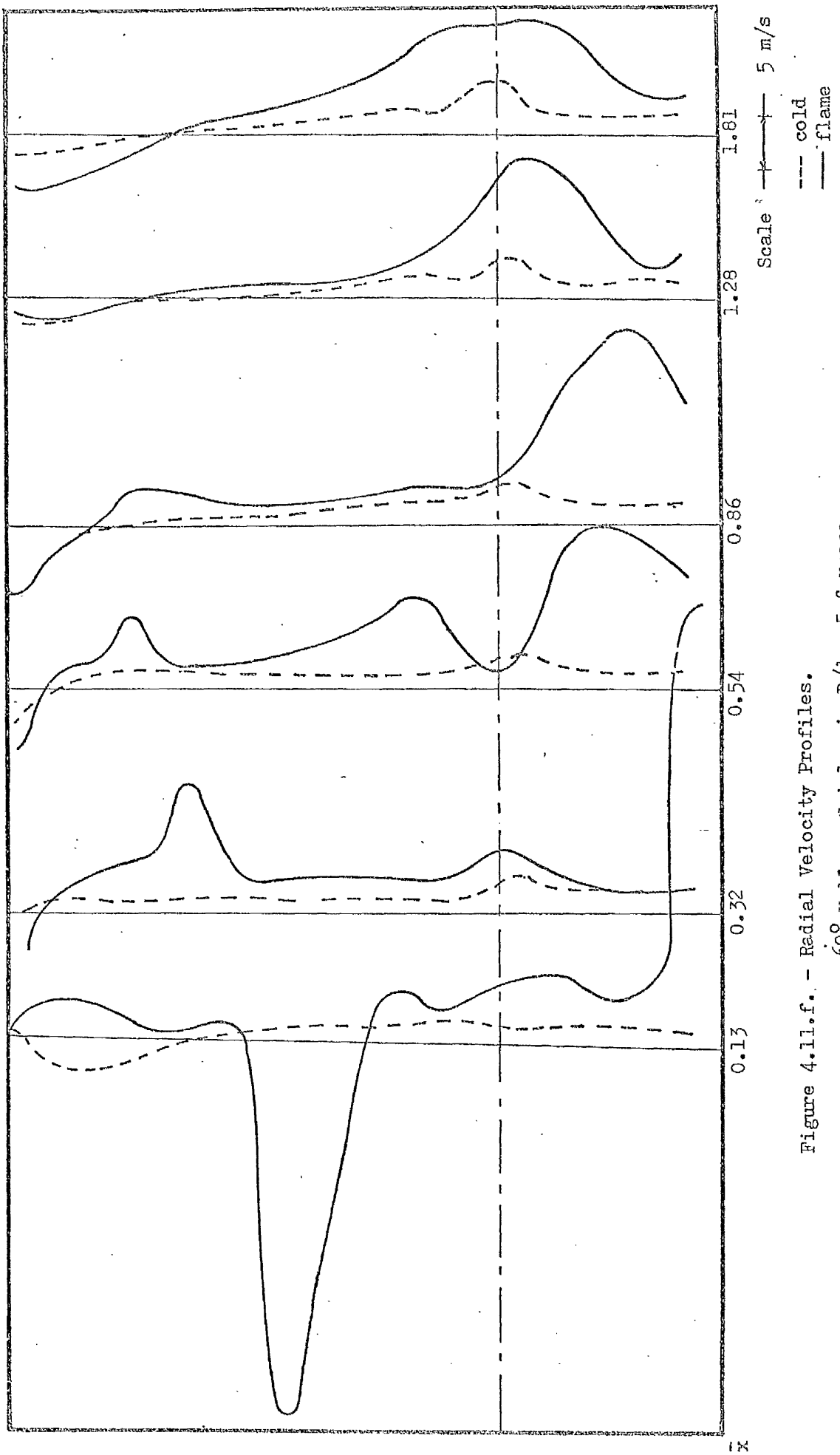

Figure 4.11.f. - Radial Velocity Profiles.
60° Hubless Swirler in D/d = 5 furnace.

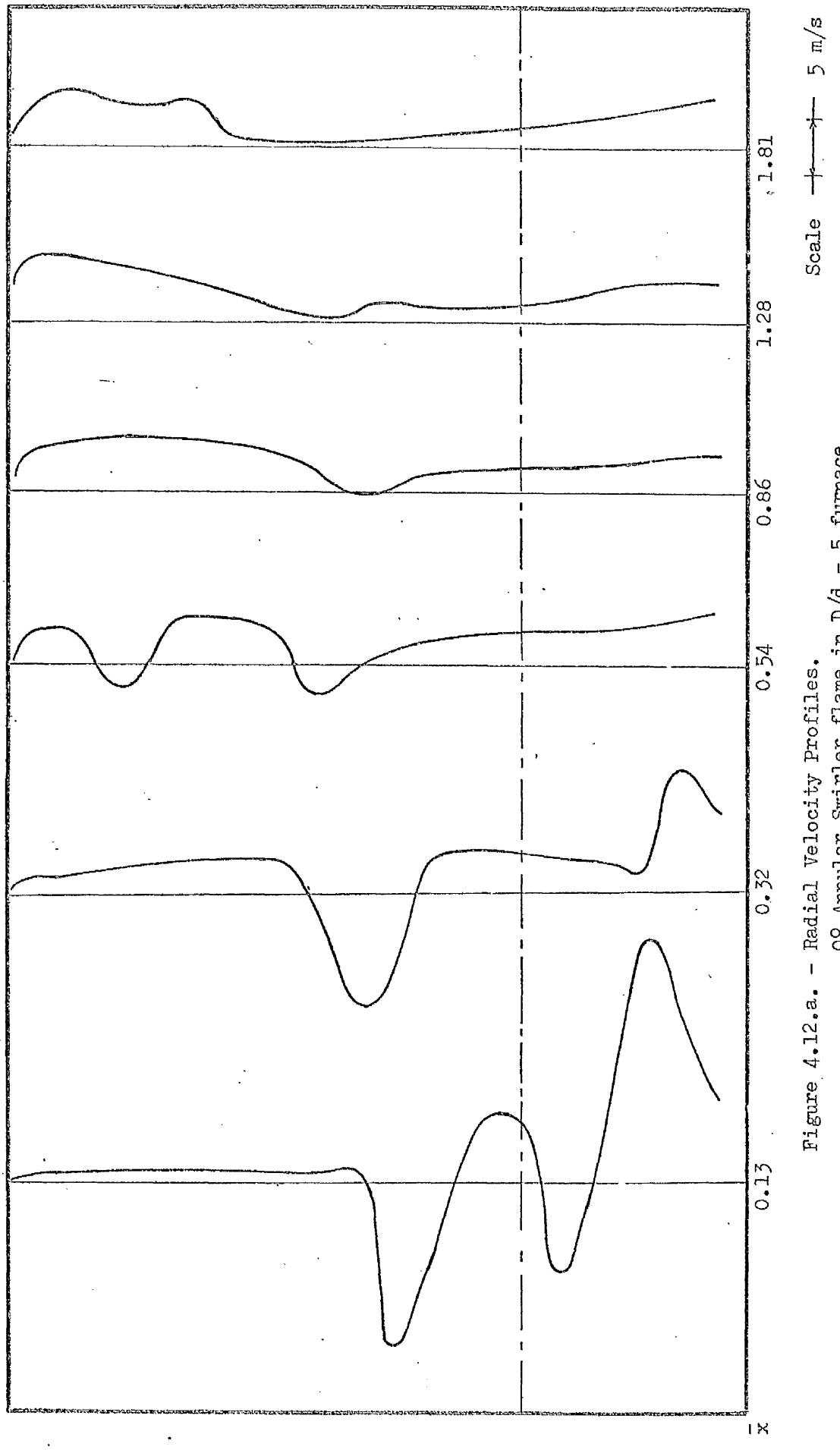

Figure 4.12.a. - Radial Velocity Profiles.
0° Annular Swirler flame in D/d = 5 furnace.

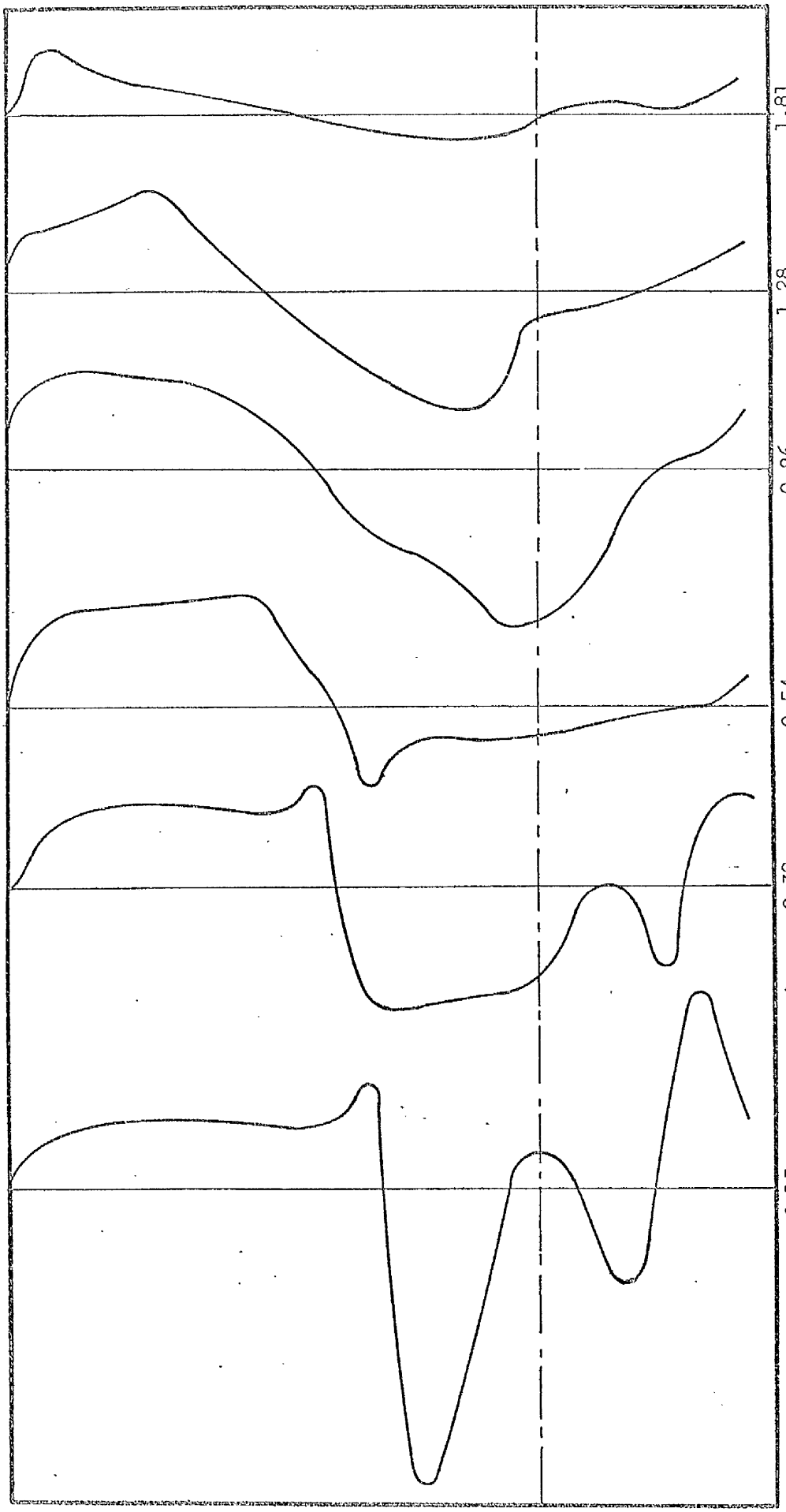

Figure 4.12.b. - Radial Velocity Profiles.
15° Annular Swirler flame in D/d = 5 furnace.

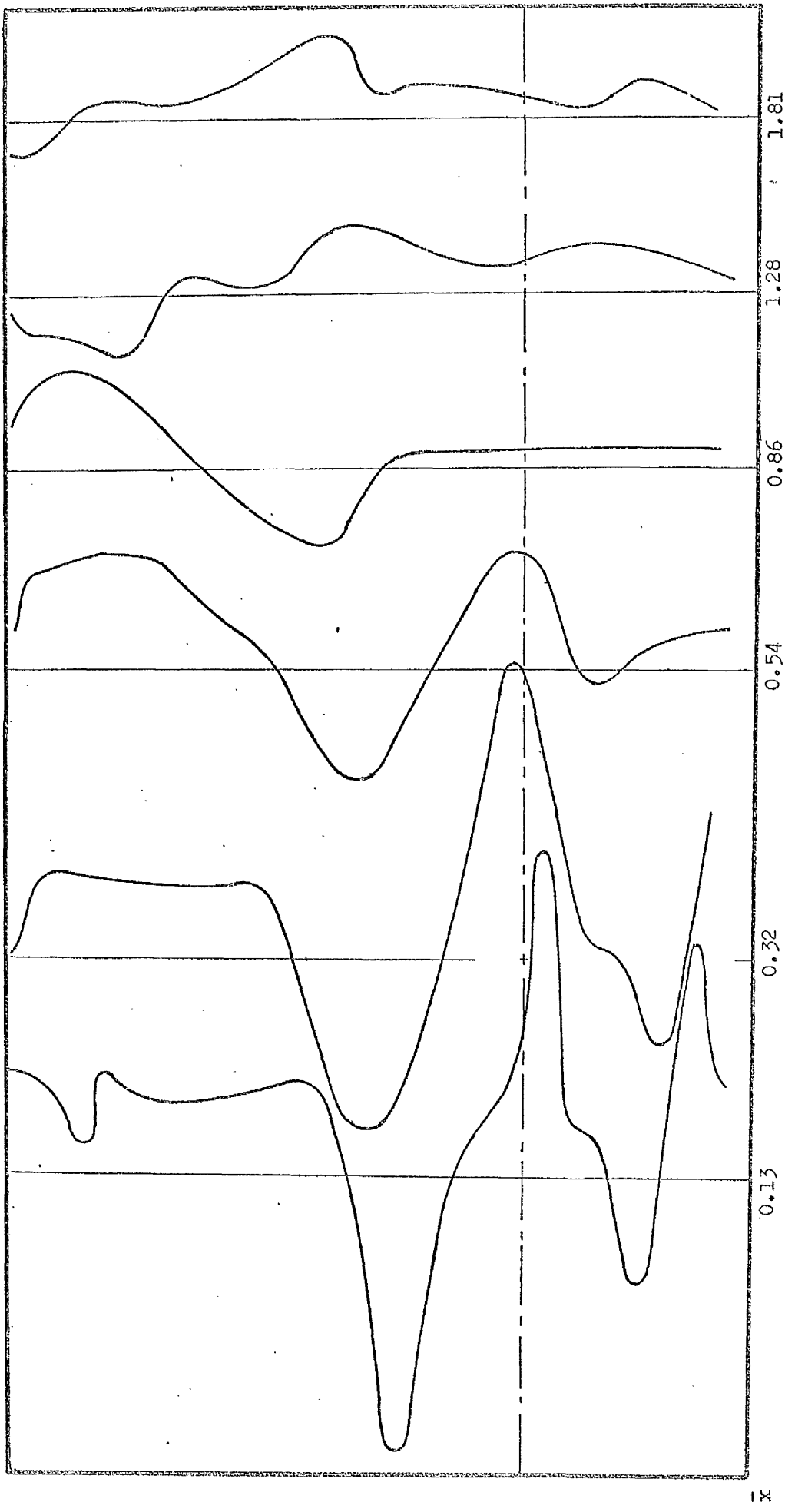

Figure 4.12.c. - Radial Velocity Profiles.
30° Annular Swirler flame in D/d = 5 furnace.

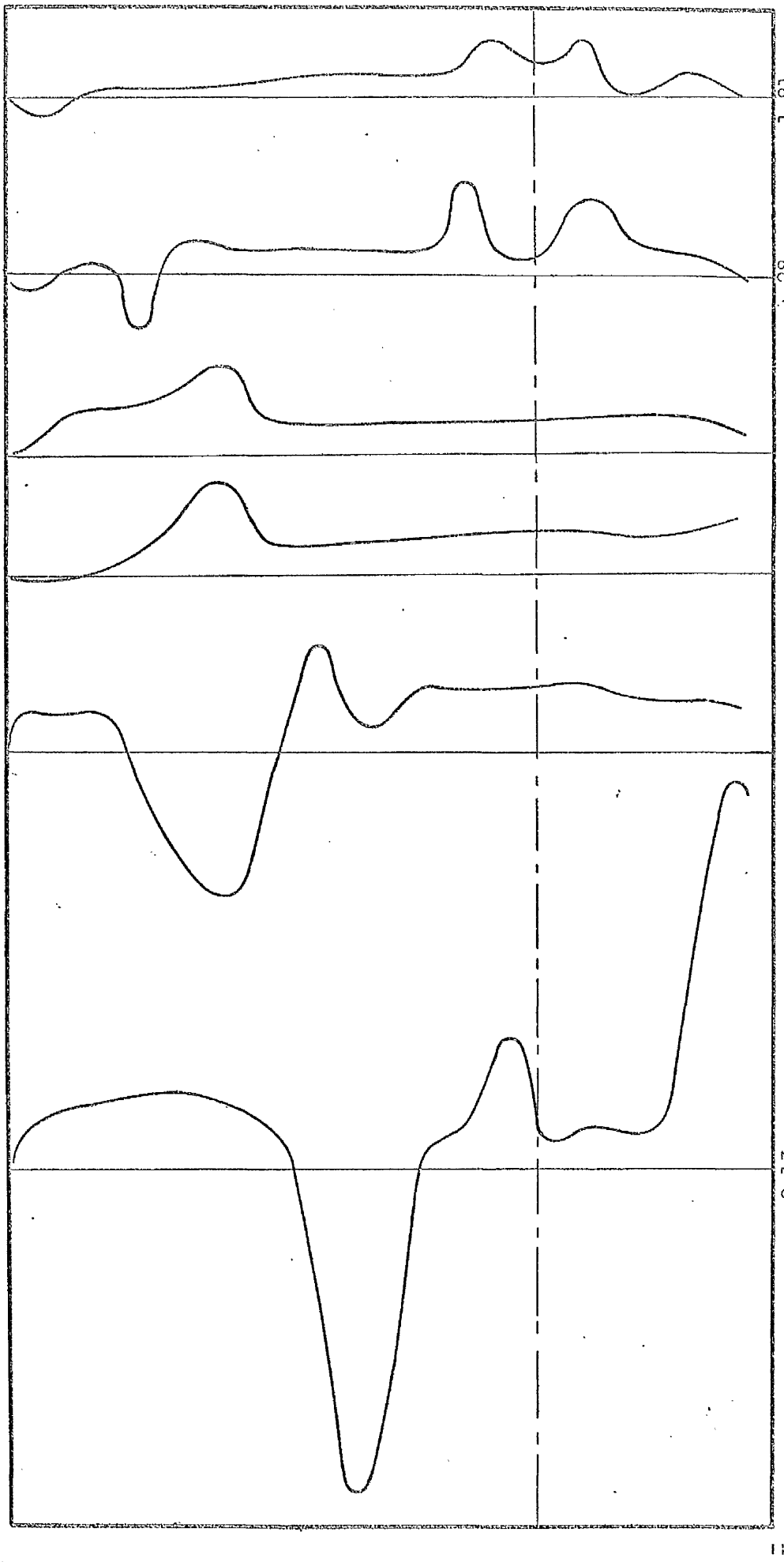

Figure 4.12.d. - Radial Velocity Profiles.
45° Annular Swirler flame in D/d = 5 furnace.

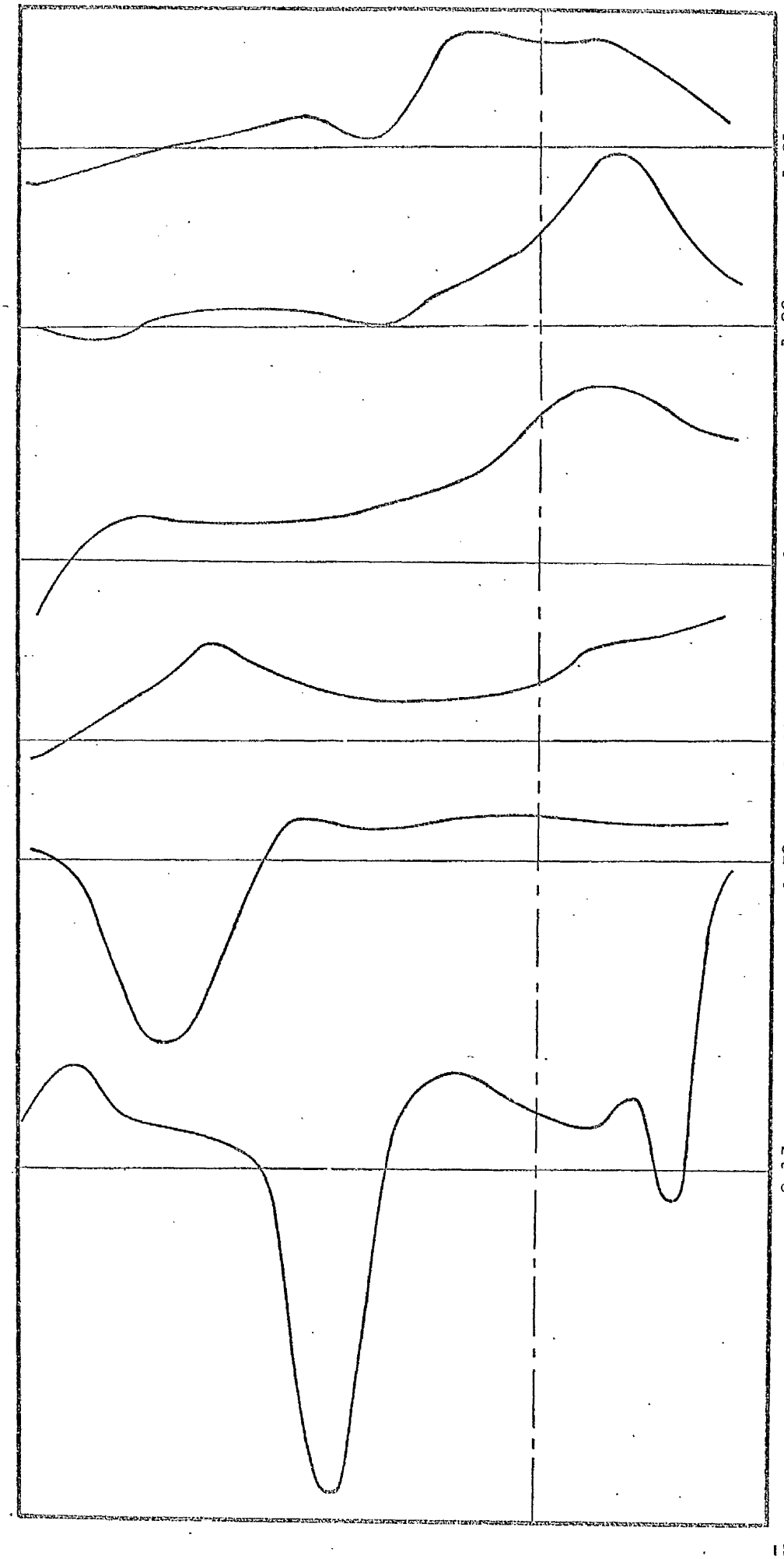

Figure 4.12.e. - Radial Velocity Profiles.
60° Annular Swirler flame in D/d = 5 furnace.

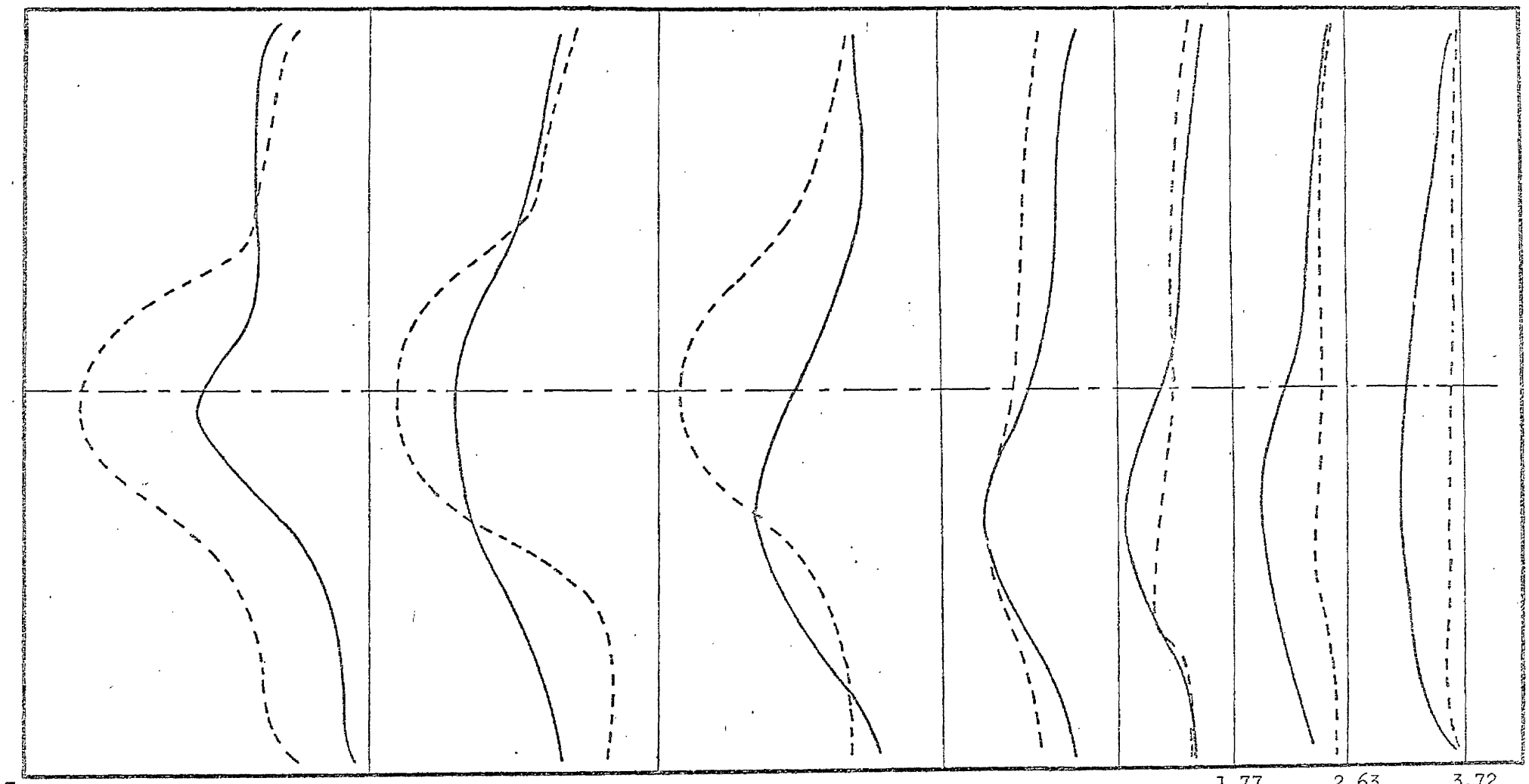

Figure 4.13.a. - Static Pressure Profiles.
15° Hubless Swirler in D/d = 2.5 furnace.

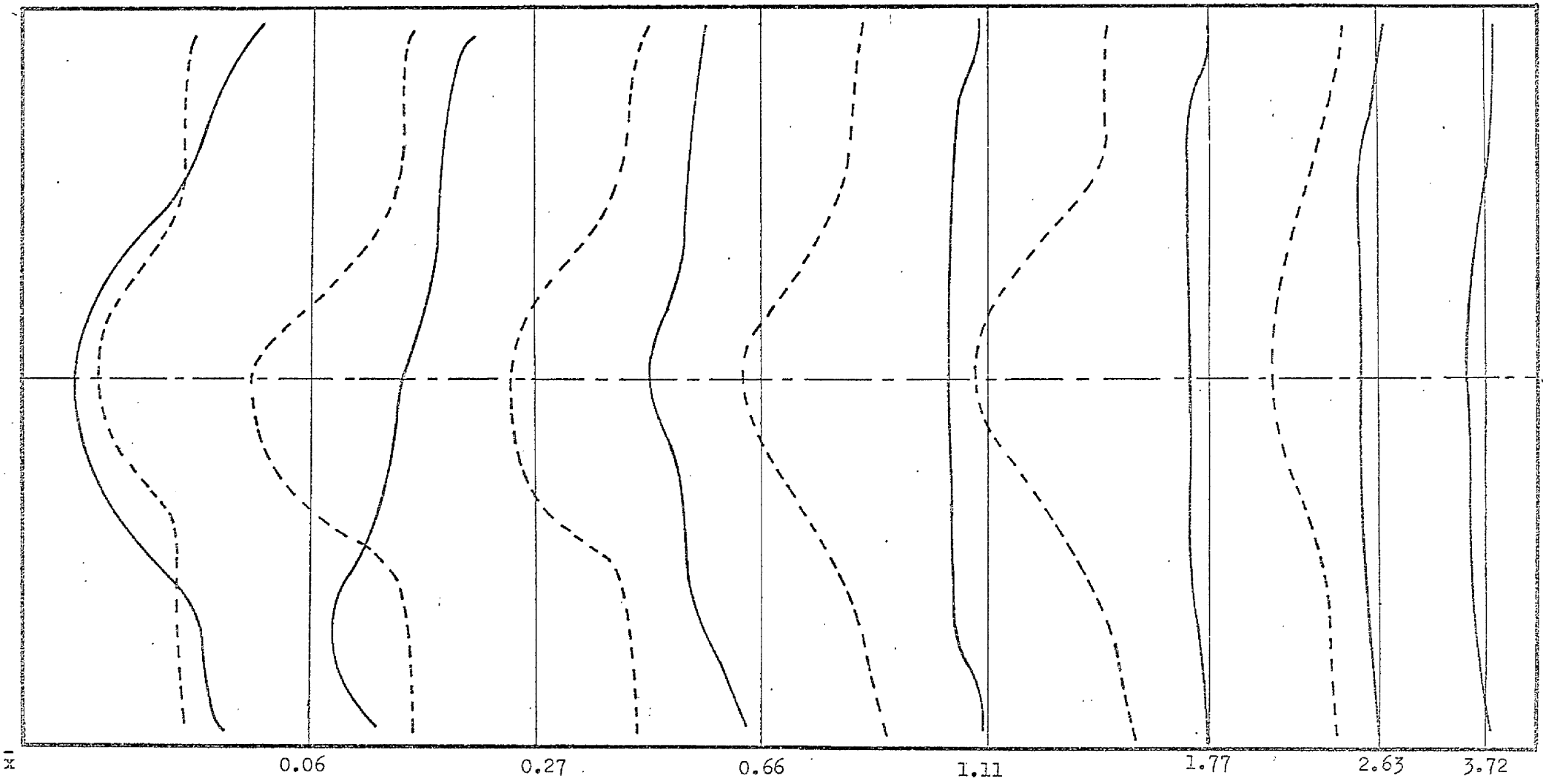

Figure 4.13.b. - Static Pressure Profiles.
0° and 22.5° Hubless Swirlers in D/d = 2.5 furnace.

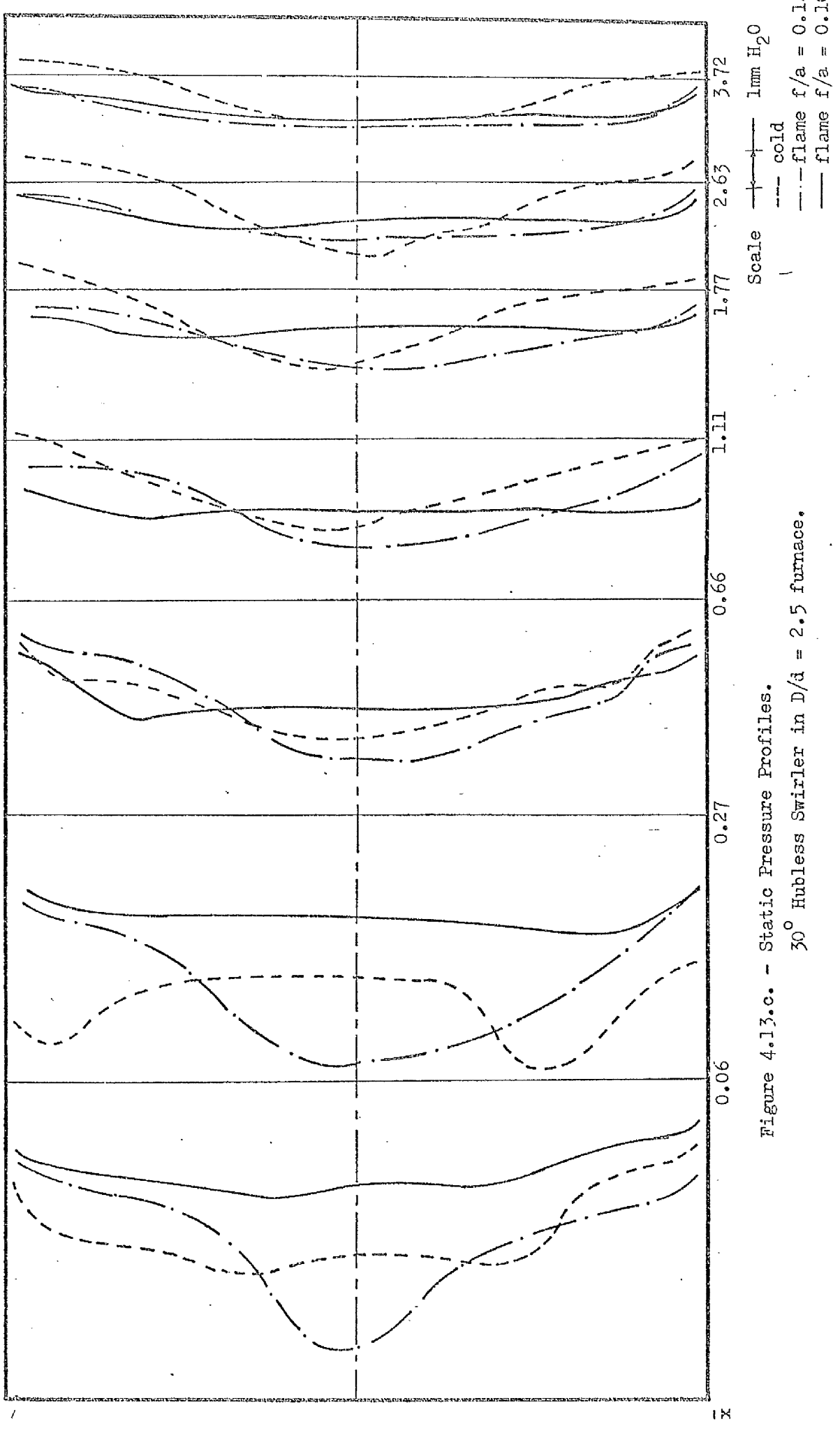

Figure 4.13.c. - Static Pressure Profiles.
30° Hubless Swirler in D/d = 2.5 furnace.

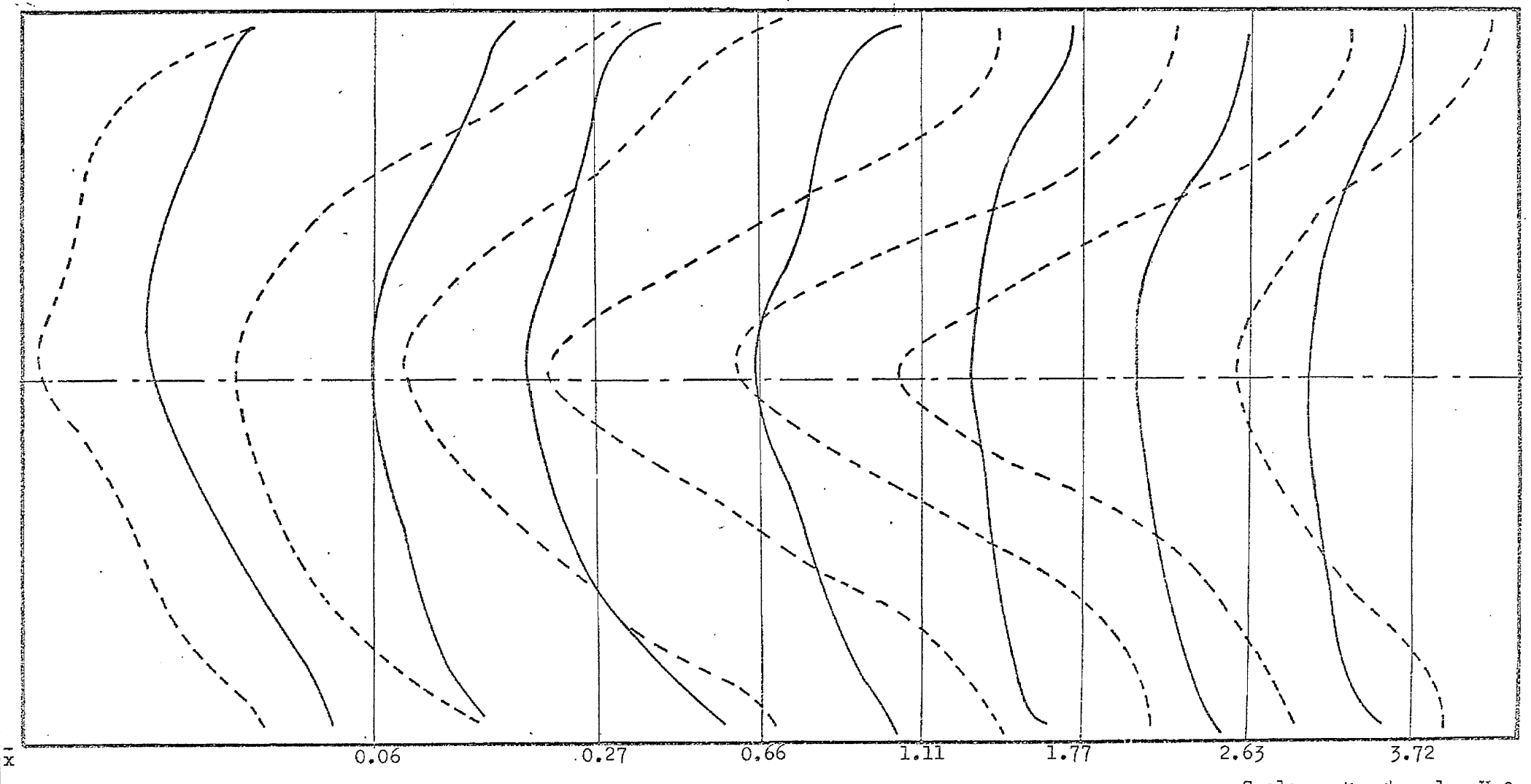

Figure 4.13.d. - Static Pressure Profiles.
45° Hubless Swirler in D/d = 2.5 furnace.

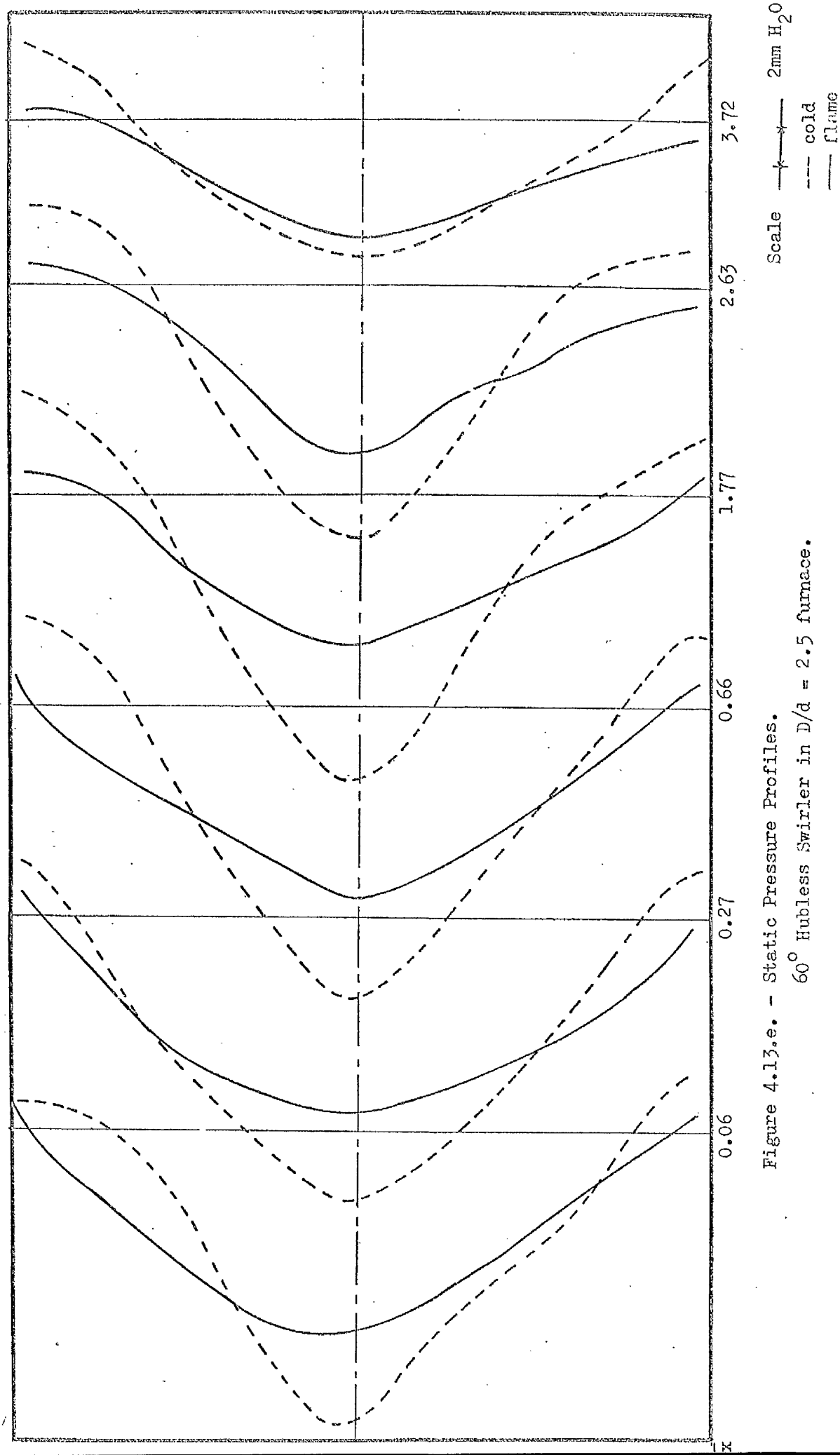

Figure 4.13.e. - Static Pressure Profiles.
60° Hubless Swirler in D/d = 2.5 furnace.

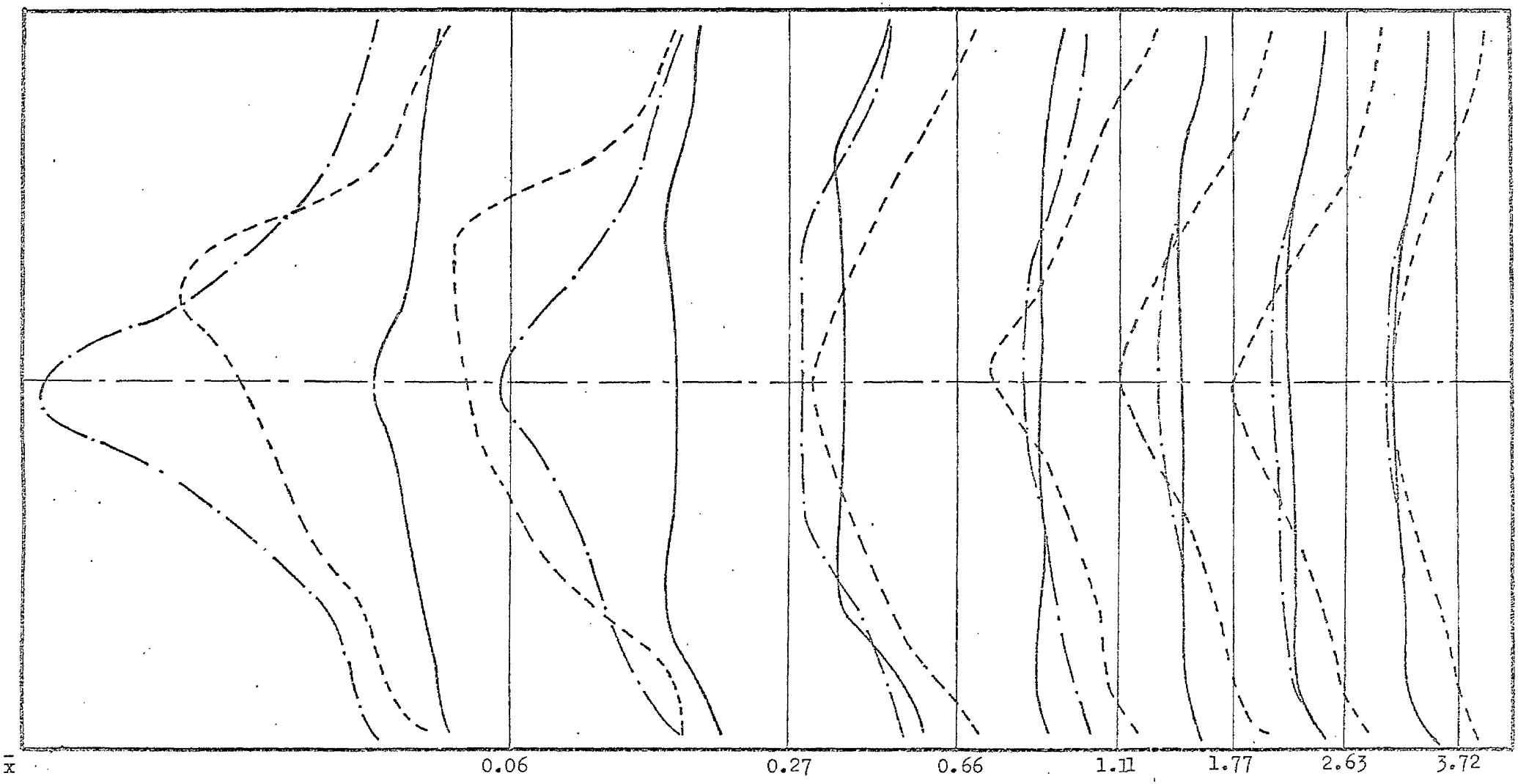

Figure 4.14.a. - Static Pressure Profiles.
30° Annular Swirler in D/d = 2.5 furnace.

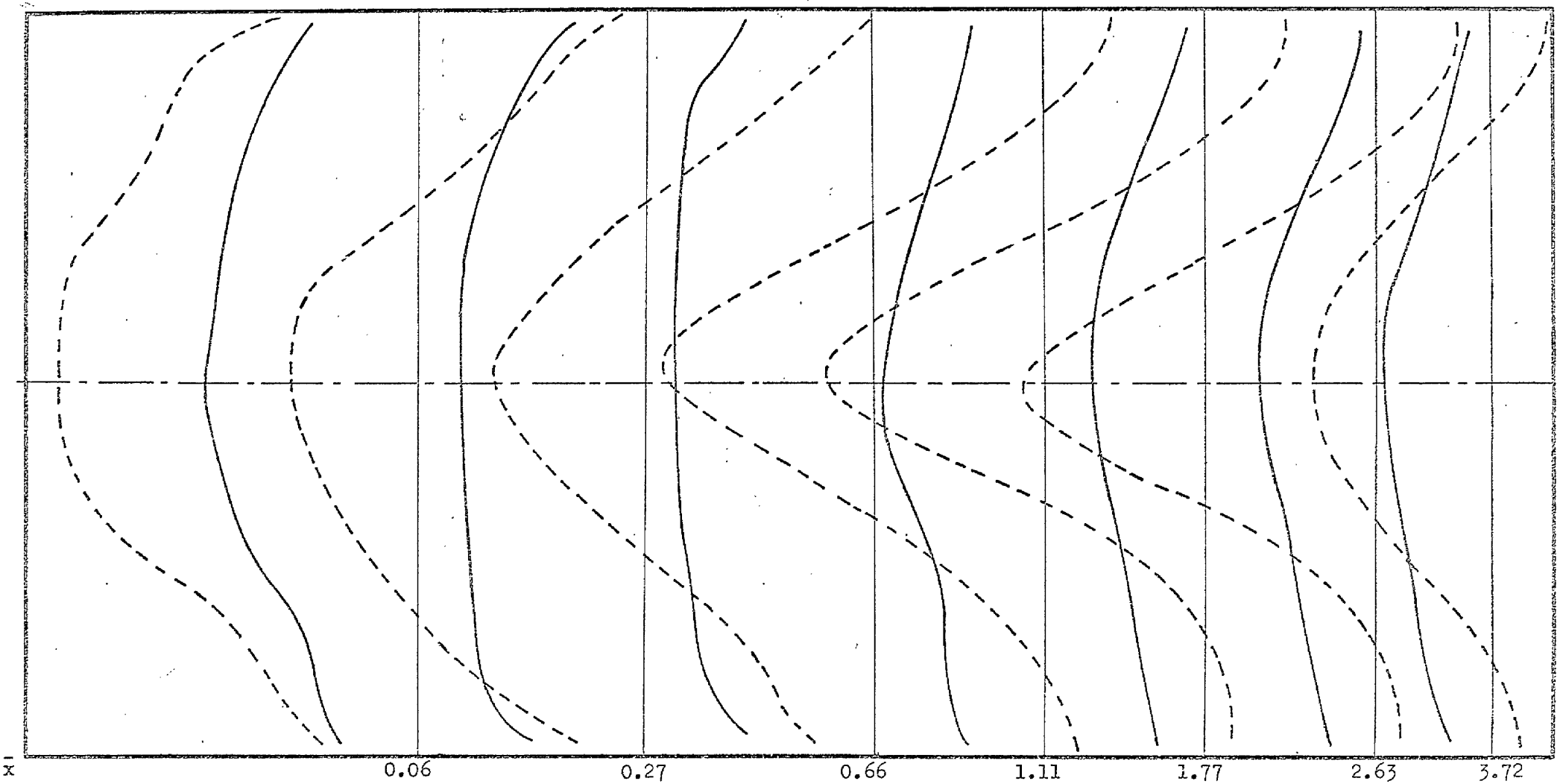

Figure 4.14.b. - Static Pressure Profiles.

45° Annular Swirler in D/d = 2.5 furnace.

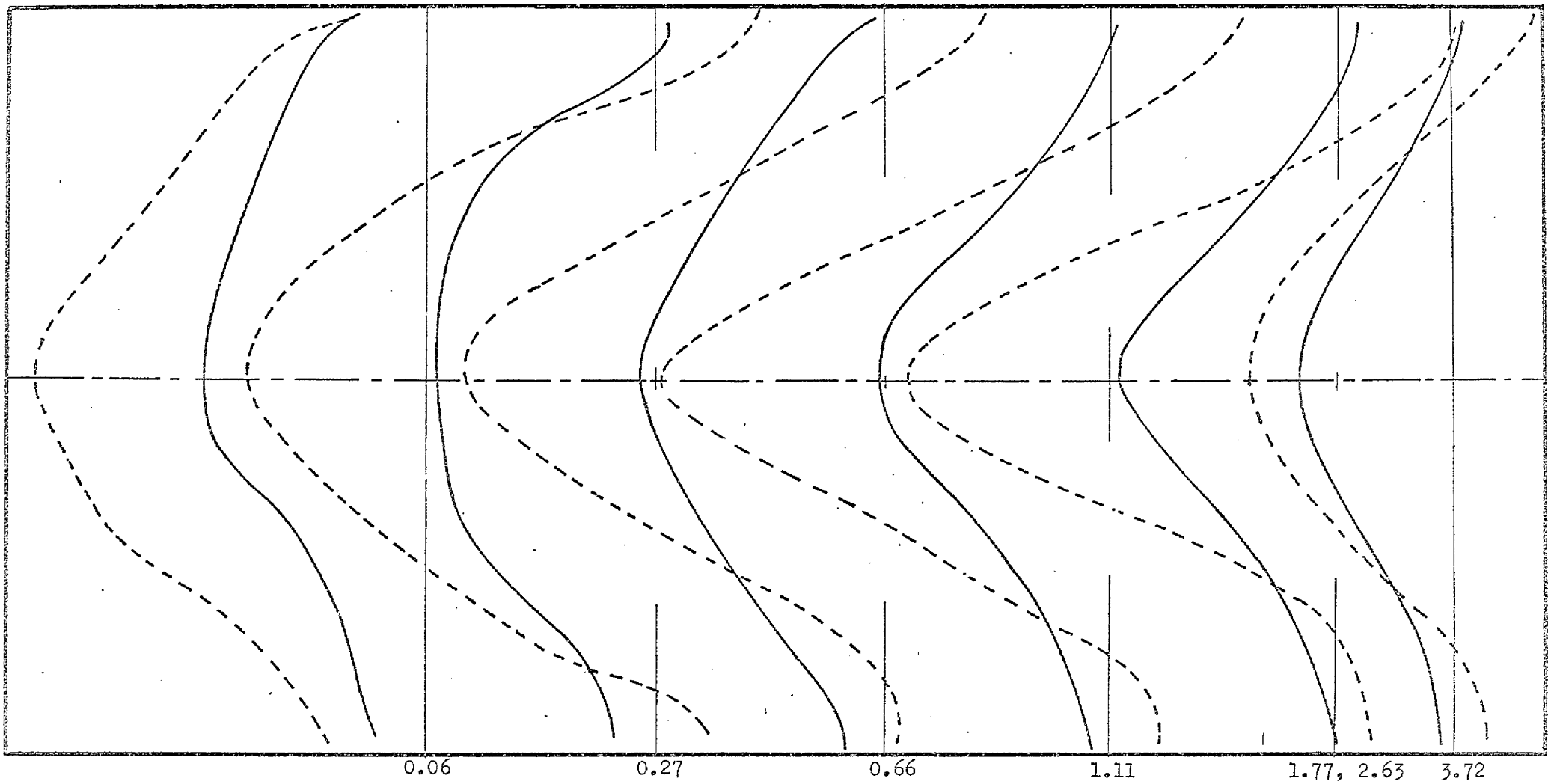

Figure 4.14.c. - Static Pressure Profiles.
60° Annular Swirler in D/d = 2.5 furnace.

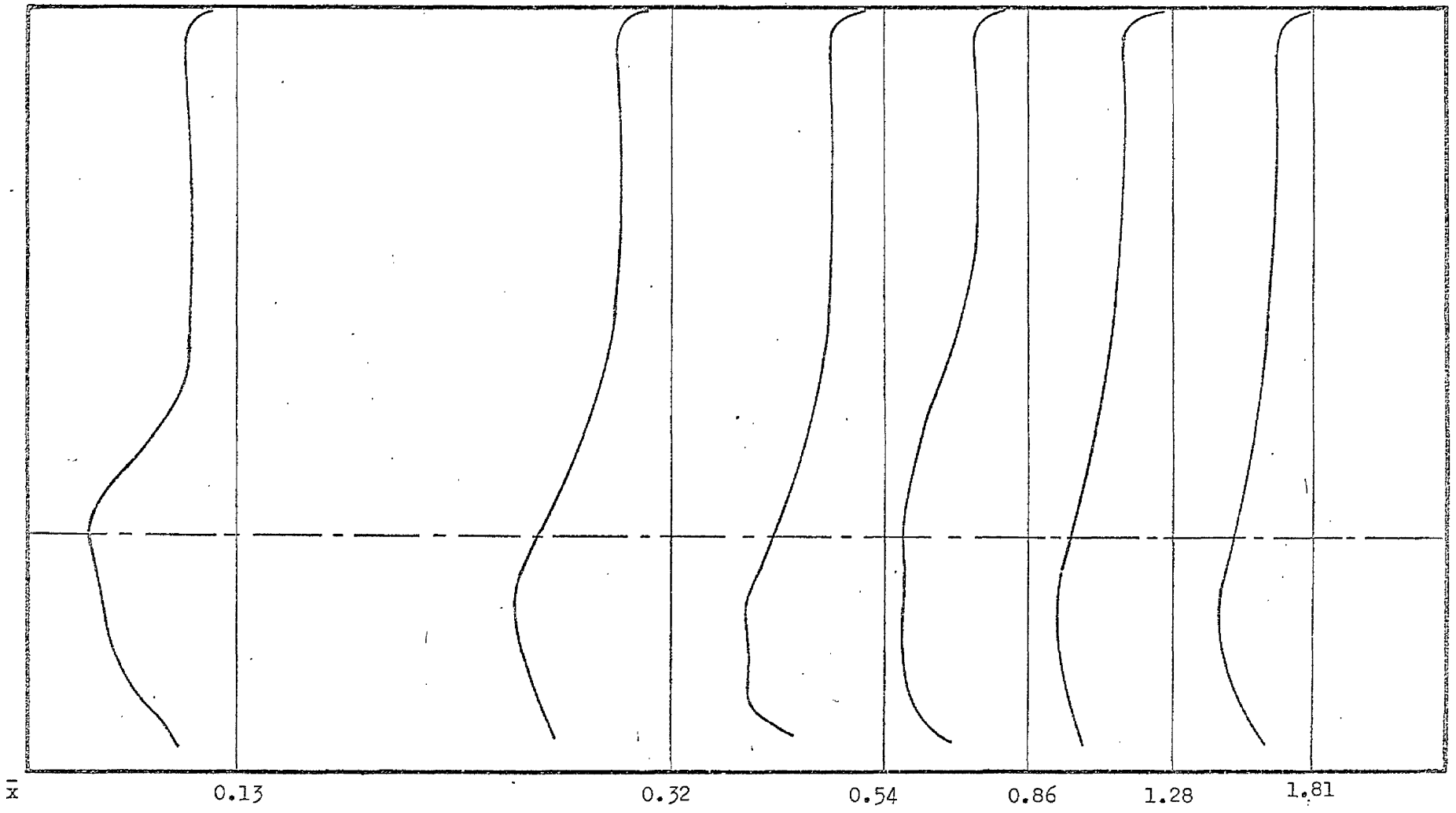

Figure 4.15.a. - Static Pressure Profiles.

0° Hubless Swirler flame in D/d = 5 furnace.

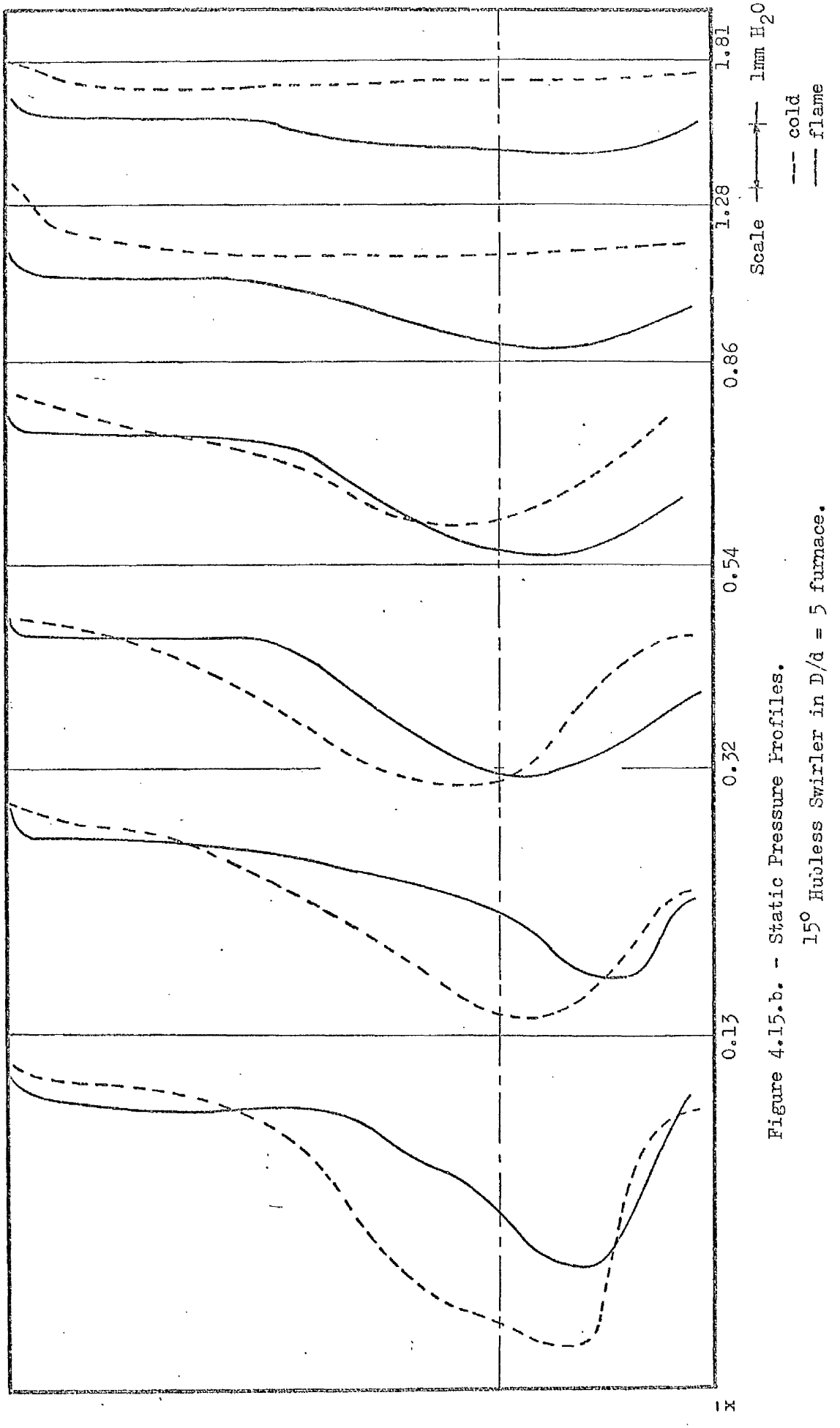

Figure 4.15.b. - Static Pressure Profiles.
15° Hubless Swirler in D/d = 5 furnace.

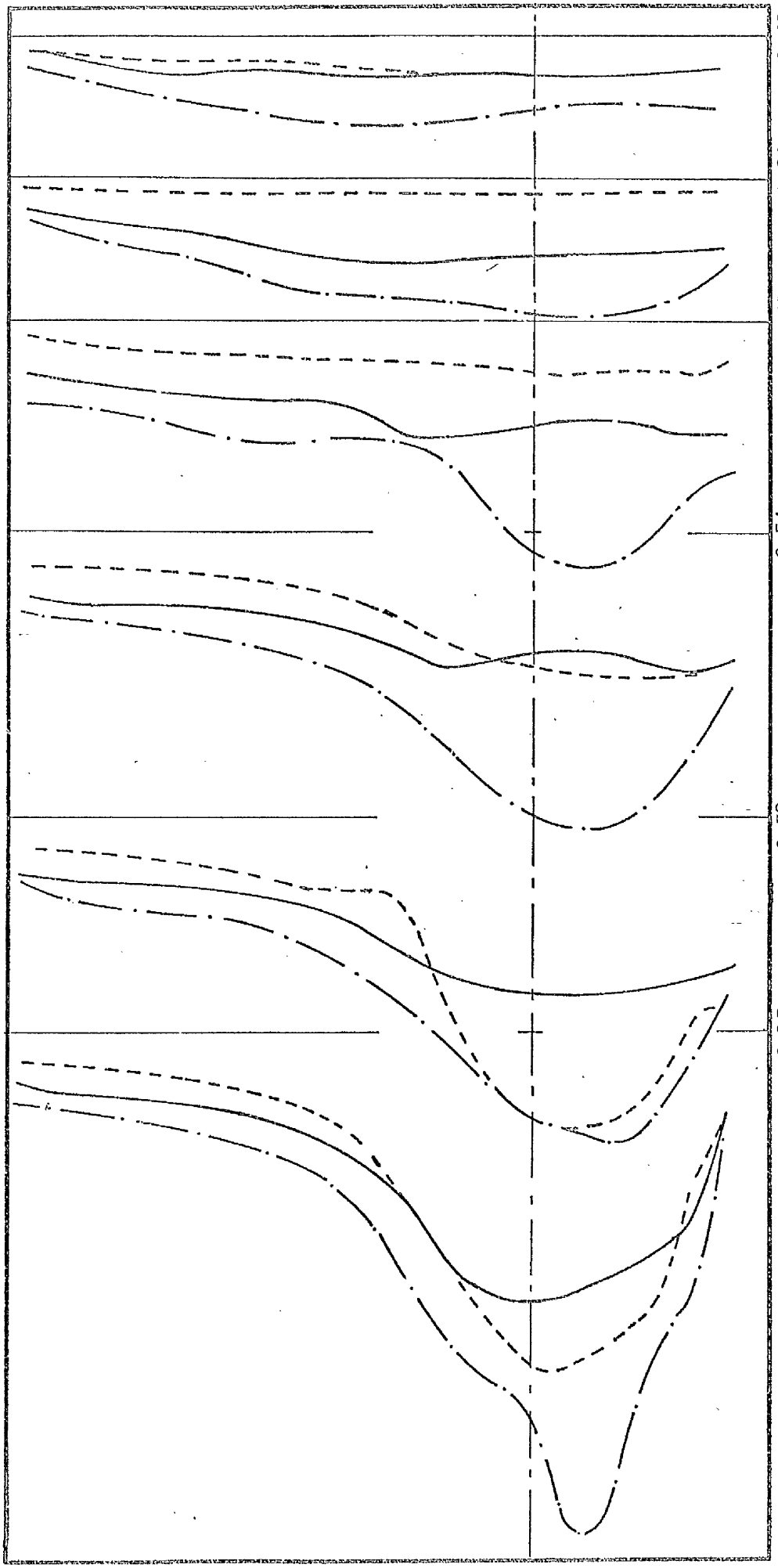

Figure 4.15.c. - Static Pressure Profiles.
22.5^{o} Hubless Swirler in D/d = 5 furnace.

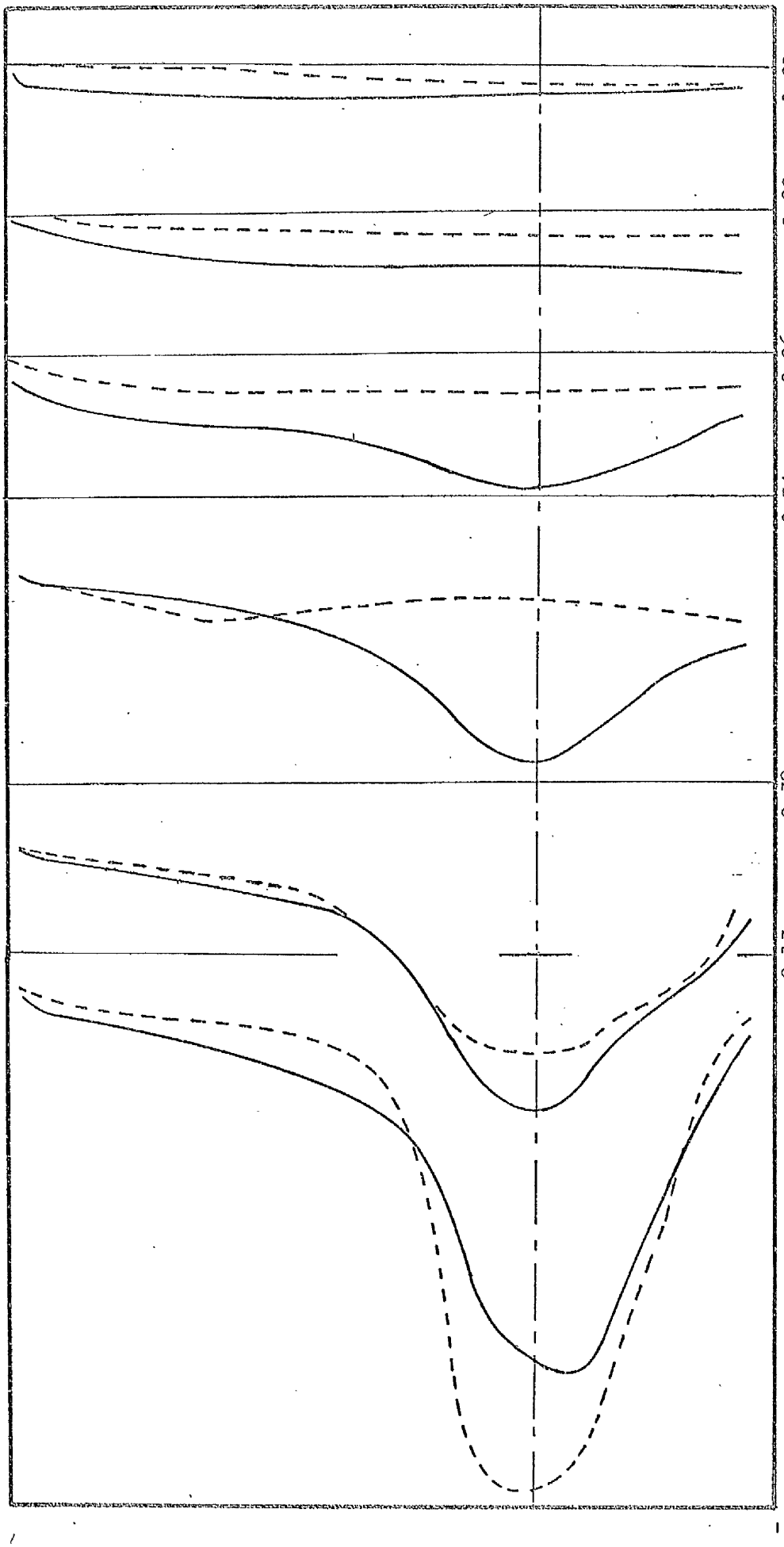

Figure 4.15.d. - Static Pressure Profiles.
30° Hubless Swirler in D/d = 5 furnace.

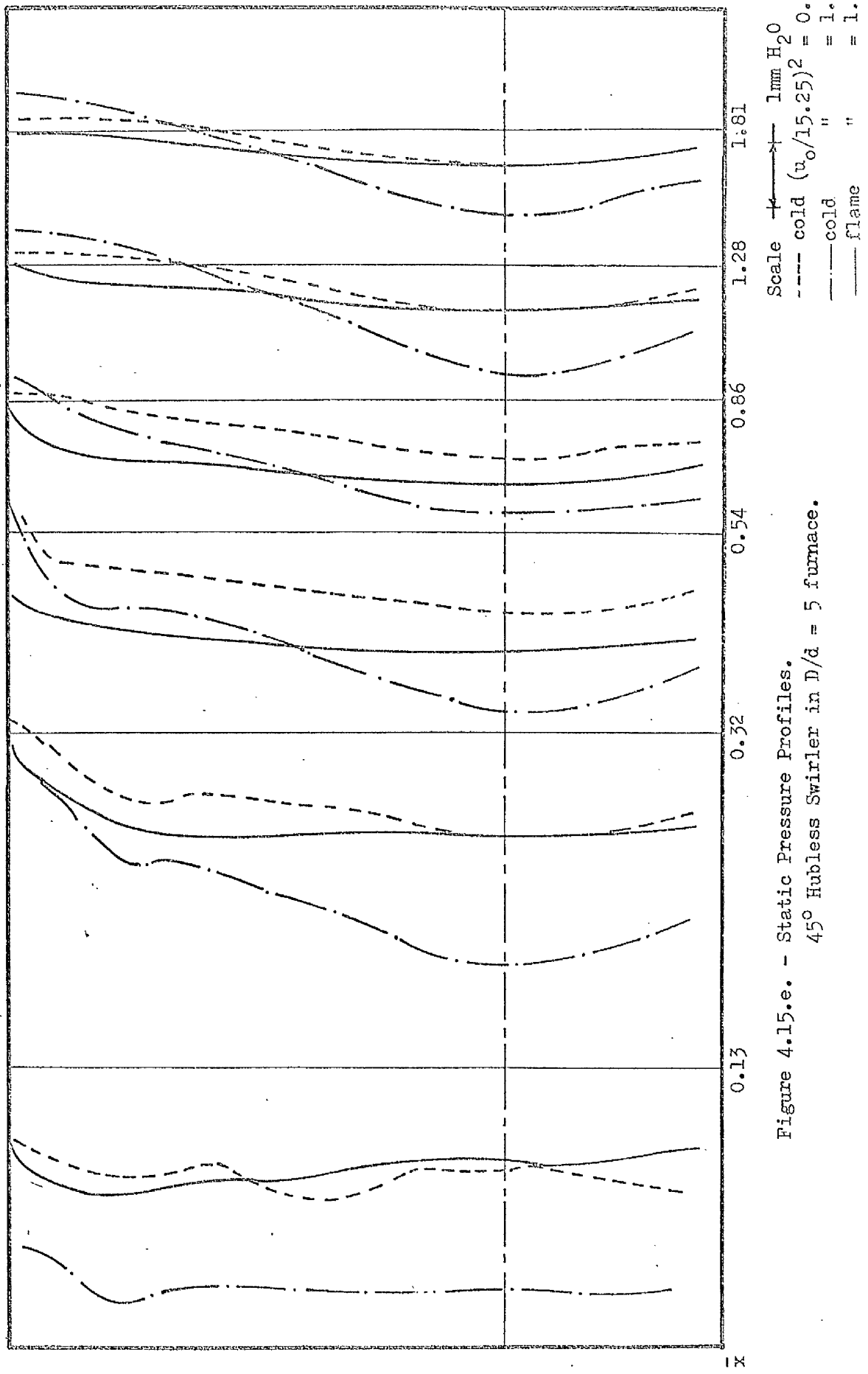

Figure 4.15.e. - Static Pressure Profiles.
45° Hubless Swirler in D/d = 5 furnace.

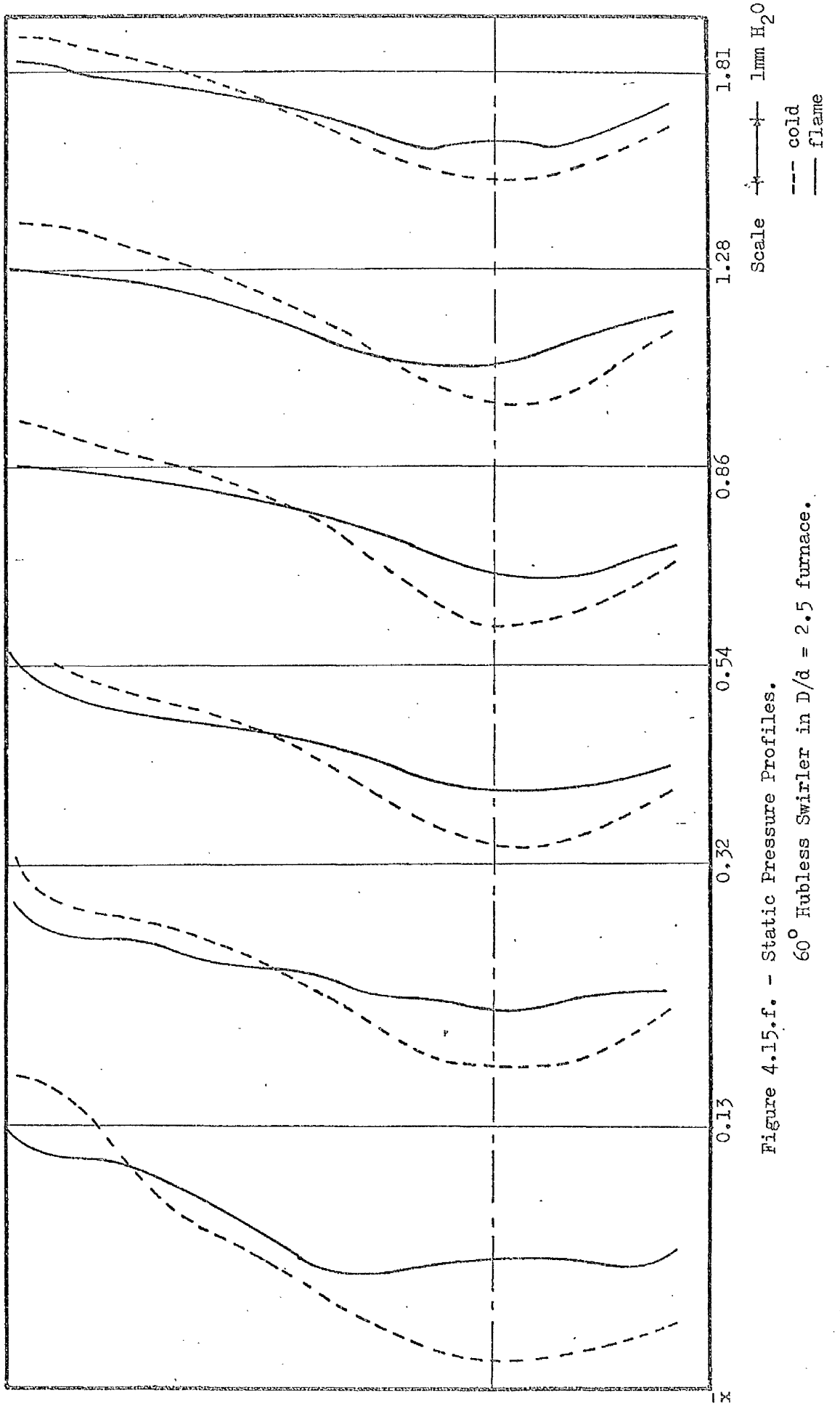

Figure 4.15.f. - Static Pressure Profiles.
60° Hubless Swirler in D/d = 2.5 furnace.

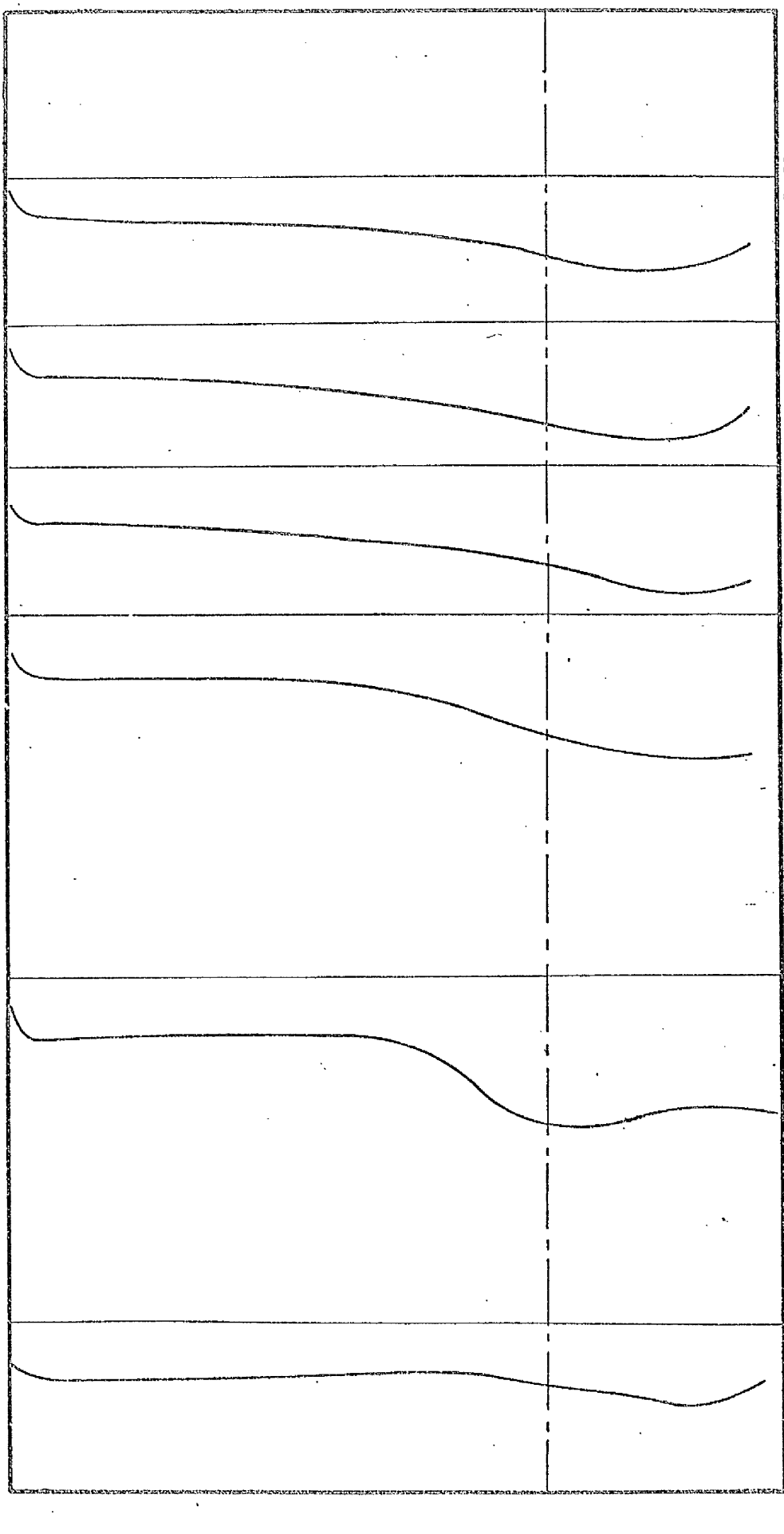

Figure 4.16.a. - Static Pressure Profiles.
0^o Annular Swirler flame in D/d = 5 furnace.

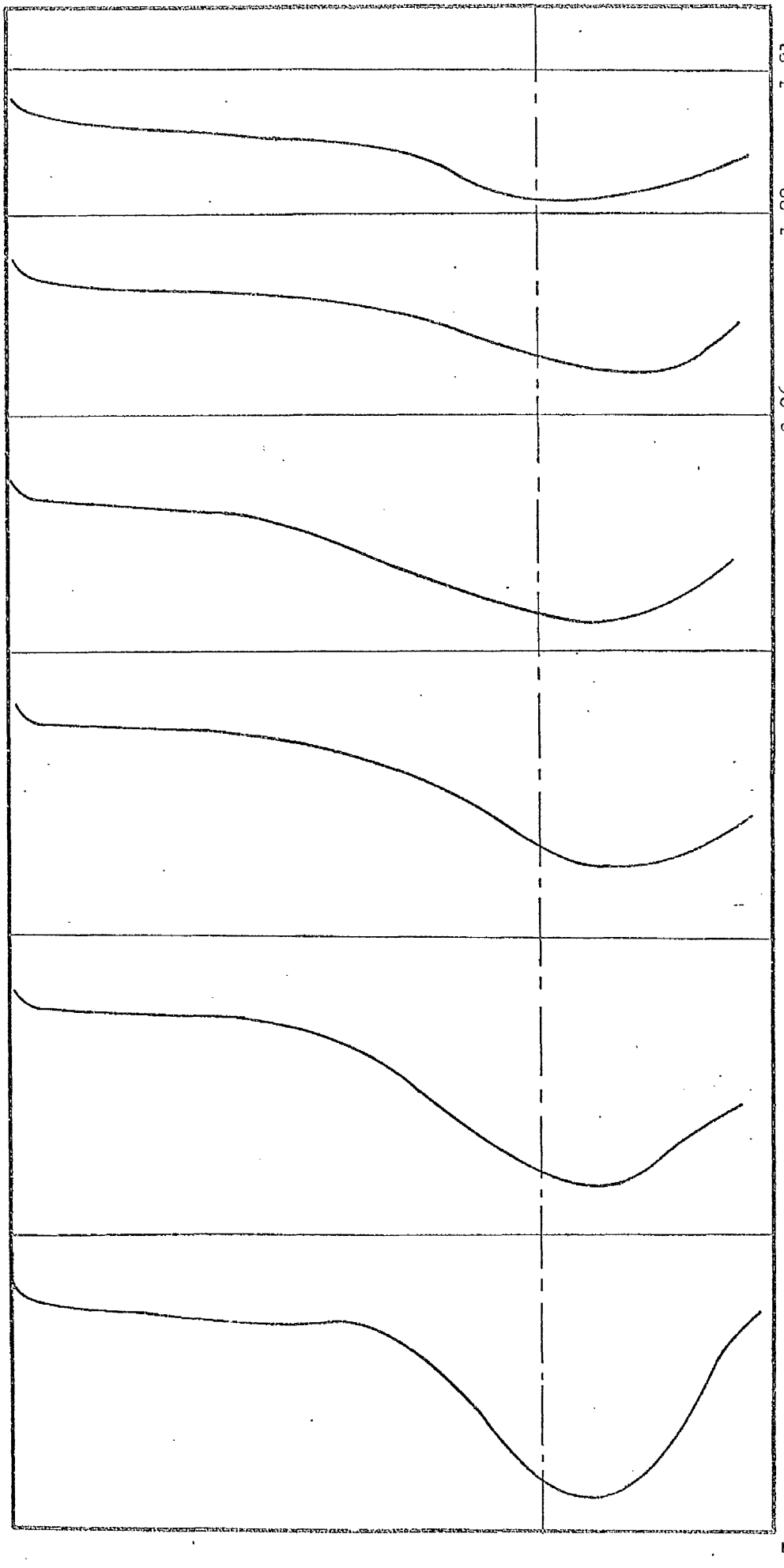

Figure 4.16.b. - Static Pressure Profiles.
15° Annular Swirler flame in D/d = 5 furnace.

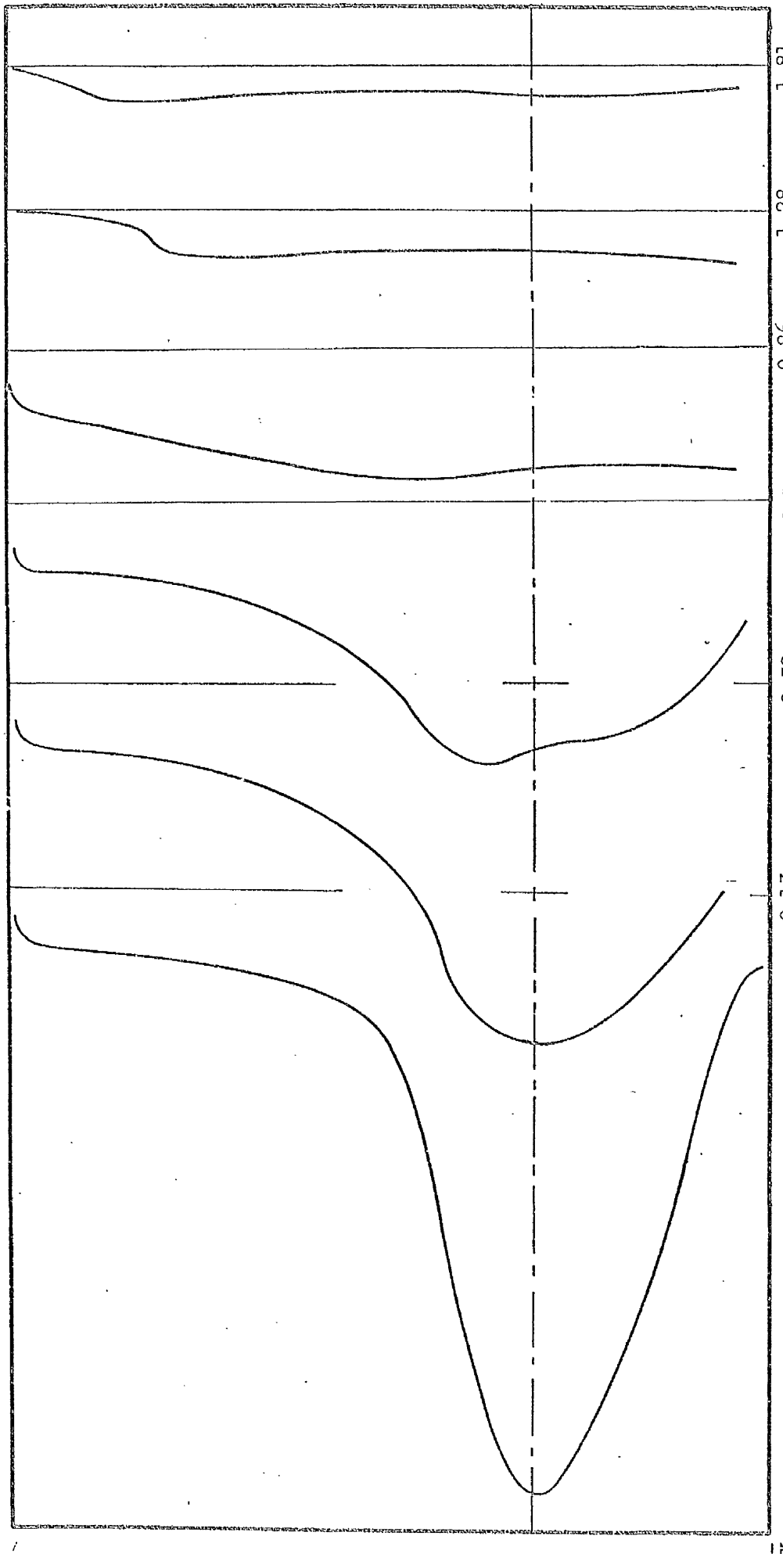

Figure 4.16.c. - Static Pressure Profiles.
30° Annular Swirler flame in D/d = 5 furnace.

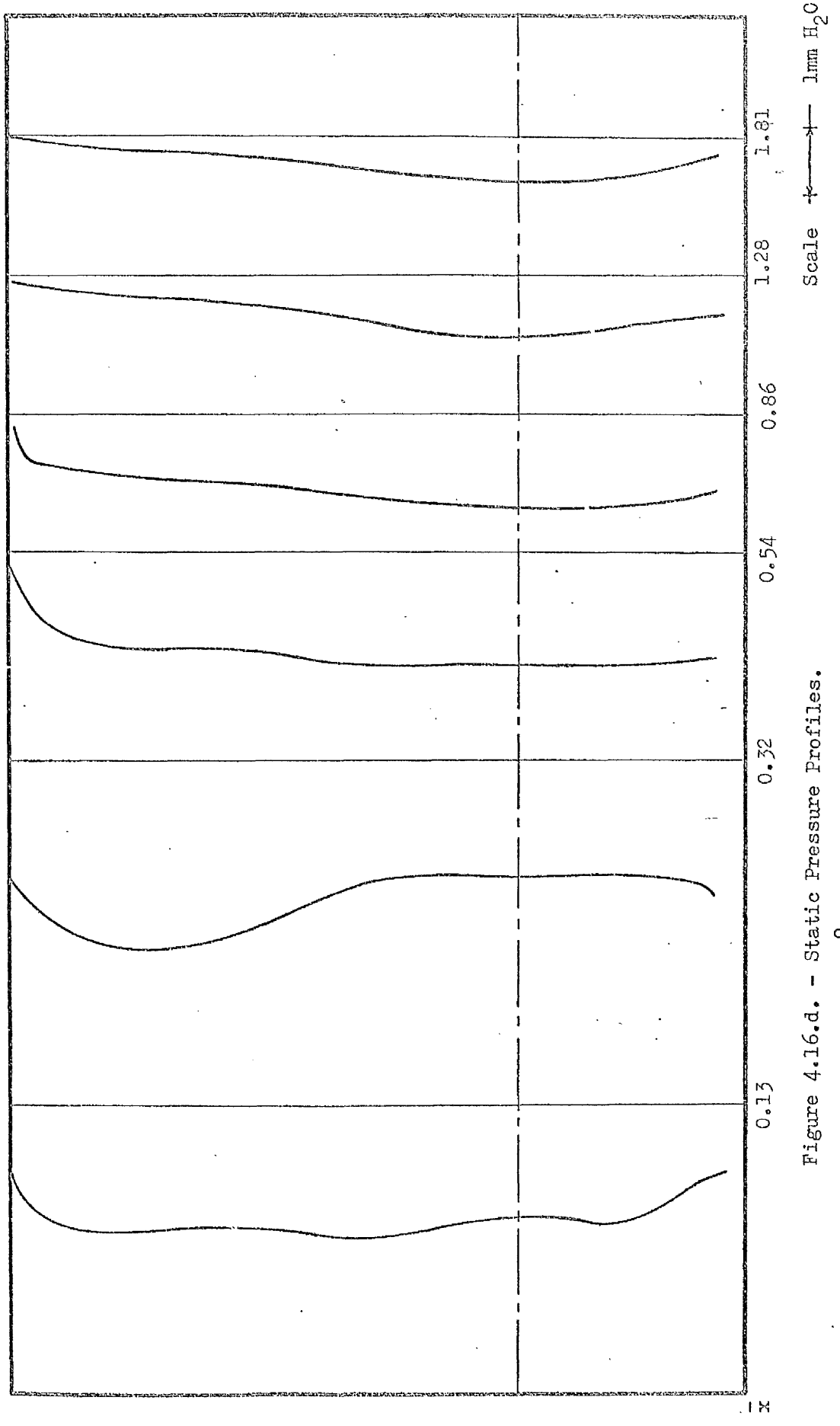

Figure 4.16.d. - Static Pressure Profiles.
45^{o} Annular Swirler flame in D/d = 5 furnace.

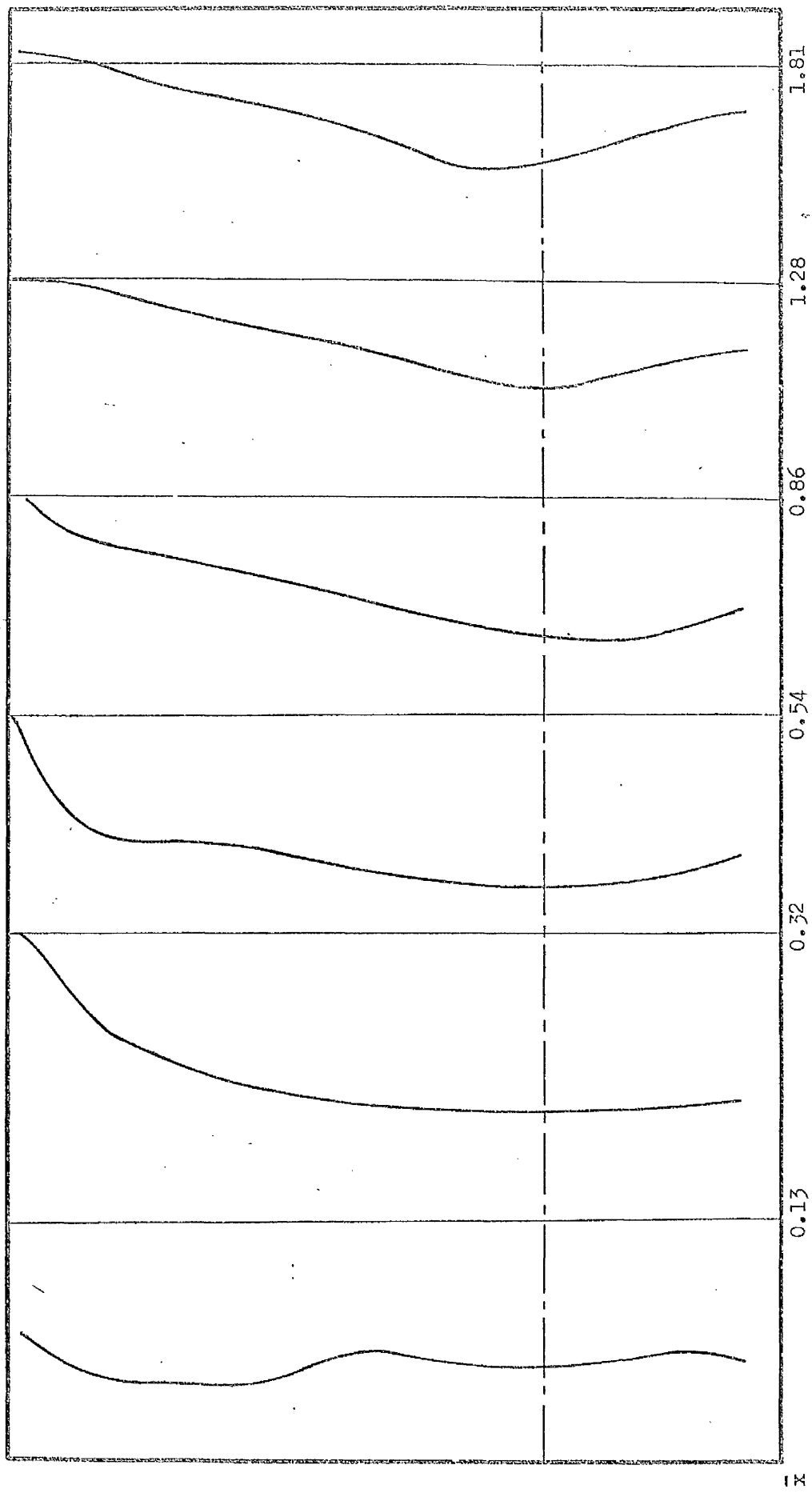

Figure 4.16.e. - Static Pressure Profiles.
60° Annular Swirler flame in D/d = 5 furnace.

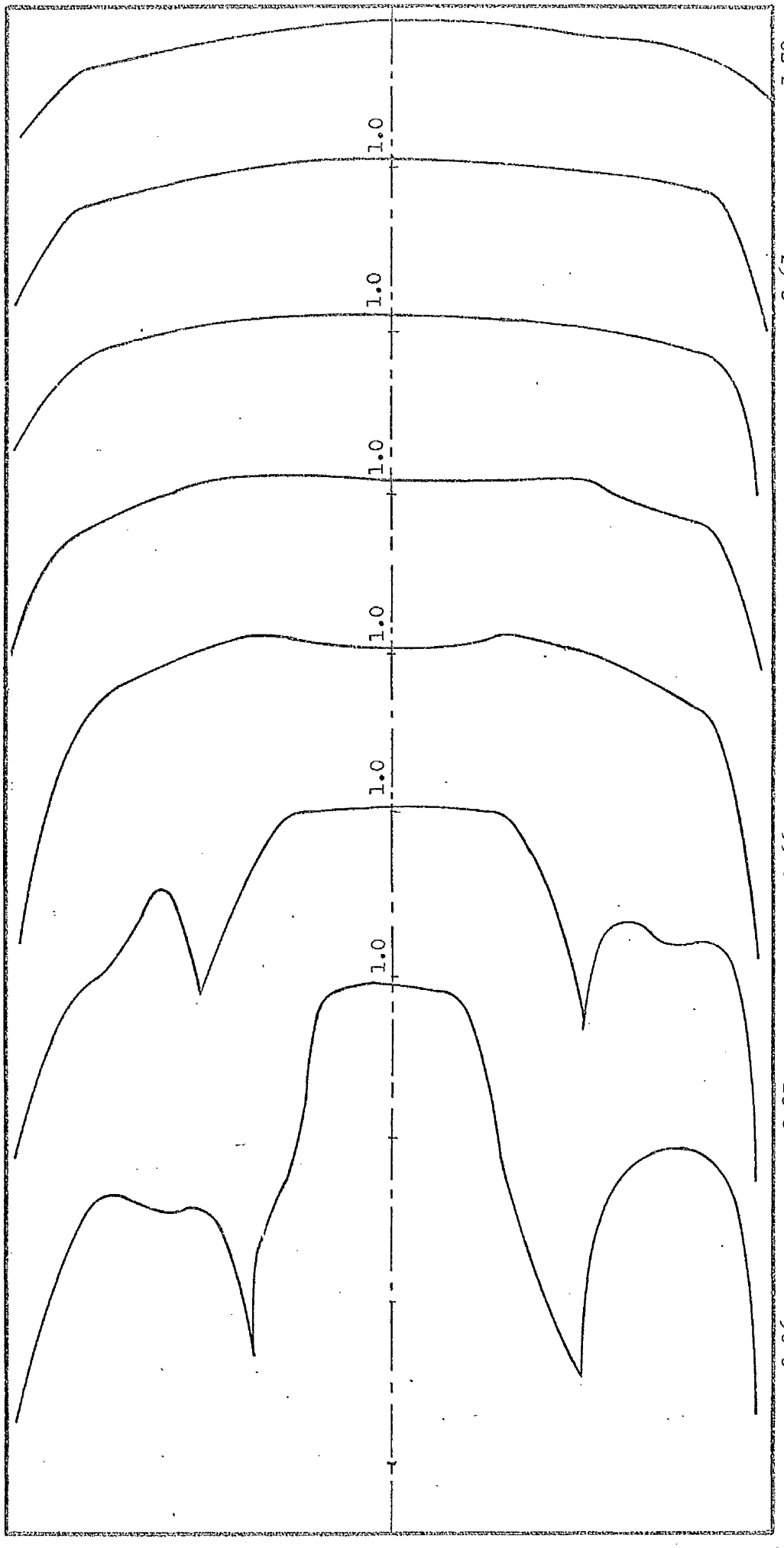

Figure 4.17.a. - Temperature Profiles.
15° Hubless Swirler in D/d = 2.5 furnace.

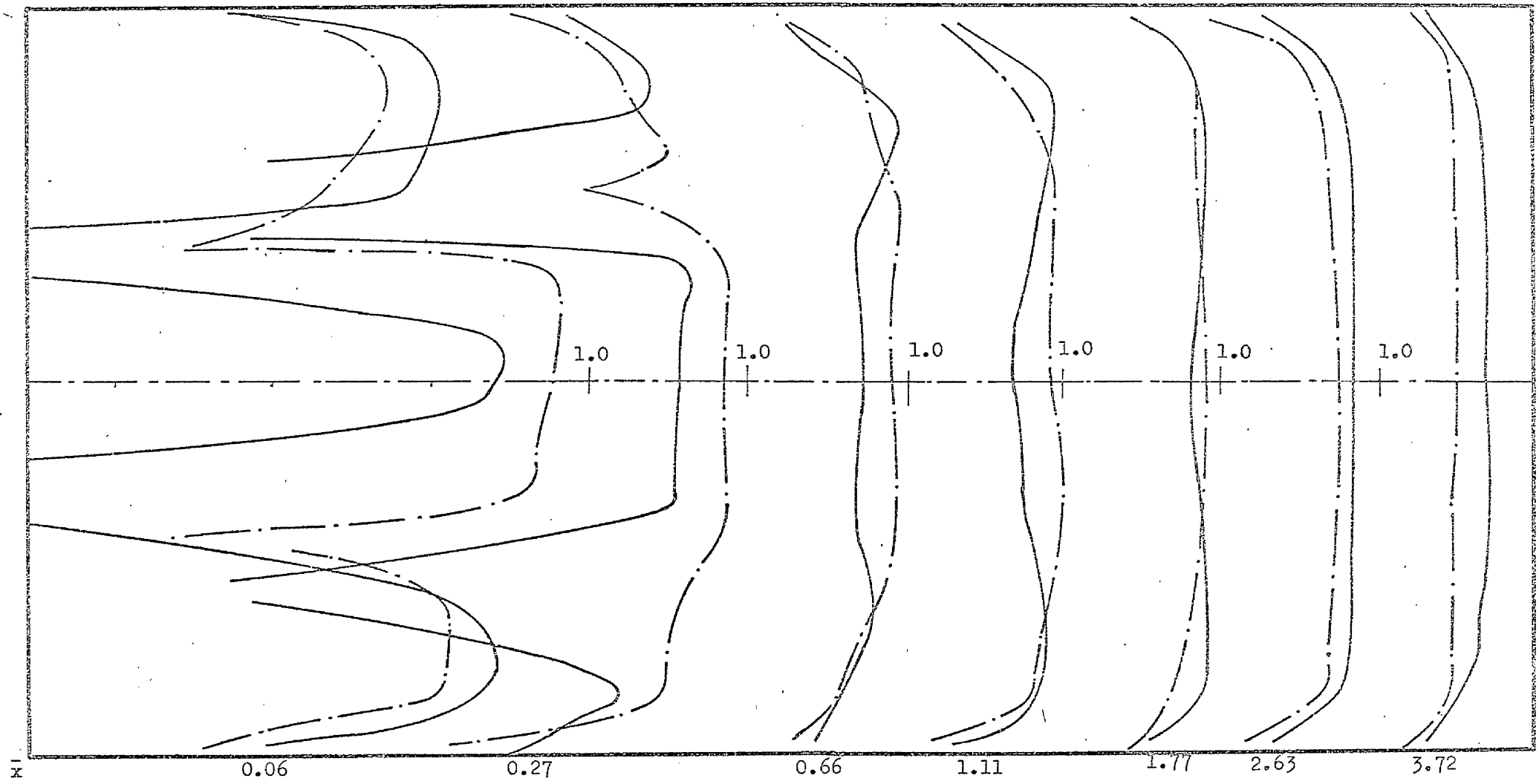

Figure 4.17.b. - Temperature Profiles.
30° Hubless Swirler in D/d = 2.5 furnace.

Scale ⟷ 0.1 T_{ad}
—·—f/a = 0.141
——f/a = 0.106

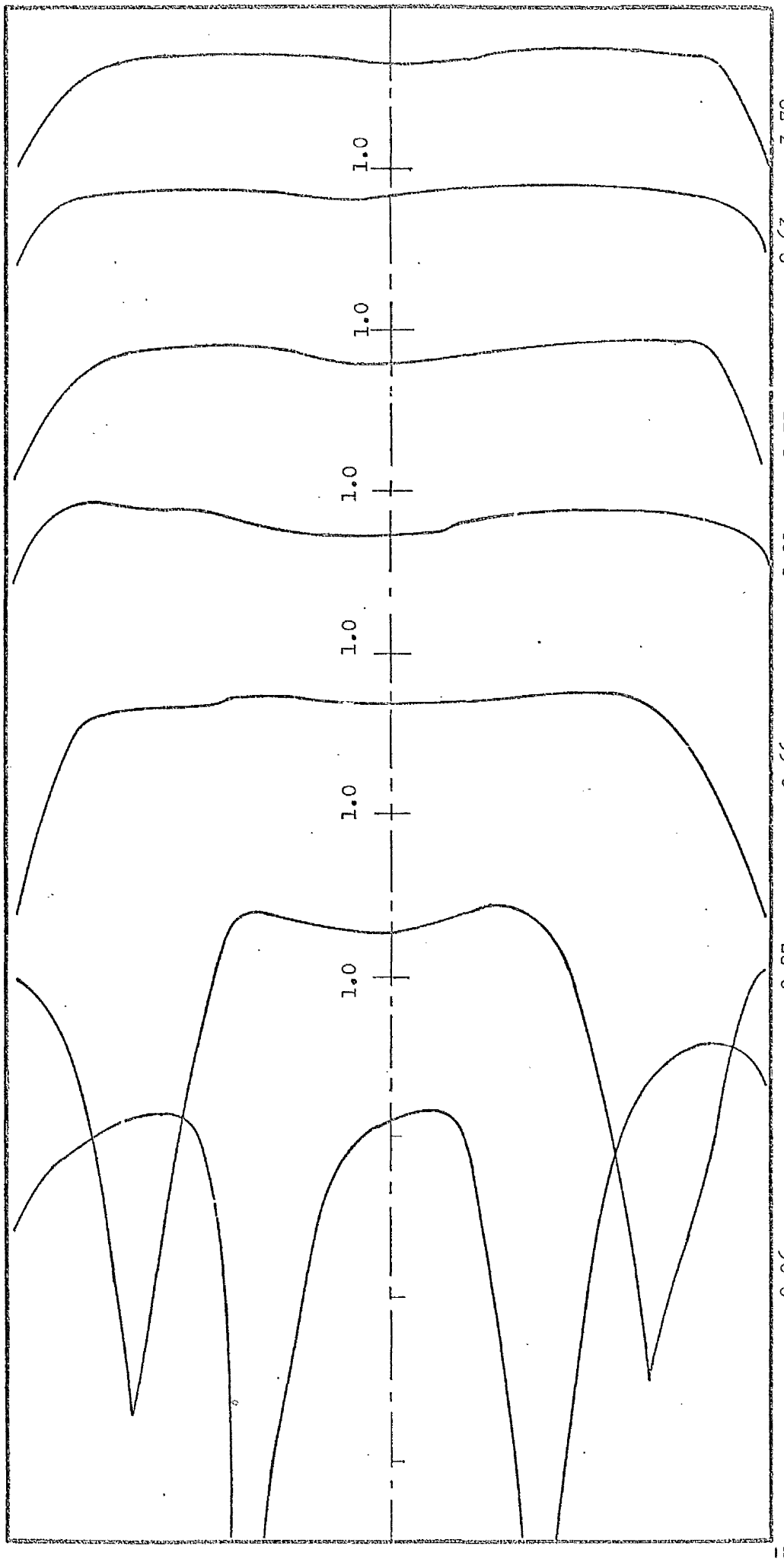

Figure 4.17.c. - Temperature Profiles.
45° Hubless Swirler in D/d = 2.5 furnace.

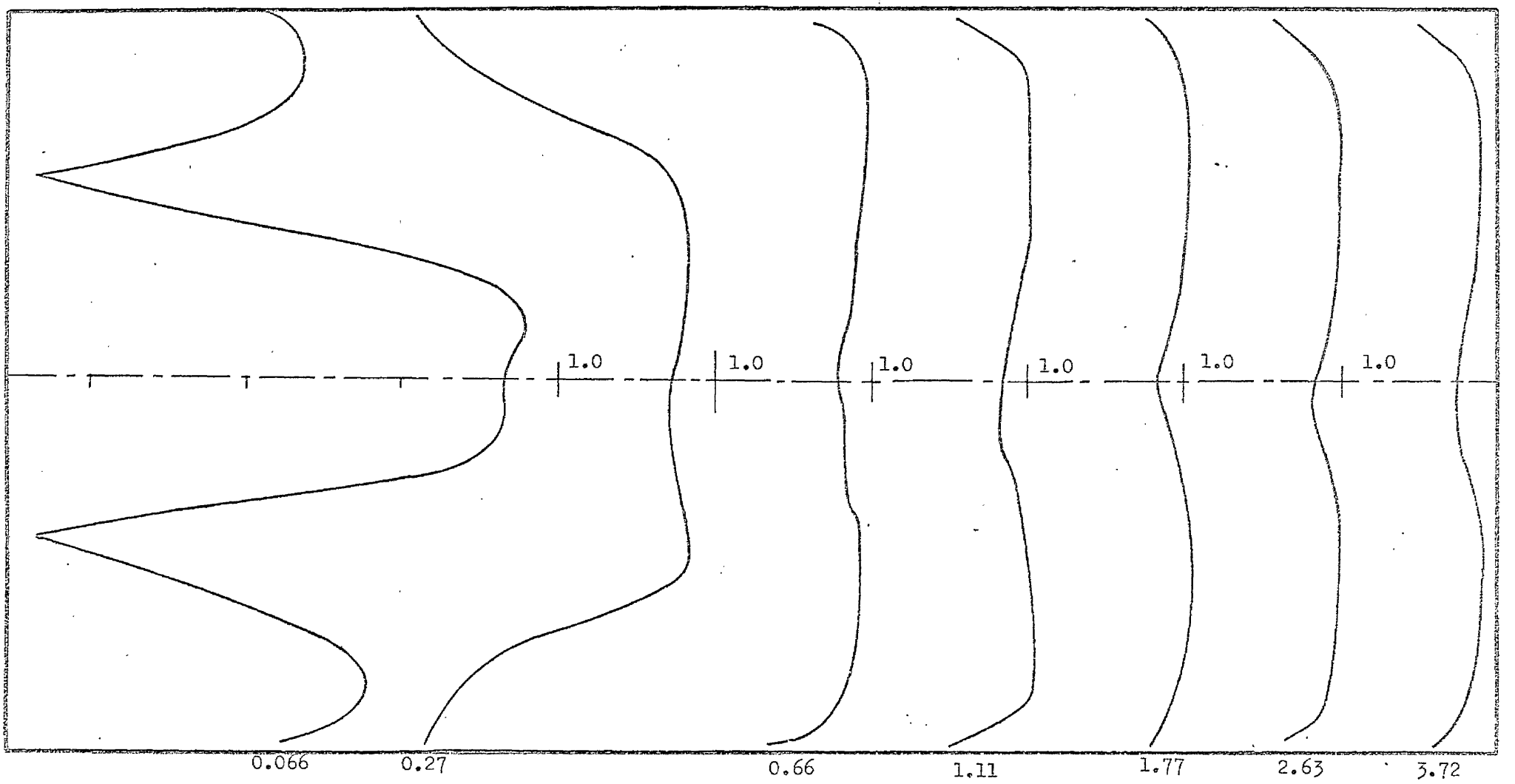

Figure 4.17.d. - Temperature Profiles.
60^{o} Hubless Swirler in D/d = 2.5 furnace.

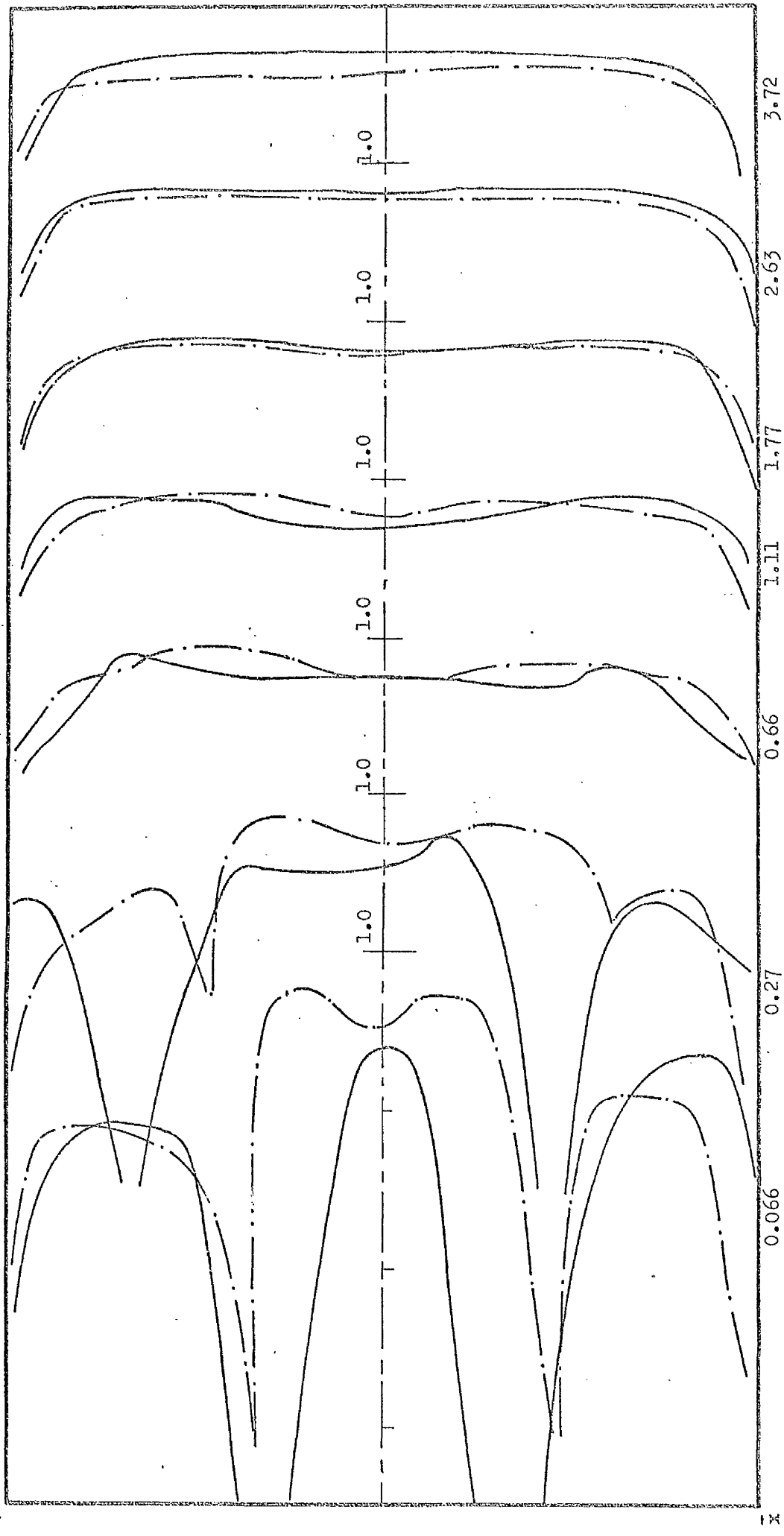

Figure 4.18.a. - Temperature Profiles.

30° Annular Swirler in D/A = 2.5 furnace.

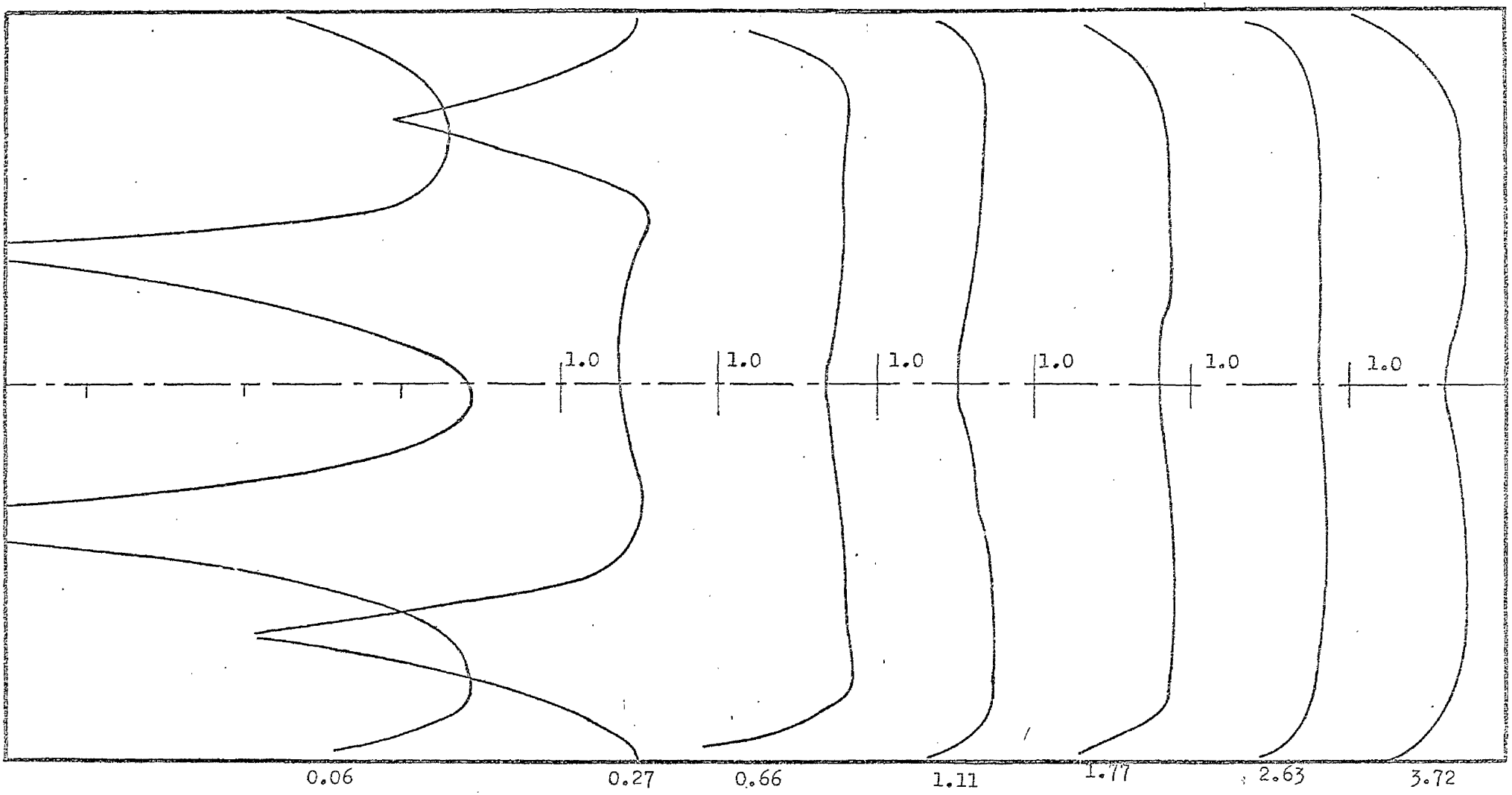

Figure 4.18.b. - Temperature Profiles.
45^{o} Annular Swirler in D/d = 2.5 furnace.

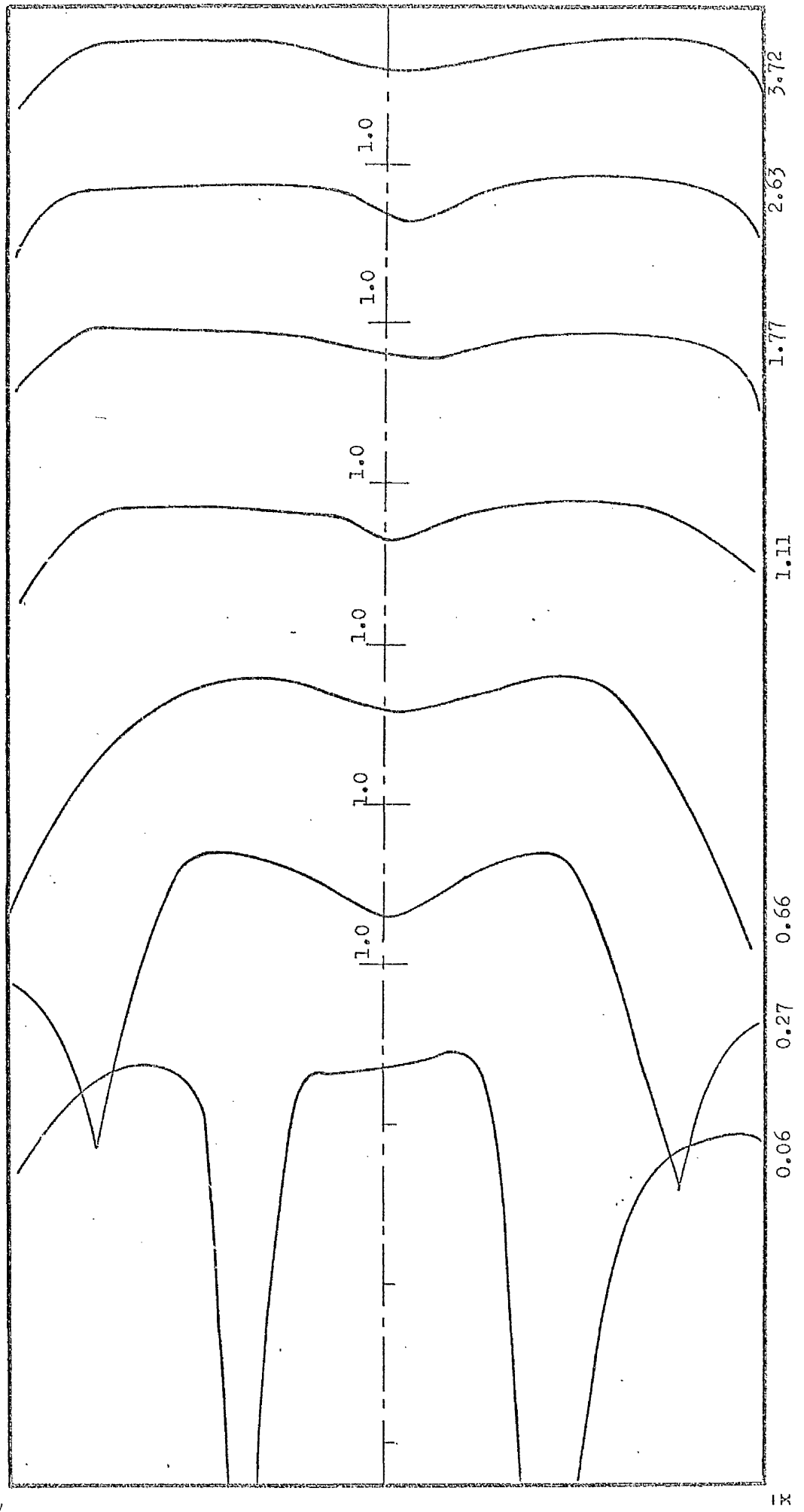

Figure 4.18.c. - Temperature Profiles.
60° Annular Swirler in D/d = 2.5 furnace.

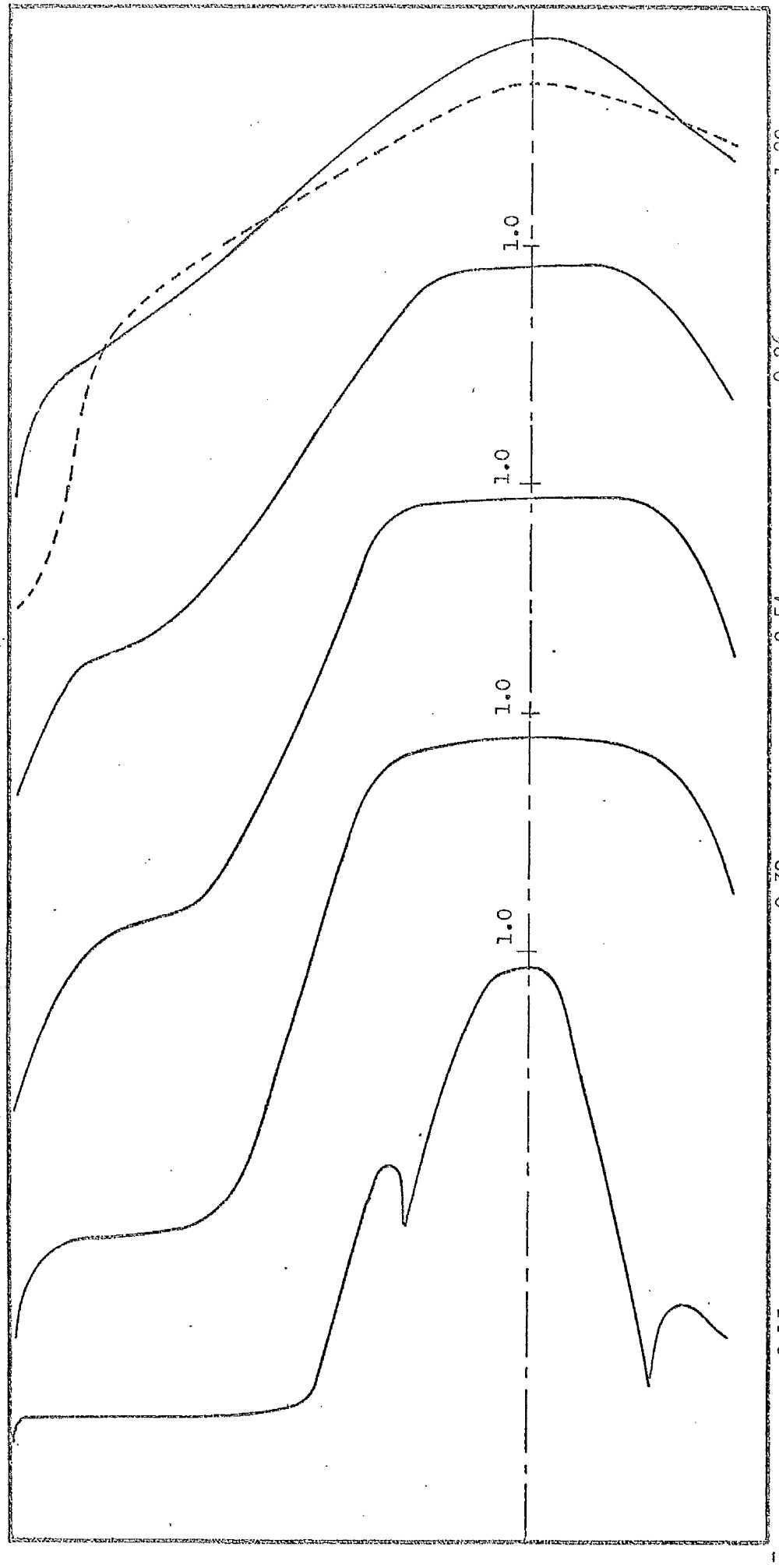

Figure 4.19.a. - Temperature Profiles.
0^{o} Hubless Swirler in D/d = 5 furnace.

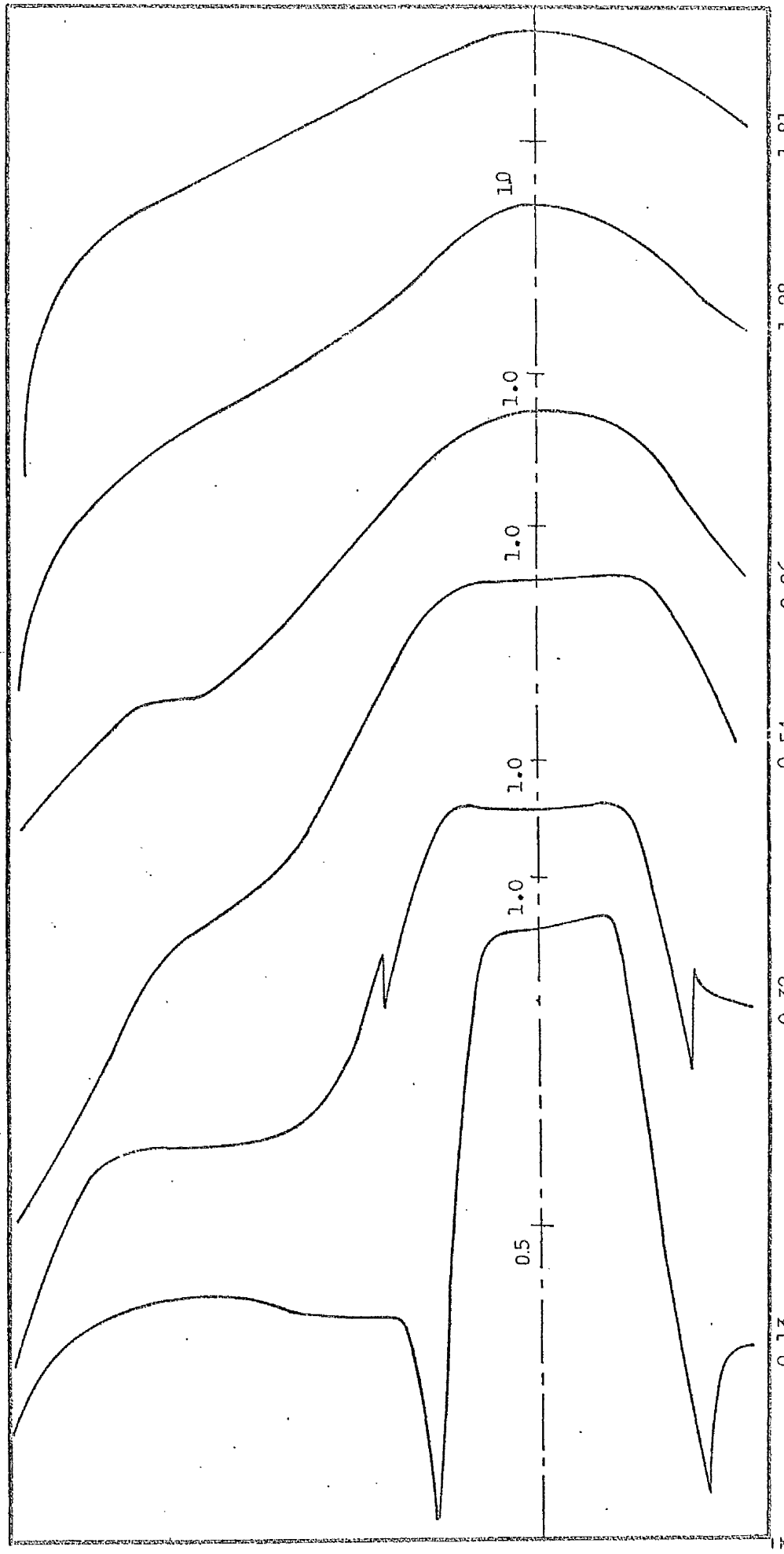

Figure 4.19.b. - Temperature Profiles.
15° Hubless Swirler in D/d = 5 furnace.

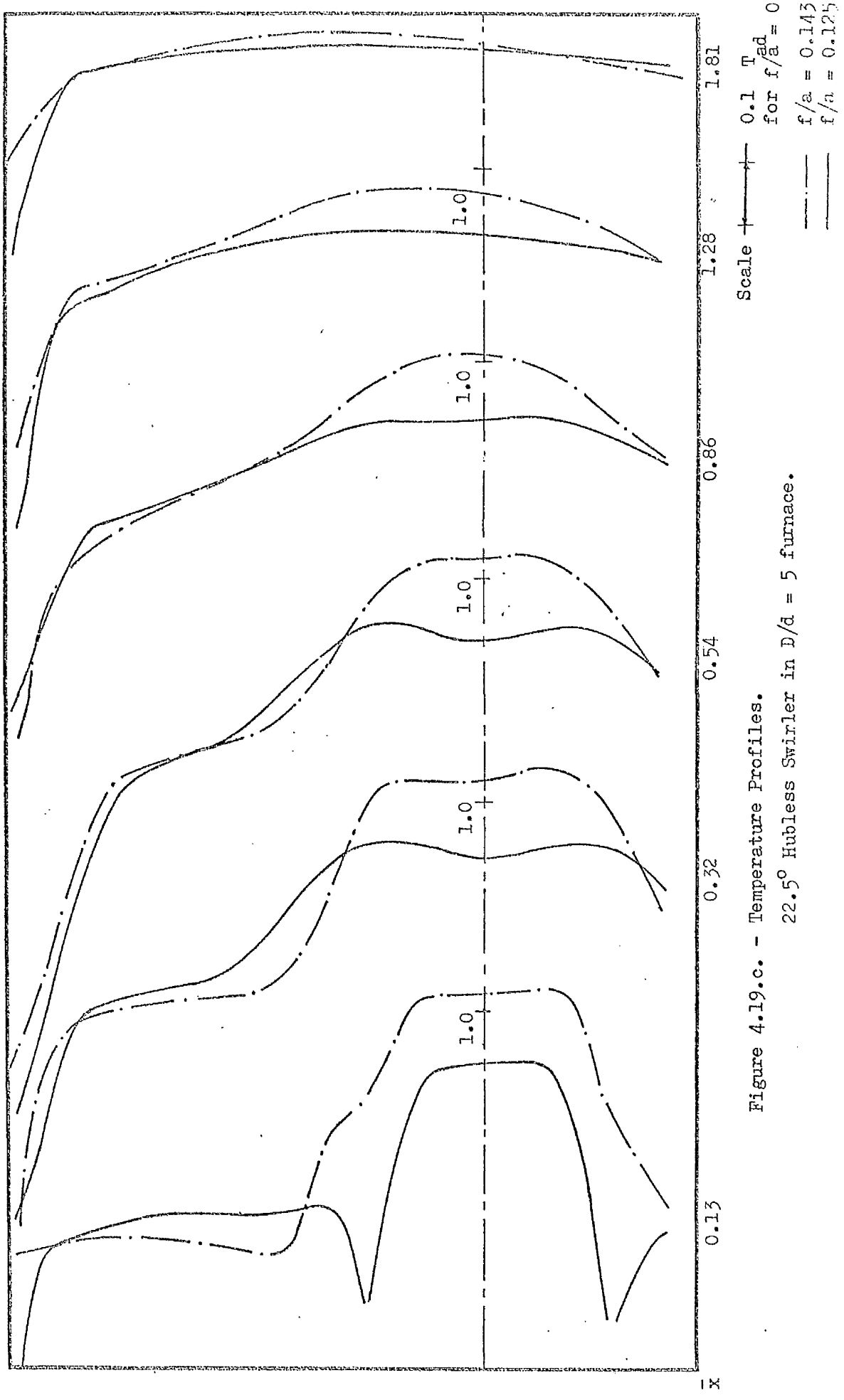

Figure 4.19.c. - Temperature Profiles.
22.5° Hubless Swirler in D/d = 5 furnace.

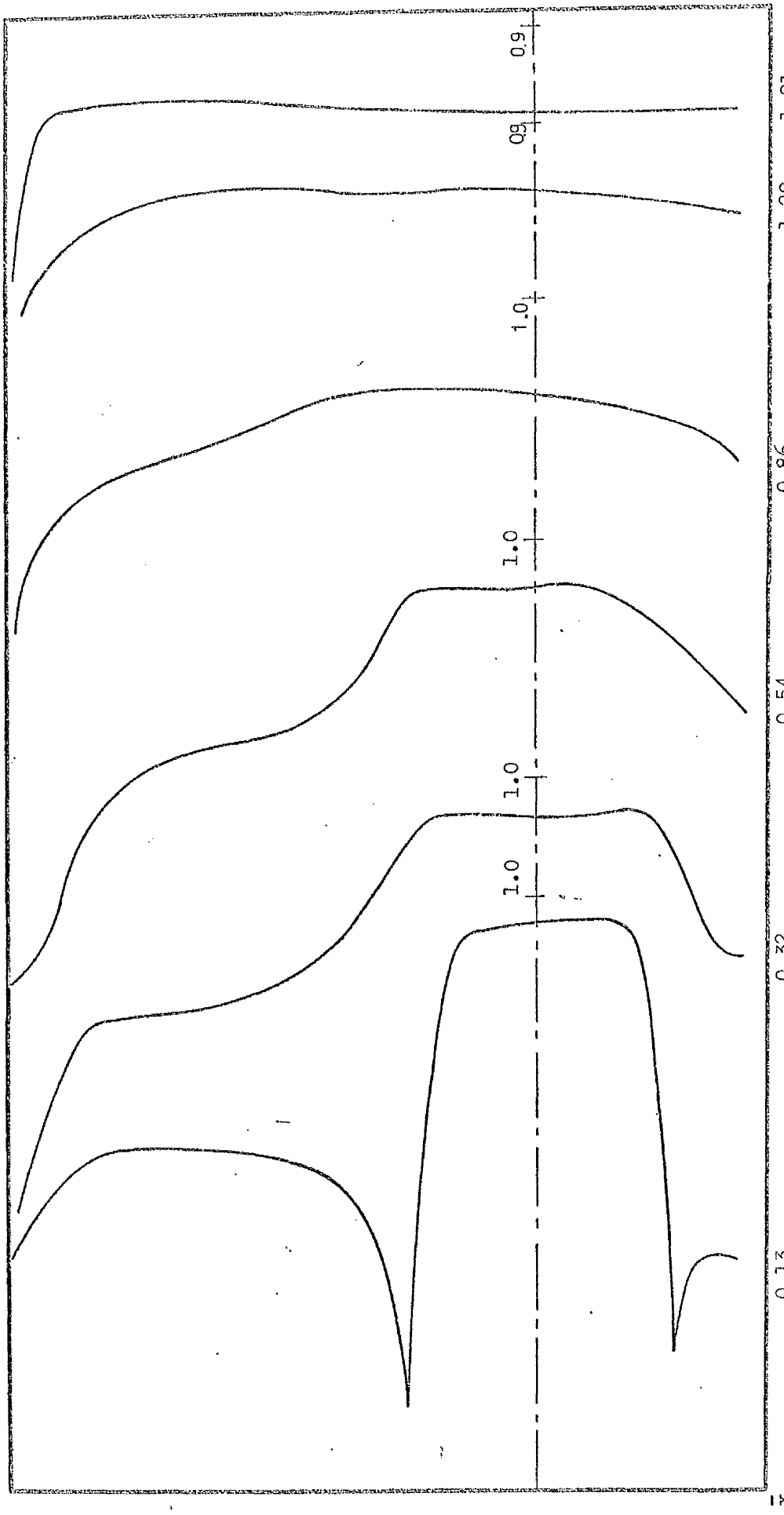

Figure 4.19.d. - Temperature Profiles.
30° Hubless Swirler in D/d = 5 furnace.

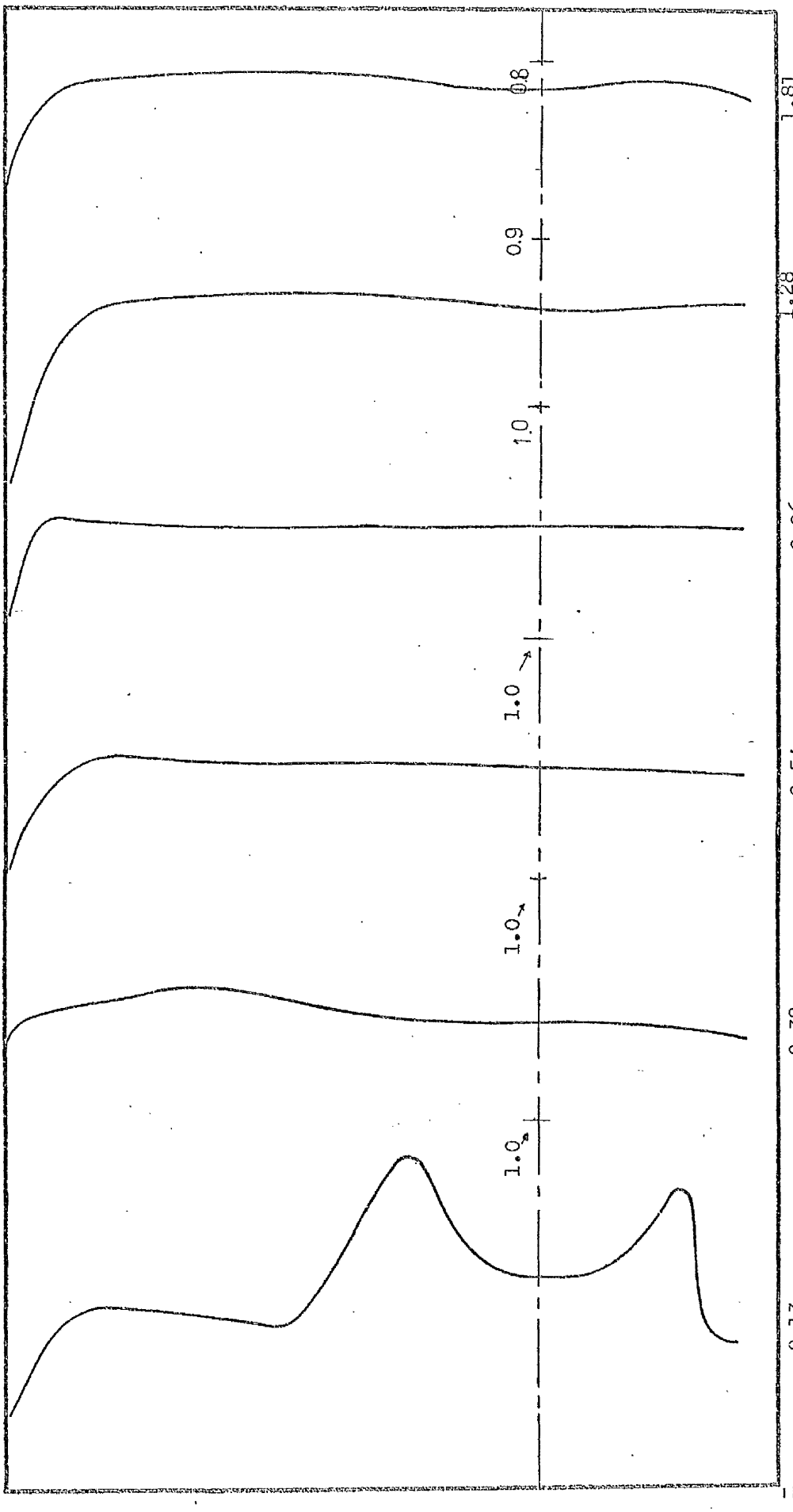

Figure 4.19.e. - Temperature Profiles.
45° Hubless Swirler in D/d = 5 furnace.

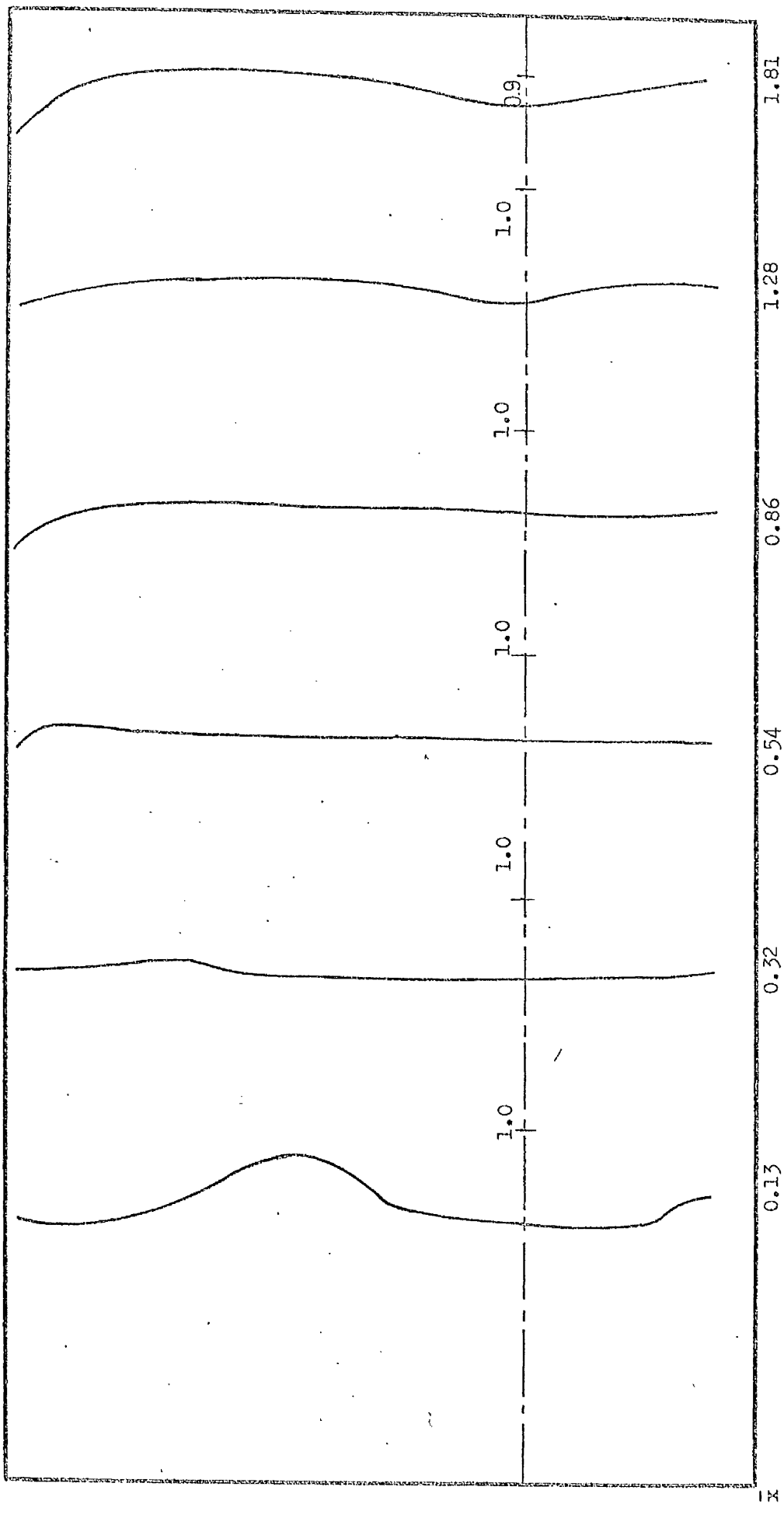

Figure 4.19.f. - Temperature Profiles.
60° Hubless Swirler in D/d = 5 furnace.

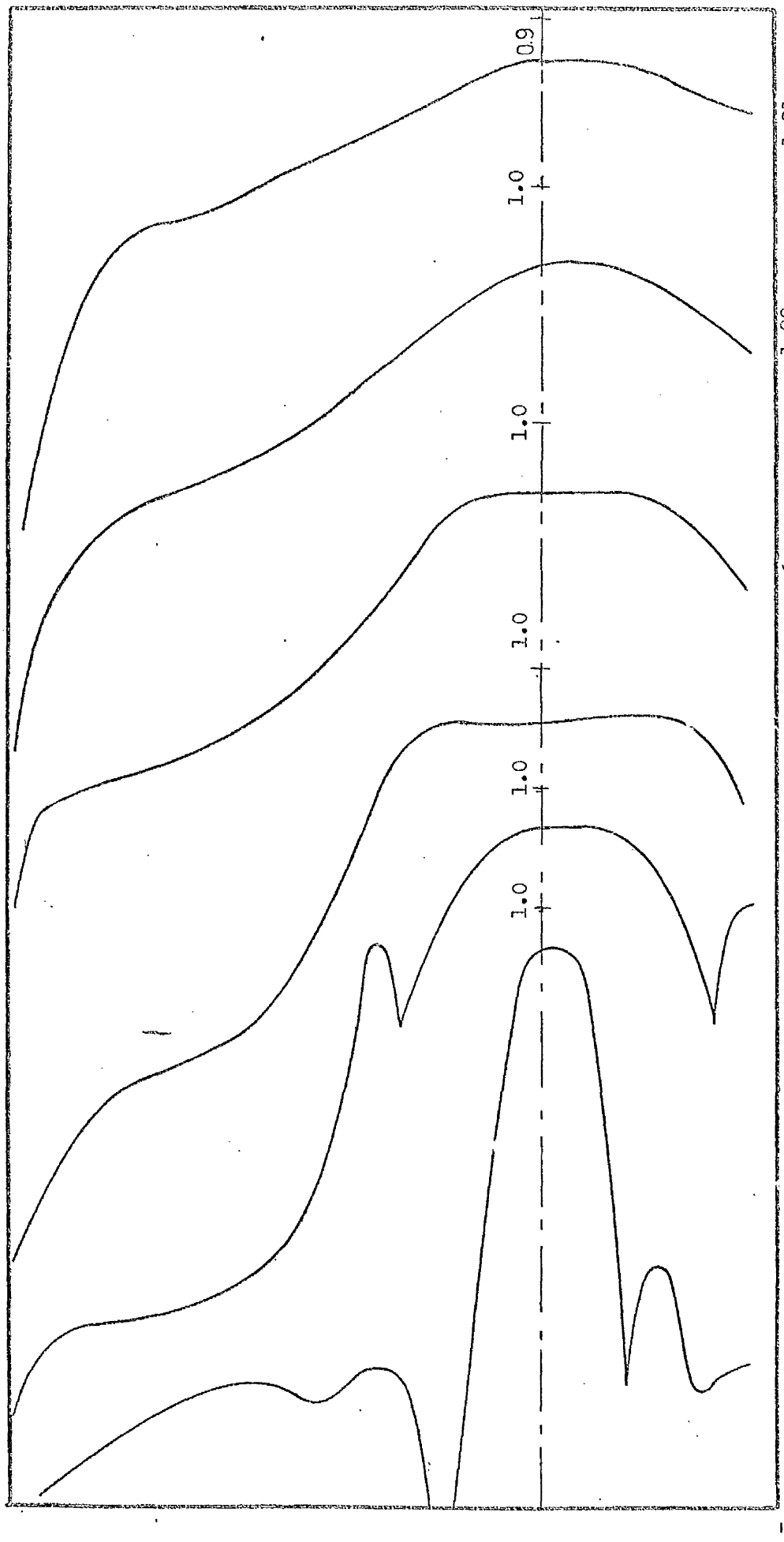

Figure 4.20.a. - Temperature Profiles.
0° Annular Swirler in D/d = 5 furnace.

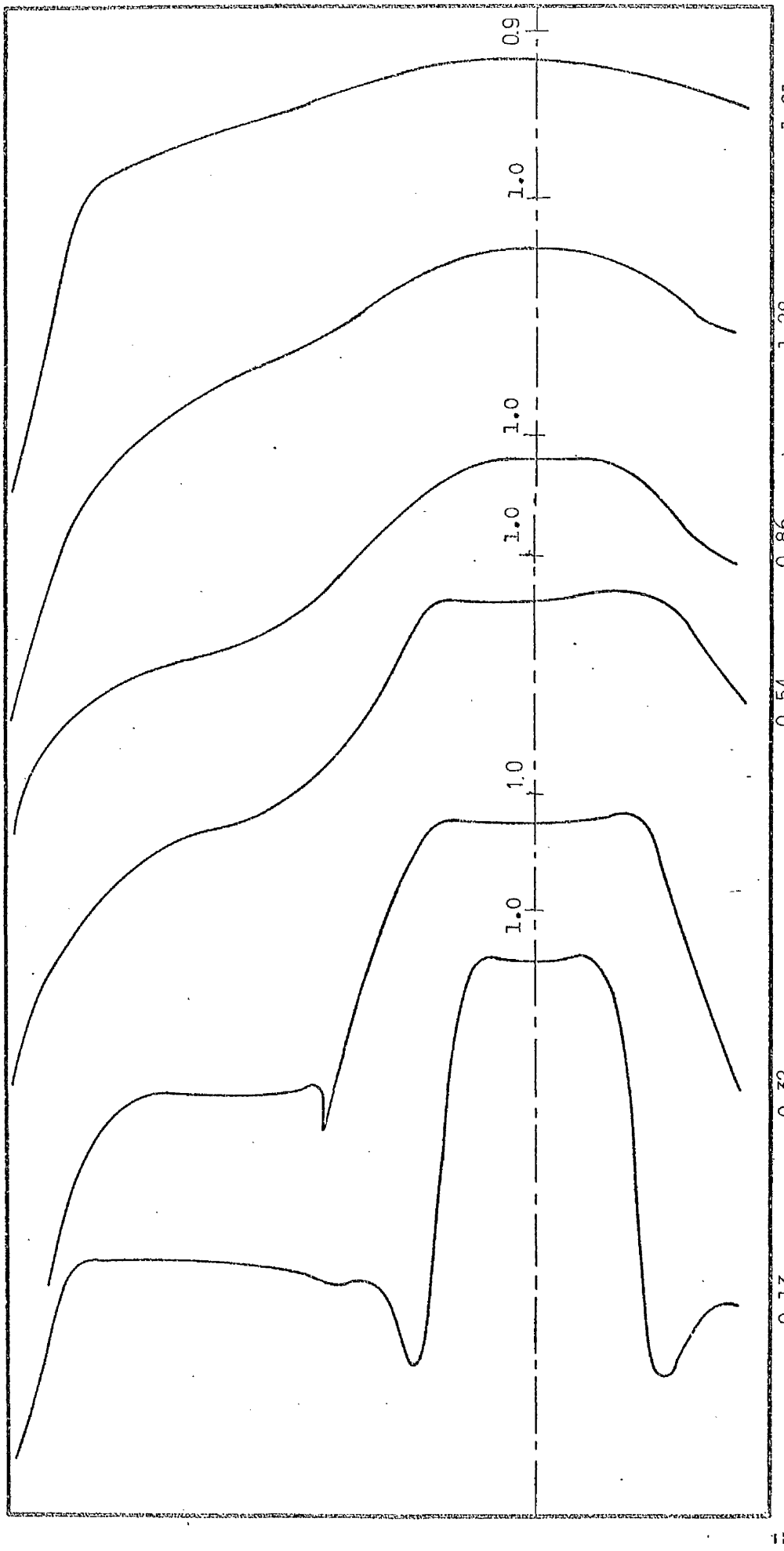

Figure 4.20.b. - Temperature Profiles.
15° Annular Swirler in D/d = 5 furnace.

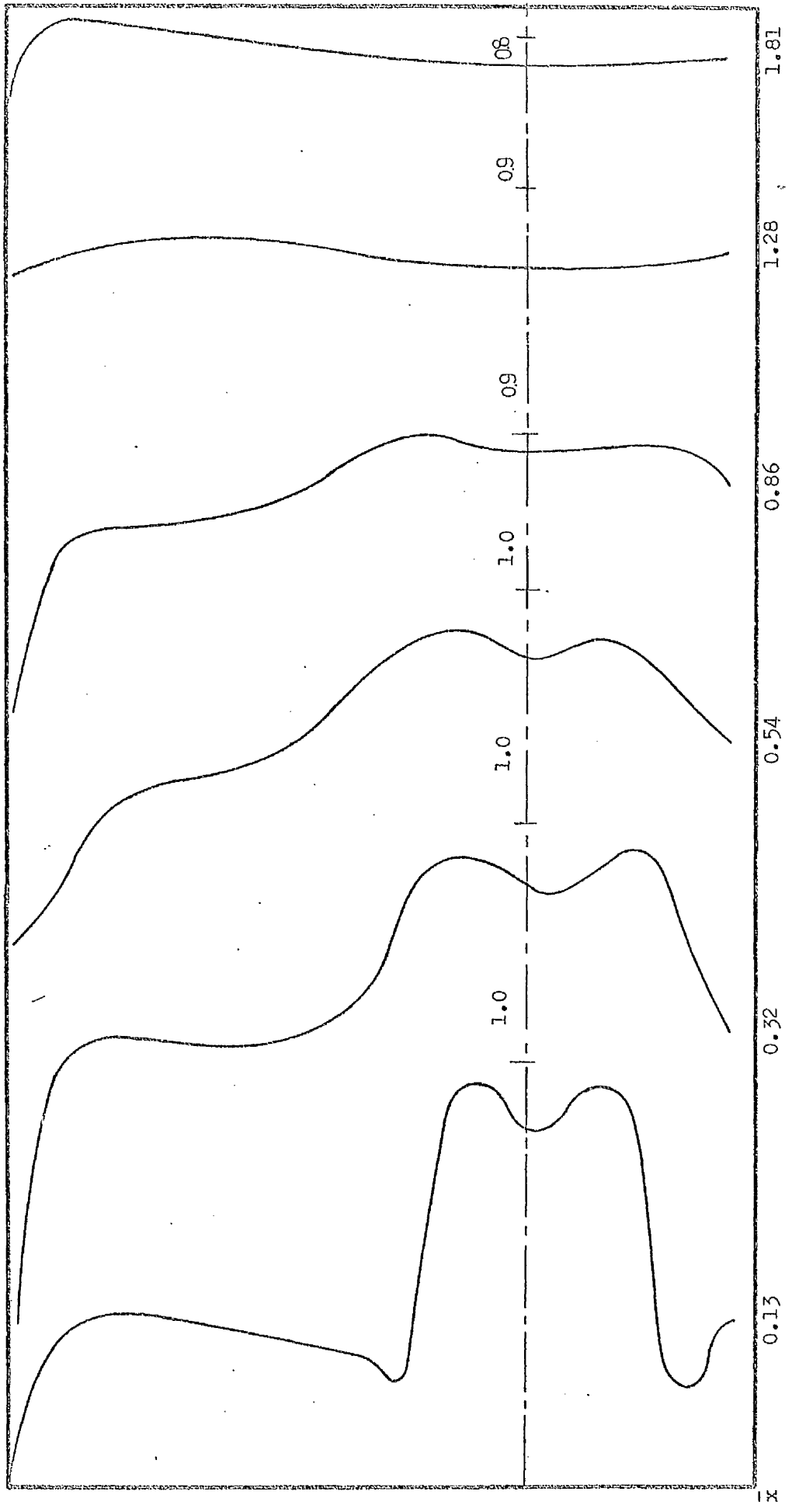

Figure 4.20.c. - Temperature Profiles.
30° Annular Swirler in D/d = 5 furnace.

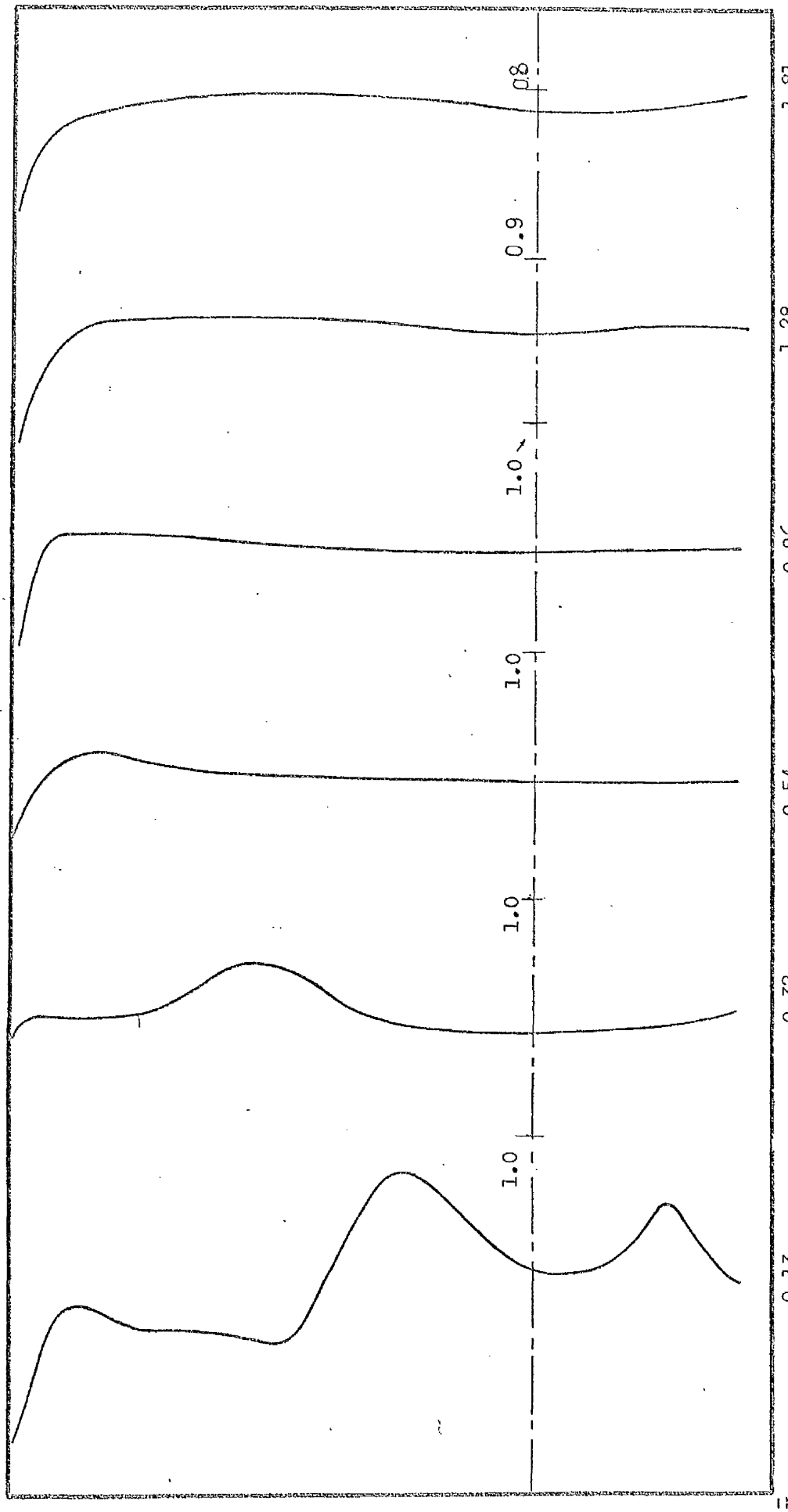

Figure 4.20.d. - Temperature Profiles.
45° Annular Swirler in D/d = 5 furnace.

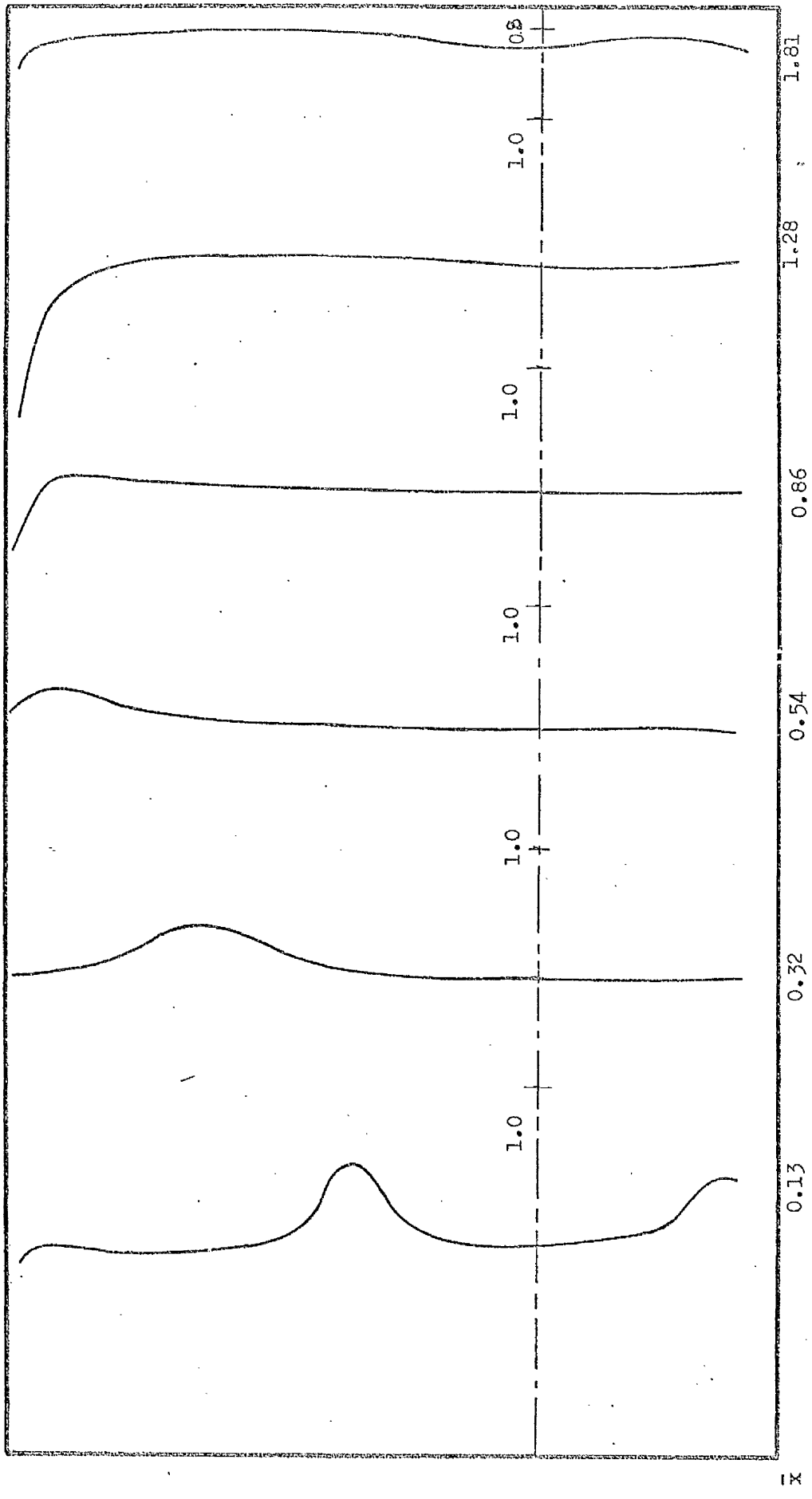

Figure 4.20.e. - Temperature Profiles.
60° Annular Swirler in D/d = 5 furnace.

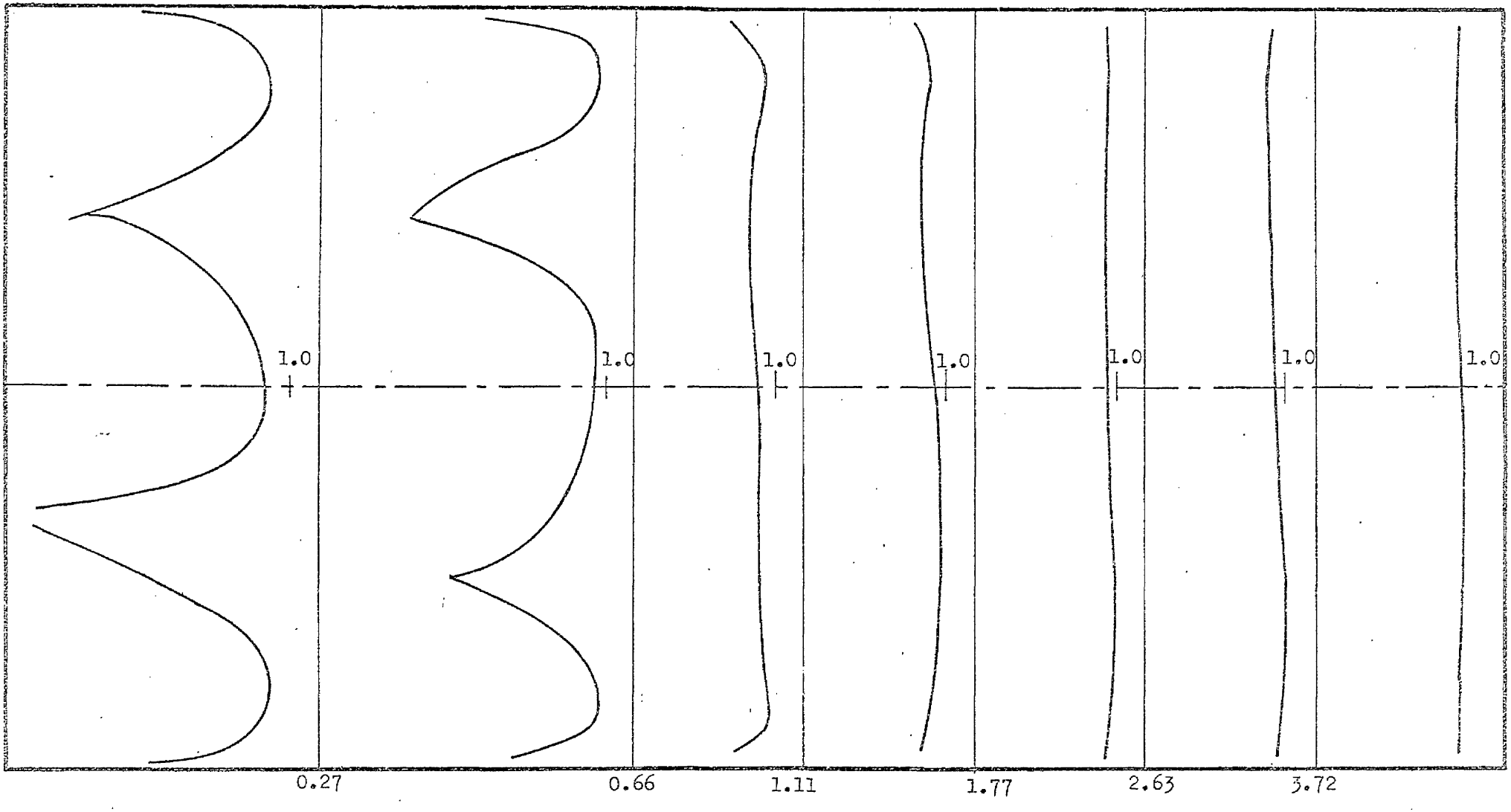

Figure 4.21.a. - CO_2 Concentration Profiles.
15^0 Hubless Swirler in D/d = 2.5 furnace.

Scale ⟷ 0.2 of complete combustion

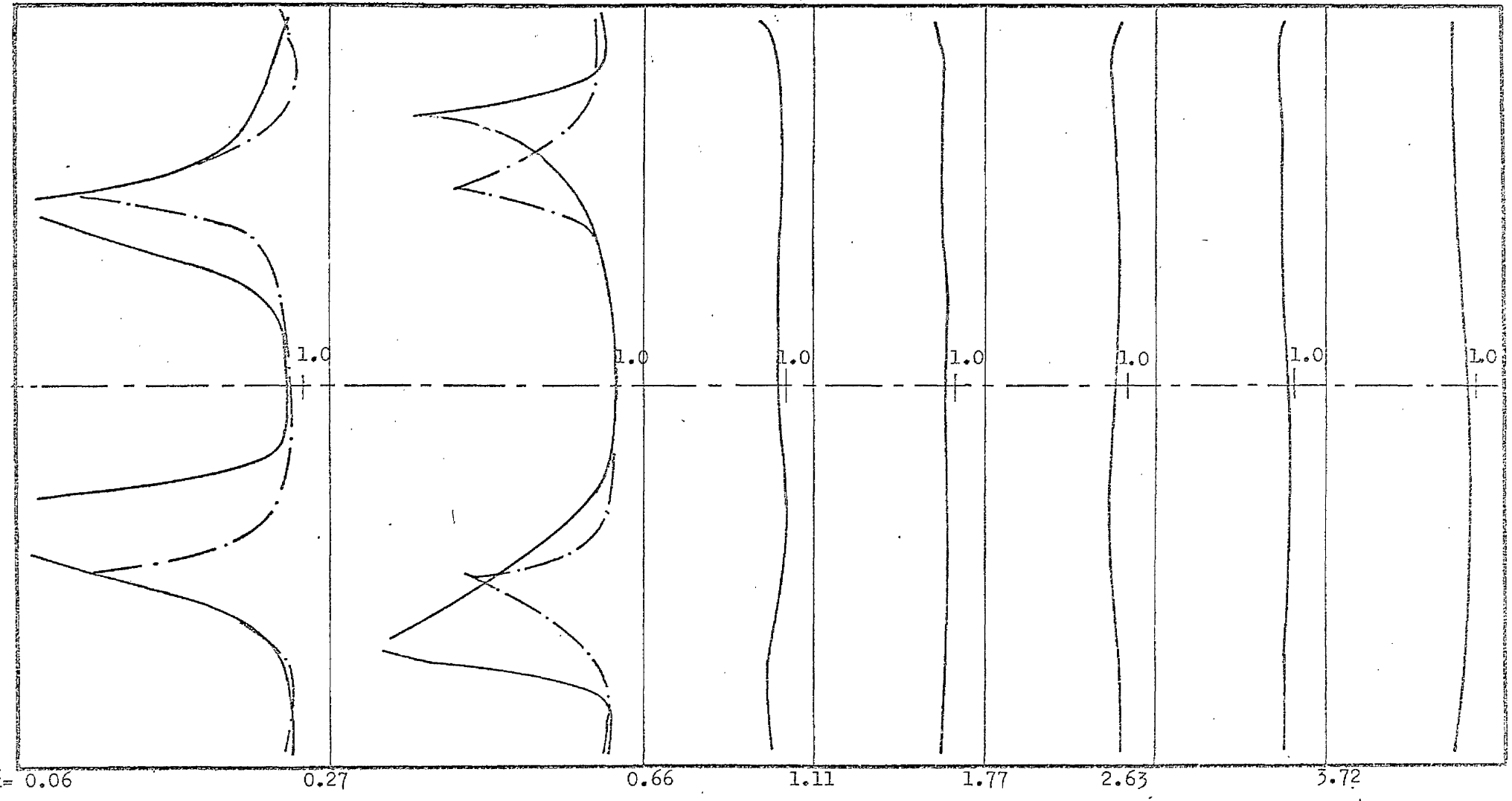

Figure 4.21.b. - Concentration Profiles.

30° Hubless Swirler in D/d = 2.5 furnace.

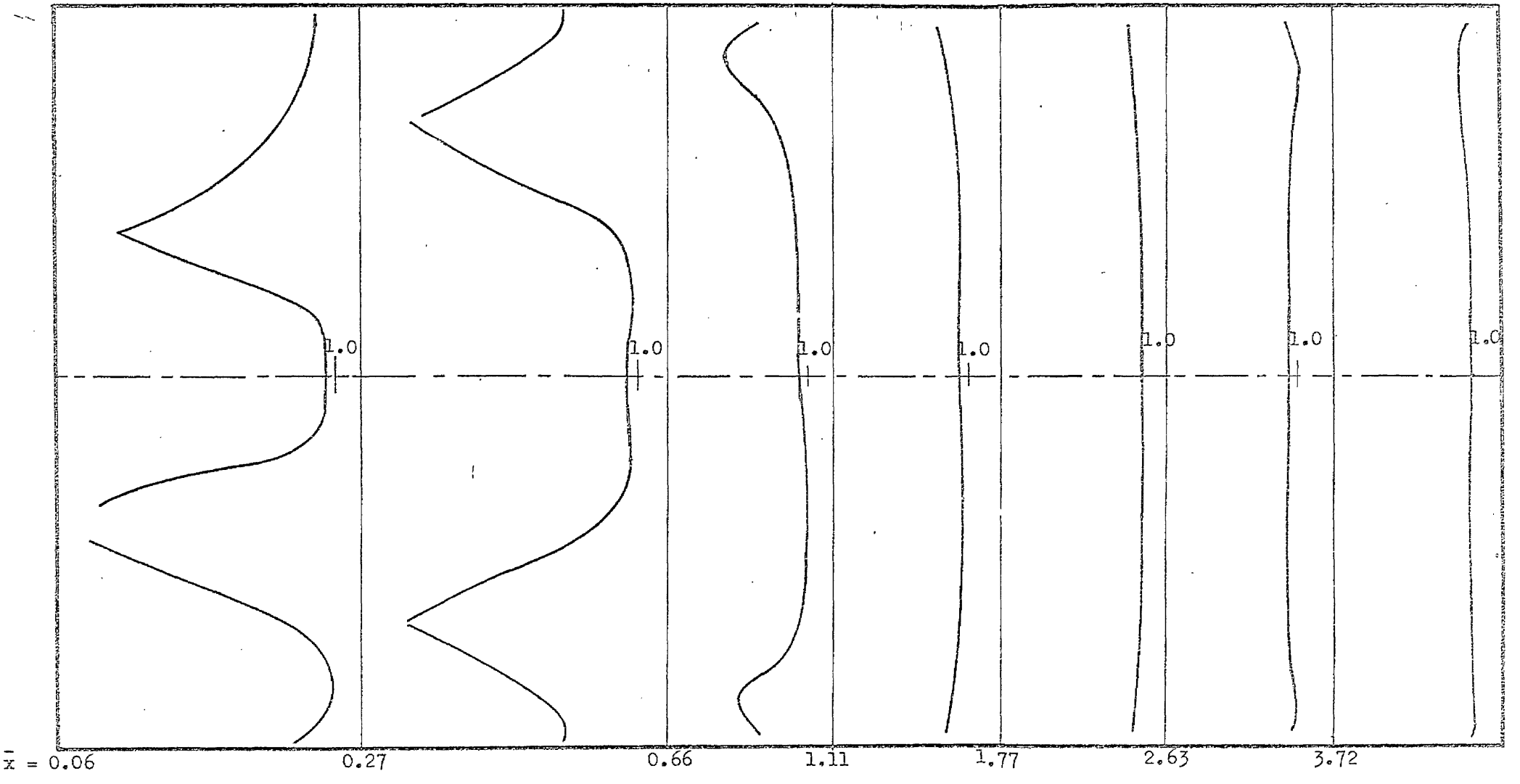

Figure 4.21.c. - CO_2 Concentration Profiles.
45° Hubless Swirler in D/d = 2.5 furnace.

Scale ⟷ 0.20 of complete combustion

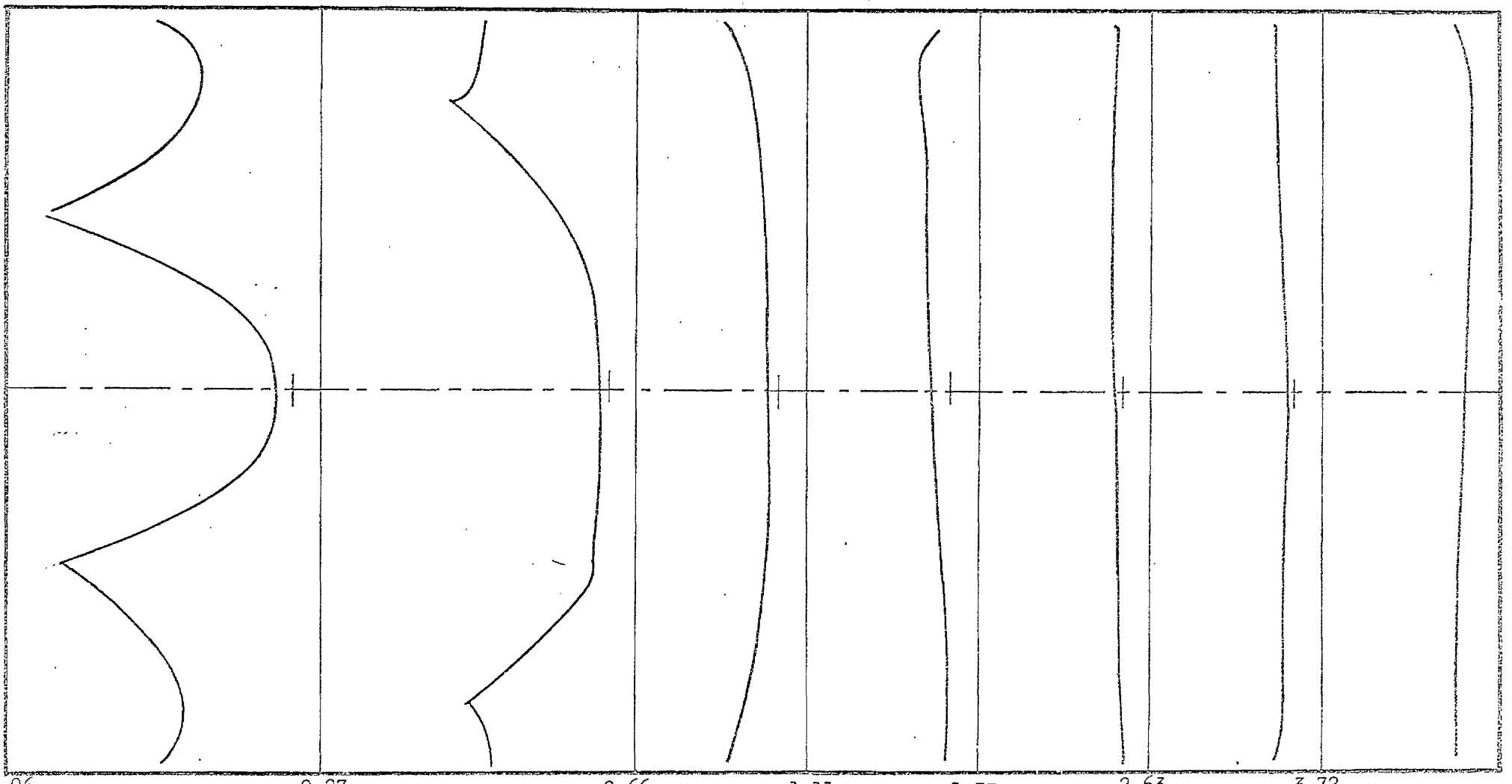

Figure 4.21.a. - CO_2 Concentration Profiles.

60° Hubless Swirler in D/d = 2.5 furnace.

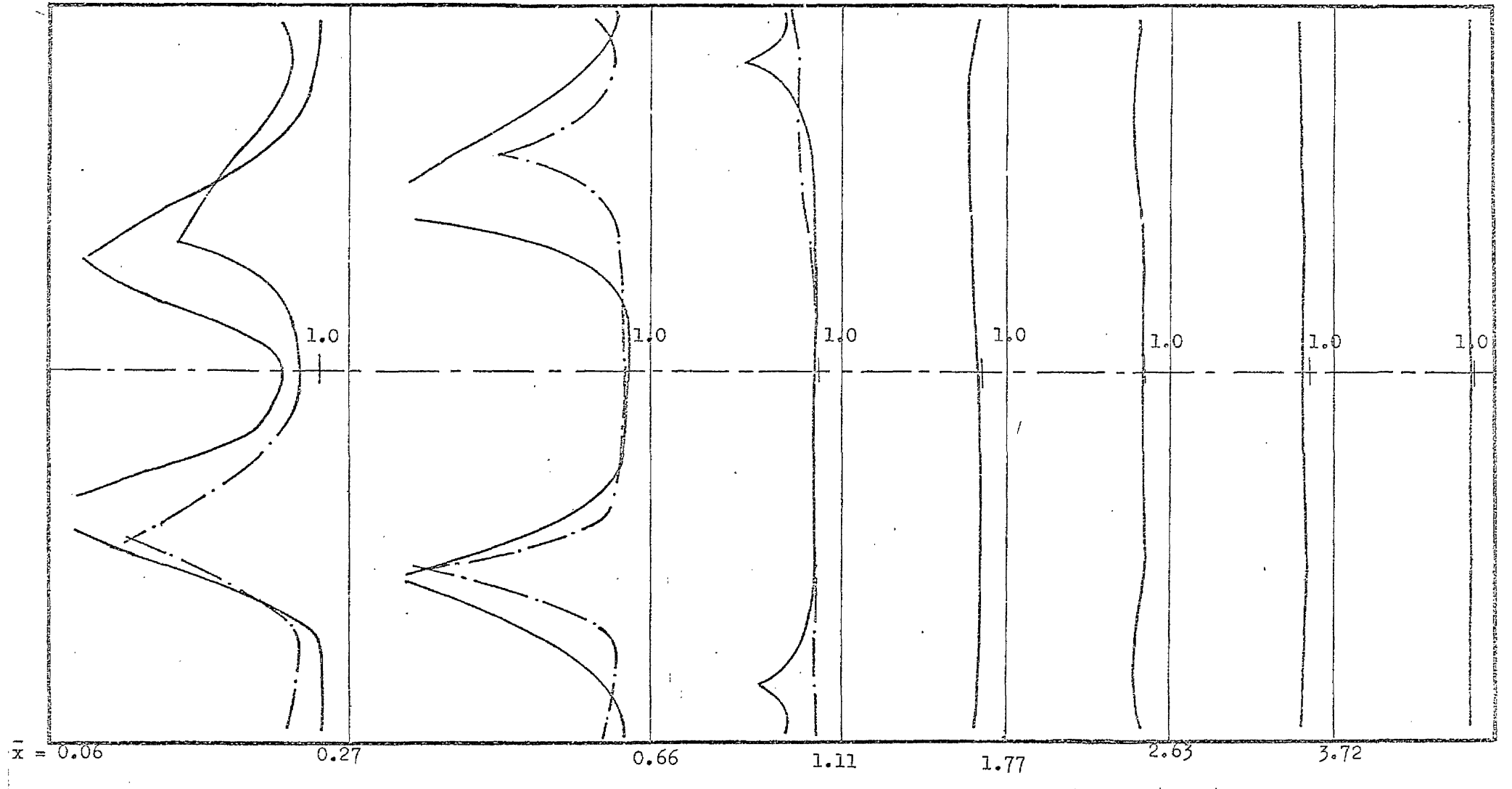

Figure 4.22.a. - CO_2 Concentration Profiles.

30° Annular Swirler in D/d = 2.5 furnace.

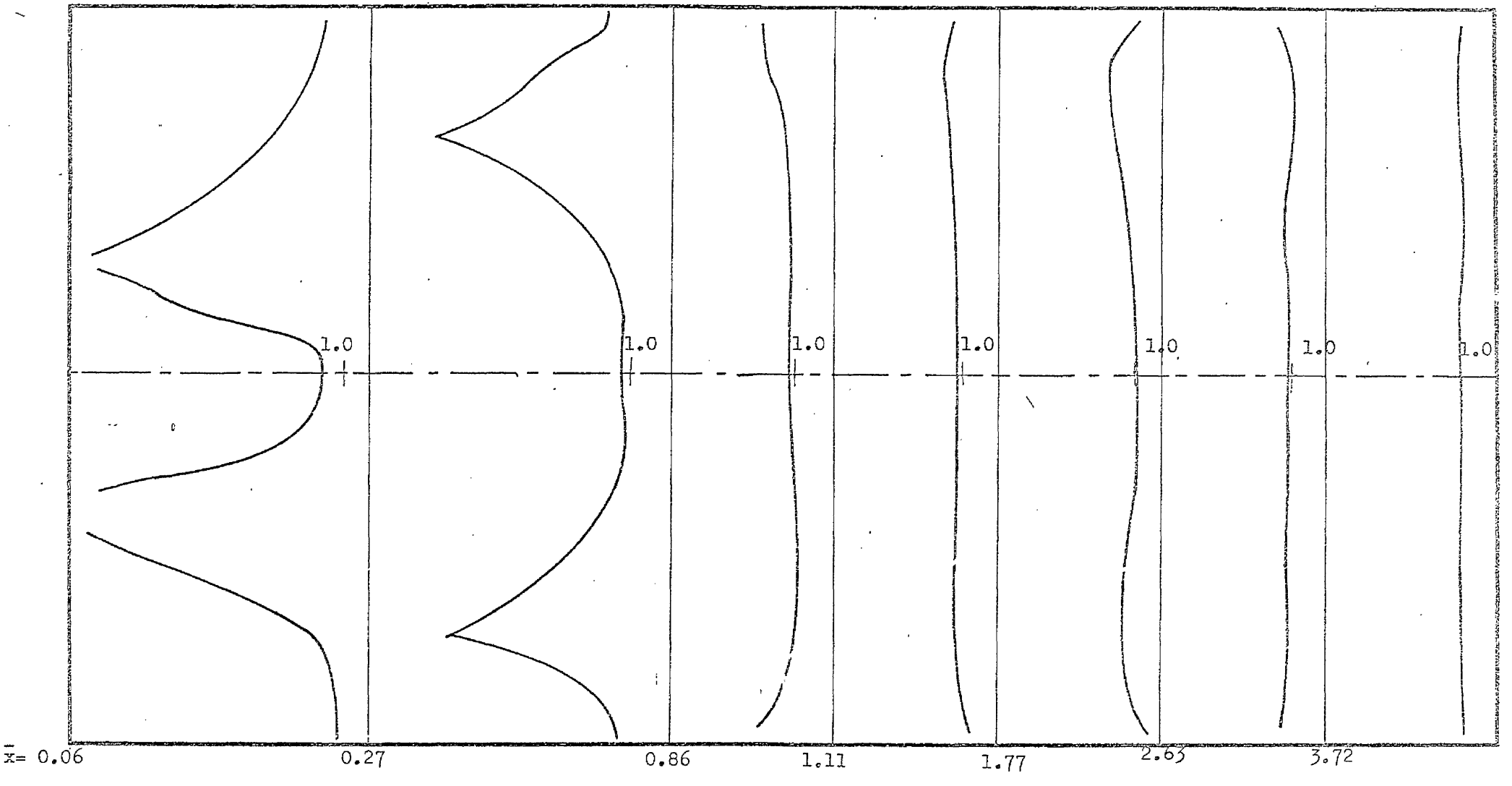

Figure 4.22.b. - CO_2 Concentration Profiles.
45° Annular Swirler in D/d = 2.5 furnace.

Scale ⟷ 0.20 of complete combustion

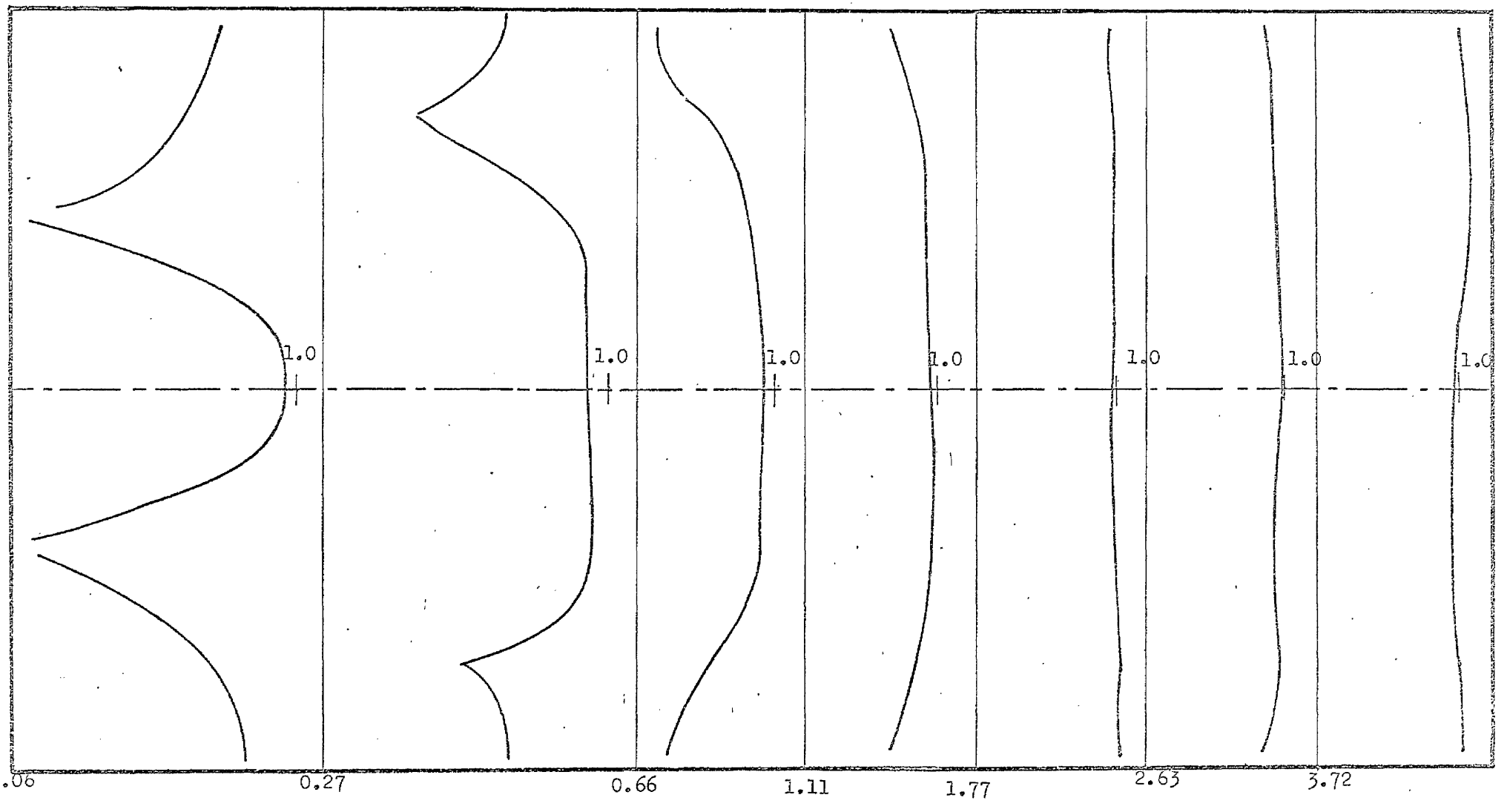

Figure 4.22.c. - CO_2 Concentration Profiles
60° Annular Swirler in D/d = 2.5 furnace.

Scale ⊣——⊢ 0.20 of complete combustion

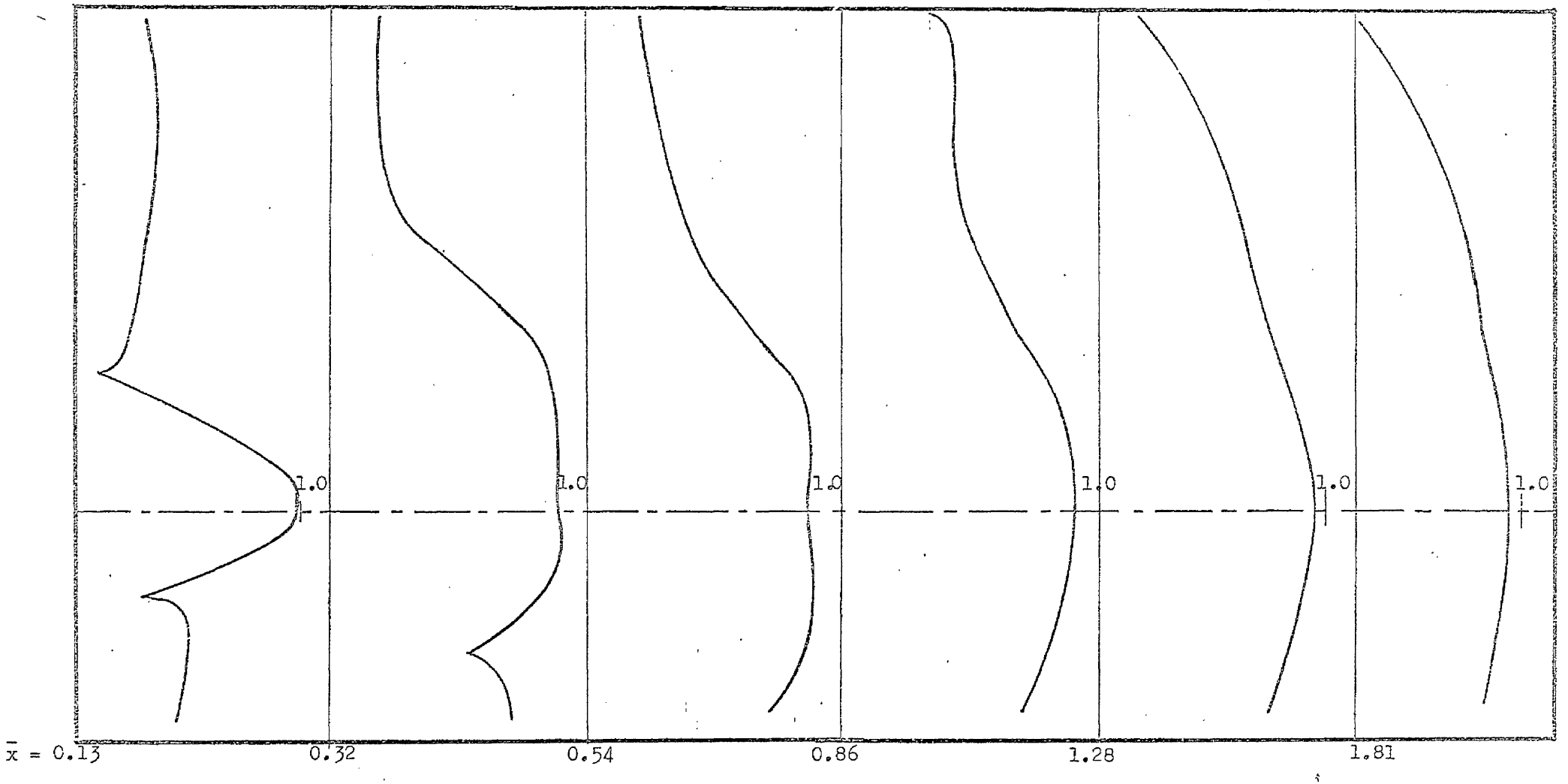

Figure 4.23.a. - CO_2 Concentration Profiles.
0^o Hubless Swirler in D/d = 5 furnace.

Scale ⊣——⊢ 0.2 of complete combustion

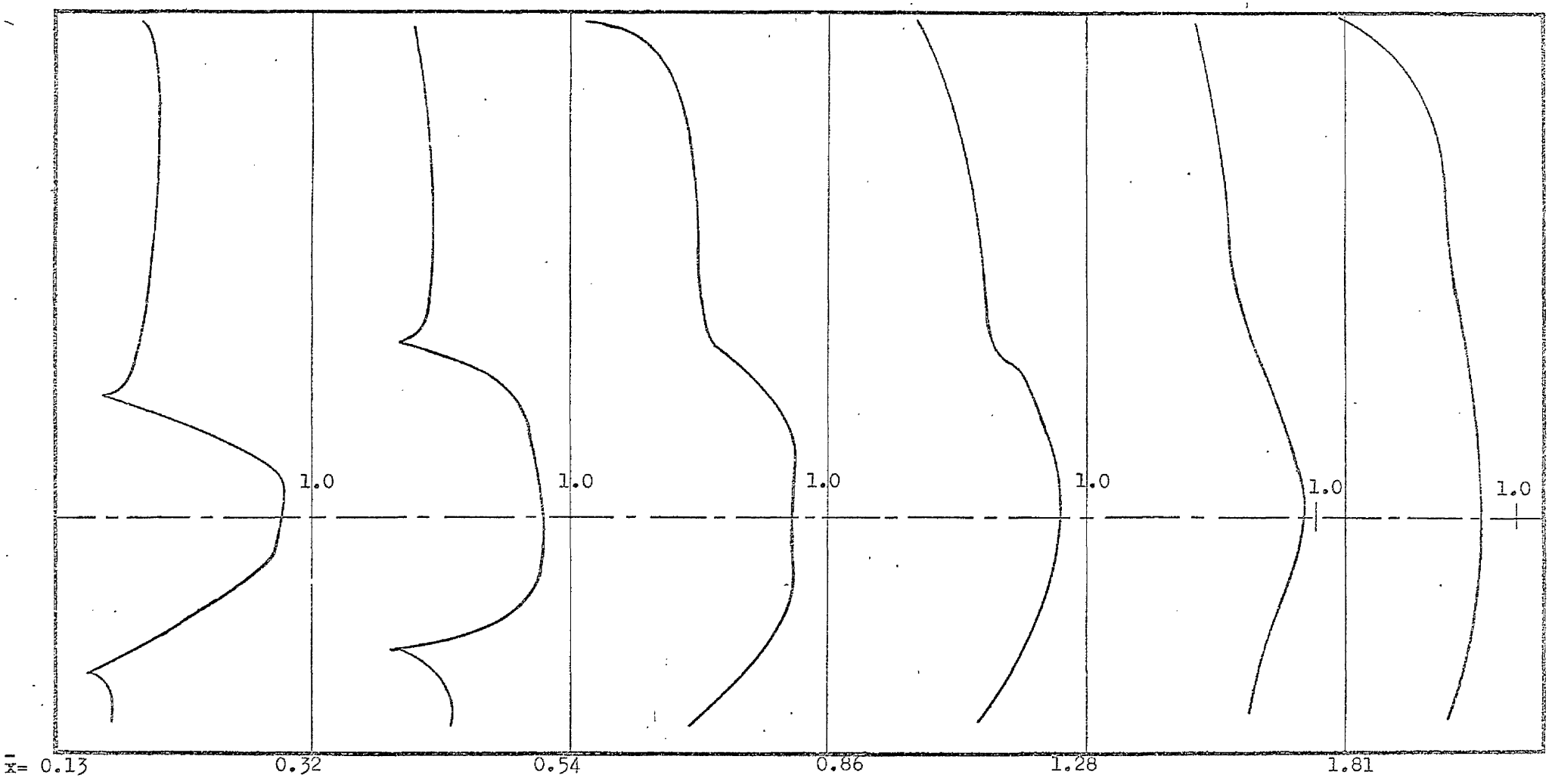

Figure 4.23.b. - CO_2 Concentration Profiles.
15° Hubless Swirler in D/d = 5 furnace.

Scale ⊢——⊣ 0.2 of complete combustion

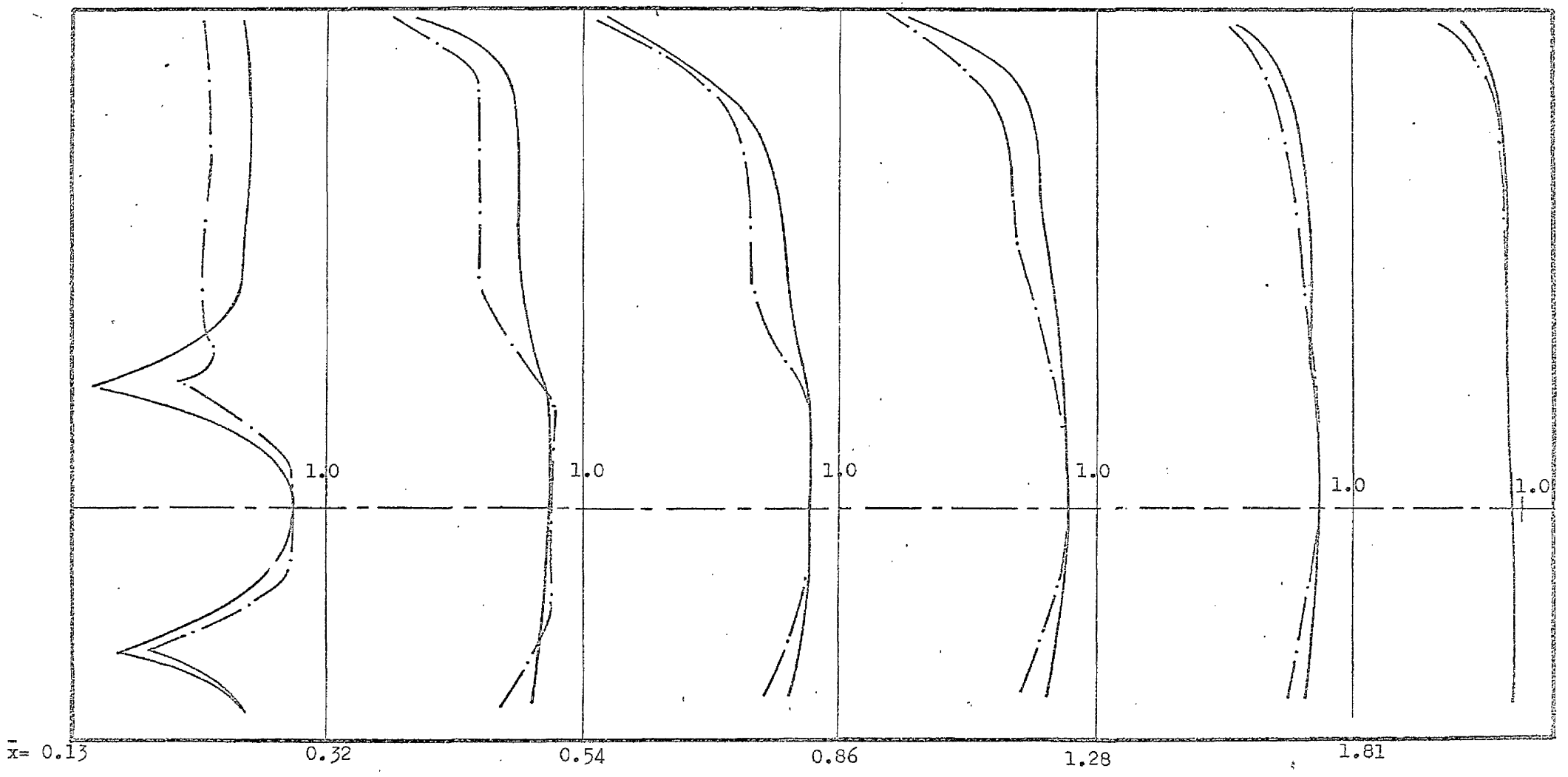

Figure 4.23.c. - CO_2 Concentration Profiles.
22.5° Hubless Swirler in D/d = 5 furnace.

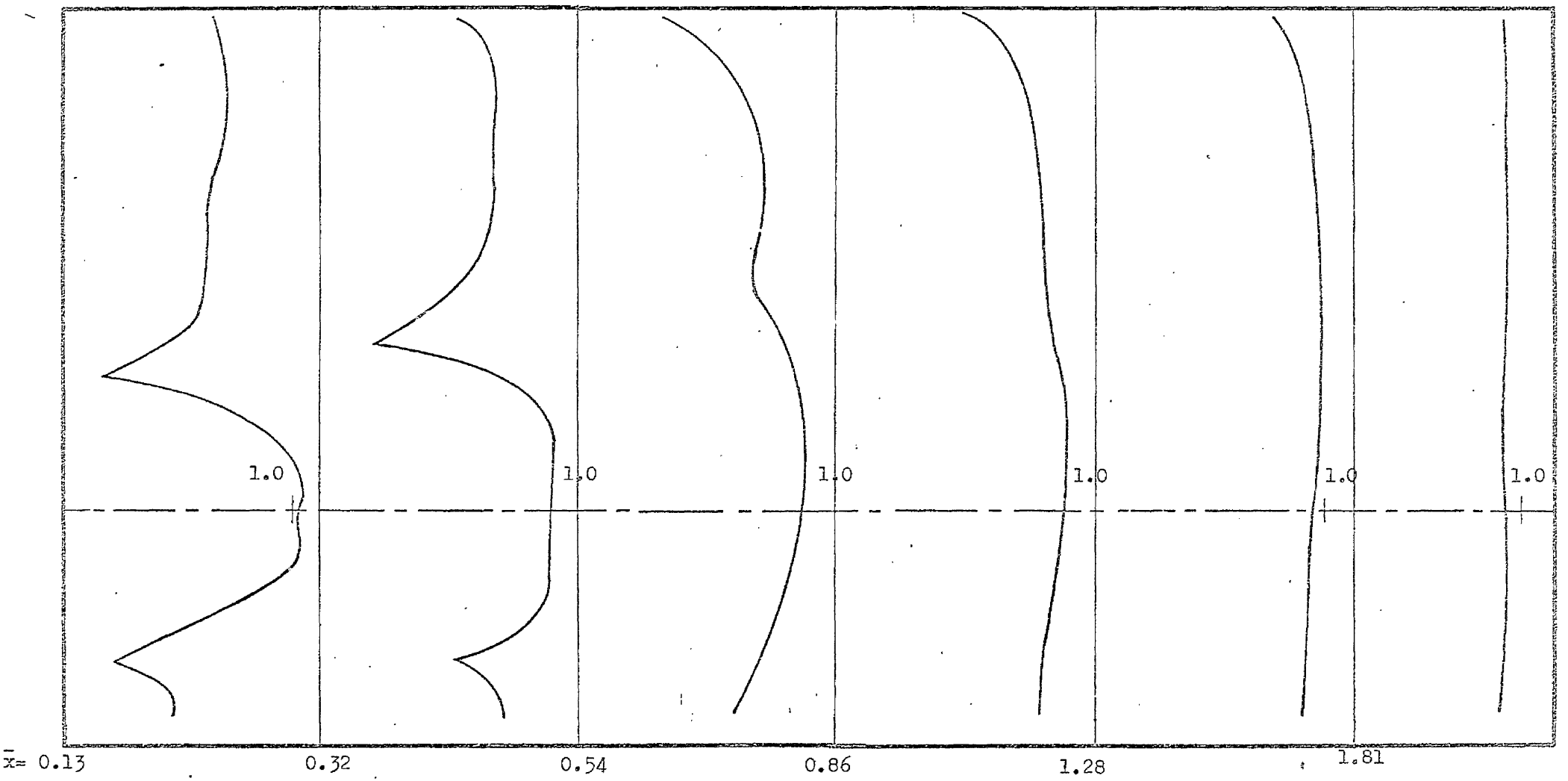

Figure 4.23.d. - CO_2 Concentration Profiles.
30^{o} Hubless Swirler in D/d = 5 furnace.

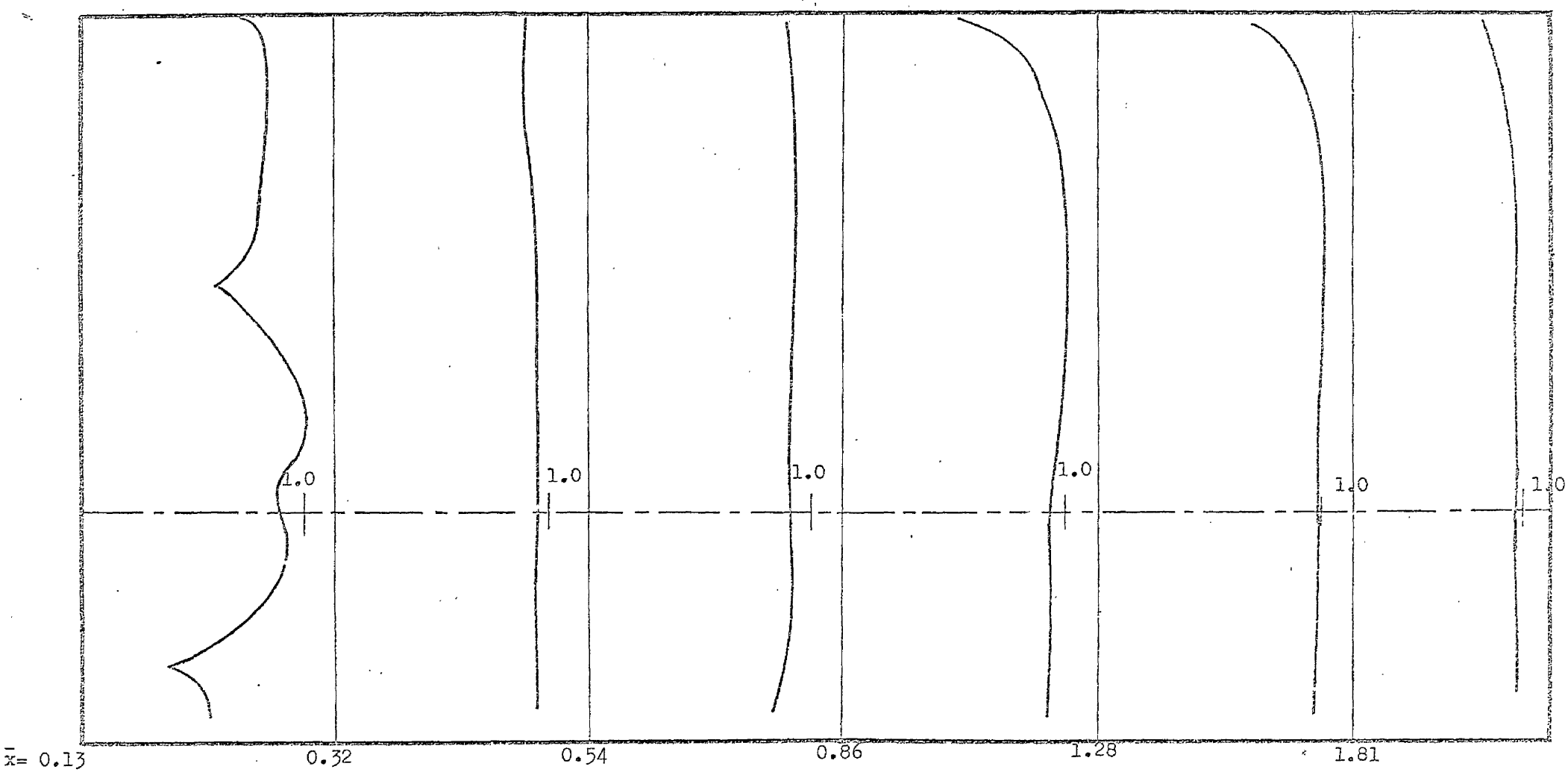

Figure 4.23.e. - CO_2 Concentration Profiles.
45° Hubless Swirler in D/d = 5 furnace.

Scale ⊣——⊢ 0.2 of complete combustion

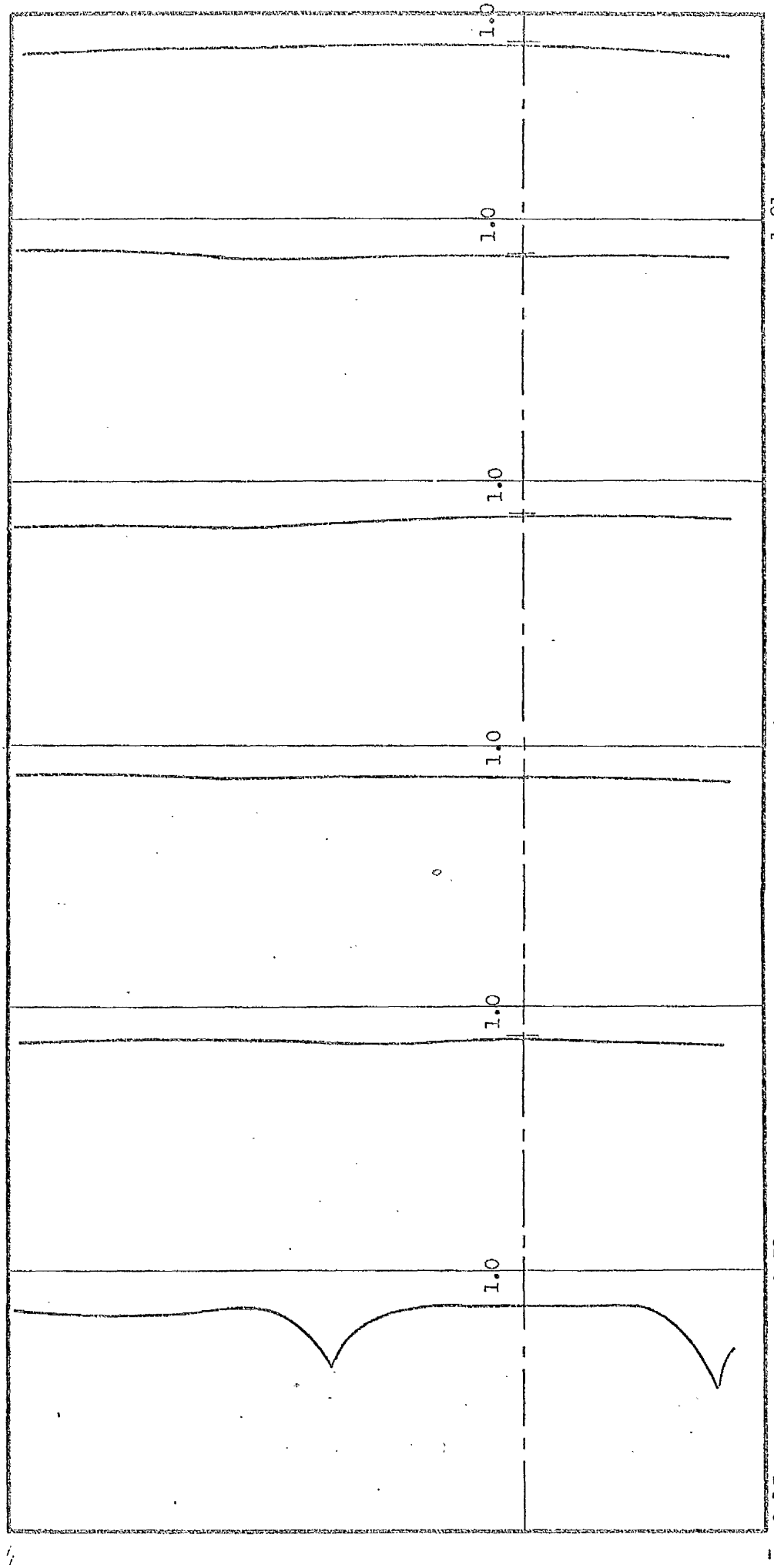

Figure 4.23.f. - CO_2 Concentration Profiles.
60° Hubless Swirler in D/d = 5 furnace.

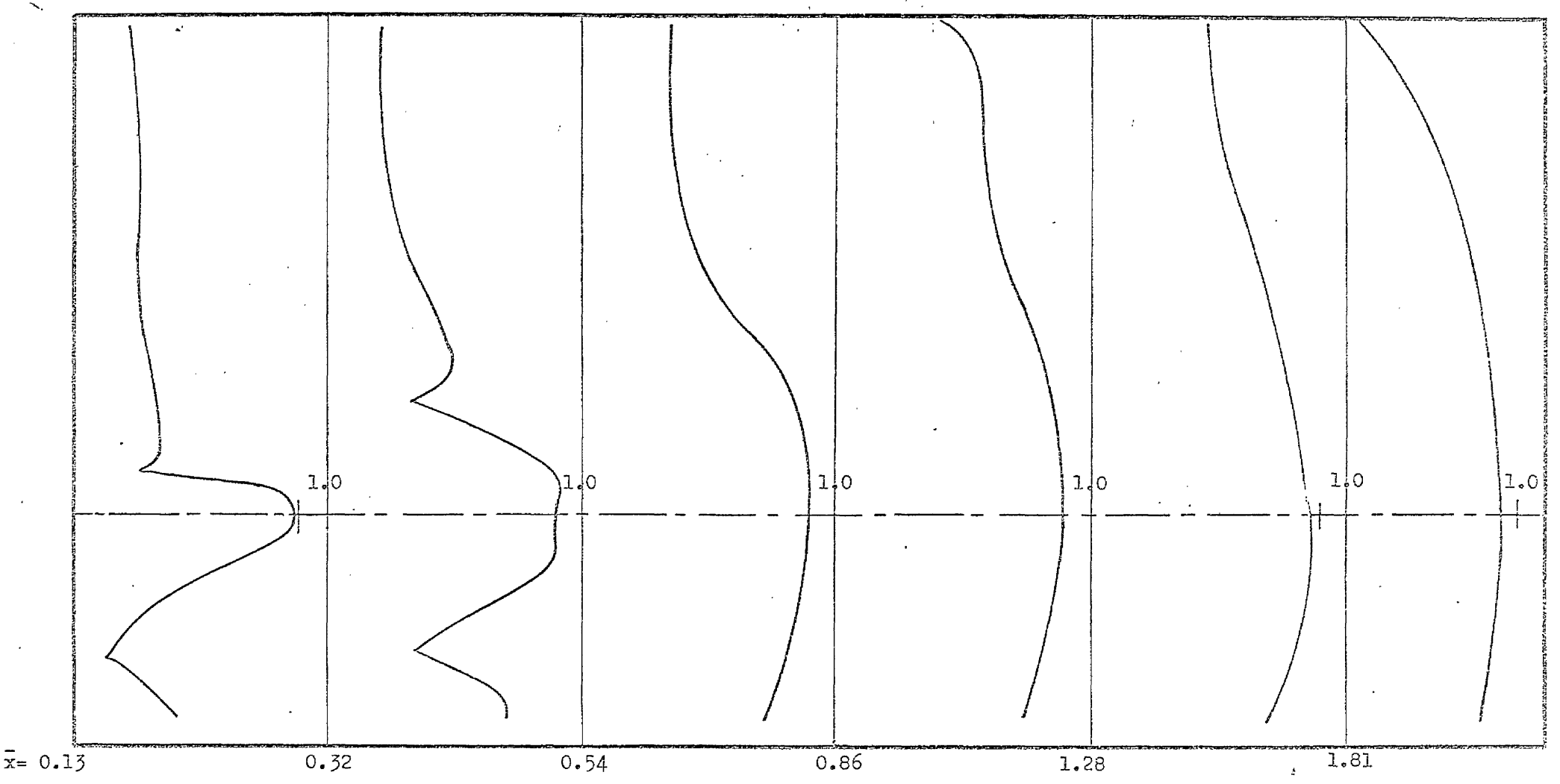

Figure 4.24.a. - CO_2 Concentration Profiles.
0^{o} Annular Swirler in D/d = 5 furnace.

Scale —|——|— 0.2 of comple
combustic

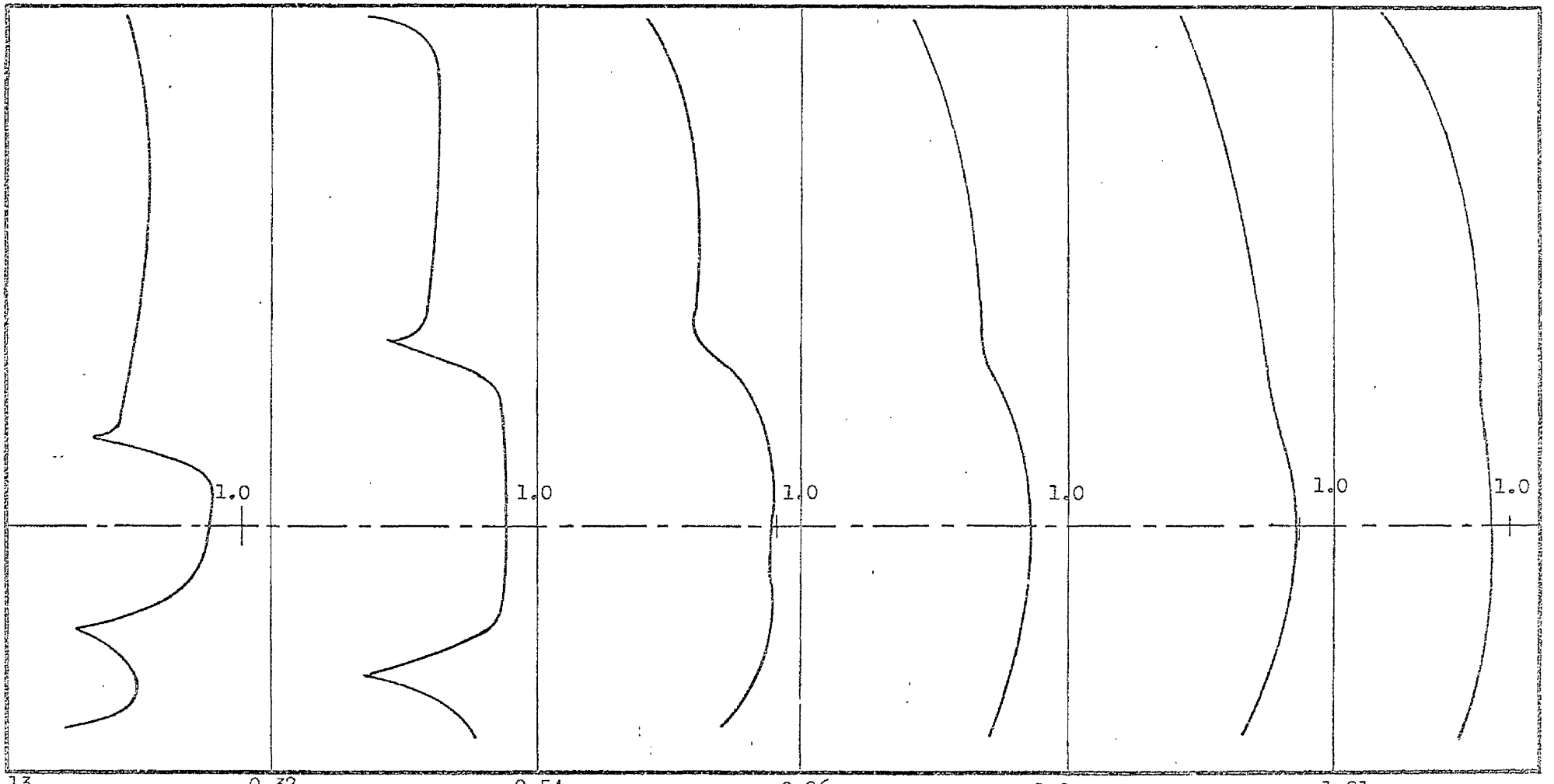

Figure 4.24.b. - CO_2 Concentration Profiles.
15° Annular Swirler in D/d = 5 furnace.

Scale ⊣——⊢ 0.2 of compl
combusti

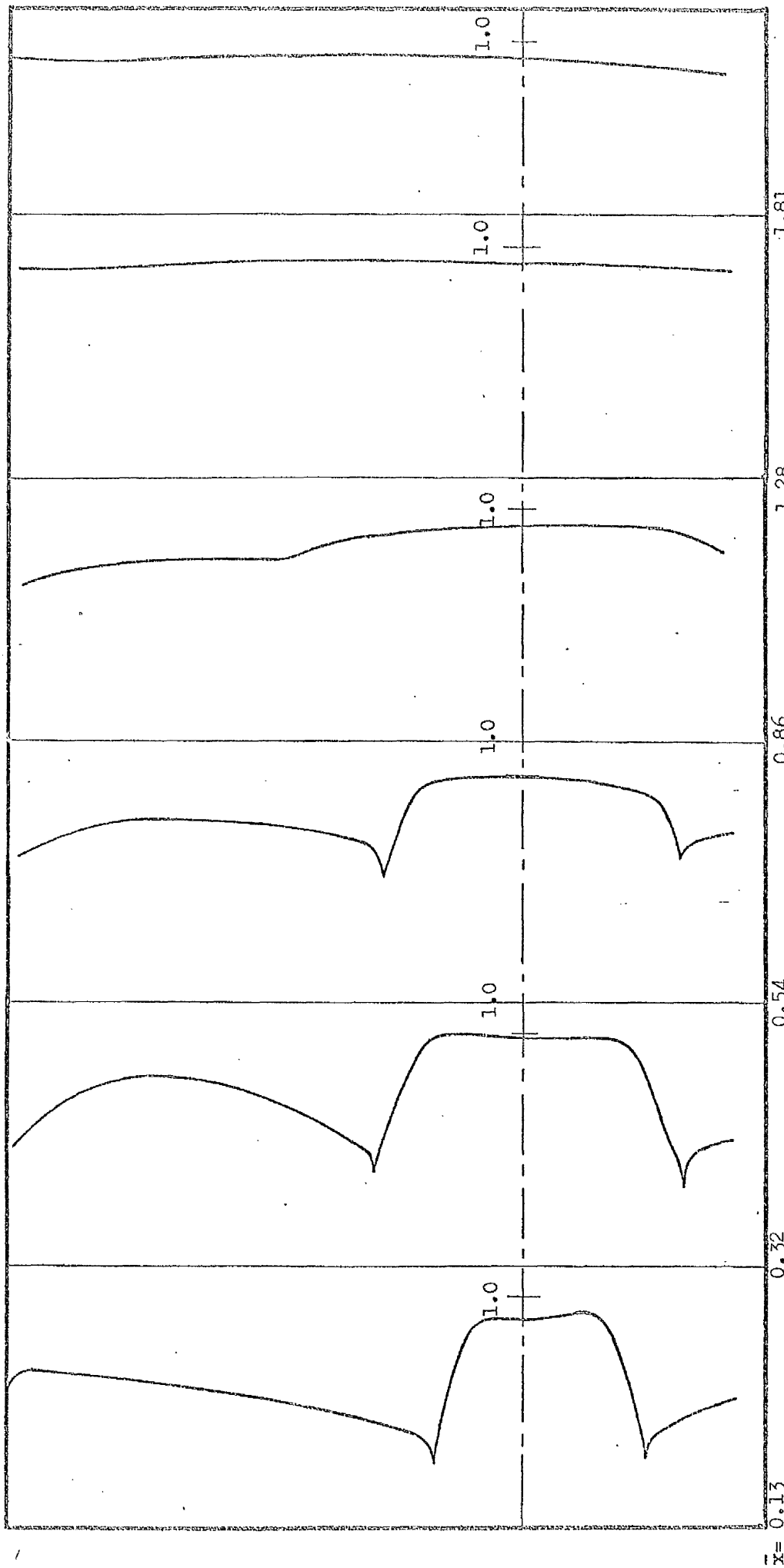

Scale ⊢—⊣ 0.2 of complet
combustion

Figure 4.24.c. - CO_2 Concentration Profiles.
30° Annular Swirler in D/d = 5 furnace.

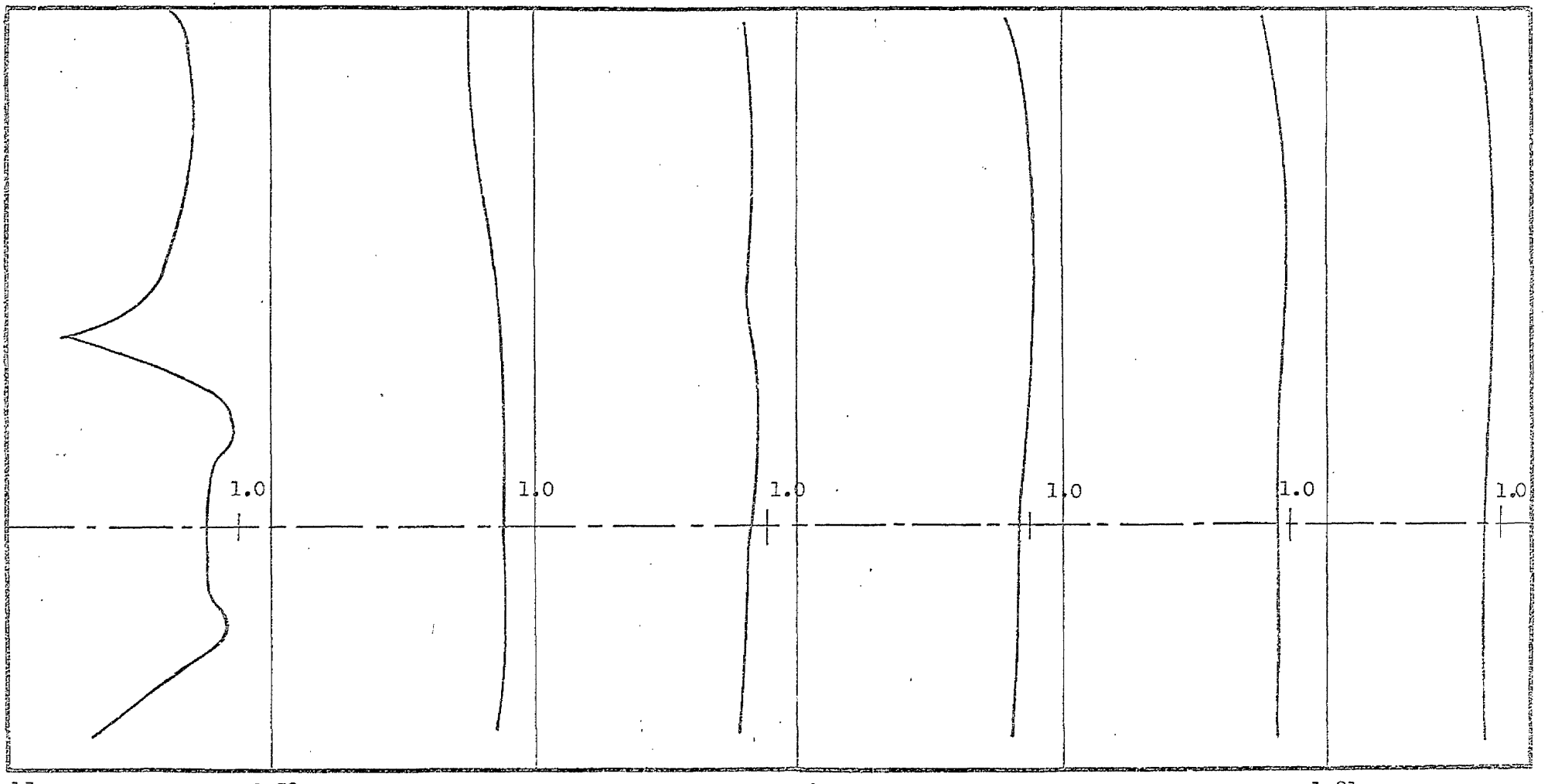

$\bar{x}$= 0.13 0.32 0.54 0.86 1.28 1.81

Figure 4.24.d. - CO_2 Concentration Profiles.
45° Annular Swirler in D/d = 5 furnace.

Scale ⟷ 0.2 of complete combustion

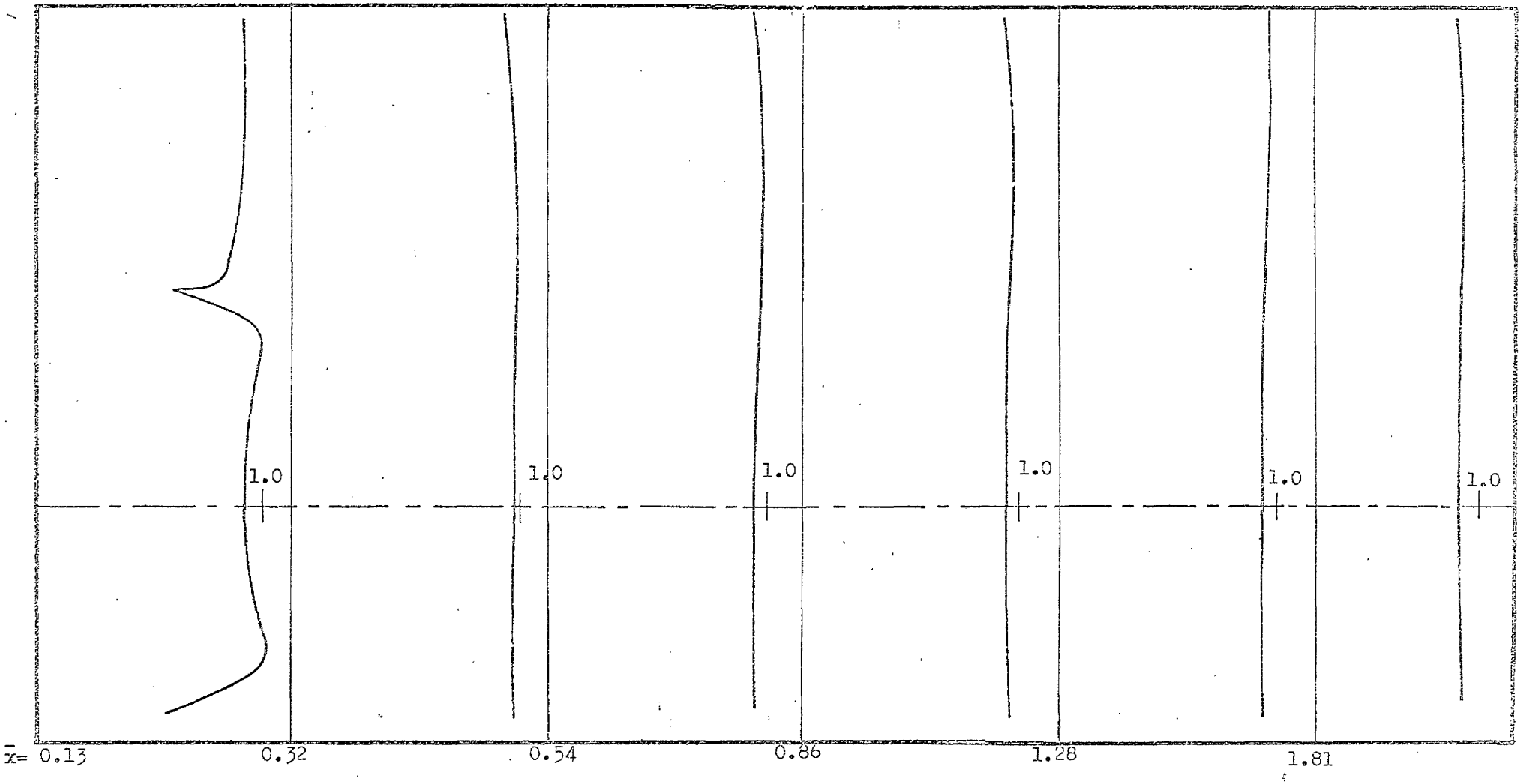

Figure 4.24.e. - CO_2 Concentration Profiles.
60^{o} Annular Swirler in D/d = 5 furnace.

Scale ⊣——⊢ 0.2 of compl
combusti

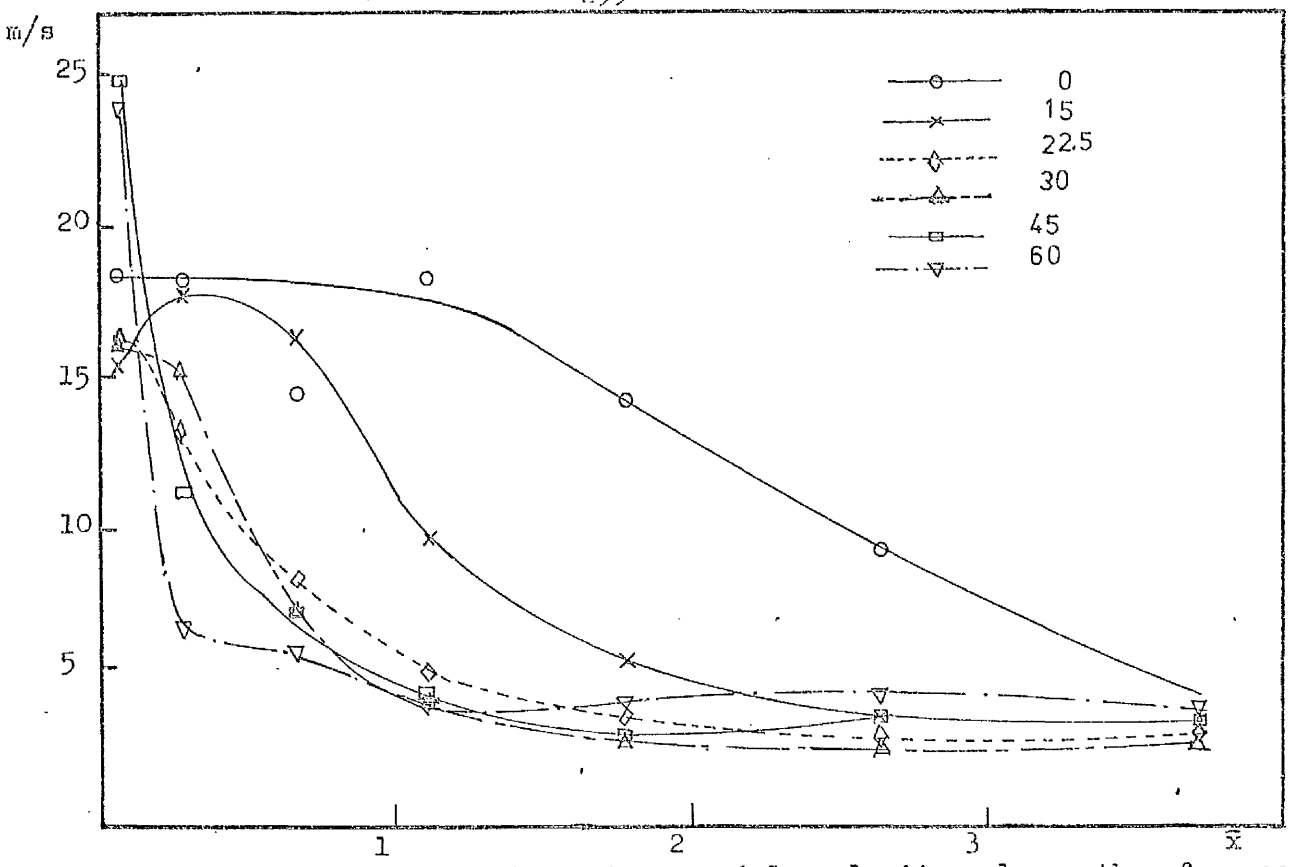

Figure 4.25.a - Decay of maximum axial velocity along the furnace Hubless swirlers cold flow in D/d = 2.5

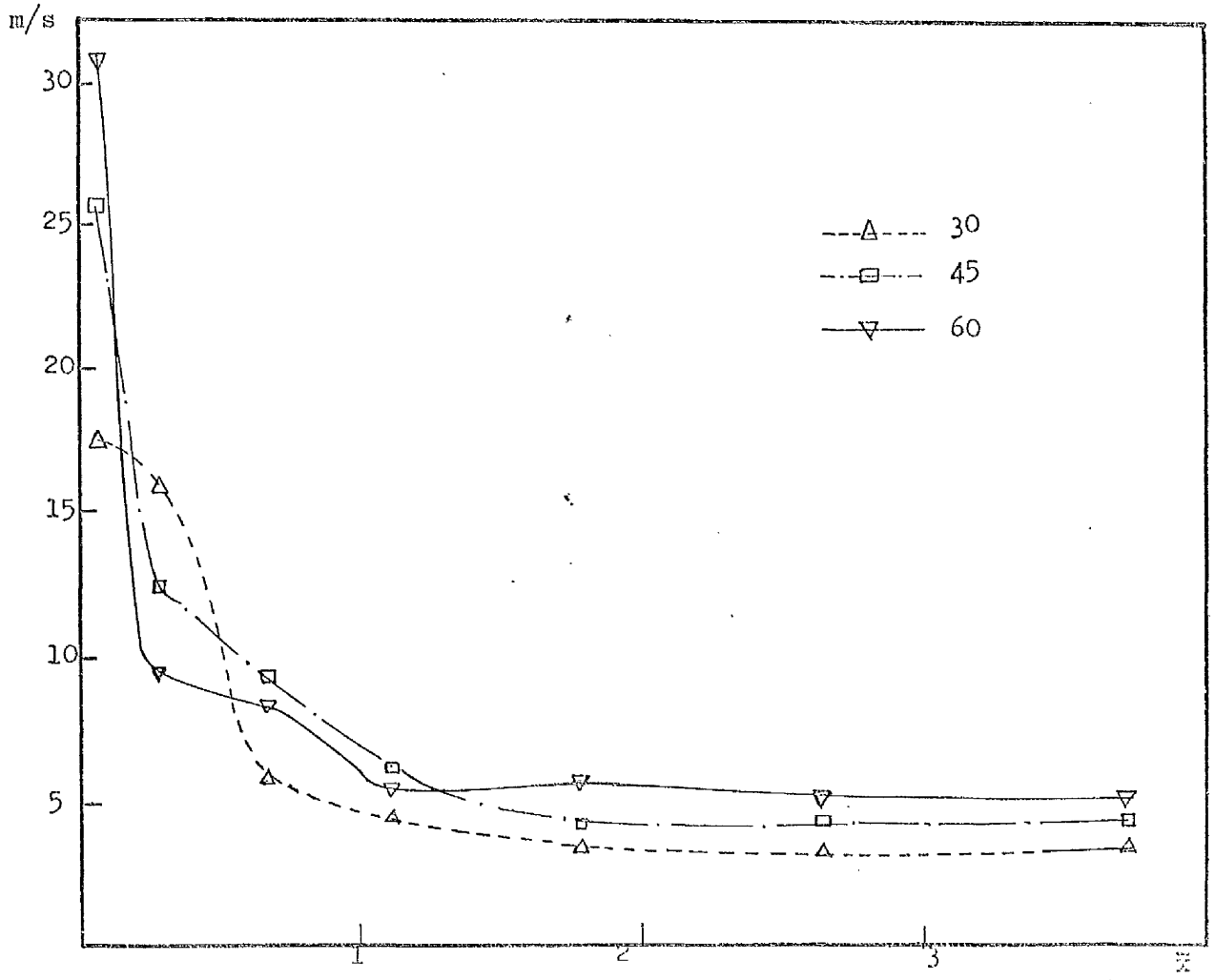

Figure 4.25.b - Decay of maximum axial velocity along the furnace Annular swirlers cold flow in D/d = 2.5

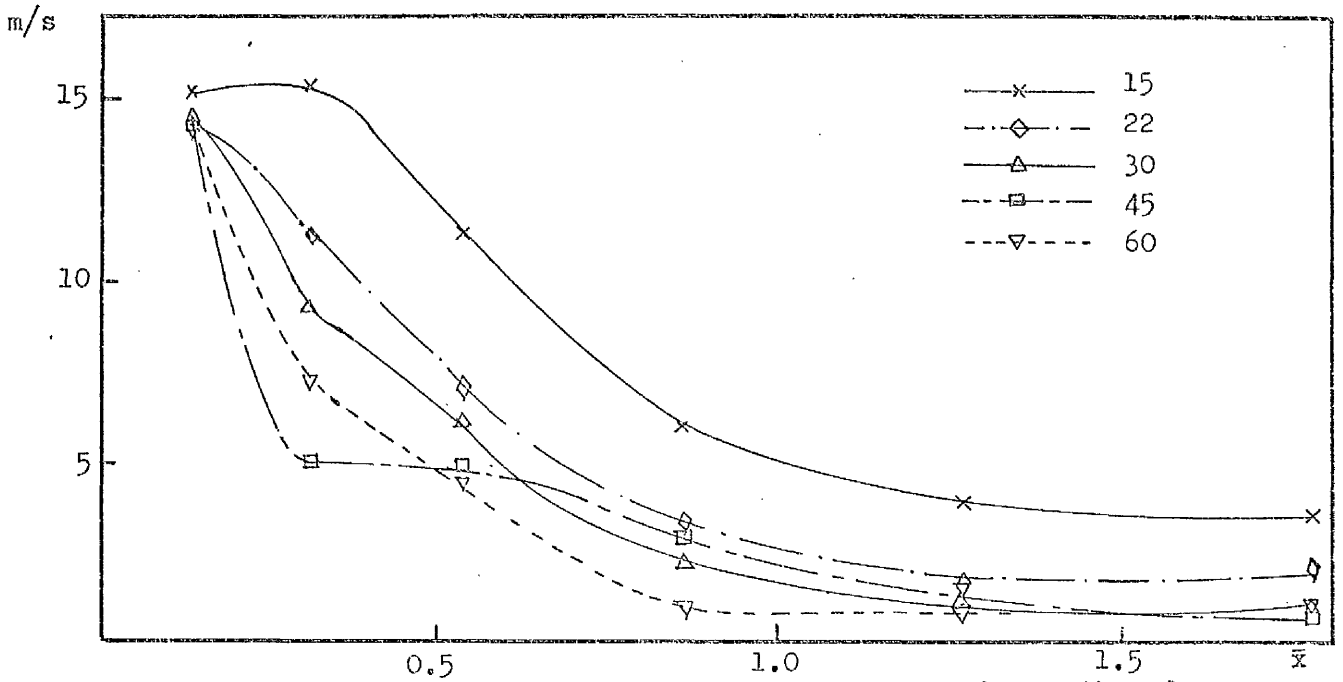

Figure 4.25.c - Decay of maximum axial velocity along the furnace Hubless swirlers cold flow in D/d = 5 furnace

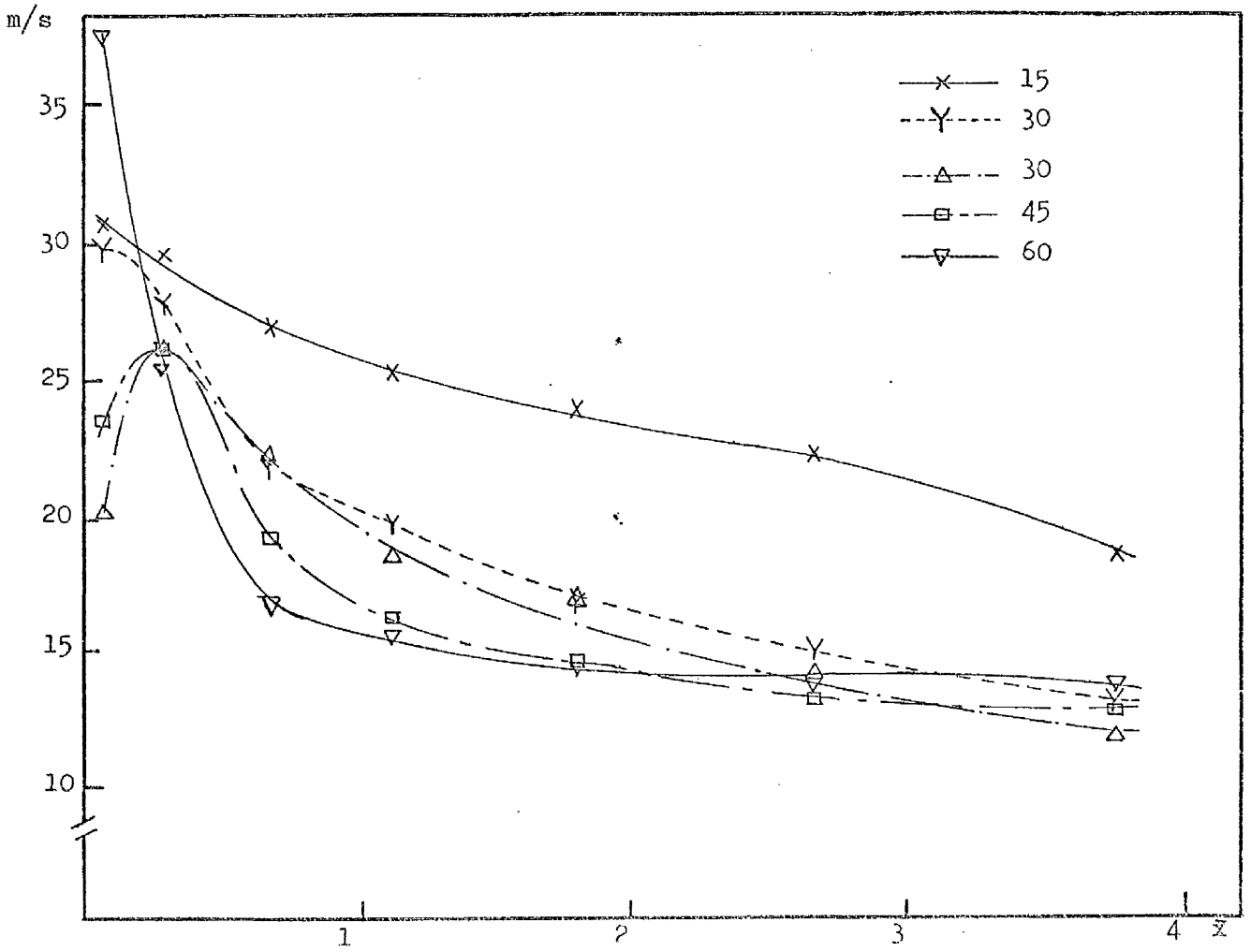

Figure 4.25.d - Decay of maximum axial velocity along the furnace Hubless swirler flames in D/d = 2.5 furnace

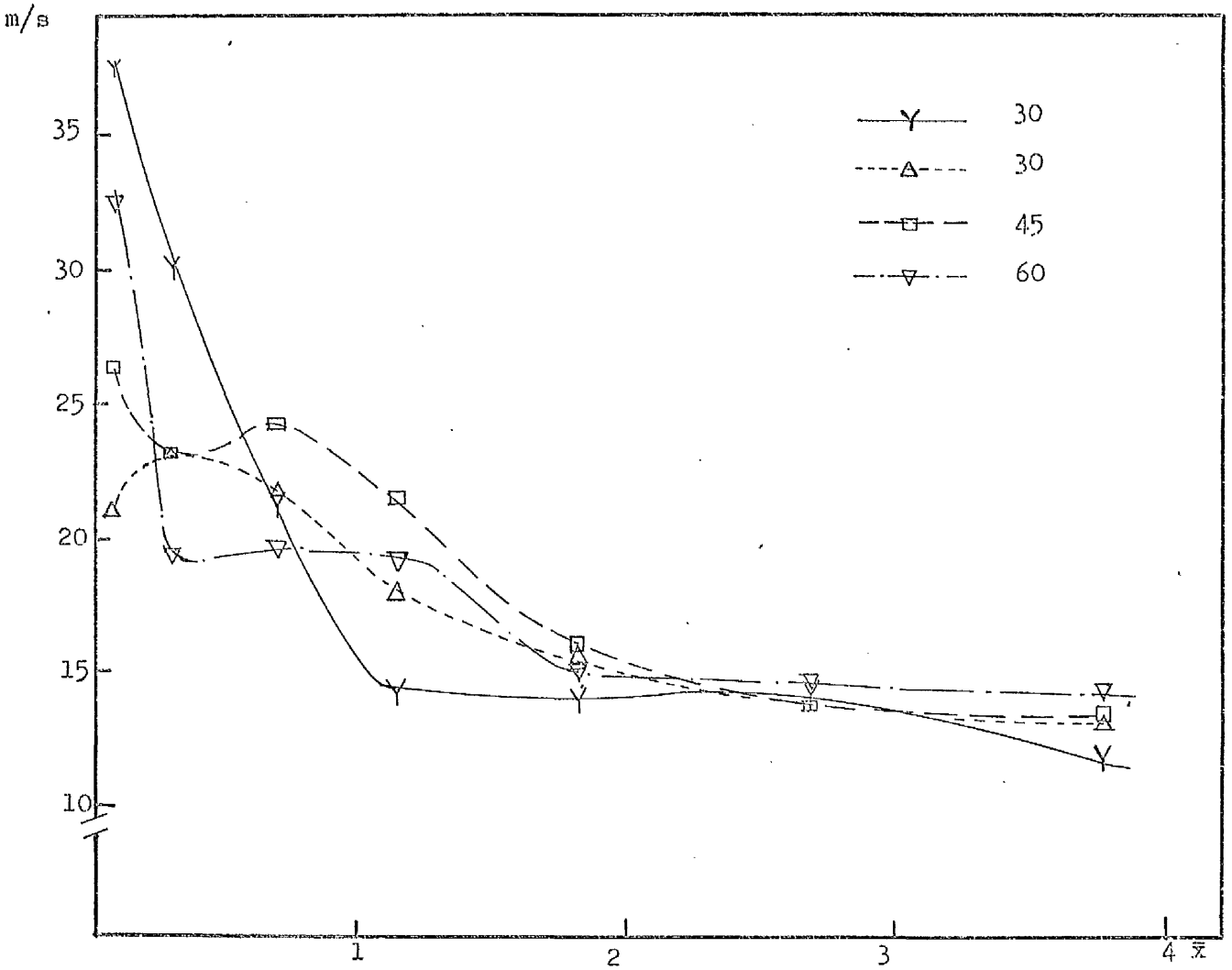

Figure 4.25.e - Decay of maximum axial velocity along the furnace
Annular swirler flames in D/d = 2.5 furnace

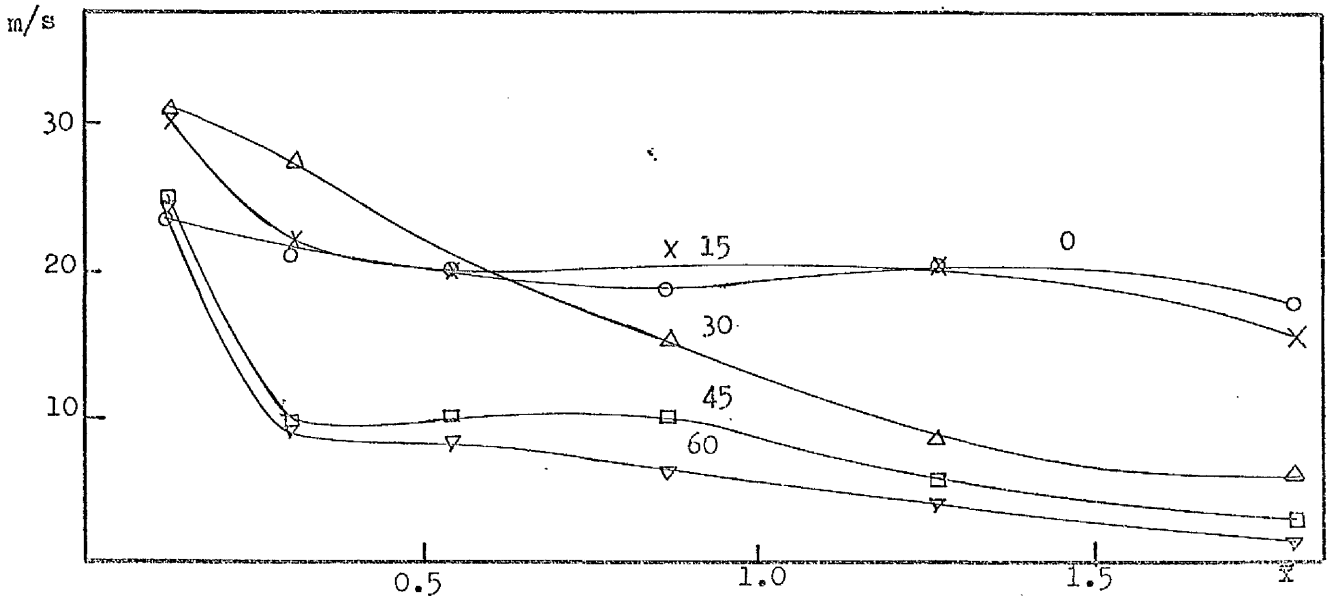

Figure 4.25.f - Decay of maximum axial velocity along the furnace
Hubless swirler flames in D/d = 5 furnace

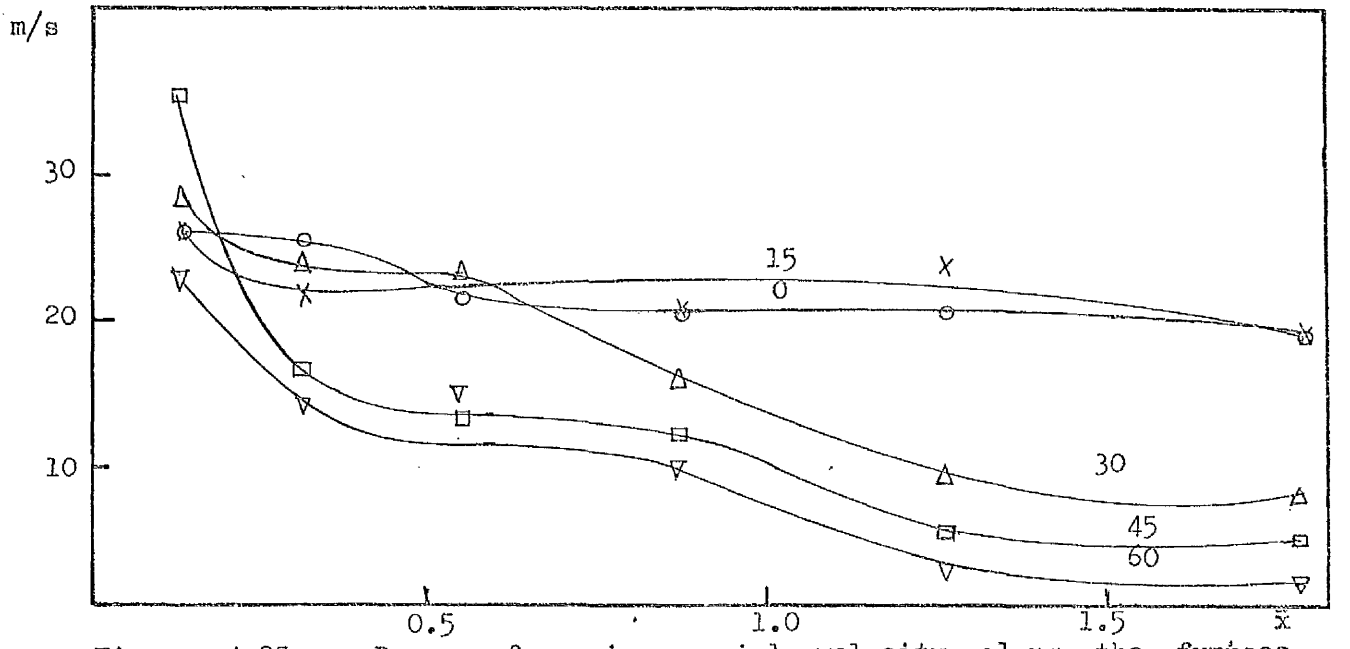

Figure 4.25.g - Decay of maximum axial velocity along the furnace Annular swirler flames in D/d = 5 furnace

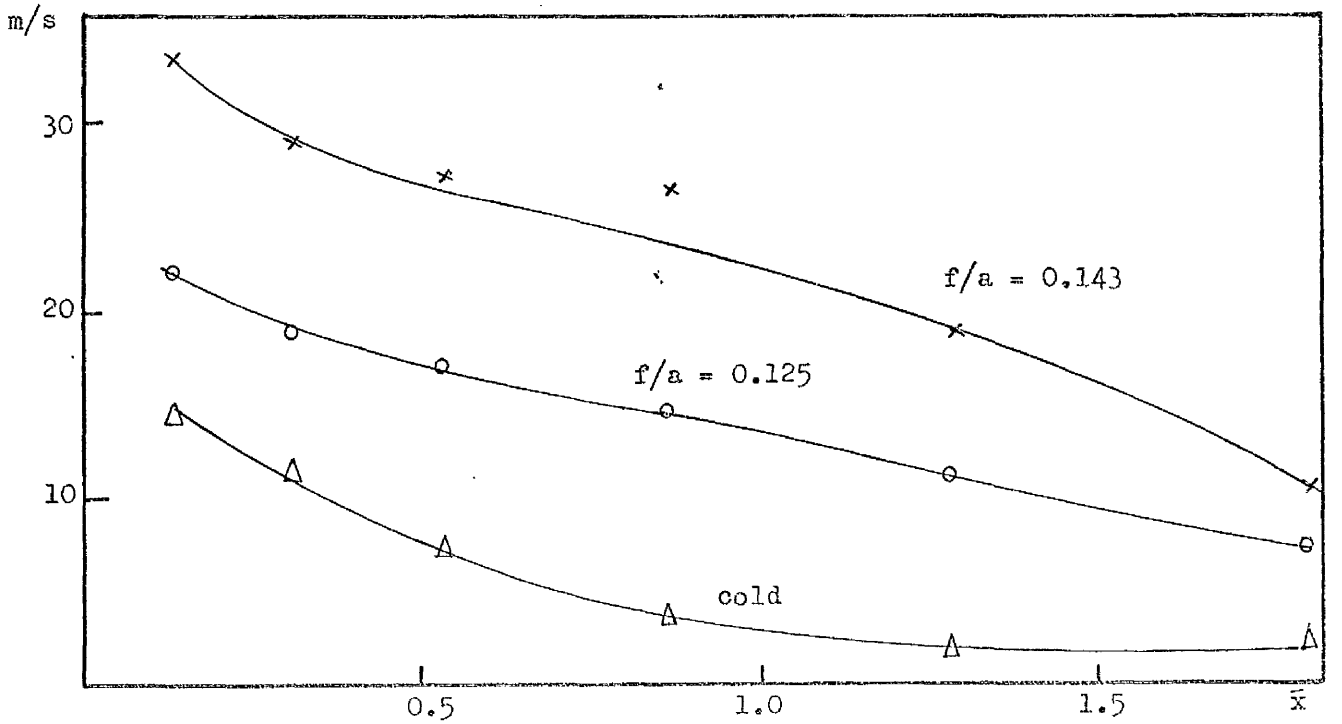

Figure 4.25.L - Decay of maximum axial velocity along the furnace 225 Hubless swirlers in D/d = 5 furnace

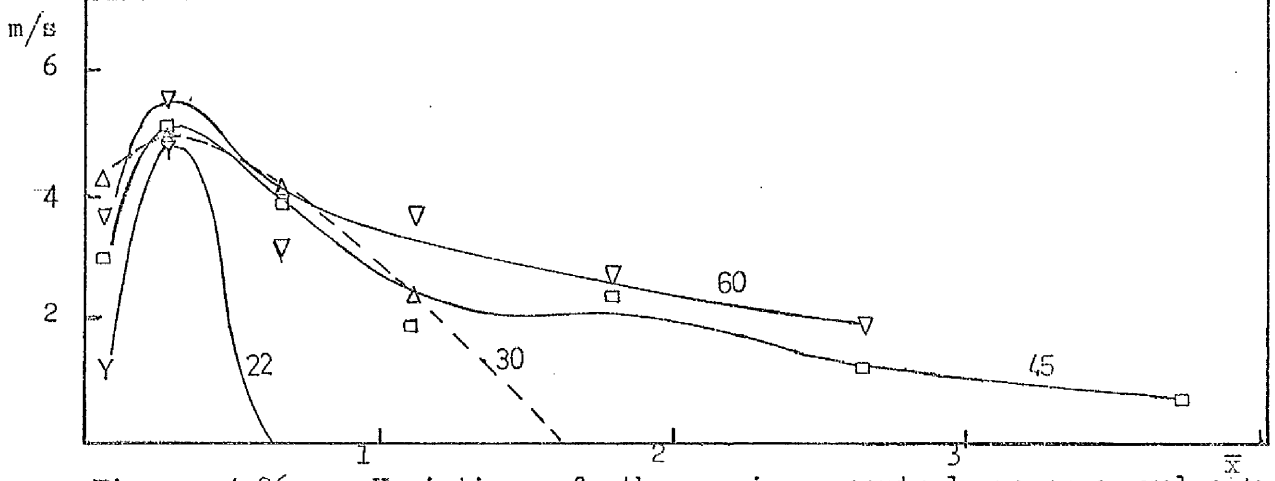

Figure 4.26.a – Variation of the maximum central reverse velocity along the furnace
Hubless swirlers cold flow in D/d = 2.5 furnace

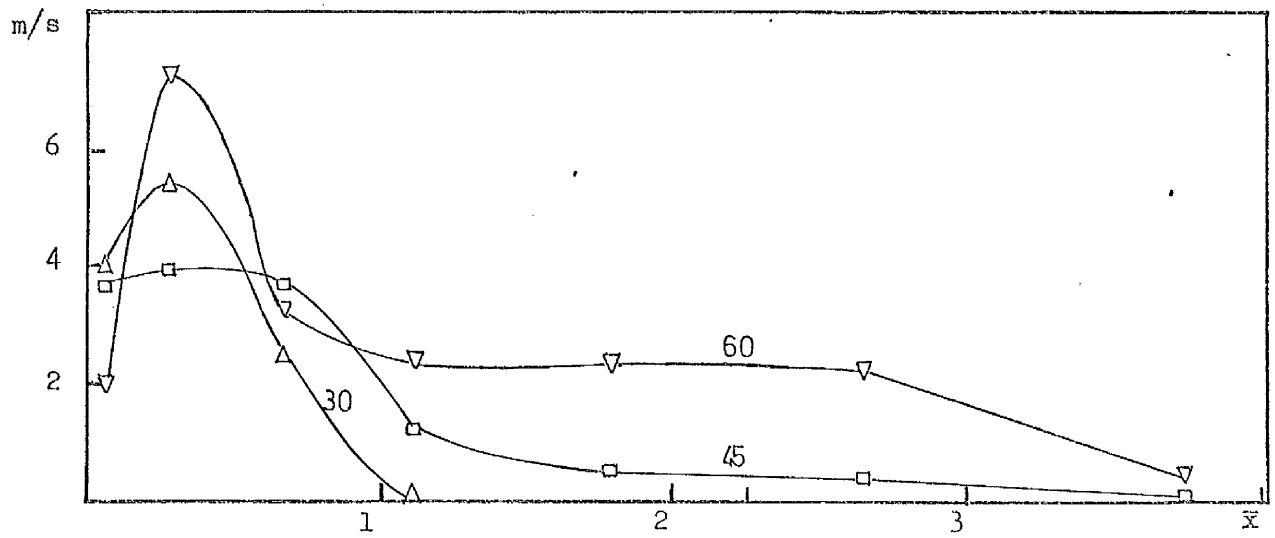

Figure 4.26.b – Variation of the maximum central reverse velocity along the furnace
Annular swirlers cold flow in D/d = 2.5 furnace

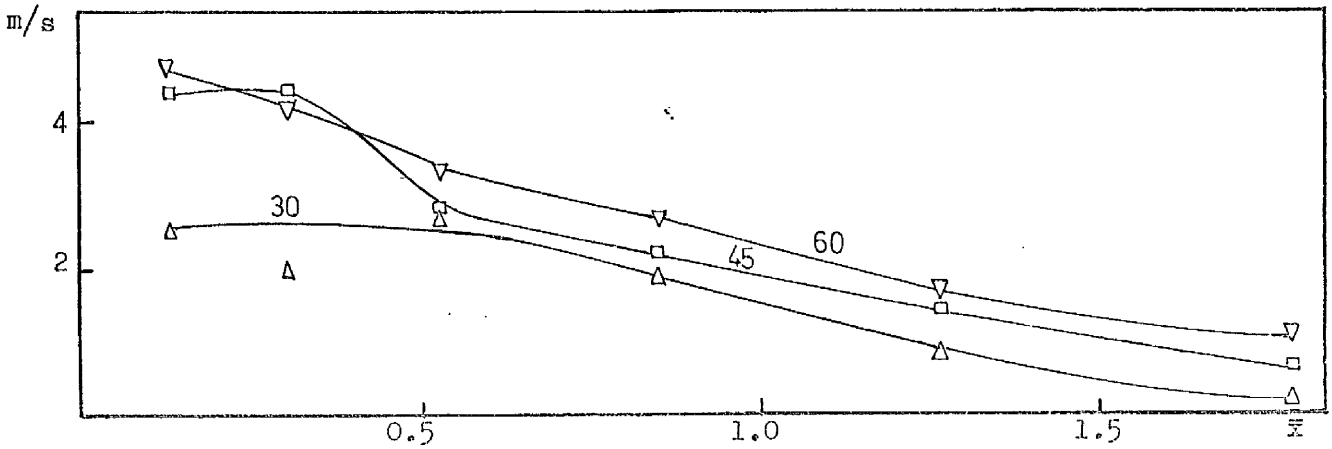

Figure 4.26.c – Variation of the maximum central reverse velocity along the furnace
Hubless swirlers cold flow in D/d = 5 furnace

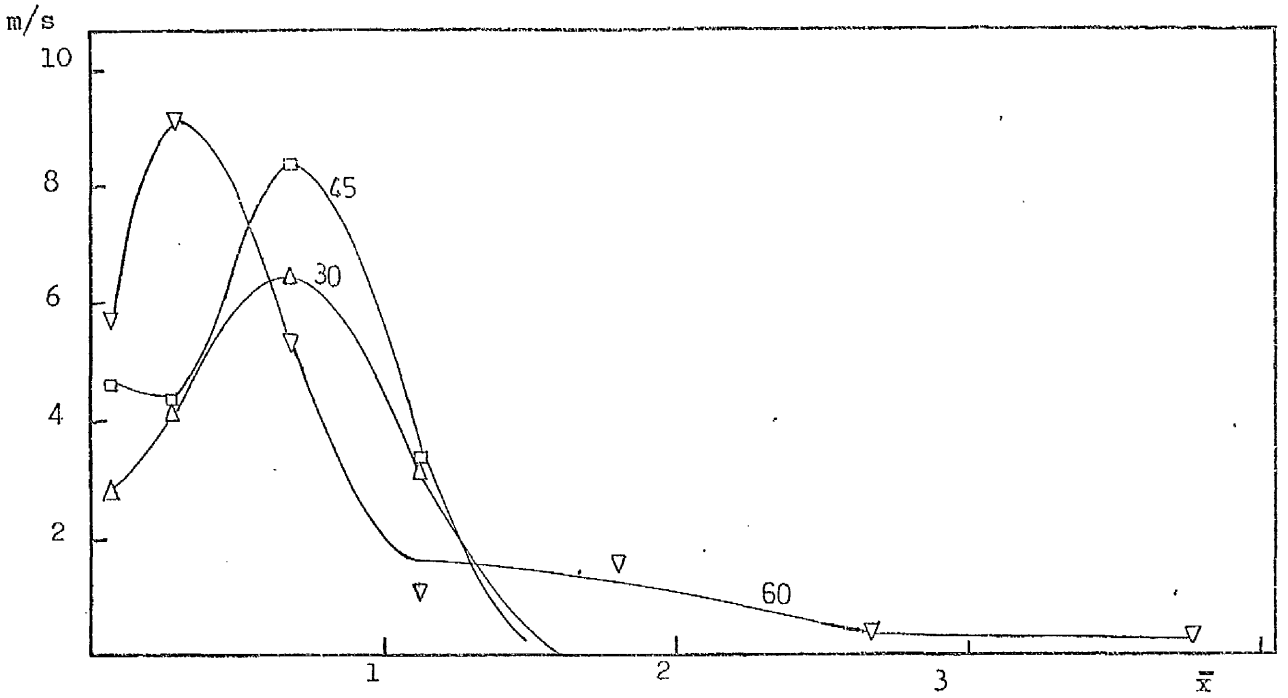

Figure 4.26.d - Variation of the maximum central reverse velocity along the furnace
Hubless swirler flames in D/d =2.5 furnace

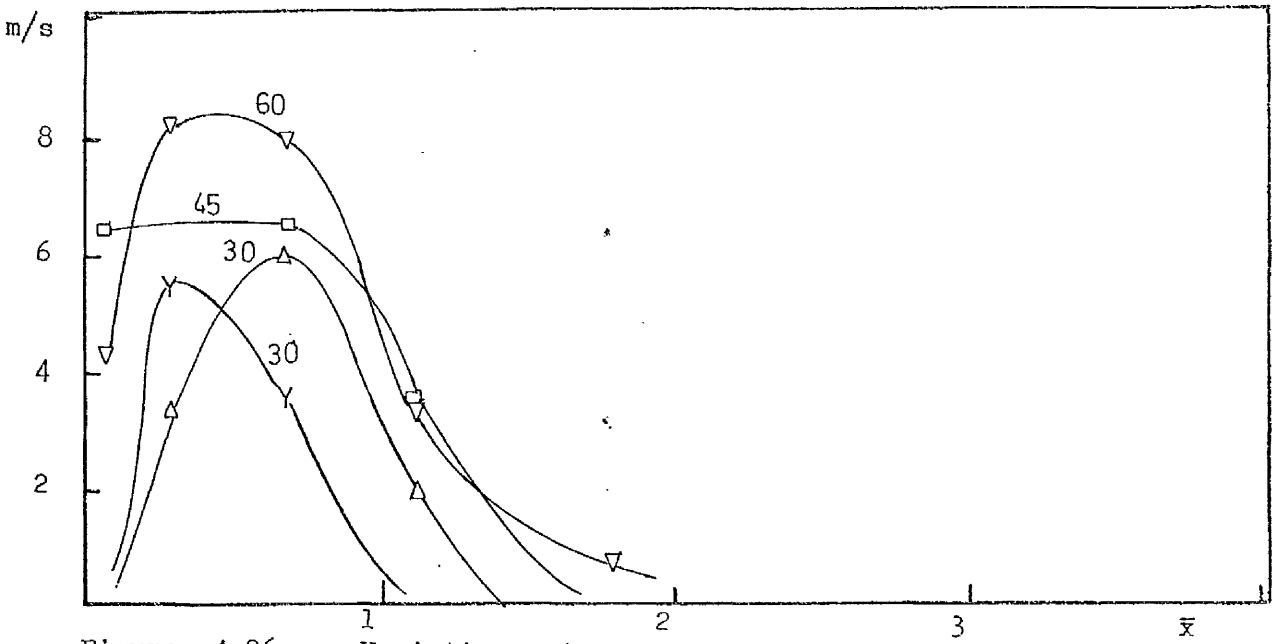

Figure 4.26.e - Variation of maximum central reverse velocity along the furnace
Annular swirler flames in D/d = 2.5 furnace

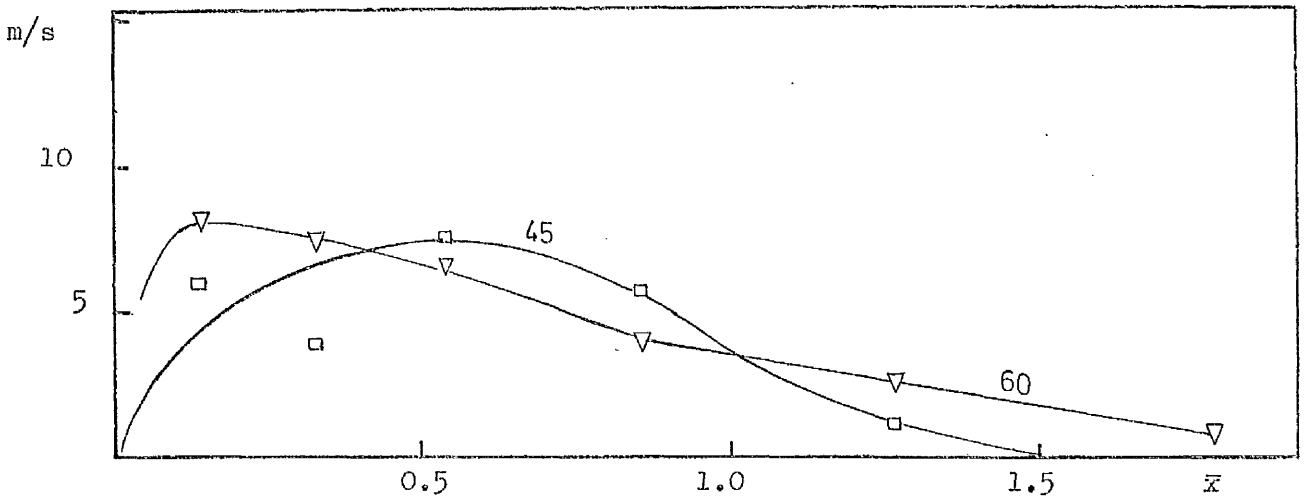

Figure 4.26.f - Variation of maximum central reverse velocity along the furnace
Hubless swirler flames in D/d =5 furnace

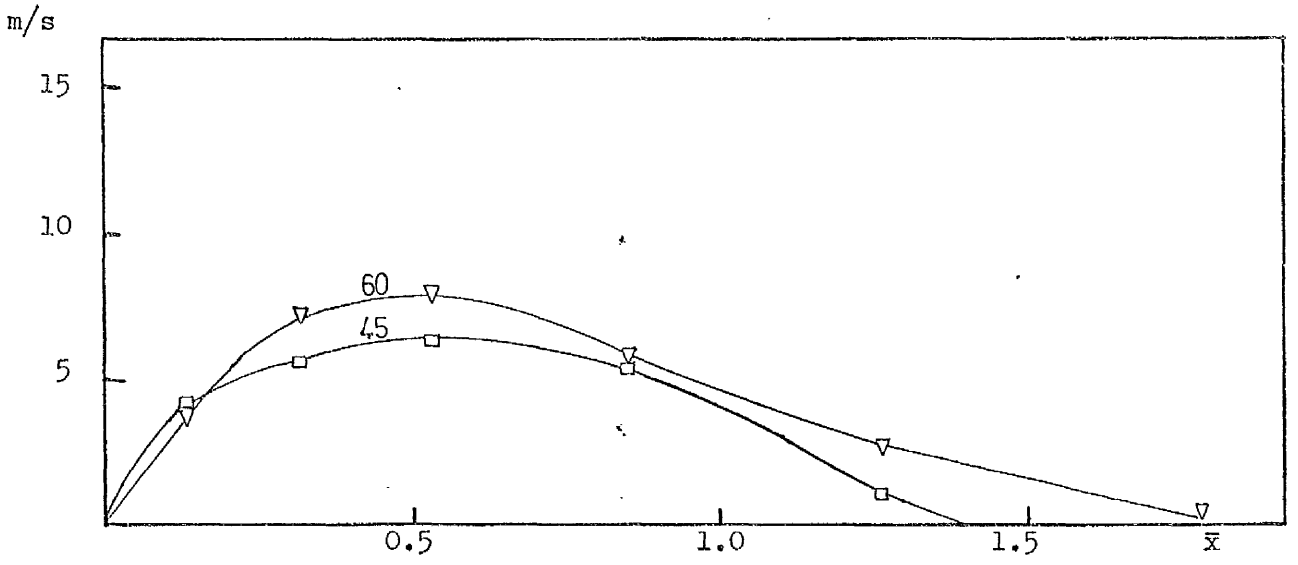

Figure 4.26.g- Variation of maximum central reverse velocity along the furnace
Annular swirler flames in D/d =5 furnace

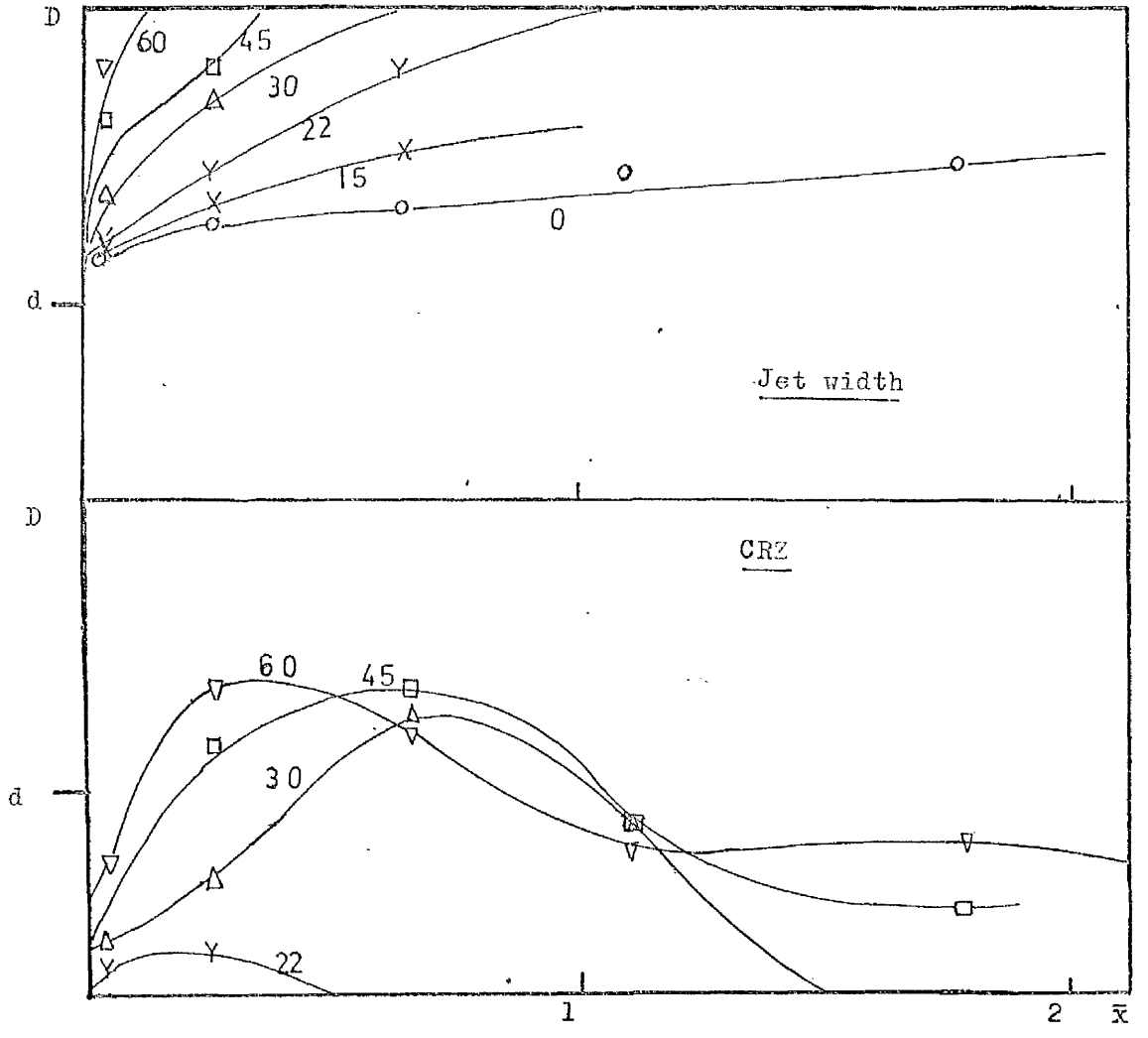

Figure 4.27.a. Jet width and CRZ dimensions
Hubless swirlers cold flow
in D/d = 2.5 furnace.

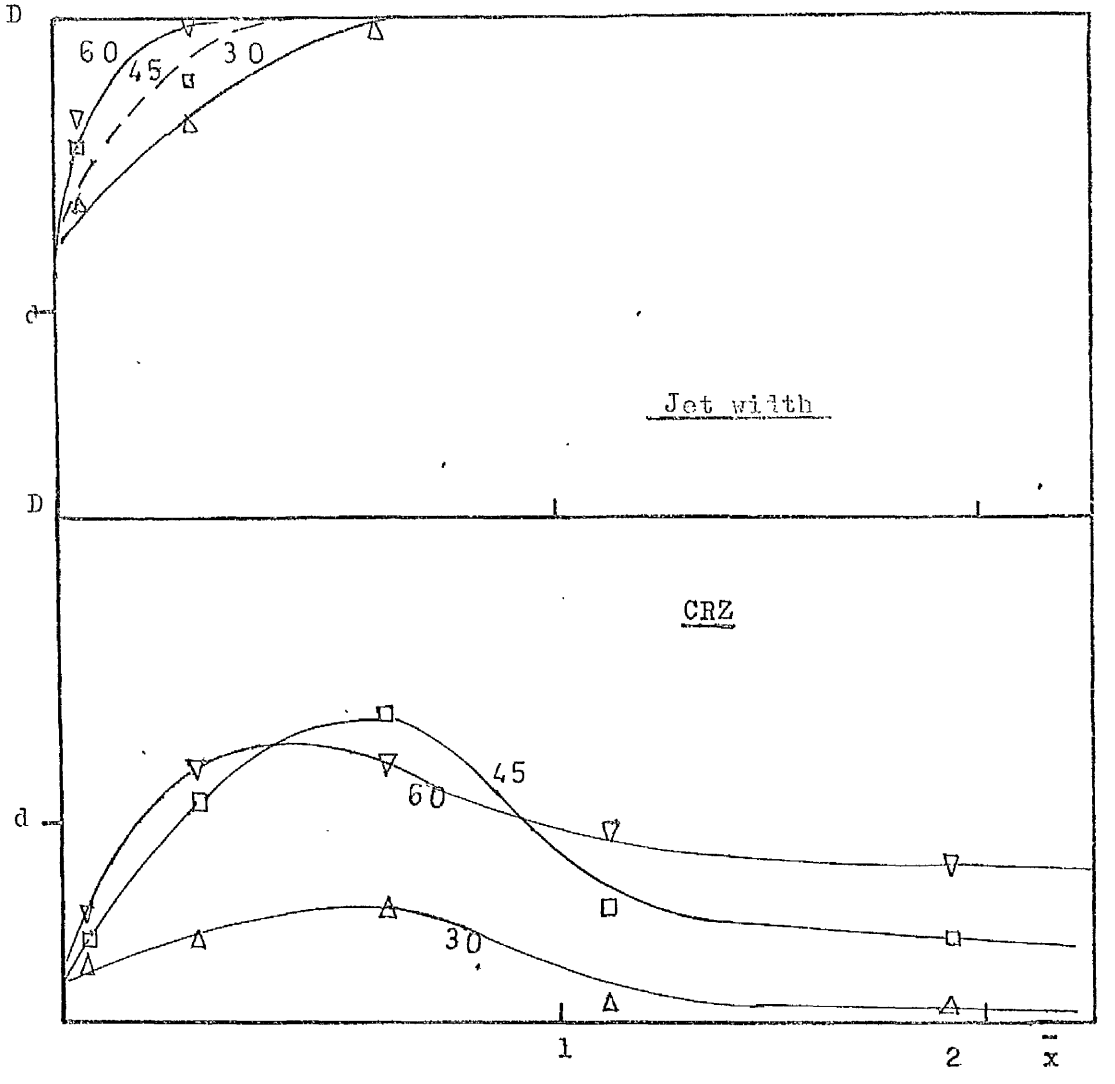

Figure 4.27.b - Jet width and CRZ dimensions
Annular swirlers cold flow in D/d = 2.5 furnace

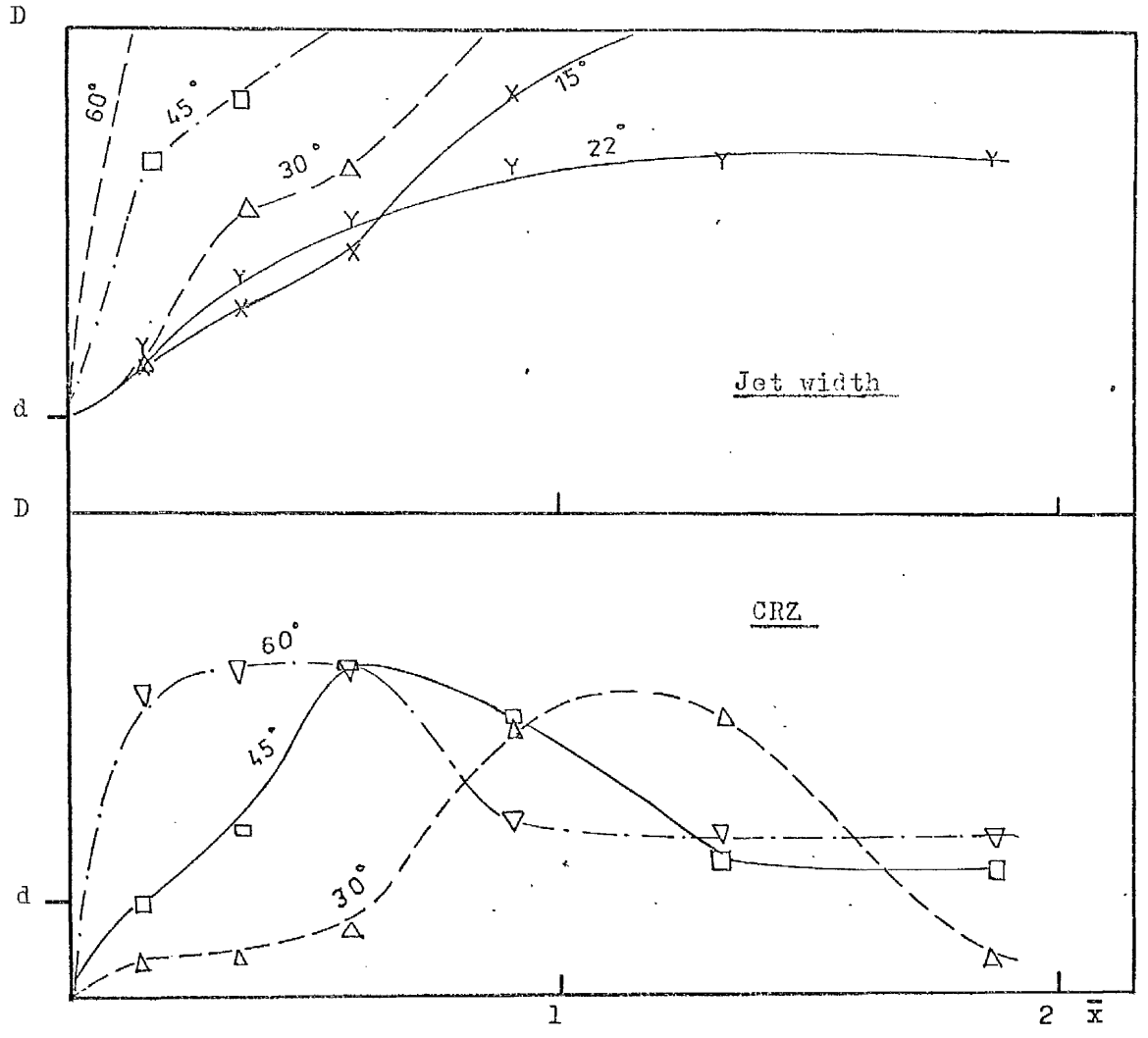

Figure 4.27.c - Jet width and CRZ dimensions
Hubless cold flow in D/d= 5 furnace.

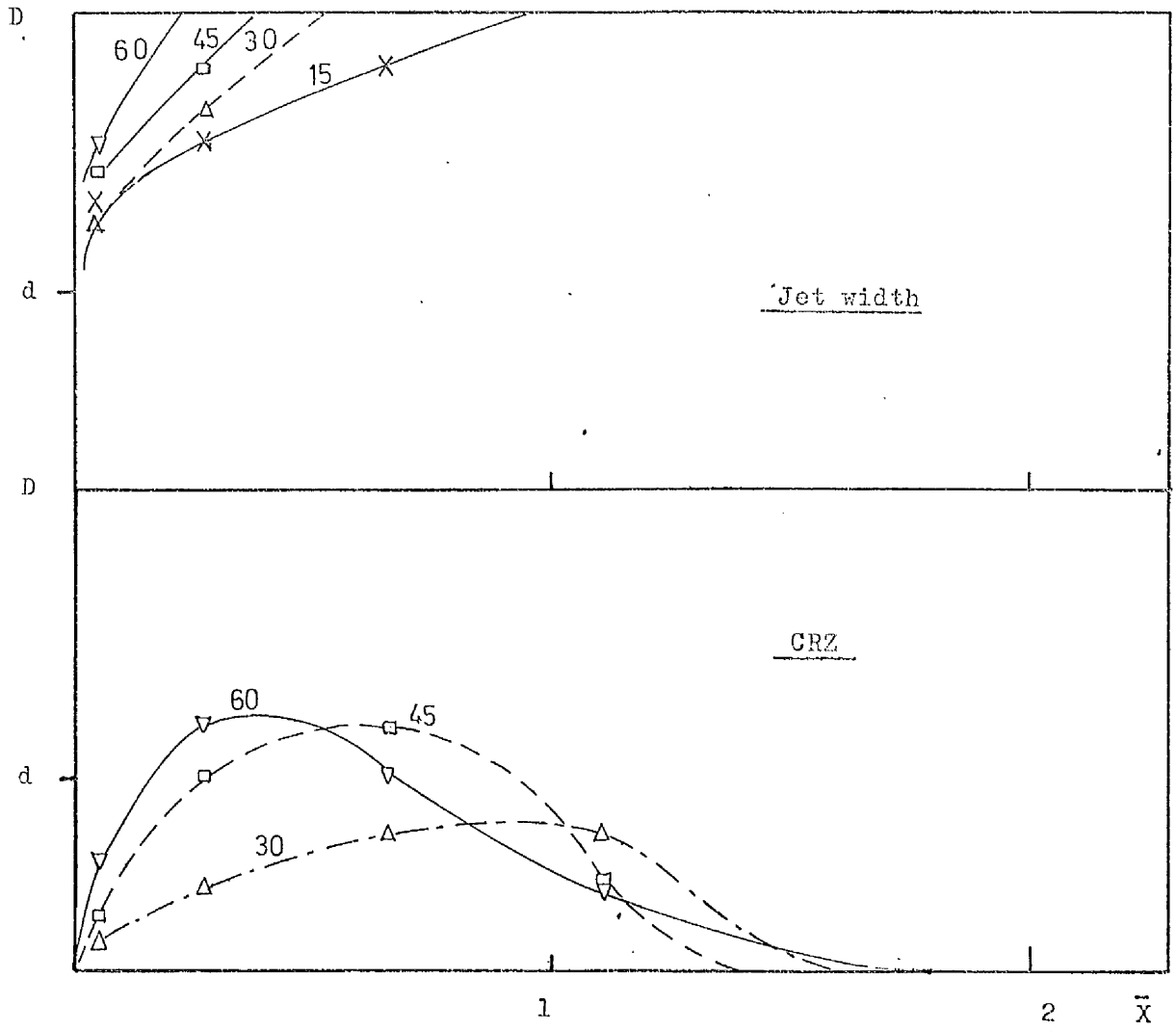

Figure 4.27.d- Jet width and CRZ dimensions
Hubless swirler flames
in D/d = 2.5 furnace.

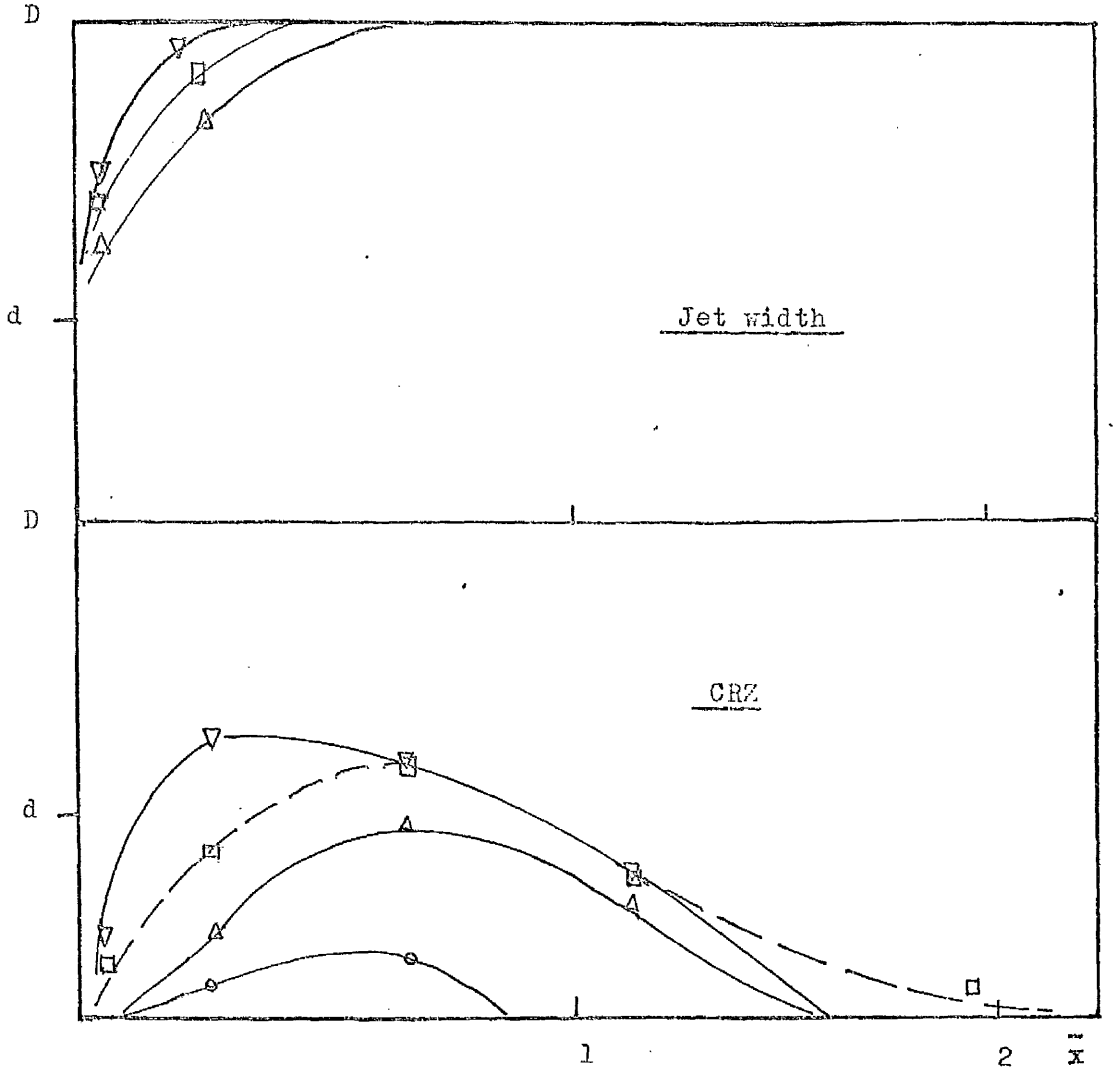

Figure 4.27.e – Jet width and CRZ dimensions
Annular swirler flames
in D/d = 2.5 furnace.

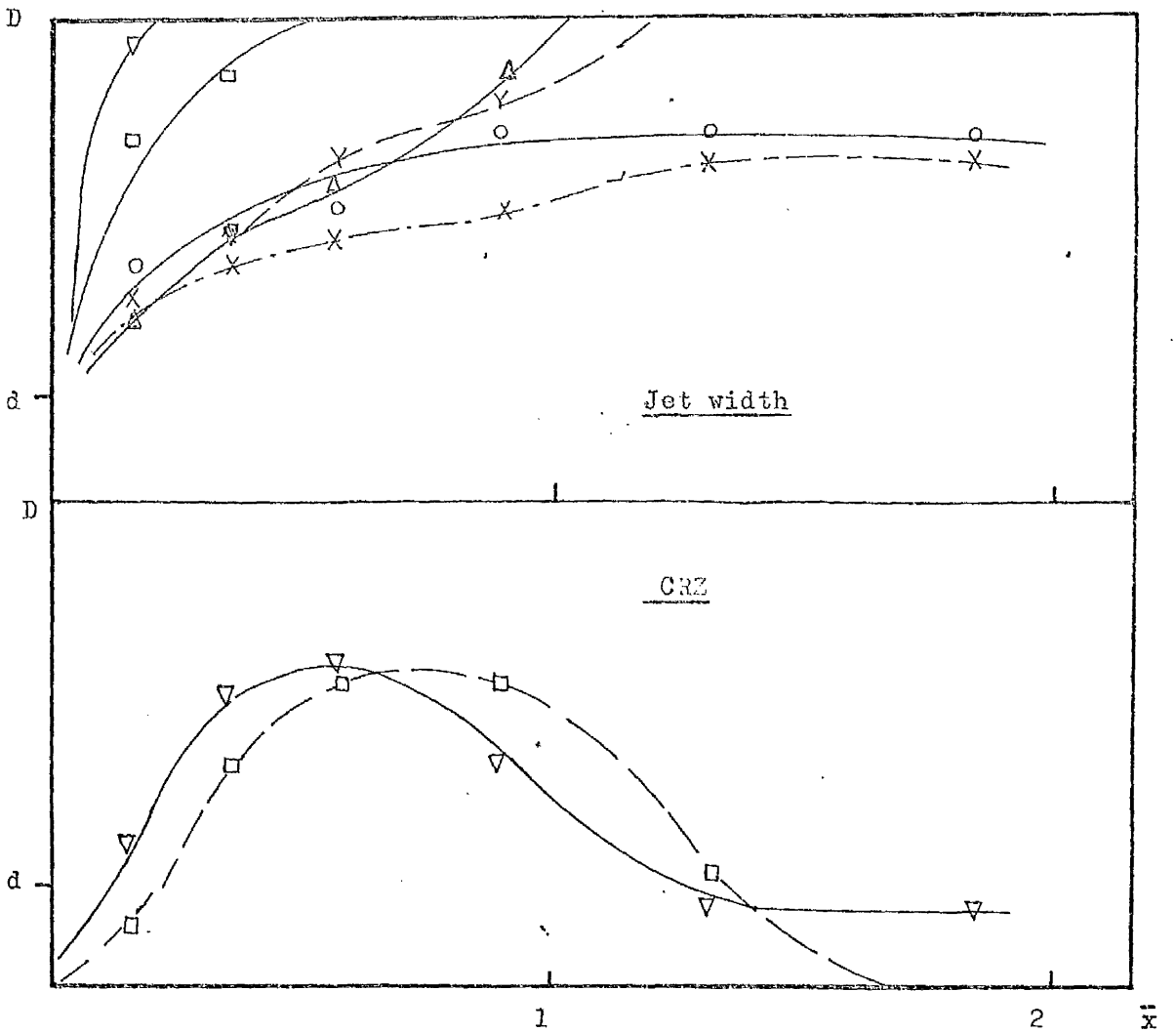

Figure 4.27.f- Jet width and CRZ dimensions
Hubless swirlers flames
in D/d = 5 furnace.

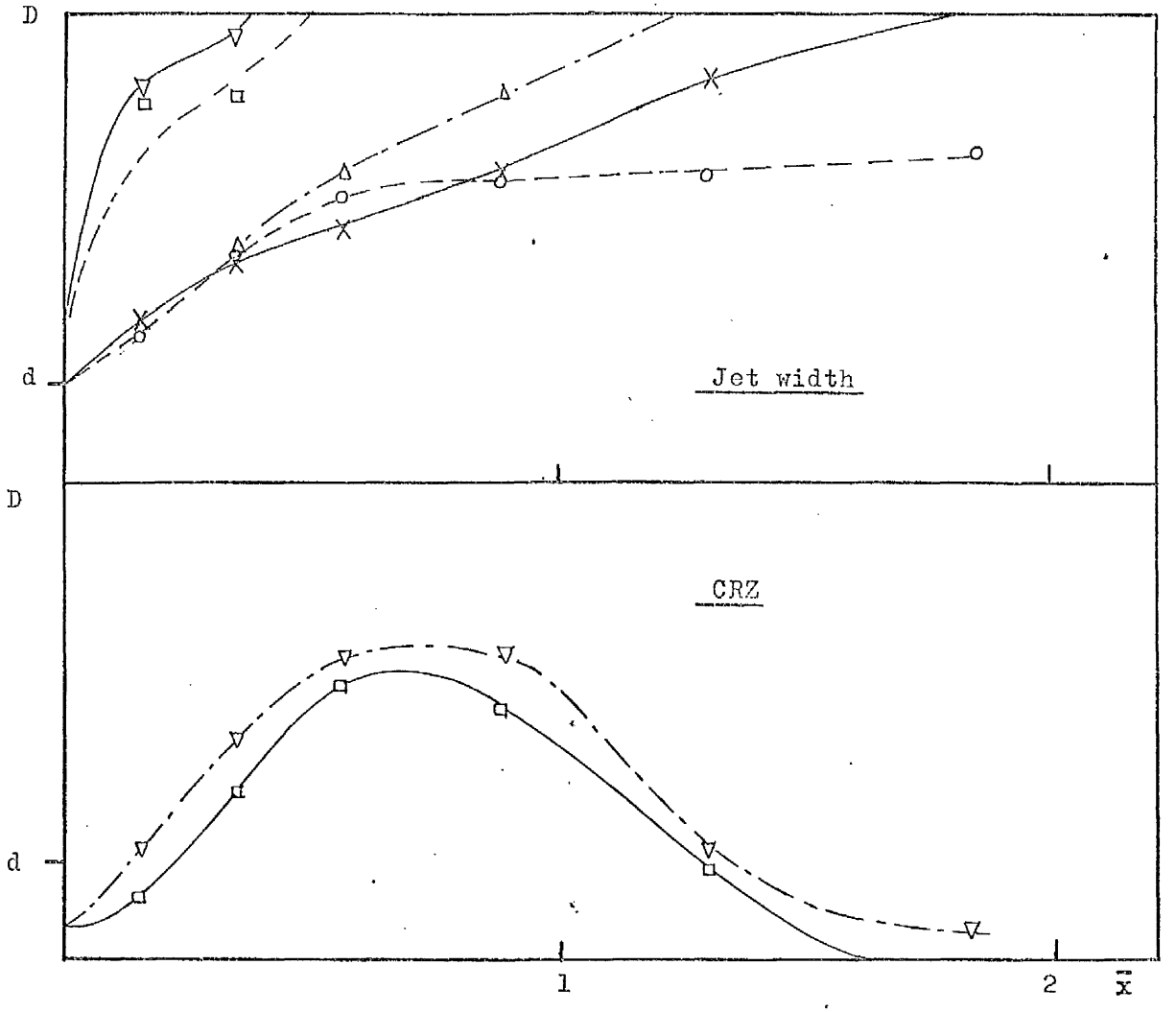

Figure 4.27.g- Jet width and CRZ dimensions
Annular swirlers flames
in D/d = 5 furnace.

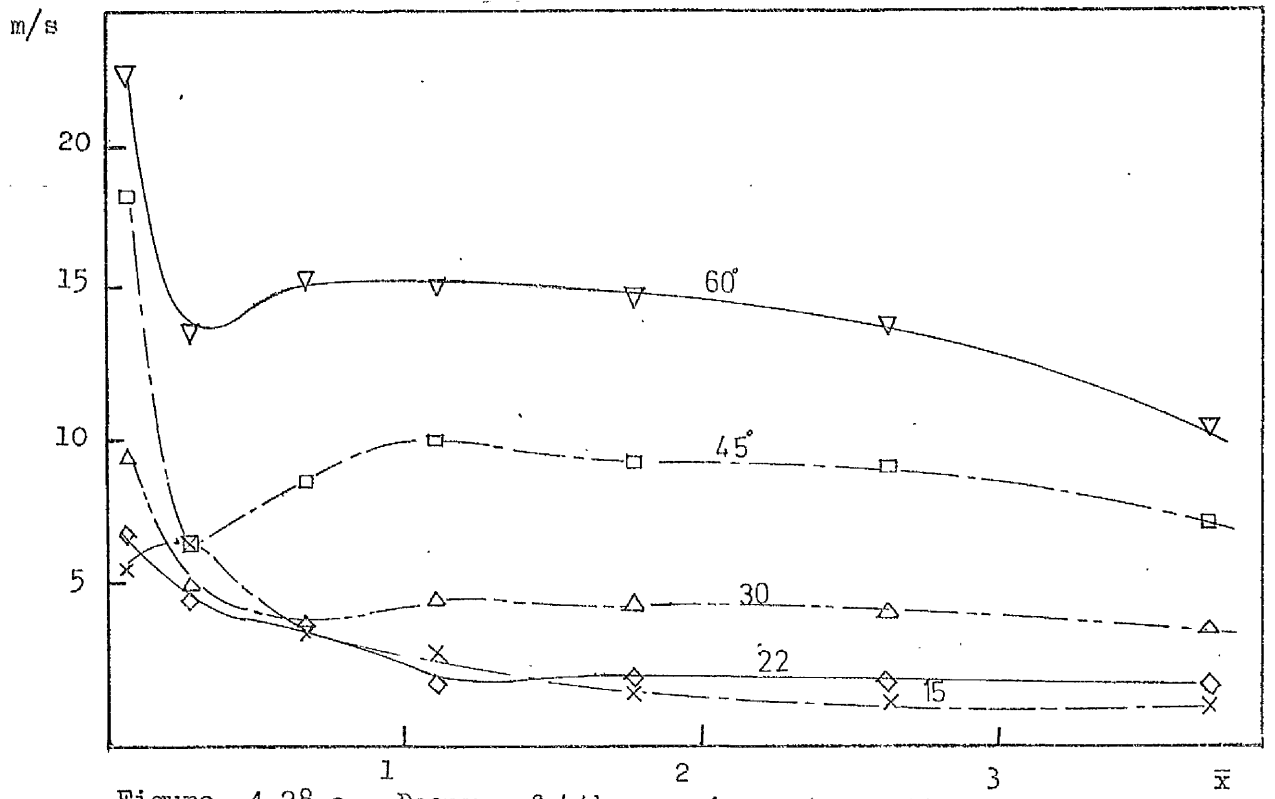

Figure 4.28.a – Decay of the maximum tangential velocity along the furnace
Hubless swirlers cold flow in D/d = 2.5 furnace

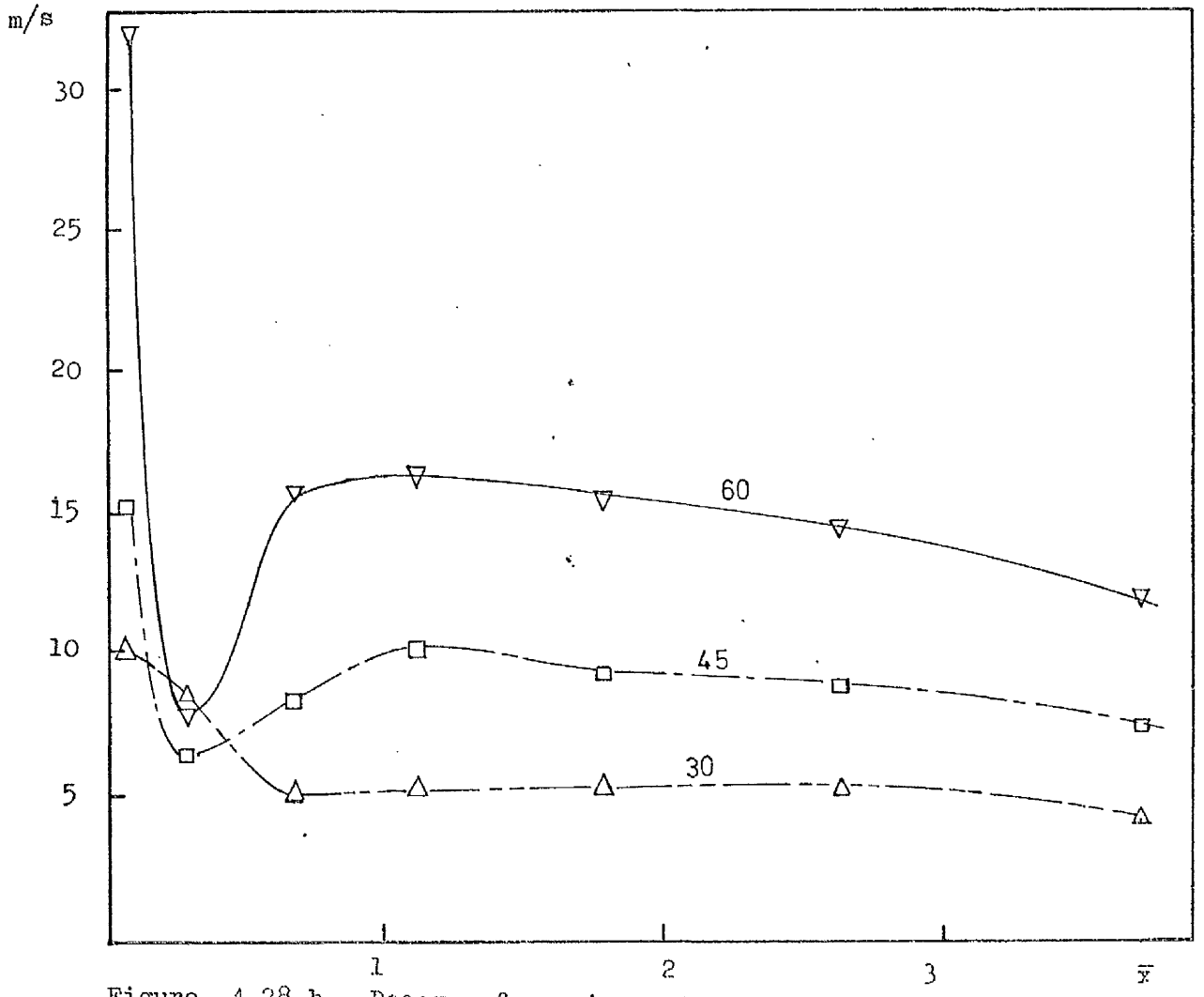

Figure 4.28.b – Decay of maximum tangential velocity along the furnace
Annular swirlers cold flow in D/d = 2.5 furnace

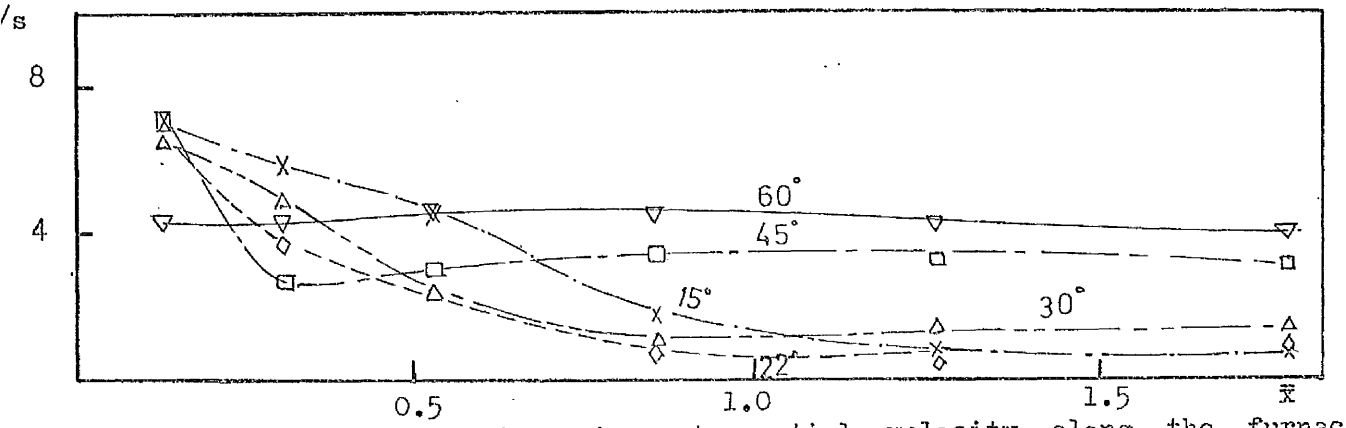

Figure 4.28.c - Decay of maximum tangential velocity along the furnace Hubless swirlers cold flow in D/d = 5 furnace

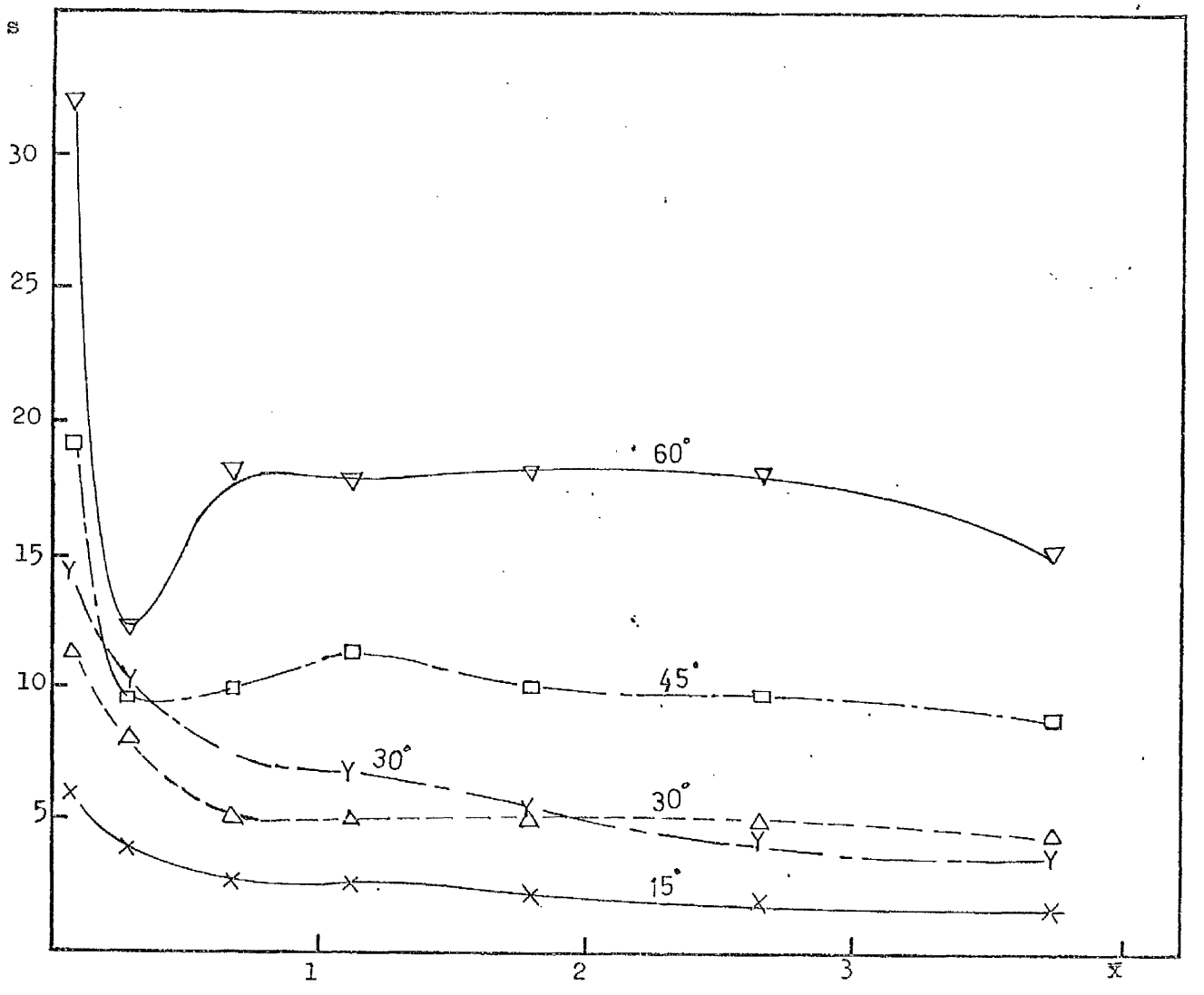

Figure 4.28.d - Decay of maximum tangential velocity along the furnace Hubless swirler flames in D/d = 2.5 furnace

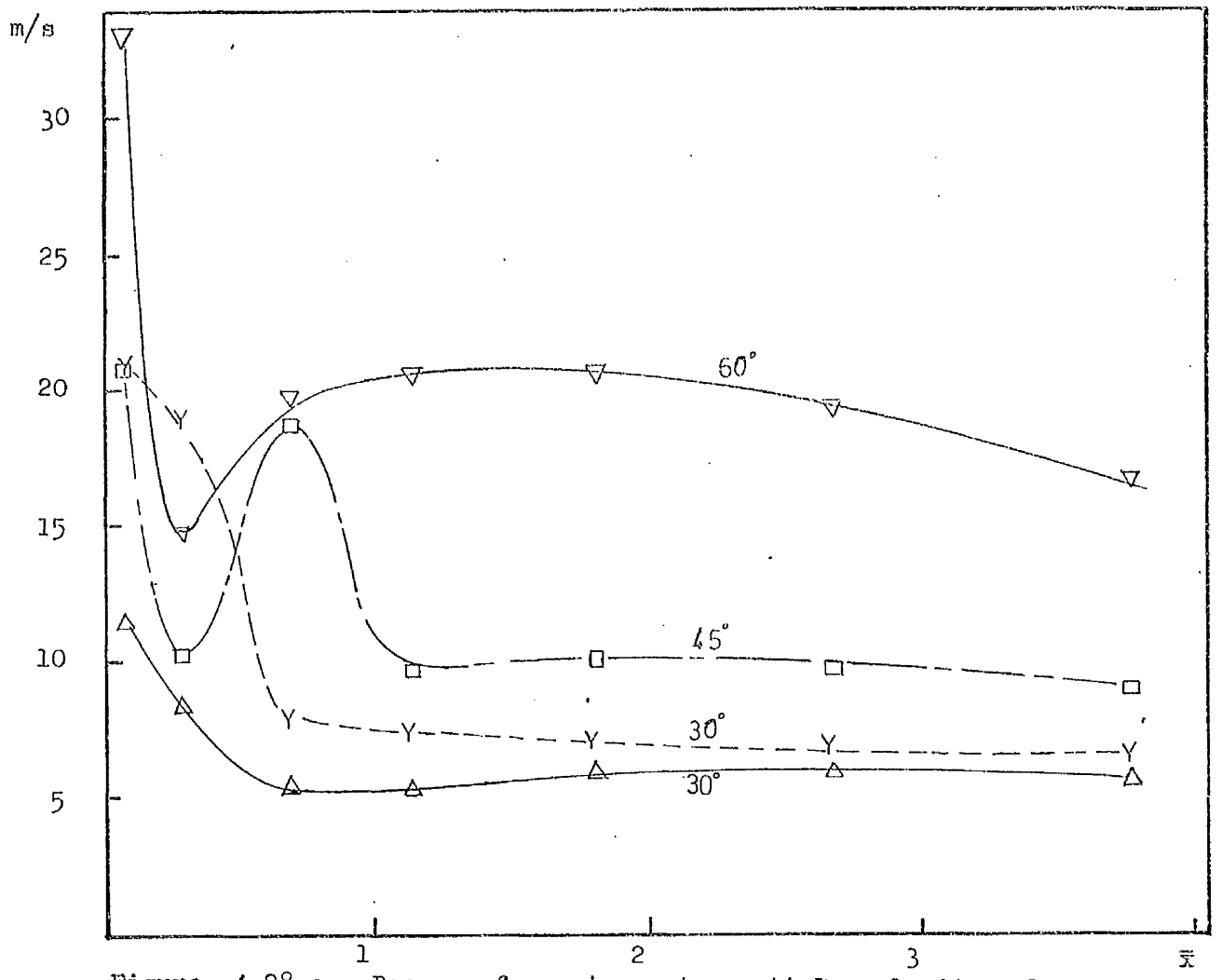

Figure 4.28.e - Decay of maximum tangential velocity along the furnace
Annular swirler flames in D/d = 2.5 furnace

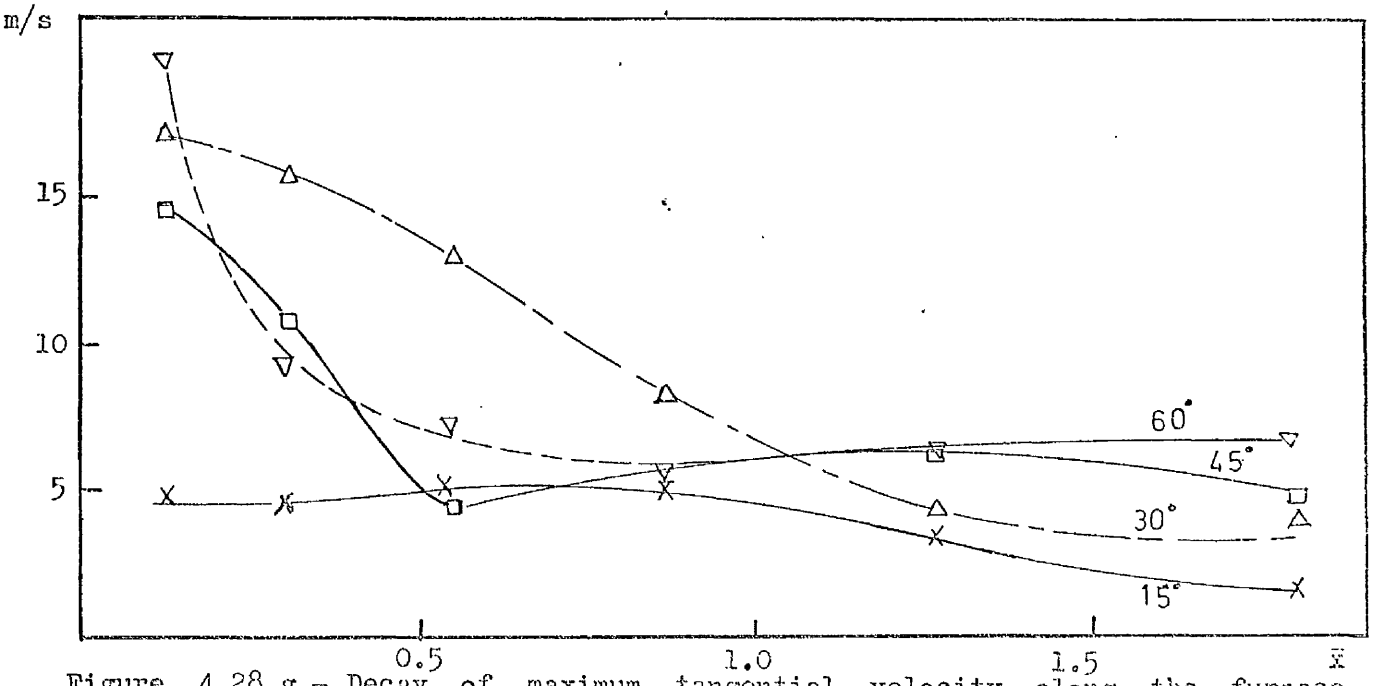

Figure 4.28.g - Decay of maximum tangential velocity along the furnace
Annular swirler flames in D/d = 5 furnace

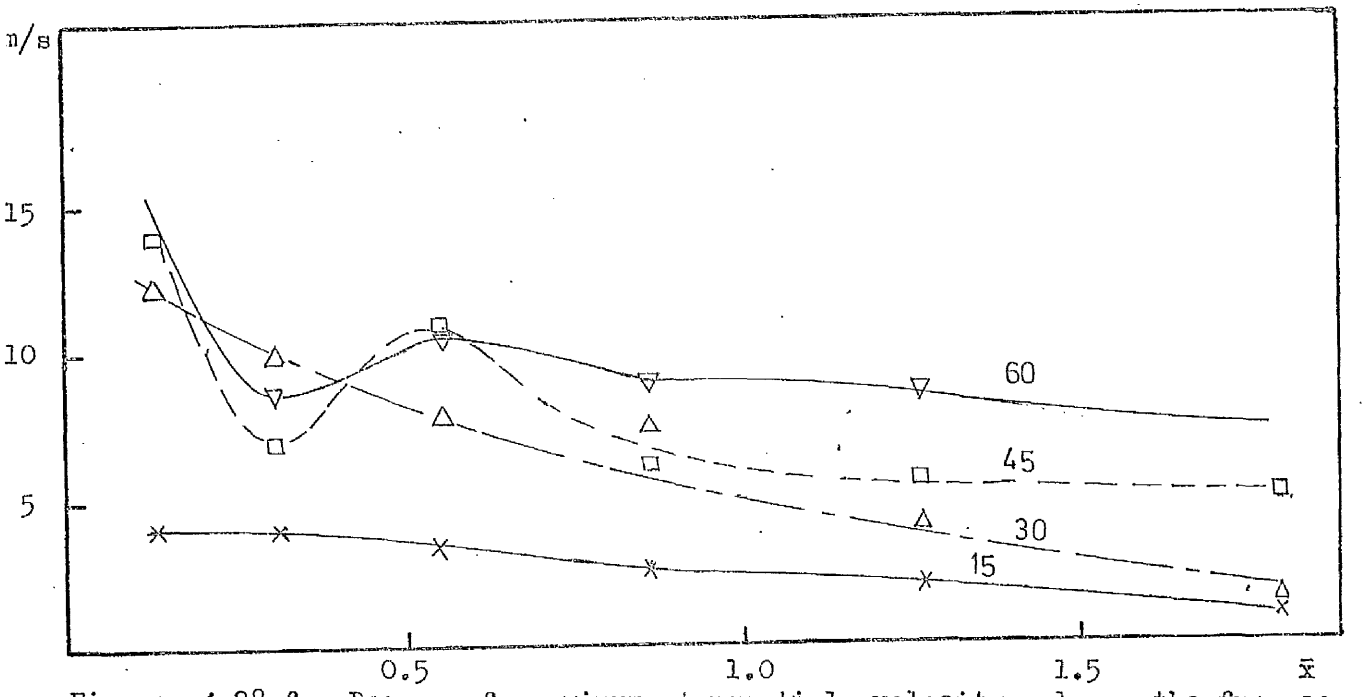

Figure 4.28.f - Decay of maximum tangential velocity along the furnace Hubless swirler flames in D/d = 5 furnace

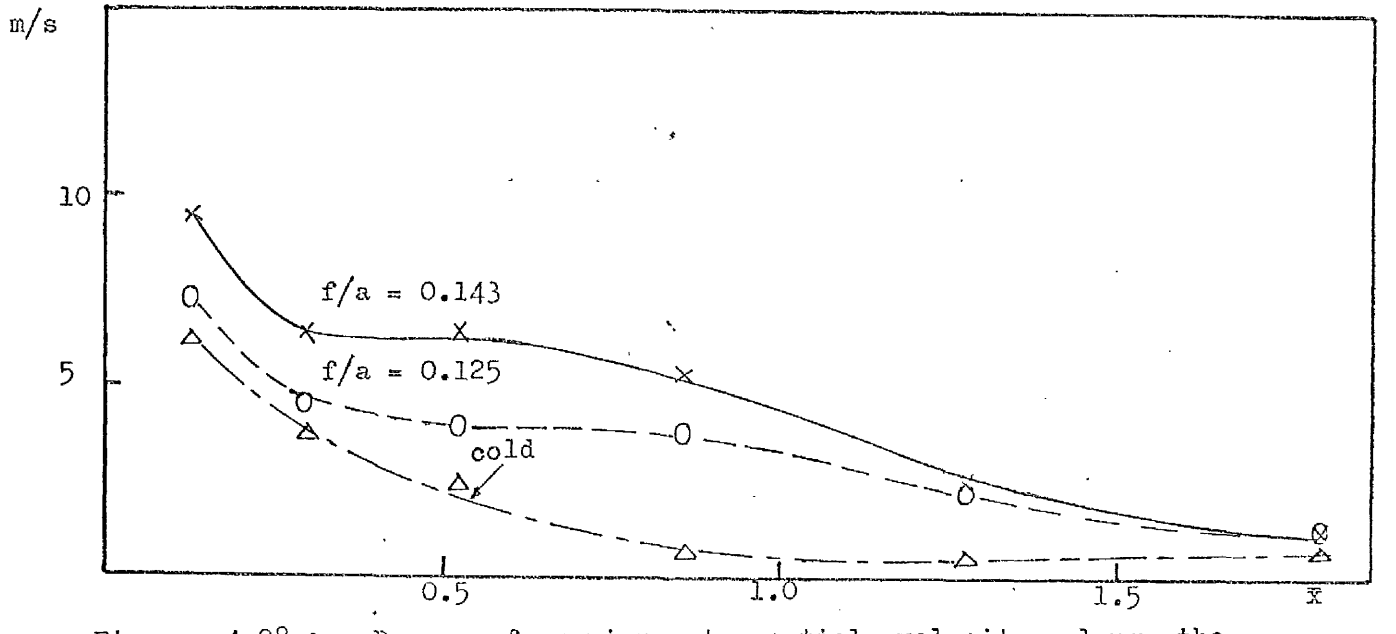

Figure 4.28.h - Decay of maximum tangential velocity along the furnace
22.5 Hubless swirler in D/d = 5 furnace

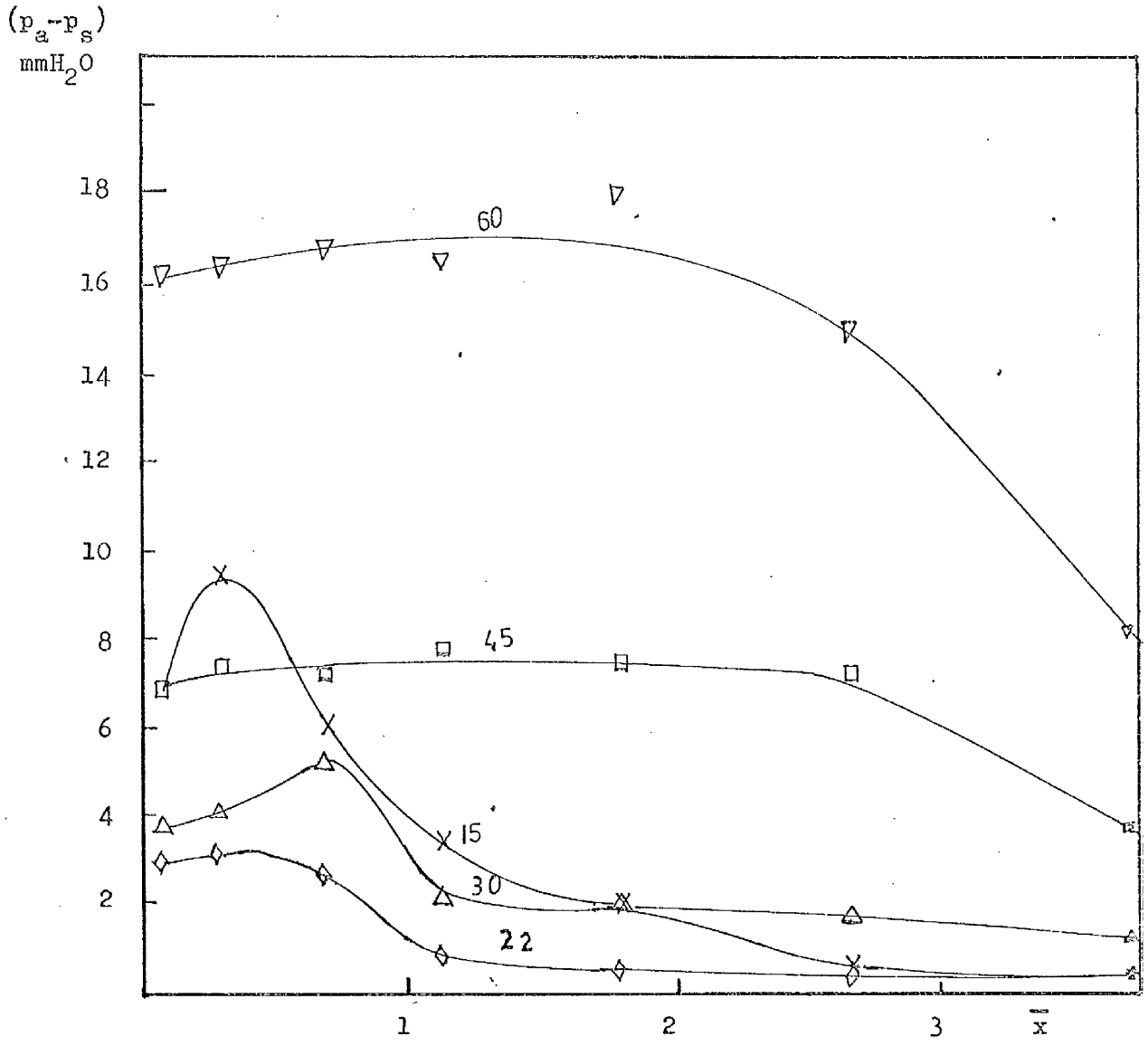

Figure 4.29.a - Recovery of centreline static pressure along the furnace Hubless swirlers cold flow in D/d = 2.5 furnace.

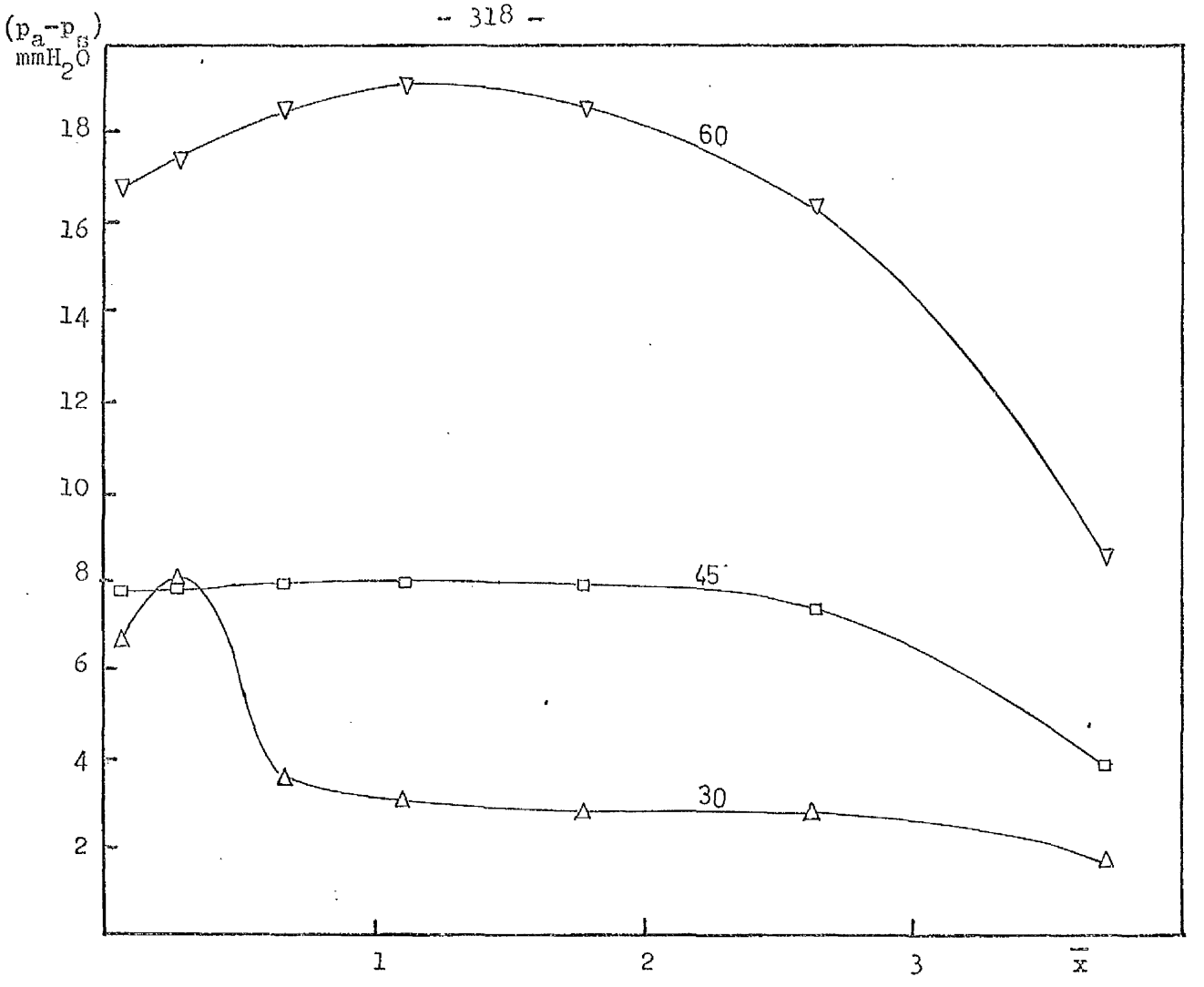

Figure 4.29.b :- Recovery of centreline static pressure along the furnace
Annular swirlers cold flow in D/d = 2.5 furnace

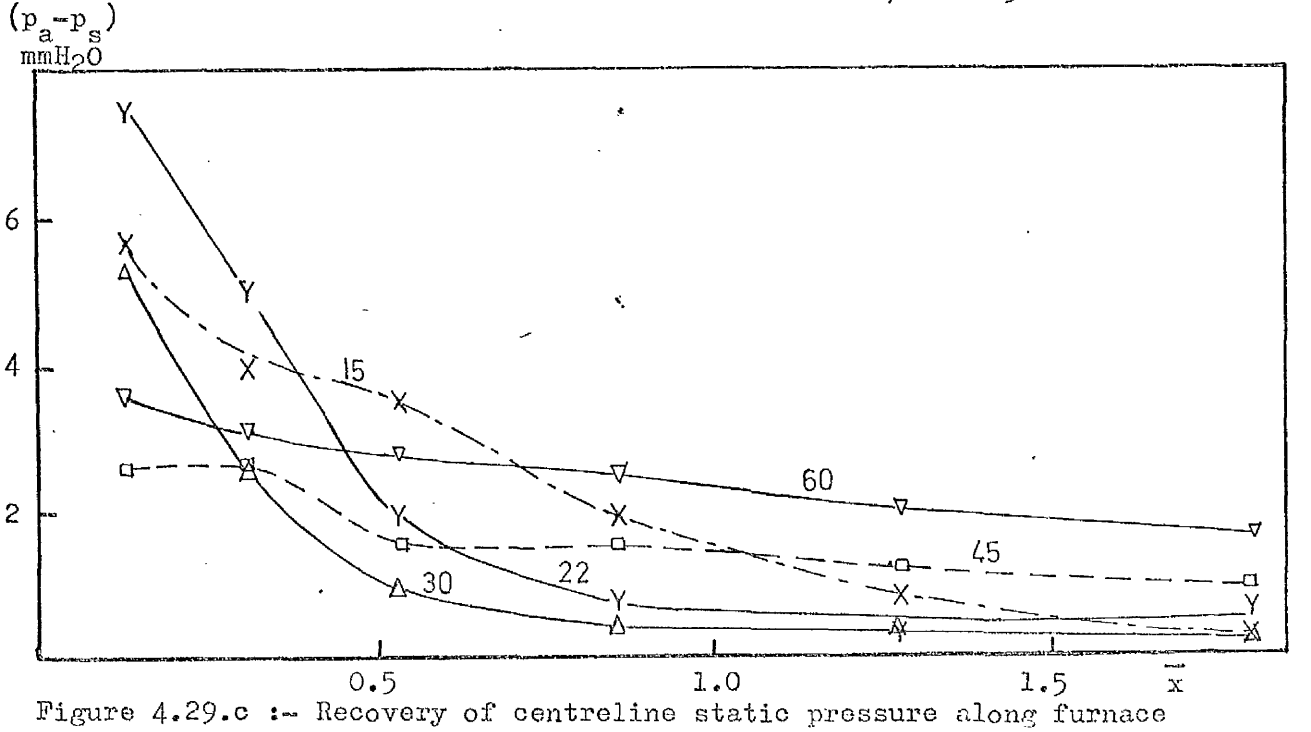

Figure 4.29.c :- Recovery of centreline static pressure along furnace
Hubless swirlers cold flow in D/d = 5 furnace.

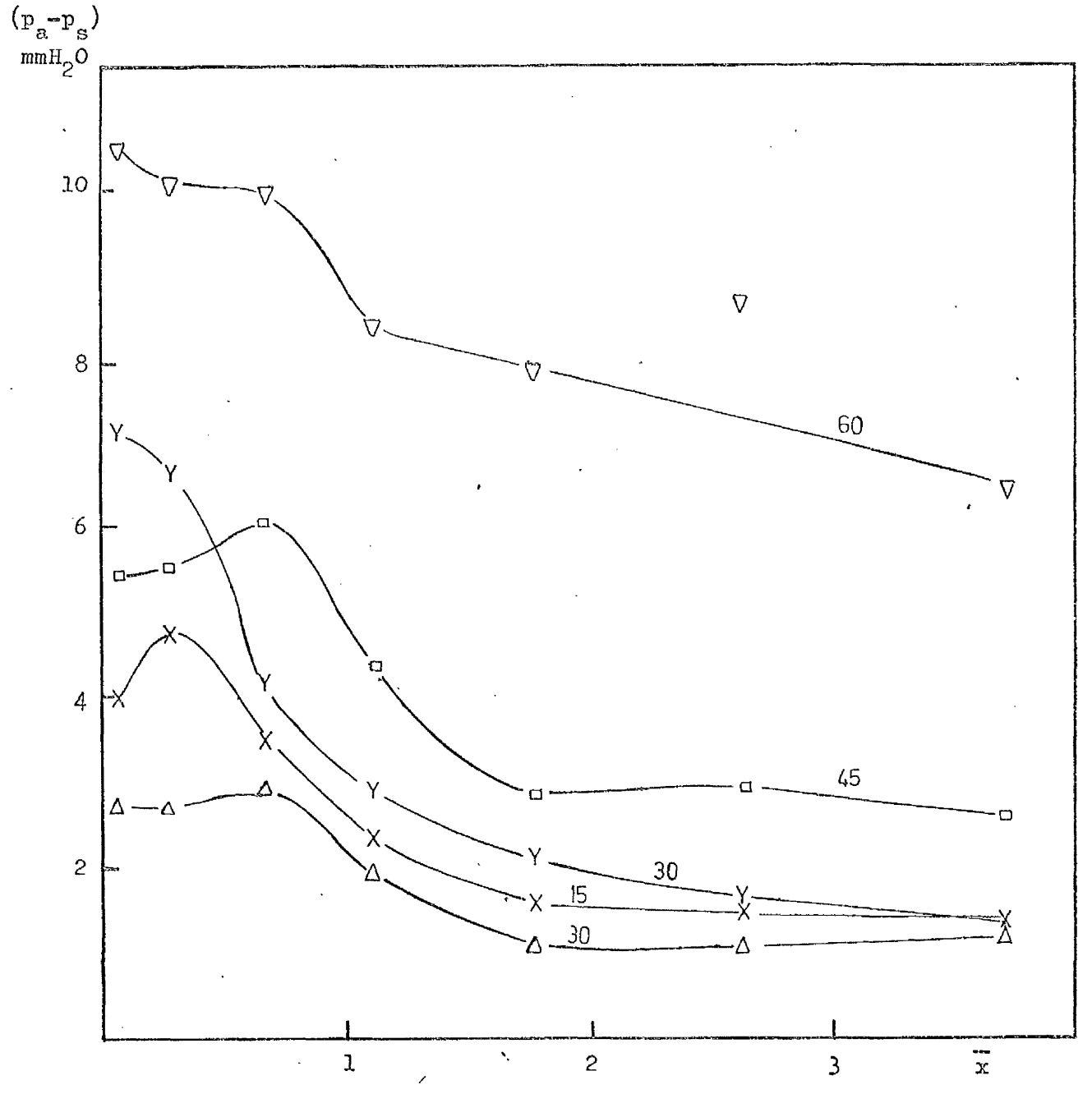

Figure 4.29.d – Recovery of centreline static pressure along the furnace Hubless swirler flames in D/d = 2.5 furnace.

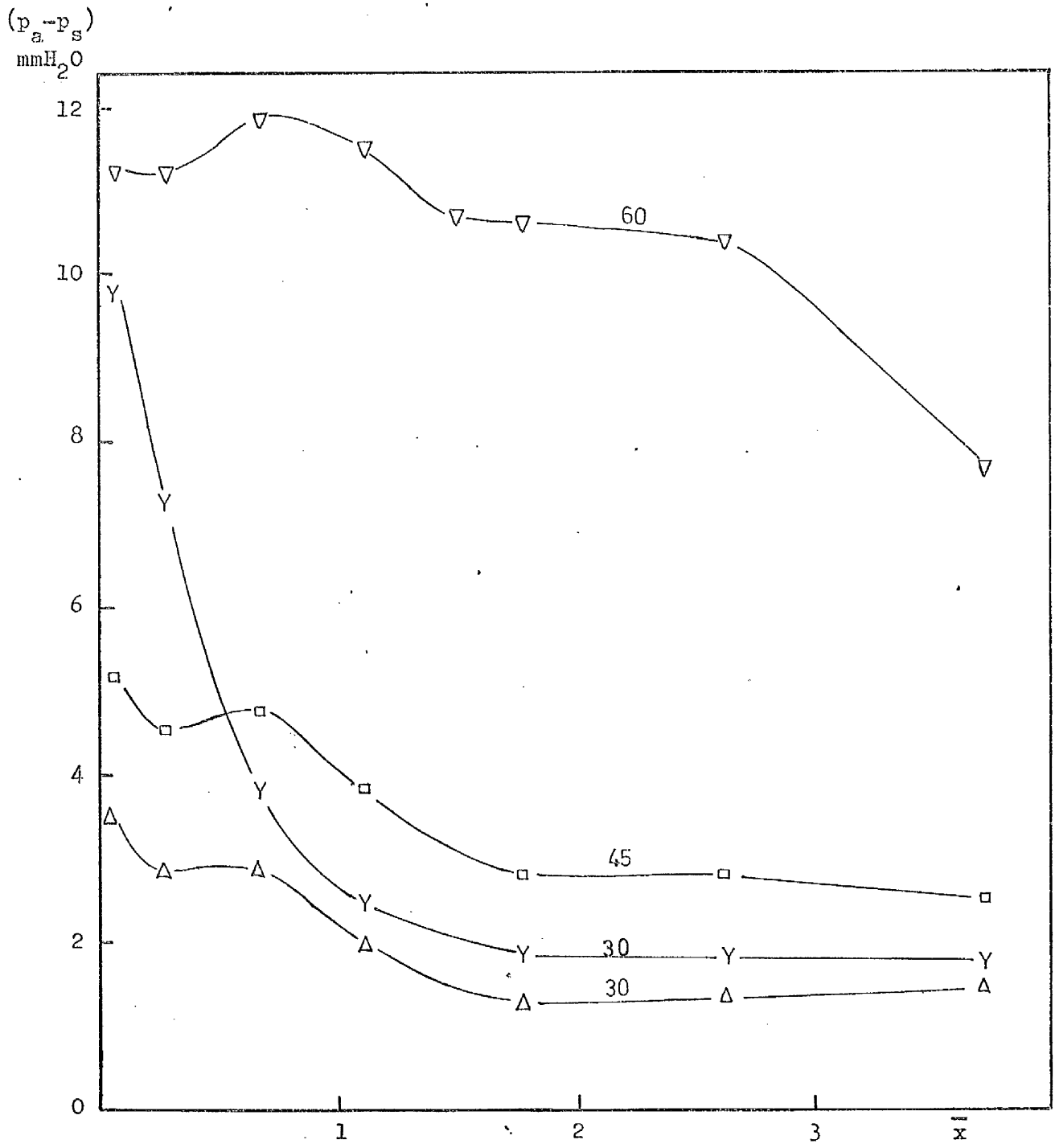

Figure 4.29.e - Recovery of centreline static pressure along the furnace
Annular swirler flames in D/d = 2.5 furnace.

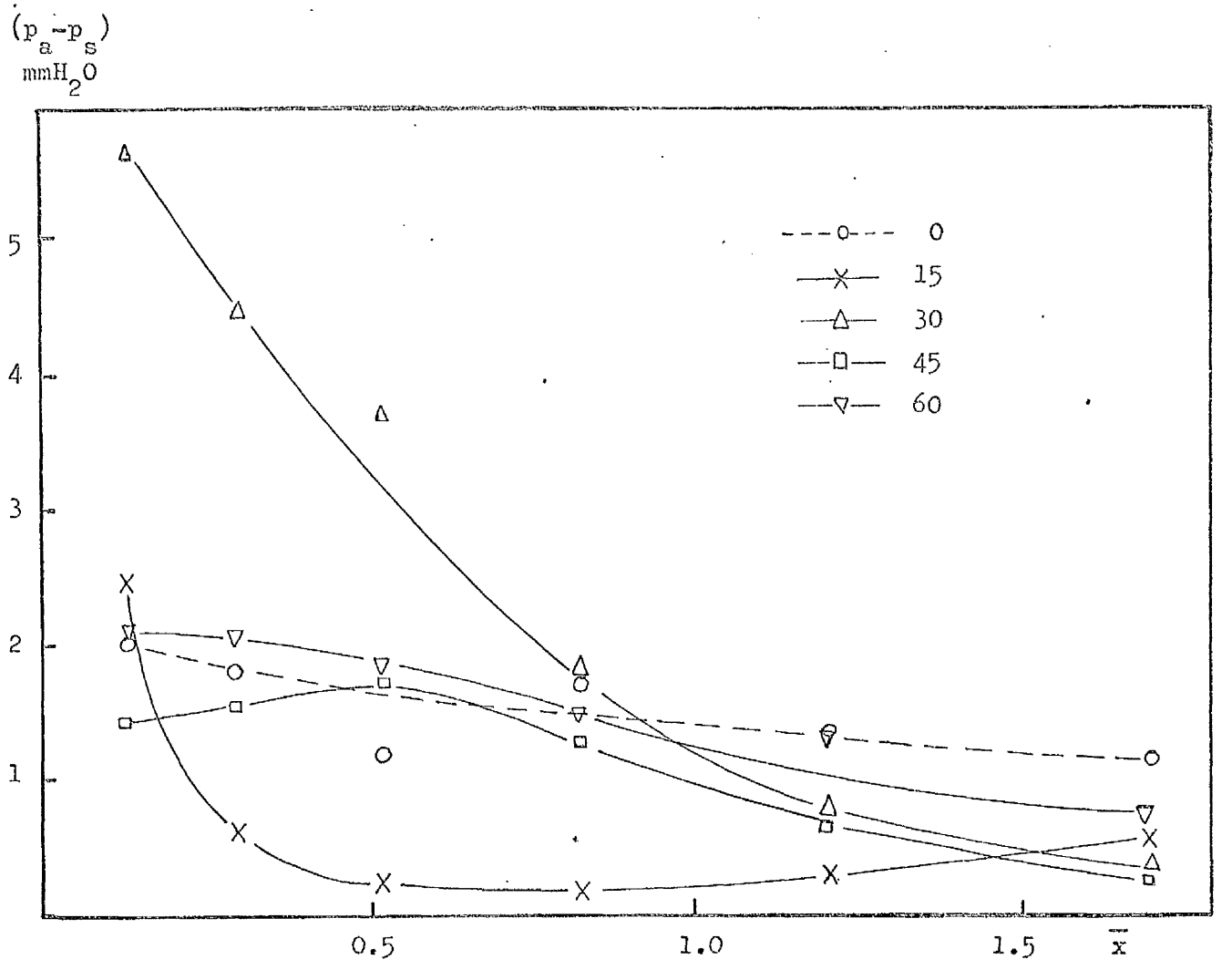

Figure 4.29.f :- Recovery of centreline static pressure along the furnace
Hubless swirler flames in D/d = 5 furnace.

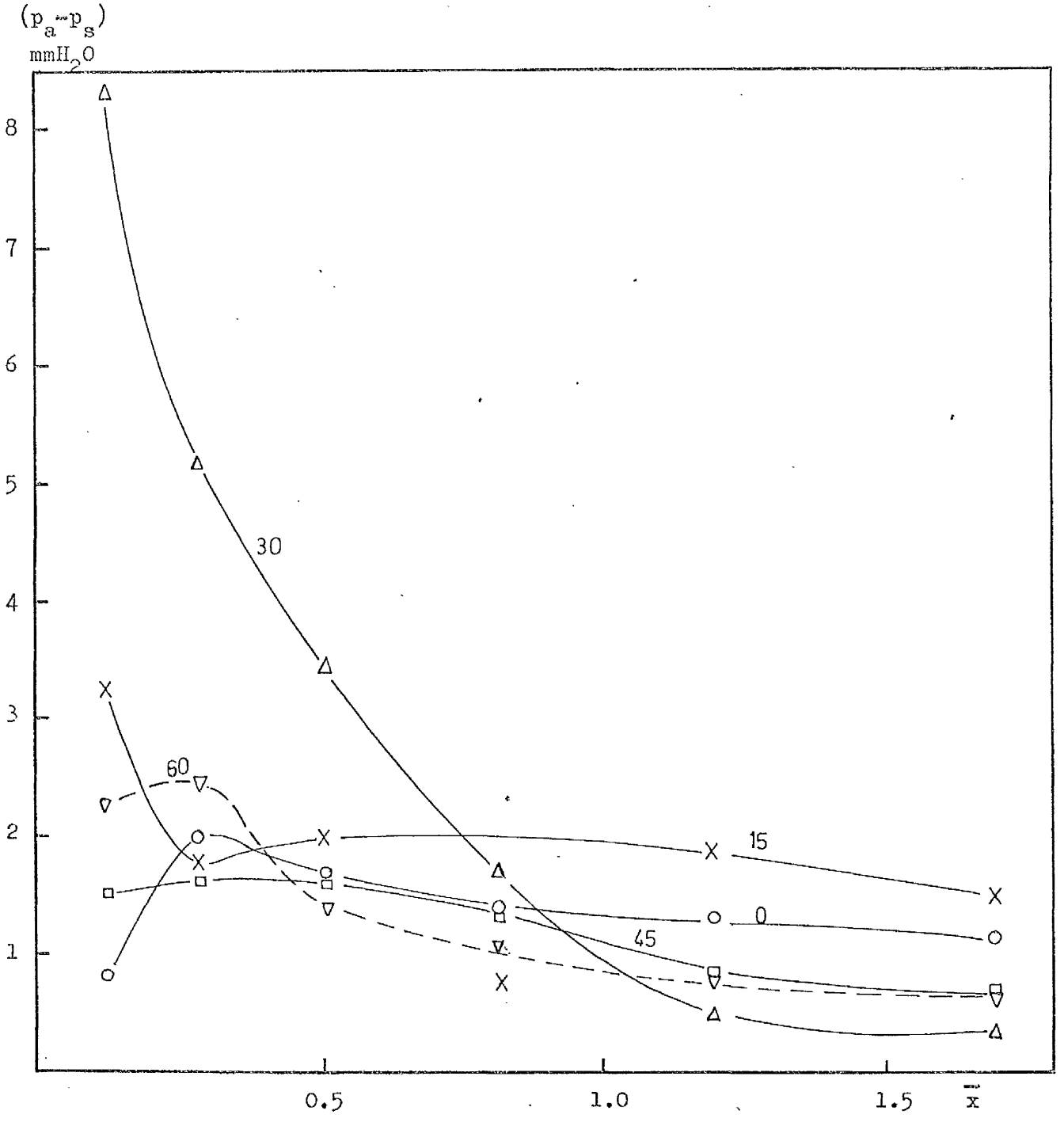

Figure 4.29.g :- Recovery of centreline static pressure along the furnace Annular swirler flames in D/d = 5 furnace.

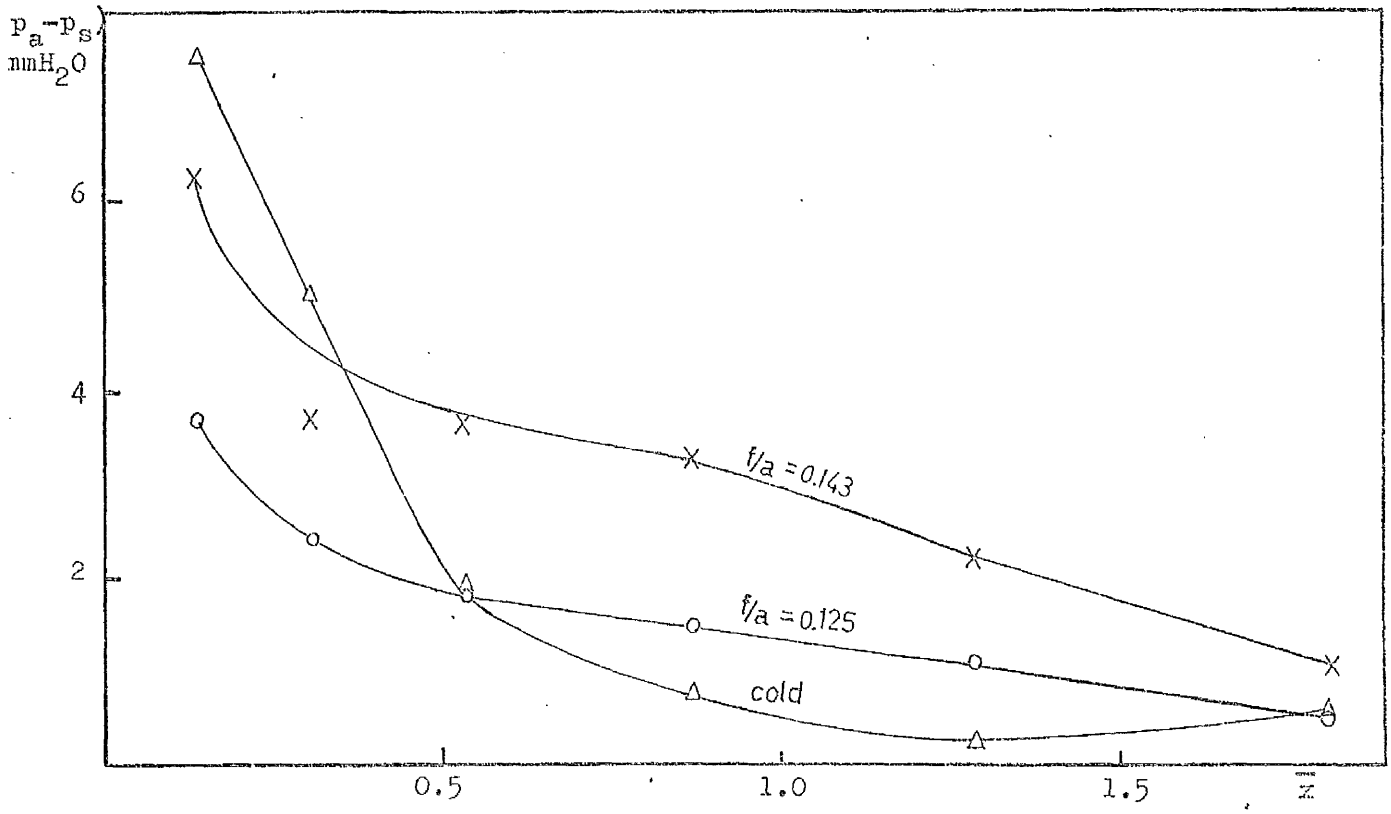

Figure 4.29.h - Recovery of centreline static pressure along the furnace 22.5 hubless swirler in D/d = 5 furnace.

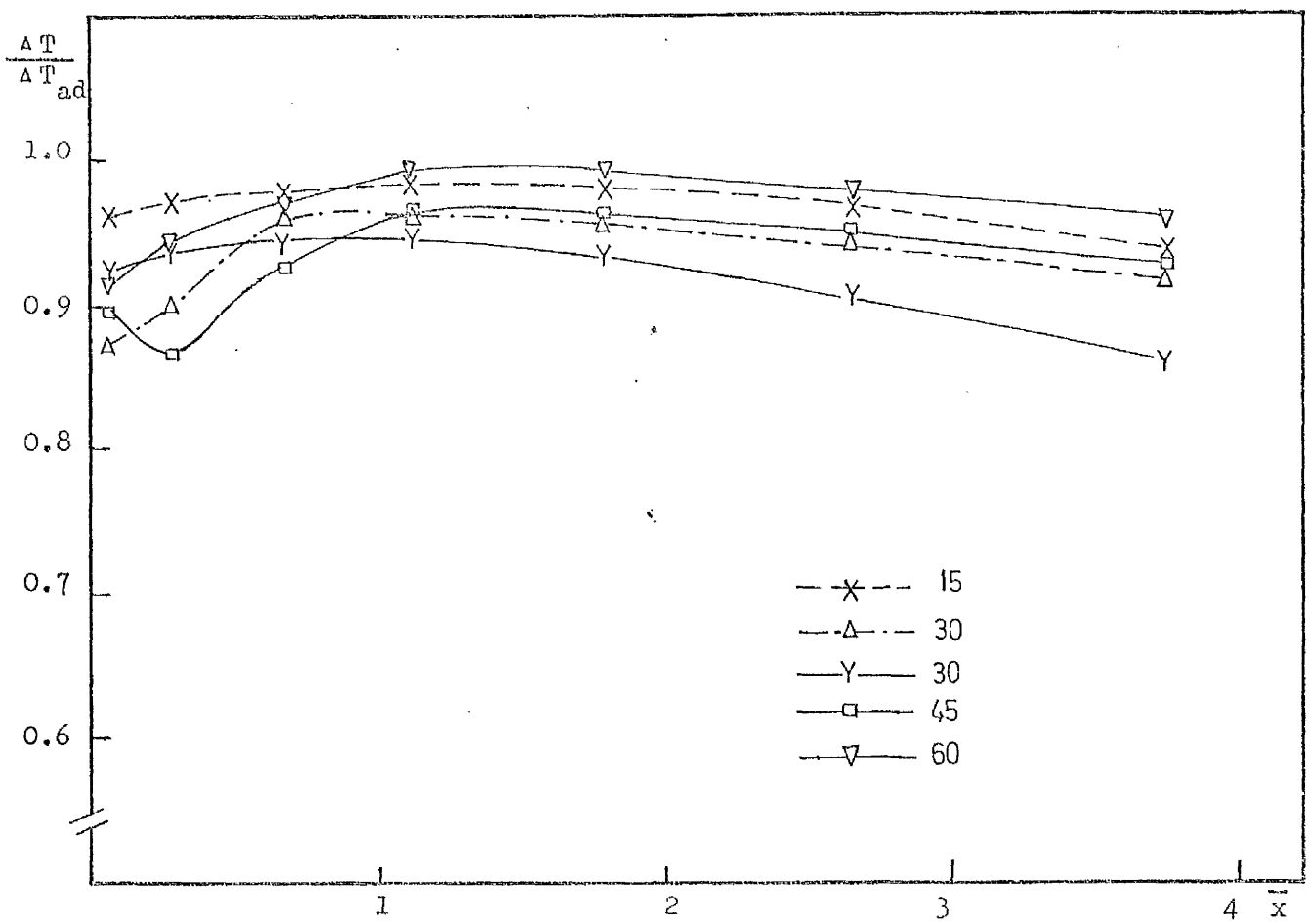

Figure 4.30.a - Maximum temperature variation along the furnace

Hubless swirlers in D/d = 2.5 furnace.

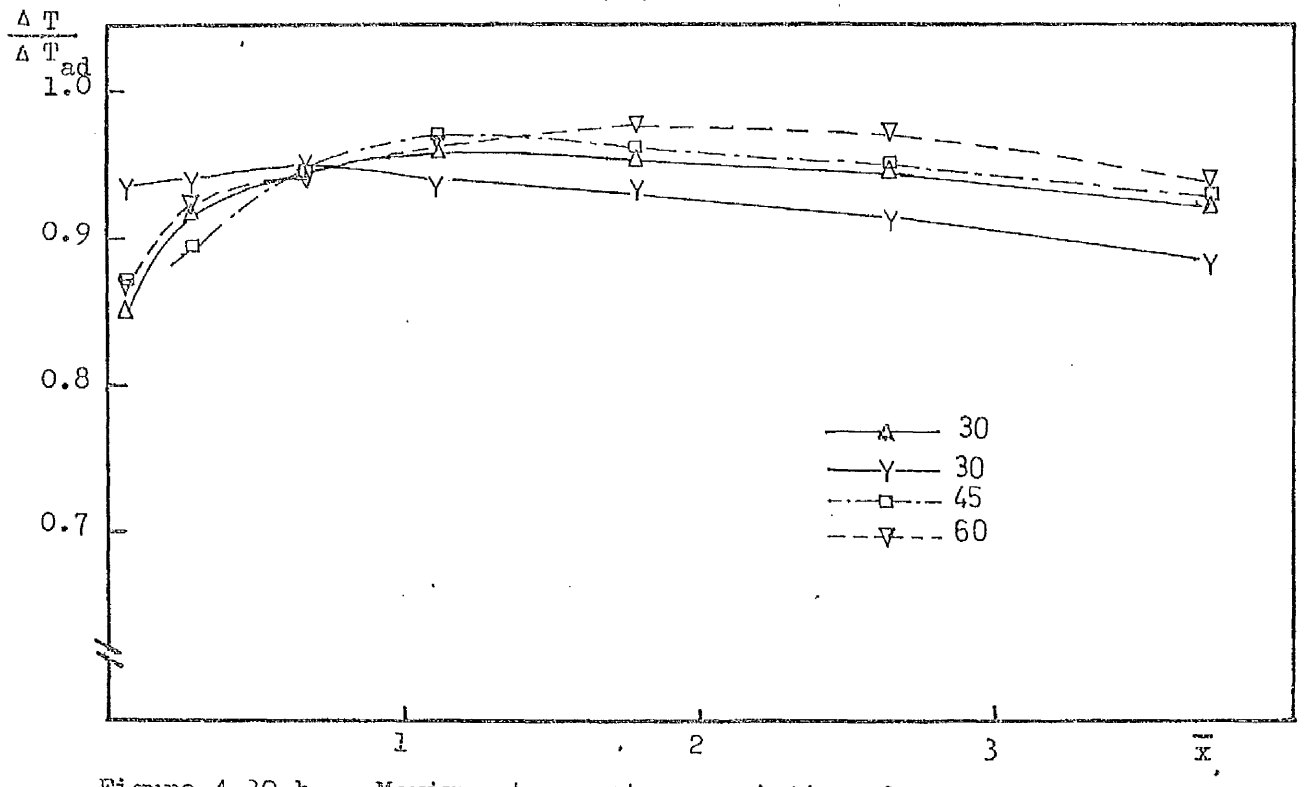

Figure 4.30.b :- Maximum temperature variation along the furnace
Annular swirlers in D/d = 2.5 furnace.

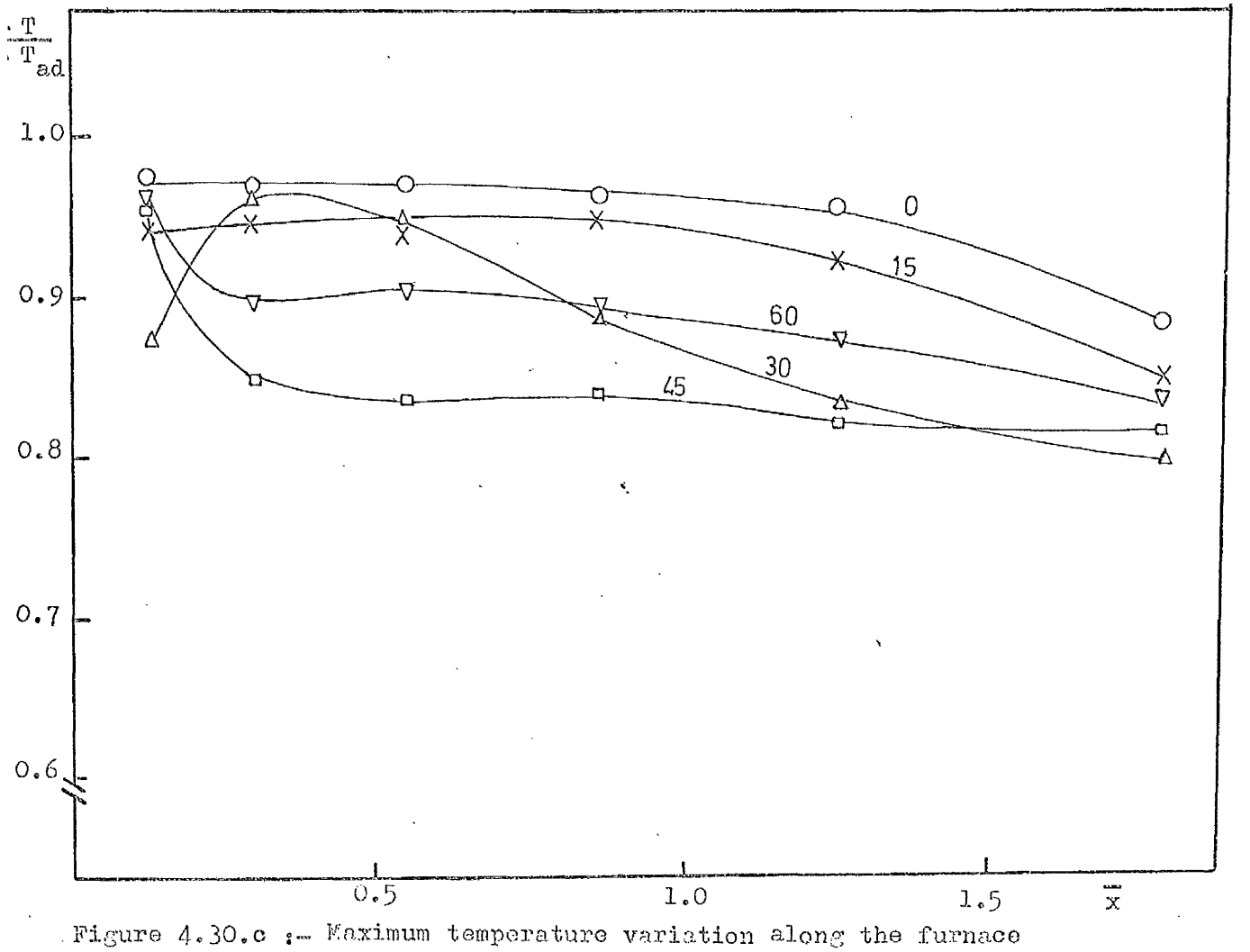

Figure 4.30.c :- Maximum temperature variation along the furnace
Hubless swirlers in D/d = 5 furnace.

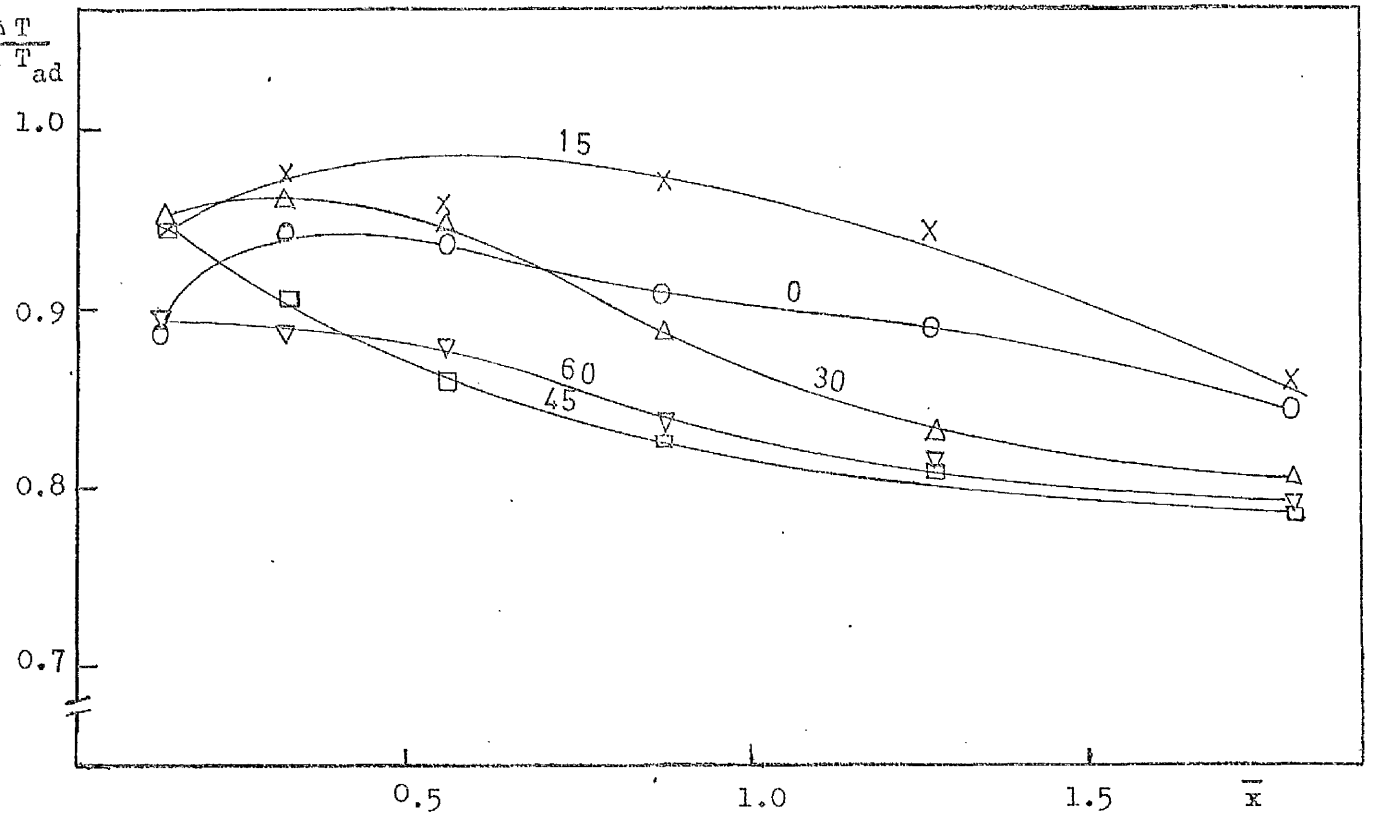

Figure 4.30.d :- Maximum temperature variation along the furnace
Annular swirlers in D/d = 5 furnace.

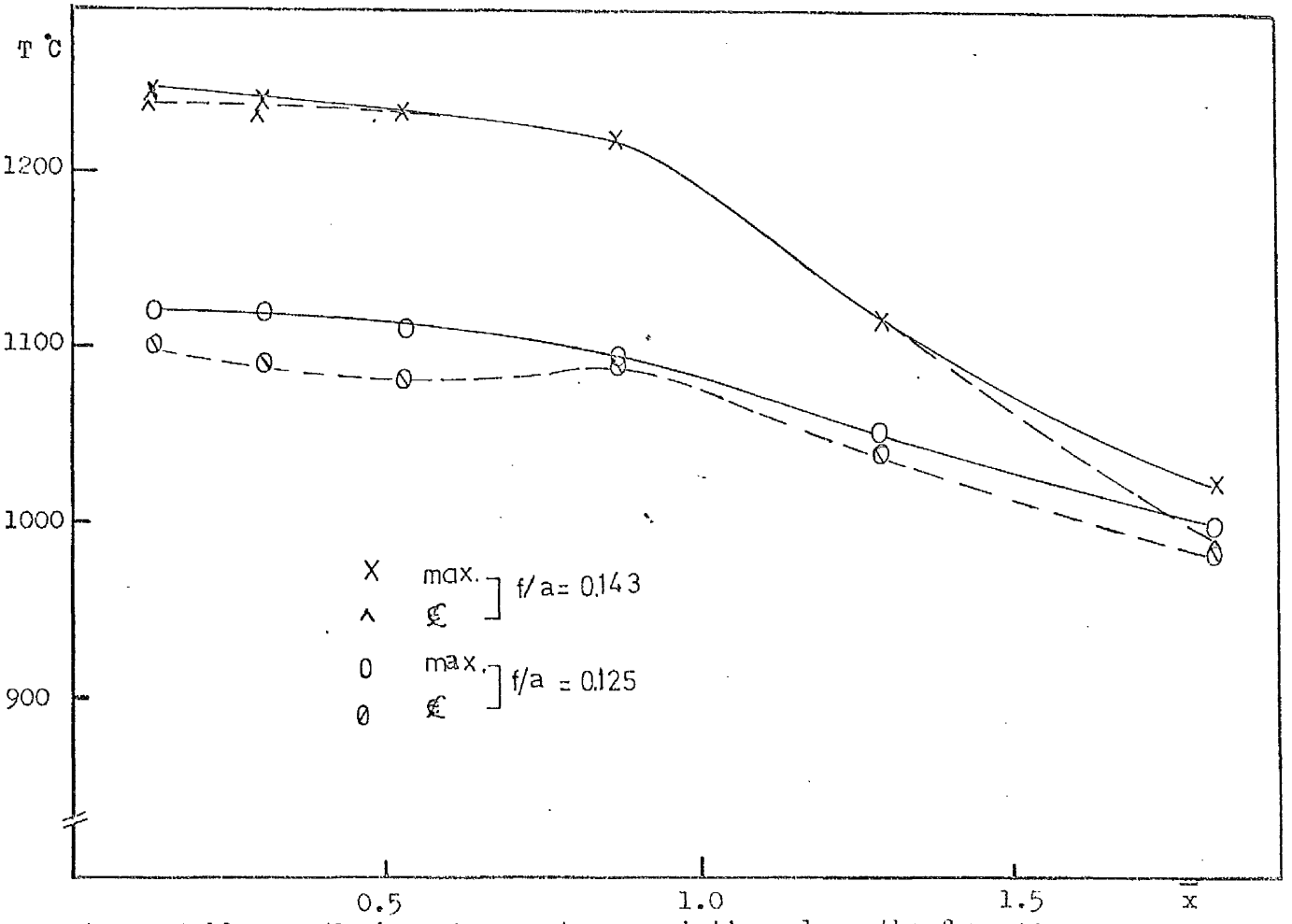

Figure 4.30.e :- Maximum temperature variation along the furnace
22.5 hubless swirler in D/d = 5 furnace.

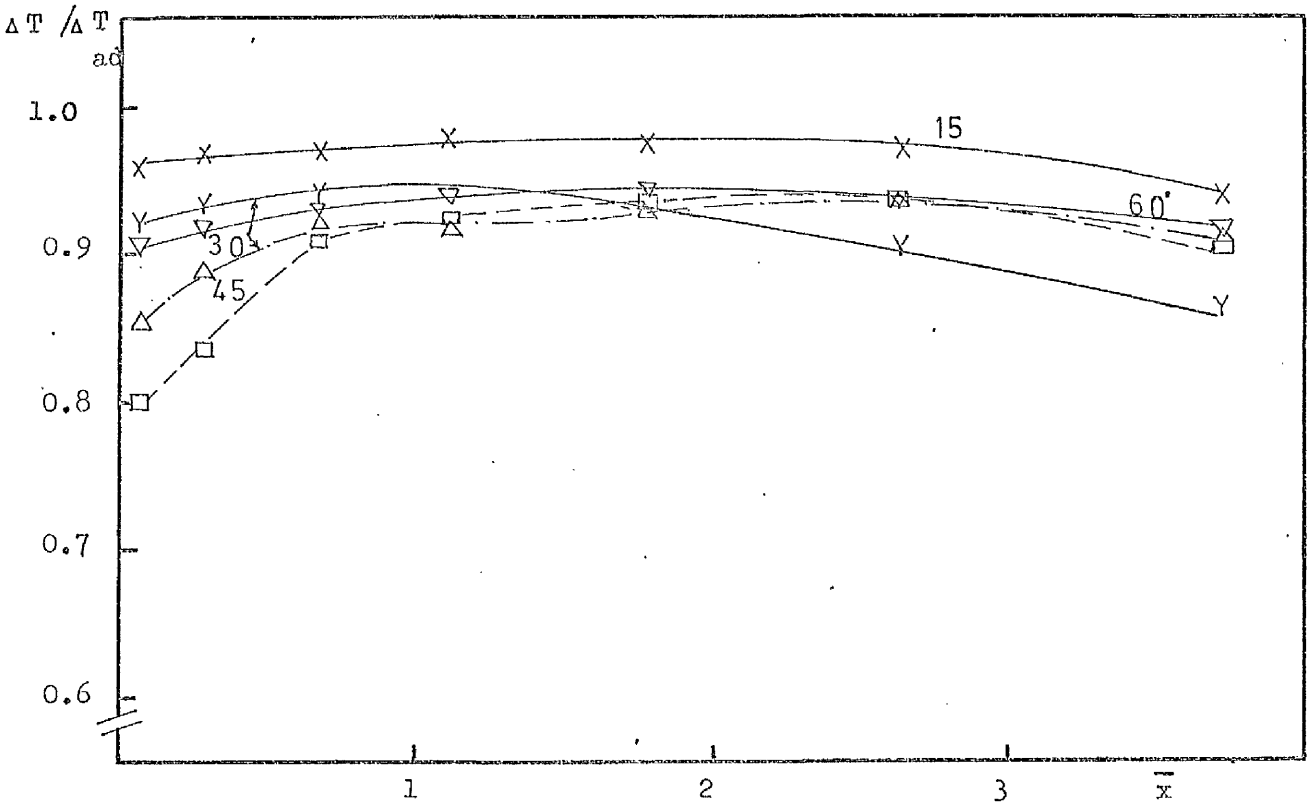

Figure 4.31.a - Centreline temperature variation along the furnace
Hubless swirlers in D/d = 2.5 furnace.

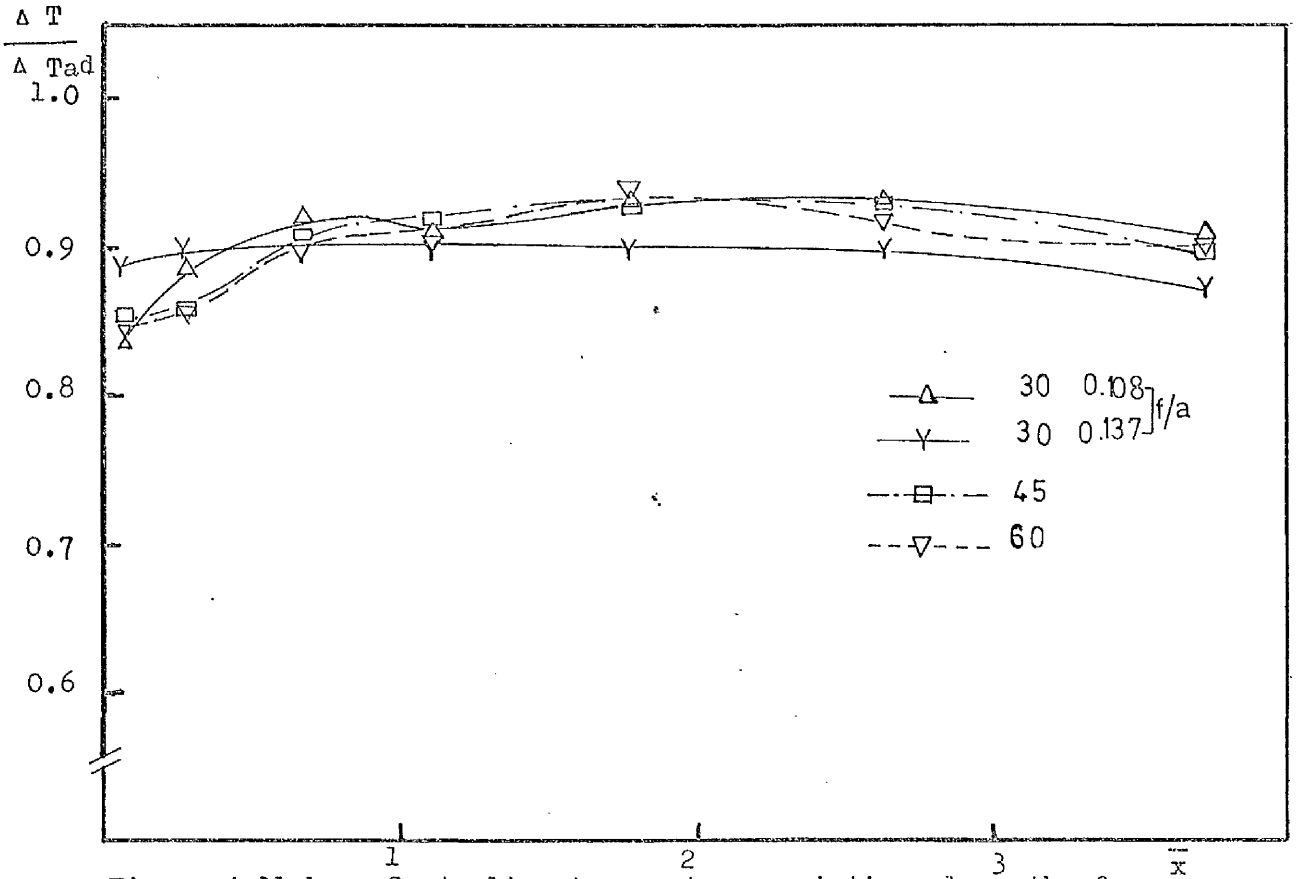

Figure 4.31.b - Centreline temperature variation along the furnace
Annular swirlers in D/d = 2.5 furnace.

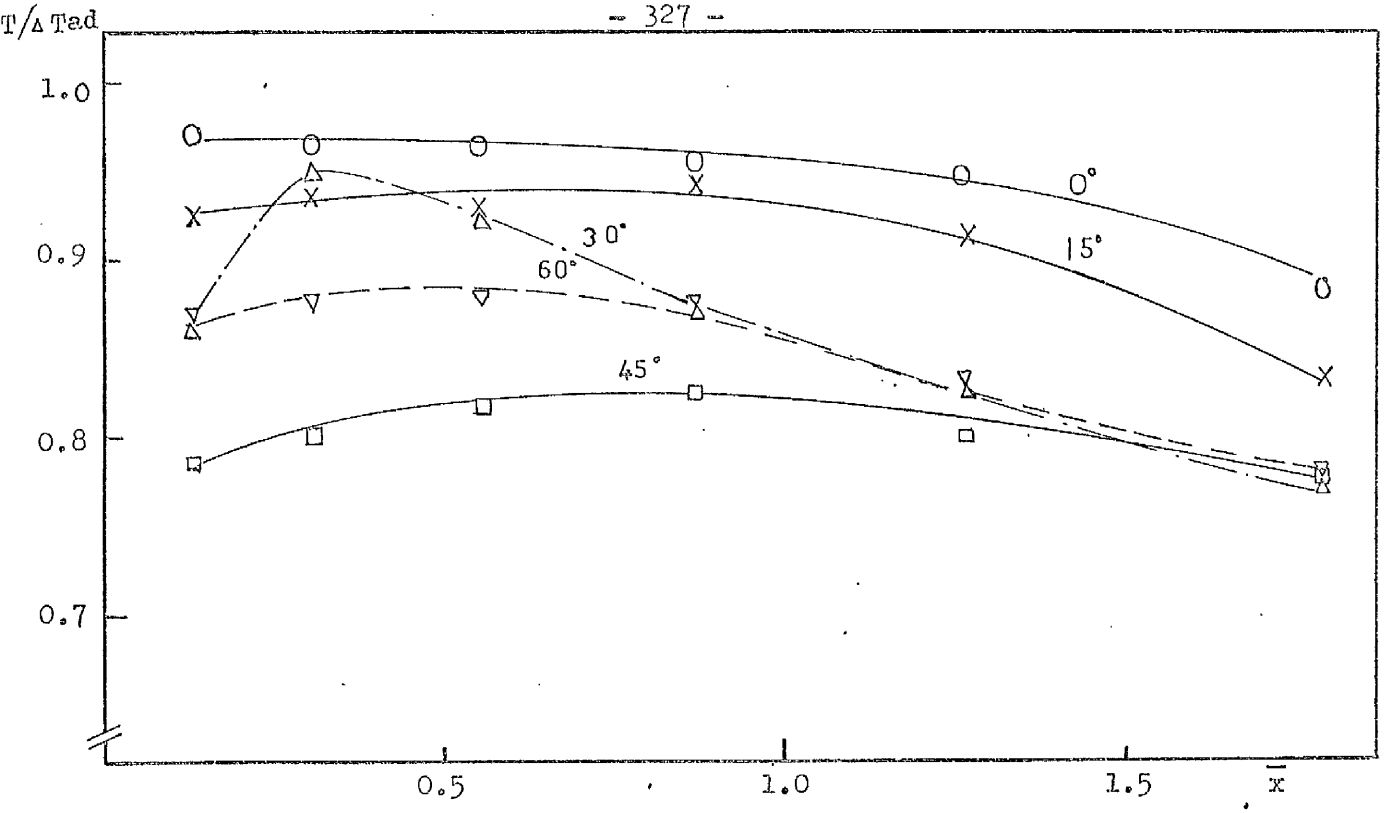

Figure 4.31.c :- Centreline temperature variation along the furnace
Hubless swirlers in D/d = 5 furnace.

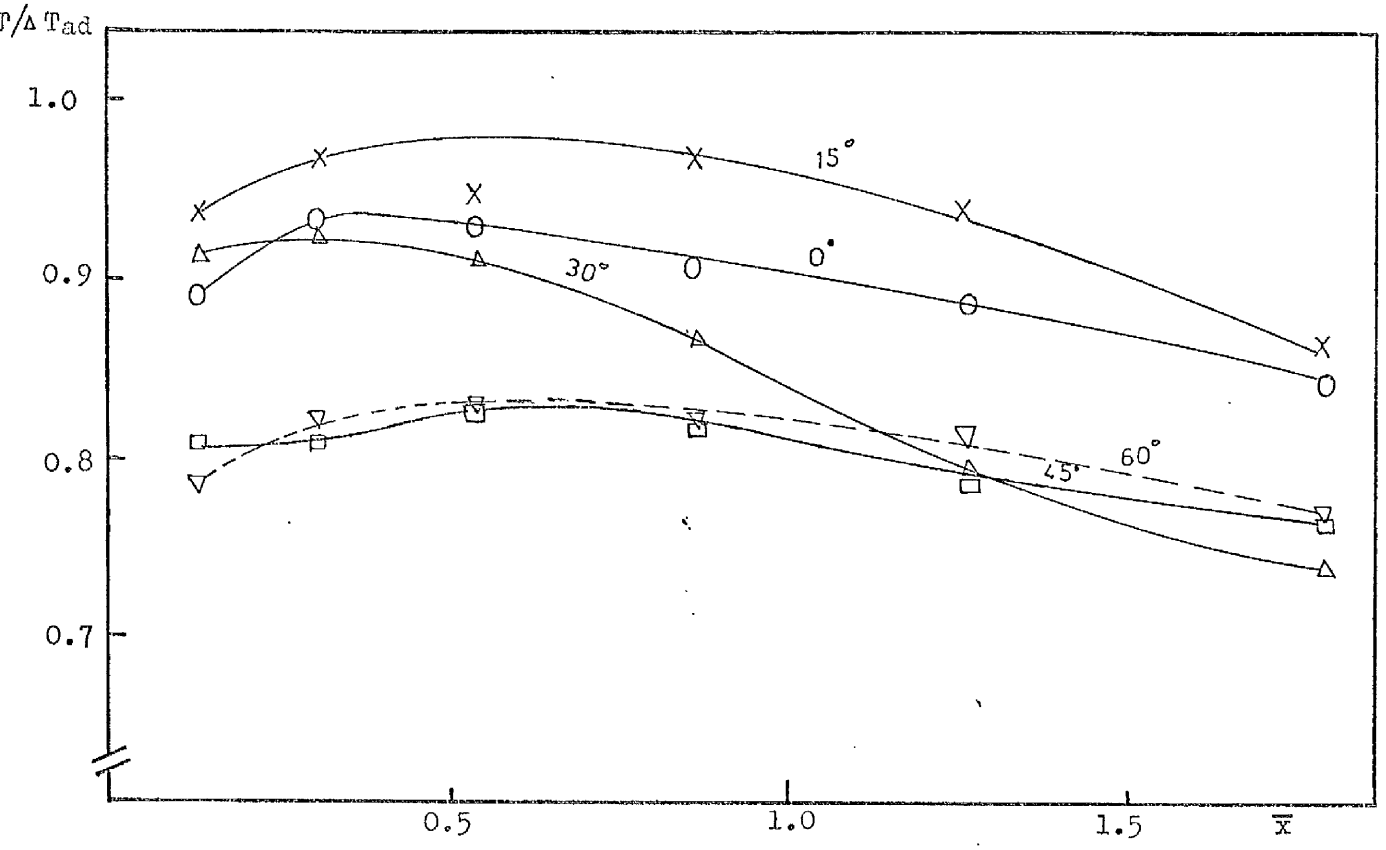

Figure 4.31.d :- Centreline temperature variation along the furnace
Annular swirlers in D/d = 5 furnace.

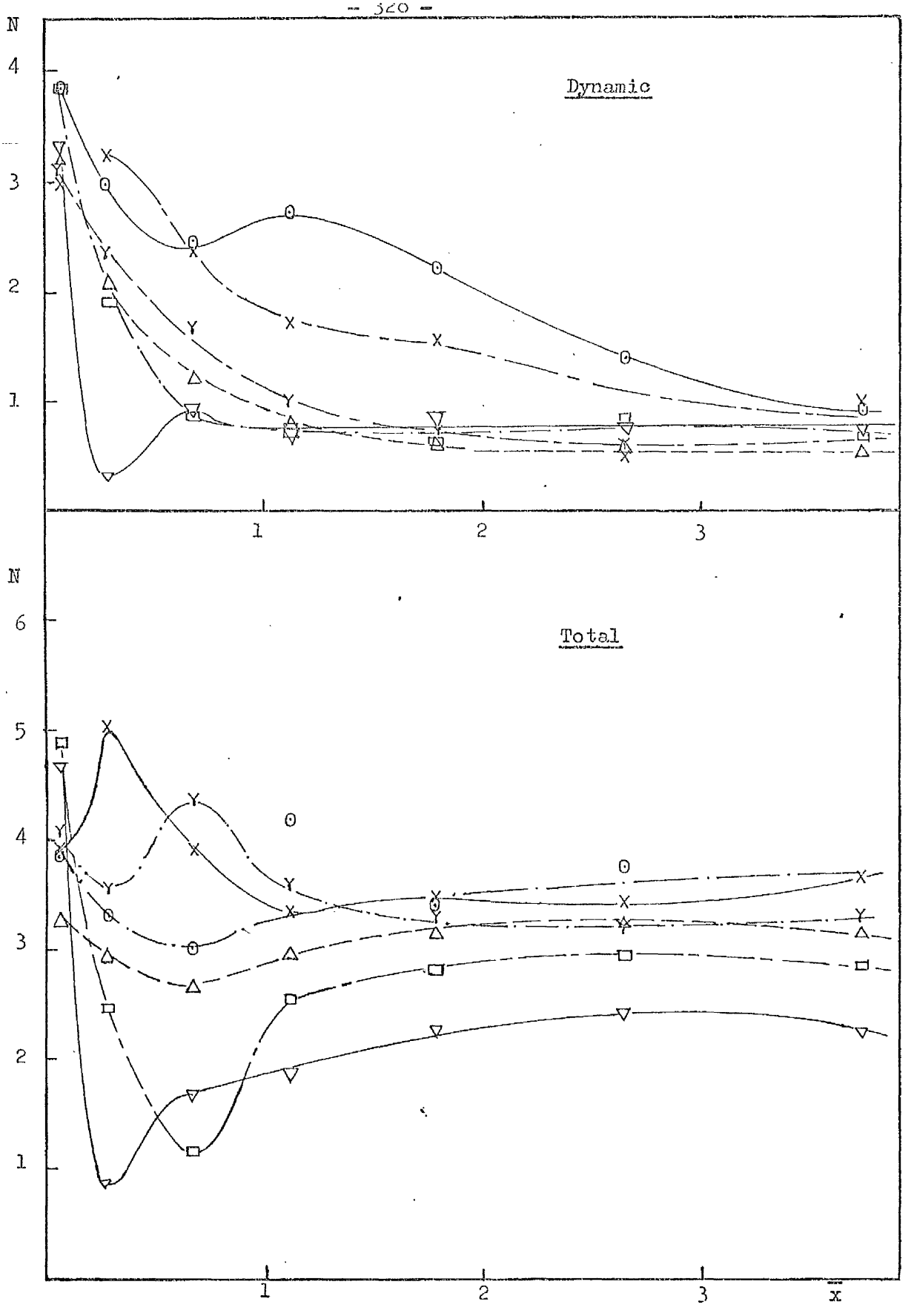

Figure 4.32.a :- Axial momentum fluxes

Hubless swirlers cold flow in D/d = 2.5 furnace.

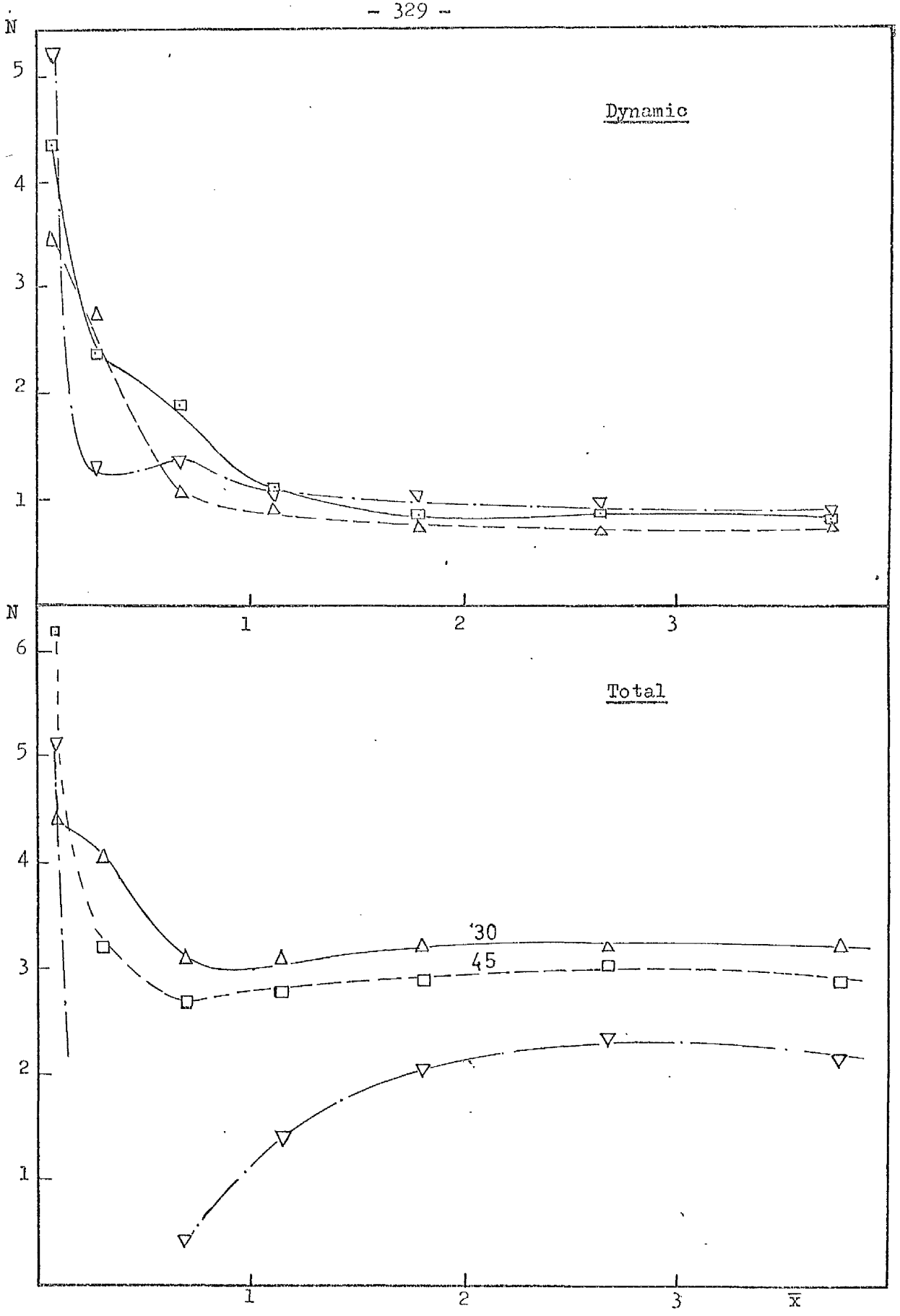

Figure 4.32.b :- Axial momentum fluxes

Annular swirlers cold flow in D/d = 2.5 furnace.

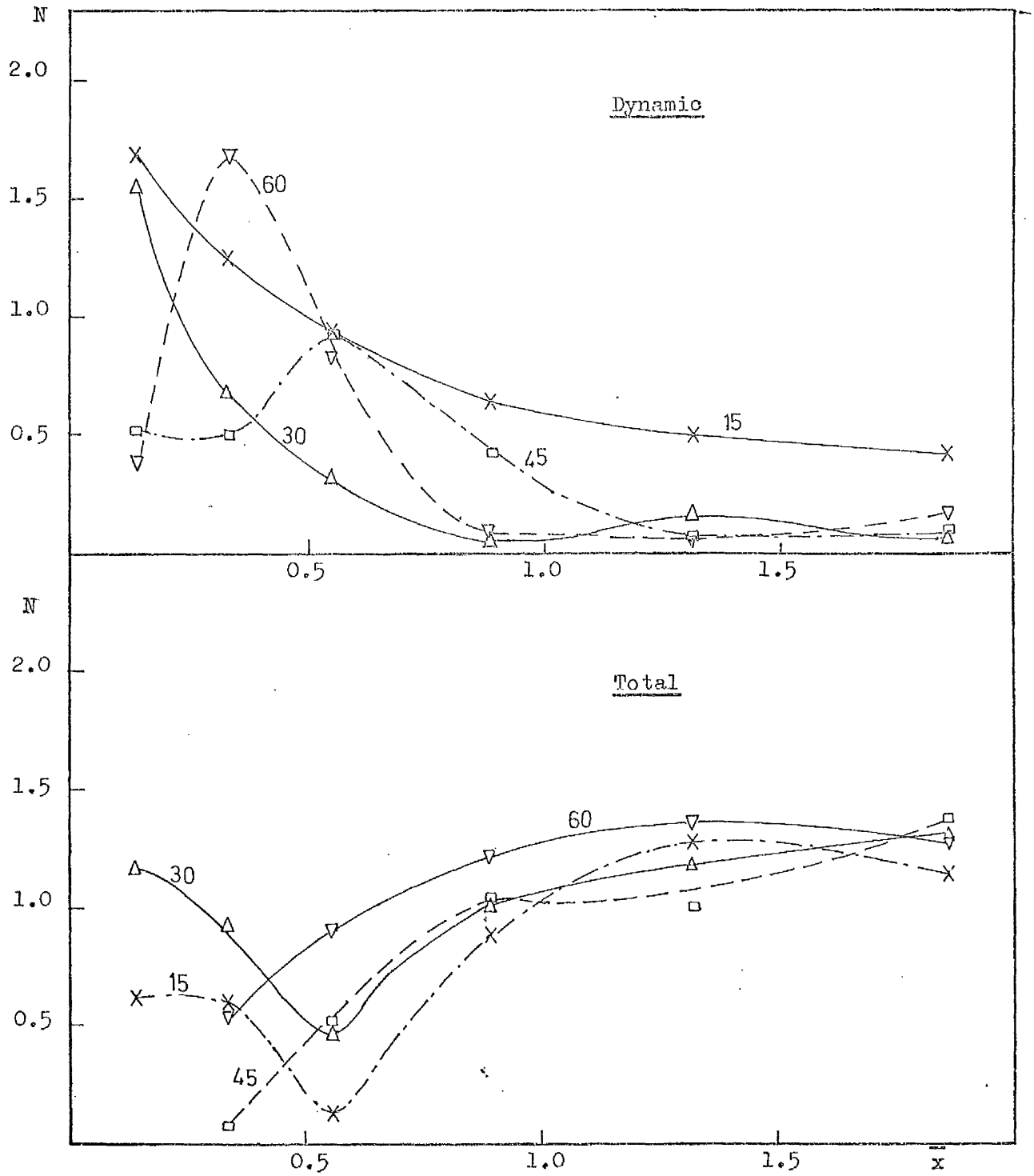

Figure 4.32.c :- Axial momentum fluxes
Hubless swirlers cold flow in D/d = 5 furnace.

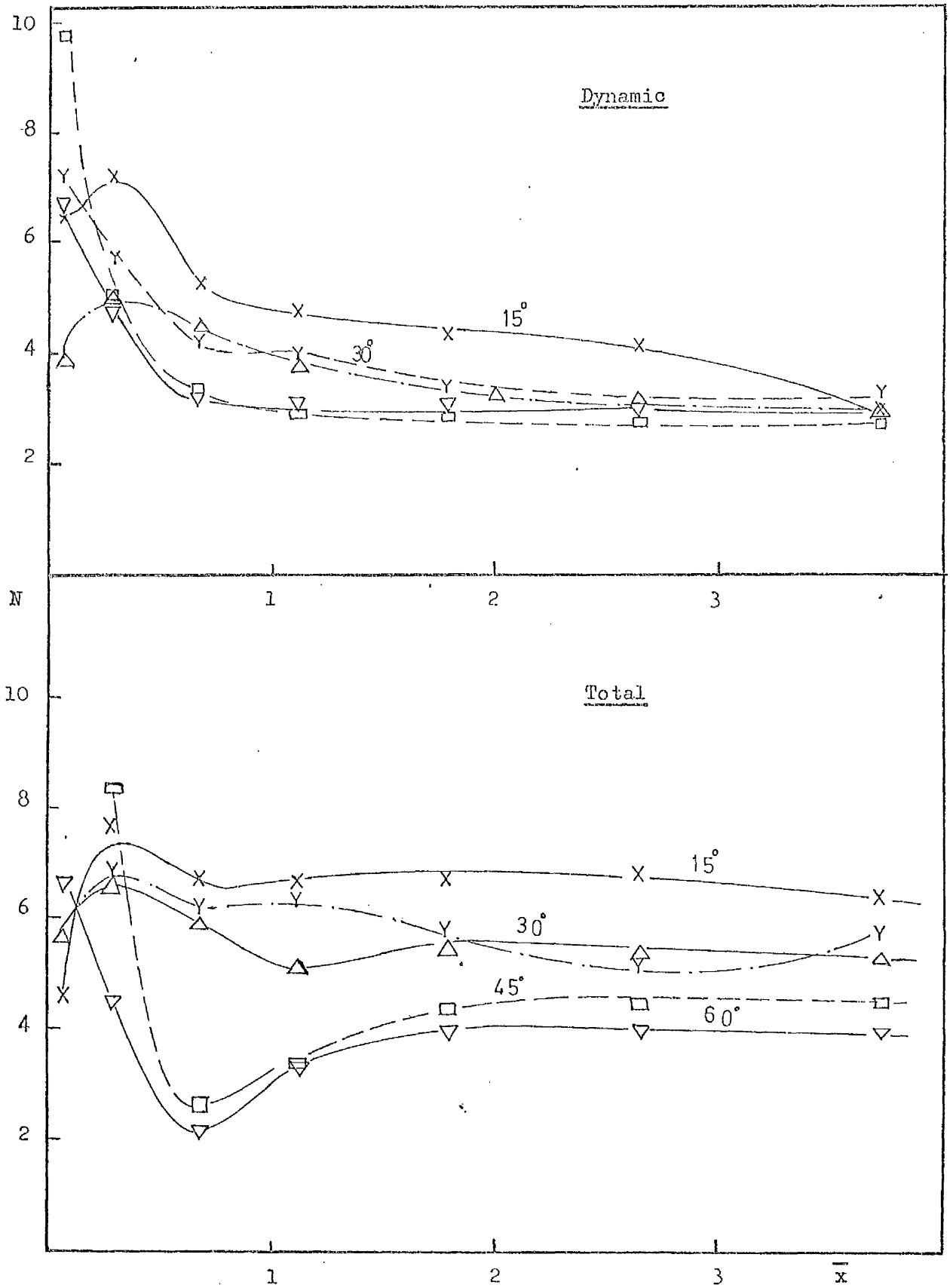

Figure 4.32.d :- Axial momentum fluxes

Hubless swirler flames in D/d = 2.5 furnace.

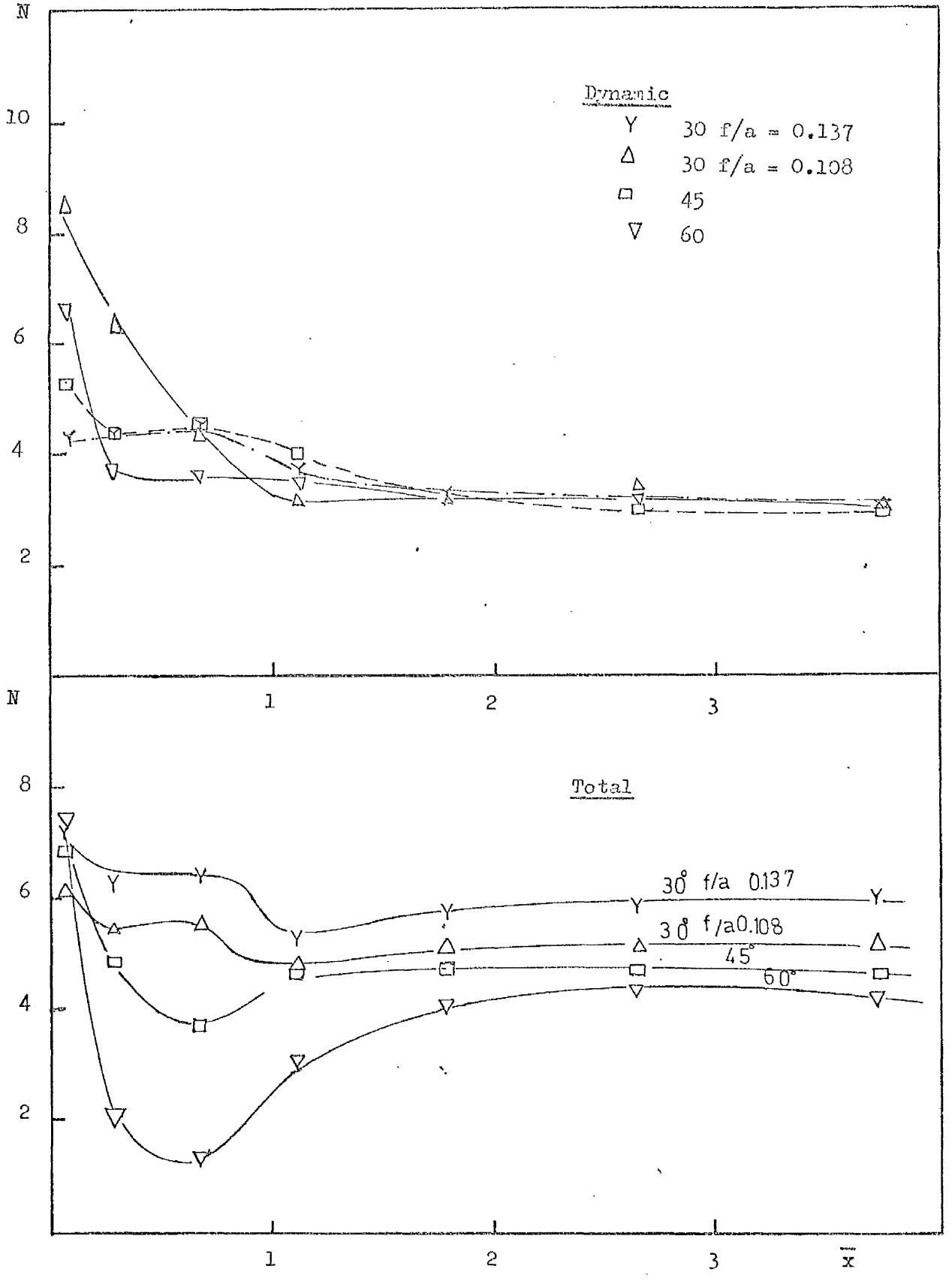

Figure 4.32.e :- Axial momentum fluxes

Annular swirler flames in D/d = 2.5 furnace.

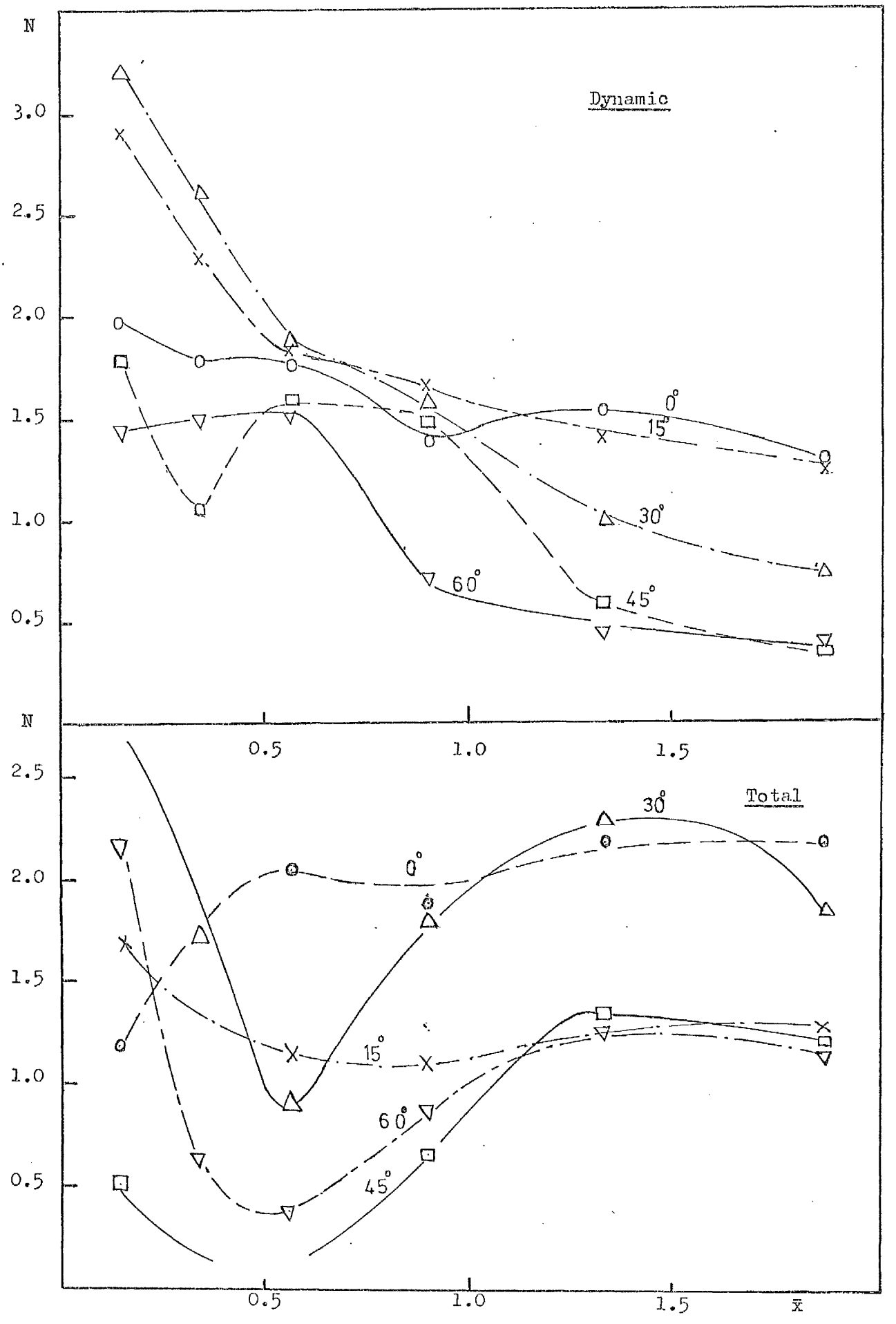

Figure 4.32.f :- Axial momentum fluxes
Hubless swirler flames in D/d = 5 furnace.

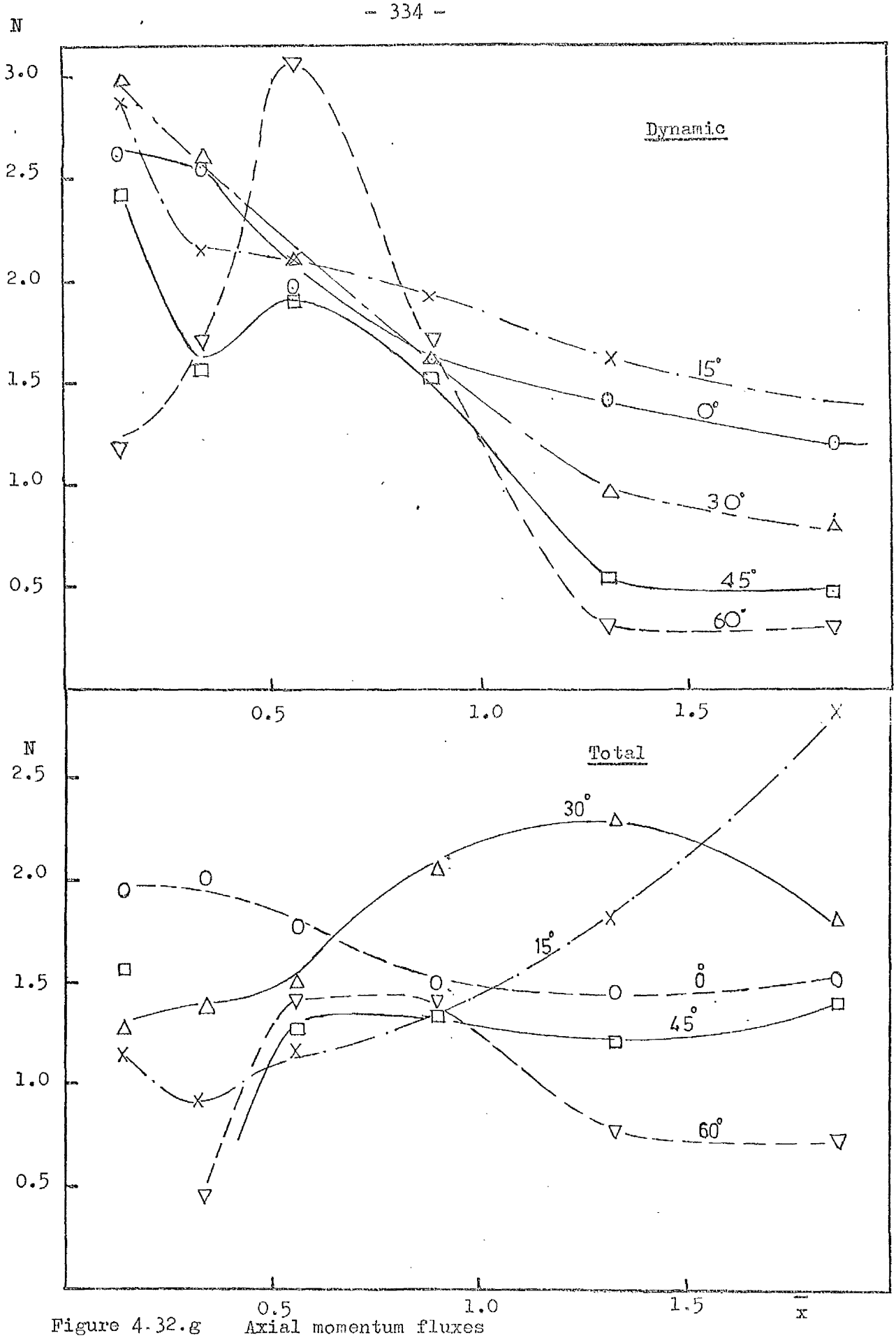

Figure 4.32.g Axial momentum fluxes
Annular swirler flames in D/d = 5 furnace.

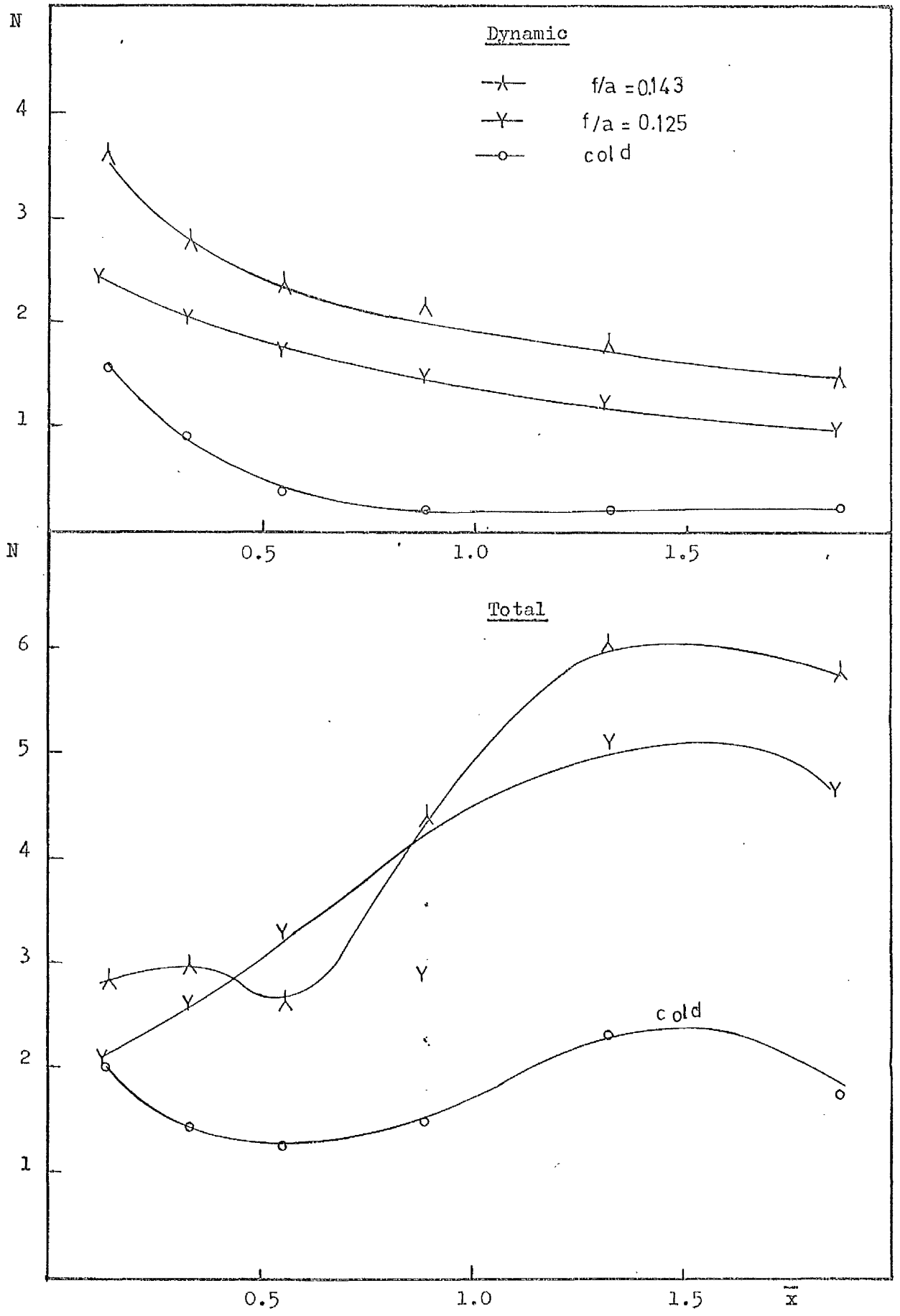

Figure 4.32.h :- Axial momentum fluxes
22.5 hubless swirler in D/d = 5 furnace.

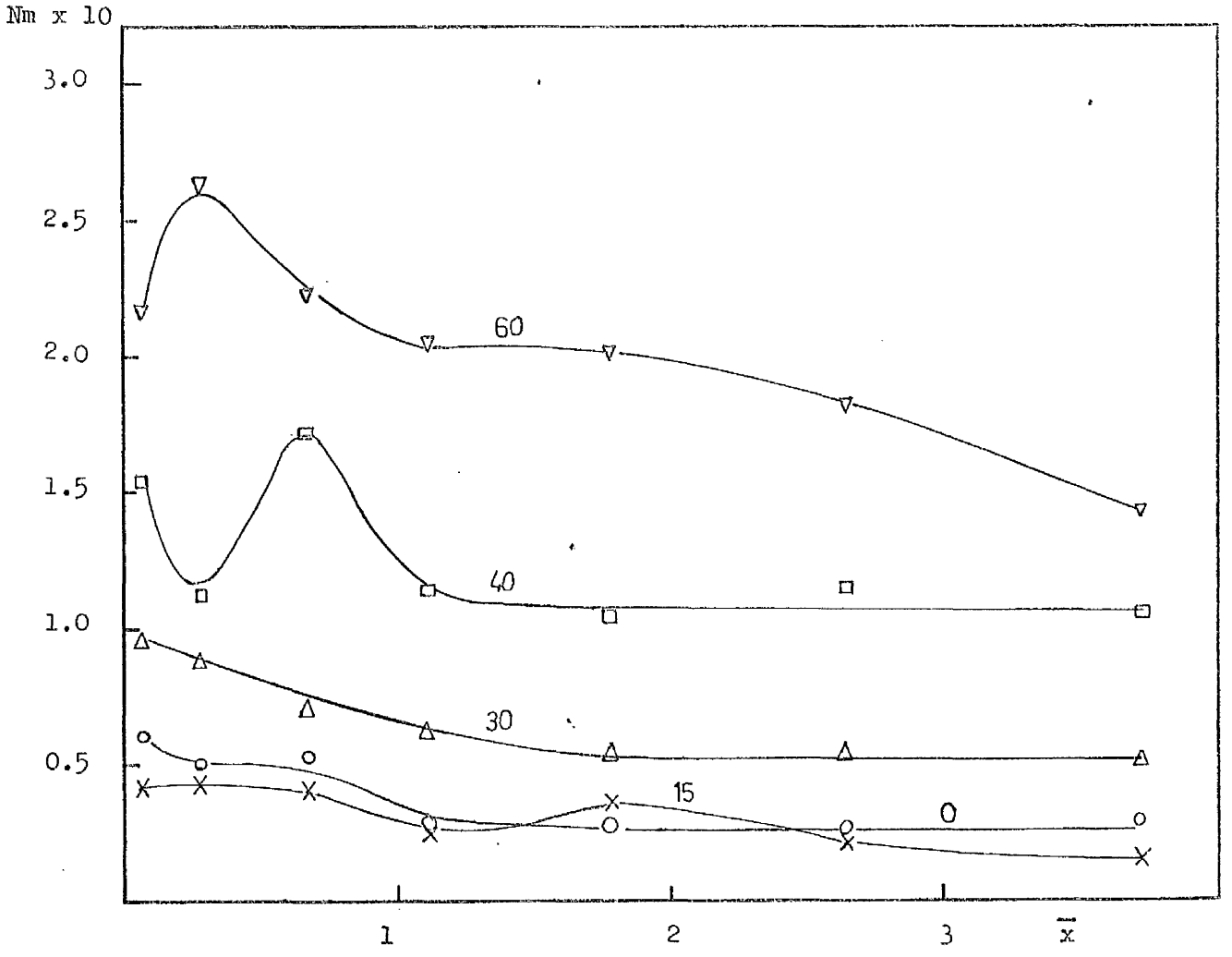

Figure 4.33.a :- Axial flux of tangential momenta
Hubless swirlers cold flow in D/d = 2.5 furnace.

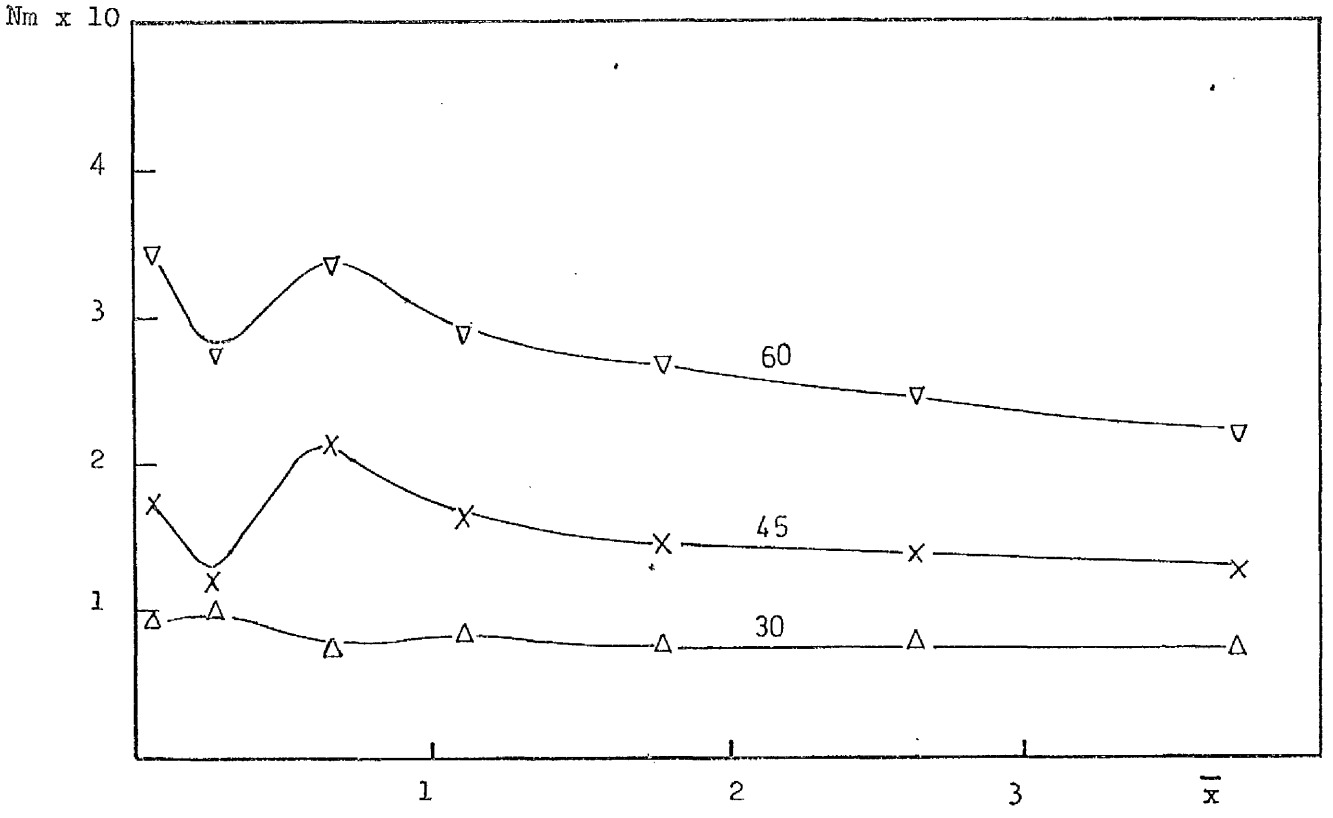

Figure 4.33.b :- Axial flux of tangential momenta
Annular swirlers cold flow in D/d = 2.5 furnace.

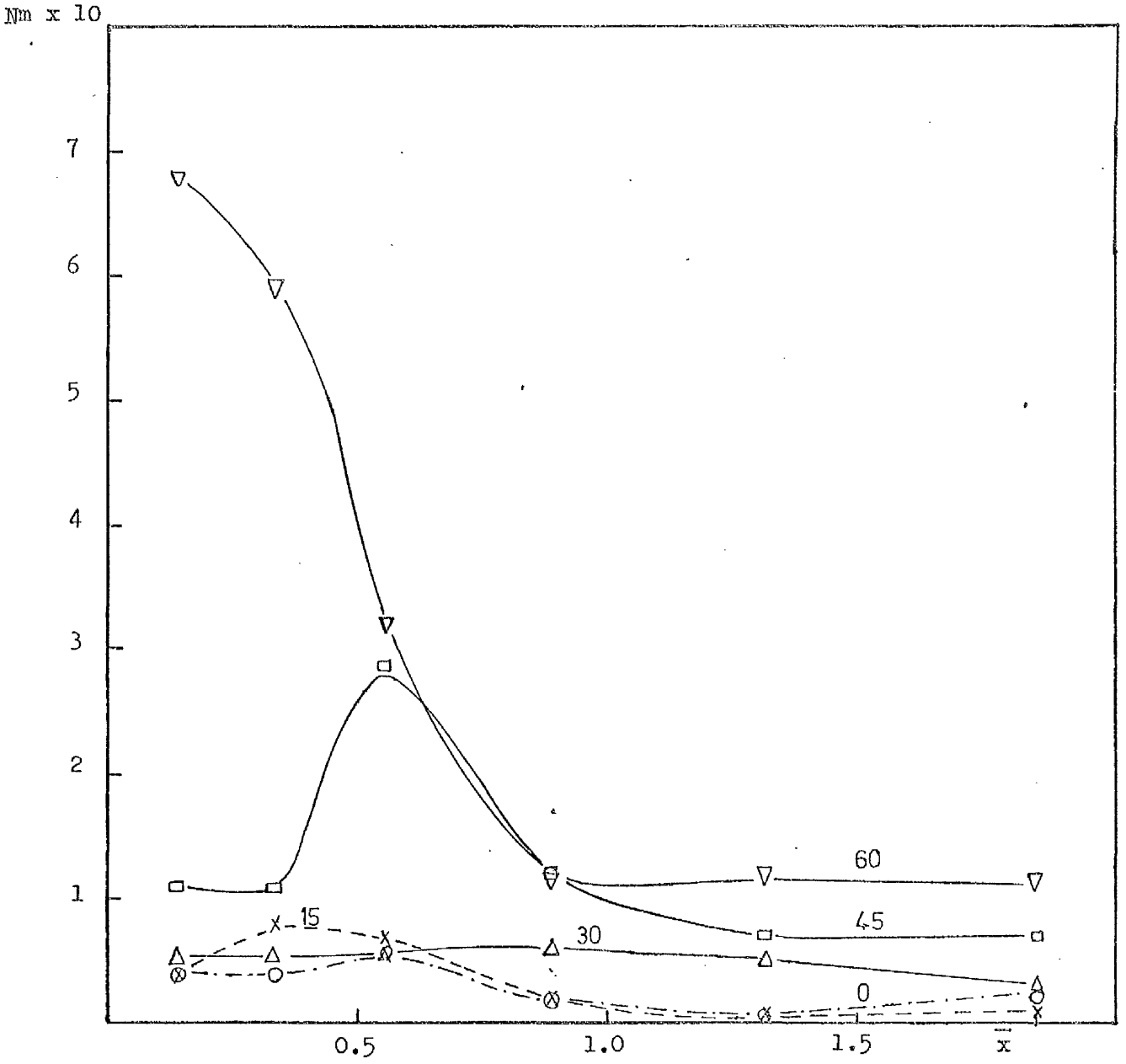

Figure 4.33.c :- Axial flux of tangential momenta
Hubless swirlers cold flow in D/d = 5 furnace.

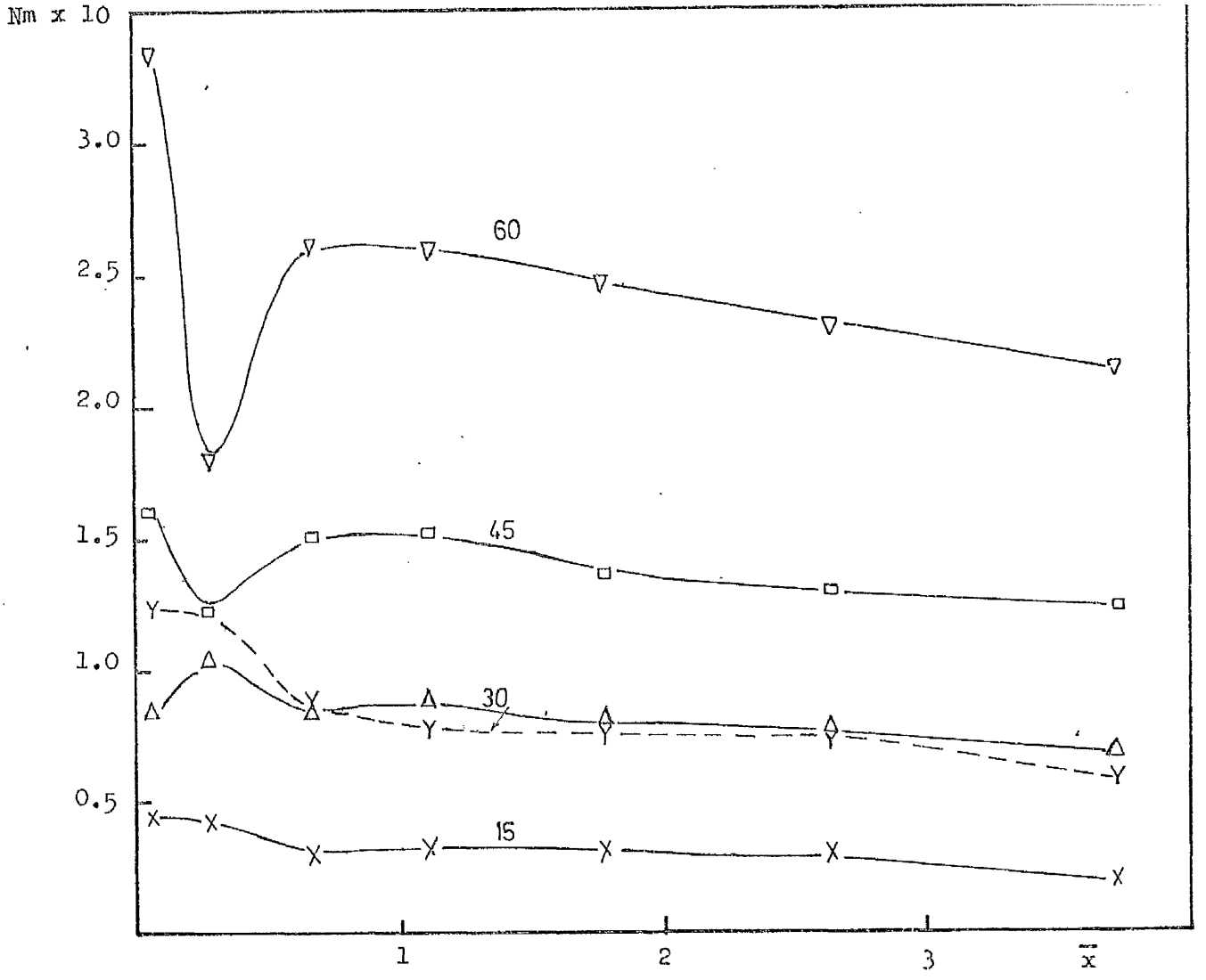

Figure 4.33.d :- Axial flux of tangential momenta
Hubless swirler flames in D/d = 2.5 furnace.

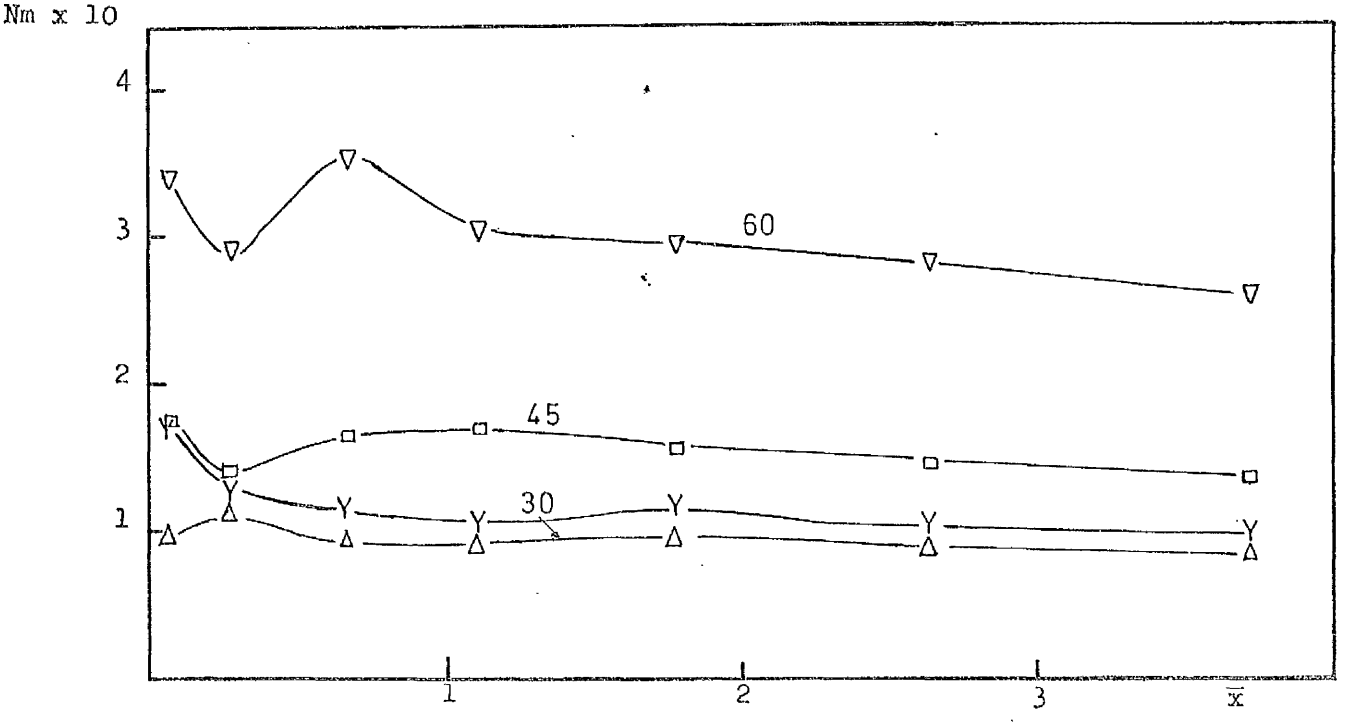

Figure 4.33.e :- Axial flux of tangential momenta
Annular swirler flames in D/d = 2.5 furnace.

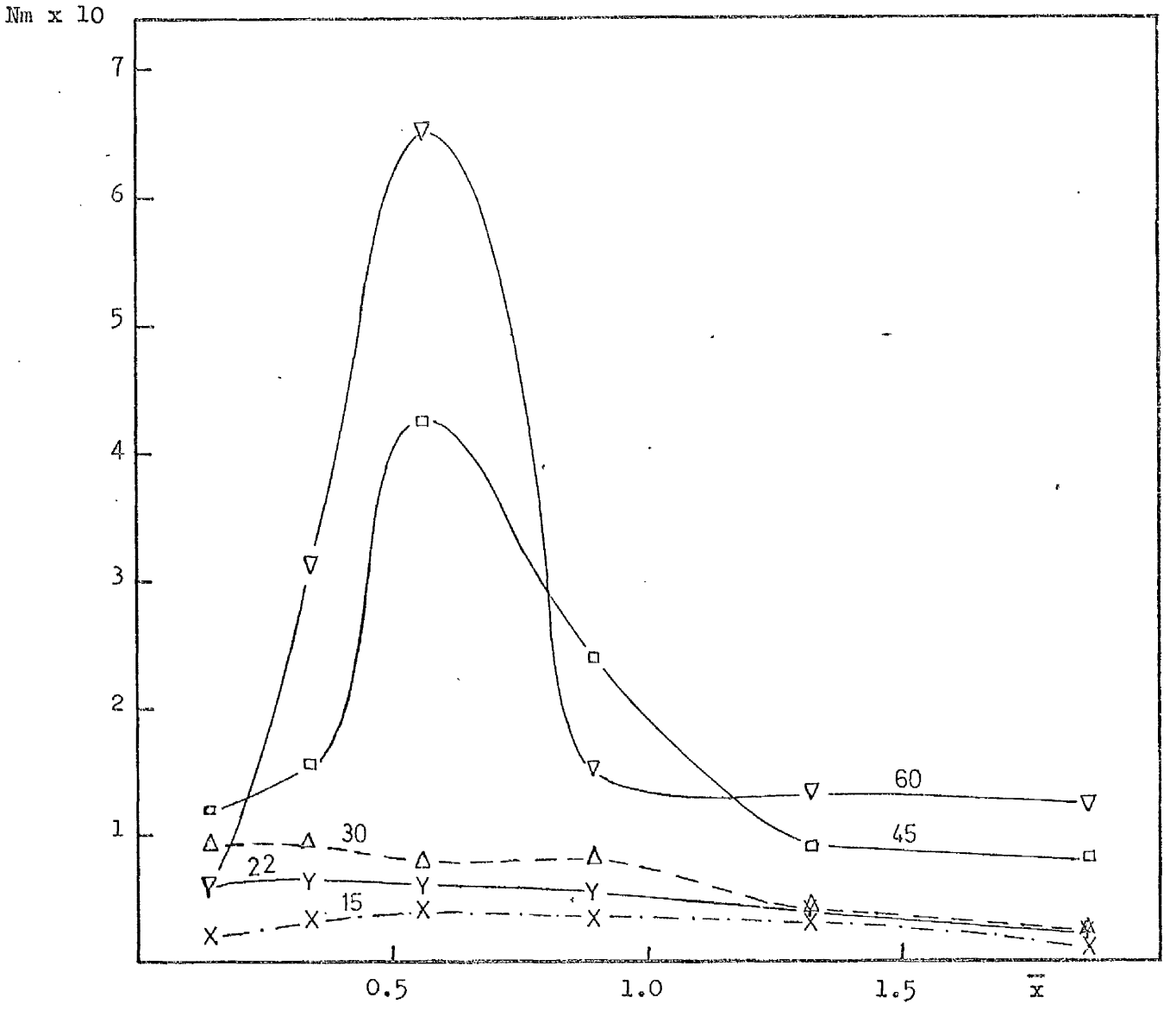

Figure 4.33.f :- Axial flux of tangential momenta
Hubless swirler flames in D/d = 5 furnace.

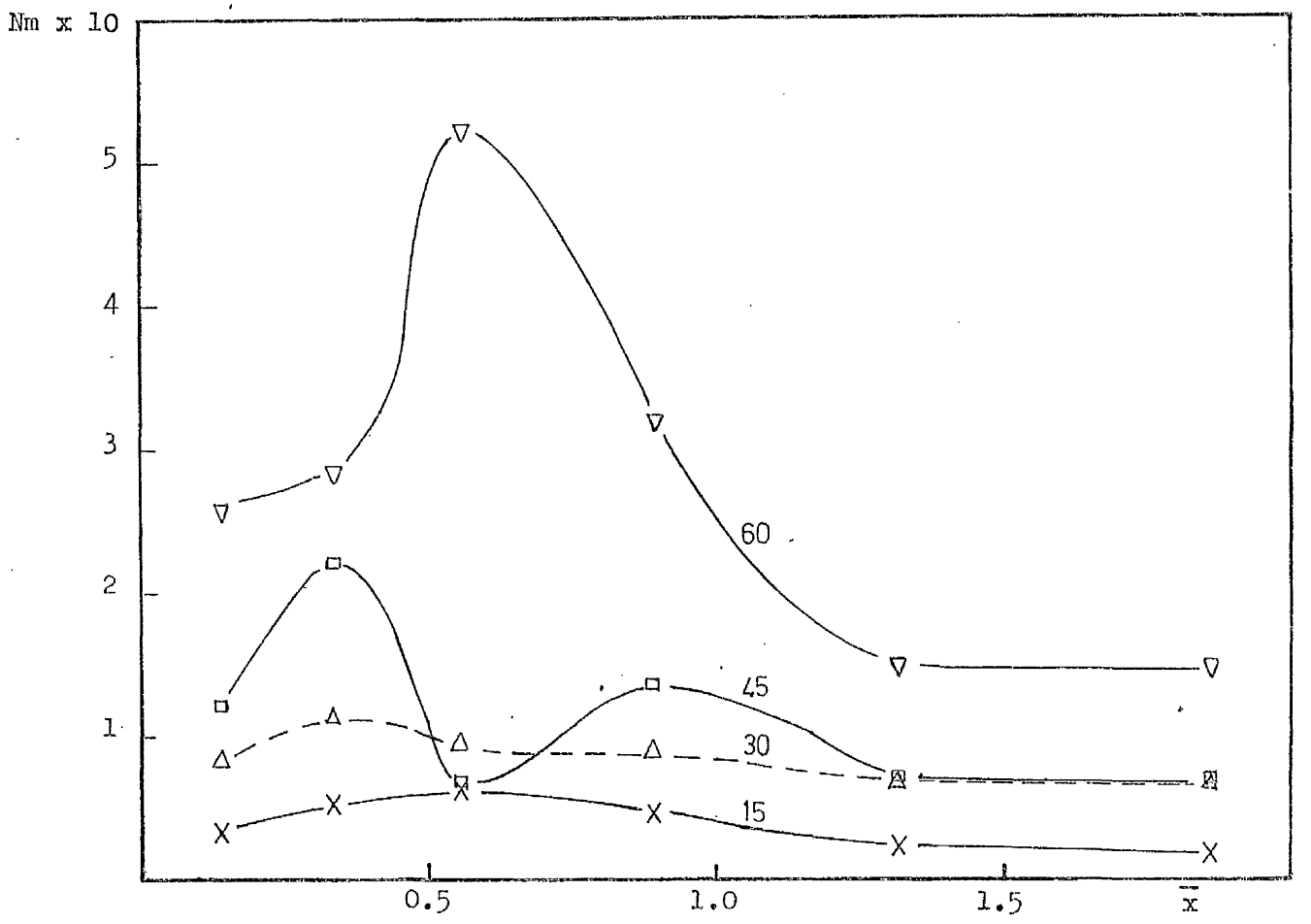

Figure 4.33.g :- Axial flux of tangential momenta
Annular swirler flames in D/d = 5 furnace.

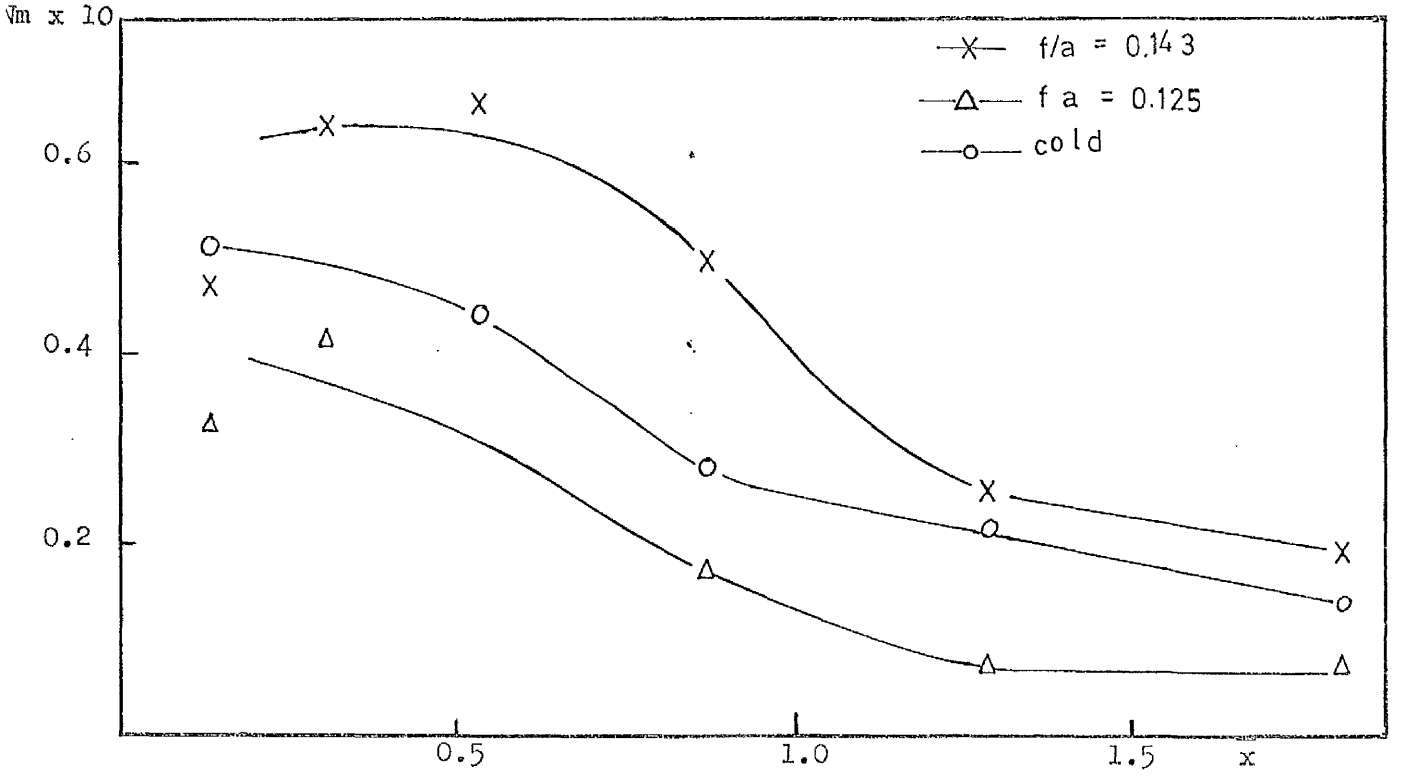

Figure 4.33.h :- Axial flux of tangential momenta
22.5 hubless swirler in D/d = 5 furnace.

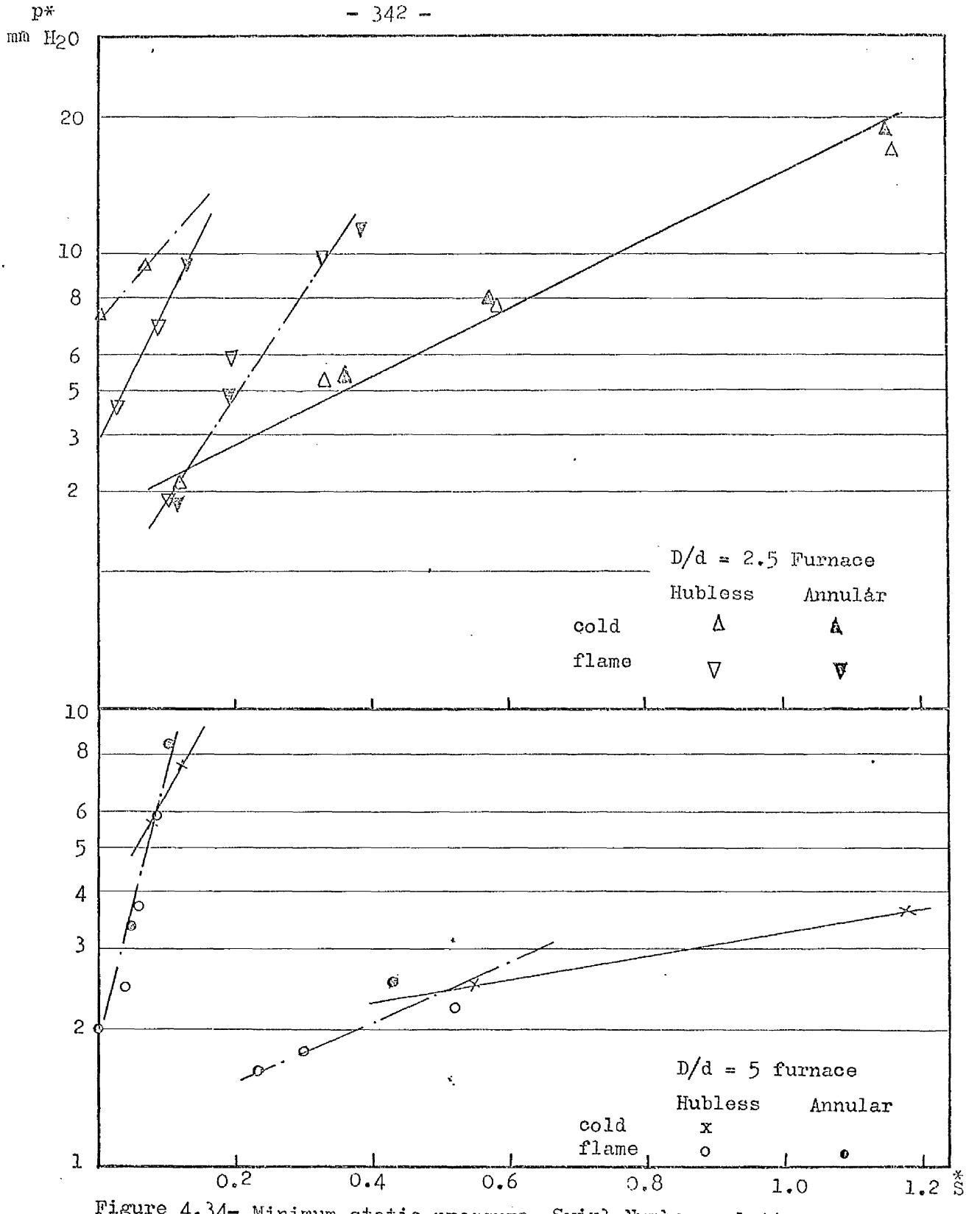

Figure 4.34- Minimum static pressure -Swirl Number relation

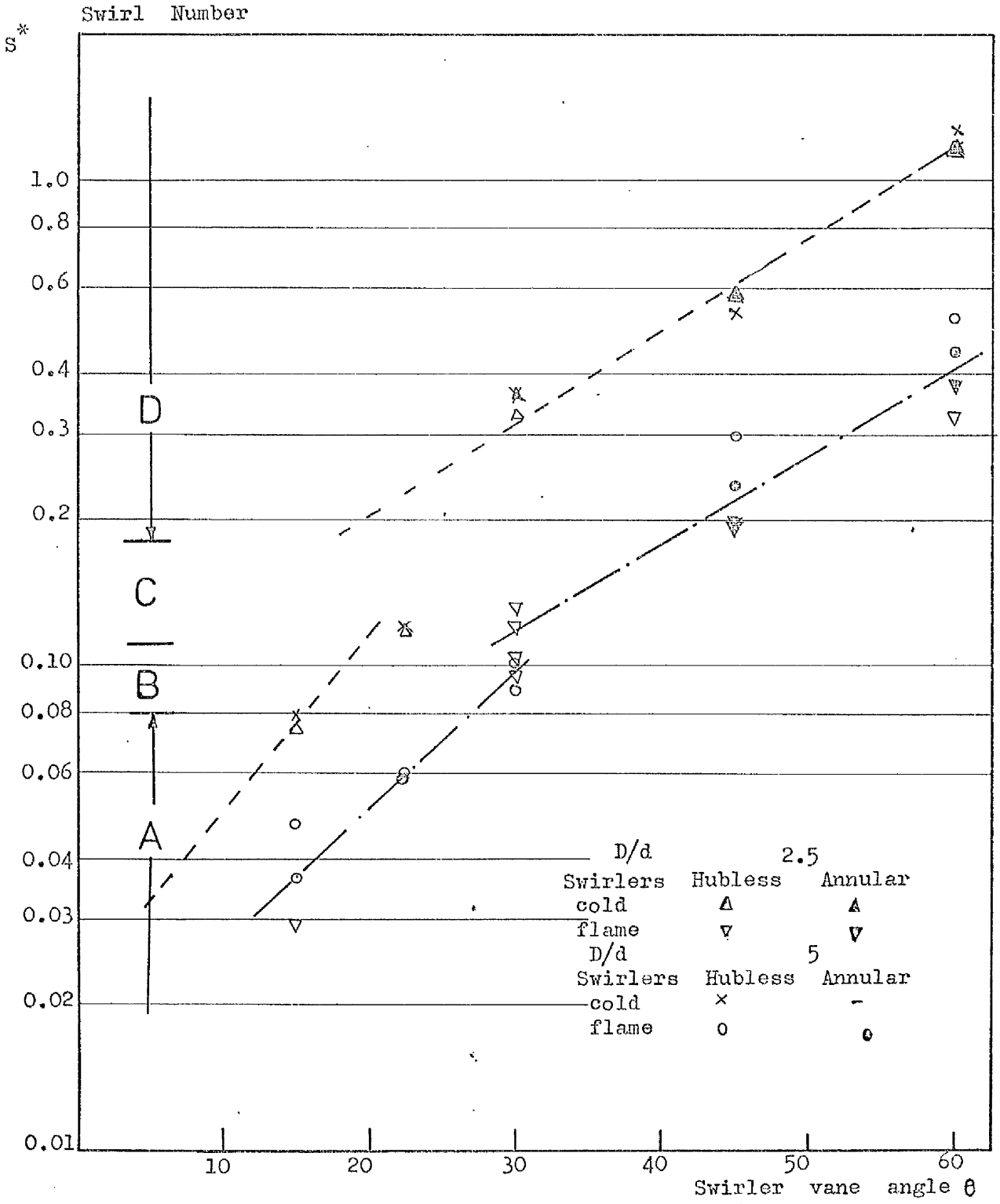

Figure 4.35 - Swirl Number relation to input conditions and flow types

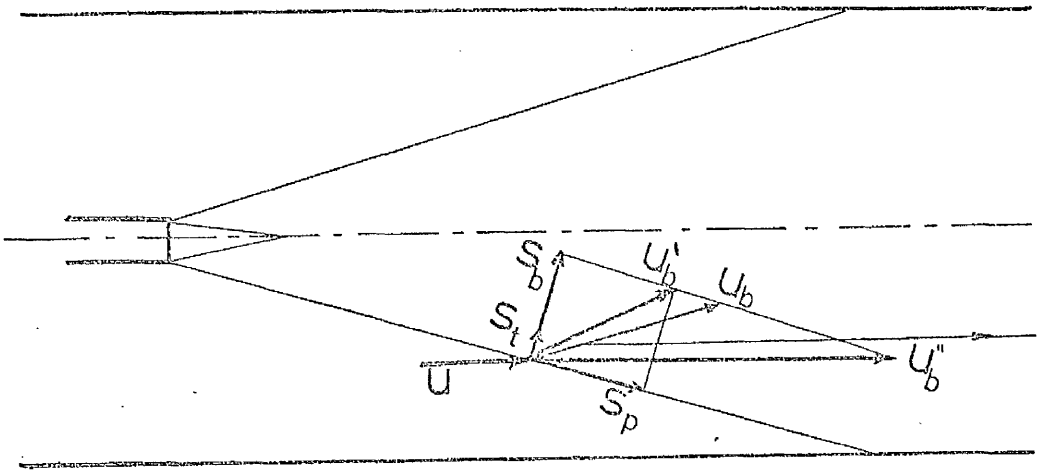

U	Total velocity of the unburnt gas
S_t	Unburnt gas velocity component normal to the flame front
S_p	Unburnt gas velocity component tangential to the flame front
U_b	Total velocity of the burnt gases, general case
U_b'	Total velocity of the burnt gases, plane wave
U_b''	Total velocity of the burnt gases, curved wave
S_b	Burnt gases velocity component normal to the flame front

Figure 5.1: Idealised flow pattern across a flame wave.

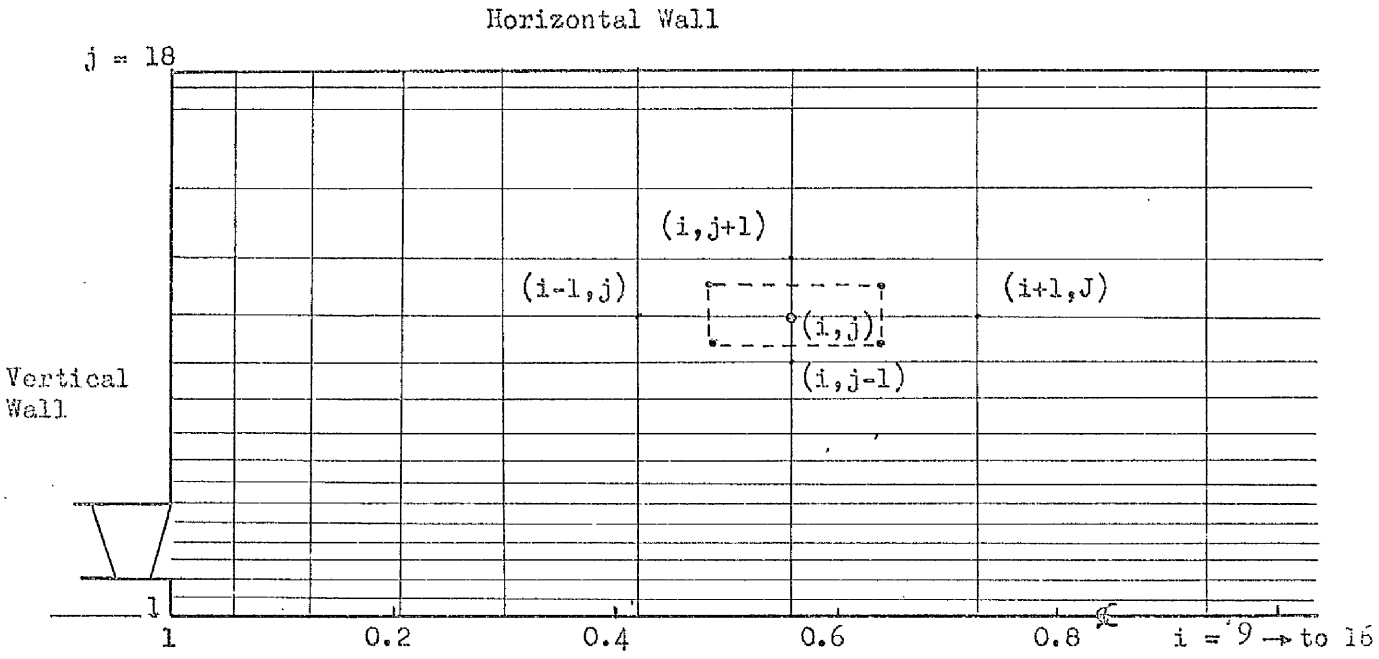

Figure 6.1 - Furnace geometry and grid arrangement

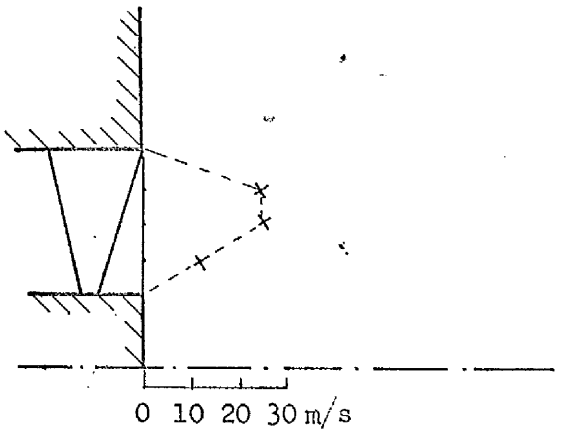

Figure 6.2. Assumed velocity distribution at swirler exit section

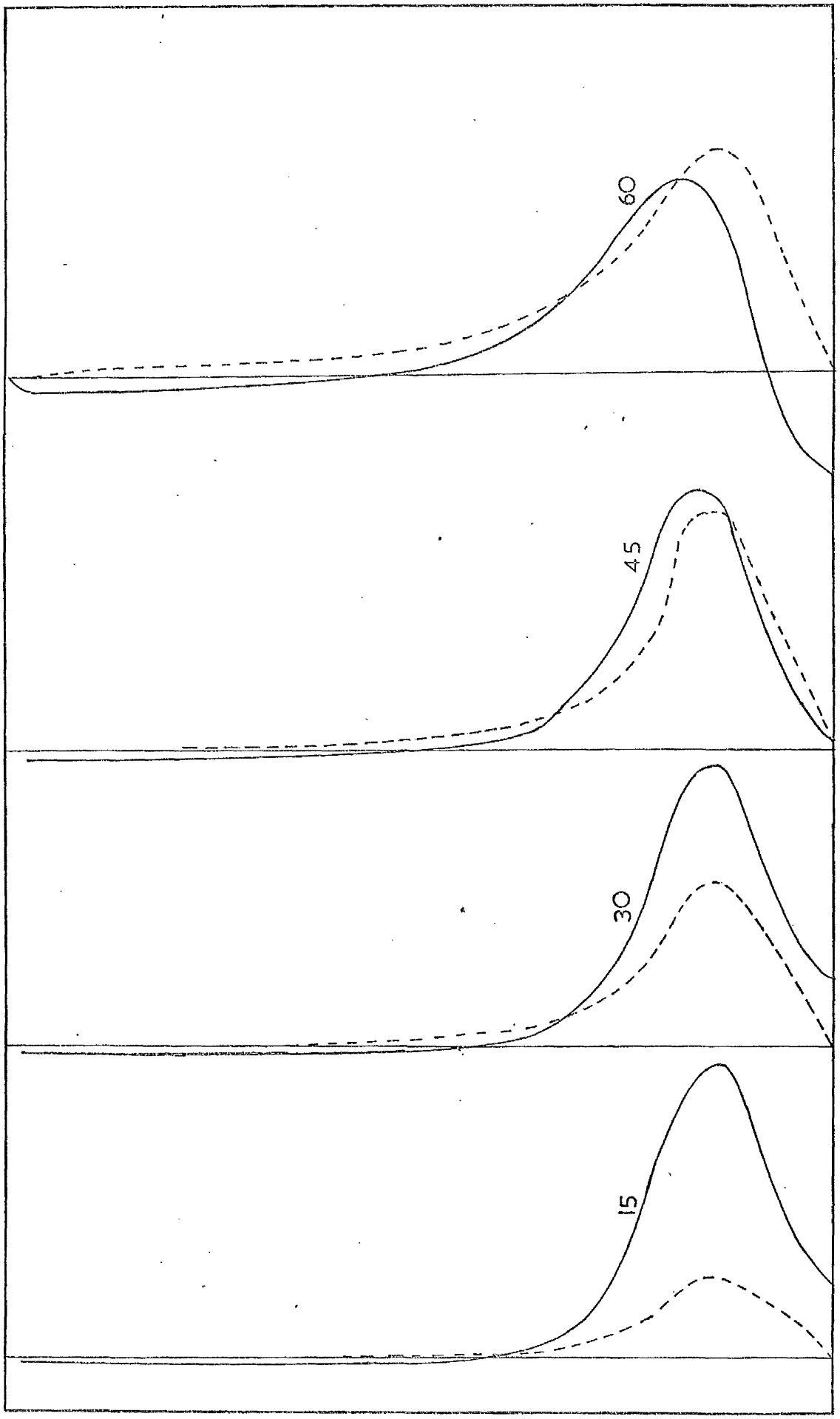

Figure 6.3.a - Predicted velocity profiles for cold flow in D/d = 5 furnace at $\bar{x}$ = 0.13

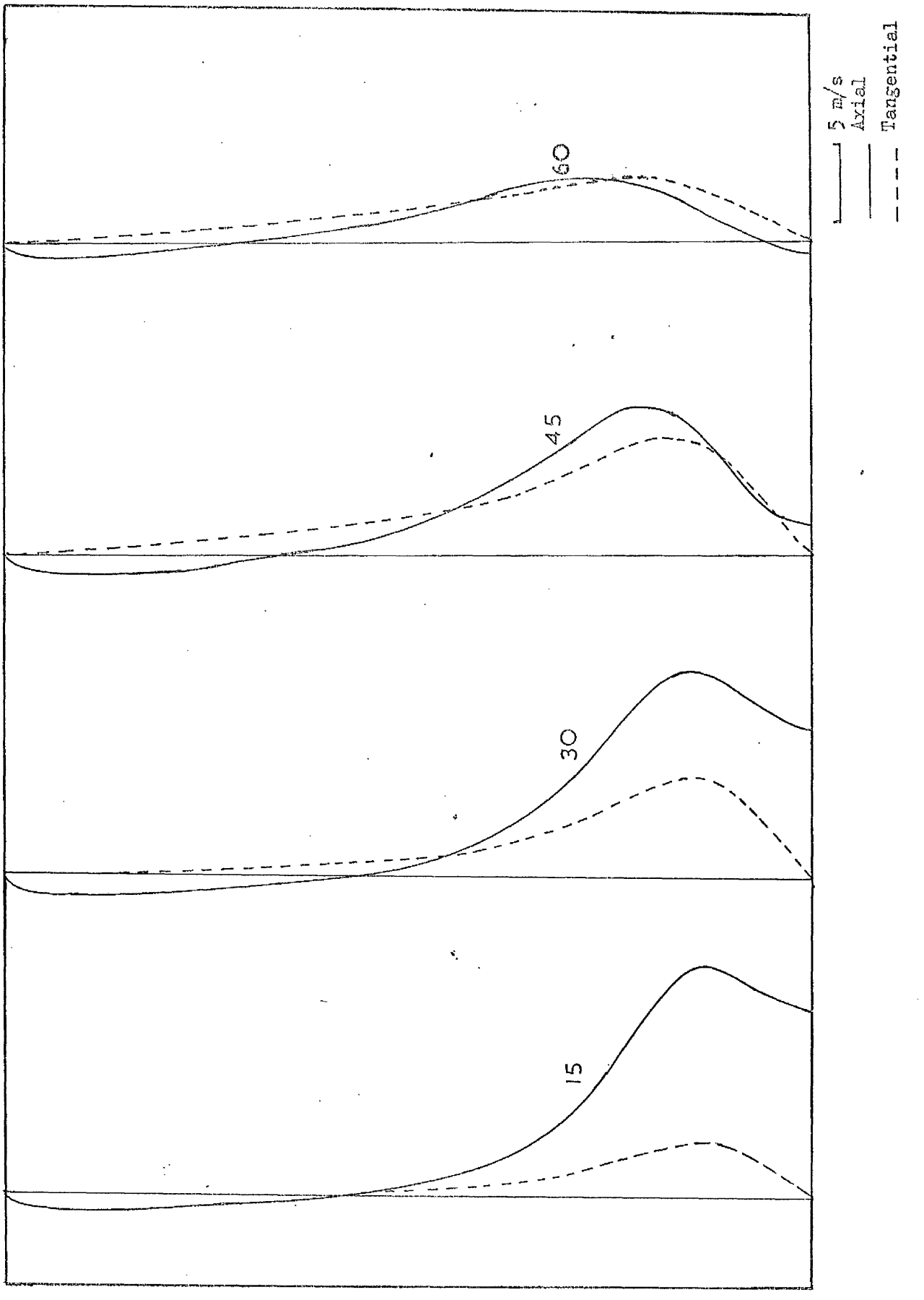

Figure 6.3.b. - Predicted velocity profiles for cold flow in D/d = 5 furnace at $\bar{x}$ = 0.3

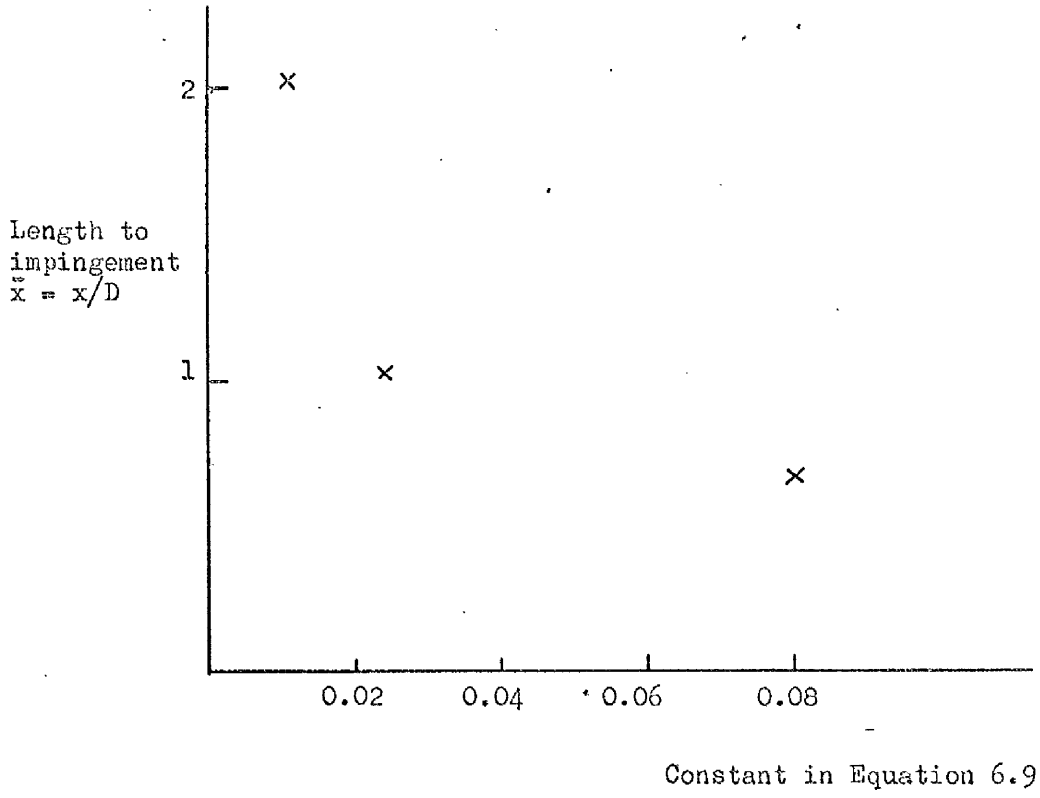

Figure 6.4. Jet spread variation with effective viscosity.

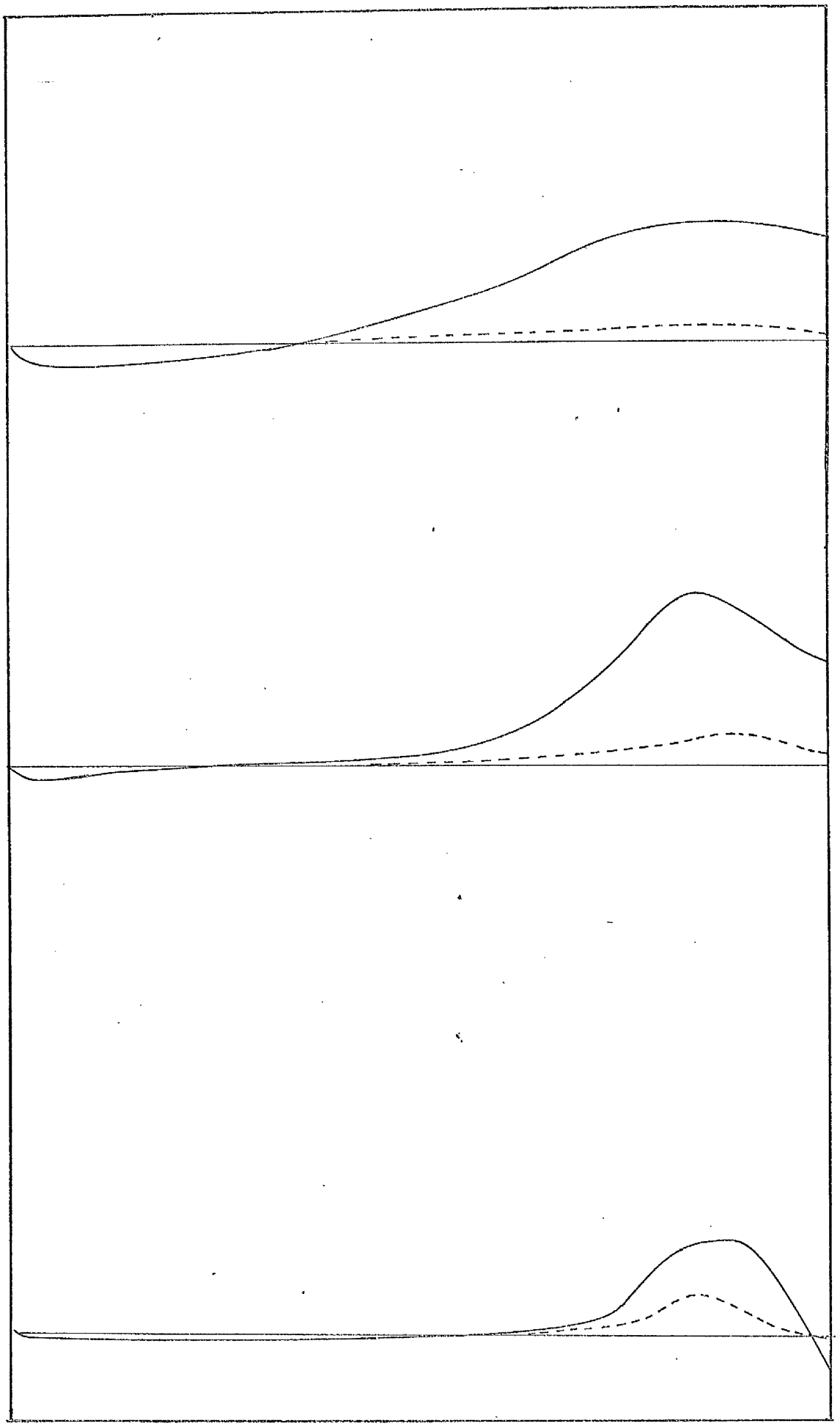

Figure 6.5.a. - Predicted velocity distributions 30° Annular Swirler flame in D/d = 5 furnace

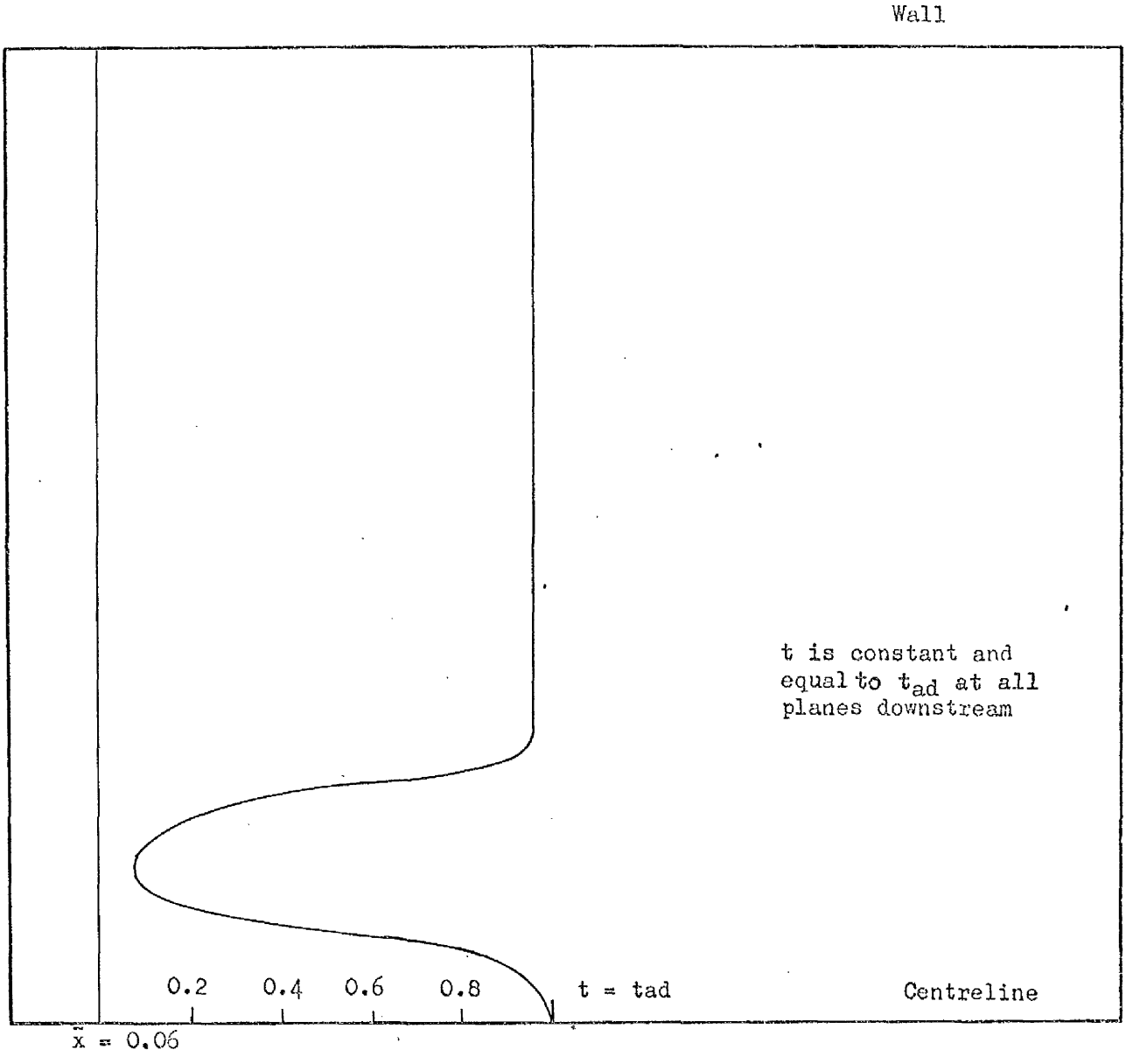

Figure 6.5.b - Predicted temperatures for 30° Annular Swirler flame in D/d = 5 furnace

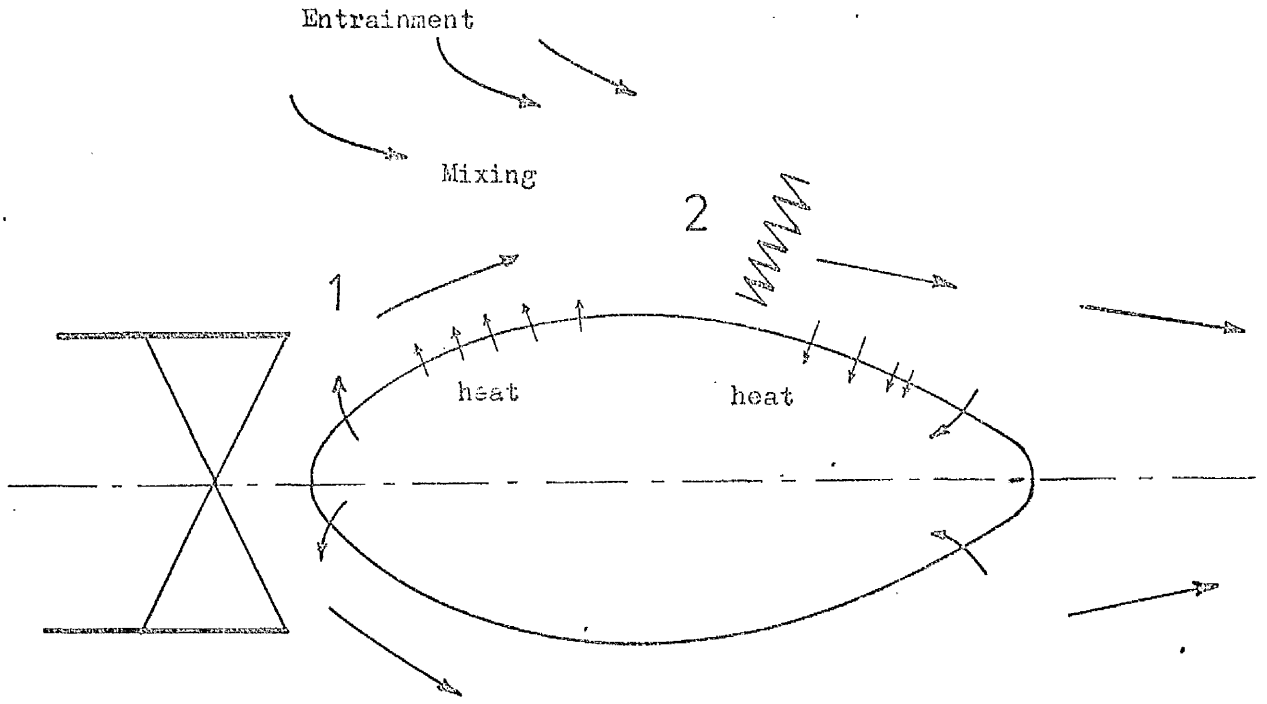

The point 2 moves progressively downstream with decreasing fuel/air ratio

(a) Flow pattern

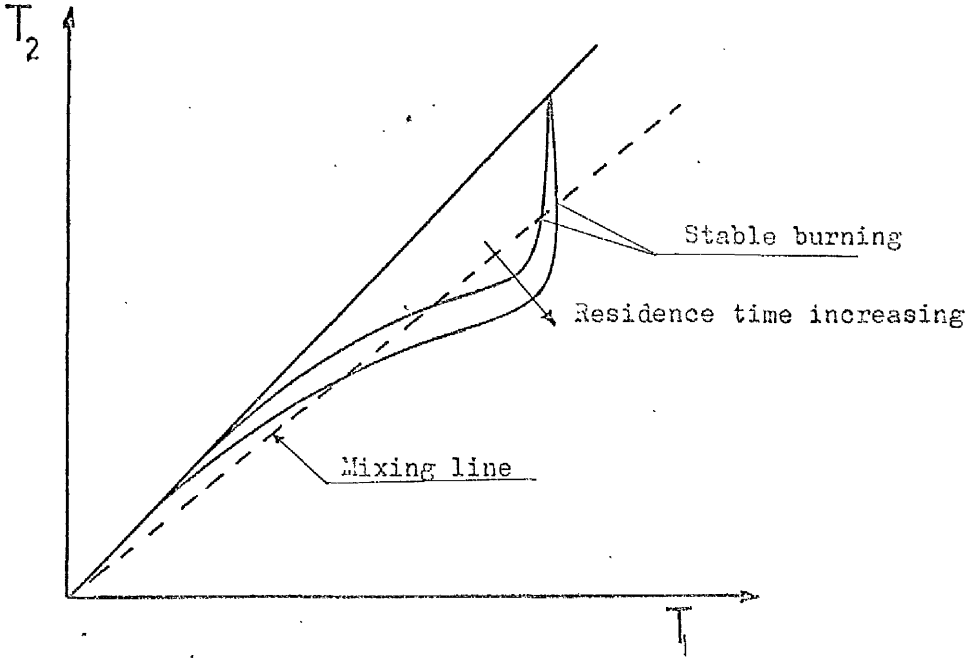

(b) Reaction Curves

Figure 7.1 - Mixing Model for flame stabilisation.

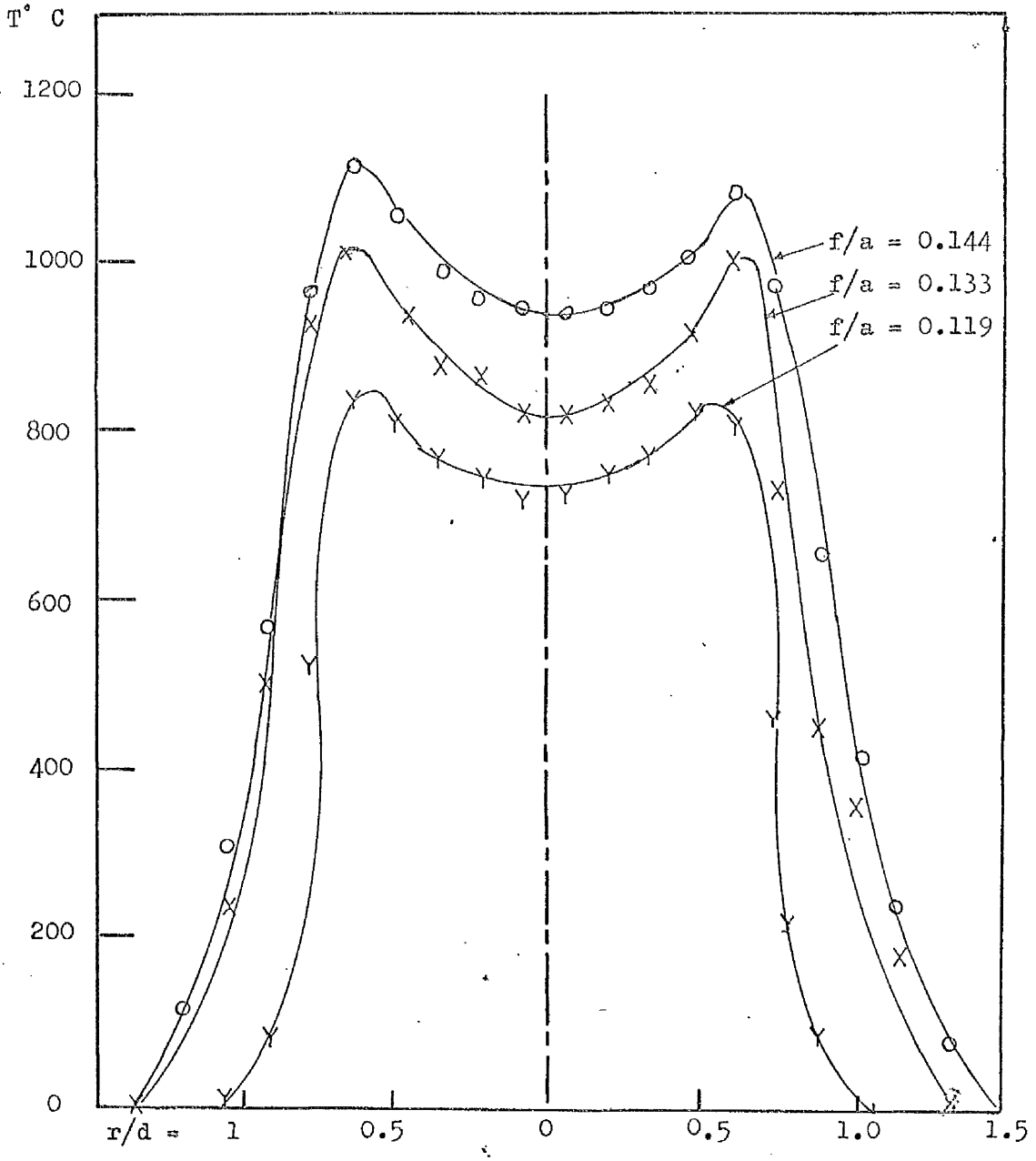

Figure 7.2 :- Temperature traverses for 45 hubless swirler free flame.

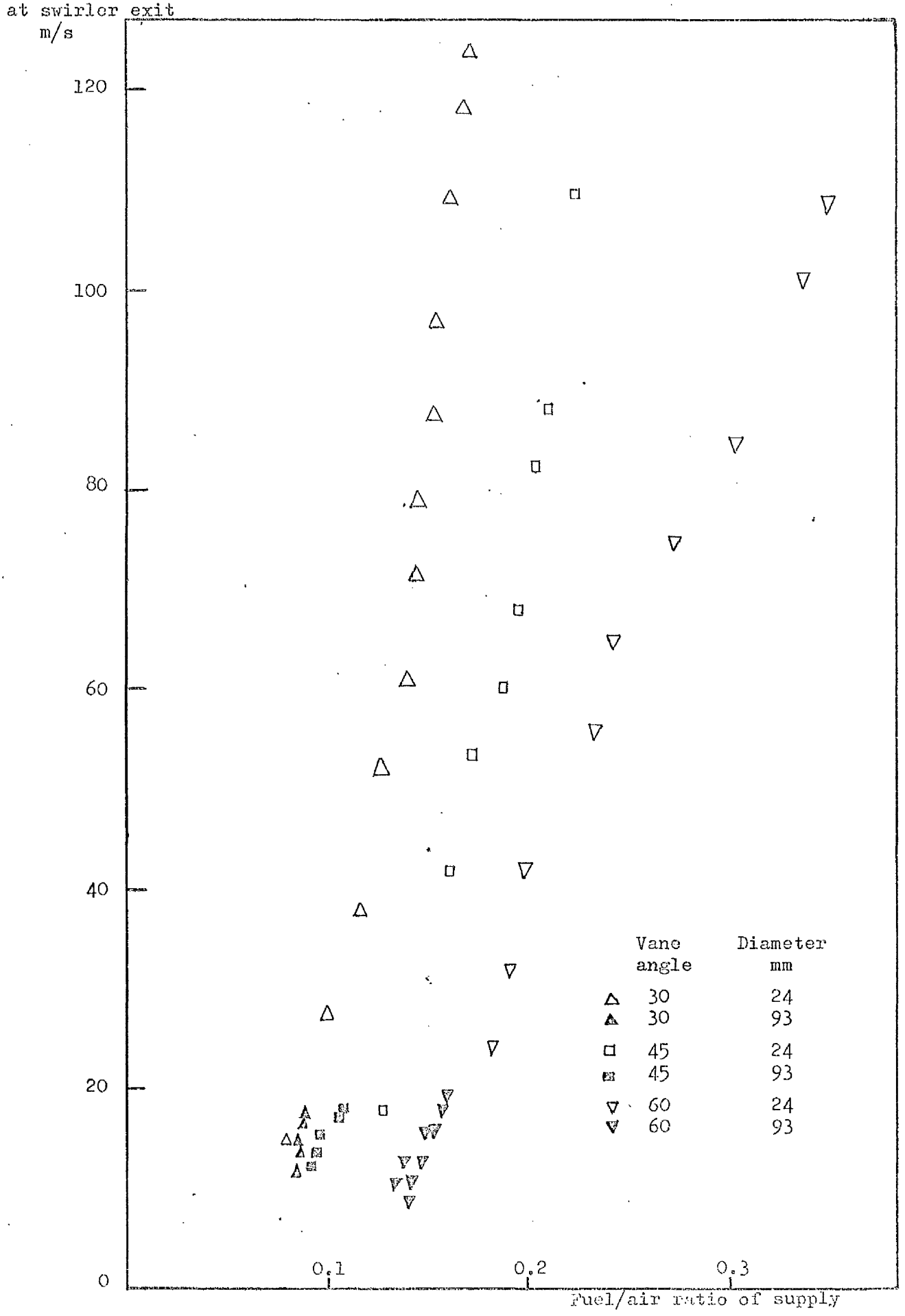

Figure 7.3 :- Effect of scale on weak stability of hubless swirler free flames.

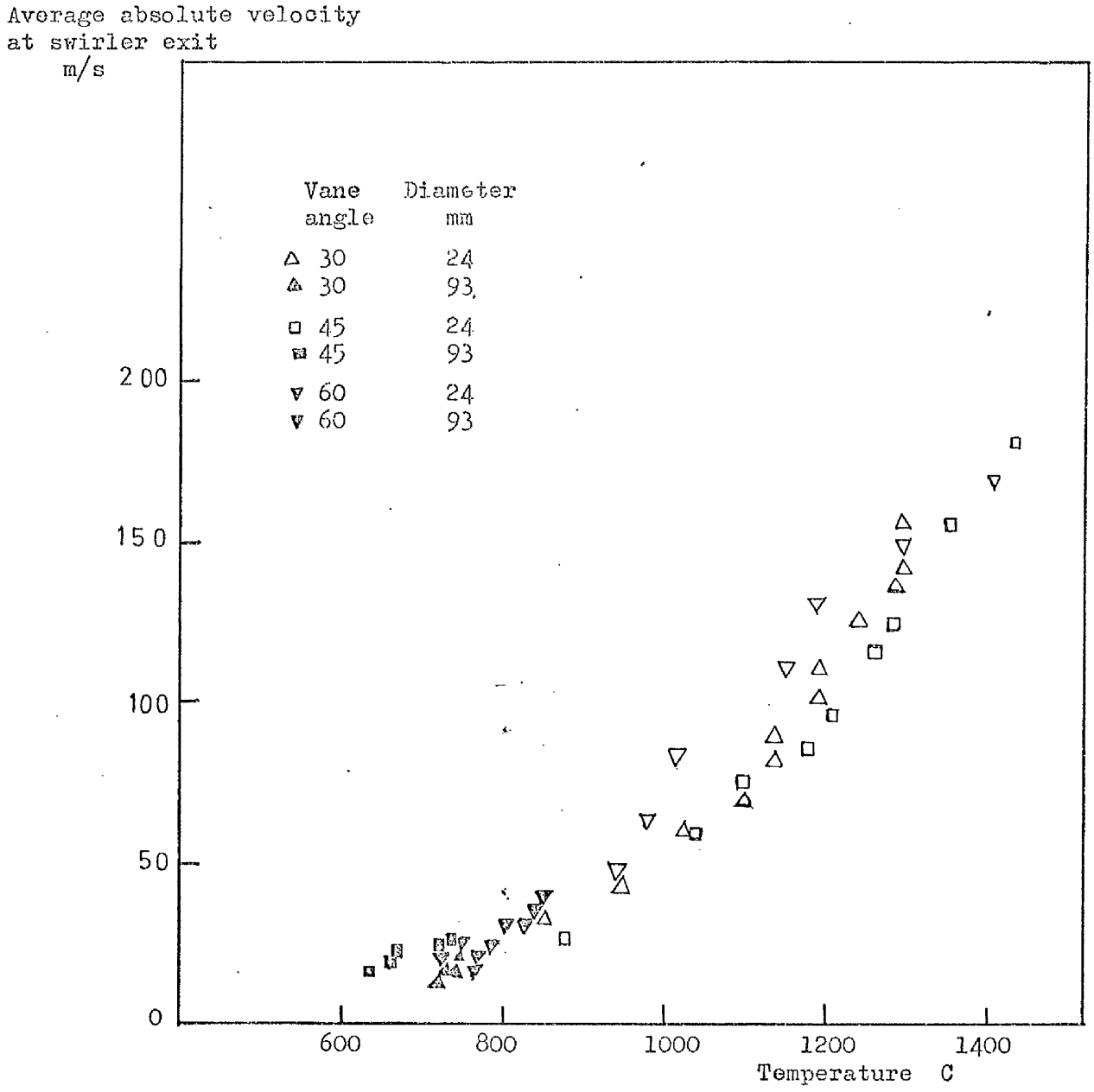

Figure 7.4 :- Correlation of weak stability limits of free flames by temperature at edge of CRZ.

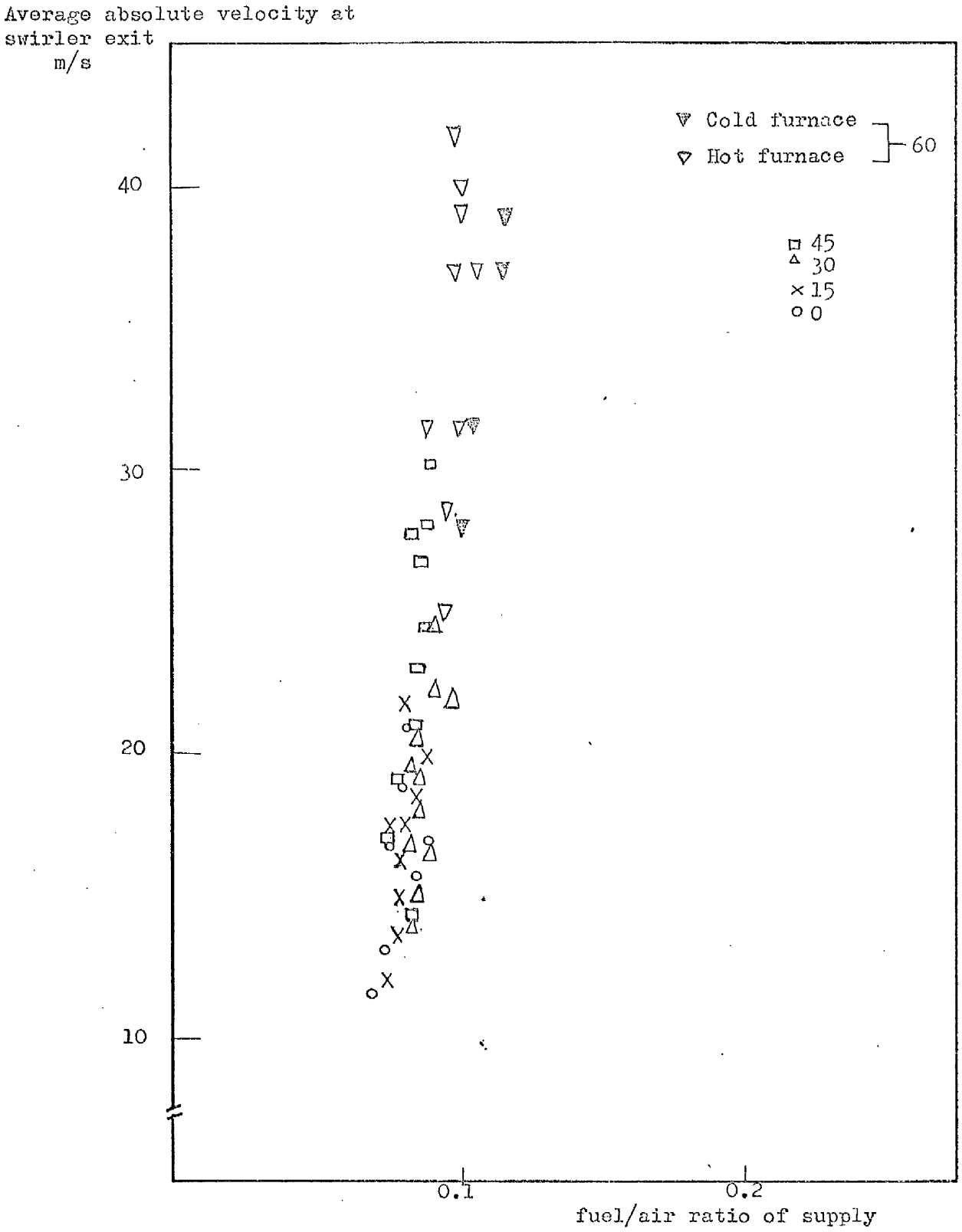

Figure 7.5.a :- Weak stability limits of enclosed swirling flames
Annular swirlers.

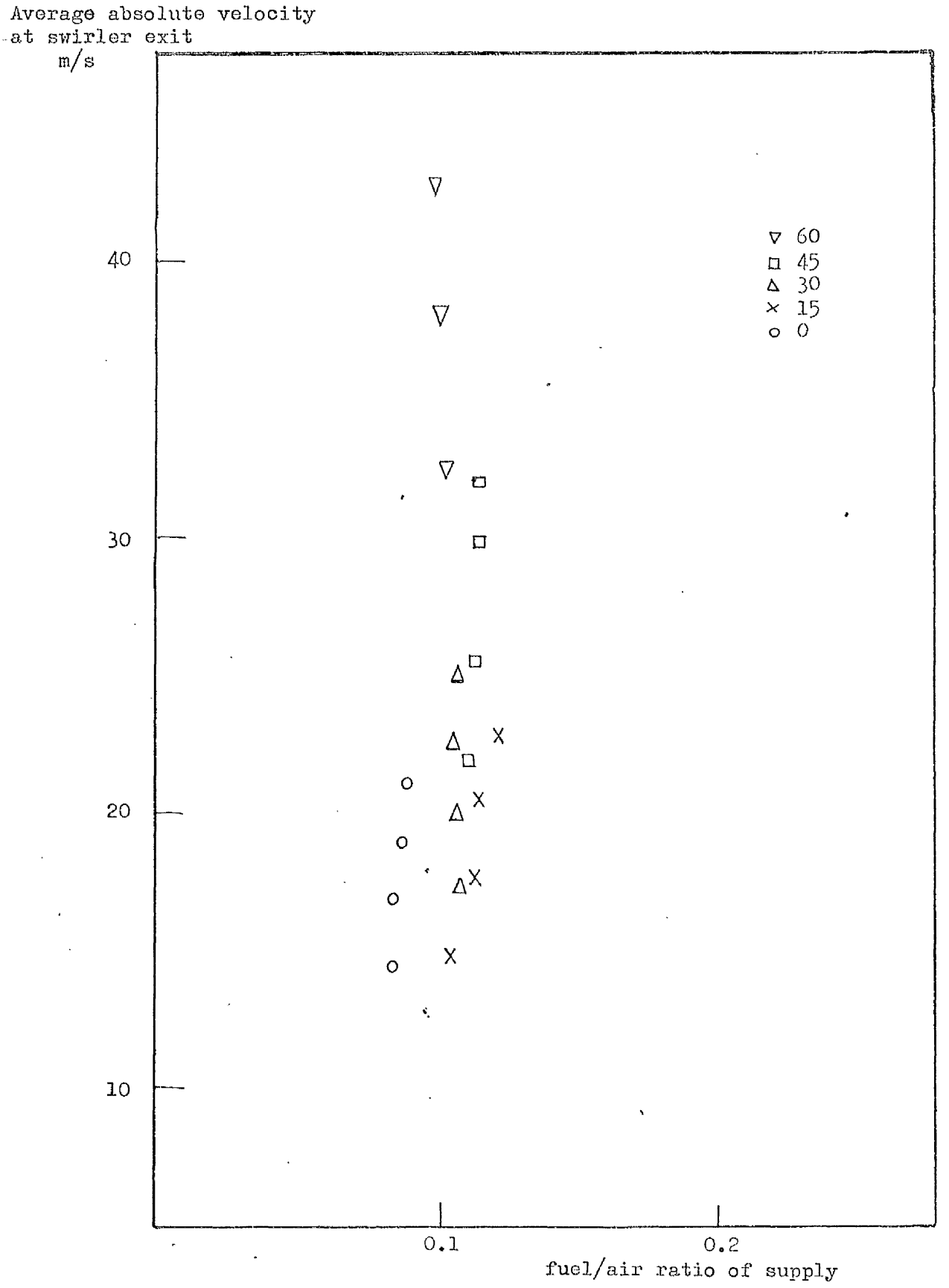

Figure 7.5.b :- Weak stability of enclosed swirling flames
Hubless swirlers.

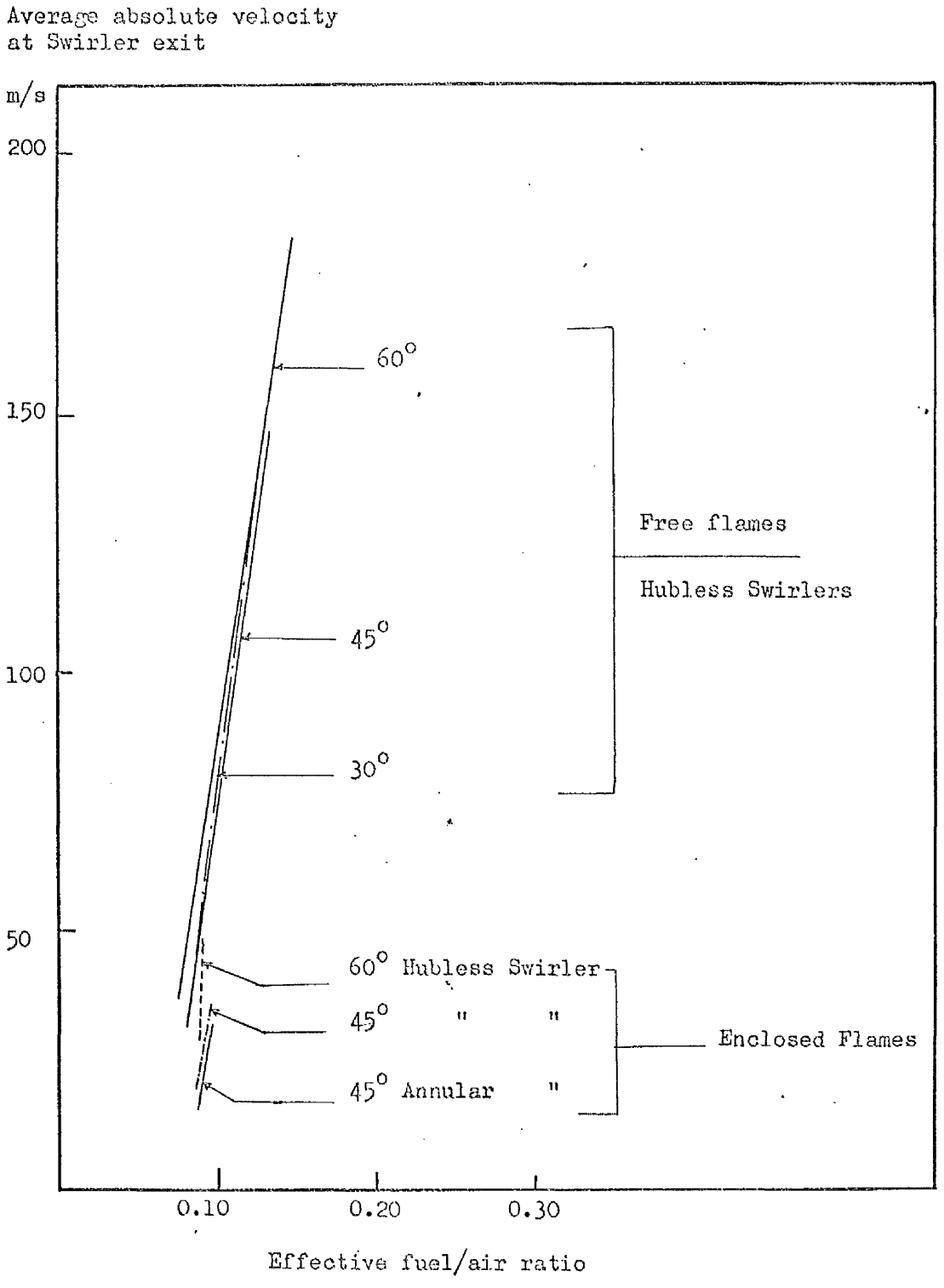

Figure 7.6 - Correlation of weak stability limits of Swirling flames

Free and enclosed

AERODYNAMICS OF SWIRLING FLAMES - VANE GENERATED TYPE

by
S.A. Beltagui and N.R.L. Maccallum
Department of Mechanical Engineering
University of Glasgow

Paper Presented at:-

The Combustion Institute European Symposium (1973)

28th March, 1973

AERODYNAMICS OF SWIRLING FLAMES - VANE GENERATED TYPE

by
S.A. Beltagui and N.R.L. Maccallum
Department of Mechanical Engineering
University of Glasgow

Introduction

Swirl produces notable effects on flames, generally making them shorter and highly stable over a wide range of air and fuel flows. This report describes research on the application of vane generated swirl to pre-mixed town gas-air flames in a furnace. The results are compared with corresponding free flames and isothermal jets.

Apparatus

Swirlers: of hubless and annular design (1), vanes placed at 15°, 30°, 45° and 60° to jet axis. diameters; hubless, 93mm; annular, 98 mm outer, 32 mm hub.

Furnace: firebrick walled, 0.46 m i.d., 1.42 m length.

Both annular and hubless swirlers were tested to provide information on the effect of the "bluff body" in the annular swirlers. The exit areas of both types were the same. The ratio of furnace diameter to burner diameter (D/d) is about 5, to provide valid comparisons with previous isothermal tests (1) at D/d of 2.6, this scaling being in accordance with Thring-Newby (2). There was no quarl and the exit from the swirler was in the plane of the end wall of the furnace.

Velocity components were measured using a 3-dimensional 3-hole water-cooled probe to the design of Hiett and Powell (3). This probe was suitably calibrated so that the static pressure was also obtained. Temperature was measured by a Pt 5% Rh - Pt 20% Rh thermocouple. Samples were analyzed for CO_2 using an Infra Red Gas Analyser.

Velocity, pressure, temperature and CO_2 distributions were observed at six radial planes at distances up to 1.8 D downstream from the burner.

The authors wish to acknowledge the financial support of the Science Research Council.

Swirling Flames

Results

The form of the results depended on whether or not a central recirculation zone (C.R.Z.) is established. There was a C.R.Z. with both the 45° and 60° swirlers (hubless and annular), but not with either the 15° or 30° swirlers. As an illustration for behaviour with a C.R.Z., the results for the 45° hubless swirler are shown in Figs. 1 and 2.

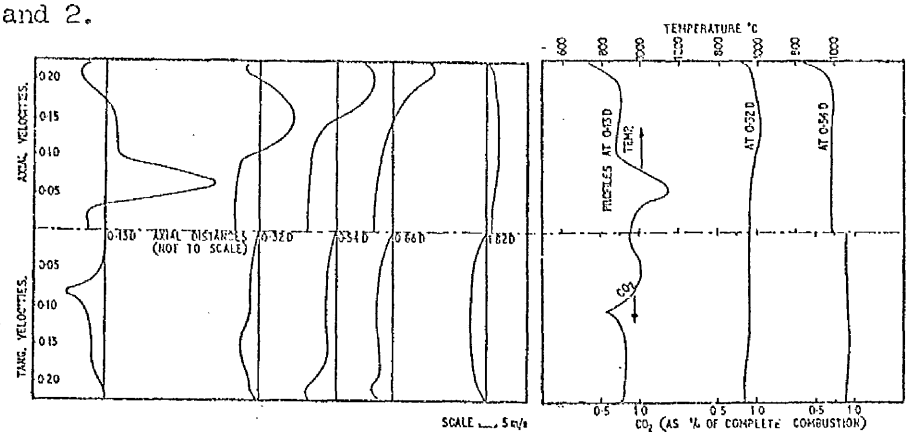

Fig. 1. VELOCITY PROFILES.

Fig. 2. PROFILES OF TEMP. AND CO_2

When there is no C.R.Z., increasing swirl increases the jet spread, but no more rapidly than in burning free jets (4). When central recirculation is established the jet spread is considerably more rapid than in the free jets. Impingement points are given in Table 1.

It is helpful to see the influence of swirl on the decays of the maximum velocities, static pressure on the axis and maximum temperature. These are shown for hubless swirlers in Figs. 3 to 6 respectively. As expected, the decays of the maximum axial velocities in the early part of the furnace are more rapid with high swirl. Once the jets have impinged on the walls of the furnace the decay is much reduced. The low swirl jets (0° and 15°) retain a central peak through the furnace. The maximum tangential velocities also decay more rapidly in the early section of the furnace with high swirl (although of course starting from initially high values). The notable feature of the variation of static pressure along the axis (Fig. 5) is how swirl initially creates a low pressure zone adjacent to the swirler, with pressure rising downstream. This gradient increases (30° swirler) until finally it is greater than the forward acting shear forces can maintain, and a central recirculation zone is formed, in which the

Swirling Flames

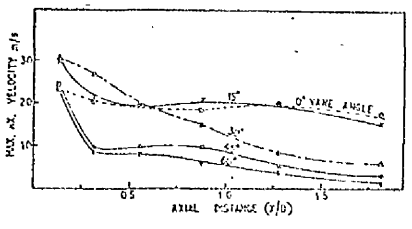

Fig.3. DECAY OF MAX. AXIAL VELOCITY.

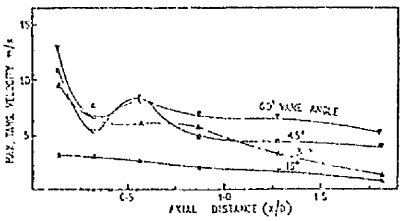

Fig.4. DECAY OF MAX. TANG. VELOCITY.

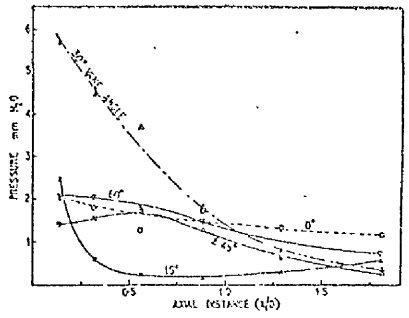

Fig.5. DECAY OF STATIC PRESSURE AT JET CENTRELINE ($P_o - P_c$)

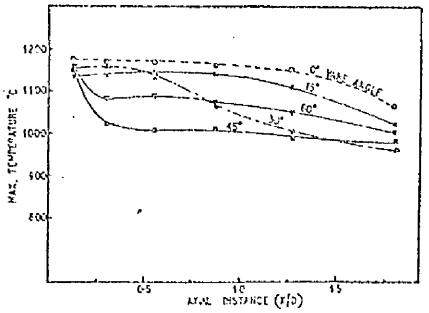

Fig.6. DECAY OF MAX. TEMPERATURE.

static pressure is much more even. Swirl tends to reduce the peaks in the temperature profiles, so that the maximum temperatures are lowered (Fig. 6).

Discussion of Results

The results arising from introducing the pre-mixed charge with swirl are found to depend on whether or not the swirl is sufficient to induce central recirculation. Central recirculation also plays an important part in flame stabilization (5). The criteria suggested from the observations for the creation of this C.R.Z. are now discussed.

As mentioned above C.R.Z's. were observed in the furnace tests only with the swirlers of vane angles of 45° and 60°. Isothermal tests in the present furnace and in the scaled furnace model (1) indicated C.R.Z.'s with the 30° and higher angle swirlers. Free jet observations, using similar swirlers, both isothermal (1) and burning (4), showed significant C.R.Z.'s only with the 45° and 60° swirlers.

Once established, the C.R.Z.'s in confined jets are seen to have dimensions which are essentially independent of further increase in swirl up to the vane angles of 60° (Table 1). The maximum diameter of the C.R.Z. is about 0.7

Swirling Flames

Swirl Angle	Enclos. diam.	Iso. or Burn.	Dist. to Impngt	C.R.Z.		U_{rmax}
				Max diam.	Length	U_o
15°	0.46	B	1.6 D	No C.R.Z.		
30°	0.46	B	1.1 D			
45°	0.46	B	0.4 D	0.6 D	1.5 D	0.43
60°	0.46	B	0.2 D	0.7 D	1.5 D	0.36
*30°	0.46	I	0.42D	0.66D	1.1 D	0.21
*45°	0.46	I	0.25D	0.73D	1.2 D	0.31
*60°	0.46	I	0.11D	0.8 D	1.2 D	0.38
30°(1)	0.25	I	0.41D	0.6 D	1.4 D	0.29
45°(1)	0.25	I	0.34D	0.65D	1.4 D	0.43
60°(1)	0.25	I	0.33D	0.65D	1.3 D	0.50

*Hubless swirlers - all others Annular.
(where both tested, results virtually identical).

TABLE 1. Impingement points and Central Recirculation Data.

of the furnace diameter, and essentially unaffected by combustion. Combustion slightly lengthens the zone, by about 20%. These results, particularly the comparison of the isothermal tests in the present furnace and in the model (1), indicate that, within the range of these tests, the C.R.Z. dimensions are a function of furnace diameter, and not of swirler diameter. This will only apply provided the walls influence the jet. If the ratio D/d exceeds some limit then the walls have negligible influence, the flow behaves as a free jet and any C.R.Z. will depend upon the swirler dimensions. It is thought that the limiting value of this diameter ratio for the enclosure to be effective might be about 8 for the 45° swirler, but will be larger at higher degrees of swirl.

When the enclosing walls have an effect, it would seem that the swirl parameter to be used in comparing flows

should be ($2\ G_t/G_x D$) rather than ($2\ G_t/G_x d$). Strictly, the axial momentum flux, G_x, includes a static pressure term in addition to the momentum term. In the previous analysis of these vane swirlers (1), the static pressure term was ignored and the swirl number based on the swirler diameter was simply ($2 \tan \theta/3$ (hubless). So the swirl parameter based on furnace diameter will be ($2d \tan \theta/(3D)$. This would indicate that for a given swirler size, the smaller the enclosure, the smaller the vane angle required to produce a C.R.Z. Unfortunately the steps in vane angles were too great to confirm this quantitatively, but the indications from the velocity distributions in the "near critical" swirlers point in this direction. The explanation for the 30° swirler in the 0.46 m enclosure giving a C.R.Z. in the isothermal test but not in the burning test is considered to lie in the effect of combustion on the static pressure. This raises the pressure in the approach stream and increases the axial momentum flux, as compared to the isothermal case. The increase depends on fuel/air ratio etc. but is probably at least 10% of the momentum component. Allowance for this static pressure shows the effective swirl parameter in the burning case to be less than in the isothermal flow (this conclusion is similar to that reached by Wu and Fricker (6)).

On comparing the initial spreads of the jets in the present furnace and in the isothermal model (1) it is seen that the impingement points in the model using the 30° swirler corresponds with the furnace using the 45° swirler. This is in fair agreement with Kerr (7) who suggested that, after scaling burner diameters according to Thring-Newby, the vane angle should be adjusted according to (ignoring hub effect)

$$\frac{\text{Tan } \theta_{mod}}{\text{Tan } \theta_{furn}} = \sqrt{\frac{\rho_{furn}}{\rho_{mod}}} \qquad (1)$$

where the model fluid is air. A problem in the application of this lies in specifying ρ_{furn}. Kerr, in deriving equation (1), considered that for equivalent flows in the enclosure, the swirl parameters based on the enclosure dimensions should be equal. The observations on C.R.Z.'s in the present work have suggested the same conclusion.

Swirling Flames

Conclusions

The confinement of swirling flames only has significant effects on the velocity profiles etc. if the combination of enclosure dimension and degree of swirl is sufficient to create a C.R.Z. If a C.R.Z. is created then the spread of the jet is more rapid than in the free case. The dimensions of the C.R.Z. are primarily functions of the enclosure dimension. The swirl parameter for the formation of the C.R.Z. should be based on the enclosure dimension. Kerr's proposal for adjustment of vane angle in isothermal models is supported.

References

1. MATHUR, M.L. and MACCALLUM, N.R.L., "Swirling air jets issuing from vane swirlers. Parts I and II". J. Inst. Fuel 40, p.214 and p.238 (1967).
2. THRING, M.W. and NEWBY, M.P., "Combustion length of enclosed turbulent jet flames". Fourth Symposium (International) on Combustion, Williams and Wilkins, Baltimore (1953), p.789.
3. HIETT, G.F. and POWELL, G.E., "Three-dimensional probe for investigation of flow patterns". The Engineer, 213, p.165 (1962)
4. BAFUWA, G.G. and MACCALLUM, N.R.L., "Turbulent swirling flames issuing from vane swirlers", 18th Meeting, Aerodynamics Panel, IFRF, Paris 1970, Doc No. G02/ca/5.
5. BAFUWA, G.G. and MACCALLUM, N.R.L., "Flame stabilization in swirling jets", Combustion Institute European Symposium, Sheffield, 1973.
6. WU, H.L. and FRICKER, N., "An investigation of the behaviour of swirling jet flames in a narrow cylindrical furnace". 2nd Members Conference, IFRF, 1971, Doc No. K20/a/61.
7. KERR, N.M., "Swirl. Part II: Effect on flame performance and the modelling of swirling flames", J. Inst. Fuel 38, p.527 (1965).

Nomenclature

D	furnace diameter
d	burner diameter
G_x	axial momentum flux
G_t	axial flux of tangential momentum
θ	vane angle (to axis)
ρ_{mod}	fluid density in model
ρ_{furn}	fluid density in furnace